Thermochromism and Photomotion of Azobenzene-Containing Polymers and Hydrogels

DISSERTATION

zur Erlangung des Grades eines Doktors

in den Naturwissenschaften

vorgelegt von

Thorben Gwydion Jaik, M. Sc.

eingereicht bei der Naturwissenschaftlich-Technischen Fakultät

der Universität Siegen

Siegen 2022

Betreuer und erster Gutachter
Prof. Dr. Ulrich Jonas
Universität Siegen

Zweiter Gutachter
Prof. Dr. Thomas Lenzer
Universität Siegen

Tag der mündlichen Prüfung
17.01.2023

The presented dissertation was prepared in the time between December 2015 and September 2022 in the Department of Chemistry and Biology of the Faculty of Natural Sciences and Engineering at the University of Siegen under the supervision of Prof. Dr. Ulrich Jonas in Macromolecular Chemistry.

Erklärung

Ich erkläre hiermit an Eides statt, dass ich die vorliegende Arbeit ohne unzulässige Hilfe Dritter und ohne Benutzung anderer, nicht angegebener Hilfsmittel angefertigt habe. Die aus anderen Quellen direkt oder indirekt übernommenen Daten und Konzepte sind unter Angabe der Quelle gekennzeichnet. Einhergehend zu jedem Kapitel ist beschrieben, wenn Teile der Arbeit in Kollaboration durchgeführt wurden und welche Anteile von mir stammen. Die Arbeit wurde weder im In- noch im Ausland in gleicher oder ähnlicher Form einer anderen Prüfungsbehörde vorgelegt. Es wurden keine Dienste eines Promotionsvermittlungsinstituts oder einer ähnlichen Organisation in Anspruch genommen. Ich habe weder früher noch gleichzeitig bei einer anderen Hochschule oder in einer anderen Fakultät ein Promotionsverfahren beantragt.
Weiterhin erkläre ich, dass mir die Promotionsordnung der Naturwissenschaftlich-Technischen Fakultät der Universität Siegen mit Stand des 10. August 2020 bekannt ist und von mir anerkannt wird.

Declaration of Authorship

I hereby declare that I have produced the present thesis without the unauthorized help of third parties and without the use of other resources, which have not been attributed. Any data or concepts taken directly or indirectly from other sources have been attributed by citing the source. Prior to each chapter my contributions are described if parts of the work have been produced in collaboration. Prior to this date, the work has not been submitted to any other examination authority either in Germany or in another country in the same or in a similar form. I have not used the services of a doctoral procurement institute or of any organization of similar nature. Moreover, I have not applied for a doctoral process neither earlier nor currently at any other university or faculty.
Furthermore, I declare that I am aware of the doctoral regulations of the Faculty of Natural Sciences and Engineering of the University of Siegen dated 10th of August 2020 and that I fully acknowledge them.

Siegen, 08.09.2022

Thorben Gwydion Jaik

And then there is Nature

List of Publications

T. G. Jaik, B. Ciubini, F. Frascella, U. Jonas, Thermal Response and Thermochromism of Methyl Red-Based Copolymer Systems - Coupled Responsiveness in Critical Solution Behaviour and Optical Absorption Properties. *Polym. Chem.* **2022**, *13*, 1186–1214.
DOI: 10.1039/D1PY01361K.

T. G. Jaik, U. Jonas, The "Tethered Solvent" Effect - H-Bonding-Controlled Thermo-Halochromism of a Push-Pull Azo Chromophore via its Secondary Amidoalkyl Acrylamide Side Chain. *ChemPhysChem* **2022**, *accepted.*
DOI: 10.1002/cphc.202200512

T. G. Jaik, U. Jonas, Thermo-Tautochromic Polymer Architectures from Tertiary Methyl Red Amides. *Macromol. Chem. Phys.* **2022**, *accepted.*
DOI: 10.1002/macp.202200201

T. G. Jaik, A. M. Flatae, N. Soltani, P. Reuschel, M. Agio, E. Descrovi, U. Jonas, Photomotion of Hydrogels with Covalently Attached Azo Dye Moieties – Thermoresponsive and Non-Thermoresponsive Gels. *Gels,* **2022**, *8*, 541-552.
DOI: 10.3390/gels8090541

Oral Contributions

Thermochromism of Methyl Red-Based Compounds – Monomers to Thermoresponsive Hydrogels, *GDCh-Wissenschaftsforum Chemie, video conference, 31st of August 2021*

Thermochromism of Methyl Red-Based Compounds – Monomers to Thermoresponsive Hydrogels, *POLY-CHAR 2022 [Halle | Siegen], video conference, 24th of May 2022*

Summary

This work describes the synthesis, and thermochromic and photoactuation properties of azobenzene-containing polymers and hydrogels.

For these polymers, monomers based on the azo dye methyl red were synthesised with varying linkages between the chromophore and the polymerizable group. These monomers showed distinct thermochromic behaviour in solution in dependence on protonation state and solvent. By determining the thermochromism of the single dyes, it was possible to elucidate the thermochromic effects of the corresponding copolymers.

The parent dye methyl red was functionalised with either an alcohol, a primary amine, or a secondary amine, yielding an ester, secondary amide, or tertiary amide attached to the aromatic ring, respectively. These exhibited largely varying thermochromic behaviours. It was possible to identify thermo-halochromism, thermo-solvatochromism, and thermo-solvato-halochromism for the ester, which provided the foundation to understand thermochromic effects and their interplay in non-thermoresponsive and lower critical solution temperature type thermoresponsive copolymers and hydrogels, which could be obtained through photocrosslinking. Both polymers in solution and gels strongly influence thermo-halochromism of this azo dye. Secondary amide functionalities on two ends of a tether between chromophore and polymerizable unit lead to intricate effects on thermo-halochromism, disturbing the simple equilibrium between neutral and protonated form by hydrogen bonding motifs in dependence on the tether length. A tertiary amide in *ortho*-position to the azo bridge results in a distinct shift in the tautomeric equilibrium between ammonium and azonium form of the protonated azo dye compared to other pseudostilbenes. Thermo-tautochromism occurs and acidic hydrolysis of the tertiary amide is catalysed through intramolecular hydrogen bonding at low temperatures, accompanied by an intense change of colour. The structure and hydrogen bonding capabilities of the corresponding copolymer or gel dictate the temperature at which hydrolysis becomes dominant.

When the azo dye-containing hydrogels were exposed to laser light instead of temperature as a trigger, intense photomotion could be observed. In thermoresponsive hydrogels with a cloud point close to room temperature, fast collapse occurred over a large area, which can be attributed to local photothermal effects. By changing the liquid medium to isopropanol instead of water, the thermoresponse can be switched off and the photomotion changed in scale to smaller but faster actuation. The same behaviour is inherent to non-thermoresponsive hydrogels. In this way, two different modes of photoactuation can be exploited by choice of the polymer matrix.

Zusammenfassung

Diese Arbeit befasst sich mit der Synthese, der Thermochromie und der Photoaktuation von azobenzolhaltigen Polymeren und Hydrogelen.

Zur Herstellung dieser Polymere wurden Monomere auf Basis des Azofarbstoffs Methylrot synthetisiert, in denen die Chromophore über unterschiedliche funktionelle Gruppen mit polymerisierbaren Gruppen verbunden wurden. Diese Monomere zeigten abhängig von Protonierung und Lösungsmittel eigenes thermochromes Verhalten. Durch Aufklärung der Thermochromie der freien Farbstoffe konnte diejenige der Copolymere erklärt werden.

Der Ausgangsfarbstoff Methylrot wurde mit einem Alkohol oder mit primären und sekundären Aminen funktionalisiert, um Ester, oder sekundäre und tertiäre Amide direkt am aromatischen Ring zu erhalten. Diese zeigten stark unterschiedliche thermochrome Effekte. Für den Ester konnten Thermohalochromie, Thermosolvatochromie und Thermosolvatohalochromie gezeigt werden, was die Aufklärung von thermochromem Verhalten in nicht-thermoresponsiven und thermoresponsiven Copolymeren und Hydrogelen mit unterer kritischer Lösungstemperatur ermöglichte. Die Hydrogele konnten durch Fotovernetzung hergestellt werden. Sowohl Polymere in Lösung als auch Gele beeinflussen Thermohalochromie des Farbstoffs stark. Sekundäre Amide an beiden Seiten einer Alkylkette zwischen Chromophor und polymerisierbarer Gruppe führten zu komplexen Effekten in Thermohalochromie, da Wasserstoffbrückenbindungen das einfache Gleichgewicht zwischen neutraler und protonierter Form verändern. Ein tertiäres Amid in *ortho*-Position zur Azobrücke führte zu einer ausgeprägten Verlagerung des Gleichgewichts zwischen Ammonium- und Azoniumion des protonierten Azofarbstoffs verglichen mit anderen Pseudostilbenen. Es trat Thermotautochromie auf und durch intramolekulare Wasserstoffbrücken wurde saure Hydrolyse des tertiären Amids schon bei niedrigen Temperaturen beobachtet. Die Struktur und Fähigkeit zur Wasserstoffbrückenbildung der zugehörigen Copolymere und Gele bestimmten die Temperatur, zu der Hydrolyse dominant wurde.

Wenn die Azohydrogele mit einem Laser bestrahlt wurden, statt einer Temperaturänderung ausgesetzt zu werden, konnte intensive Photobewegung beobachtet werden. In thermoresponsiven Hydrogelen wurde ein schneller Kollaps auf großer Fläche beobachtet, der lokalen photothermalen Effekten zugeschrieben wurde. Durch Austausch des Mediums zu Isopropanol wurde die Thermoresponsivität unterdrückt und eine sehr viel kleinere, aber schnellere Bewegung beobachtet. Dieses Verhalten trat auch bei nicht-thermoresponsiven Hydrogelen auf. Auf diese Weise konnten zwei verschiedene Modi der Photoaktuation durch Wahl der Polymermatrix gezeigt werden.

Table of Contents

1 Preface

This dissertation is a combination of published material and yet unpublished material that is compiled in the form of manuscripts. These manuscripts make up five chapters, which are each structured into abstract, introduction, optionally an experimental section, and results and discussion, as well as a conclusion. Each chapter also contains a supporting information, which directly follows the chapter, features experimental details, and supporting data.

In a preface to each chapter, the contributions of the author are stated and, if published, where the chapter has been published or accepted for publication.

The five chapters are parenthesised by the state of knowledge and an overarching outlook after the last chapter. Some information found in the introductions of the separate manuscripts may be presented in the general state of knowledge as well.

The chapters describe three different topics. Chapters 3-5 are concerned with the thermochromism of azo dyes based on the pseudostilbene methyl red (MR) and polymers thereof. Chapter 6 deals with photomotion in with laser light irradiated, MR-containing gels. Chapters 3-6 have been published in different journals.

Chapter 7 contains a proof-of-principle, which presents preliminary results regarding systems containing both coumarin- and benzophenone-based crosslinkers and their reversible crosslinking behaviour in a concise manner. This material has not been published yet.

Supporting information documents containing experimental details and additional results were attached directly to the articles or manuscripts, as some information provided in these sections is crucial for understanding.

2 Introduction and State of Knowledge

2.1 Thermochromism

The term thermochromism, coming from the Greek words “thermós” (engl. “hot”) and “chrõma” (engl. “colour”), describes the phenomenon of reversible or irreversible change of colour in response to temperature variation.[1–3]

The temperature-dependent optical behaviour of inorganic compounds is a subject of research for more than a century already.[2] This is a lasting topic of research and the influences by temperature on colour have been determined early on as changes in the crystal structure, equilibria between several ligands, or solvent effects on metalorganic complexes.[4] However, recent literature is dominated by vanadium oxide (VO_2).[5] VO_2 switches from a metallic to a

semiconductor phase at a critical transition temperature of 68 °C.[6] The phase change leads to heightened reflectivity for infrared radiation, making this material interesting for smart coatings.[5,7,8]

In organic molecules, the origin of thermochromic phenomena lies in several possible mechanisms. These may be phase transitions, e.g., in thermochromic liquid crystals,[9] chemical equilibria between different structures of the same molecule,[10–22] changes in conformation or vibronic structure,[23–26] aggregation,[27,28] or a change in the solvation shell with temperature variation.[29–31]

The oldest class of thermochromic organic molecules are spiropyrans, which are thermochromic, solvatochromic, and photochromic dyes. These dyes go from the colourless spiropyran form at low temperatures to the coloured merocyanine form when heated, depending on substituents (cf. Scheme 1).[32] Solvatochromism describes a change in colour in dependence on the solvent,[33] while photochromism refers to a change in absorption behaviour in response to irradiation.[34]

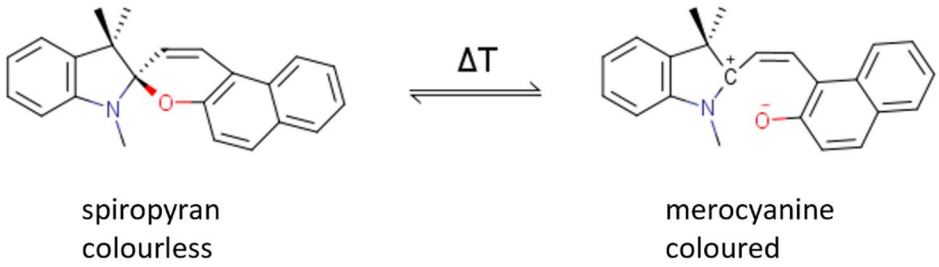

Scheme 1: Thermochromism of a spiropyran via a reversible ring-opening to a merocyanine form when heating. Here indolino-β-naphthospiropyran as an example, which turns blue in the melt or intensely red coloured in an inert solvent.[1]

Another class of thermochromic materials are photonic structures that may be either of a single material, e.g., structured polymers,[35–37] or of composites.[38–45] In these materials, the colour evolution mainly originates from a shift in the distance between the structural elements, adjusting the interference colour.[3]

A particularly interesting example is the combination of a photonic crystal with a photo- and thermoresponsive polymeric hydrogel.[42] In this system, an azo dye was copolymerised with *N*-isopropyacrylamide (NiPAAm) and *N,N´*-methylenebisacrylamide as a crosslinker inside of a colloidal crystal as template. Owing to the thermoresponsive properties of poly-NiPAAm, which undergoes lower critical solution temperature (LCST)-behaviour, the distance between the colloids could be adjusted by influencing the swelling state of the gel with temperature. The azo dye furthermore imparts a base colour, as well as photoresponsivity. Azo dyes undergo

optically induced *cis-trans*-isomerisation, which results in changes in the molecular volume, the dipole moment, and the absorption behaviour.[46,47] This additional responsivity leads to a composite system, which can be adjusted in colour over the whole visible range.

The first transparent, thermochromic hydrogel was a borax-crosslinked polyvinyl alcohol gel that was developed with the solvato- and thermochromic dye 2^5-(2,4,6-triphenylpyridin-1-ium-1-yl)[1^1,2^1:2^3,3^1-terphenyl]-2^2-olate, better known at betaine 30 or Reichardt's dye, or with another chromic dye, the pH indicator Cresol Red. A surfactant was added to solubilise both dyes.[48] The colour change was explained by protonation at the phenolate of both dyes at elevated temperatures. This temperature-dependent protonation equilibrium only occurred at specific pH values and only when the dyes were embedded in the hydrogel, making the matrix a critical factor for thermochromism. A change in colour depending on protonation of a dye is referred to as "halochromism",[49] which is sometimes also called "acidochromism".[50–52]

Similar hydrogel systems were developed since then that function on principles of interaction of the matrix with a dye.[3,19–21,53]

An application, which exploits thermochromism, are optical thermometers, which are also called ratiometric thermometers. While these are often based on fluorescent dyes, which change their emission behaviour depending on temperature,[10–12,54–63] coupling of fluorescent dyes with LCST-behaviour of polymers[64,65] or on semi-conjugated polymers,[66,67] there are also examples that employ non-fluorescent azo dyes.[68–87]

In these systems, a combination of thermoresponsive polymers and azo dyes is utilised. The azo dyes change their absorption behaviour owing to scattering effects and because their local environment becomes more or less hydrophobic after a volume phase transition depending on LCST- or upper critical solution temperature (UCST)-behaviour. The dyes exhibit perichromism, a variation in colour in response to the local environment.[88] However, a drawback of these systems is that a large colour change occurs over a narrow temperature region in dependence on the critical solution temperature, limiting the operation temperature.

A mechanism resulting in a larger dynamic range, i.e., the temperature range in which colour change is noticeable, is the azo-hydrazone tautomerism of some phenolic azo dyes,[17,89–93] or special tricyanofuran hydrazone dyes, which are in equilibrium with their anionic form.[13–16]

The azo-hydrazone tautomerism of phenolic azo dyes is an equilibrium between the yellow enol (azo) form, in which the hydrogen is bound to the oxygen of the naphthol ring and the red keto (hydrazone) form, in which the hydrogen is bound to the azo bridge (cf. Scheme 2). The equilibrium shifts from the hydrazone form at low temperatures to the azo form at higher temperatures in suitable solvents, accompanied by a distinct blue shift of the spectra.[89]

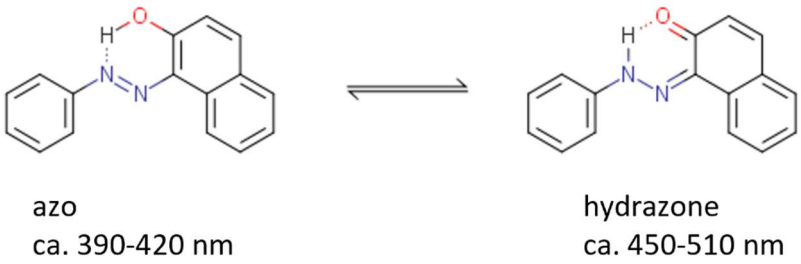

Scheme 2: Tautomeric azo-hydrazone equilibrium with the example of 1-phenylazo-2-naphthol.[89]

The tricyanofuran hydrazone dyes behave similarly. Here, a deprotonated hydrazone anion in a quinoid form is the more stable form at increased temperatures. However, strong electron-withdrawing groups[15,16] or embedding in gels[13] are necessary for this type of dye to be thermochromic.

Another instance of an azo dye being thermochromic because of its environment are ion-exchange micelles containing the pH indicator chromoionophore IV or 5-octadecanoyloxy-2-(4-nitrophenylazo)-phenol and an anion exchanger.[18] In this example, instead of deprotonation, protonation occurs with increasing temperatures. This mechanism was attributed to a partitioning effect of water in the wall of the micelle, which harboured the anion exchanger. At higher temperatures, the block copolymer micelles contain less water in the hydrophilic corona, inhibiting the action of the ion exchanger. These systems show a strong change in colour over only a few Kelvins.

For 2-{[4-(dimethylamino)phenyl]diazenyl}benzoic acid, more commonly known as (*ortho*-)methyl red, two thermochromic mechanisms have been described. These were explained in parts with the other chromic behaviours, which are halochromism on the one hand and solvatochromism on the other.

As mentioned above, halochromism is the phenomenon of pH-dependent colour change, as typical of pH indicators like *o*-methyl red. This azo dye exists primarily in three protonation states in aqueous solution: a protonated, a neutral and an anionic state (cf. Scheme 3). The monoprotonated state exists below pH 4.4 in a tautomeric equilibrium between the colourless ammonium ion (abs. max. ~325 nm) and the intensely red azonium ion (abs. max. ~525 nm). Ammonium ion refers to protonation of the amine group of the chromophore and azonium ion to protonation of the azo bridge. This protonation occurs at the *β*-nitrogen of the azo bridge in 4-aminoazobenzene- and push-pull azobenzene-type dyes, which *o*-methyl red belongs to.[94–98] Owing to stabilisation by intramolecular hydrogen bonding and a quinoidal resonance structure, the tautomeric equilibrium of this dye lies strongly on the side of the azonium ion, leading to

an intensely coloured solution.[96] The neutral form has very low solubility in water but is of orange colour. Above pH 6.2, the dye is completely deprotonated and soluble again, showing yellow colour (abs. max. ~430 nm).[99,100]

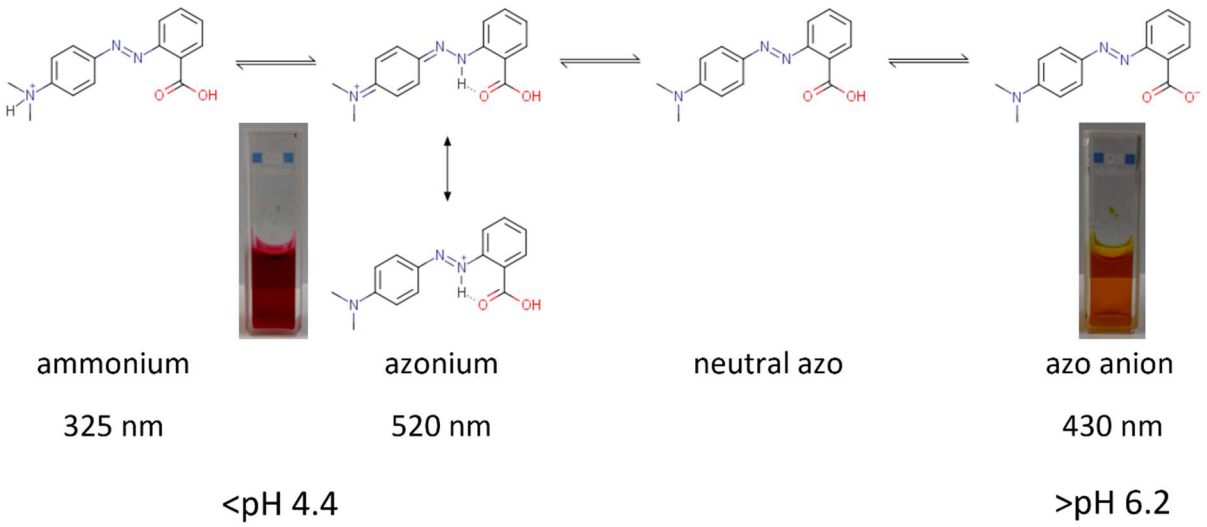

Scheme 3: Protonation equilibrium of o-methyl red in aqueous solution at different pH with an ammonium, azonium, neutral, and deprotonated form. The pictures are of solutions of the dye in aqueous hydrochloric acid (1.2 M, left, red, product of a tautomer mixture of ammonium and azonium forms) and in aqueous sodium hydroxide solution (0.1 M, right, orange).

Apart from the pH-induced halochromism, also solvatochromism of *o*-methyl red has been described based on the prototropic equilibrium of the dye.[101] Depending on different solvent parameters like polarity, hydrogen bonding capabilities like hydrogen bond accepting and hydrogen bond donating parameters, and Kamlet-Taft-parameters,[33,101–103] the neutral dye shows either absorption in the red (~500 nm) or further in the blue (~400-440 nm). This has been explained by the influence of the solvent on intramolecular hydrogen bonding between the carboxylic acid and the azo bridge in *ortho*-position. If intramolecular hydrogen bonding is enhanced by the solvent, the proton of the carboxylic acid is located on the azo bridge, forming a zwitterion with a quinoid character, thus absorbing in the red. If intermolecular hydrogen bonding to the solvent is enhanced and intramolecular hydrogen bonding is suppressed, the proton is located on the carboxylic acid and the dye is neutral, absorbing further in the blue.

The first thermochromic mechanism is a temperature-dependent, competitive complexation of a *β*-cyclodextrin (*β*-CD) derivative of *o*-methyl red.[104] In this system, the azo chromophore primarily exists as its azonium form at lower temperatures if a competitive guest like adamantan-1-ol is in solution as well. Only the azo form and the ammonium form of *o*-methyl red are complexed by the host, protecting the dye against protonation at the azo bridge.[105] A competitive guest displaces the azo form, which results in higher degrees of protonation of the

dye. When the temperature is increased, the guest is expelled from the cavity of *β*-CD and the dye can enter the host as the neutral form again. This process of temperature-dependent complexation leads to a blue-shift with increasing temperatures, as the equilibrium between the red azonium form and the orange azo form is shifted towards the orange azo form.[104]

For the second thermochromic study, the dye was adsorbed on silica gel that was treated with acetic acid to adsorb the protonated form of *o*-methyl red. It was observed that heating the gel led to a decrease in the absorption band of the protonated form and an increase in the absorption band of the neutral form. This was attributed to two effects. First, the basic sites of the silica gel increase with temperature when adhering water is evaporated and second, the acidity of the protonated dye increases at higher temperatures.[106]

In summary, while there are several methods to obtain thermochromism from azo dyes, mostly by employing a matrix, thermochromic effects from the dyes themselves, and especially the combination of intrinsic and matrix phenomena, are little explored, and knowledge is limited.

2.2 Photomotion of Azo Dye-Containing Systems

While there are several different mechanisms to achieve photomotion of azo dye-containing materials, they all rely on the same property of azobenzenes. A process common to all photoactuated systems based on azobenzenes is the *trans* → *cis* isomerisation of the dye, which proceeds after absorption of a photon with high quantum yields. In most azo compounds, the *trans*-state is the thermodynamically more stable conformation. Because of this, the *cis* → *trans* isomerisation may occur either by absorption of as second photon or by thermal relaxation. The *cis*-isomer has considerably different properties from the *trans*-isomer, foremost the size of the chromophore decreases and the dipole moment increases (cf. Scheme 4). The majority of this discussion is a summary of a comprehensive review.[47]

The geometric pathway for photoisomerisation, as well as the half-life time of the excited *cis*-state strongly depend on the substituents on the chromophore.[107] Azobenzenes are categorised by their substitution pattern, which strongly influences absorption, photoisomerization, and especially thermal relaxation of the *cis*-state to the *trans*-state. There are three categories of azobenzenes: First, azobenzenes, which entail unsubstituted azobenzene, most monosubstituted, and symmetrically substituted azobenzenes. Second, aminoazobenzenes, which are azobenzenes substituted in 4- or 4- and 4'-positions with amines. And third, pseudostilbenes, which are also referred to as donor-acceptor (D-π-A)- or push-pull azobenzenes. As the latter two names suggest, the chromophores are substituted with an electron-accepting group on one ring and with an electron-donating group on the other ring.

In azobenzenes, two main transitions can be observed in UV-vis spectra. A π-π*-transition, which absorbs below 400 nm, and a longer wavelength n-π*-transition. In aminoazobenzenes and especially in pseudostilbenes, these transitions are either almost or actually degenerate in energy, yielding a strong absorption band in the visible region. This absorption band leads to the intense orange or red colours, which are typical for these types of azo dyes. The absorption bands of the *cis*-isomer in azobenzenes are red-shifted but usually degenerate in aminoazobenzenes and pseudostilbenes.

Four models have been proposed for the geometric pathway of photoisomerisation. Rotation, inversion, concerted inversion, and inversion-assisted rotation. All these models have been suggested for the different types of azobenzenes and have been contested by different measurements or calculations. This is also a consequence of the pathways being strongly influenced by conditions like solvent, pressure, and temperature. The only uncontested systems are pseudostilbenes, which isomerise *via* rotation.

More important for applications than the exact pathway of isomerisation is the lifetime of the *cis*-state. This lifetime is longest in azobenzenes, where it may be minutes to days, or even months in derivatives persubstituted in *ortho*-positions.[107] The lifetime decreases over aminoazobenzenes to pseudostilbenes, which show a lifetime of seconds or milliseconds. As a consequence, aminoazobenzenes and pseudostilbenes are not utilisable for applications in which the *cis*-state has to persist for longer times. However, they switch back and forth between *trans* and cis more quickly, which may be advantageous for some types of photomotion, as outlined below.

Protonation has a strong influence on absorption behaviour and photoisomerisation as well. Protonation of any azobenzene leads to the chromophore being considered as a pseudostilbene, as the absorption bands are red-shifted and the thermal relaxation of the *cis*-state becomes faster.

The *cis* → *trans*-isomerisation is also the reason for the low fluorescence quantum yields that most azobenzenes show. The energy taken up by the dye is converted into the change of geometry instead of being released by fluorescence. Only if the *trans* → *cis*-isomerisation is hindered by, for example, low temperatures or a stiff matrix, do these dyes fluoresce.

The unique photochemistry of azobenzenes has led to interesting photomechanical effects that will be discussed in the following.

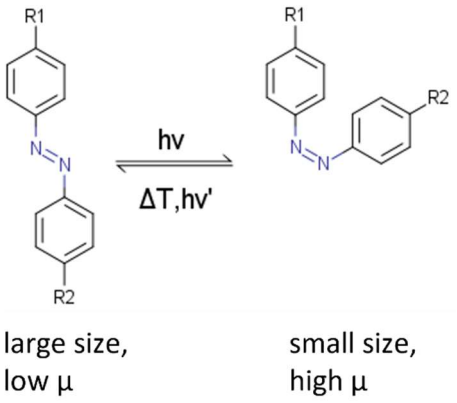

Scheme 4: Photoisomerisation process of an unspecified azo dye involving trans to cis isomerisation upon absorption of a photon and cis to trans isomerisation upon thermal relaxation or absorption of a second photon. R1 and R2 determine the type of azo dye, e.g., R1=NH_2, R2=H is aminoazobenzene, also known as Aniline Yellow and R1=NO_2, R2=$N(C_2H_5)(C_2H_4OH)$ is a common pseudostilbene known as Disperse Red 1.

2.2.1 Surface Relief Grating Formation of Glassy Azobenzene-Compounds and Azobenzene-Polymers

Likely the most intriguing photomotion azobenzene-containing materials (azo materials) exhibit is the photoinduced mass migration leading to surface relief gratings (SRGs).[108–110] SRG formation is a phenomenon observed upon irradiation of azobenzene-containing thin films with laser light of appropriate wavelength. As the term implies, a periodical grating pattern is inscribed into glassy azobenzene-containing materials well below the glass transition temperature T_g. Classically, this can be achieved by interference patterns of two lasers in a certain angle, where destructive interference leads to dark regions and constructive interference to bright regions (cf. Scheme 5).[108,110] This pattern is also referred to as "writing beams".

The process behind the formation of SRGs is still under discussion and several models attempt to describe the phenomenon, which are discussed later. But until now none have succeeded to explain all systems in the same model. Phenomenologically, mass in form of azopolymers, azobenzene glasses or liquid crystalline azo materials moves either away from or towards illuminated regions. In this manner, highly regular structures are formed, which only depend on the wavelength of the writing beams employed and the angle between them. SRG formation is not limited to one dimension either and gratings with more elaborate symmetry can be formed by exposing the same film to a laser interference pattern at different angles.[110–114]

Another notable feature of SRG formation is a strong dependency on polarisation of the writing beams, which may be exploited to introduce topographical features in the thin films.[111,115–121] The polarisation dependence stems from the absorption probability of the chromophores being proportional to the angle of the electromagnetic field to the dipole axis of the chromophore. Linearly polarised light can only act with chromophores parallel to the electromagnetic field vector, while circularly polarised light can only interact with those that are not parallel.[122]

An interesting and useful characteristic of SRGs is that it is not only possible to inscribe them easily with light but that they can also be erased thermally[123] or with light.[110–114,120,121]

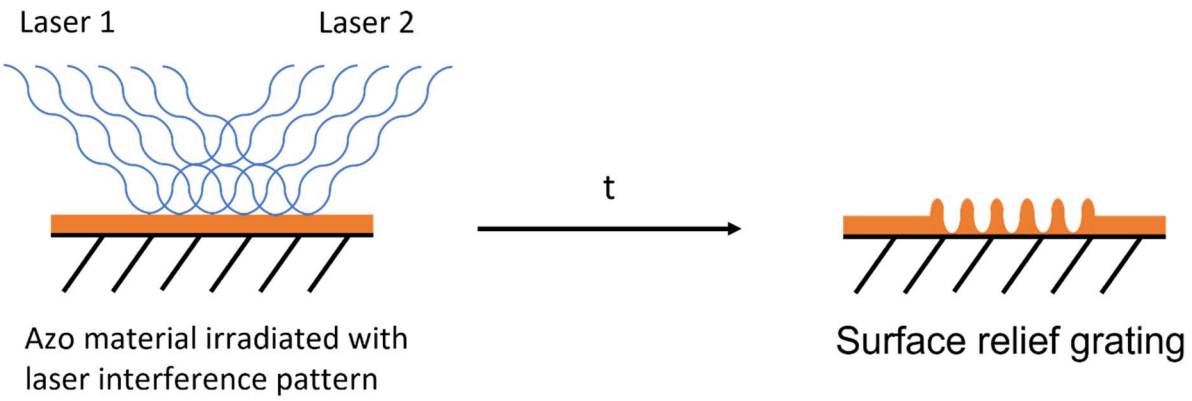

Scheme 5: Schematic description of the formation of a surface relief grating in an azo material via a laser interference pattern.

The models attempting to unify the different effects in the interaction of light with azo materials all consider the aforementioned trans → cis photoisomerization of azo dyes. More specifically, fast trans-cis-trans cycling is necessary for efficient mass transport. This requires spectral overlap of the absorption bands of the trans- and the cis-isomer, which is best provided by pseudostilbenes. As mentioned in the introduction of Chapter 2.2., these dyes are also characterised by a short thermal lifetime of the cis-isomer. Combined with the overlap of the absorption bands of the two isomers, a photostationary state is reached, which exhibits quick cycling between the two forms.

There are seven main models, which will be described briefly in the following.[111,113,114,120,122,124–134]

Thermal model: In this model, the temperature increase of azopolymer thin films under irradiation is described. However, while the temperature rise under irradiation with high power can be substantial, the temperature gradient between the bright and the dark regions is minimal with only 10^{-4} K. It has been concluded that photothermal effects are not the main reason for SRG formation and only play a minimal role.[130]

Pressure gradient model: The pressure gradient model is the oldest model to describe SRG formation.[122] This model is based on the increase in free volume occurring upon isomerisation from the trans- to the cis-state. It assumes that this increase leads to free volume-induced pressure gradient in the bright regions of interference patterns, pushing the material past the point of visco-elastic flow. Consequently, the mass migration occurs towards the dark regions of the interference pattern. This model, however, is unable to explain photoinduced mass migration towards bright regions, the formation of purely polarisation dependent gratings and the reconfiguration of free-standing objects like azo polymeric micropillars that can be deformed and then reshaped to their original dimensions.[135]

Mean-field model: The mean-field model[128,129] assumes that the chromophores will orient themselves according to the mean-field of the electromagnetic field induced by the writing beam. Under certain conditions, attractive forces between the chromophores in the orientation process can lead to mass transport. However, this model has only been described for liquid crystalline polymers and has not been specifically demonstrated for other azo materials. It also only describes motion towards bright regions and not away from them.

Optical-field gradient force model: This model assumes a strong polarisation dependency of SRG formation and that trans-cis-trans cycling leads to softening of the surface of the azo material.[127] Here, as consequence of polarisation patterns, a gradient in the electric field induces a small force, leading to mass migration to regions with a lower force, i.e., from bright to dark regions. While this model has been used to explain the formation of holes in azo polymeric thin films,[126] the predicted force densities are low, and the model is unable to explain mass migration towards bright regions.

Asymmetric diffusion or "Inchworm" model: The "inchworm" model describes photoinduced mass migration by anisotropic movement of the chromophores with each trans-cis-trans cycle.[125] Each cycle, the molecule moves slightly forward along the polarisation direction. Yet, this also means that the model is not actually suitable for macromolecules, and it does not consider effects like orientational diffusion under irradiation.

Photoinduced molecular diffusion (PIMD) model: In the PIMD model,[124] two previously described models are referenced, the "inchworm" and the mean-field model. Like in the "inchworm" model, the mode of motion is translation via isomerisation along the axis of the molecule, which is set at the direction of the molecular dipole. In contrast to the "inchworm" model, interaction of the dipole with the optically induced electric field is taken into account, as well as that the chromophore is attached to a polymeric chain. This is considered by random reorientation of the rest of the macromolecule whenever the modelled chromophore moves, as well as by the molecule only being allowed to move from one "hole" in the polymer matrix to another. While this model is applicable to many systems and can reliably reproduce hole burning, motion away from the light, and different illumination conditions like far-field and near-field illumination, it cannot account for motion towards the bright areas. Another shortcoming is that the model is optimised for a temperature close to the T_g of the material in question, which is rarely the case in experiments.

Orientation approach: The orientation approach is the most recent model proposed for SRG formation and related effects.[131–134] This model is based on reorientation of the chromophores attached to a macromolecular chain by trans-cis-trans cycling until they are perpendicular to

the incoming light. The reorientation directly leads to the macromolecule being forced to move as well, inducing optomechanical stress in the bulk material. This process is described by a time-dependent effective orientation potential. The orientation approach is able to describe all photomechanical effects for glassy and liquid crystalline azo materials through minor modifications and reproduces experimental results well. It is especially powerful in predicting polarisation effects in such materials.

Models based on the semi-implicit moving-particle method[136,137] and on a random-walk approach[138] have been proposed as well but did not come to fruition.

While the models have limitations and are not in use for full prediction of SRG formation yet, the practical use of SRGs is not inhibited. The strict periodicity and simple production from nano- to microscale of SRGs makes these materials interesting for several applications, such as transmissive or reflective diffraction gratings used in optics and photonics, photochemical imaging to reproduce electromagnetic fields in thin films, nano- and micropatterning, e.g., for lithography, or to introduce reconfigurable surface structures for wettability and adhesive properties.[111,113,114]

2.2.2 Azobenzene-Containing Liquid Crystalline Elastomers

Another class of azobenzene-based photoactuators are liquid crystalline elastomers (LCEs), which employ azobenzenes either as crosslinkers or as side groups.[111,114,139–142]

In the simplest case of nematic phases, the rod-like *trans*-isomer acts like a mesogen and does not disturb the liquid crystalline phase. However, upon photoisomerisation to the *cis*-state, the chromophore loses its rod-like configuration and disrupts the mesophase. Consequently, the loss of order leads to a volume change.

Most commonly, film or cantilever configurations are used to investigate the photomechanical behaviour following irradiation. The thickness of these materials is in the order of up to 100 µm, which, in combination with the high absorption coefficients of the dye, leads to light only penetrating the surface layer of the material. The loss of order on only one side of the strip results in a mechanical deformation, which makes these materials actuators (cf. Scheme 6).

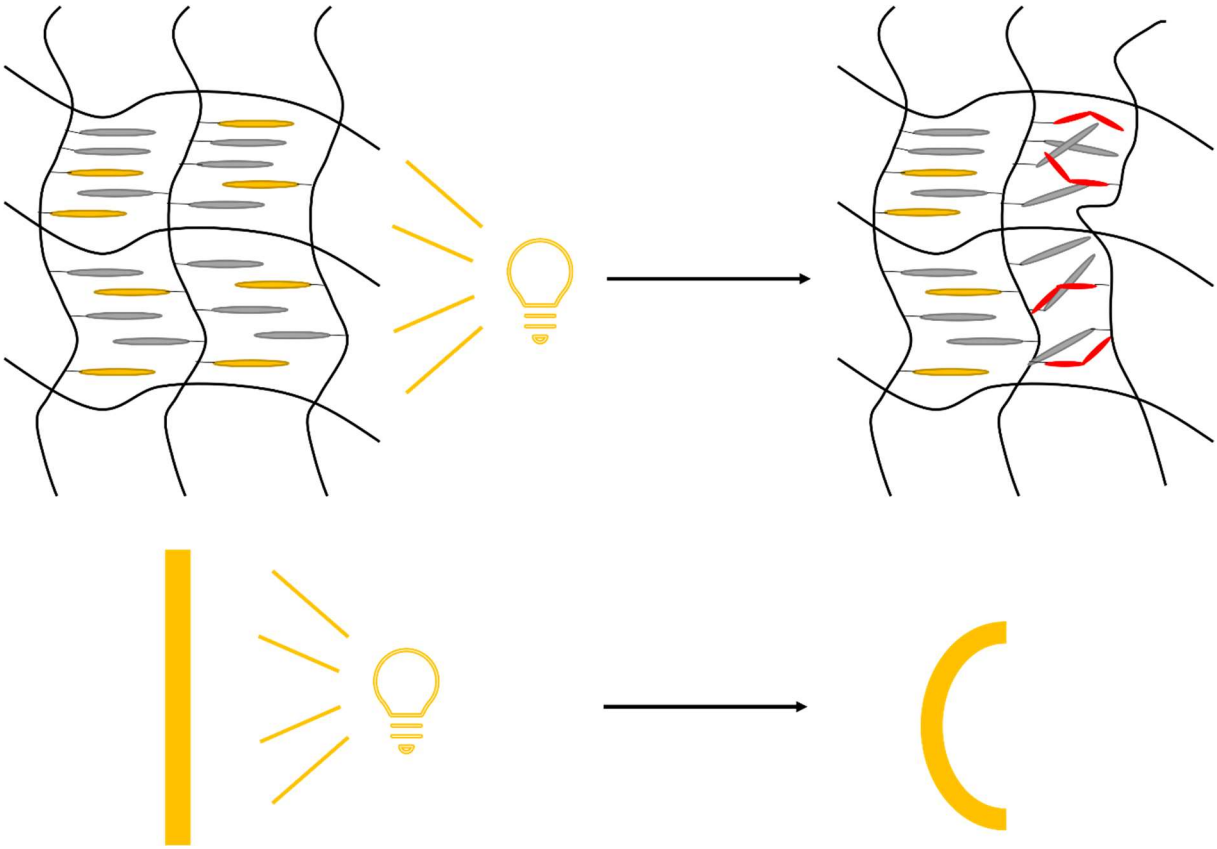

Scheme 6: Cartoon of the photoactuation of azobenzene-containing liquid crystalline elastomers by disruption of the mesophase of the network via trans-cis isomerisation. Top: Microscopic change from a nematic to an isotropic phase after irradiation from one side. Bottom: The respective macroscopic change upon irradiation from one side.

This deformation is fully reversible upon either thermal relaxation of the *cis*- to the *trans*-state or by irradiation with appropriate wavelength to restore the *trans*-configuration. As usually the deformation should not be lost immediately after the irradiation is stopped, there are different requirements for the dye. In LCEs, azobenzene-type dyes are employed, which exhibit longer thermal lifetimes for the metastable *cis*-isomer.

Several factors influence the efficacy of photoactuation. Apart from the exact azo dye utilised, which is defined by its molecular shape and the thermal lifetime of the *cis*-state, the dye-content in the LCE, as well as side chain or main-chain substitution strongly affect bending of the material. This can even lead to bending towards or away from the light.[143] Also, not only nematic liquid crystals may be used, but other mesophases as well.[111,114,139–142]

Another factor is whether the liquid crystalline elastomer is monodomain or polydomain. This can even completely change the photoactuation from a polarisation-independent one (polydomain)[144] to a polarisation-dependent one (monodomain), which even shows oscillation upon irradiation with a laser.[145,146] Closely related to the domain-dependence is the influence of the director of the liquid crystal, which can change the bending direction as well.[141]

By patterning the material with dye-containing regions and regions without dyes, also more complex bending can be induced, allowing for elaborate shape-changes upon irradiation.[147]

Applications of such materials are mostly found for artificial muscles[141] or other soft robotics applications.[111,114,139,141,148]

2.3 Photoresponsive Hydrogels

Hydrogels are three-dimensional, physically or chemically crosslinked networks of a synthetic or natural, hydrophilic material, that are swollen in water. The high water-content and mechanical properties, with the gels behaving similarly to elastomers in the swollen state, allow for using them in tissue engineering and other biomedical applications. Other properties like biocompatibility, anti-fouling properties and stealth behaviour, the ability not to be identified and rejected by an organism, play an important role for applicability as well. This similarity of hydrogels to biological tissue leads to suitability for several fields from biomedical devices,[149–151] to applications in bionanotechnology,[150] to drug delivery,[150] protein delivery,[152] and self-healing materials.[153]

An interesting class of hydrogels are photoresponsive hydrogels. A recent review sheds some light on this type of materials[154] and will be used here to highlight some important examples.

These photoresponsive hydrogels change one or several properties under the influence of light. Light as a trigger is a convenient and "clean" tool to influence a system. It is cheap, can be manipulated precisely in energy and flux and has high spatial and temporal control. It has the additional advantages that it is, depending on the wavelength, non-invasive and harmless for biological systems. In contrast to other stimuli, it can be employed orthogonally as well, if different processes are controlled with light of different wavelengths.

The photoresponses can be a change in the swelling ratio, crosslinking density, or completely reversible crosslinking. Other possibilities are photothermal effects, controlled release of a substrate or the activation of functional groups or active sites. The active compounds that are activated or triggered by light vary, as well as the mechanism of their photoresponse.

An example for photolabile groups is *o*-nitrobenzyl esters. Under irradiation, these esters are photolyzed into a carboxylic acid and an *o*-nitrosobenzaldehyde. This photolysis can then be used, for example, to change the mechanical properties of a gel[155] or even to decompose the gel in a controlled manner.[156,157] The latter process is irreversible.

A reversible mechanism is based on photocrosslinkers functioning *via* cycloadditions like cinnamates,[158] coumarins[159–161] and anthracenes.[162,163] They can be crosslinked at one wavelength and the crosslinks can then, theoretically, be cleaved at another wavelength. While this approach was used for the anthracene examples in the references here, the cinnamate was cleaved under light to moderate mechanical stress. The coumarin-containing hydrogels showed even more possible pathways of application. While one was used to release a dye as an example for phototriggered release,[160] a specific coumarin-derivative was used similarly to *o*-nitrobenzyl esters to completely degrade a gel,[161] and in a third case reversible crosslinking was employed to design a self-healing material.[159]

The opposite approach to reversible crosslinking or photocleavage is taken in the case of thiol-ene "click" reactions. There, the photoresponse is the formation, or hardening, of a gel. The thiol-ene click reaction has three components. A thiol, a double-bond and either a base for a Michael-addition-type reaction or a photoinitiator for a radically sensitised reaction. Like this, crosslinks can be formed simply by controlling the dose of light in a certain region, allowing, for example, to crosslink a material in tissue.[164–166]

The mechanisms described until now, however, are either irreversible or require the interaction of two or several molecules. Photoresponses that involve only one molecule and light are based on isomerisations of those molecules. For this, several classes of molecules can be used. While recently shape-memory hydrogels on the basis of dithienylethene have been developed,[167,168] more common and robust dye classes are spiropyrans that isomerise reversibly to merocyanines

under irradiation, and azobenzenes, which, as has been mentioned before, have a *cis-trans*-isomerisation, with the *cis*-isomer being thermally instable.

While spiropyrans have numerous applications and responsivities,[32,169–173] the focus here will be on the two most important modes of operation.[174] The first is the isomerisation of the less hydrophilic spiropyran to the more hydrophilic, zwitterionic merocyanine under UV-light that can be reversed by irradiation with visible light. This change in hydrophilicity can be used for several things. For example, it can be used to control cell adhesion reversibly on the surface of a spiropyran-containing hydrogel. By irradiating with UV-light, the spiropyran opens to the hydrophilic merocyanine and cells detach. When the illumination is changed to visible light, the isomerisation reverses and the cells can attach to the surface again. [175] Another possibility is to form a thin interface between a hydrogel and a liquid phase by attaching the spiropyran at a water-oil-interface to the gel *via* quaternisation of tertiary amines at the surface of the swollen gel. This photoresponsive layer then allows to control release of dye loaded into the gel into liquid surroundings.[176]

The second mode of operation is, in principle, a modification of the first one. Introducing an acid in the equation changes the stability of the different isomers considerably. At room temperature, the protonated form of merocyanine is more stable than the spiropyran in aqueous solution, meaning that the equilibrium shifts to the merocyanine. This, however, opens new possibilities compared to the simple equilibrium. If the protonated merocyanine is exposed to visible light, it will isomerise to the spiropyran, which then in turn slowly protonates and opens into the merocyanine form again.[177–179] This mechanism can be used to have temporal control over the swelling of a hydrogel,[180] reversibly switch surface topographies[181] or generate valves for microfluidic devices.[182]

As it has been mentioned before, the process of thermal reversibility that can be induced in spiropyrans, is an inherent property of azobenzenes with the lifetime of the thermally instable *cis*-isomer depending on the substituents of the dye.

One interesting use of azobenzenes in hydrogels is the combination with cyclodextrins. Many azobenzene-derivatives have a high affinity for cyclodextrin in the *trans*-configuration but a low affinity in the *cis*-configuration. This allows for using this combination of a host-guest complex as a reversible binding motif.

If azobenzenes and cyclodextrins are used as side groups in polymer chains, this motif leads to interesting applications. These range from controlling the viscosity of a polymer solution (high viscosity in *trans*, when the azobenzenes bind to cyclodextrin and low viscosity in *cis*, when the host-guest complexes decompose),[183] to dissolving and reforming supramolecular

hydrogels with the same reasoning,[184–186] to artificial muscles.[187,188] The process of reversible host-guest interactions is depicted in Scheme 7.

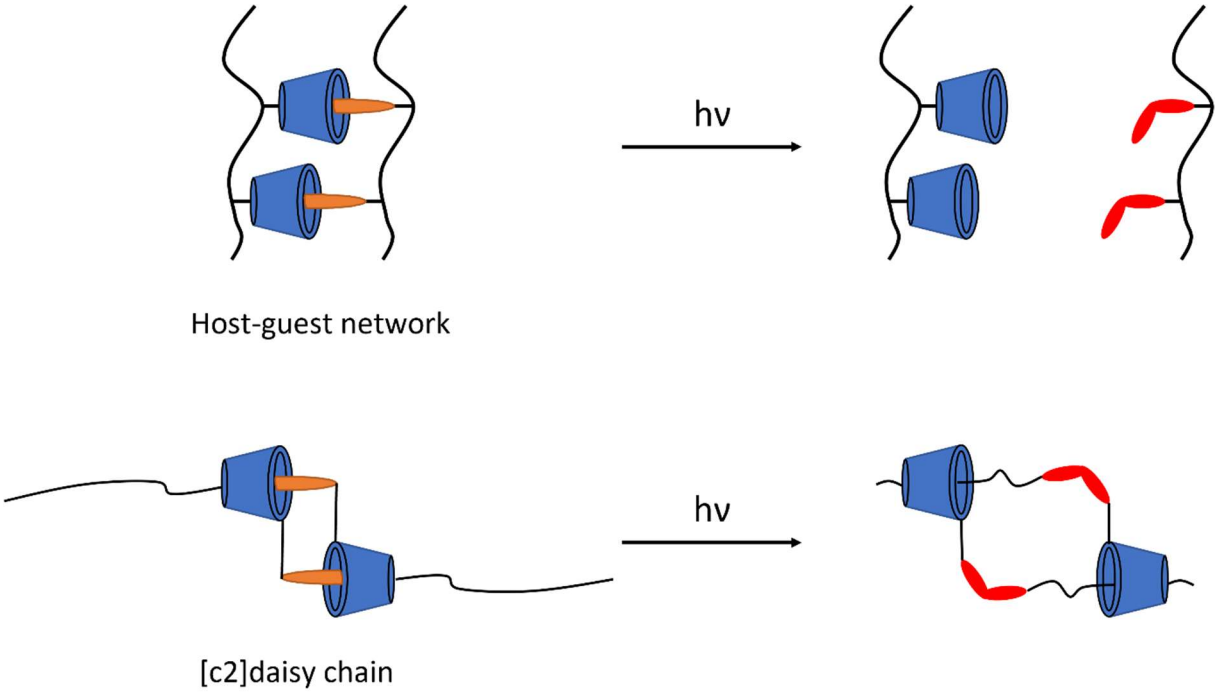

Scheme 7: Photoresponse of two different systems containing both azobenzene- and cyclodextrin-moieties. Top: Host-guest network, which is crosslinked when the azobenzene is in the trans-state and can act as a guest to the host cyclodextrin. The network dissolves upon irradiation, when the azo dye isomerises into the cis-state and does not fit the host anymore. Bottom: A [c2]daisy chain, which is in a relaxed state when the azo dye is in trans-configuration and can act as the guest and contracts an attached system when the dye isomerises into the cis-state and leaves the cyclodextrin-moieties.

The artificial muscles are, in principle, a special case of dissolving and reforming hydrogels. In contrast to a complete gel-to-sol transition, they employ polymer networks that include the binding motifs but do not use them as their primary crosslinks. Therefore, the formation or decomposition of the host-guest complexes primarily affect the swelling of those gels.

To increase response times, the artificial muscles rely on confining the system. By restricting the mobility of the host and the guest, e.g. by forming a static network[188] or with a [c2]daisy chain,[187] the proximity of the host and guest is ensured. This means that when the *cis*-azobenzene is switched back to the *trans*-state with visible light, the reformation of the host-guest-complex does not rely on diffusion control, cutting that diffusion time off the response time. The [c2]daisy chain is a more advanced system here, as the cyclodextrin and azobenzene are direct neighbours in a cycle (cf. Scheme 7).

However, the swelling behaviours under irradiation of a ‘simple’ host-guest complex modified gel and a [c2]daisy chain modified gel are opposite to each other. When the simple host-guest complex is decomposed, the crosslinking density is reduced, and the gel swells more. If the

complex on a [c2]daisy chain is decomposed, the host and guest cannot separate and as they are essentially threaded on a macrocycle, the crosslinking density stays the same. The *cis*-azobenzene and the cyclodextrin still avoid each other, shortening the chain and, thus, contracting the gel.

In a strip configuration, the swollen strip can be bent by using an appropriate dose of light for illuminating swollen strips of those gels. If more of the host-guest complex is decomposed in one region of the strip than it is in the others, strain will be formed on the object, and it will bend towards the light source. On the other hand, if a system with simple host-guest complexes or even without host-guest complexes is employed under the same conditions the strip bends away from the light source when switching from trans to cis, as the hydrophilicity and swelling increases.[187,188]

In a series of crosslinked and non-crosslinked poly(NiPAAm)-*co*-(azobenzene-4-acrylamide) copolymers without cyclodextrin as host, a miniscule effect of the azobenzene has been shown on the phase transition for small amounts of azobenzene in the chain (up to 0.3 mol%). Contrary to the expectation that swelling should be similarly unaffected, swelling and the mechanical properties are severely affected even by these small percentages of azobenzene. It has also been shown in this context, that release of bovine serum albumin from the gel can be influenced by irradiating and, thus, switching the azo-moiety from *trans* to *cis*.[189]

In summary, photoactive molecules and especially azobenzenes allow for elaborate photoactuation of gels if they are used under appropriate conditions or with suitable additives.

2.4 Aim of this Thesis

The high versatility of azobenzene-containing polymer systems with their potential in chromism and photoactuation demonstrate their worth as a class of smart materials. Yet, while parts of their chromism and photoactuation have been explored already, many facets remain untouched.

Especially a mechanistic explanation of thermochromism, the combination of different kinds of chromism, and the combination with polymeric systems are still lacking insights in the field of colour changing systems. Also, descriptions of photoactuated gels that rely on a combination of polymer properties and inherent effects of azobenzenes, in particular pseudostilbenes, are far and few between.

In this light, the development of copolymers bearing both a chromic azo dye, as well as a crosslinker is an interesting goal. In this way, several different effects can be investigated in the

same system. For this purpose, synthesis of a monomer based on the pH indicator *o*-methyl red was targeted, as this is a chromic dye and a pseudostilbene at the same time. The next step is the integration of this dye monomer in a copolymer containing benzophenone moieties as photocrosslinker to obtain a gel after photocrosslinking with UV-light and swelling. Lastly, the obtained copolymers and gels are to be analysed regarding chromic, especially thermochromic, behaviour and photoactuation under irradiation with a focussed laser.

On the one hand, the influence of chemical structure on thermochromism can be determined by variation of the linkage of the dye with a polymerisable unit *via* the free acid of *o*-methyl red. On the other hand, variation of the copolymer structure to obtain either lower critical solution (LCST)-type thermoresponsive or non-thermoresponsive systems is a convenient way to influence the microenvironment of the dye in a chromic context. In relation to photoactuation, thermoresponsiveness allows to imbue a gel matrix with inherent, polymer-specific properties.

The complex interplay of polymer properties, dye responses to thermal influences or irradiation, as well as chemical triggers in form of pH is to be unravelled in this thesis.

References

1 J. H. Day, Thermochromism, *Chem. Rev.*, 1963, **63**, 65–80.

2 J. H. Day, Thermochromism of inorganic compounds, *Chem. Rev.*, 1968, **68**, 649-657.

3 A. Seeboth, D. Lötzsch, R. Ruhmann and O. Muehling, Thermochromic polymers-function by design, *Chem. Rev.*, 2014, **114**, 3037–3068.

4 A. Hakami, S. S. Srinivasan, P. K. Biswas, A. Krishnegowda, S. L. Wallen and E. K. Stefanakos, Review on thermochromic materials: development, characterization, and applications, *J. Coat. Technol. Res.*, 2022, **19**, 377–402.

5 T.-C. Chang, X. Cao, S.-H. Bao, S.-D. Ji, H.-J. Luo and P. Jin, Review on thermochromic vanadium dioxide based smart coatings: from lab to commercial application, *Adv. Manuf.*, 2018, **6**, 1–19.

6 F. J. Morin, Oxides Which Show a Metal-to-Insulator Transition at the Neel Temperature, *Phys. Rev. Lett.*, 1959, **3**, 34–36.

7 E. K. Barimah, A. Boontan, D. P. Steenson and G. Jose, Infrared optical properties modulation of VO2 thin film fabricated by ultrafast pulsed laser deposition for thermochromic smart window applications, *Sci. Rep.*, 2022, **12**, 11421.

8 J. Kim and T. Paik, Recent Advances in Fabrication of Flexible, Thermochromic Vanadium Dioxide Films for Smart Windows, *Nanomaterials*, 2021, **11**.

9 I. Sage, Thermochromic liquid crystals, *Liq. Cryst.*, 2011, **38**, 1551–1561.

10 N. Bar and P. Chowdhury, A Brief Review on Advances in Rhodamine B Based Chromic Materials and Their Prospects, *ACS Appl. Electron. Mater.*, 2022.

11 M. M. A. Mazza and F. M. Raymo, Structural designs for ratiometric temperature sensing with organic fluorophores, *J. Mater. Chem. C*, 2019, **7**, 5333–5342.

12 Y. Zheng, Y. Meana, M. M. A. Mazza, J. D. Baker, P. J. Minnett and F. M. Raymo, Fluorescence Switching for Temperature Sensing in Water, *J. Am. Chem. Soc.*, 2022, **144**, 4759–4763.

13 M. S. Abdelrahman, T. A. Khattab and S. Kamel, Development of a novel colorimetric thermometer based on poly(N-vinylcaprolactam) with push–π–pull tricyanofuran hydrazone anion dye, *New J. Chem.*, 2021, **45**, 5382–5390.

14 T. A. Khattab, From chromic switchable hydrazones to smart materials, *Mater. Chem. Phys.*, 2020, **254**, 123456.

15 T. A. Khattab, M. E. El-Naggar, M. S. Abdelrahman, A. Aldalbahi and M. R. Hatshan, Simple Development of Novel Reversible Colorimetric Thermometer Using Urea Organogel Embedded with Thermochromic Hydrazone Chromophore, *Chemosensors*, 2020, **8**, 132.

16 T. A. Khattab, B. D. B. Tiu, S. Adas, S. d. Bunge and R. C. Advincula, Solvatochromic, thermochromic and pH-sensory DCDHF-hydrazone molecular switch: response to alkaline analytes, *RSC Adv.*, 2016, **6**, 102296–102305.

17 M. Nepraš, M. Titz, M. Nečas, S. Luňák, R. Hrdina and A. Lyčka, Study of the azo-hydrazone tautomeric equilibrium by electronic spectroscopy and quantum chemistry. I. Electronic spectra, *Collect. Czech. Chem. Commun.*, 1988, **53**, 213–226.

18 X. Du, C. Zhu and X. Xie, Thermochromic Ion-Exchange Micelles Containing H+ Chromoionophores, *Langmuir*, 2017, **33**, 5910–5914.

19 A. Seeboth, J. Kriwanek, D. Lötzsch and A. Patzak, Chromogenic polymer gels for reversible transparency and color control with temperature at a constant volume, *Polym. Adv. Technol.*, 2002, **13**, 507–512.

20 A. Seeboth, D. Lötzsch and R. Ruhmann, First example of a non-toxic thermochromic polymer material – based on a novel mechanism, *J. Mater. Chem. C*, 2013, **1**, 2811.

21 A. Seeboth, J. Kriwanek and R. Vetter, Novel Chromogenic Polymer Gel Networks for Hybrid Transparency and Color Control with Temperature, *Adv. Mat.,* 2000, **12**, 1424–1426.

22 J. Catalán, J. L. Garcia de Paz and C. Reichardt, On the molecular structure and UV/vis spectroscopic properties of the solvatochromic and thermochromic pyridinium-N-phenolate betaine dye B30, *J. Phys. Chem. A*, 2010, **114**, 6226–6234.

23 W. Chi, W. Yin, Q. Qi, Q. Qiao, Y. Lin, Z. Zhu, S. Vijayan, M. Hashimoto, G. Udayakumar, Z. Xu and X. Liu, Ground-state conformers enable bright single-fluorophore ratiometric thermometers with positive temperature coefficients, *Mater. Chem. Front.*, 2017, **1**, 2383–2390.

24 Š. Sršeň, J. Sita, P. Slavíček, V. Ladányi and D. Heger, Limits of the Nuclear Ensemble Method for Electronic Spectra Simulations: Temperature Dependence of the (E)-Azobenzene Spectrum, *J. Chem. Theory Comput.*, 2020, **16**, 6428–6438.

25 S. Lunák, M. Nepraš, R. Hrdina and H. Mustroph, Excited states of azo compounds. II. Vibrational structure of the electronic absorption spectra of 4,4′-di-substituted azobenzene derivatives, *Chem. Phys.*, 1994, **184**, 255–260.

26 M. Nepraš, S. Luňák, R. Hrdina and J. Fabian, Electronic excited states of azo compounds: Strong ππ* fluorescence of bis-4,4′-diethylaminoazobenzene, *Chem. Phys. Lett.*, 1989, **159**, 366–370.

27 S. Liang, Y. Wang, L. Mu, G. She and W. Shi, Robust liquid-core nanocapsules as biocompatible and precise ratiometric fluorescent thermometers for living cells, *Nanotechnology*, 2020, **31**, 365502.

28 S. Wu, L. Niu, J. Shen, Q. Zhang and C. Bubeck, Aggregation-Induced Reversible Thermochromism of Novel Azo Chromophore-Functionalized Polydiacetylene Cylindrical Micelles, *Macromolecules*, 2009, **42**, 362–367.

29 M. S. Antonious, E. B. Tada and O. A. E. Seoud, Thermo-solvatochromism in aqueous alcohols: effects of the molecular structures of the alcohol and the solvatochromic probe, *J. Phys. Org. Chem.*, 2002, **15**, 403–412.

30 E. B. Tada, P. L. Silva, C. Tavares and O. A. El Seoud, Thermo-solvatochromism of zwitterionic probes in aqueous aliphatic alcohols and in aqueous 2-alkoxyethanols: relevance to the enthalpies of activation of chemical reactions, *J. Phys. Org. Chem.*, 2005, **18**, 398–407.

31 E. B. Tada, P. L. Silva and O. A. El Seoud, Thermo-solvatochromism of betaine dyes in aqueous alcohols: explicit consideration of the water-alcohol complex, *J. Phys. Org. Chem.*, 2003, **16**, 691–699.

32 L. Kortekaas and W. R. Browne, The evolution of spiropyran: fundamentals and progress of an extraordinarily versatile photochrome, *Chem. Soc. Rev.*, 2019, **48**, 3406–3424.

33 C. Reichardt, *Solvents and Solvent Effects in Organic Chemistry (Third Edition)*, Wiley-VCH, Weinheim, 3rd edn., 2003.

34 V. I. Minkin, A. V. Tsukanov, A. D. Dubonosov and V. A. Bren, Tautomeric Schiff bases: Iono-, solvato-, thermo- and photochromism, *J. Mol. Struct.*, 2011, **998**, 179–191.

35 W. Zhang, A. P. Schenning, A. J. Kragt, G. Zhou and L. T. de Haan, Thermochromic Multicolored Photonic Coatings with Light Polarization- and Structural Color-Dependent Changes, *ACS Appl. Polym. Mater.*, 2022, **4**, 537–545.

36 W. Zhang, A. P. H. J. Schenning, A. J. J. Kragt, G. Zhou and L. T. de Haan, Reversible Thermochromic Photonic Coatings with a Protective Topcoat, *ACS App. Mater. Interfaces*, 2021, **13**, 3153–3160.

37 A. J. J. Kragt, N. C. M. Zuurbier, D. J. Broer and A. P. H. J. Schenning, Temperature-Responsive, Multicolor-Changing Photonic Polymers, *ACS App. Mater. Interfaces*, 2019, **11**, 28172–28179.

38 B. Ding, P. Zeng, Z. Huang, L. Dai, T. Lan, H. Xu, Y. Pan, Y. Luo, Q. Yu, H.-M. Cheng and B. Liu, A 2D material-based transparent hydrogel with engineerable interference colours, *Nat. Commun.*, 2022, **13**, 1212.

39 H. Chen, Y. Jin, A. Zhong, J. Wu, H. Yan and R. Li, Reversible thermochromic behavior and mechanism of Congo red/palygorskite nanohybrid induced by mechanochromism, *J. Porous Mater.*, 2022, **29**, 215–227.

40 Y. Ohtsuka, M. Sakai, T. Seki, R. Ohnuki, S. Yoshioka and Y. Takeoka, Stimuli-Responsive Structural Colored Gel That Exhibits the Three Primary Colors of Light by Using Multiple Photonic Band Gaps Acquired from Photonic Balls, *ACS App. Mater. Interfaces*, 2020, **12**, 54127–54137.

41 K. Ueno, K. Matsubara, M. Watanabe and Y. Takeoka, An Electro- and Thermochromic Hydrogel as a Full-Color Indicator, *Adv. Mater.*, 2007, **19**, 2807–2812.

42 K. Matsubara, M. Watanabe and Y. Takeoka, A thermally adjustable multicolor photochromic hydrogel, *Angew. Chem. Intl. Ed.*, 2007, **46**, 1688–1692.

43 Y. Wu, Y. Wang, S. Zhang and S. Wu, Artificial Chameleon Skin with Super-Sensitive Thermal and Mechanochromic Response, *ACS Nano*, 2021, **15**, 15720–15729.

44 X. Liang, M. Chen, Q. Wang, S. Guo, L. Zhang and H. Yang, Active and passive modulation of solar light transmittance in a hybrid thermochromic soft-matter system for energy-saving smart window applications, *J. Mater. Chem. C*, 2018, **6**, 7054–7062.

45 Weissman, Sunkara, Tse and Asher, Thermally Switchable Periodicities and Diffraction from Mesoscopically Ordered Materials, *Science*, 1996, **274**, 959–960.

46 A. A. Beharry and G. A. Woolley, Azobenzene photoswitches for biomolecules, *Chem. Soc. Rev.*, 2011, **40**, 4422–4437.

47 H. M. D. Bandara and S. C. Burdette, Photoisomerization in different classes of azobenzene, *Chem. Soc. Rev.*, 2012, **41**, 1809–1825.

48 A. Seeboth, J. Kriwanek and R. Vetter, The first example of thermochromism of dyes embedded in transparent polymer gel networks, *J. Mater. Chem.*, 1999, **9**, 2277–2278.

49 in *The IUPAC Compendium of Chemical Terminology*, ed. V. Gold, International Union of Pure and Applied Chemistry (IUPAC), Research Triangle Park, NC, 2019.

50 K. Hofmann, S. Brumm, C. Mende, K. Nagel, A. Seifert, I. Roth, D. Schaarschmidt, H. Lang and S. Spange, Solvatochromism and acidochromism of azobenzene-functionalized poly(vinyl amines), *New J. Chem.*, 2012, **36**, 1655.

51 H. Detert and V. Schmitt, Acidochromism of stilbenoid chromophores with ap-aminoaniline centre, *J. Phys. Org. Chem.*, 2006, **19**, 603–607.

52 H. Detert, O. Sadovski and E. Sugiono, Acidochromism of C 2 -symmetrical aza-analogues of 1,4-distyrylbenzene, *J. Phys. Org. Chem.*, 2004, **17**, 1046–1050.

53 J. Kriwanek, D. Lötzsch, R. Vetter and A. Seeboth, Influence of a zwitterionic surfactant on the chromogenic behavior of a dye-containing aqueous PVA-polyether gel network, *Polym. Adv. Technol.*, 2003, **14**, 79–82.

54 M. M. A. Mazza, F. Cardano, J. Cusido, J. D. Baker, S. Giordani and F. M. Raymo, Ratiometric temperature sensing with fluorescent thermochromic switches, *Chem. Commun.*, 2019, **55**, 1112–1115.

55 S. Uchiyama, C. Gota, T. Tsuji and N. Inada, Intracellular temperature measurements with fluorescent polymeric thermometers, *Chem. Commun.*, 2017, **53**, 10976–10992.

56 S. Uchiyama, N. Kawai, A. P. de Silva and K. Iwai, Fluorescent polymeric AND logic gate with temperature and pH as inputs, *J. Am. Chem. Soc.*, 2004, **126**, 3032–3033.

57 S. Uchiyama and Y. Makino, Digital fluorescent pH sensors, *Chem. Commun.*, 2009, 2646–2648.

58 M. Peng, A. M. Kaczmarek and K. van Hecke, Ratiometric Thermometers Based on Rhodamine B and Fluorescein Dye-Incorporated (Nano) Cyclodextrin Metal-Organic Frameworks, *ACS applied materials & interfaces*, 2022, **14**, 14367–14379.

59 Y. Wu, J. Liu, Y. Wang, K. Li, L. Li, J. Xu and D. Wu, Novel Ratiometric Fluorescent Nanothermometers Based on Fluorophores-Labeled Short Single-Stranded DNA, *ACS App. Mater. Interfaces*, 2017, **9**, 11073–11081.

60 D. Mao, X. Liu, Q. Qiao, W. Yin, M. Zhao, J. M. Cole, J. Cui and Z. Xu, Coumarin 545: an emission reference dye with a record-low temperature coefficient for ratiometric fluorescence based temperature measurements, *Analyst*, 2015, **140**, 1008–1013.

61 S. Otto, N. Scholz, T. Behnke, U. Resch-Genger and K. Heinze, Thermo-Chromium: A Contactless Optical Molecular Thermometer, *Chem. Eur. J.*, 2017, **23**, 12131–12135.

62 N. Zhou, Y. Zhang, Z. Chen, X. Zhu and X. He, Developing luminescent ratiometric thermometers based on copolymers containing Platinum(II) isocyanide complex, *Dyes Pigm.*, 2021, **184**, 108815.

63 A. Mills and A. Lepre, Development of novel thermochromic plastic films for optical temperature sensing, *Analyst*, 1999, **124**, 685–689.

64 C. Pietsch, U. S. Schubert and R. Hoogenboom, Aqueous polymeric sensors based on temperature-induced polymer phase transitions and solvatochromic dyes, *Chem. Commun.*, 2011, **47**, 8750–8765.

65 H. Ren, D. Chen, Y. Shi, H. Yu and Z. Fu, Multi-responsive fluorescence of amphiphilic diblock copolymer containing carboxylate azobenzene and N-isopropylacrylamide, *Polymer*, 2016, **97**, 533–542.

66 G. H. Darwish, A. Koubeissi, T. Shoker, S. Abou Shaheen and P. Karam, Turning the heat on conjugated polyelectrolytes: an off-on ratiometric nanothermometer, *Chem. Commun.*, 2016, **52**, 823–826.

67 C. Bellacanzone, J. R. Otaegui, J. Hernando, D. Ruiz-Molina and C. Roscini, Tunable Thermofluorochromic Sensors Based on Conjugated Polymers, *Adv. Optical Mater.*, 2022, **10**, 2102423.

68 C. Pietsch, R. Hoogenboom and U. S. Schubert, Soluble polymeric dual sensor for temperature and pH value, *Angew. Chem. Intl. Ed.*, 2009, **48**, 5653–5656.

69 C. Pietsch, R. Hoogenboom and U. S. Schubert, PMMA based soluble polymeric temperature sensors based on UCST transition and solvatochromic dyes, *Polym. Chem.*, 2010, **1**, 1005.

70 M. Irie and D. Kungwatchakun, Stimuli-responsive Polymers. Photostimulated Reversible Phase Separation of Aqueous Solutions of Poly(N-isopropylacrylamide) with Pendant Azobenzene Groups, *Proc. Jpn. Acad. Ser. B*, 1992, **68**, 127–132.

71 D. Kungwatchakun and M. Irie, Photoresponsive polymers. Photocontrol of the phase separation temperature of aqueous solutions of poly-[N-isopropylacrylamide-co-N-(4-phenylazophenyl)acrylamide], *Makromol. Chem., Rapid Commun.*, 1988, **9**, 243–246.

72 R. Kröger, H. Menzel and M. L. Hallensleben, Light controlled solubility change of polymers, *Macromol. Chem. Phys.*, 1994, **195**, 2291–2298.

73 H. Akiyama and N. Tamaoki, Polymers derived fromN-isopropylacrylamide and azobenzene-containing acrylamides: Photoresponsive affinity to water, *J. Polym. Sci. A Polym. Chem.*, 2004, **42**, 5200–5214.

74 W. Yuan, G. Jiang, J. Wang, G. Wang, Y. Song and L. Jiang, Temperature/Light Dual-Responsive Surface with Tunable Wettability Created by Modification with an Azobenzene-Containing Copolymer, *Macromolecules*, 2006, **39**, 1300–1303.

75 A. Desponds and R. Freitag, Synthesis and Characterization of Photoresponsive N - Isopropylacrylamide Cotelomers, *Langmuir*, 2003, **19**, 6261–6270.

76 P. Ravi, S. L. Sin, L. H. Gan, Y. Y. Gan, K. C. Tam, X. L. Xia and X. Hu, New water soluble azobenzene-containing diblock copolymers: synthesis and aggregation behavior, *Polymer*, 2005, **46**, 137–146.

77 H. Akiyama and N. Tamaoki, Synthesis and Photoinduced Phase Transitions of Poly(N - isopropylacrylamide) Derivative Functionalized with Terminal Azobenzene Units, *Macromolecules*, 2007, **40**, 5129–5132.

78 F. D. Jochum and P. Theato, Temperature and light sensitive copolymers containing azobenzene moieties prepared via a polymer analogous reaction, *Polymer*, 2009, **50**, 3079–3085.

79 F. D. Jochum and P. Theato, Thermo- and light responsive micellation of azobenzene containing block copolymers, *Chem. Commun.*, 2010, **46**, 6717–6719.

80 F. D. Jochum, L. zur Borg, P. J. Roth and P. Theato, Thermo- and Light-Responsive Polymers Containing Photoswitchable Azobenzene End Groups, *Macromolecules*, 2009, **42**, 7854–7862.

81 F. D. Jochum, F. R. Forst and P. Theato, PNIPAM Copolymers Containing Light-Responsive Chromophores: A Method Toward Molecular Logic Gates, *Macromol. Rapid Commun.*, 2010, **31**, 1456–1461.

82 P. Schattling, F. D. Jochum and P. Theato, Multi-stimuli responsive polymers – the all-in-one talents, *Polym. Chem.*, 2014, **5**, 25–36.

83 C. Luo, F. Zuo, X. Ding, Z. Zheng, X. Cheng and Y. Peng, Light-triggered reversible solubility of α-cyclodextrin and azobenzene moiety complexes in PDMAA-co-PAPA via molecular recognition, *J. Appl. Polym. Sci.*, 2008, **107**, 2118–2125.

84 X. Tang, X. Liang, L. Gao, X. Fan and Q. Zhou, Water-soluble triply-responsive homopolymers of N,N -dimethylaminoethyl methacrylate with a terminal azobenzene moiety, *J. Polym. Sci. A Polym. Chem.*, 2010, **48**, 2564–2570.

85 Y. Xiang, X. Xue, J. Zhu, Z. Zhang, W. Zhang, N. Zhou and X. Zhu, Fluorescence behavior of an azobenzene-containing amphiphilic diblock copolymer, *Polym. Chem.*, 2010, **1**, 1453.

86 J. Wang, Q. Li, S. Yi and X. Chen, Visible-light/temperature dual-responsive hydrogel constructed by α-cyclodextrin and an azobenzene linked surfactant, *Soft Matter*, 2017, **13**, 6490–6498.

87 E.-M. Lee, S.-Y. Gwon, B.-C. Ji and S.-H. Kim, Temperature and acid/base-driven dual switching of poly(N-isopropylacrylamide) hydrogel with Azo dye, *Fibers Polym.*, 2011, **12**, 142–144.

88 C. Reichardt, Solvatochromic Dyes as Solvent Polarity Indicators, *Chem. Rev.*, 1994, **94**, 2319–2358.

89 H. Joshi, F. S. Kamounah, G. van der Zwan, C. Gooijer and L. Antonov, Temperature dependent absorption spectroscopy of some tautomeric azo dyes and Schiff bases, *J. Chem. Soc. Perkin Trans. 2*, 2001, 2303–2308.

90 P. Gilli, V. Bertolasi, L. Pretto, A. Lycka and G. Gilli, The nature of solid-state N-H···O/O-H···N tautomeric competition in resonant systems. Intramolecular proton transfer in low-barrier hydrogen bonds formed by the ···O=C-C=N-NH··· ⇌ ···HO-C=C-N=N··· Ketohydrazone-Azoenol system. A variable-temperature X-ray crystallographic and DFT computational study, *J. Am. Chem. Soc.*, 2002, **124**, 13554–13567.

91 E. Fischer and Y. F. Frei, Tautomerism and geometrical isomerism of arylazo-phenols and -naphthols. Part I. 4-phenylazo-1-naphthol, *J. Chem. Soc.*, 1959, 3159.

92 G. Gabor, Y. Frei, D. Gegiou, M. Kaganowitch and E. Fischer, Tautomerism and Geometric Isomerism in Arylazo-Phenols and Naphthols. Part III. Orthohydroxy Derivatives and their Reversible Photochemical Reactions, *Isr. J. Chem.*, 1967, **5**, 193–211.

93 A. C. Olivieri, R. B. Wilson, I. C. Paul and D. Y. Curtin, Carbon-13 NMR and x-ray structure determination of 1-(arylazo)-2-naphthols. Intramolecular proton transfer between nitrogen and oxygen atoms in the solid state, *J. Am. Chem. Soc.*, 1989, **111**, 5525–5532.

94 E. Sawicki, Physical Properties of the Aminoazobenzene Dyes. IV. The Position of Proton Addition 1, *J. Org. Chem.*, 1957, **22**, 365–367.

95 E. Sawicki, The Physical Properties of the Aminoazobenzene Dyes. III. Tautomerism of 4-Aminoazobenzene Salt Cations in Acid Solution, *J. Org. Chem.*, 1956, **21**, 605–609.

96 E. Sawicki, Physical Properties of Aminoazobenzene Dyes. V. The C ϵ /A ϵ Ratio, *J. Org. Chem.*, 1957, **22**, 621–625.

97 G. E. Lewis, Structures of the mono-acid cations of 4-aminoazobenzene and its derivatives, *Tetrahedron*, 1960, **10**, 129–134.

98 I. Y. Bershtein and O. F. Ginzburg, Tautomerism of Aromatic Azo-compounds, *Russ. Chem. Rev.*, 1972, **41**, 97–110.

99 K. M. Tawarah and H. M. Abu-Shamleh, A spectrophotometric study of the acid-base equilibria of o-methyl red in aqueous solutions, *Dyes Pigm.*, 1991, **17**, 203–215.

100 J. A. Dean and N. A. Lange, *Lange's handbook of chemistry*, McGraw-Hill; Knovel, New York, 15th edn., 1999.

101 G. Seu, Spectrophotometric study of the prototropic equilibrium of methyl red in organic solvents, *Dyes Pigm.*, 1995, **29**, 227–240.

102 R. W. Taft, J.-L. M. Abboud, M. J. Kamlet and M. H. Abraham, Linear solvation energy relations, *J. Solut. Chem.*, 1985, **14**, 153–186.

103 A. R. Katritzky, D. C. Fara, H. Yang, K. Tämm, T. Tamm and M. Karelson, Quantitative measures of solvent polarity, *Chem. Rev.*, 2004, **104**, 175–198.

104 T. Kuwabara, A. Nakamura, A. Ueno and F. Toda, Supramolecular Thermochromism of a Dye-appended P-Cyclodextrin, *J. Chem. Soc. Chem. Commun.*, 1994, 689–690.

105 A. Ueno, T. Kuwabara, A. Nakamura and F. Toda, A modified cyclodextrin as a guest responsive colour-change indicator, *Nature*, 1992, **356**, 136–137.

106 M. Tajima, M. Sugai, K. Matsunaga, T. Yamashita, H. Inoue and M. Hida, Thermochromism of dyes on silica gel, *Dyes Pigm.*, 1998, **39**, 97–109.

107 P. Weis and S. Wu, Light-Switchable Azobenzene-Containing Macromolecules: From UV to Near Infrared, *Macromol. Rapid Commun.*, 2018, **39**.

108 P. Rochon, E. Batalla and A. Natansohn, Optically induced surface gratings on azoaromatic polymer films, *Appl. Phys. Lett.*, 1995, **66**, 136–138.

109 D. Y. Kim, S. K. Tripathy, L. Li and J. Kumar, Laser-induced holographic surface relief gratings on nonlinear optical polymer films, *Appl. Phys. Lett.*, 1995, **66**, 1166–1168.

110 A. Natansohn and P. Rochon, Photoinduced Motions in Azo-Containing Polymers, *Chem. Rev.*, 2002, **102**, 4139–4176.

111 S. L. Oscurato, M. Salvatore, P. Maddalena and A. Ambrosio, From nanoscopic to macroscopic photo-driven motion in azobenzene-containing materials, *Nanophotonics*, 2018, **7**, 1387–1422.

112 N. S. Yadavalli, T. König and S. Santer, Selective mass transport of azobenzene-containing photosensitive films towards or away from the light intensity, *J. Soc. Inf. Disp.*, 2015, **23**, 154–162.

113 A. Priimagi and A. Shevchenko, Azopolymer-based micro- and nanopatterning for photonic applications, *J. Polym. Sci. Part B: Polym. Phys.*, 2014, **52**, 163–182.

114 A. Priimagi, C. J. Barrett and A. Shishido, Recent twists in photoactuation and photoalignment control, *J. Mater. Chem. C*, 2014, **2**, 7155.

115 X. L. Jiang, L. Li, J. Kumar, D. Y. Kim and S. K. Tripathy, Unusual polarization dependent optical erasure of surface relief gratings on azobenzene polymer films, *Appl. Phys. Lett.*, 1998, **72**, 2502–2504.

116 H. Audorff, R. Walker, L. Kador and H.-W. Schmidt, Polarization dependence of the formation of surface relief gratings in azobenzene-containing molecular glasses, *J. Phys. Chem. B*, 2009, **113**, 3379–3384.

117 J. Aleksejeva, A. Gerbreders, U. Gertners, M. Reinfelde and J. Teteris, Polarization holographic recording in Disperse Red1 doped polyurethane polymer film, *IOP Conf. Ser.: Mater. Sci. Eng.*, 2011, **23**, 12006.

118 J. Zhou, J. Shen, J. Yang, Y. Ke, K. Wang and Q. Zhang, Fabrication of a pure polarization grating in a cross-linked azopolymer by polarization-modulated holography, *Opt. Lett.*, 2006, **31**, 1370–1372.

119 N. Zettsu, T. Fukuda, H. Matsuda and T. Seki, Unconventional polarization characteristic of rapid photoinduced material motion in liquid crystalline azobenzene polymer films, *Appl. Phys. Lett.*, 2003, **83**, 4960–4962.

120 S. Lee, H. S. Kang and J.-K. Park, Directional photofluidization lithography: micro/nanostructural evolution by photofluidic motions of azobenzene materials, *Adv. Mat.*, 2012, **24**, 2069–2103.

121 S. Lee, H. S. Kang and J.-K. Park, High-Resolution Patterning of Various Large-Area, Highly Ordered Structural Motifs by Directional Photofluidization Lithography: Sub-30-nm Line, Ellipsoid, Rectangle, and Circle Arrays, *Adv. Funct. Mater.*, 2011, **21**, 1770–1778.

122 C. J. Barrett, A. L. Natansohn and P. L. Rochon, Mechanism of Optically Inscribed High-Efficiency Diffraction Gratings in Azo Polymer Films, *J. Phys. Chem.,* 1996, **100**, 8836-8842.

123 P. U. Veer, U. Pietsch and A. D. Mueller, Alteration of the mechanical properties of azopolymer film in the process of surface relief grating formation, *Appl. Phys. Lett.*, 2009, **94**, 231911.

124 M. L. Juan, J. Plain, R. Bachelot, P. Royer, S. K. Gray and G. P. Wiederrecht, Multiscale model for photoinduced molecular motion in azo polymers, *ACS Nano*, 2009, **3**, 1573–1579.

125 P. Lefin, C. Fiorini and J.-M. Nunzi, Anisotropy of the photo-induced translation diffusion of azobenzene dyes in polymer matrices, *Pure Appl. Opt.*, 1998, **7**, 71–82.

126 S. Bian, L. Li, J. Kumar, D. Y. Kim, J. Williams and S. K. Tripathy, Single laser beam-induced surface deformation on azobenzene polymer films, *Appl. Phys. Lett.*, 1998, **73**, 1817–1819.

127 J. Kumar, L. Li, X. L. Jiang, D.-Y. Kim, T. S. Lee and S. Tripathy, Gradient force, *Appl. Phys. Lett.*, 1998, **72**, 2096–2098.

128 T. G. Pedersen, P. M. Johansen, N. C. R. Holme, P. S. Ramanujam and S. Hvilsted, Mean-Field Theory of Photoinduced Formation of Surface Reliefs in Side-Chain Azobenzene Polymers, *Phys. Rev. Lett.*, 1998, **80**, 89–92.

129 T. G. Pedersen and P. M. Johansen, Mean-Field Theory of Photoinduced Molecular Reorientation in Azobenzene Liquid Crystalline Side-Chain Polymers, *Phys. Rev. Lett.*, 1997, **79**, 2470–2473.

130 K. G. Yager and C. J. Barrett, Temperature modeling of laser-irradiated azo-polymer thin films, *J. Chem. Physics*, 2004, **120**, 1089–1096.

131 S. Loebner, B. Yadav, N. Lomadze, N. Tverdokhleb, H. Donner, M. Saphiannikova and S. Santer, Local Direction of Optomechanical Stress in Azobenzene Containing Polymers During Surface Relief Grating Formation, *Macromol. Mater. Eng.*, 2022, 2100990.

132 B. Yadav, J. Domurath and M. Saphiannikova, Modeling of Stripe Patterns in Photosensitive Azopolymers, *Polymers*, 2020, **12**.

133 B. Yadav, J. Domurath, K. Kim, S. Lee and M. Saphiannikova, Orientation Approach to Directional Photodeformations in Glassy Side-Chain Azopolymers, *J. Phys. Chem. B*, 2019, **123**, 3337–3347.

134 V. Toshchevikov, J. Ilnytskyi and M. Saphiannikova, Photoisomerization Kinetics and Mechanical Stress in Azobenzene-Containing Materials, *J. Phys. Chem. Lett.*, 2017, **8**, 1094–1098.

135 F. Pirani, A. Angelini, F. Frascella, R. Rizzo, S. Ricciardi and E. Descrovi, Light-Driven Reversible Shaping of Individual Azopolymeric Micro-Pillars, *Sci. Rep.*, 2016, **6**, 31702.

136 D. Barada, T. Fukuda, M. Itoh and T. Yatagai, Numerical Analysis of Photoinduced Surface Relief Grating Formation by Particle Method, *Opt. Rev.*, 2005, **12**, 271–273.

137 D. Barada, M. Itoh and T. Yatagai, Computer simulation of photoinduced mass transport on azobenzene polymer films by particle method, *J. Appl. Phys.*, 2004, **96**, 4204–4210.

138 B. Bellini, J. Ackermann, H. Klein, C. Grave, P. Dumas and V. Safarov, Light-induced molecular motion of azobenzene-containing molecules, *J. Phys. Condens. Matter*, 2006, **18**, S1817-S1835.

139 T. J. White, Photomechanical effects in liquid crystalline polymer networks and elastomers, *J. Polym. Sci. Part B: Polym. Phys.*, 2018, **56**, 695–705.

140 H. K. Bisoyi and Q. Li, Light-Driven Liquid Crystalline Materials: From Photo-Induced Phase Transitions and Property Modulations to Applications, *Chem. Rev.*, 2016, **116**, 15089–15166.

141 T. Ikeda, J.-I. Mamiya and Y. Yu, Photomechanics of liquid-crystalline elastomers and other polymers, *Angew. Chem. Intl. Ed.*, 2007, **46**, 506–528.

142 C. Ohm, M. Brehmer and R. Zentel, Liquid crystalline elastomers as actuators and sensors, *Advanced materials (Deerfield Beach, Fla.)*, 2010, **22**, 3366–3387.

143 A. Priimagi, A. Shimamura, M. Kondo, T. Hiraoka, S. Kubo, J.-I. Mamiya, M. Kinoshita, T. Ikeda and A. Shishido, Location of the Azobenzene Moieties within the Cross-Linked Liquid-Crystalline Polymers Can Dictate the Direction of Photoinduced Bending, *ACS Macro Lett.*, 2012, **1**, 96–99.

144 Y. Yu, M. Nakano and T. Ikeda, Photomechanics: directed bending of a polymer film by light, *Nature*, 2003, **425**, 145.

145 T. J. White, S. V. Serak, N. V. Tabiryan, R. A. Vaia and T. J. Bunning, Polarization-controlled, photodriven bending in monodomain liquid crystal elastomer cantilevers, *J. Mater. Chem.*, 2009, **19**, 1080–1085.

146 T. J. White, N. V. Tabiryan, S. V. Serak, U. A. Hrozhyk, V. P. Tondiglia, H. Koerner, R. A. Vaia and T. J. Bunning, A high frequency photodriven polymer oscillator, *Soft Matter*, 2008, **4**, 1796.

147 B. A. Kowalski, T. C. Guin, A. D. Auguste, N. P. Godman and T. J. White, Pixelated Polymers: Directed Self Assembly of Liquid Crystalline Polymer Networks, *ACS Macro Lett.*, 2017, **6**, 436–441.

148 D. Tang, L. Zhang, X. Zhang, L. Xu, K. Li and A. Zhang, Bio-Mimetic Actuators of a Photothermal-Responsive Vitrimer Liquid Crystal Elastomer with Robust, Self-Healing, Shape Memory, and Reconfigurable Properties, *ACS Appl. Mater. Interfaces*, 2022, **14**, 1929–1939.

149 A. S. Hoffman, Hydrogels for biomedical applications, *Adv. Drug Deliv. Rev.*, 2002, **54**, 3–12.

150 N. A. Peppas, J. Z. Hilt, A. Khademhosseini and R. Langer, Hydrogels in Biology and Medicine: From Molecular Principles to Bionanotechnology, *Adv. Mat.*, 2006, **18**, 1345–1360.

151 H. Yao, J. Wang and S. Mi, Photo Processing for Biomedical Hydrogels Design and Functionality: A Review, *Polymers*, 2017, **10**.

152 T. Vermonden, R. Censi and W. E. Hennink, Hydrogels for protein delivery, *Chem. Rev.*, 2012, **112**, 2853–2888.

153 Z. Wang, L. Scheres, H. Xia and H. Zuilhof, Developments and Challenges in Self-Healing Antifouling Materials, *Adv. Funct. Mater.*, 2020, 1908098.

154 L. Li, J. M. Scheiger and P. A. Levkin, Design and Applications of Photoresponsive Hydrogels, *Adv. Mater.*, 2019, **31**, e1807333.

155 A. M. Rosales, S. L. Vega, F. W. DelRio, J. A. Burdick and K. S. Anseth, Hydrogels with Reversible Mechanics to Probe Dynamic Cell Microenvironments, *Angew. Chem. Intl. Ed.,* 2017, **56**, 12132–12136.

156 D. R. Griffin and A. M. Kasko, Photodegradable macromers and hydrogels for live cell encapsulation and release, *J. Am. Chem. Soc.*, 2012, **134**, 13103–13107.

157 A. M. Kloxin, A. M. Kasko, C. N. Salinas and K. S. Anseth, Photodegradable hydrogels for dynamic tuning of physical and chemical properties, *Science*, 2009, **324**, 59–63.

158 H. Zhang, X. Li, Y. Lin, F. Gao, Z. Tang, P. Su, W. Zhang, Y. Xu, W. Weng and R. Boulatov, Multi-modal mechanophores based on cinnamate dimers, *Nat. Commun.*, 2017, **8**, 1147.

159 L. Yu, K. Xu, L. Ge, W. Wan, A. Darabi, M. Xing and W. Zhong, Cytocompatible, Photoreversible, and Self-Healing Hydrogels for Regulating Bone Marrow Stromal Cell Differentiation, *Macromol. Biosci.*, 2016, **16**, 1381–1390.

160 W. Ji, M. Qin and C. Feng, Photoresponsive Coumarin-Based Supramolecular Hydrogel for Controllable Dye Release, *Macromol. Chem. Phys.*, 2018, **219**, 1700398.

161 M. A. Azagarsamy, D. D. McKinnon, D. L. Alge and K. S. Anseth, Coumarin-Based Photodegradable Hydrogel: Design, Synthesis, Gelation, and Degradation Kinetics, *ACS Macro Lett.*, 2014, **3**, 515–519.

162 L. A. Wells, M. A. Brook and H. Sheardown, Generic, anthracene-based hydrogel crosslinkers for photo-controllable drug delivery, *Macromol. Biosci.*, 2011, **11**, 988–998.

163 Y. Zheng, M. Micic, S. V. Mello, M. Mabrouki, F. M. Andreopoulos, V. Konka, S. M. Pham and R. M. Leblanc, PEG-Based Hydrogel Synthesis via the Photodimerization of Anthracene Groups, *Macromolecules*, 2002, **35**, 5228–5234.

164 P. M. Kharkar, M. S. Rehmann, K. M. Skeens, E. Maverakis and A. M. Kloxin, Thiol-ene click hydrogels for therapeutic delivery, *ACS Biomater. Sci. Eng.*, 2016, **2**, 165–179.

165 A. B. Lowe, Thiol-ene "click" reactions and recent applications in polymer and materials synthesis, *Polym. Chem.*, 2010, **1**, 17–36.

166 A. B. Lowe, Thiol–ene "click" reactions and recent applications in polymer and materials synthesis: a first update, *Polym. Chem.*, 2014, **5**, 4820–4870.

167 Z. Li, G. Davidson-Rozenfeld, M. Vázquez-González, M. Fadeev, J. Zhang, H. Tian and I. Willner, Multi-triggered Supramolecular DNA/Bipyridinium Dithienylethene Hydrogels Driven by Light, Redox, and Chemical Stimuli for Shape-Memory and Self-Healing Applications, *J. Am. Chem. Soc.*, 2018, **140**, 17691–17701.

168 A. Vlasceanu, M. Cacciarini and M. B. Nielsen, Photo/thermochromic macrocycles based on dihydroazulenes, dithienylethenes, and spiropyrans, *Tetrahedron*, 2018, **74**, 6635–6646.

169 A. D. Pugachev, E. L. Mukhanov, I. V. Ozhogin, A. S. Kozlenko, A. V. Metelitsa and B. S. Lukyanov, Isomerization and changes of the properties of spiropyrans by mechanical stress: advances and outlook, *Chem. Heterocycl. Compd.*, 2021, **57**, 122–130.

170 N. Deneke, M. L. Rencheck and C. S. Davis, An engineer's introduction to mechanophores, *Soft Matter*, 2020, **16**, 6230–6252.

171 G. A. Leith, C. R. Martin, A. Mathur, P. Kittikhunnatham, K. C. Park and N. B. Shustova, Dynamically Controlled Electronic Behavior of Stimuli-Responsive Materials: Exploring Dimensionality and Connectivity, *Adv. Energy Mater.*, 2022, **12**, 2100441.

172 A. S. Kozlenko, A. D. Pugachev, I. V. Ozhogin, I. M. El-Sewify and B. S. Lukyanov, Spiropyrans: molecules in motion, *Chem. Heterocycl. Compd.*, 2021, **57**, 984–989.

173 B. S. Lukyanov and M. B. Lukyanova, Spiropyrans: Synthesis, Properties, and Application. (Review), *Chem. Heterocycl. Compd.*, 2005, **41**, 281–311.

174 R. Klajn, Spiropyran-based dynamic materials, *Chem. Soc. Rev.*, 2014, **43**, 148–184.

175 N. Wang, Y. Li, Y. Zhang, Y. Liao and W. Liu, High-strength photoresponsive hydrogels enable surface-mediated gene delivery and light-induced reversible cell adhesion/detachment, *Langmuir*, 2014, **30**, 11823–11832.

176 L. Chen, X. Yao, Z. Gu, K. Zheng, C. Zhao, W. Lei, Q. Rong, L. Lin, J. Wang, L. Jiang and M. Liu, Covalent tethering of photo-responsive superficial layers on hydrogel surfaces for photo-controlled release, *Chem. Sci.*, 2017, **8**, 2010–2016.

177 F. M. Raymo and S. Giordani, Signal processing at the molecular level, *J. Am. Chem. Soc.*, 2001, **123**, 4651–4652.

178 J. T. C. Wojtyk, A. Wasey, N.-N. Xiao, P. M. Kazmaier, S. Hoz, C. Yu, R. P. Lemieux and E. Buncel, Elucidating the mechanisms of acidochromic spiropyran-merocyanine interconversion, *J. Phys. Chem. A*, 2007, **111**, 2511–2516.

179 B. Ziółkowski, L. Florea, J. Theobald, F. Benito-Lopez and D. Diamond, Self-protonating spiropyran-co-NIPAM-co-acrylic acid hydrogel photoactuators, *Soft Matter*, 2013, **9**, 8754.

180 J. ter Schiphorst, M. van den Broek, T. de Koning, J. N. Murphy, A. P. H. J. Schenning and A. C. C. Esteves, Dual light and temperature responsive cotton fabric functionalized with a surface-grafted spiropyran–NIPAAm-hydrogel, *J. Mater. Chem. A*, 2016, **4**, 8676–8681.

181 J. E. Stumpel, B. Ziółkowski, L. Florea, D. Diamond, D. J. Broer and A. P. H. J. Schenning, Photoswitchable ratchet surface topographies based on self-protonating spiropyran-NIPAAM hydrogels, *ACS Appl. Mater. Interfaces*, 2014, **6**, 7268–7274.

182 J. Ter Schiphorst, S. Coleman, J. E. Stumpel, A. Ben Azouz, D. Diamond and A. P. H. J. Schenning, Molecular Design of Light-Responsive Hydrogels, For in Situ Generation of Fast and Reversible Valves for Microfluidic Applications, *Chem. Mater.*, 2015, **27**, 5925–5931.

183 G. Pouliquen, C. Amiel and C. Tribet, Photoresponsive viscosity and host-guest association in aqueous mixtures of poly-cyclodextrin with azobenzene-modified poly(acrylic)acid, *J. Phys. Chem. B*, 2007, **111**, 5587–5595.

184 S. Tamesue, Y. Takashima, H. Yamaguchi, S. Shinkai and A. Harada, Photoswitchable supramolecular hydrogels formed by cyclodextrins and azobenzene polymers, *Angew. Chem. Intl. Ed.*, 2010, **49**, 7461–7464.

185 X. Liao, G. Chen, X. Liu, W. Chen, F. Chen and M. Jiang, Photoresponsive pseudopolyrotaxane hydrogels based on competition of host-guest interactions, *Angew. Chem. Intl. Ed.*, 2010, **49**, 4409–4413.

186 H. Yamaguchi, Y. Kobayashi, R. Kobayashi, Y. Takashima, A. Hashidzume and A. Harada, Photoswitchable gel assembly based on molecular recognition, *Nat. Commun.*, 2012, **3**, 603.

187 K. Iwaso, Y. Takashima and A. Harada, Fast response dry-type artificial molecular muscles with c2daisy chains, *Nat. Chem.*, 2016, **8**, 625–632.

188 Y. Takashima, S. Hatanaka, M. Otsubo, M. Nakahata, T. Kakuta, A. Hashidzume, H. Yamaguchi and A. Harada, Expansion-contraction of photoresponsive artificial muscle regulated by host-guest interactions, *Nat. Commun.*, 2012, **3**, 1270.

189 Y.-S. Lin, C.-H. Lin and W.-F. Lee, Investigation of the synthesis and properties of the copolymeric hydrogels based on N-isopropyl acrylamide and acrylamidoazobenzene, *J. Polym. Res.*, 2014, **21**.

3 Thermal response and thermochromism of methyl red-based copolymer systems – coupled responsiveness in critical solution behaviour and optical absorption properties

Thorben Gwydion Jaik, Betty Ciubini, Francesca Frascella, Ulrich Jonas

Polym. Chem., 2022, **13**, 1186-1214
https://doi.org/10.1039/D1PY01361K

A correction to the article was published under:

Polym. Chem., 2022, **13**, 1282-1282
https://doi.org/10.1039/D2PY90024F

Published by the *Royal Society of Chemistry* as Open Access articles under the terms of the Creative Commons CC BY 3.0 license, which permits even commercial use, distribution, and reproduction in any medium, provided the original work is properly cited (CC BY 3.0, https://creativecommons.org/licenses/by/3.0/). The article was not modified in any way. The Electronic Supporting Information (ESI) was attached directly to the article.

Contributions of the authors to this project:

- All UV-vis measurements, data analysis, synthesis of monomers and polymers, specimen preparation and method design, as well as interpretation were done by me.
- The project was mainly initiated by me with help from Betty Ciubini and Francesca Frascella. The complete draft was written by me and completed, refined, and edited together with Prof. Dr. Jonas.

Corrections:

- The unit in Table 7 for the energies calculated for thermochromic processes should read kJ mol^{-1}.
- It was erroneously stated on page 1191 of the paper that in derivative spectroscopy the negative peaks in the fourth derivative locate sub-bands. Instead, positive peaks do.

Polymer Chemistry

ROYAL SOCIETY OF CHEMISTRY

PAPER

View Article Online
View Journal | View Issue

Check for updates

Cite this: *Polym. Chem.*, 2022, **13**, 1186

Open Access Article. Published on 14 January 2022. Downloaded on 1/30/2023 11:32:10 AM.
This article is licensed under a Creative Commons Attribution 3.0 Unported Licence.

Thermal response and thermochromism of methyl red-based copolymer systems – coupled responsiveness in critical solution behaviour and optical absorption properties†

Thorben Gwydion Jaik, [a] Betty Ciubini,[b] Francesca Frascella [b] and Ulrich Jonas *[a]

Until now, only limited experimental knowledge and sparse theoretical treatment about the mechanisms of thermochromism of azo dyes in solution has been available. Especially the coupling of thermoresponsiveness of polymers with the inherent thermochromism of azo dyes is attractive to enhance the optical response for applications like polymeric optical pH- and temperature-dual sensors. To elucidate the different mechanisms contributing to the thermochromism of such azo chromophores, we synthesised monomers based on the constitutional isomers of the common pH indicator methyl red. The *ortho*-isomer was copolymerised with hydrophilic monomers and the photocrosslinker benzophenone acrylamide, with the resulting copolymers being converted to networks by irradiation with UV-light and yielding hydrogels after swelling with water. *N*-Isopropylacrylamide was used as comonomer to introduce thermoresponsiveness in the polymers in form of a lower critical solution temperature (LCST) behaviour. Three different dye systems with varying protonation states were investigated by temperature-dependant UV-vis spectroscopy: as monomers in solution, as part of copolymers in solution, and as photocrosslinked hydrogels. Consequently, we were able to identify the four different mechanisms of vibronic thermochromism, thermo-solvatochromism, thermo-perichromism and thermo-halochromism. Their interplay was investigated by choosing appropriate combinations of solvents, acid and comonomers. The LCST behaviour of the *N*-isopropylacrylamide copolymers could be exploited to strongly influence thermochromism, providing insight into the mechanisms of critical solution behaviour of polymers and thermochromism alike. The experimental data suggest that various thermochromic mechanisms act simultaneously and mutually influence each other, specifically with thermo-solvato- and thermo-perichromism affecting thermo-halochromism. These effects are best described by the terms *thermo-solvato-halochromism* and *thermo-peri-halochromism*. Notably, on the basis of the identified thermochromic mechanisms prevailing in the monomer solutions, the behaviour of the more complex polymer systems can be elucidated, and consequently, the distinct properties of the dye in combination with polymer-inherent phenomena can be deduced. To our knowledge, this is the first comprehensive study to harmonise the understanding of the different thermochromic mechanisms in azobenzene, their mutual action, and the strong influence of thermoresponse on thermochromism.

Received 11th October 2021,
Accepted 1st January 2022

DOI: 10.1039/d1py01361k

rsc.li/polymers

1. Introduction

A large number of materials show a change of colour with temperature, which is generally termed thermochromism. This has been observed and exploited to sense temperature in systems like dye-based luminescent sensors for biological and biomedical applications,[1–3] nanomaterials,[4] supramolecular systems[5] and dye aggregates.[6] Generally, thermochromism describes the change of colour due to a change of temperature and depending on the scientific community, this is defined as being either purely reversible or both reversible and irreversible processes.[7–9] Polymeric materials exhibiting thermochromic behaviour are particularly versatile and can be used in a variety of systems to achieve a change in absorption, emittance, or reflectance of a system. The term thermochromic

[a]*Department of Chemistry and Biology, University of Siegen, Adolf-Reichwein-Strasse 2, D-57076 Siegen, Germany. E-mail: jonas@chemie.uni-siegen.de*
[b]*Department of Applied Science and Technology, Politecnico di Torino, Corso Duca degli Abruzzi 24, IT-10129 Torino, Italy*

†Electronic supplementary information (ESI) available. See DOI: 10.1039/d1py01361k

This journal is © The Royal Society of Chemistry 2022

Open Access Article. Published on 14 January 2022. Downloaded on 1/30/2023 11:32:10 AM.
This article is licensed under a Creative Commons Attribution 3.0 Unported Licence.

polymers entails a manifold of systems with either the polymer itself being thermochromic or the polymer being a matrix for thermochromic dyes, complexes or particles.[7] The thermochromic mechanism relevant for the work presented in this paper is based on the change in absorption of organic dyes in dependence on temperature.

One class of optical thermometers entails solvatochromic dyes coupled to a polymer phase transition. Owing to the change in polarity in the polymer coil during the transition, either the fluorescence or absorption change with temperature.[10]

Another established thermochromic system consists of a pH-sensitive dye embedded in a hydrogel matrix that changes colour reliant on a thermally dependant protonation equilibrium, notably alkaline PVA-borax hydrogels with cresol red or Reichardt's dye as indicator dyes.[11,12]

Azo dyes are a particularly interesting class of photochromic molecules that show additional mechanisms for a colorimetric response with respect to external stimuli, besides light, such as thermochromism (responding to a temperature change), halochromism (pH change) and solvatochromism (change of solvent interaction). Thermochromism in azobenzene derivatives is often coupled to a thermochromic matrix, with the azobenzene only enhancing the optical effects in the matrix material. In one example, this was realised by adding azobenzene to an LCST polymer–opal composite to tune the transmission band over the whole visible spectrum *via trans–cis*-isomerisation and temperature. The polymer volume phase transition changes the distance between the particles in the opals, effectively tuning the optical interference, while the photochromism of the azobenzene influences the base colour of the composite.[13] In other studies, azobenzenes were combined with photochromic polyelectrolytes based on polythiophenes or polydiacetylenes (PDA), enhancing the thermochromic behaviour of the polymers or enhancing thermal reversibility, apparently by acting as controlled defects or as stabilising groups, in the case of PDA micelles.[14–20]

A thermochromic effect solely relying on the azo dye core has been investigated for several phenylazonaphthols.[21] The tautomeric equilibrium between the enol and quinone forms was followed in solution in dependence of temperature, with the quinone form absorbing at longer wavelengths and being more stable at low temperatures.

For pH-sensitive and thus halochromic azobenzenes, thermochromism has been observed in different environments. In one of the first examples, the well-known pH indicator methyl red (2-{[4-(dimethylamino)phenyl]diazenyl}benzoic acid, in short here MR) was adsorbed on silica gel. In aqueous solution, the MR chromophore changes from a red protonated form with an absorption maximum at ~525 nm at pH 4.4 to a yellow, deprotonated form above pH 6.2 (abs. max. ~430 nm).[22,23] Protonated MR exists in two different tautomeric cations, namely an ammonium ion with a protonated tertiary amine, and an azonium structure protonated at the azo bridge. In MR, the azonium form is stabilised *via* a quinoidal resonance structure and intramolecular hydrogen bonding, rendering it the preferred structure.[24] Adsorption on silica gel results in a colour change of MR from red (acidic) to orange (neutral/basic) upon heating. The authors attribute this effect to an increase of basic sites at the silica gel surface at low temperatures due to release of water and an increase in acidity of the dye at higher temperatures.[25] Another halochromic azobenzene has been shown to have the opposite behaviour when immobilised in ion-exchange micelles: the protonated form was more stable than the deprotonated form. This was explained by a change in the partition of water between the aqueous bulk and the periphery of the micelle.[26] An example for a dual colorimetric sensor to measure simultaneously pH and temperature is established with the azobenzene derivative Disperse Red 1 in thermoresponsive copolymers.[27,28]

Besides halochromism, MR also shows an intense solvatochromism. An absorption band at ~425 nm dominates the spectrum in polar solvents, while in apolar solvents an absorption band at ~500 nm prevails. The coexistence of the two absorption bands characterises the spectra in dependence of several solvent parameters, such as solvent composition, solvent polarity, hydrogen bonding and Kamlet–Taft-parameters.[29,30]

Two scenarios have been proposed to explain the solvatochromic behaviour of MR.[31,32] In both studies, the change in absorption has been attributed to the change in the ratio of intermolecular hydrogen bonding to solvent molecules *versus* intramolecular hydrogen bonding of the carboxylic acid in *ortho*-position to the azo bridge. The reasoning for the change in absorption wavelength, however, is vastly different in the two publications, as outlined below. The first study[31] assumes solvatochromism to result from a solvent-dependant, intramolecular prototropic equilibrium by relocating a proton between the azobenzene and an azonium form. The azonium ion absorbs at longer wavelengths than the azobenzene, owing to its quinoid character with lower energy of the π^* orbital. The author showed that the dominance of either the azonium or the azobenzene band does not only depend on solvent polarity but on several other solvent parameters, like hydrogen bonding and polarizability. Accordingly, prediction of the spectral features is only reliable withing the same solvent family (hydrogen bond donating or accepting, halogenated aliphatic and aromatic solvents). The second study[32] attributes the solvatochromic shifts solely to the balance between the hydrogen bond accepting parameter β and donating parameter α of the solvent. According to the authors, these parameters dictate whether intermolecular (to the solvent molecules) or intramolecular hydrogen bonding is preferred in MR. The absorption band at ~425 nm is considered here as the $\pi \rightarrow \pi^*$ transition of MR, while the band at ~500 nm is considered to be the $n \rightarrow \pi^*$ transition. Based on the presented calculations, intramolecular hydrogen bonding, which is increased in apolar solvents, spreads the π^* orbital over a larger part of the molecule and lowers its energy. With that, the $n \rightarrow \pi^*$ transition is energetically preferred.

The interpretation of the first study appears more plausible based on the detailed UV-vis absorption behaviour of azobenzenes as discussed in the following.[31] Owing to a quinoid orbital structure, the main absorption band of protonated MR

Open Access Article. Published on 14 January 2022. Downloaded on 1/30/2023 11:32:10 AM.
This article is licensed under a Creative Commons Attribution 3.0 Unported Licence.

lies at longer wavelengths than the absorption band of neutral or anionic MR.[23] Both the azonium ion of MR as well as a strongly intramolecularly hydrogen bonded MR show a strong absorption band around 500 nm. The similarity between the absorption behaviour of the azonium ion of MR compared to the intramolecular hydrogen-bonded MR in certain solvents suggests that an intramolecular hydrogen shift leads to a quinoid character of the zwitterionic molecule, which is accompanied by a redshift. The existence of the long wavelength absorption band of the azonium ion corresponds to the $\pi \rightarrow \pi^*$ and conforms to the general observation that the $\pi \rightarrow \pi^*$ transition is lowered in energy upon protonation of azobenzenes.[33] This is supported by the fact, that MR belongs to the class of pseudostilbenes, in which the $n \rightarrow \pi^*$ and $\pi \rightarrow \pi^*$ transitions are energetically nearly degenerate. Furthermore, the $n \rightarrow \pi^*$ transition is generally weaker in azobenzenes.[34] A large shift in absorption without a considerable decrease of the extinction coefficients involving the non-bonding orbitals is, therefore, unlikely.

Concluding from the various experimental results found in literature, the coexistence of several chromic mechanisms in MR renders this dye a suitable candidate for sensing applications. Yet, a detailed understanding of the mechanistic interplay would be required for effective exploitation, but a comprehensive picture is still lacking. An early application example, which is still in use today, is the determination of acid production by some bacteria during glucose digestion by MR, referred to in microbiology as the Methyl Red test.[35] Immobilisation of the MR probe is preferred for many sensing applications, yet direct contact with a liquid medium is mandatory, which can be provided by the open network structure of swollen polymer gels. As such, polymer matrices based on poly-*N*-isopropylacrylamide (PNiPAAm)[36] and poly-*N*-(2-hydroxyethyl)acrylamide (PHEAm)[37] are interesting candidates in biomedicine, as they are known to be biocompatible and even non-fouling in the case of PHEAm.

PNiPAAm is additionally interesting owing to its lower critical solution temperature (LCST)-type thermoresponsive behaviour in solution. It is soluble at low temperatures and undergoes a volume phase transition when increasing the temperature, leading to insolubility of the macromolecule beyond the transition temperature. This transition temperature can be influenced by copolymerisation and added solutes, like salts or small organic molecules that undergo hydrogen bonding.[38,39] Recently, a new polymerisation method on the basis of reversible activation-deactivation of the surface of Ni–Co alloy nanoparticles has been proposed for the synthesis of poly-methacrylate, which may become an interesting candidate in the near future as well.[40]

These research accounts inspired our present study about the thermochromic behaviour of MR-containing polymer systems. Here, the synthesis of a series of MR-based azobenzene monomers with acrylamide functionalities is reported, from which copolymers were prepared, utilising *N*-(2-hydroxyethyl)acrylamide (HEAm) or *N*-isopropylacrylamide (NiPAAm) monomers and a benzophenone acrylamide (BPAAm) photocrosslinker. By irradiation with UV-light, crosslinked networks were formed from these polymers, yielding hydrogels after swelling with water. For the monomeric and polymeric systems, the thermochromic behaviour was investigated in alcoholic and aqueous media under neutral, slightly acidic, and strongly acidic conditions.

2. Experimentals

2.1. Materials and equipment

All solvents used were of Milli-Q®, spectroscopic, or HPLC-grade. Absolute ethanol was purchased from VWR Chemicals. Tetrahydrofurane was dried and distilled over potassium. Trifluoroacetic acid was purchased from Carl Roth (Germany) in PEPTIPURE® ≥99.9% quality. Sulfuric acid (≥95%, Fisher Chemical), hydrochloric acid (37%, Anal. Reag. Gr., Fisher Chemical), acetic acid (Anal. Reag. Gr., ChemSolute), methyl red (Alfa Aesar), carbonyldiimidazole (97%, Alfa Aesar), *N*-(2-hydroxyethyl)acrylamide (97%, Sigma Aldrich), 4-aminobenzoic acid (Merck) and 3-aminobenzoic acid (98%, Merck) were used as received. 1,8-Diazabicyclo[5.4.0]undec-7-ene was dried over calciumchloride (anhydrous, technical, Bernd Kraft) and distilled *in vacuo*. *N*-Isopropylacrylamide was recrystallised from *n*-hexane. Azobisisobutyronitrile was recrystallised from methanol. 4-Benzophenoneacrylamide was synthesised according to literature.[41] 4-(3-Triethoxysilyl)propoxybenzophenone was synthesised by Mr Daniel John according to literature.[42]

UV-vis measurements were performed on a Thermo Scientific™ Evolution™ 220 UV-Vis-spectrophotometer. If not stated otherwise, the measurements were done with 100 nm min^{-1} and a resolution of 1 nm.

NMR-measurements were performed on either a Bruker AV 400 or a Jeol EZC 500. Detailed assignments of peaks are given in the ESI† in the corresponding spectra.

GPC/SEC was measured on a PSS GRAM linM column (Polymer Standards Service GmbH, Mainz, Germany) in dimethylacetamide with LiBr (0.1 g L^{-1}) at 60 °C with PMMA-standards as reference.

Only selected monomer and polymer syntheses are shown here to illustrate the synthetic process. Full experimental details and NMR-data are given in the ESI.†

Synthesis of methyl red imidazolide. Methyl red (1 mol eq.) was dissolved in tetrahydrofuran (0.1 mmol L^{-1}), carbonyldiimidazole (1.8 mol eq.) was added and the solution was stirred until no more gas evolution occurred, typically overnight or for three hours at 45 °C. The solution was used without purification for further syntheses (adapted from literature[43–45]).

Synthesis of 2-(prop-2-enamido)ethyl-2-[(1*E*)-2-[4-(dimethylamino)phenyl]diazen-1-yl]benzoate (*o*-methyl red ester of *N*-(2-hydroxyethyl)acrylamide, *o*-MREAm). To a solution of methyl red imidazolide in tetrahydrofuran (0.1 mmol L^{-1}), *N*-(2-hydroxyethyl)acrylamide (2 mol eq.) and 1,8-diazabicyclo[5.4.0]undec-7-ene (1.5 mol eq.) were added. The reaction mixture was stirred overnight, before the reaction was stopped by addition of acetic acid. The solvent was removed azeotropically with toluene and the remaining solid extracted with water. The

 This journal is © The Royal Society of Chemistry 2022

Open Access Article. Published on 14 January 2022. Downloaded on 1/30/2023 11:32:10 AM.
This article is licensed under a Creative Commons Attribution 3.0 Unported Licence.

product was purified *via* column chromatography on neutral AlOx in ethyl acetate, followed by column chromatography on silica in diethylether. The yield was 90%.

δH(400 MHz; $CDCl_3$) 7.82 (d, J = 9.3 Hz, 2H; Ph–*H*), 7.74 (dd, J = 7.9, 1.1 Hz, 1H; Ph–*H*), 7.56 (qd, J = 7.9, 1.6 Hz, 2H; Ph–*H*), 7.39 (ddd, J = 7.6, 6.7, 1.9 Hz, 1H; Ph–*H*), 6.72 (d, J = 9.3 Hz, 2H; Ph–*H*), 6.12 (dd, J = 17.0, 1.5 Hz, 1H; CHC*H*H(trans)), 5.85 (s, br, 1H; CON*H*), 5.63 (dd, J = 17.0, 10.4 Hz, 1H; C*H*CHH), 5.43 (dd, J = 10.4, 1.5 Hz, 1H; CHCH*H*(*cis*)), 4.39 (t, J = 5.0 Hz, 2H; COOCH_2), 3.59 (q, J = 5.3 Hz, 2H; CONHCH_2), 3.07 (s, 6H; N(Me)$_2$).

δC(101 MHz; $CDCl_3$) δ 168.61 (COO), 165.49 (CONH), 152.99 (Ph), 152.54 (Ph), 143.54 (Ph), 132.08 (Ph), 130.59 (CO*C*HCH$_2$), 129.70 (Ph), 128.50 (Ph), 127.72 (Ph), 126.36 (COCH*C*H$_2$), 125.35 (Ph), 119.50 (Ph), 111.70 (Ph), 64.35 (COO*C*H$_2$), 40.35 (N(Me)$_2$), 38.79 (CONH*C*H$_2$).

Copolymerisations with *o*-MREAm. The different copolymers were obtained by radical polymerisation. The monomers (0.6 mol L^{-1}) and azobisisobutyronitrile were dissolved in 1,4-dioxane or methanol. The solutions were purged with nitrogen for 30 minutes and heated in an oil bath at 75 °C for 1,4-dioxane or 60 °C for methanol for 24 to 63 hours. The polymers were then precipitated up to three times in a non-solvent. The details are summarised in ESI Table S1.†

P1 (poly(HEAm-*co*-*o*-MREAm-*co*-BPAAm)): δH(500 MHz, MeOD) 8.5–6.5 (br, aromatic H), 4.57 (COOCH_2), 4.38 (Ar–CONHCH_2), 3.66 (CH$_2$CH_2OH), 3.51–3.12 (CONHCH_2), 2.4–1.25 (backbone).

P2 (poly(NiPAAm-*co*-HEAm-*co*-*o*-MREAm-*co*-BPAAm)): δH (500 MHz, D_2O) 8.0–6.5 (br, aromatic H), 4.41 (COOCH_2), 3.91 (NHC*H*(CH$_3$)$_2$), 3.68 (CH$_2$CH_2OH), 3.36 (CONHCH_2), 2.3–1.25 (backbone), 1.16 (NHCH(CH_3)$_2$).

P2b (poly(NiPAAm-*co*-HEAm-*co*-*o*-MREAm-*co*-BPAAm)): δH (400 MHz, MeOD) 8.0–6.75 (br, aromatic H), 4.38 (COOCH_2), 3.96 (NHC*H*(CH$_3$)$_2$), 3.65 (CH$_2$CH_2OH), 3.12 (N(Me)$_2$), 2.3–1.25 (backbone), 1.16 (NHCH(CH_3)$_2$).

P3 (poly(HEAm-*co*-MAA-*co*-*o*-MREAm-*co*-BPAAm)): δH (400 MHz, D_2O) 8.5–6.5 (br, aromatic H), 4.42 (COOCH_2), 3.66 (CH$_2$CH_2OH), 3.34 (CONHCH_2), 2.4–1.25 (backbone), 1.00 (backbone-CH_3).

P4 (poly(NiPAAm-*co*-MAA-*co*-*o*-MREAm-*co*-BPAAm)): δH (500 MHz, MeOD) 8.0–6.5 (br, aromatic H), 4.58 (COOCH_2), 4.38 (Ar–CONHCH_2), 3.91 (NHC*H*(CH$_3$)$_2$), 3.12 (N(Me)$_2$), 2.3–1.25 (backbone), 1.16 (NHCH(CH_3)$_2$).

Film preparation. The glass slides used in photocrosslinking experiments were cleaned with fresh Carothers' acid (sulfuric acid : hydrogen peroxide, 3 : 1) and rinsed thoroughly with water. The slides were dried under a nitrogen stream. They were submerged in an ethanolic solution of benzophenone silane (1 mmol L^{-1}) for 24 hours before they were rinsed thrice with absolute ethanol and finally dried under a nitrogen stream.

Polymers were drop-casted on the glass slides from methanolic solution (1 w%, 200 μL on 2.4 cm × 2.4 cm slides). Photocrosslinking was performed at 302 nm with an energy of 20.3 J cm^{-2}. The polymer films of P1 and P2 were annealed at 170 °C prior to photocrosslinking. All films were washed with water until the supernatant remained colourless before thermochromicity measurements.

3. Results and discussion

The synthesis of the MR-based monomers and polymers is briefly discussed first, followed by the analysis of their thermochromic behaviour. The optical characteristics are described for the individual monomers and then elaborated in relation to the more complex thermochromism of the polymers in the following order:

(i) The dye monomers in simple solvents.
(ii) The dye monomers in binary solvent mixtures.
(iii) Copolymers bearing the dye in solution.
(iv) Photocrosslinked, water–swollen polymer gels.

3.1. Synthesis of methyl red-based monomers and polymers

The monomers in this study were synthesised in a one-pot synthesis in two successive steps by first reacting the parent compound methyl red with carbonyldiimidazole (CDI) and subsequent coupling of the resulting imidazolide with the monomer *N*-(2-hydroxyethyl)acrylamide without intermediate workup (*cf.* Scheme 1). The imidazolide synthesis was based on a previously reported reaction procedure by Staab.[43,45] The subsequent esterification step of the MR imidazolide with an alcohol does not occur spontaneously at room temperature upon mixing, but only after addition of 1,8-diazabicyclo[5.4.0]undec-7-ene (DBU) as strong base. DBU has previously been reported to be an excellent catalyst for the amidation of aromatic acids employing CDI[48] and proved here to be efficient for the esterification with HEAm as well. The yields for the target compounds around 90% were only achieveable upon adding an excess of acetic acid before further purification by extraction with water-dichloromethane. The obtained esters are base labile and extraction with water without prior acidification substantially reduced the yield by hydrolysis. It is worthwhile to note, that synthesis attempts for the target monomers employing either *N*-hydroxysuccinimide (NHS) active esters, acyl chlorides or carbodiimides were not satisfactory. The active ester- and acyl chloride-routes failed to yield any product. The target compound could be synthesised in reasonable yields around 68% when utilising the coupling reagent 1-ethyl-3-(3-dimethylaminopropyl)carbodiimide hydrochloride (EDCI) with 4-dimethylaminopyridine as a catalyst. Yet, the more convenient reaction conditions and higher yields, as well as more affordable coupling reagents rendered the imidazolide route as the preferred procedure. Overall, we established a simple, high-yield synthesis for acrylamide monomers carrying an azobenzene chromophore that is equally applicable to all constitutional isomers of the parent compound MR.

Free radical copolymerisation of the *ortho*-MR monomer with NiPAAm, HEAm, MAA and BPAAm comonomers in solution was successful, while attempts at homopolymerisation of only the *o*-MR monomer failed. The obtained copolymers have

Open Access Article. Published on 14 January 2022. Downloaded on 1/30/2023 11:32:10 AM.
This article is licensed under a Creative Commons Attribution 3.0 Unported Licence.

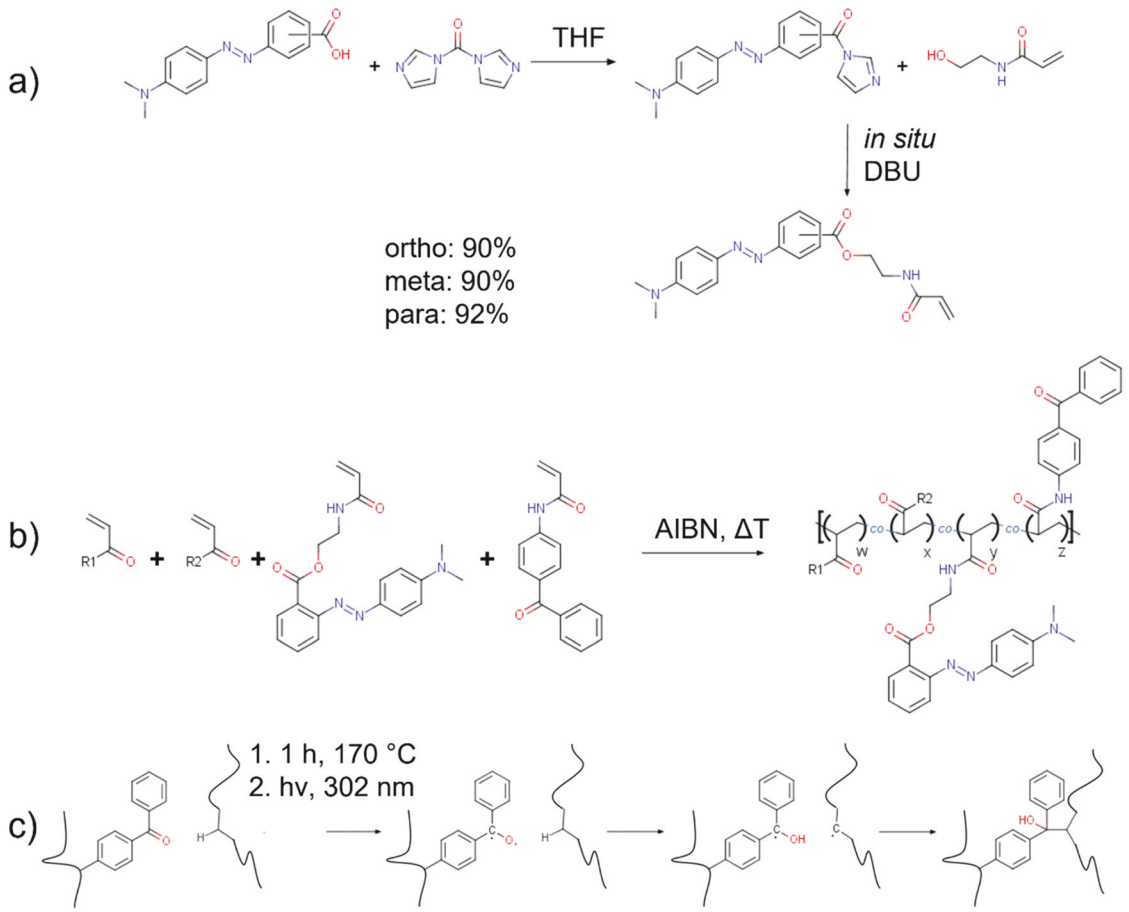

Scheme 1 a) Carbonyldiimidazole-mediated one-pot synthesis yielding the constitutional isomers of the methyl red ester of *N*-(2-hydroxyethyl) acrylamide. (b) Free radical copolymerisation of two generic acrylic monomers, *o*-MREAm and BPAAm. (c) Benzophenone-based photocrosslinking process optimised for the polymers containing an azobenzene chromophore, involving formation of a biradical, hydrogen abstraction, and cross-linking with a second chain.[46,47]

dispersities $Đ > 2$ and only about two thirds of the dye monomer feed were built into the copolymers. With a M_n of 15–22 kDa the copolymers remain rather small as well (*cf.* Table 1). All these observations agree with previous studies about the retardation effect of aromatic azo compounds on free radical polymerisations.[49–53] This effect was attributed to the formation of stable radicals at the azo group, increasing the rate of transfer, and lowering the overall polymerisation rate and degree of polymerisation. Furthermore, the rather high initiator concentration of 2 mol% was used to offset the retardation effects and obtain polymers in reasonable time frames. The high initiator concentration, as well as the retardation effects, increase the dispersity of the copolymers.

The built-in ratio of the photocrosslinker BPAAm, on the other hand, was close to the feed ratio. For the chemical structures provided in the figures, the numbers given after parentheses relate to the nominal feed composition and do not necessarily reflect the built-in ratios.

The preparation of the photocrosslinked gels is discussed further below in the context of their optical characterisation.

Table 1 Copolymer characteristics as determined by UV-vis spectroscopy and GPC. The built-in ratios for *o*-MREAm and BPAAm are given in weight percentages and the percentage of the monomer built-in compared to the feed composition

Polymer	*o*-MREAm [w%]	BPAAm [w%]	M_n [10^3 Da]	M_w [10^3 Da]	$Đ$	Yield [%]
1	4.5 (65%)	1.9 (94%)	17.4	37.7	2.17	79
2	4.9 (63%)	2.0 (91%)	14.9	32.2	2.16	70
2b	5.2 (67%)	2.1 (96%)	22.1	51.9	2.35	81
3	4.8 (63%)	2.0 (95%)	15.5	31.7	2.04	85
4	4.4 (62%)	1.8 (88%)	16.0	51.4	3.21	86

3.2. Proton-induced thermochromism of the constitutional isomers of methyl red derivatives in solution

The major incentive of this section is the elucidation of a structure–property relationship for three dye monomers with respect to the influence of their positional isomerism on thermo-halochromism and vibronic thermochromism. For this purpose, we specifically investigated the three isomers of the methyl red ester derived from *N*-(2-hydroxyethyl)acrylamide (MREAm), that bear the ester linkage in *ortho*-, *meta*- or *para*-

 This journal is © The Royal Society of Chemistry 2022

Open Access Article. Published on 14 January 2022. Downloaded on 1/30/2023 11:32:10 AM.
This article is licensed under a Creative Commons Attribution 3.0 Unported Licence.

position to the azo-bridge. All three derivatives show similar absorption behaviours in the UV-visible range in neat ethanol. The magnitudes of the extinction coefficients follow the order *ortho* < *meta* < *para*. The absorption maxima for *ortho*- and *meta*-derivatives lie almost at the same wavelength, while the maximum is slightly red shifted for the *para*-isomer. These derivatives show only minimal thermochromism in neat ethanol (no acid present). With increasing temperature, the maximum does not shift considerably (~0.5 nm/10 °C), but the absorption bands slightly broaden and their asymmetric shape decreases (*cf.* ESI Fig. S17†).

In ethanolic trifluoroacetic acid at a concentration of 1 v/v%, the different constitutional isomers of MREAm are *partially* protonated (*cf.* Fig. 1). The azonium form is generated upon addition of an acid by protonation of the azobenzene, which acts as the base in the system. With rising temperature, the absorption band of the protonated form, the azonium ion (longer wavelength), diminishes for all isomers. In particular for the *ortho*-isomer, the band corresponding to the neutral azobenzene (shorter wavelength) visibly increases. This thermochromic phenomenon involves deprotonation of the azonium form (the conjugated acid of the azobenzene) upon increasing the temperature. We refer to this process involving a temperature-dependant ionisation/protonation equilibrium as "thermo-halochromism" in relation to previous reports on salt-concentration dependant thermochromism of betaine dyes[54,55] and the IUPAC definition of halochromism.[56] The main absorption band of *p*-MREAm is at 438 nm, with devolving shoulders at around 505 nm and 540 nm upon increasing temperatures. These shoulders correspond to the azonium cation. *m*-MREAm shows a similar behaviour compared to *p*-MREAm, with the main absorption band lying at a shorter wavelength of 417 nm. The attenuating shoulders are localised at 506 nm and 537 nm and the bands of the neutral azobenzene and the azonium are better separated for this isomer. In comparison to the *para*-isomer, the shoulders are overall lower in intensity with respect to the main absorption band. *o*-MREAm has a reversed ratio of the absorption of the protonated species and the neutral species compared to the other isomers. Here, the main absorption band is that of the azonium ion (522 nm) while the absorption band of the neutral species (~425 nm) is about a third in intensity.

Two analysis tools for UV-vis spectroscopy can be employed to elucidate the origin of the small shift of the maximum in neat ethanol and the spectral behaviour upon the changes of the equilibrium between the neutral and the protonated species with temperature variation. Derivative spectroscopy as the first method allows to identify sub-band structures convoluted under an absorption peak by the appearance of negative peaks in the second and fourth derivative at the position of the sub-band maxima.[57] Difference spectroscopy represents the second tool. With this method, spectral differences occurring upon variation of a system parameter are determined by subtracting the UV-vis spectrum of a reference state from all following variants. This has been shown to be effective in determining the vibronic fine-structure in temperature-dependant UV-vis measurements of neat *trans*-azobenzene.[58]

In neat ethanol, a slight change of the absorption band asymmetry at 420 nm for *ortho*, at 419 nm for *meta*, or at 438 nm for *para* with temperature variation can be observed,

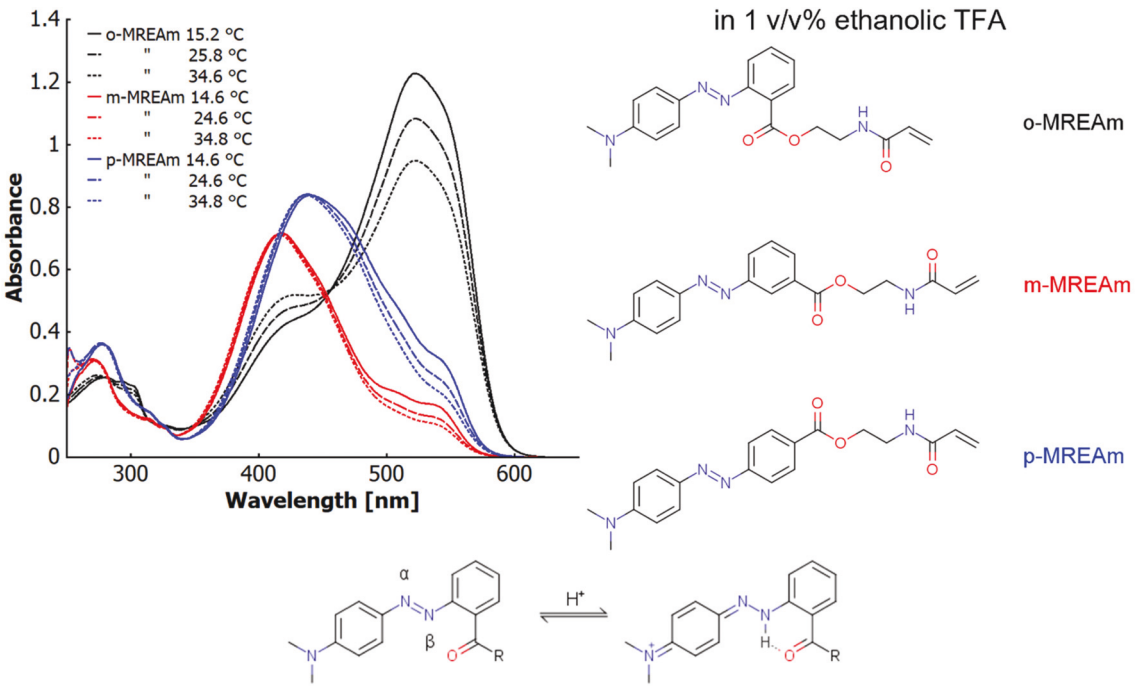

Fig. 1 UV-vis spectra showing thermo-halochromism of *ortho*-, *meta*- and *para*-methyl red ester of *N*-(2-hydroxyethyl)acrylamide (2.7×10^{-5} mol L^{-1}) at different temperatures in ethanolic trifluoroacetic acid (1 v/v%) with a depiction of the underlying azobenzenze–azonium ion equilibrium.

Open Access Article. Published on 14 January 2022. Downloaded on 1/30/2023 11:32:10 AM.
This article is licensed under a Creative Commons Attribution 3.0 Unported Licence.

suggesting an underlying equilibrium of transitions between energetically similar states (*cf.* ESI Fig. S17, S31 and S32†). These transitions are expressed by a sub-band structure, which are convoluted in the observed asymmetric absorption band. The concomitantly observed decrease in absorbance may be ascribed to the temperature-dependant change of the solvent density or in the variation of the population of states with pronounced differences in the extinction coefficients. To analyse this behaviour, the second spectral derivatives were generated for the main UV-vis bands at several temperatures. The wavelengths of the observable minima in these second derivatives are summarised in Table 2. They lie at slighty shorter and longer wavelengths than the convoluted maxima in the parent UV-vis spectra and change in intensity with temperature (*cf.* red arrows and colourful triangles in ESI Fig. S31 and S32†). The energy difference between these sub-bands is around 1590 cm^{-1} (*ortho*) to 1870 cm^{-1} (*meta*). A third sub-band may be concealed by overlap with the second sub-band, being visible only as a shoulder at 400 nm in the derivative spectra.

For the explanation of the sub-band structure, we consider three possibilities:

First possibility: The observed spectroscopic features correspond to a vibronic fine structure. The vibronic fine structure of azobenzenes strongly depends on the substituents of the aromatic rings. It has been shown before that azobenzene and aminoazobenzene dyes have a more pronounced fine structure than pseudostilbenes (push–pull-type azobenzenes). This vibronic structure has also been demonstrated to be temperature-dependant.[59–61] Recently, the temperature-dependence of vibronic transitions has been studied for neat *trans*-azobenzene.[58] For *o*-MREAm in ethanol, the determined energy difference between the two sub-bands is in accordance with a vibronic origin of the spectral features. Specifically, some stretching modes of the aromatic rings as well as the –N=N– stretching mode are found around that particular energy range (*ca.* 1400 cm^{-1}) in the parent compound (MR).[62,63] Even though the energy difference between the sub-bands is higher than the energy of the –N=N– stretching mode, coupling of the involved vibrational modes is likely to influence the observed maximum. This is indicated by significant broadening of the sub-bands and their apparent overlap, which is apparent even in the derivative spectra.

Second possibility: A temperature-induced shift of the equilibrium between several stable rotamers causes the sub-band structure. This effect has been ascribed to the features in the fine structure of the optical absorption of isophthalaldehyde,[64] but also to absorption[65] or fluorescence characteristics of stilbenes[66–68] and to azo compounds.[69]

Third possibility: The thermal peak shift may be associated with a temperature-induced change in the structure of the solvent shell, which has been reported for the related azo dye methyl orange.[70]

Considering previous studies[58,59,61–63] about vibrational and vibronic behaviour of azobenzenes, the first possibility is the most probable explanation. Thus, we attribute these spectral features to vibronic sub-bands.

The spectral changes with temperature are best scrutinised by difference spectroscopy. For this purpose, the spectra at the respective lowest temperature were taken as reference and subtracted from each spectrum at higher temperatures (*cf.* ESI Fig. S32g–i†). The positive bands in the difference spectra result from an increase in absorbance at wavelengths well below the absorption maximum in the parent UV-vis spectra (~400 nm) at higher temperatures, which coincides with the shoulder visible in the derivative spectra (*cf.* ESI Fig. S32d–f†). The negative bands correspond to a decrease in absorbance and vary between the positional isomers. For the *ortho*- and *meta*-isomers, the decrease occurs at wavelengths related to both the 0–0 (vibrational ground state of the electronic ground state S_0 to vibrational ground state of the first excited electronic state S_1) transition as well as the 0–1 transition (vibrational ground state in S_0 to first excited vibrational state in S_1). Owing to the involvement of at least two vibronic sub-bands, this leads to a considerable asymmetric band structure. For the *para*-isomer, on the other hand, the negative band is highly symmetric with its minimum at the wavelength of the 0–0 transition, indicating an absorbance change related to a single vibronic sub-band. This suggests a correlation between the symmetry of the molecule and the vibronic changes with temperature.

Summarising these results, we conclude that the observed thermochromism is of vibronic origin, where vibronic sub-bands of lower energy decrease and those of higher energy increase with higher temperature. We call this phenomenon "vibronic thermochromism".

Besides the vibronic thermochromism of the neutral dyes, as discussed above, thermochromism of the azonium ion must be understood as well to fully embrace the underlying mechanism of the thermo-halochromic behaviour in a *par-*

Table 2 Absorbance maximum at low temperatures (λ_{max}), vibronic sub-bands as determined by derivative spectroscopy ($0–0_{max}$,$0–1_{max}$), energy difference between the sub-bands ($\tilde{\nu}_{01}$) and wavelength shift (λ-shift) of the absorbance maximum with temperature increase from around 10 °C to around 50 °C of neutral *o*-, *m*- and *p*-MREAm in ethanol or binary water–ethanol mixtures (X_{EtOH} = 0.31)

Derivative	Solvent	λ_{max}[nm]	$0–0_{max}$ [nm]	$0–1_{max}$ [nm]	$\tilde{\nu}_{01}$ [cm^{-1}]	λ-shift [nm]
o-MREAm	EtOH	420	450	420	1590	420 → 417
m-MREAm	EtOH	419	451	416	1870	418 → 415
p-MREAm	EtOH	437	470	434	1760	437 → 435
o-MREAm	H_2O : EtOH	441	460	420	2070	441 → 430
m-MREAm	H_2O : EtOH	449	462	417	2340	449 → 432
p-MREAm	H_2O : EtOH	470	483	438	2130	470 → 461

 This journal is © The Royal Society of Chemistry 2022

Open Access Article. Published on 14 January 2022. Downloaded on 1/30/2023 11:32:10 AM.
This article is licensed under a Creative Commons Attribution 3.0 Unported Licence.

tially protonated system. Compared to the neutral isomers of the MREAm dye, the corresponding azonium ions show a red-shifted absorption band at 510–520 nm (*cf.* ESI Fig. S33a–c†). In the case of 4-aminoazobenzene-derived dyes, protonation primarily occurs at the β-nitrogen of the azo-bridge (*cf.* Fig. 1 and ESI Scheme S1†). The resulting azonium ion has a partial quinoid structure, lowering the energy of the electronic transition. However, alternatively protonation may occur at the amino substituent, forming an ammonium ion, which absorbs at ~320 nm. For the parent compound *ortho*-methyl red, the tautomeric equilibrium between the ammonium and the azonium form lies on the side of the azonium ion owing to intramolecular hydrogen bonding to the carbonyl in *ortho*-position.[71–75] The same can be observed for the MR-monomers discussed here, where the effect is particularly pronounced for the *ortho*-isomer (*cf.* ESI Fig. S33a–c†). The maxima of the main absorption band of the azonium ions of all positional isomers of MREAm at 510–520 nm do not shift with temperature. However, the fine structure of these bands, which is more apparent than for the neutral dyes, changes characteristically. Especially in the *meta*- and the *para*-isomers, sub-bands are clearly visible in the unprocessed absorption spectra (*cf.* ESI Fig. S33a–c†).

The derivative and difference spectra of the azonium ions in ethanolic solution can be analysed in the same way as the neutral dye above (Table 3). This detailed analysis can be found in the ESI (ESI below Fig. S33†).

The temperature-dependant protonation equilibrium between the azonium ion and the neutral dye were also analysed with derivative and difference spectroscopy. As stated above, the fundamental process is a shift of the equilibrium towards the neutral dye with increasing temperature (*cf.* ESI Fig. S34a–c†). This trend is visible both in the derivative spectra (*cf.* ESI Fig. S34d–f†) and difference spectra (*cf.* ESI Fig. S34g–i†) as follows. In dependence of their initial degree of protonation, the shape of the positive and negative peaks in the difference spectra vary between the positional isomers. For the *ortho*-isomer, the negative bands in the difference spectra resemble the shape of the absorption band of the azonium ion, just with the opposite sign (*cf.* ESI Fig. S33a and S34g†). The position of the positive band coincides with the one of the main absorption band of the neutral species (*cf.* ESI Fig. S32a and S34g†). On the other hand, the samples of the initially less protonated *meta*- and *para*-isomers exhibit spectral features of thermo-halochromism and additionally of vibronic thermochromism from the neutral population. The negative band in the difference spectra appears like a combination of the negative bands in vibronic thermochromism (*cf.* ESI Fig. S32h and i†) with the absorption band of the corresponding azonium ions of opposite sign (*cf.* ESI Fig. S33b and c and S34h and i†). We assume that the positive bands are related to the vibronic thermochromism found for the neutral species (*cf.* ESI Fig. S32h and i†). The appearance of overlapping features is mainly a consequence of vibronic thermochromism acting simultaneously to thermo-halochromism resulting from the shift of the protonation equilibrium, which affect the absorption spectra with similar magnitudes under the conditions of weak protonation. In the case of the *ortho*-isomer, thermo-halochromism is prevalent, overshadowing vibronic effects.

It is worthwhile to mention that the difference spectra of the *partially* protonated *meta*- and *para*-isomers in ethanolic TFA show more pronounced vibronic features in the negative peaks than would be expected from a simple subtraction of the azonium ion spectra (*cf.* ESI Fig. S34h and i†). This suggests a vibronic contribution to thermo-halochromism.

3.3. Relationship of pK_a and thermochromicity in MR monomers

To determine a possible correlation between pK_a and thermochromicity (meaning the quantification of the extent of thermochromism[76]), the different constitutional isomers of the MR derivative were titrated in H_2O : EtOH (X_{EtOH} = 0.31) with 5 M HCl in H_2O : EtOH (X_{EtOH} = 0.31) (*cf.* Fig. 2). Water/ethanol mixtures were chosen as solvent because the solubility in pure water was too low for UV-vis measurements, and according to literature, the pK_a values of azo dyes do not change severely with different percentages of ethanol.[77]

All three isomers show similar spectral changes upon titration. In the neutral state, they have an absorption maximum at around 450 nm and with lower pH values, shoulders evolve around 515 nm, which eventually result in distinct absorption bands. In all three cases, the extinction coefficients are higher for the azonium ion than for the neutral forms, following the order *meta* < *para* < *ortho*. In contrast, the red shifts of the absorption maxima are in the order *para* < *meta* < *ortho*. Therefore, at similar degrees of protonation the visible change in colour is strongest for the *ortho*-isomer (*cf.* Fig. 2a, c and e,

Table 3 Absorbance maximum at low temperatures (λ_{max}) and vibronic sub-bands ($0–0_{max}$, $0–1_{max}$, $0–2_{max}$) as determined by derivative spectroscopy, as well as the energy difference between the sub-bands ($\tilde{\nu}_{01}$, $\tilde{\nu}_{12}$) of the protonated *o*-, *m*- and *p*-MREAm in ethanolic sulfuric acid (1 v/v%) or binary water–ethanol mixtures (X_{EtOH} = 0.31) with hydrochloric acid (5 M)

Derivative	Solvent	λ_{max} [nm]	$0–0_{max}$ [nm]	$0–1_{max}$ [nm]	$0–2_{max}$ [nm]	$\tilde{\nu}_{01}$ [cm^{-1}]	$\tilde{\nu}_{12}$ [cm^{-1}]
o-MREAm	EtOH	519	549	513	482	1280	1250
m-MREAm	EtOH	511	544	508	477	1300	1280
p-MREAm	EtOH	516	548	511	480	1320	1260
o-MREAm	H_2O : EtOH	522	553	516	485	1300	1240
m-MREAm	H_2O : EtOH	511	543	508	477	1270	1280
p-MREAm	H_2O : EtOH	514	546	510	479	1290	1270

Open Access Article. Published on 14 January 2022. Downloaded on 1/30/2023 11:32:10 AM.
This article is licensed under a Creative Commons Attribution 3.0 Unported Licence.

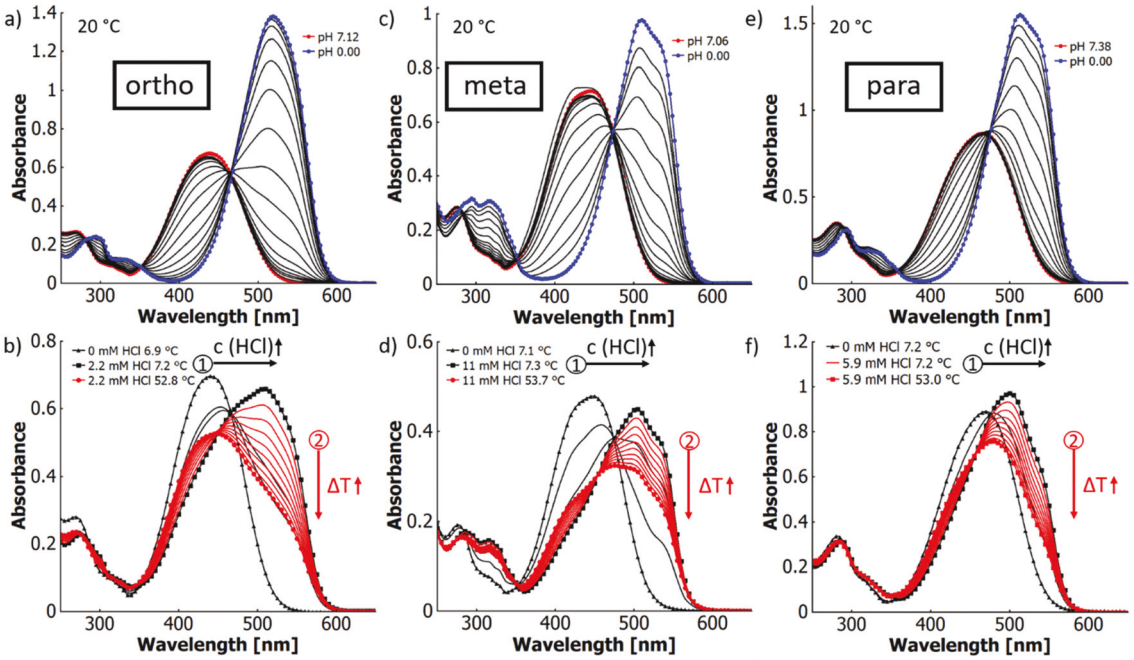

Fig. 2 UV-vis spectra in H_2O : EtOH (X_{EtOH} = 0.31) at different pH values at 20 °C for (a) *o*-MREAm, (c) *m*-MREAm and (e) *p*-MREAm (all 2.7 × 10^{-5} mol L^{-1}); and the spectra after titration (black arrow 1) with hydrochloric acid at ~6–7 °C to ~50% protonation at different temperatures (red arrow 2) for (b) *o*-MREAm, (d) *m*-MREAm and (f) *p*-MREAm (all 2.7 × 10^{-5} mol L^{-1}). The black curves in (b), (d) and (e) are spectra of intermediate titration steps to emphasise the isosbestic points.

Table 4). The pK_a values of the configurational isomers of MREAm in H_2O : EtOH (X_{EtOH} = 0.31) can be determined from the spectral changes upon titration (*ortho*-isomer: pK_a 2.24, *para*-isomer: 1.83, *meta*-isomer: 1.54; *cf.* ESI Fig. S18† and Table 4). This trend can be explained by two factors: firstly, the mesomeric stabilisation of the azonium cation is higher for the *para*- and the *ortho*-than for the *meta*-isomer. Secondly, the *ortho*-isomer has the additional option for intramolecular hydrogen bonding of the β-protonated azo bridge with the carbonyl oxygen, further stabilising the cation as observed for the parent MR.[73] The same tendency can be found for the pK_a values previously reported in the parent isomers in water (*cf.* ESI Table S2†).[23,24,78,79] In the *ortho*-isomer (ΔpK_a 0.14), the difference between the parent compound and the derivative is small and may be explained with the change in solvent. This difference, however, increases with the acidity of the isomer (*para*: ΔpK_a 0.25; *meta*: ΔpK_a 0.45). This suggests that intramolecular hydrogen bonding is the dominating influence that stabilises the *ortho*-azonium ion, while mesomeric and inductive effects lower the pK_a changing from the free acid (MR) to an ester (MREAm).

In Fig. 2(b), (d) and (f), the dyes were first titrated (black arrow 1) at low temperatures (6–7 °C) to a degree of 50% protonation followed by a successive temperature increase (red arrow 2) in order to observe maximal thermochromic variations. We refer to this process as "thermotitration". Under these conditions, all isomers of MREAm show similar thermochromic behaviour. The decrease in absorbance of the protonated species upon heating is in the same order of magnitude. With increasing temperatures, the absorption bands around 515 nm decrease in intensity while those around 450 nm increase, leading to an overall blueshift (*cf.* Fig. 2b, d and f).

To determine the correlation between thermochromicity and pK_a, the thermochromicity must be quantified. For this purpose, van't Hoff analysis was chosen. Fig. 4(d) shows for the *ortho*-isomer the van't Hoff plot of the natural logarithm of the absorbances ratio of the azonium ion and the neutral azobenzene *R versus* the inverse of the absolute temperature. The

Table 4 Compilation of pK_a-values, extinction coefficients, and absorption maxima for the neutral and protonated forms of the different MREAm isomers, measured in H_2O : EtOH (X_{EtOH} = 0.31) acified with HCl

Isomer	pK_a	ε(dye) [L mol^{-1} cm^{-1}]	ε(H^+dye) [L mol^{-1} cm^{-1}]	ε(H^+dye)/ε(dye)	λ_{max}(dye) [nm]	λ_{max}(H^+dye) [nm]	Δλ_{max} [nm]
ortho	2.2	24 600	50 600	2.06	438	519	81
meta	1.6	26 300	35 900	1.37	445	510	65
para	1.8	31 800	56 800	1.79	467	513	46

This journal is © The Royal Society of Chemistry 2022

Open Access Article. Published on 14 January 2022. Downloaded on 1/30/2023 11:32:10 AM.
This article is licensed under a Creative Commons Attribution 3.0 Unported Licence.

specifically selected absorbance wavelengths were chosen to avoid a large spectral overlap.

While van't Hoff plots of $\ln K$ *vs.* T^{-1} usually provide a linear relationship, the plots in the present examples are non-linear, suggesting a significant temperature dependence of the reaction enthalpy. In order to account for this non-linearity, the plots were fitted by eqn (1) according to previously reported procedures for protein titrations and complexation studies.[80,81]

$$\ln\left(\frac{R}{R_0}\right) = \frac{\Delta H_0 - T_0\Delta C_p}{R}\left(\frac{1}{T_0} - \frac{1}{T}\right) + \frac{\Delta C_p}{R}\ln\left(\frac{T}{T_0}\right) \quad (1)$$

A simplified representation of this equation introduces the parameters "*a*", "*b*" and "*c*" as follows: $\ln(R) = a - b \times 1/T + c \times \ln(T)$. These fit parameters together with the extracted values for ΔH_0 and ΔC_p are summarised in Table 7 and will be discussed in further detail after introducing all systems. The enthalpy ΔH_0 may be used as a measure of the extent of protonation (and in turn deprotonation) at 25 °C. It also tells whether the process is endothermic or exothermic. The heat capacity of ionisation ΔC_p quantifies how temperature-dependant the enthalpy is. This provides information about whether deprotonation becomes more favourable or disfavourable with increasing temperatures. Both values may be considered as thermochromicity parameters.

Plotting ΔH_0 and ΔC_p for the different consitutional isomers *vs.* their pK_a shows an almost linear correlation with both thermochromicity parameters (*cf.* ESI Fig. S19†). As direct consequences, both the magnitude of the thermochromic effects as well as the pH, at which they can be observed, depend on the pK_a.

3.4. Variants of thermochromism for the MREAm monomers in binary solvent mixtures

In order to analyse the individual thermochromic mechanisms that contribute to the overall optical behaviour, we investigate the effect of the different permutations for the combination of ethanol, water, and acid as constituents for the liquid medium. Isosbestic points can be observed in UV-vis absorption spectra when titrating the MREAm monomers in water–ethanol mixtures with hydrochloric acid, which shifts the azobenzene protonation equilibrium between the neutral dye (around 455 nm) and the azonium cation (around 515 nm). At ~20 °C these isosbestic points (*cf.* Fig. 2a, c and e) are at the same wavelength as those found for thermotitration (following the black arrow 1 in Fig. 2b, d and f) at low temperature (6–7 °C) when *partially* titrating to 50% protonation. Surprisingly, when raising the temperature from 6–7 °C to above 50 °C for the *partially* protonated sample in the binary solvent mixture, no isosbestic point is visible. Instead, the intersections of the corresponding absorption spectra continuously blueshift, which is particularly pronounced at lower temperatures *(cf.* Table 5).

Table 5 Isosbestic points in titrations at different temperatures and regions of intersections upon temperature change for the different MREAm isomers in H_2O : EtOH (X_{EtOH} = 0.31) acidified with HCl, and for *o*-MREAm in ethanol acidified with TFA

Isomer	Isosbestic point ΔpH 19.8 °C [nm]	Isosbestic point ΔpH 6–7 °C [nm]	Regions of intersections [nm]
ortho	465	465	455–434
meta	474	475	457–440
para	474	476	463–448

Since chemical equilibria are established between the free proton, the azobenzene and the azonium ion upon titration as well as during temperature variation, isosbestic points would be expected for both cases. Apparently, a fundamental difference must exist between the proton concentration-influenced and temperature-controlled equilibria to cause the blueshift. To elucidate this phenomenon, we separately expatiate on the individual mechanisms of thermochromism that coexist for the dye in acidified water–ethanol-mixtures. For this purpose, the following three scenarios are contrasted with each other: (1) vibronic thermochromism (neat ethanol), (2) thermo-halochromism (one solvent with added acid) and (3) thermo-solvatochromism (binary solvent mixture without acid). The additional fourth scenario (4) combines the case of a binary solvent mixture with that of added acid. It will be discussed with respect to the findings of the first three scenarios.

In the first scenario (1) of neat ethanolic solution, the azobenzene monomers show only minimal thermochromism (*cf.* Fig. 3a). This phenomenon has been discussed above and involves changes in the sub-band structure that is likely of vibronic origin. Thus, we call it vibronic thermochromism.

The second scenario (2) of the monomer in a single solvent with added acid (here ethanol with trifluoroacetic acid, *cf.* Fig. 3b) has already been discussed above. As no appreciable wavelength shift of the maxima with temperature is observed for neither the protonated species (522 nm) nor the neutral species (419 nm), a pure protonation equilibrium is more likely than a change in the quality of solvation.

The third scenario (3) is the monomer in the binary solvent system (H_2O : EtOH, X_{EtOH} = 0.31) without addition of acid (*cf.* Fig. 3c). In this case, a blueshift from 441 nm to 431 nm can be observed over a temperature range of 46 K (7.5–53.5 °C). With higher temperatures, the spectra shift towards that of the dye in neat ethanol (*cf.* Fig. 3a and c). This effect may be attributed to a temperature-dependant change of the solvent–dye interactions at different rates for the two solvents. Such behaviour was first described for betaine– and other zwitterionic dyes in binary water–organic solvent mixtures and has been termed "thermosolvatochromism".[82–86] In contrast to the present MR systems, the literature suggests for the zwitterionic structures with large dipole moments a quicker change of the balance between hydrogen bonding and hydrophobic interactions for various alcohols than for water, leading to a depletion of the alcohol in the solvation complex.[84] The inverse behaviour in our case apparently results from the less polar MR dye being more

Open Access Article. Published on 14 January 2022. Downloaded on 1/30/2023 11:32:10 AM.
This article is licensed under a Creative Commons Attribution 3.0 Unported Licence.

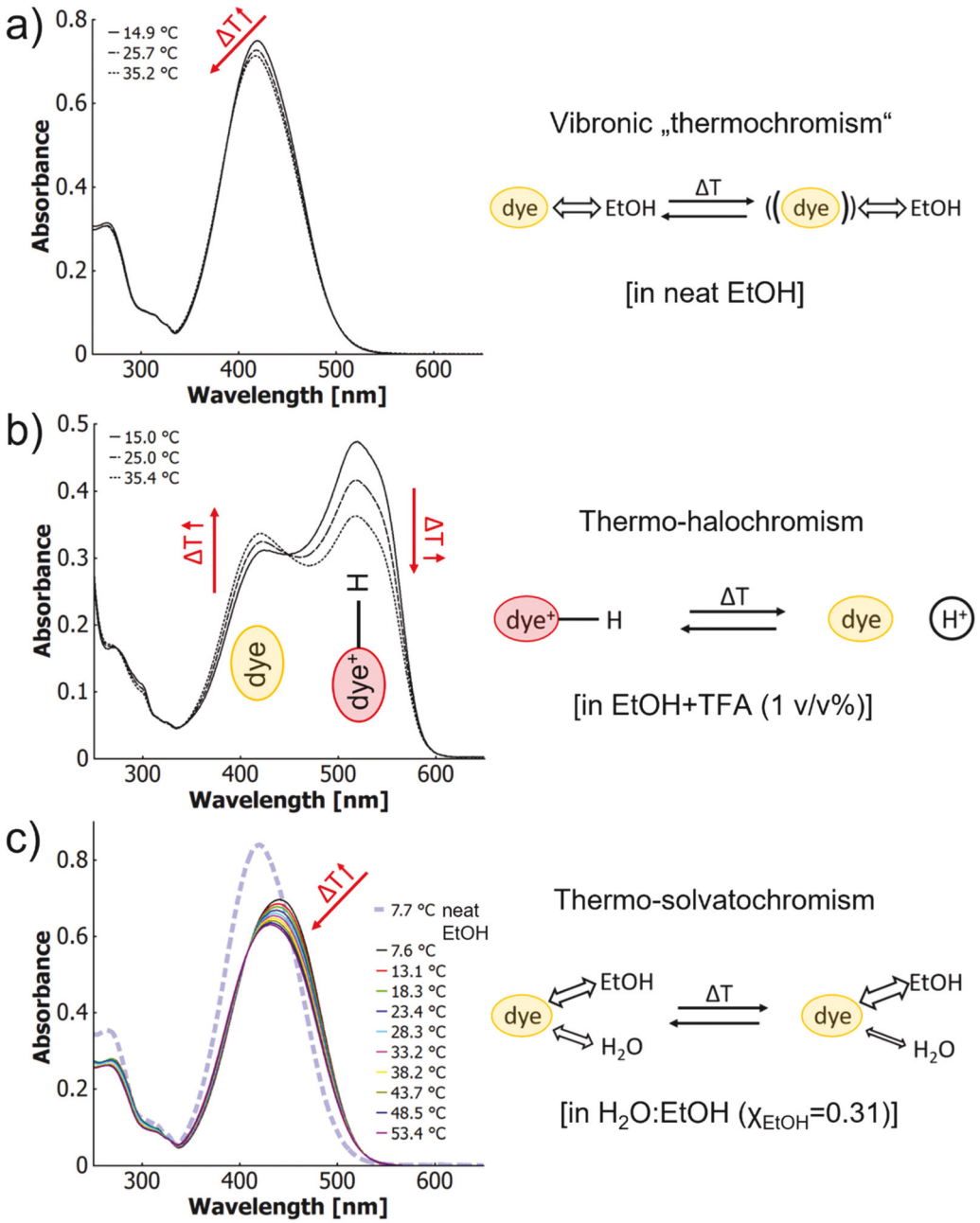

Fig. 3 UV-vis spectra of *o*-MREAm (2.7×10^{-5} mol L^{-1}) at different temperatures with cartoons showing the corresponding thermochromic processes involving (a) vibronic thermochromism in neat ethanol; (b) thermo-halochromism in ethanolic trifluoroacetic acid (1 v/v%); and (c) thermo-solvatochromism in H_2O : EtOH (X_{EtOH} = 0.31).

soluble in ethanol, while being practically insoluble in water. Thus, as the interactions of both solvents change with temperature and water being a non-solvent, the net result will be dominated by the good solvent ethanol. The temperature-induced change in solvent composition in the solvation shell also affects the vibronic characteristics of the dye and as such thermo-solvatochromism resembles features of vibronic thermochromism (1) for the neutral MR dye (*cf.* ESI Fig. S32 and S35†).

Detailed analysis was performed with derivative and difference spectroscopy to show the exact differences between vibronic thermochromism and thermo-solvatochromism. Interestingly, the thermochromic properties of the azonium ion are not affected by the particular solvent systems in contrast to the neutral azo dye. The detailed analysis can be found in the ESI (below Fig. S35†).

In the fourth scenario (4) a more complex behaviour occurs for the binary solvent mixture water–ethanol (X_{EtOH} = 0.31) when adding free acid, for which the results are shown in Fig. 4(a). Upon heating, the maximum of the azonium ion at around 510 nm gradually decreases, while the absorption

 This journal is © The Royal Society of Chemistry 2022

Open Access Article. Published on 14 January 2022. Downloaded on 1/30/2023 11:32:10 AM.
This article is licensed under a Creative Commons Attribution 3.0 Unported Licence.

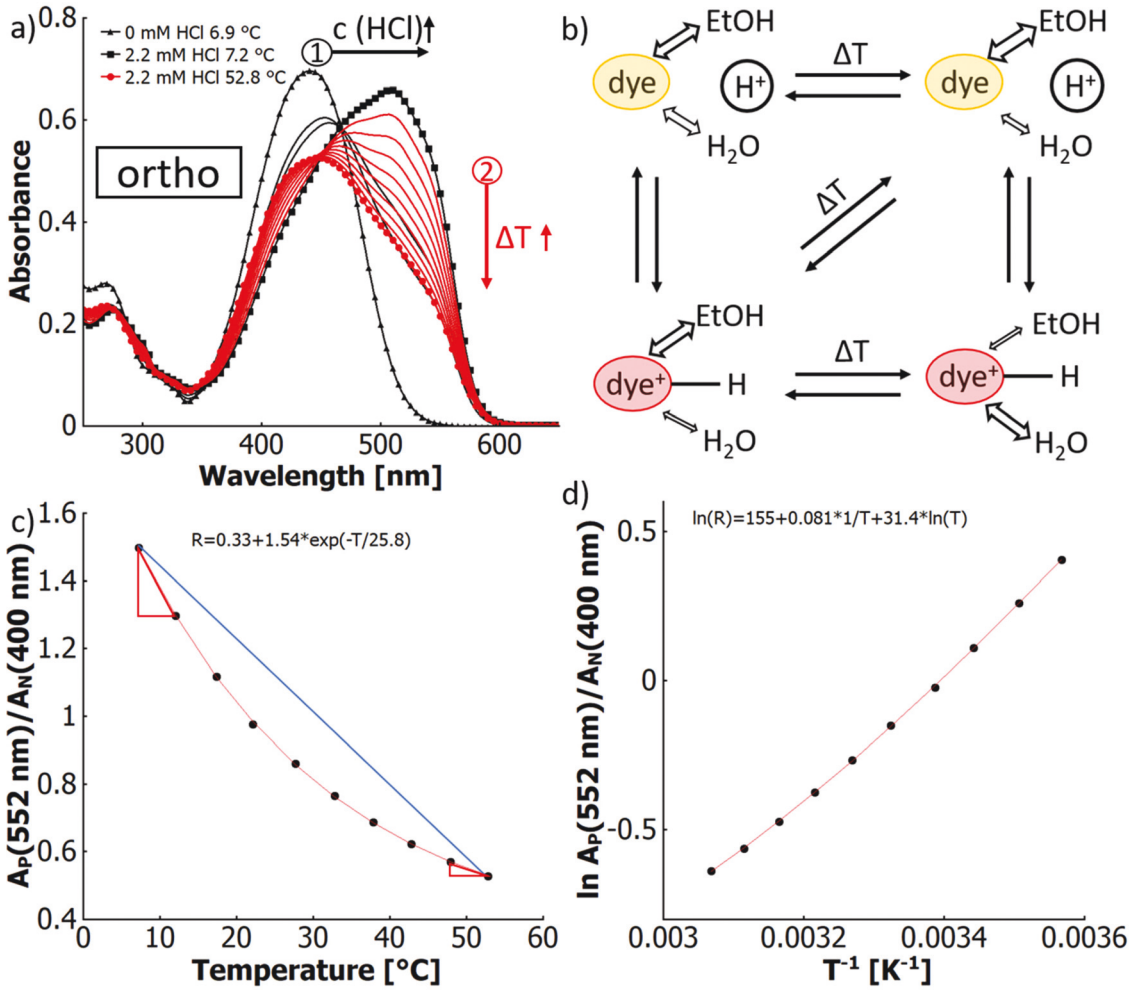

Fig. 4 (a) UV-vis spectra demonstrating thermo-solvato-halochromism of *o*-MREAm (2.7×10^{-5} mol L^{-1}) in H_2O : EtOH (X_{EtOH} = 0.31) after titration (black arrow 1) with hydrochloric acid at ~6–7 °C to ~50% protonation at different temperatures (red arrow 2) with; (b) cartoon of competing processes; (c) ratio of the absorption of the protonated species (552 nm) and the neutral species (400 nm) ("*R*" in the equation) *vs*. temperature, fitted with a first order exponential decay function. The blue line along with the red slope triangles serve as a reference to emphasise the non-linearity of the graphs; (d) natural logarithm of the ratio of the absorption of the protonated species (552 nm) and the neutral species (400 nm) *vs*. the inverse of the absolute temperature, fitted with a function $\ln(R) = a - b \times 1/T + c \times \ln(T)$.

band corresponding to the neutral species around 450 nm increases in intensity. However, no isosbestic point is observed, but rather a region of intersecting spectra, which shift to shorter wavelengths. In the ratiometric approach shown in Fig. 4(c), the ratio of the absorbance of the azonium ion and the neutral azobenzene *R versus* temperature is characterised by a non-linear (exponential) decrease. This characteristic signifies a temperature dependence of the protonation equilibrium between the azonium form and the neutral form. The equilibrium shifts at different rates for different temperatures. In essence, more of the azonium ion is deprotonated per temperature increment at lower temperatures, as indicated by the red slope triangles.

To explain this behaviour mechanistically, the coexisting species and their equilibria in the system must be analysed separately and then harmonised. Owing to the presence of free acid, two species exist: the neutral azobenzene and the positively charged azonium ion. Each species has its distinct interaction with the binary solvent mixture. In the binary solvent mixture, the protonation equilibrium follows the same trend as in a single solvent with added acid (*cf.* Fig. 3b). With rising temperature, the protonation equilibrium shifts towards the neutral azobenzene.

However, the thermally dependant equilibrium of the water–ethanol composition in the solvent shell of each dye species gains a new aspect. The blueshift indicative for the negative thermo-solvatochromism of the neutral species has been described previously in the third scenario (*cf.* Fig. 3c), with the effective influence of the solvent shell resembling that of neat ethanol at higher temperatures. In contrast, the polar azonium ion does not show any significant thermochromism neither in ethanol with sulfuric acid nor water with HCl nor in the binary mixture of water and ethanol with HCl (*cf.* ESI Fig. S20†). The effective influence of the solvation shell and its

Open Access Article. Published on 14 January 2022. Downloaded on 1/30/2023 11:32:10 AM.
This article is licensed under a Creative Commons Attribution 3.0 Unported Licence.

stabilisation of the ground and excited states does not change. On the other hand, the ethanol–water ratio in the solvation shell does most likely change, as has been described in the literature for zwitterionic dyes.[84] This effect may be explained by the fact that both water and ethanol are good solvents for the azonium ion.

The thermal equilibrium between all solvated species is reflected in the combined emergence of thermo-solvatochromism and thermo-halochromism. This equilibrium and the competing processes guiding their interconversion are schematically depicted in Fig. 4(b). The temperature effects on both the protonation equilibrium as well as on the composition of the solvation shell of the *neutral azobenzene* can be followed by changes of spectral features. However, for the *azonium ion* no spectroscopic signature is observed for a conceivable temperature effect on the solvation shell, since in this case water and ethanol are both good solvents. Yet, as with increasing temperature water dominates the interactions in the solvation shell for the binary solvent mixture,[84] the solvated and less polar azobenzene is destabilised in relation to the more polar azonium ion. Consequently, the two species have a different proton affinity in dependence of their solvation shell composition, which in turn is differently affected by temperature. This means that also the shift of the protonation equilibrium within a given temperature interval is differently affected at low compared to high temperatures. Thus, at higher temperatures, the protonated species (azonium ion) shows a lower incremental concentration decrease by the halochromic pathway, which is characterised by the exponential dependence in the non-linear reduction of its absorbance in Fig. 4(c).

Additionally, the difference in the extent of thermo-solvatochromism between the neutral and the protonated species results in the region of intersections of absorption curves for different temperatures instead of an expected isosbestic point, as visible in Fig. 4(a). An isosbestic point could be observed if at least two absorbing species have an equal absorbance upon variation of a system parameter like temperature.[87–90] Yet, in our present system, the absorbing species is not simply represented by only an isolated molecular framework of the dye, but the chromophore being strongly influenced in its conformation and electronic structure by its solvation shell in dependence of the temperature. This fact is expressed by the observed thermo-solvatochromism. Consequently, the protonation equilibrium does not simply comprise two static absorbing species, which would result in only thermo-halochromism, but the equilibrium exists between the azobenzene with a temperature-variable solvation shell and the azonium ion, whose absorption is temperature invariant. We define the here witnessed, combined effects of thermo-solvatochromism and thermo-halochromism as *thermo-solvato-halochromism*, which leads to the above-mentioned continuous shift of the curve intersections with the absence of an isosbestic point.

As a further consequence, the graphs of A(protonated)/A(neutral) *vs*. temperature in Fig. 4c and ESI Fig. S42† are non-linear insofar that the shift of the protonation equilibrium becomes smaller with increasing temperatures. Consequently, the magnitude of thermochromism is reduced and we refer to this process as *diminishing* thermo-solvato-halochromism.

The difference spectra from the thermotitrations in ESI Fig. S37g–i† indicate distinct reaction pathways that establish the protonation/deprotonation equilibrium in dependence of either the proton concentration or temperature. Such spectra exhibit a significantly different vibronic structure for several proton concentrations compared to those resulting from temperature variation. This suggests that a change in the molecular gestalt, defined here as the conformation of the dye and the structure of its solvent shell, is differently influenced by titration or temperature variation.

In essence, the results above corroborate the existence of three different mechanisms of thermochromism of methyl red (MR)-based azobenzene monomers in solution. The first and simplest thermochromism on the basis of vibronic transitions was identified *via* derivative and difference spectroscopy (*cf.* Fig. 3a and ESI Fig. S31†). The second mechanism is thermo-halochromism. Solutions of *partially* protonated MR-monomers (*e.g.*, in ethanolic trifluoroacetic acid) show a temperature-dependant equilibrium between the neutral azobenzene and the ionic azonium species. The equilibrium shifts towards the neutral species at elevated temperatures (*cf.* Fig. 3b). The third mechanism is thermo-solvatochromism in binary solvent mixtures like H_2O : EtOH (X_{EtOH} = 0.31). Here, the spectra shift towards that in pure ethanol at higher temperatures (*cf.* Fig. 3c).

The obtained data suggest that these mechanisms do coexist and influence each other in binary solvent mixtures containing free acid. Under these conditions, thermo-solvatochromism affects substantially the extent of thermo-halochromism. In other words, the extent of deprotonation upon heating is different at low and at high temperatures (*cf.* Fig. 4). As such and stated above, this process may be best described by the term *thermo-solvato-halochromism*.

3.5. Thermochromism of methyl red-containing copolymers in solution

When transitioning from the individual dye monomer to a macromolecular architecture, the polymer chain provides a further contribution to the microenvironment of the polymer-bound dye in addition to the solvent, which is reflected in the concept of *thermo-perichromism*. The particular effects resulting from this transition will be elaborated for different polymer systems in the following. Various copolymers were prepared from the MR-based monomers by free radical polymerisation. By proper choice of the comonomers a thermoresponsive behaviour can be imparted and with this an associated polarity change upon temperature variation. Furthermore, copolymerisation of carboxylic acid-containing comonomers provide the possibility of an intrinsic proton source.

As a reference, the first system (P1) comprises a *non-thermoresponsive*, *acid-free copolymer* made from the azo-chromophore *o*-MREAm, the hydrophilic main monomer HEAm, and the photocrosslinker benzophenone acrylamide (BPAAm). HEAm

 This journal is © The Royal Society of Chemistry 2022

Open Access Article. Published on 14 January 2022. Downloaded on 1/30/2023 11:32:10 AM.
This article is licensed under a Creative Commons Attribution 3.0 Unported Licence.

imparts a polar character to the copolymer, and thus the polymer facilitates dissolution of the attached hydrophobic dye in water. BPAAm is a versatile photocrosslinker that forms covalent bonds between the polymer chains *via* C,H-insertion upon UV irradiation.[46,91] In the second copolymer system (P2), NiPAAm was copolymerised together with HEAm, *o*-MREAm and BPAAm to introduce *thermoresponsive solution behaviour*. In the third polymer (P3), *carboxylic acid functions* were introduced into the HEAm-based P1 system by copolymerisation with methacrylic acid (MAA). For the fourth system (P4), *o*-MREAm, NiPAAm, BPAAm, and MAA were copolymerised, yielding an *intrinsically acidic*, *thermoresponsive polymer*.

The thermochromism of all copolymers P1–P4 was investigated in aqueous and in ethanolic solution. Furthermore, all four copolymers were also studied after transformation into hydrogels by photocrosslinking and swelling with water. In the following, the four different copolymers are discussed in order of increasing complexity: (P1) non-thermoresponsive without intrinsic acid moieties; (P2) thermoresponsive without intrinsic acid moieties; (P3) non-thermoresponsive with intrinsic acid moieties and (P4) thermoresponsive with intrinsic acid moieties.

The description will be provided in two parts. First, the thermochromic behaviour of the polymers will be described phenomenologically for each polymer before the systems are quantified *via* van't Hoff analysis and compared to each other.

Copolymer P1: no intrinsic acid, no thermoresponsive behaviour. For the simplest, non-thermoresponsive copolymer system P1 without acid moieties, thermochromism shows a similar dependency on solvents as the free monomer. The macromolecule acts like a local solvent and influences the spectral changes with temperature. To illustrate this behaviour, the thermochromic behaviour was first studied in neat ethanol and in pure water. While the hydrophobic MR-monomer itself is not soluble in water, indeed the polar copolymer P1 with the integrated dye is well soluble. Apparently, the polymer provides a microenvironment analogous to ethanol and acts as a solubilizer for the hydrophobic dye.

The P1 solutions both in ethanol and in water show a thermochromic effect visible as a blueshift in Fig. 5 with temperature increase. In ethanol, the wavelength of the maximum shifts from 423 nm at 7.5 °C to 420 nm at 48.5 °C (*cf.* Fig. 5a). The behaviour of the copolymer and the free dye are essentially identical under these conditions. In aqueous solution, the maximum blue-shifts from 454 nm at 7.4 °C to 448 nm at 48.7 °C (*cf.* Fig. 5b). This observation is reminiscent of thermosolvatochromism in the binary solvent mixture. However, the more general term *thermo-perichromism* should be used here, as perichromism describes a colour shift related to a change in the local molecular environment (here, the macromolecular structure behaves analogously to a solvent molecule interacting with the dye).[92]

By addition of TFA as acid to solutions of P1, which does not contain any intrinsic acid-moieties in the polymer backbone, thermo-halochromism can be induced. This was demonstrated by partial protonation leading to the coexistence of neutral dye and azonium ion (*cf.* Fig. 6). The general behaviour is similar to the isolated dye monomer discussed above (*cf.* Fig. 3 and 4). The absorbance related to the azonium ion decreases and the one of the neutral azobenzene correspondingly increases with higher temperatures. While an analogous trend is observed for ethanol and for water, the details of thermochromism vary considerably between the two solvents.

In ethanol with added acid (TFA), the absorption bands of the neutral species at ~423 nm and the protonated species at ~525 nm are well separated (*cf.* Fig. 6a), which facilitates calculation of the peak ratios (*cf.* ESI Fig. S43†). The occurrence of an isosbestic point at 452 nm instead of a region of intersections suggests that the influence of the thermo-perichromic mechanism on the thermo-halochromic mechanism is negligible in ethanolic solution. Under these conditions of partial protonation, the wavelength maximum of the absorption band of the azonium ion does not shift appreciably upon temperature variation. Also, the polymer-bound, pure azonium ion present in ethanolic sulfuric acid does not show a wavelength shift upon temperature increase (*cf.* ESI Fig. S24a†), yet the measurement is affected by a stronger scattering background because of reduced solubility.

In aqueous solutions of the same polymer P1 with added acid (TFA) the overlap between the absorption bands of the neutral dye at ~453 nm and the protonated species at ~500 nm is high, which leads to only a shoulder in the main absorption band (*cf.* Fig. 6b). Similar to the spectral behaviour of the parent dye monomer in binary solvent mixtures of water and ethanol (*cf.* Fig. 4), a region of intersections exists instead of an isosbestic point. The intersections of the curves between adjacent temperature steps gradually blue-shift from 452 nm at the lowest temperatures (6.2 °C) to 443 nm at the highest temperatures (52.6 °C, *cf.* Fig. 6b and ESI Fig. S44†). The existence of the region of intersections for the dye monomer was attributed to the mutual influence of thermo-solvatochromism and thermo-halochromism, with the former being only observable for the neutral azobenzene and not the azonium ion.

Interestingly, the *completely* protonated dye monomer (azonium ion) shows no thermo-solvatochromism, while the same azonium unit incorporated into the polymer is characertised by a change in absorption upon temperature variation. The wavelength maximum for the *completely* protonated polymer P1 in aqueous HCl red shifts from 500 nm at 7.8 °C to 507 nm at 59.4 °C, while the absorbance of the shoulder at around 530 nm increases slightly (*cf.* Fig. S25a†). Furthermore, the P1 absorption maximum is considerably blue-shifted compared to the one of the dye monomer at around 520 nm in different solvent systems (*cf.* Table 6). With the redshift upon heating, the spectroscopic features of the polymer approach those of the parent dye monomer. This significant difference in thermochromic behaviour must result from specific interactions between the polymer-bound azonium ion and the macromolecular framework. In particular, the hydrophilic OH– and amide side groups in the polymer can form polar and hydrogen bonding interactions while the (CH_2–CHR) backbone provides a hydrophobic character.

Open Access Article. Published on 14 January 2022. Downloaded on 1/30/2023 11:32:10 AM.
This article is licensed under a Creative Commons Attribution 3.0 Unported Licence.

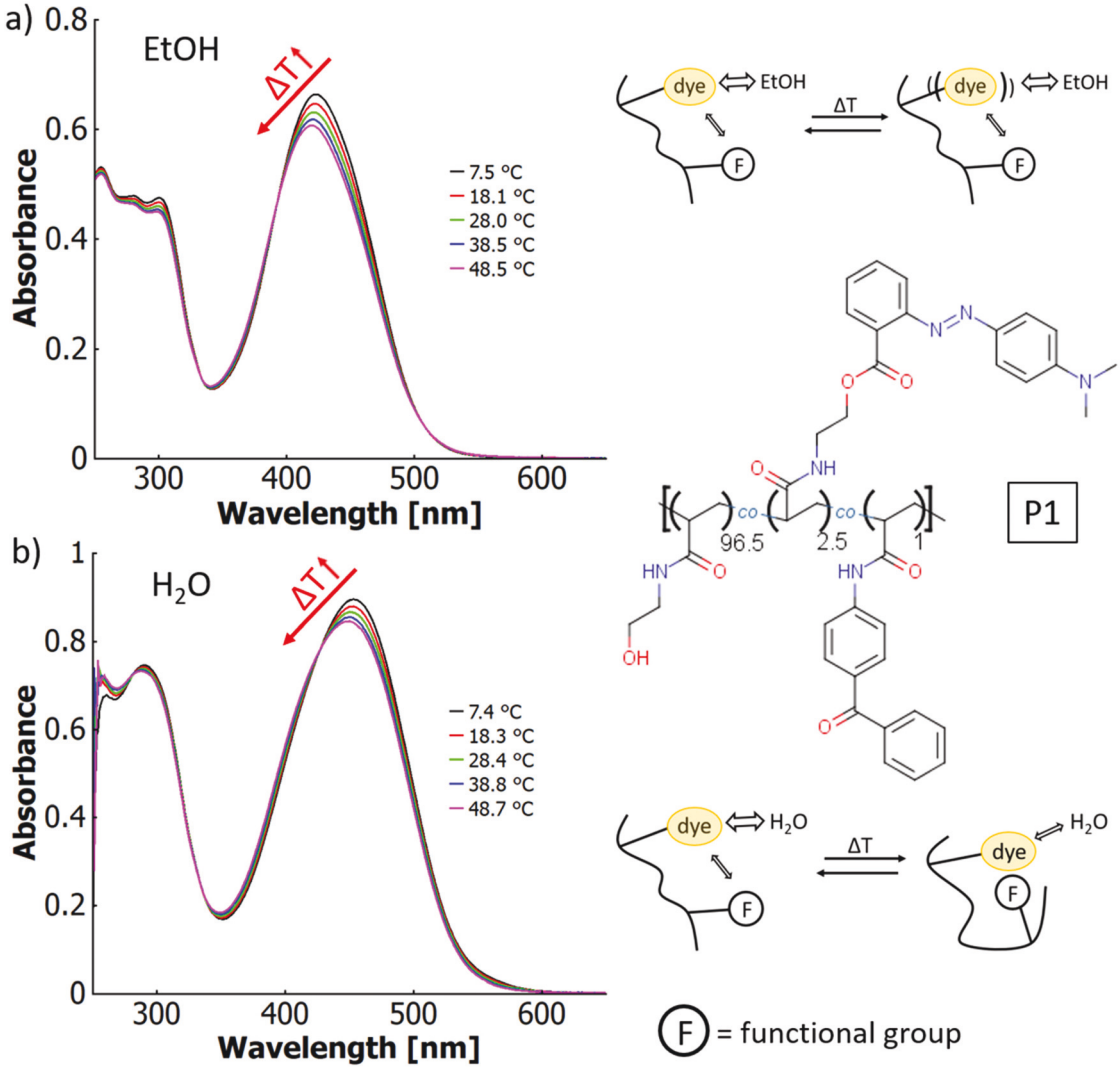

Fig. 5 UV-vis spectra of a poly(HEAm-*co*-*o*-MREAm-*co*-BPAAm) copolymer P1 at different temperatures (a) in neat ethanol (0.02 w% polymer) and (b) in pure water (0.03 w% polymer), with the chemical structure of the copolymer and thermo-perichromic mechanism sketched on the right side.

This difference is also signified in derivative spectroscopy, where the monomer shows three vibronic sub-bands in all solvents, while the polymer only shows two vibronic sub-bands (*cf.* ESI Fig. S39†). The balance of the individual contributions from the water–dye, water–macromolecule and dye–macromolecule interactions is affected by temperature and with this the associated thermochromic mechanisms. Apparently, the solvation of the dye substituent by water increases at higher temperatures.

The similarity between thermo-solvatochromic and thermo-perichromic behaviour can be revealed with derivative spectroscopy. In ethanolic solution, the second derivative of P1 evolves similarly to that of the dye monomer, with both sub-bands decreasing uniformly (*cf.* ESI Fig. S32d and S38c†). In aqueous solution, the 0–0 sub-band of the copolymer shows a stronger decrease compared to the other sub-bands, as in the case of the dye monomer in the binary solvent mixture (*cf.* ESI Fig. S35d and S38d†).

Copolymers P2 and P2b: no intrinsic acid, thermoresponsive behaviour. When combining thermoresponsiveness in polymers, as expressed by a lower critical solution temperature (LCST), with the particular optical features of thermochromism, the experiments discussed below indicate that the thermoresponsive behaviour dictates the magnitude and temperature range of thermochromism. For this purpose, the same measurement conditions used for the characterisation of the non-thermoresponsive polymer system P1 were applied to the thermoresponsive polymer system P2 without intrinsic acid moieties. The thermochromic behaviour of P2 was studied either in water and in ethanol or with acid added to induce thermo-halochromism. As a reminder, the thermoresponsiveness (specifically, the LCST behaviour) of this particular polymer is only present in aqueous solutions and is not observed in ethanol.

In ethanol, the temperature-induced changes in the absorption spectra are virtually the same for the polymer systems P1

 This journal is © The Royal Society of Chemistry 2022

Open Access Article. Published on 14 January 2022. Downloaded on 1/30/2023 11:32:10 AM.
This article is licensed under a Creative Commons Attribution 3.0 Unported Licence.

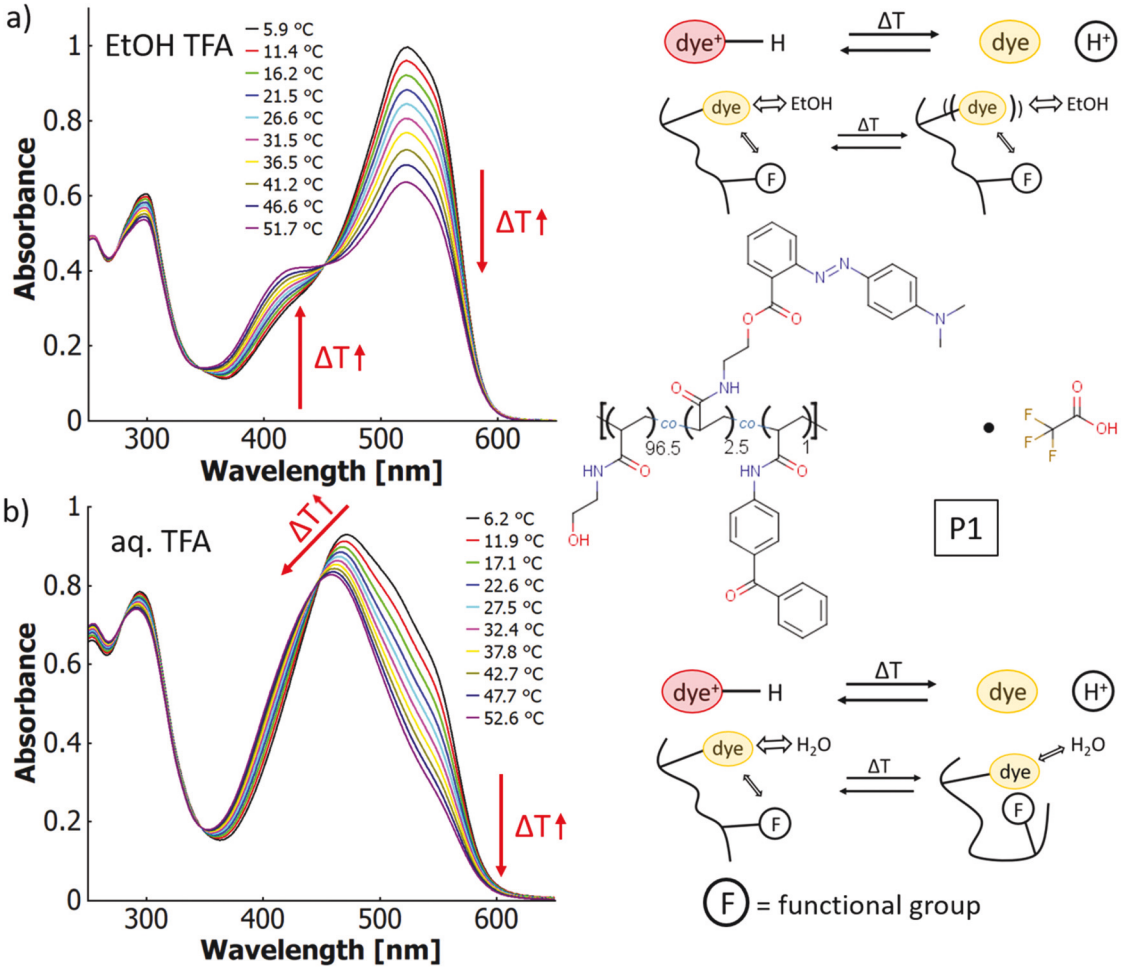

Fig. 6 UV-vis spectra of a poly(HEAm-*co*-*o*-MREAm-*co*-BPAAm) copolymer P1 at different temperatures (a) 0.02 w% in ethanolic trifluoroacetic acid (1 v/v%) and (b) 0.03 w% in aqueous trifluoroacetic acid (0.001 v/v%), with the chemical structure of the copolymer and thermo-*peri*-halochromic mechanism sketched on the right side.

Table 6 Absorption maxima of the monomer *o*-MREAm and copolymers containing *o*-MREAm for different measurement conditions (solvent, protonation state) at low temperatures (7–10 °C) below the cloud point

	Neutral aq.	Neutral EtOH	Neutral binary mixture	Azonium aq.	Azonium EtOH	Azonium binary mixture
o-MREAm	—	420 nm	441 nm	522 nm	519 nm	519 nm
P1	453 nm	423 nm	—	500 nm	520 nm	—
P2	452 nm	422 nm	—	499 nm	518 nm	—
P3	—	422 nm	—	501 nm	520 nm	—
P4	—	421 nm	—	501 nm	517 nm	—

and P2 both for the neutral and the *partially* protonated form. Thus, the same arguments as discussed above apply here (*cf.* ESI Fig. S43, S23 and S45†). Yet, the behaviour of the *completely* protonated polymer in ethanolic sulfuric acid deviates slightly between P1 and P2 (*cf.* ESI Fig. S24†). Under these conditions, polymer system P2 has a higher solubility than polymer system P1 and thus shows no scattering effects (opposed to the inverse wavelength dependence of the baseline in P1 due to scattering, *cf.* ESI Fig. S24a and b†). Upon increasing the temperature of the P2 solution, the absorption maximum slightly red-shifts from 517 nm at 5.7 °C to 520 nm at 44.8 °C.

In aqueous solutions, the thermochromic behaviour of P1 and P2 differs considerably. For P2 and without the addition of acid, the wavelength of the absorption maximum blue-shifts from 450 nm at 7.0 °C to 443 nm at 53.4 °C. However, the absolute value of absorbance at the peak maximum decreases until ~43 °C to then sharply increase again upon further heating (*cf.* Fig. 7a and c). This can be explained by the LCST phase transition of the P2 copolymer in aqueous solution.

Open Access Article. Published on 14 January 2022. Downloaded on 1/30/2023 11:32:10 AM.
This article is licensed under a Creative Commons Attribution 3.0 Unported Licence.

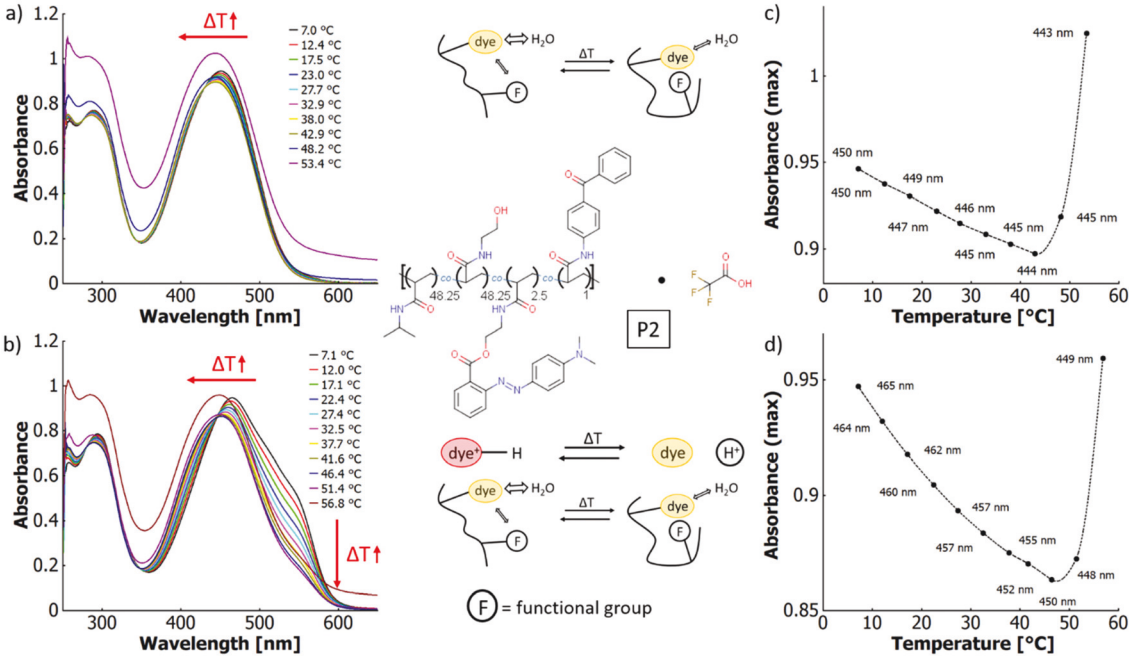

Fig. 7 UV-vis spectra of a poly(NiPAAm-*co*-HEAm-*co*-*o*-MREAm-*co*-BPAAm) copolymer (P2) 0.03 w% in (a) pure water, and (b) aqueous trifluoroacetic acid (0.001 v/v%) at different temperatures (direction of shifts in absorbance upon heating marked with red arrows); absorbance at maximum (wavelength indicated in graph) *vs*. temperature for (c) pure water and (d) aqueous trifluoroacetic acid (0.001 v/v%). The lines are generated by a non-rounded Akima interpolation and only serve as guide to the eye. The structure of the copolymer (acid optional) and cartoons of the ongoing thermochromic processes are shown in the middle section.

When the macromolecule passes the coil-to-globule transition, the system starts to scatter, which increases the overall absorbance. As large agglomerates are absent at these low mass concentrations of the polymer,[93] the absorbance increase can be attributed to stronger Rayleigh scattering (λ^{-4} dependence) due to the change of refractive index between coil and globule.[94] When adding acid to these aqueous P2 solutions, thermo-halochromism is induced. Because of the large spectral overlap between the neutral azobenzene and the azonium ion in aqueous solutions, the presence of the azonium ion is reflected by a shoulder of the main absorption band at around 550 nm. The absorbance decreases over a large temperature range (7.1 °C to 51.4 °C) before scattering effects dominate, leading to an overall absorbance increase again (*cf.* Fig. 7 and ESI Fig. S46a and b†). In comparison to the non-protonated P2, the absorption maximum of the *partially* protonated polymer shifts more strongly to shorter wavelengths upon heating (465 nm at 7.1 °C to 449 nm at 56.8 °C). Owing to the large spectral overlap, this blueshift occurs when the azonium ion content decreases by the thermo-halochromic pathway. The absorbance at maximum shows the same general behaviour as the neutral polymer, since it decreases until the phase transition temperature, to then drastically increase again by scattering upon the coil-to-globule transition. Yet, the associated minimum occurs at higher temperatures in the *partially* protonated case (~48–49 °C) compared to the neutral case.

According to the literature, the cloud point of neat polyNiPAAm homopolymer solutions is constant or decrease with lower pH values and higher anion concentrations.[95,96] Therefore, addition of trifluoroacetic acid should not influence the phase transition significantly. Thus, the observed disparate behaviour of the neutral and the *partially* protonated P2 copolymer is attributed to the charge effect of the azonium ion. As a direct consequence, the protonation equilibrium of thermo-halochromism affects the LCST behaviour since the cloud point temperature depends on the residual azonium content, which directly accounts for the charge of the polymer and with this its degree of hydrophilicity. The more hydrophilic the polymer, the higher the transition temperature.[97,98]

With the thermoresponsive transition, the polarity of the polymer changes and with this the interaction with the dye. Consequently, the thermo-perichromism is directly affected by the thermoresponsiveness. To investigate this effect in further detail, a more hydrophobic copolymer P2b with the same constitutents but a reduced HEAm content was studied in aqueous solutions. For this copolymer P2b without added acid, the minimum in the graph of the absorbance maximum *vs*. temperature lies at around 21 °C (*cf.* ESI Fig. S22b†), which is about 20 K lower than that of the more hydrophilic P2. This trend follows the decrease of the cloud point temperature being affected by a reduction in hydrophilicity. At the same time, the absorption maxima shift from 447 nm at 7.7 °C to 436 nm at 28.0 °C (*cf.* ESI Fig. S22†). Here, the blueshift of the wavelength ($\Delta\lambda$ = −11 nm) for P2b in the temperature interval of ΔT = 20 K is larger compared to copolymer P2 (ΔT = 46 K, $\Delta\lambda$ = −7 nm).

This journal is © The Royal Society of Chemistry 2022

Open Access Article. Published on 14 January 2022. Downloaded on 1/30/2023 11:32:10 AM.
This article is licensed under a Creative Commons Attribution 3.0 Unported Licence.

These data clearly support the hypothesis that the thermo-perichromic shift directly depends on the thermoresponse. The range of the wavelength shift is related to the difference in hydrophobicity of the microenvironment of the dye below and above the coil-to-globule transition. This difference is larger in more hydrophobic polymers that show a lower cloud point temperature, as in these systems the polarity change between the hydrophilic coil and the hydrophobic globule is expected to be larger.

When acid (TFA, 0.13 mM) is added to the P2b solution, thermo-halochromism dominates the temperature-dependant spectral changes in analogy to P2 and P1. At the same acid concentration, the degree of protonation at low temperatures is roughly the same for both copolymers P2 and P2b. Yet, the temperature dependence of the protonation equilibrium is different for the two copolymers. The lowest degree of protonation is reached around the minimum in the graph of the absorbance maximum *vs.* temperature, which we associate with the coil-to-globule transition (*cf.* Fig. 7b and ESI Fig. S22b†). Apparently, the temperature influence on the protonation equilibrium levels off around the cloud point and the corresponding coil-to-globule transition. Inside the collapsed globule, the water content is reduced and hydrophobic interactions dominate.[98,99] As the neutral species partitions into the hydrophobic regions, it is depleted from the protonation equilibrium with the azonium ion in the aqueous phase. Consequently, the concentration of the azonium ion, which favours a polar environment, decreases. Therefore, the characteristic LCST behaviour for a given polymer determines the temperature range of thermo-halochromism.

These measurements suggest that apart from the rather abrupt cloud point transition during the LCST-type collapse, the polymer polarity changes gradually with temperature. This gradual change is signified by the following two observations. Firstly, the steady decrease in concentration of the azonium species with increasing temperature for *partial* protonation in acidic solutions, and secondly, by the gradual blueshift of the main absorption band upon heating in acid-free aqueous solutions (*cf.* Fig. 7 and ESI Fig. S22†). This continuous transition has been shown in the literature for other PNiPAAm-based systems with several methods, *e.g.*, EPR (electron paramagnetic resonance spectroscopy),[99] AFM (atomic force microscopy),[100] and fluorescence/NRET (non-radiative energy transfer).[101]

Copolymer P3: intrinsic acid and without thermoresponsiveness. The thermochromic behaviour of the copolymer systems P3 (non-thermoresponsive) and P4 (thermoresponsive) with intrinsic acid moieties (integrated MAA comonomer) in the main chain was studied in pure water. In ethanol, the acid strength and concentration was insufficient to protonate the azobenzene moiety (*cf.* ESI Fig. S23c and d†). The non-thermoresponsive copolymer P3 in pure water shows the same thermochromic features as P1 in aqueous solution with added acid (TFA) (*cf.* Fig. 6b and 8a). Upon temperature increase, the wavelength maximum gradually blue-shifts from 460 nm at 7.5 °C to 455 nm at 32.7 °C and its absorbance decreases linearly with temperature. At the same time, the absorbance of the shoulder (~550 nm) corresponding to the azonium ion decreases as well (*cf.* Fig. 8a and c). Again, no isosbestic point, but a continuous shift of intersections between the spectra of adjacent temperature steps is found. The intersections shift spans a region from 442 nm at the lowest temperature (7.5 °C) to 438 nm at the highest temperature (32.7 °C). This behaviour can be explained by the interplay of thermo-perichromism and thermo-halochromism, as discussed above for P1 in aqueous solution with added acid.

Copolymers P4: intrinsic acid, thermoresponsive behaviour. The thermochromic behaviour of the thermoresponsive copolymer P4 with intrinsic acid in aqueous solution is similar to that of the thermoresponsive copolymer P2b with a low LCST in aqueous solution with added acid (*cf.* ESI Fig. S22b† and Fig. 8b), which is in contrast to the characteristics of non-thermoresponsive P3 with intrinsic acid. For P4, the wavelength of the maximum shifts from 458 nm at 2.4 °C (455 nm at 7.6 °C) to 442 nm at 23.3 °C. At the same time, the absorbance maximum decreases nearly linearly to around 18 °C and then increases again upon heating (*cf.* Fig. 8d). This can be attributed to scattering effects of the collapsed macromolecules at higher temperatures, as in the case of P2 and P2b. Under these conditions, the absorbance of the shoulder at around 550 nm (azonium ion) decreases, like in all other examples of *partially* protonated polymers shown before.

Compared to the non-thermoresponsive system P3, the thermoresponsive copolymer P4 shows a stronger decrease in absorbance per temperature increment (*cf.* Fig. 8a and b). Apparently, the LCST transition in P4 augments both the thermo-perichromic and thermo-halochromic effect. Upon thermal collapse, the macromolecule provides a more hydrophobic environment in which the neutral dye is preferentially accommodated over the charged azonium ion. Consequently, the protonation equilibrium shifts towards the neutral dye, as described above for P2 and P2b. Since the cloud point depends on the polymer concentration, thermochromism of P4 was measured at different concentrations. Upon decreasing the polymer fraction below the concentration at the LCST point, the cloud point, respectively the coil-to-globule transition temperature increases.[102,103] Accordingly, with lower polymer concentration the position of the minimum in the absorbance-maximum-*vs.*-temperature plot shifts to higher temperatures (*cf.* ESI Fig. S26a–f†), which we associate with a shift of the coil-to-globule transition. In the globular state the hydrophobicity of the polymer increases substantially, modifying the interactions with the dye and therefore serving as a measure for thermo-perichromism as well.

To understand whether polymer concentration affects the thermo-halochromism, the evolution of two features upon temperature variation can be considered. First, the change in the degree of protonation can be determined by the ratio of absorbance at 552 nm (azonium ion) and at 420 nm (neutral dye), referred to as *ratiometric approach*. Second, the relative variation in azonium ion content per temperature interval can be determined *via* the change in absorbance at 552 nm. For this purpose, the band is normalised by dividing the absor-

Open Access Article. Published on 14 January 2022. Downloaded on 1/30/2023 11:32:10 AM.
This article is licensed under a Creative Commons Attribution 3.0 Unported Licence.

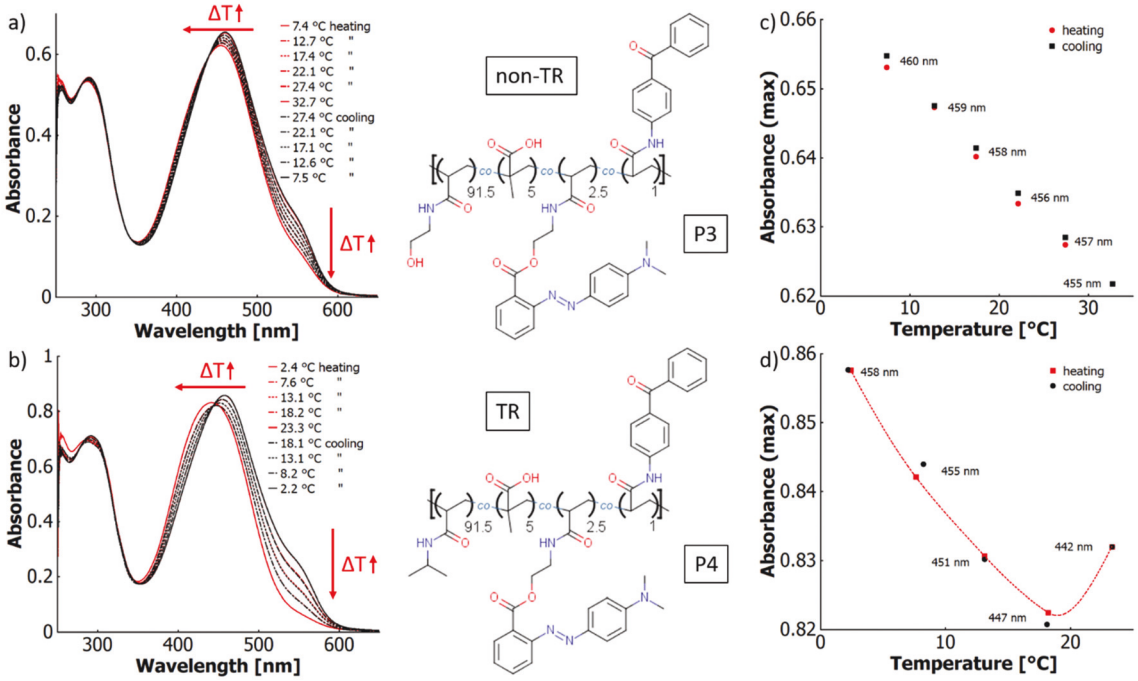

Fig. 8 UV-vis spectra in water at different temperatures of (a) poly(HEAm-*co*-MAA-*co*-*o*-MREAm-*co*-BPAAm) (P3, 0.02 w%) and (b) poly(NiPAAm-*co*-MAA-*co*-*o*-MREAm-*co*-BPAAm) (P4, 0.03 w%); absorbance at maximum (wavelength indicated in plot) *versus* temperature of (c) P3 and (d) P4 ("TR" = thermoresponsive). The lines are generated by a non-rounded Akima interpolation and only serve as guide to the eye. The structures of the copolymers are displayed in the middle section.

bance at each temperature by the absorbance at the lowest temperature, termed *normalisation approach*. These parameters were determined for three concentrations (0.15 g L^{-1}, 0.2 g L^{-1} and 0.3 g L^{-1}; *cf.* ESI Fig. S26g–i†). There are at least five components in the acid–base equilibrium of this system comprising the neutral dye, the azonium ion, methacrylic acid, its anion and H_3O^+ as a proton shuttle (ignoring low concentrations of OH^- from self-dissociation of water). The equilibrium between these components depends on temperature and on polymer concentration, with higher concentrations leading to higher degrees of protonation. At all concentrations, the degree of protonation decreases with increasing temperatures and the plots of the ratio of absorbances *vs.* temperature converge around the coil-to-globule transition (*cf.* ESI Fig. S26g†). Simultaneously, the normalised absorbances overlap and decrease linearly up to 20 °C to then level off at around 25 °C (*cf.* ESI Fig. S26e†), indicating almost complete conversion of the azonium ion into the azobenzene.

It follows, that the ratiometric approach shows a dependence of thermochromism on polymer concentration, while the normalisation approach is independent of polymer concentration. The seeming discrepancy between these approaches may be explained by the effects of both the thermo-perichromic and the thermoresponsive behaviour of the copolymer P4. To rationalise this apparent discrepancy, the position of the reference wavelengths, at which the ratiometric approach is performed, as well as the respective protonation state of the chromophore in the spectrum of a *partially* protonated copolymer in water must be discussed (*cf.* ESI Fig. S27†). The spectra of P4 result from a combination of the absorption of the neutral azobenzene and the azonium ion with considerable overlap of the absorption bands. This overlap leads to an apparent redshift of the maximum in the *partially* protonated case compared to the neutral copolymer. On the other hand, the pronounced shoulder at long wavelengths in these spectra results from the absorption of the azonium ion with only minor contributions of the neutral species. The wavelength selected for the normalisation approach is located in this shoulder. Even though minor contributions of the neutral species do change the absorbance here, these changes are small, and we assume that they are caused by density fluctuations. Therefore, the variations are, relative for both species, independent of the concentration. As the absorption of both the neutral and the protonated species is barely affected by temperature changes at this long wavelength (*cf.* ESI Fig. S27†), thermo-perichromism plays apparently a negligible role.

Accordingly, the decrease in normalised absorbance at 552 nm upon temperature increase for the *partially* protonated case (*cf.* ESI Fig. S26h†) is solely caused by thermo-halochromism, and consequently unaffected by concentration. On the other hand, the azonium ion has a low absorbance at the shorter wavelength of 420 nm and is almost unaffected by temperature variation. Thus, the observed thermal effect is attributed to thermo-perichromism in consequence of the thermoresponse of the polymer in solution, which primarily

 This journal is © The Royal Society of Chemistry 2022

Open Access Article. Published on 14 January 2022. Downloaded on 1/30/2023 11:32:10 AM.
This article is licensed under a Creative Commons Attribution 3.0 Unported Licence.

affects the absorbance of the neutral species (*cf.* Fig. S26i†). Since the thermoresponse is concentration-dependent, the ratiometric approach must be concentration-dependant as well.

Notably, the concentration dependence of the absorbance ratio between 552 nm and 420 nm (*i.e.*, the slopes in the curves of ESI Fig. S26g†) is smaller for higher concentrations than for lower concentrations. This trend follows the variation of the cloud point at low volume fractions in the phase diagramme of LCST-type polymers in solution before the critical point. In this phase diagramme, the slope increases with decreasing polymer concentration.

Based on the observations above, the thermochromic behaviour of the thermoresponsive P4 with intrinsic acid moieties can be explained by the interplay of two mechanisms: thermo-halochromism and thermo-perichromism. Thermo-halochromism reflects the temperature-dependant protonation equilibrium between the azobenzene and the azonium ion and is polymer concentration independant. Thermo-perichromism is a consequence of the modulation of the immediate environment of the dye that varies with temperature. This effect is enhanced by the LCST-behaviour of the copolymer, which steadily decreases its polarity upon heating towards the phase transition. As the polymer phase transition is concentration-dependant, the thermo-perichromic effect is as well.

In their concerted action, thermo-perichromism strongly affects thermo-halochromism *via* the thermoresponsiveness of the polymer. Thus, upon the induced polarity shift in the microenvironment of the dye, the susceptibility for protonation is greatly altered. As a consequence, thermo-halochromism is strongly enhanced below the cloud point and vanishes above it, as the neutral dye is protected from protonation by the collapsed polymer.

3.6. Thermochromism in photocrosslinked films of methyl red copolymers

Gel preparation. Both the non-thermoresponsive copolymers P1 and P3, and the thermoresponsive systems P2 and P4 were photocrosslinked at 302 nm (20.3 J cm^{-2}) *via* their benzophenone side groups. This wavelength was chosen to match the optical window with low absorption of the azobenzene chromophore. In order to achieve covalent attachment of the polymer network simultaneously to photocrosslinking, the utilised glass substrates were treated with a benzophenone silane prior to polymer deposition and irradiation. To improve the film stability, the dried polymer layers of P1 and P2 were annealed before irradiation. All crosslinked films were washed with water and their thermochromic behaviour was analysed in the swollen state. The resulting hydrogel films are termed P*X*gel (X = 1 to 4 being the polymer number).

Irradiating an unannealed, dry film of P1 reduced the absorbance of the azobenzene chromophore by about 20% (*cf.* Fig. S54a†). After irradiation, the films were sufficiently crosslinked to swell in water, but their mechanical integrity and surface attachment were low, deeming measurements in the swollen state impossible. As a remedy, annealing above the glass temperature was found to result in a substantial increase in film stability to allow such measurements. This annealing procedure leads to a slight decrease in absorbance and a small blueshift (1 nm) of the absorption maximum alongside a change in band asymmetry. Irradiation of such annealed films reduced the absorbance by just about 10% instead of 20% in the untreated films (*cf.* Fig. S54b†). For P2 the same increase in film stability was observed after annealing. Both P3 and P4 showed sufficiently high intrinsic film stability after solvent casting, drying, and crosslinking, thus no heat treatment was required prior to photocrosslinking. Upon irradiation, the azobenzene content in the dry film of P3 decreased by about 20% as for unannealed P1. Washing the crosslinked P3 film until the supernatant remained colourless decreased the azobenzene content in the film by about 70%, indicating polymer leaching as a consequence of a less efficient photocrosslinking process (*cf.* ESI Fig. S55†). The analogous leaching behaviour was observed for the other polymer samples.

A factor that likely influences the crosslinking is the *cis–trans* isomerism of the azobenzene dye. Although the dye itself does not strongly absorb at the crosslinking wavelength (302 nm, *cf.* ESI Fig. S56†), there is still residual absorption. As *cis–trans* isomerisation occurs regardless of the wavelength at which the chromophore is excited, albeit at varying efficacies,[34] the dye will use up a certain amount of UV-light either in the isomerisation process or in radiationless decay. The *cis*-isomer thermally relaxes relatively fast to the *trans*-isomer even in a rigid matrix,[104] which means that absorption processes can be repeated. This secondary pathway of energy consumption may decrease the crosslinking efficiency. Yet, sufficient crosslinking is observed with the given conditions.

Comparison between gels and solution. When comparing the gels and solutions a disparity in thermo-halochromism is found, which can be related to the marked difference in their protonation behaviour. This effect is further enhanced by the critical phase transition characteristics in the thermoresponsive polymer systems.

The most prominent effect that can be identified in the gel systems is the strong halochromic effect of the integrated carboxylic acid function at much lower concentrations compared to the cases of externally added acid, which is required in much higher concentrations. This effect is much less pronounced in polymer solutions and may be explained by a proximity effect of the integrated carboxylic acid functions on the neighbouring dye moieties, which apparently results in a considerably more efficient protonation process. This peculiarity originating from the characteristic network architecture will be elucidated in the frame of the individual polymer systems.

As already described for the dye monomers and the polymers in solution, addition of acid to the polymer systems leads to an "induced thermo-halochromism" (P1 and P2) upon temperature variation, while in the copolymer systems with integrated acid moieties we speak about "intrinsic thermo-halochromism" (P3 and P4).

From an experimental point of view, two general differences between the temperature-dependant measurements of the

Open Access Article. Published on 14 January 2022. Downloaded on 1/30/2023 11:32:10 AM.
This article is licensed under a Creative Commons Attribution 3.0 Unported Licence.

swollen gels compared to the polymer solutions have to be considered. First, the gels may show substantial scattering even in the swollen state, for which we applied a simplified baseline correction by subtracting the absorbance at 750 nm (neglecting the wavelength dependence of scattering as a first approximation). Second, since the chromophore is directly bound to the surface-attached polymer network the absorbance does not inherently decrease with temperature, which is the case for the corresponding solutions due to a reduced dye concentration by the thermal volume expansion of the solvent. Owing to the confinement by surface-attachment, the average number of chromophores in the illumination volume remains essentially constant independent of potential temperature effects on the swelling state.

Induced thermo-halochromism in P1gel and P2gel. The non-thermoresponsive P1gel and the thermoresponsive P2gel both without intrinsic acid were swollen and measured in pure water, aqueous HCl (1 M) and aqueous TFA (0.01 v/v% or 1.3 mM). The P1gel and the P1 copolymer in solution show the same behaviour upon temperature variation at both protonation limits, when neutral and when *completely* protonated. The absorption maxima for the neutral and for the *completely* protonated gel are blue-shifted by 4–5 nm compared to the P1 solution. Upon temperature increase under neutral conditions, the absorption maximum shifts to shorter wavelengths by 6–7 nm for both in solution (*cf.* ESI Fig. S38b†) and in the gel (*cf.* ESI Fig. S28a†). For the *completely* protonated systems (gel and solution), the absorption maxima red-shift by 6–7 nm (*cf.* ESI Fig. S25a and S28b†). We attribute the wavelength shifts for the neutral and *completely* protonated case to thermo-perichromism in relation to a change of the ratio of the vibronic sub-bands. The reasoning for the gel is the same as discussed above for the solution case, in that the polymer–dye interactions vary with temperature.

In the *partially* protonated gel system thermo-halochromism dominates. While the azonium ion content in the gel as well as in solution decreases with increasing temperatures, the degree of protonation differs considerably between both systems. An order-of-magnitude higher acid concentration is required in the gel to reach similar degrees of protonation as in solution. Concomitantly, the decrease in the degree of protonation per temperature increment is lower for the gel compared to the solution (*cf.* ESI Fig. S30a†). This may result from the substantially higher polymer volume fraction in the gel network compared to the polymer chains in solution, increasing the local dye concentration in the network. Higher degrees of protonation amplify the Coulomb repulsion between the like-charged azonium ions, in turn raising the osmotic pressure, which is thermodynamically unfavourable. Consequently, a higher acid concentration is required for protonation of the gel.

For the thermoresponsive copolymer P2, thermo-perichromism of the neutral and the *completely* protonated gel is similar to that in solution (*cf.* Fig. 7a; ESI Fig. S25b and S28c and d†). At low temperatures, the *partially* protonated P2gel and the P2 solution show a lower degree of protonation at the same acid concentration, and a higher variation in the degree of protonation per temperature increment compared to the P1gel and P1 solution (*cf.* ESI Fig. S29†). Partially replacing HEAm of P1 by the less polar NiPAAm comonomer decreases the overall hydrophilicity of P2. Assuming a weaker hydration, a higher polymer volume fraction of P2 owing to a more compact coil in solution and a lower swelling ratio in the gel is expected compared to P1. At the same acid concentration, the degree of protonation in P2 is thus lower because of the higher proximity of the charged groups and the resulting stronger Coulomb repulsion.

The differences in behaviour of thermoresponsive P2 in solution and in the gel state are more pronounced than for the non-responsive P1 system. While an absorbance increase because of scattering is observed for the P2 solution upon the coil-to-globule transition (*cf.* Fig. 7), this scattering effect is absent in the P2gel (*cf.* ESI Fig. S51†). Yet, based on the thermoresponsiveness of P2 in water, a variation of hydrophilicity with temperature should still occur for the P2gel. This is experimentally supported by the aforementioned higher variation of the degree of protonation per temperature increment compared to the P1gel (*cf.* Fig. S29b†). This variation is similar for both the P2gel and P2 in solution (*cf.* ESI Fig. S30b†). The absence of scattering in the P2gel may be explained by the higher polymer volume fraction in the gel compared to the solvated coil. Thus, upon collapse, the refractive index variation in the gel is smaller than in the polymer solution.

Intrinsic thermo-halochromism in P3gel and P4gel. The non-thermoresponsive P3gel and the thermoresponsive P4gel networks both with intrinsic acid functions show the same general thermochromic behaviour as the respective polymers in solution. The absorbance shoulder at 550 nm, relating to the azonium ion, decreases upon increasing temperature with the absorption maximum simultaneously shifting to shorter wavelengths (*cf.* Fig. 9). However, distinct differences exist between the gels and the corresponding polymer solutions and must be discussed individually for each polymer system.

For the P3gel, the absorbance at maximum decreases linearly from 10 °C to 50 °C. At temperatures beyond, the absorbance stagnates and the absorption band broadens significantly (*cf.* Fig. 9a and c). The reason for this behaviour may lie in fluctuations of the film thickness due to an increased gel mobility by Brownian motion at higher temperatures. The degree of protonation at low temperatures is higher in the P3gel than in P3 solution (*cf.* Fig. 8a and 9a). Two factors may be considered to explain this observation. On the one hand, photobleaching upon UV-irradiation during the crosslinking step already leads to a relative decrease in the number of the dye side groups in the network compared to the acid moieties. On the other hand, for P1gel and P2gel without intrinsic acid much higher acid concentrations are required to protonate the non-bleached dye compared to their aqueous solutions. This completely opposite behaviour suggests that the increase in the degree of protonation for the P3gel is not solely due to photobleaching. We hypothesise that the proximity between the intrinsic carboxylic moieties and dye side groups in the

 This journal is © The Royal Society of Chemistry 2022

Open Access Article. Published on 14 January 2022. Downloaded on 1/30/2023 11:32:10 AM.
This article is licensed under a Creative Commons Attribution 3.0 Unported Licence.

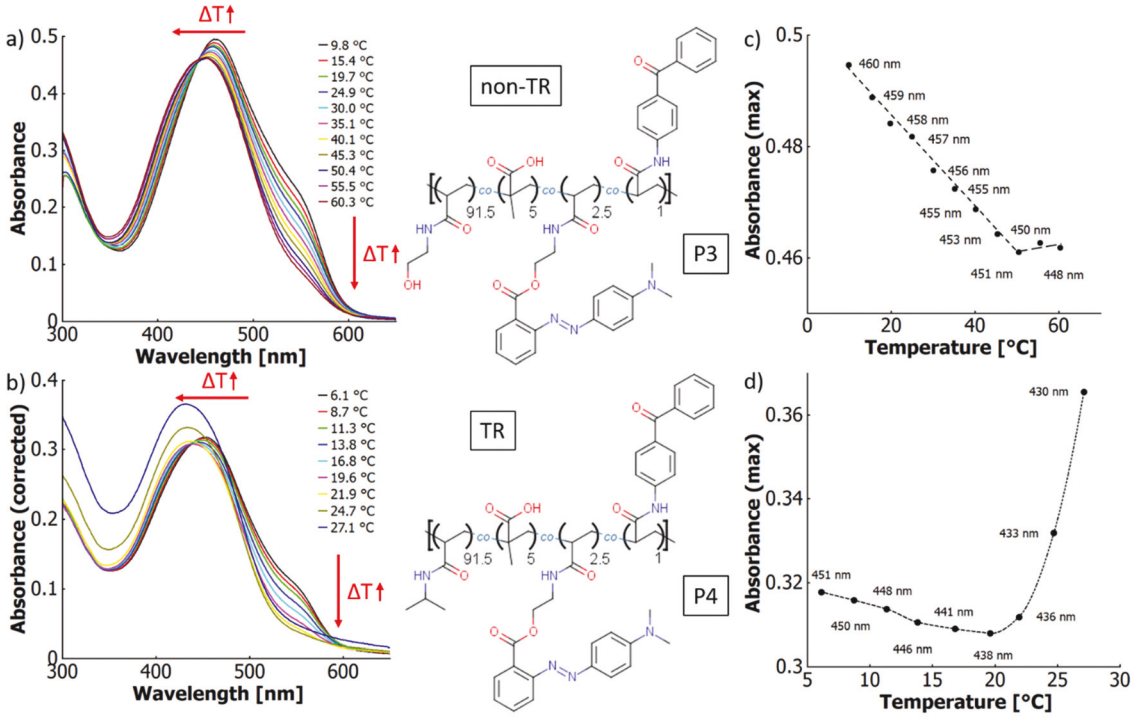

Fig. 9 UV-vis spectra at different temperatures of water–swollen, photocrosslinked films of (a) poly(HEAm-*co*-MAA-*co*-*o*-MREAm-*co*-BPAAm) P3 and (b) poly(NiPAAm-*co*-MAA-*co*-*o*-MREAm-*co*-BPAAm) P4. Plot of the absorbance at maximum (wavelength indicated in plot) *versus* temperature for (c) P3 and (d) P4 ("TR" = thermoresponsive). The line in (c) was generated by hand, the one in (d) by a non-rounded Akima interpolation. Both serve as guide to the eye. The absorbance was baseline-corrected by subtracting the absorbance at 750 nm.

P3gel and P4gel network offsets the requirement of higher free acid concentration observed in P1gel and P2gel. The temperature range in which thermochromic behaviour may be observed, is also larger in the P3gel than in the P3 solution. Temperature-induced deprotonation leads to the same degree of protonation at ~40 °C in solution and ~60 °C in the gel (*cf.* ESI Fig. S48 and S52†). As the initial degree of protonation in the gel system is higher but the extent of deprotonation per temperature increment is similar, the larger dynamic range cannot be attributed to the network architecture itself but is a consequence of the acid proximity effects.

In the thermoresponsive P4gel, the temperature dependence of the absorbance at maximum changes from a negative to a positive slope between 20 °C and 21 °C (*cf.* Fig. 9d). This point assumably matches the transition temperature, as it corresponds to the thermoresponsive behaviour in more concentrated solutions of P4 (0.3 g L^{-1}, *cf.* ESI Fig. S26h†). The degree of protonation in P4 at low temperature is similar for the solution and the gel. However, the deprotonation behaviour differs considerably between the two (*cf.* ESI Fig. S26e, S53b and S30d†).

Except for the P4gel, in all other systems (monomers, polymers P1–P4, and P1–P3gels) the protonation equilibrium shifts stronger to the deprotonated form at lower temperatures than at higher temperatures, especially for the monomers in the binary mixture of water and ethanol. This is documented in Fig. 4c and ESI Fig. S52c† by the decrease in slope of *A*(protonated)/*A*(neutral) *vs.* temperature curves at higher temperature as indicated by the red slope triangles. On the other hand, specifically P4gel exhibits the opposite behaviour with a stronger reduction of the degree of protonation per temperature interval with increasing temperature (red slope triangles in ESI Fig. S53c†). With the P4gel collapse at higher temperatures, the polymer environment becomes more hydrophobic and thus more unfavourable for the polar azonium ion. This drives deprotonation towards the neutral and less polar azobenzene form, which is better accommodated in the hydrophobic environment. Yet, the formation of hydrophobic compartments from collapsing polymer chain segments is no abrupt process. The gradual change in the degree of protonation with temperature suggests that the hydrophobicity increases over a large temperature range. The same effect has been observed for the solution of P4 (*cf.* Fig. 7 and ESI Fig. S26†). In LCST hydrogels, EPR measurements involving spin probe decomposition also suggest the formation of hydrophobic nanocompartments.[99]

The rising hydrophobicity with temperature involving the formation and growth of hydrophobic compartments, eventually leading to the gel collapse, can explain the differences between the polymer in solution and as hydrogel. In solution, the polymer chains have sufficient conformational freedom for the azonium ion side groups to orient towards solvent rich regions *via* chain rearrangement. In contrast, with gels, movement of chain segments is considerably reduced by the cross-

Open Access Article. Published on 14 January 2022. Downloaded on 1/30/2023 11:32:10 AM.
This article is licensed under a Creative Commons Attribution 3.0 Unported Licence.

linked polymer network. Under these conditions the dye substituent cannot partition freely between the solvent-rich regions and the hydrophobic compartments. Thus, with the volume fraction of the collapsed gel growing upon heating, a larger fraction of the dye is surrounded by a hydrophobic environment, which increasingly shifts the protonation equilibrium from the azonium ion to the neutral azobenzene.

The particular thermochromic behaviour of this P4 gel system manifests in a thermo-halochromism that is amplified along the temperature axis by a contribution from the thermo-perichromic mechanism. In other words, the temperature-dependant change of the microenvironment as the underlying mechanism of thermo-perichromism does modulate the protonation equilibrium of thermo-halochromism. The resulting *augmenting* thermo-*peri*-halochromism of the thermo-responsive P4gel behaves inversely to the *diminishing* thermo-solvato-halochromism of the monomers in the binary solvent mixture. The term "augmenting" indicates an increase in the magnitude of thermo-halochromism with temperature.

3.7. Comparison of thermochromicity in different systems

In order to allow the quantification of the phenomenological observations for all different combinations of solvents, dyes, and dye-containing polymers, temperature-dependant van't Hoff analysis was applied to the temperature-dependant UV-vis measurements of acidified, thermochromic solutions. For this, the natural logarithm of the ratio of the absorbances of the azonium ion and the azobenzene $\ln(R)$ was plotted against the inverse of the absolute temperature K^{-1} and fitted according to eqn (1) to extract ΔH_0 and ΔC_p, as described above in the context of pK_a values of the dye monomers. In the case of thermoresponsive systems, only the data below the coil-to-globule transition was fitted because scattering effects prevent accurate fitting. This analysis yields the enthalpy of protonation under standard conditions and the heat capacity of ionisation, which is connected to the interconversion between the azonium ion and the neutral azobenzene and the corresponding optical changes. It is important to note that this analysis is only viable to determine the magnitude of thermo-halochromism, as only in this thermochromic mechanism an equilibrium between different chemical species is of main relevance. The enthalpy ΔH_0 may be regarded here as a measure of the extent of protonation at 25 °C. It also tells whether the process is endothermic or exothermic. A negative ΔH_0 means that the equilibrium shifts away from the product, which refers to the deprotonation of the azonium ion to yield the neutral azobenzene. The heat capacity of ionisation ΔC_p quantifies the temperature dependence of the enthalpy change. As such, it provides information about whether deprotonation becomes more favourable (negative value) or unfavourable (positive value) with increasing temperatures. Both values can be considered as thermochromicity parameters.

We define here the linearity factor T_L as a third quantity, which is associated with the linearity of the thermo-halochromic process. To obtain this value, the ratio of the absorbances of the azonium ion to that of the azobenzene R was plotted against the temperature in °C. The resulting plot was fitted with an exponential decay function

$$R = A + R_0 \times e^{-\frac{T}{T_L}} \quad (2)$$

where R_0 is the ratio of absorbances at 0 °C, A is the offset, and T_L is the linearity factor. With increasing value of the linearity factor, the curvature decreases towards a linear dependency. The linearity factor in eqn (2) is positive in all cases indicating a curvature shift below the line between start and end values (diminished thermo-halochromism), except for the thermo-responsive gel P4, where a negative T_L represents a curvature shift above the line between start and end values (augmented thermo-halochromism). Examples are indicated in ESI Fig. S52b and S53b.†

Based on these analyses the systems can be categorised into four sub-groups highlighted by a colour code in Table 7, in accordance with their tendencies regarding the enthalpy ΔH_0 and the heat capacity of ionisation ΔC_p.

o-MREAm, *m*-MREAm, *p*-MREAm, P1, and P2 all in ethanol, as well as the photocrosslinked and water swollen gels P1gel, P2gel, and P3gel have a negative ΔH_0 and negative ΔC_p. This category has been highlighted by an orange hue in Table 7.

P1, P2, and P3 in water have a small positive value both for ΔH_0 and ΔC_p, represented by the white entries in Table 7.

The constitutional isomers of the MREAm monomers in the binary solvent mixture of water and ethanol have large positive values both in ΔH_0 and ΔC_p. These entries are marked in green.

The thermoresponsive systems P2b, and P4 for all measured concentrations in aqueous solution, as well as the photocrosslinked and water swollen P4gel have large negative values of ΔH_0 and ΔC_p, shaded in blue.

The linearity factor T_L shows less variation between the different dye monomer and polymer systems than the corresponding thermochromicity parameters ΔH_0 and ΔC_p. In general, T_L is larger for the systems with a low influence of thermo-solvatochromism and thermo-perichromism on thermo-halochromism for the two categories with small negative (orange) or positive (white) ΔC_p. Consequently, T_L is smaller for those systems with a strong influence on thermo-halochromism, as represented by the two categories green with moderate positive ΔC_p and blue with strongly negative ΔC_p.

Several conclusions can be drawn from this categorisation. First, incorporation of the dye by copolymerisation has little to no influence on thermochromism in ethanolic solution with added acid. Under these conditions both polymers, the non-thermoresponsive P1 and the thermoresponsive P2, yield the same negative thermochromicity parameters as the free dye monomer. The water swollen gels P1gel, P2gel and P3gel also have similar negative values for the thermochromicity parameters ΔH_0 and ΔC_p, while the corresponding polymers in solution have positive values for both parameters. The thermo-halochromic behaviour of these gel networks is reminiscent to that of the free dye monomers dissolved in acidified ethanol.

 This journal is © The Royal Society of Chemistry 2022

Open Access Article. Published on 14 January 2022. Downloaded on 1/30/2023 11:32:10 AM.
This article is licensed under a Creative Commons Attribution 3.0 Unported Licence.

Table 7 Overview of the relevant parameters obtained from van't Hoff analyses of thermochromic solutions of methyl red-based monomers and different polymer systems. "*a*", "*b*", and "*c* term" refer to the raw data from the van't Hoff analyses and the colour code is applied to distinguish categories of thermo-halochromic systems with similar behaviour, both discussed in the main text

System	Solvent	Acid	*a* term	*b* term	*c* term	ΔH_0 [kJ]	ΔC_p [kJ K^{-1}]	Linearity factor [°C]
o-MREAm	EtOH	130 mM TFA	−55.7	0.071	−13.7	−34	−0.11	47
m-MREAm	EtOH	130 mM TFA	−56.7	0.062	−13.0	−32	−0.11	84
p-MREAm	EtOH	130 mM TFA	−41.8	0.054	−10.0	−25	−0.08	62
o-MREAm	H_2O : EtOH	2.2 mM HCl	155	−0.081	31.4	78	0.26	26
m-MREAm	H_2O : EtOH	11 mM HCl	102	−0.049	20.4	51	0.17	33
p-MREAm	H_2O : EtOH	5.9 mM HCl	125	−0.063	25.3	63	0.21	28
P1	EtOH	130 mM TFA	−55.5	0.063	−13.2	−33	−0.11	83
P1	H_2O	0.13 mM TFA	13.0	0.016	1.48	3.7	0.01	45
P1gel	H_2O	1.3 mM TFA	−11.6	0.024	−3.23	−8.0	−0.03	97
P2	EtOH	130 mM TFA	−55.4	0.061	−13.0	−32	−0.11	92
P2	H_2O	0.13 mM TFA	14.8	0.023	1.51	3.7	0.01	36
P2gel	H_2O	1.3 mM TFA	−52.7	0.066	−12.6	−31	−0.11	51
P2b	H_2O	0.13 mM TFA	−538	0.46	−119	−295	−0.99	29
P3	H_2O	MAA	18.7	0.014	2.79	6.9	0.02	39
P3gel	H_2O	MAA	−73	0.076	−16.6	−41	−0.14	75
P4 0.15 g L^{-1}	H_2O	MAA	−367	0.35	−82.2	−204	−0.68	23
P4 0.2 g L^{-1}	H_2O	MAA	−544	0.48	−120	−298	−1.00	27
P4 0.3 g L^{-1}	H_2O	MAA	−633	0.55	−139	−345	−1.2	30
P4gel	H_2O	MAA	−1950	1.53	−422	−1046	−3.51	−34

Yet, this behaviour is contrary to the thermo-halochromism of the constituting, non-crosslinked polymers in aqueous solution in a *partially* protonated state, which is affected by their thermo-perichromism as reflected in the change of sign to negative values of ΔH_0 and ΔC_p. Apparently, this strong effect of crosslinking is a consequence of the more uniform microenvironment in the gel network and the reduced mobility of the dye attached to the crosslinked polymer segments. In contrast to the free polymer coil, no sufficient conformational rearrangement of the macromolecular segments in the network is possible, inhibiting favourable interactions with the surrounding medium. As the heat capacity of ionisation ΔC_p is negative for this category (orange in Table 7), deprotonation becomes more favourable at higher temperatures.

Considering the similar thermochromicity values for aqueous P3 (intrinsic acid) and for P1 and P2 (no intrinsic acid) in acidic aqueous solution, there is no obvious difference between intrinsic and induced thermo-halochromism. Additionally, below the transition temperature the thermoresponsive polymer P2 with high cloud point behaves the same as the non-thermoresponsive P1. All three polymers P1, P2, and P3 in water show almost no temperature dependence, with their heat capacity of ionisation ΔC_p being close to 0.

The next category comprising the positional isomers of MREAm in H_2O : EtOH (X_{EtOH} = 0.31) is highlighted in green in Table 7. For these systems, the influence of thermo-solvatochromism on thermo-halochromism in the binary solvent mixture of water and ethanol has been discussed above in the context of Fig. 4. With increasing temperature, their thermo-solvatochromism results in a reduction of the extent of deprotonation per temperature increment, which is reflected in the positive heat capacity of ionisation ΔC_p in these systems. Both thermochromicity parameters ΔH_0 and ΔC_p correlate linearly with the pK_a of the constitutional isomers of MREAm, increasing from *meta* over *para* to *ortho* (*cf.* ESI Fig. S19†). Even though the difference spectra from thermotitration (*cf.* ESI Fig. S37g–i†) show considerable deviation in the protonation mechanism between the positional isomers, the linear relationship between ΔC_p and pK_a corroborate the dominance of the acidity (*i.e.* pK_a) of the dye monomers on their thermo-halochromism in the binary solvent mixture.

Comparing the thermochromicity parameters of P1, P2, and P3 in acidic aqueous solutions (white category in Table 7) and the configurational isomers of the dye monomer in the binary solvent mixture suggests that thermo-perichromism in these particular polymers is analogous to thermo-solvatochromism of the monomers. All these systems share positive values for ΔH_0 and ΔC_p, which evidences stabilisation of the azonium ion by the respective microenvironment with increasing temperature.

The strongest impact of either thermo-solvatochromism or thermo-perichromism on thermo-halochromism can be found in the category of thermoresponsive polymers in aqueous solution and hydrogels, coloured blue in Table 7, for which the absolute values of both thermochromicity parameters are the highest among all categories. These parameters become more negative with decreasing cloud point temperatures. This has been observed for solutions of P4 with a concentration increase, as well as for solutions of P2 (higher cloud point) in comparison to those of P2b (lower cloud point), where even the sign of ΔH_0 and ΔC_p switches from positive to negative. With lower cloud point temperatures, the coil-to-globule transition takes place in a narrower temperature interval, accompanied by a more pronounced change in interactions of the dyes with their microenvironment. This, in turn, results in larger absolute values of the thermochromicity parameters with lower cloud points. This hypothesis is further substan-

Open Access Article. Published on 14 January 2022. Downloaded on 1/30/2023 11:32:10 AM.
This article is licensed under a Creative Commons Attribution 3.0 Unported Licence.

tiated by the P4gel, for which the absolute values of the thermochromicity parameters are yet larger by an order of magnitude compared to the respective thermoresponsive polymer solutions, agreeing well with the phenomenological discussion above about thermo-halochromism of immobilised dyes in thermoresponsive gels containing intrinsic acid.

The obtained knowledge can be combined into the following conclusions:

1. Varying the microenvironment of a dye *via* the liquid medium or polymer composition provides the possibility to control the protonation equilibrium by the corresponding azonium ion concentration in dependence of the temperature for *partially* protonated systems.

2. When the dye microenvironment shifts to a more hydrophilic state upon a temperature increase, which is the case for the binary solvent mixture of water and ethanol, the azonium ion persists against thermally driven deprotonation owing to a better solubilisation.

3. *Vice versa*, when the dye microenvironment becomes more hydrophobic at higher temperatures, occurring with LCST-type polymers, the azonium ion is deprotonated more easily to yield the less polar azobenzene. This effect becomes particularly obvious for a thermoresponsive polymer in solution, when the azonium ion concentration vanishes close to the coil-to-globule transition at the cloud point.

4. Summary and conclusion

A synthesis route to novel azo dye monomers by esterification of methyl red to *N*-(2-hydroxyethyl)acrylamide (MREAm) *via* carbonyldiimidazole coupling could be established for all three positional isomers of the dye. From these monomers, copolymers were obtained by free radical polymerisation employing *N*-(2-hydroxyethyl)acrylamide (HEAm), *N*-isopropylacrylamide (NiPAAm), methacrylic acid (MAA), and 4-benzophenoneacrylamide (BPAAm). Here, HEAm provides water-solubility, NiPAAm thermoresponsivity in aqueous solution, MAA the intrinsic acid group as proton donor, and BPAAm the photocrosslinker unit for network formation. Thermochromism was studied for solutions of the monomer and polymer systems in pure water, ethanol, and the mixture thereof. For hydrogels prepared from these polymers by photocrosslinking and subsequent swelling in water, the thermochromic behaviour was investigated.

In these experiments three different mechanisms of thermochromism, namely vibronic thermochromism, thermo-solvatochromism, and thermo-halochromism, were identified for the constitutional isomers of the azo dye monomer MREAm. Depending on the particular system and the experimental conditions, various combinations of these thermochromic mechanisms were found. In neat ethanol, the MREAm dyes show vibronic thermochromism by a blueshift of a few nanometers upon temperature increase that can be attributed to a change in the vibronic sub-bands, as observed *via* derivative spectroscopy and difference spectroscopy. In the binary solvent mixture of ethanol and water, the observed thermo-solvatochromism shows similarities to the vibronic mechanism as a consequence of the competition of the two solvent species in the solvation shell, also suggested by temperature-dependant derivative and difference spectra. By addition of extrinsic acid (trifluoroacetic acid) to a MREAm dye solution in ethanol, thermo-halochromism can be induced. When such a system is titrated to *partial* protonation with coexisting neutral azobenzene and azonium ion, the protonation equilbrium shifts towards the neutral azobenzene at higher temperatures. However, thermo-halochromism is strongly influenced by the nature of the solvent. Particularly, in the binary solvent mixture with added acid, two phenomena are observed with increasing temperatures: 1. instead of an isosbestic point, a blue-shifting region of intersections exists for consecutive spectra of adjacent temperature steps; 2. the extent of deprotonation per temperature increment decreases. Both phenomena result from the influence of thermo-solvatochromism on thermo-halochromism, which we termed in this particular combination "diminishing thermo-solvato-halochromism".

Similarly, solutions of copolymers bearing *o*-MREAm units show thermo-perichromism as the polymer-related analogon to thermo-solvatochromism observed for solutions of the free monomers. The thermo-perichromic effect is stronger in water than in ethanol, which is most pronounced in LCST-type thermoresponsive polymers that undergo a coil-to-globule transition alongside strong changes in the hydrophobicity of the polymers in aqueous solution. The coil-to-globule transition for these systems can be best followed *via* the change of absorbance at maximum by an increase in scattering. No major differences in thermochromism can be identified for the polymers in solution by the van't Hoff analysis, neither with added (extrinsic) nor with copolymerised (intrinsic) acid. Thermoresponsive LCST behaviour in solution strongly affects thermo-halochromism, which scales with the cloud point, while in non-thermoresponsive polymers thermo-halochromism is almost identical to that of the isolated dye monomers. As the hydrophobicity of the LCST-type polymers increases with temperature and reaches its maximum at the coil-to-globule transition, the attached dyes are completely deprotonated at this point. For polymers with a lower cloud point, a smaller temperature interval is available during this transition for the deprotonation process, thus increasing the extent of deprotonation per temperature increment. Consequently, thermo-halochromism can be conveniently tailored by the design of the molecular architecture of the copolymer.

All hydrogels prepared from the different copolymers also show thermochromic behaviour. Remarkably, the thermoresponsive hydrogels from the LCST polymers with intrinsic acid exhibit the strongest thermochromic behaviour of all examined systems. Here, the extent of deprotonation per temperature increment increases strongly with temperature, and we termed the resulting effect "augmenting thermo-peri-halochromism". We ascribe this behaviour to an azonium-destabilising change of the microenvironment towards a more hydrophobic character of the polymer.

In conclusion, we identified multiple mechanisms of thermochromism for various azobenzene systems of moderate pK_a

 This journal is © The Royal Society of Chemistry 2022

Open Access Article. Published on 14 January 2022. Downloaded on 1/30/2023 11:32:10 AM.
This article is licensed under a Creative Commons Attribution 3.0 Unported Licence.

in solution and in the gel state, and elaborated the influence of solvent, polymer architecture and especially LCST behaviour. Employing van't Hoff analysis, a scaling of thermo-halochromism with the pK_a could be demonstrated and the contributing effects were categorised with respect to thermo-solvatochromism and thermo-perichromism. Detailed understanding of the underlying mechanisms is of great value for potential applications of these dye–polymer systems, for example as macromolecular optical thermometers, or in any other scenario involving azobenzenes and temperature variation.

Conflicts of interest

There are no conflicts to declare.

Acknowledgements

We thank the Faculty IV of the University of Siegen for funding, Dr Thomas Paululat for NMR measurements, and Silvia Freese for extensive discussions.

References

1 X. Wang, O. S. Wolfbeis and R. J. Meier, Luminescent probes and sensors for temperature, *Chem. Soc. Rev.*, 2013, **42**, 7834–7869.
2 A. Steinegger, I. Klimant and S. M. Borisov, Purely Organic Dyes with Thermally Activated Delayed Fluorescence-A Versatile Class of Indicators for Optical Temperature Sensing, *Adv. Opt. Mater.*, 2017, **5**, 1700372.
3 L. Yin, C. He, C. Huang, W. Zhu, X. Wang, Y. Xu and X. Qian, A dual pH and temperature responsive polymeric fluorescent sensor and its imaging application in living cells, *Chem. Commun.*, 2012, **48**, 4486–4488.
4 X. Wang, R. J. Meier and O. S. Wolfbeis, A Fluorophore-Doped Polymer Nanomaterial for Referenced Imaging of pH and Temperature with Sub-Micrometer Resolution, *Adv. Funct. Mater.*, 2012, **22**, 4202–4207.
5 A. Malfait, F. Coumes, D. Fournier, G. Cooke and P. Woisel, A water-soluble supramolecular polymeric dual sensor for temperature and pH with an associated direct visible readout, *Eur. Polym. J.*, 2015, **69**, 552–558.
6 H. Sun, J. Xiang, X. Zhang, H. Chen, Y. Shi, L. Yu, Q. Yang, Q. Li, A. Guan and Y. Tang, A colorimetric temperature sensor of a cyanine dye supramolecule and its application in reversible switch, *Appl. Phys. Lett.*, 2014, **105**, 71914.
7 A. Seeboth, D. Lötzsch, R. Ruhmann and O. Muehling, Thermochromic polymers–function by design, *Chem. Rev.*, 2014, **114**, 3037–3068.
8 W. Theilacker, G. Kortüm and G. Friedheim, Zur Frage der Thermochromie; ein Beispiel für eine echte Valenztautomerie, *Chem. Ber.*, 1950, **83**, 508–519.
9 J. H. Day, Thermochromism, *Chem. Rev.*, 1963, **63**, 65–80.
10 C. Pietsch, U. S. Schubert and R. Hoogenboom, Aqueous polymeric sensors based on temperature-induced polymer phase transitions and solvatochromic dyes, *Chem. Commun.*, 2011, **47**, 8750–8765.
11 A. Seeboth, J. Kriwanek and R. Vetter, The first example of thermochromism of dyes embedded in transparent polymer gel networks, *J. Mater. Chem.*, 1999, **9**, 2277–2278.
12 J. Kriwanek, D. Lötzsch, R. Vetter and A. Seeboth, Influence of a zwitterionic surfactant on the chromogenic behavior of a dye-containing aqueous PVA-polyether gel network, *Polym. Adv. Technol.*, 2003, **14**, 79–82.
13 K. Matsubara, M. Watanabe and Y. Takeoka, A thermally adjustable multicolor photochromic hydrogel, *Angew. Chem., Int. Ed.*, 2007, **46**, 1688–1692.
14 X. Zhao, Synthesis, characterization and structure dependence of thermochromism of polythiophene derivatives, *J. Mater. Sci.*, 2005, **40**, 3423–3428.
15 X. Y. Zhao and M. Z. Wang, Structure dependence of photochromism and thermochromism of azobenzene-functionalized polythiophenes, *eXPRESS Polym. Lett.*, 2007, **1**, 450–455.
16 X. Yu, Y. Luo, W. Wu, Q. Yan, G. Zou and Q. Zhang, Synthesis and reversible thermochromism of azobenzene-containing polydiacetylenes, *Eur. Polym. J.*, 2008, **44**, 3015–3021.
17 S. Wu, L. Niu, J. Shen, Q. Zhang and C. Bubeck, Aggregation-Induced Reversible Thermochromism of Novel Azo Chromophore-Functionalized Polydiacetylene Cylindrical Micelles, *Macromolecules*, 2009, **42**, 362–367.
18 S. Wu, Q. Zhang and C. Bubeck, Solvent Effects on Structure, Morphology, and Photophysical Properties of an Azo Chromophore-Functionalized Polydiacetylene, *Macromolecules*, 2010, **43**, 6142–6151.
19 M. Leclerc and K. Faid, Electrical and optical properties of Processable Polythiophene Derivatives: Structure-Property relationships, *Adv. Mater.*, 1997, **9**, 1087–1094.
20 I. Lévesque and M. Leclerc, Novel Dual Photochromism in Polythiophene Derivatives, *Macromolecules*, 1997, **30**, 4347–4352.
21 H. Joshi, F. S. Kamounah, G. van der Zwan, C. Gooijer and L. Antonov, Temperature dependent absorption spectroscopy of some tautomeric azo dyes and Schiff bases, *J. Chem. Soc., Perkin Trans. 2*, 2001, 2303–2308.
22 J. A. Dean and N. A. Lange, *Lange's handbook of chemistry*, McGraw-Hill; [Distributed by] Knovel, New York, [Norwich, N.Y.], 15th edn, 1999.
23 K. M. Tawarah and H. M. Abu-Shamleh, A spectrophotometric study of the acid-base equilibria of o-methyl red in aqueous solutions, *Dyes Pigm.*, 1991, **17**, 203–215.
24 T. Kuwabara, A. Nakamura, A. Ueno and F. Toda, Inclusion Complexes and Guest-Induced Color Changes of pH-Indicator-Modified beta.-Cyclodextrins, *J. Phys. Chem.*, 1994, **98**, 6297–6303.
25 M. Tajima, M. Sugai, K. Matsunaga, T. Yamashita, H. Inoue and M. Hida, Thermochromism of dyes on silica gel, *Dyes Pigm.*, 1998, **39**, 97–109.

Open Access Article. Published on 14 January 2022. Downloaded on 1/30/2023 11:32:10 AM.
This article is licensed under a Creative Commons Attribution 3.0 Unported Licence.

26 X. Du, C. Zhu and X. Xie, Thermochromic Ion-Exchange Micelles Containing H + Chromoionophores, *Langmuir*, 2017, **33**, 5910–5914.
27 C. Pietsch, R. Hoogenboom and U. S. Schubert, Soluble polymeric dual sensor for temperature and pH value, *Angew. Chem., Int. Ed.*, 2009, **48**, 5653–5656.
28 L. Liu, W. Li, K. Liu, J. Yan, G. Hu and A. Zhang, Comblike Thermoresponsive Polymers with Sharp Transitions: Synthesis, Characterization, and Their Use as Sensitive Colorimetric Sensors, *Macromolecules*, 2011, **44**, 8614–8621.
29 R. W. Taft, J.-L. M. Abboud, M. J. Kamlet and M. H. Abraham, Linear solvation energy relations, *J. Solution Chem.*, 1985, **14**, 153–186.
30 A. R. Katritzky, D. C. Fara, H. Yang, K. Tämm, T. Tamm and M. Karelson, Quantitative measures of solvent polarity, *Chem. Rev.*, 2004, **104**, 175–198.
31 G. Seu, Spectrophotometric study of the prototropic equilibrium of methyl red in organic solvents, *Dyes Pigm.*, 1995, **29**, 227–240.
32 L. Zhang, J. M. Cole and X. Liu, Tuning Solvatochromism of Azo Dyes with Intramolecular Hydrogen Bonding in Solution and on Titanium Dioxide Nanoparticles, *J. Phys. Chem. C*, 2013, **117**, 26316–26323.
33 H. Jaffé, S.-J. Yeh and R. Gardner, The electronic spectra of azobenzene derivatives and their conjugate acids, *J. Mol. Spectrosc.*, 1958, **2**, 120–136.
34 H. M. D. Bandara and S. C. Burdette, Photoisomerization in different classes of azobenzene, *Chem. Soc. Rev.*, 2012, **41**, 1809–1825.
35 S. T. Cowan, Micromethod for the methyl red test, *J. Gen. Microbiol.*, 1953, **9**, 101–109.
36 Z. Guo, S. Li, C. Wang, J. Xu, B. Kirk, J. Wu, Z. Liu and W. Xue, Biocompatibility and cellular uptake mechanisms of poly(N -isopropylacrylamide) in different cells, *J. Bioact. Compat. Polym.*, 2017, **32**, 17–31.
37 H. Chen, C. Zhao, M. Zhang, Q. Chen, J. Ma and J. Zheng, Molecular Understanding and Structural-Based Design of Polyacrylamides and Polyacrylates as Antifouling Materials, *Langmuir*, 2016, **32**, 3315–3330.
38 F. Doberenz, K. Zeng, C. Willems, K. Zhang and T. Groth, Thermoresponsive polymers and their biomedical application in tissue engineering - a review, *J. Mater. Chem. B*, 2020, **8**, 607–628.
39 S. Chen, K. Wang and W. Zhang, A new thermoresponsive polymer of poly(N-acryloylsarcosine methyl ester) with a tunable LCST, *Polym. Chem.*, 2017, **8**, 3090–3101.
40 S. A. Mohammad, S. Dolui, D. Kumar, S. R. Mane and S. Banerjee, Facile access to functional polyacrylates with dual stimuli response and tunable surface hydrophobicity, *Polym. Chem.*, 2021, **12**, 3042–3051.
41 J. Jia, M. Sarker, M. G. Steinmetz, R. Shukla and R. Rathore, Photochemical elimination of leaving groups from zwitterionic intermediates generated via electrocyclic ring closure of alpha,beta-unsaturated anilides, *J. Org. Chem.*, 2008, **73**, 8867–8879.
42 M. Gianneli, R. F. Roskamp, U. Jonas, B. Loppinet, G. Fytas and W. Knoll, Dynamics of swollen gel layers anchored to solid surfaces, *Soft Matter*, 2008, **4**, 1443–1447.
43 H. A. Staab and A. Mannschreck, Synthese von Carbonsäureestern nach der Imidazolidmethode, *Chem. Ber.*, 1962, **95**, 1284–1297.
44 D. E. Bergbreiter, P. L. Osburn and C. Li, Soluble Polymer-Supported Catalysts Containing Azo Dyes, *Org. Lett.*, 2002, **4**, 737–740.
45 H. A. Staab, M. Lüking and F. H. Dürr, Darstellung von Imidazoliden. Synthese von Amiden, Hydraziden und Hydroxamsäuren nach der Imidazolidmethode, *Chem. Ber.*, 1962, **95**, 1275–1283.
46 G. Dormán, H. Nakamura, A. Pulsipher and G. D. Prestwich, The Life of Pi Star: Exploring the Exciting and Forbidden Worlds of the Benzophenone Photophore, *Chem. Rev.*, 2016, **116**, 15284–15398.
47 Marvin was used for drawing and displaying chemical structures, substructures and reactions, Marvin 18.30, ChemAxon (https://www.chemaxon.com).
48 C. Larrivée-Aboussafy, B. P. Jones, K. E. Price, M. A. Hardink, R. W. McLaughlin, B. M. Lillie, J. M. Hawkins and R. Vaidyanathan, DBU catalysis of N, N'-carbonyldiimidazole-mediated amidations, *Org. Lett.*, 2010, **12**, 324–327.
49 O. F. Olaj, J. W. Breitenbach and I. Hofreiter, Über einen bimolekularen Mechanismus der Radikalbildung bei der durch Di-(3-benzolazobenzoyl-)peroxid angeregten Polymerisation von Styrol, *Monatsh. Chem.*, 1967, **98**, 997–1016.
50 O. F. Olaj, J. W. Breitenbach and I. Hofreiter, Die Einführung von Starterbruchstücken in das Polymere bei der durch Di-(3-benzolazobenzoyl-)peroxyd angeregten Styrolpolymerisation, *Makromol. Chem.*, 1966, **91**, 264–280.
51 O. F. Olaj, J. W. Breitenbach and I. Hofreiter, Der Einfluß aromatischer Azoverbindungen auf die Polymerisation von Vinylacetat, Vinylchlorid und Methylmethacrylat, *Makromol. Chem.*, 1967, **110**, 72–83.
52 D. Braun, G. Arcache, R. J. Faust and W. Neumann, Darstellung und Polymerisationsverhalten von einigen neuen Vinylverbindungen, *Makromol. Chem.*, 1968, **114**, 51–69.
53 D. Braun and G. Arcache, Über den Einfluß aromatischer Azoverbindungen auf die radikalische Polymerisation von Styrol, *Makromol. Chem.*, 1971, **148**, 119–129.
54 M. C. Rezende and A. Aracena, In search of the thermo/halochromism of the E(T)(30) pyridinium-N-phenolate betaine dye, *Spectrochim. Acta, Part A*, 2012, **98**, 18–22.
55 L. Hermosilla, M. C. Rezende, V. G. Machado and R. I. Stock, Thermohalochromism of phenolate dyes conjugated with nitro-substituted aryl groups, *Spectrochim. Acta, Part A*, 2017, **173**, 556–561.
56 V. Gold, *The IUPAC Compendium of Chemical Terminology*, International Union of Pure and Applied Chemistry (IUPAC), Research Triangle Park, NC, 2019.

 This journal is © The Royal Society of Chemistry 2022

Open Access Article. Published on 14 January 2022. Downloaded on 1/30/2023 11:32:10 AM.
This article is licensed under a Creative Commons Attribution 3.0 Unported Licence.

57 L. Antonov and D. Nedeltcheva, Resolution of overlapping UV–Vis absorption bands and quantitative analysis, *Chem. Soc. Rev.*, 2000, **29**, 217–227.
58 Š. Sršeň, J. Sita, P. Slavíček, V. Ladányi and D. Heger, Limits of the Nuclear Ensemble Method for Electronic Spectra Simulations: Temperature Dependence of the (E)-Azobenzene Spectrum, *J. Chem. Theory Comput.*, 2020, **16**, 6428–6438.
59 H. Mustroph, Studies on the UV-vis Absorption Spectra of Azo Dyes: Part 25. Analysis of the Fine Structure of the π_1 -> π_1* Band of 4′-Donor-Substituted 4-*N,N*-Diethylaminoazobenzenesa, *Dyes Pigm.*, 1991, **15**, 129–137.
60 M. Nepraš, S. Luňák, R. Hrdina and J. Fabian, Electronic excited states of azo compounds: Strong ππ* fluorescence of bis-4,4′-diethylaminoazobenzene, *Chem. Phys. Lett.*, 1989, **159**, 366–370.
61 S. Lunák, M. Nepraš, R. Hrdina and H. Mustroph, Excited states of azo compounds. II. Vibrational structure of the electronic absorption spectra of 4,4′-di-substituted azobenzene derivatives, *Chem. Phys.*, 1994, **184**, 255–260.
62 S.-K. Park, C.-K. Lee, K.-C. Min and N.-S. Lee, Fourier Transform Raman Studies of Methyl Red Adsorbed on γ-Alumina and Silica-Alumina, *Bull. Korean Chem. Soc.*, 2004, **25**, 1817–1821.
63 S. Bell, A. Bisset and T. J. Dines, Ab initio and density functional study of the resonance Raman spectra of Methyl Red, Ethyl Red and their protonated derivatives, *J. Raman Spectrosc.*, 1998, **29**, 447–462.
64 T. Itoh, Ground-state, excited-singlet-state, and excited-triplet-state energy levels and photophysics of the three rotational isomers of isophthalaldehyde vapor, *J. Phys. Chem. A*, 2007, **111**, 8439–8444.
65 A. Cesaretti, B. Carlotti, F. Elisei, C. G. Fortuna, G. Consiglio and A. Spalletti, A cationic naphthyl derivative defies the non-equilibrated excited rotamers principle, *Phys. Chem. Chem. Phys.*, 2017, **19**, 5262–5272.
66 M. Quick, A. L. Dobryakov, I. N. Ioffe, F. Berndt, R. Mahrwald, N. P. Ernsting and S. A. Kovalenko, Rotamer-Specific Photoisomerization of Difluorostilbenes from Transient Absorption and Transient Raman Spectroscopy, *J. Phys. Chem. B*, 2018, **122**, 1049–1059.
67 E. Fischer, Emission spectroscopy evidenvce for the existence of rotamers in solutions of trans-diarylethylenes and related compounds, *J. Photochem.*, 1981, **17**, 331–340.
68 N. Castel and E. Fischer, Frozen-in non-equilibrium rotamer mixtures in 1,2-diarylethylenes obtained by low-temperature irradiation, *J. Mol. Struct.*, 1985, **127**, 159–166.
69 N. Castel and E. Fischer, Rotamers in azonaphthalenes? A combined photochemical and UV-absorption spectrophotometric study in rigid media, *J. Mol. Struct.*, 1986, **140**, 365–369.
70 J.-F. Boily and T. M. Seward, On the Dissociation of Methyl Orange: Spectrophotometric Investigation in Aqueous Solutions from 10 to 90 °C and Theoretical Evidence for Intramolecular Dihydrogen Bonding, *J. Solution Chem.*, 2005, **34**, 1387–1406.
71 E. Sawicki, Physical Properties of the Aminoazobenzene Dyes. IV. The Position of Proton Addition 1, *J. Org. Chem.*, 1957, **22**, 365–367.
72 E. Sawicki, The Physical Properties of the Aminoazobenzene Dyes. III. Tautomerism of 4-Aminoazobenzene Salt Cations in Acid Solution, *J. Org. Chem.*, 1956, **21**, 605–609.
73 E. Sawicki, Physical Properties of Aminoazobenzene Dyes. V. The C ϵ /A ϵ Ratio, *J. Org. Chem.*, 1957, **22**, 621–625.
74 G. E. Lewis, Structures of the mono-acid cations of 4-aminoazobenzene and its derivatives, *Tetrahedron*, 1960, **10**, 129–134.
75 I. Y. Bershtein and O. F. Ginzburg, Tautomerism of Aromatic Azo-compounds, *Russ. Chem. Rev.*, 1972, **41**, 97–110.
76 D. G. Hafeman, K. L. Crawford and L. J. Bousse, Fundamental thermochromic properties of buffered pH-indicator solutions and the formulation of "athermochromic" systems, *J. Phys. Chem.*, 1993, **97**, 3058–3066.
77 R. K. Srour and L. M. McDonald, Determination of the Acidity Constants of Methyl Red and Phenol Red Indicators in Binary Methanol– and Ethanol–Water Mixtures, *J. Chem. Eng. Data*, 2008, **53**, 116–127.
78 K. Tawarah, The tautomeric and acid-base equilibria of p-methyl red in aqueous solutions, *Dyes Pigm.*, 1992, **20**, 261–270.
79 S. J. Khouri, I. A. Abdel-Rahim, E. M. Alshamaileh and A. M. Altwaiq, Equilibrium and Structural Study of m-Methyl Red in Aqueous Solutions: Distribution Diagram Construction, *J. Solution Chem.*, 2013, **42**, 1844–1853.
80 H. Naghibi, A. Tamura and J. M. Sturtevant, Significant discrepancies between van't Hoff and calorimetric enthalpies, *Proc. Natl. Acad. Sci. U. S. A.*, 1995, **92**, 5597–5599.
81 Y. Liu and J. M. Sturtevant, Significant discrepancies between van't Hoff and calorimetric enthalpies. II, *Protein Sci.*, 1995, **4**, 2559–2561.
82 E. B. Tada, L. P. Novaki and O. A. El Seoud, Solvatochromism in pure and binary solvent mixtures: effects of the molecular structure of the zwitterionic probe, *J. Phys. Org. Chem.*, 2000, **13**, 679–687.
83 M. S. Antonious, E. B. Tada and O. A. E. Seoud, Thermo-solvatochromism in aqueous alcohols: effects of the molecular structures of the alcohol and the-solvatochromic probe, *J. Phys. Org. Chem.*, 2002, **15**, 403–412.
84 E. B. Tada, P. L. Silva and O. A. El Seoud, Thermo-solvatochromism of betaine dyes in aqueous alcohols: explicit consideration of the water-alcohol complex, *J. Phys. Org. Chem.*, 2003, **16**, 691–699.
85 E. B. Tada, P. L. Silva, C. Tavares and O. A. El Seoud, Thermo-solvatochromism of zwitterionic probes in aqueous aliphatic alcohols and in aqueous 2-alkoxyetha-

Open Access Article. Published on 14 January 2022. Downloaded on 1/30/2023 11:32:10 AM.
This article is licensed under a Creative Commons Attribution 3.0 Unported Licence.

nols: relevance to the enthalpies of activation of chemical reactions, *J. Phys. Org. Chem.*, 2005, **18**, 398–407.

86 P. L. Silva, E. L. Bastos and O. A. El Seoud, Solvation in binary mixtures of water and polar aprotic solvents: theoretical calculations of the concentrations of solvent-water hydrogen-bonded species and application to thermosolvatochromism of polarity probes, *J. Phys. Chem. B*, 2007, **111**, 6173–6180.

87 C. Chylewski, Verallgemeinerung des isosbestischen Punktes, *Angew. Chem., Int. Ed. Engl.*, 1971, **83**, 214–215.

88 J. R. Morrey, Fused Salt Spectrophotometry. III. Isosbestic Points Generated By Variation In Temperature, *J. Phys. Chem.*, 1962, **66**, 2169–2173.

89 J. Brynestad and G. P. Smith, Isosbestic points and internally linear spectra generated by changes in solvent composition or temperature, *J. Phys. Chem.*, 1968, **72**, 296–300.

90 M. D. Cohen and E. Fischer, 588. Isosbestic points, *J. Chem. Soc.*, 1962, 3044.

91 S. K. Christensen, M. C. Chiappelli and R. C. Hayward, Gelation of Copolymers with Pendent Benzophenone Photo-Cross-Linkers, *Macromolecules*, 2012, **45**, 5237–5246.

92 C. Reichardt, Solvatochromic Dyes as Solvent Polarity Indicators, *Chem. Rev.*, 1994, **94**, 2319–2358.

93 A. V. Gorelov, A. Du Chesne and K. A. Dawson, Phase separation in dilute solutions of poly (N-isopropylacrylamide), *Phys. A*, 1997, **240**, 443–452.

94 P. W. Atkins and J. de Paula, *Atkins' physical chemistry*, Oxford Univ. Press, Oxford u.a, 9th edn, 2010.

95 M. J. Tiera, G. R. dos Santos, V. A. O. Tiera, N. A. B. Vieira, E. Frolini, R. C. da Silva and W. Loh, Aqueous solution behavior of thermosensitive (N-isopropylacrylamide-acrylic acid-ethyl methacrylate) terpolymers, *Colloid Polym. Sci.*, 2005, **283**, 662–670.

96 L. Liu, Y. Shi, C. Liu, T. Wang, G. Liu and G. Zhang, Insight into the amplification by methylated urea of the anion specificity of macromolecules, *Soft Matter*, 2014, **10**, 2856–2862.

97 M. L. Ohnsorg, J. M. Ting, S. D. Jones, S. Jung, F. S. Bates and T. M. Reineke, Tuning PNIPAm self-assembly and thermoresponse: roles of hydrophobic end-groups and hydrophilic comonomer, *Polym. Chem.*, 2019, **10**, 3469–3479.

98 Q. Zhang, C. Weber, U. S. Schubert and R. Hoogenboom, Thermoresponsive polymers with lower critical solution temperature: from fundamental aspects and measuring techniques to recommended turbidimetry conditions, *Mater. Horiz.*, 2017, **4**, 109–116.

99 M. J. N. Junk, U. Jonas and D. Hinderberger, EPR spectroscopy reveals nanoinhomogeneities in the structure and reactivity of thermoresponsive hydrogels, *Small*, 2008, **4**, 1485–1493.

100 M. J. N. Junk, R. Berger and U. Jonas, Atomic force spectroscopy of thermoresponsive photo-cross-linked hydrogel films, *Langmuir*, 2010, **26**, 7262–7269.

101 F. M. Winnik, Phase transition of aqueous poly-(N-isopropylacrylamide) solutions: a study by non-radiative energy transfer, *Polymer*, 1990, **31**, 2125–2134.

102 T. Kawaguchi, Y. Kojima, M. Osa and T. Yoshizaki, Cloud Points in Aqueous Poly(N-isopropylacrylamide) Solutions, *Polym. J.*, 2008, **40**, 455–459.

103 T. Kawaguchi, K. Kobayashi, M. Osa and T. Yoshizaki, Is a "cloud-point curve" in aqueous poly(N-isopropylacrylamide) solution binodal?, *J. Phys. Chem. B*, 2009, **113**, 5440–5447.

104 G. J. Lee, D. Kim and M. Lee, Photophysical properties and photoisomerization processes of Methyl Red embedded in rigid polymer, *Appl. Opt.*, 1995, **34**, 138–143.

This journal is © The Royal Society of Chemistry 2022

Electronic Supplementary Material (ESI) for Polymer Chemistry.
This journal is © The Royal Society of Chemistry 2022

Electronic Supporting Information (ESI)

Thermal Response and Thermochromism of Methyl Red-Based Copolymer Systems - Coupled Responsiveness in Critical Solution Behaviour and Optical Absorption Properties

Thorben Jaik[1]; Betty Ciubini[2]; Francesca Frascella[2]; Ulrich Jonas[1*]

[1] Department Chemistry - Biology, University of Siegen, Adolf-Reichwein-Strasse 2, D-57076, Siegen, Germany

[2] Department of Applied Science and Technology, Politecnico di Torino, Corso Duca degli Abruzzi 24, IT-10129, Torino, Italy

*Corresponding author: Prof. Dr. Ulrich Jonas, jonas@chemie.uni-siegen.de

This document contains experimental details like syntheses and sample preparations, additional optical analysis data, graphs from the van't Hoff analyses, etc.

Experimentals:

Materials and equipment:

All solvents used were of Milli-Q®, spectroscopic or HPLC-grade. Absolute ethanol was purchased from VWR Chemicals. Tetrahydrofurane was dried and distilled over potassium. Trifluoroacetic acid was purchased from Carl Roth (Germany) in PEPTIPURE® ≥99,9% quality. Sulfuric acid (≥95%, Fisher Chemical), hydrochloric acid (37%, Anal. Reag. Gr., Fisher Chemical), acetic acid (Anal. Reag. Gr., ChemSolute), methyl red (Alfa Aesar), carbonyldiimidazole (97%, Alfa Aesar), *N*-(2-hydroxyethyl)acrylamide (97%, Sigma Aldrich), 4-aminobenzoic acid (Merck) and 3-aminobenzoic acid (98%, Merck) were used as received. 1,8-Diazabicyclo[5.4.0]undec-7-ene was dried over calciumchloride (anhydrous, technical, Bernd Kraft) and distilled *in vacuo*. *N*-Isopropylacrylamide was recrystallised from n-hexane. Azobisisobutyronitrile was recrystallised from methanol. 4-Benzophenoneacrylamide was synthesised according to literature.[1] 4-(3-

Triethoxysilyl)propoxybenzophenone was synthesised by Mr. Daniel John according to literature.[2]

UV-vis measurements were performed on a Thermo Scientific™ Evolution™ 220 UV-Vis-spectrophotometer. If not stated otherwise, the measurements were done with 100 nm/min and a resolution of 1 nm.

NMR-measurements were performed on either a Bruker AV 400 or a Jeol EZC 500. Detailed assignments of peaks are given in the ESI in the corresponding spectra.

GPC/SEC was measured on a PSS GRAM linM column (Polymer Standards Service GmbH, Mainz, Germany) in dimethylacetamide with LiBr (0.1 g/L) at 60 °C with PMMA-standards as reference.

Synthesis of methyl red imidazolide:

Methyl red (1 mol eq.) was dissolved in tetrahydrofuran (0.1 mmol/L), carbonyldiimidazole (1.8 mol eq.) was added and the solution was stirred until no more gas evolution occurred, typically overnight or for three hours at 45 °C. The solution was used without purification for further syntheses. (Adapted from literature[3-5])

Synthesis of 2-(prop-2-enamido)ethyl-2-[(1E)-2-[4-(dimethylamino)phenyl]diazen-1-yl]benzoate (o-methyl red ester of N-(2-hydroxyethyl)acrylamide, o-MREAm):

To a solution of methyl red imidazolide in tetrahydrofuran (0.1 mmol/L), *N*-(2-hydroxyethyl)acrylamide (2 mol eq.) and 1,8-diazabicyclo[5.4.0]undec-7-ene (1.5 mol eq.) were added. The reaction mixture was stirred overnight, before the reaction was stopped by addition of acetic acid. The solvent was removed azeotropically with toluene and the remaining solid extracted with water. The product was purified via column chromatography on neutral AlOx in ethyl acetate, followed by column chromatography on silica in diethylether. The yield was 90%.

δH(400 MHz; $CDCl_3$) 7.82 (d, J = 9.3 Hz, 2H; Ph-*H*), 7.74 (dd, J = 7.9, 1.1 Hz, 1H; Ph-*H*), 7.56 (qd, J = 7.9, 1.6 Hz, 2H; Ph-*H*), 7.39 (ddd, J = 7.6, 6.7, 1.9 Hz, 1H; Ph-*H*), 6.72 (d, J = 9.3 Hz, 2H; Ph-*H*), 6.12 (dd, J = 17.0, 1.5 Hz, 1H; CHC*H*H(trans)), 5.85 (s, br, 1H; CON*H*), 5.63 (dd, J = 17.0, 10.4 Hz, 1H; C*H*CHH), 5.43 (dd, J = 10.4, 1.5 Hz, 1H; CHCH*H*(cis)), 4.39 (t, J = 5.0 Hz, 2H; COOCH_2), 3.59 (q, J = 5.3 Hz, 2H; CONHCH_2), 3.07 (s, 6H; $N(Me)_2$).

δC(101 MHz; $CDCl_3$) δ 168.61 (COO), 165.49 (CONH), 152.99 (Ph), 152.54 (Ph), 143.54 (Ph), 132.08 (Ph), 130.59 ($COCHCH_2$), 129.70 (Ph), 128.50 (Ph), 127.72 (Ph), 126.36 ($COCHCH_2$), 125.35 (Ph), 119.50 (Ph), 111.70 (Ph), 64.35 ($COOCH_2$), 40.35 ($N(Me)_2$), 38.79 ($CONHCH_2$).

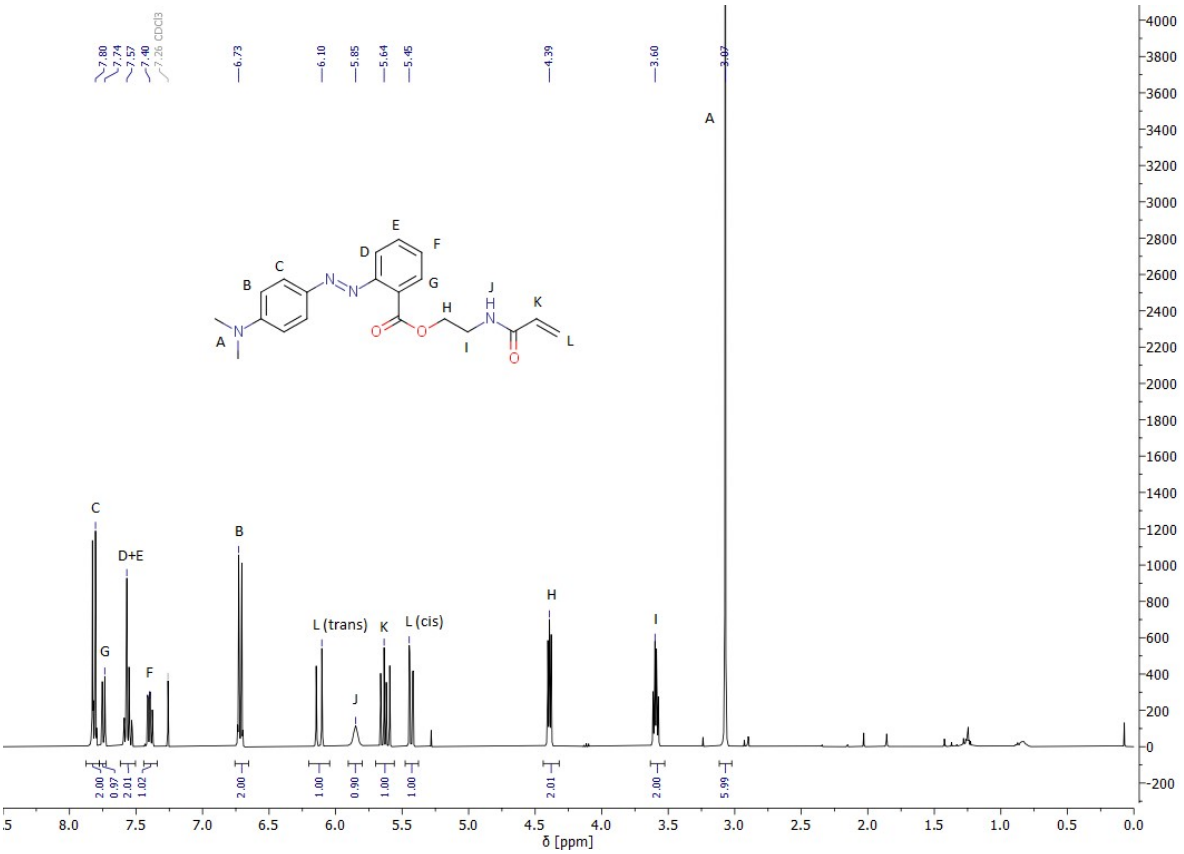

Figure S 1: [1]H-NMR spectrum (400 MHz) in $CDCl_3$ of 2-(prop-2-enamido)ethyl-2-[(1E)-2-[4-(dimethylamino)phenyl]diazen-1-yl]benzoate (o-methyl red ester of N-(2-hydroxyethyl)acrylamide, o-MREAm).

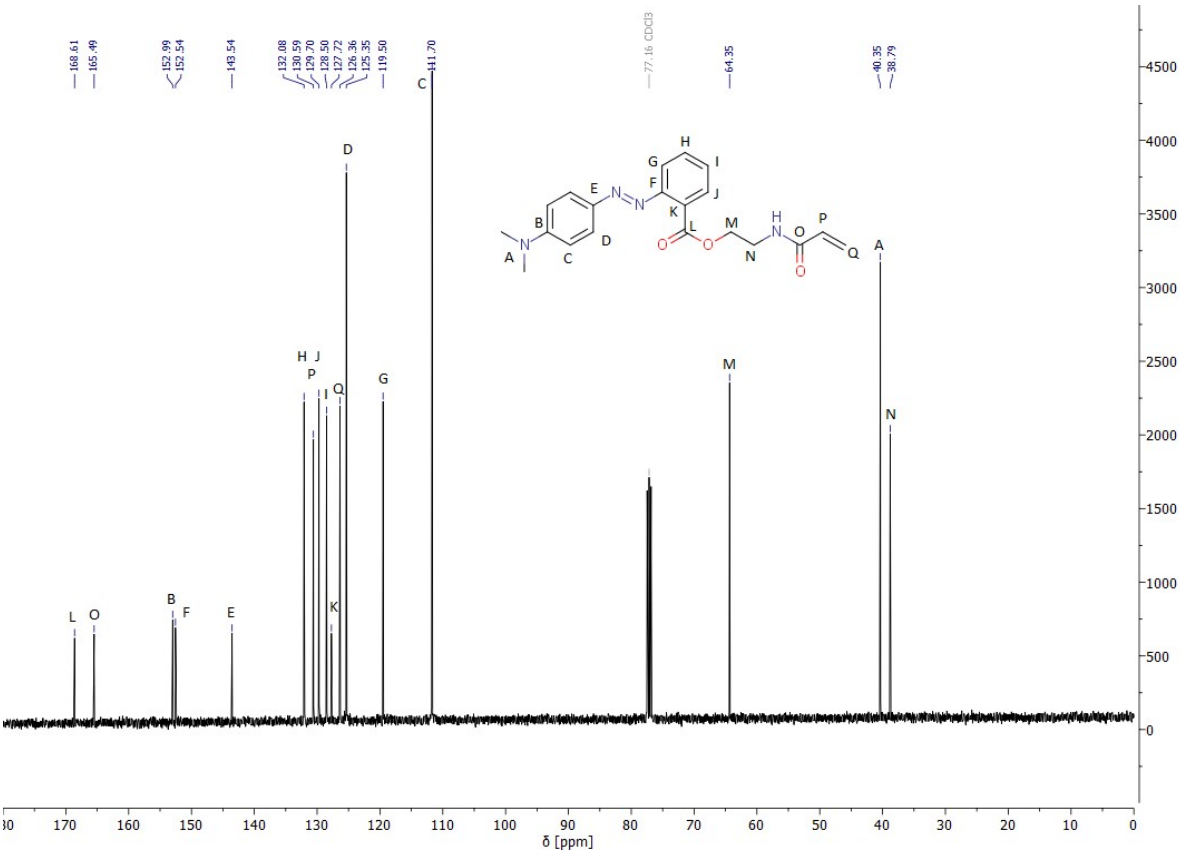

Figure S 2: ^{13}C-NMR spectrum (133 MHz) in $CDCl_3$ of 2-(prop-2-enamido)ethyl-2-[(1E)-2-[4-(dimethylamino)phenyl]diazen-1-yl]benzoate (o-methyl red ester of N-(2-hydroxyethyl)acrylamide, o-MREAm).

Synthesis of 4-[(1E)-2-[4-(dimethylamino)phenyl]diazen-1-yl]benzoic acid (p-methyl red, p-MR):

4-Aminobenzoic acid (1412 mg, $1.0*10^{-2}$ mol) was dispersed in concentrated hydrochloric acid (4.5 mL) and cooled to 0 °C. An aqueous solution of sodium nitrite (713 mg, $1.0*10^{-2}$ mol) was added dropwise to the slurry over the course of 40 minutes and the resulting turbid mixture was stirred at 0 °C for another 40 minutes. Five minutes after the cooling was removed, it was added to a solution of N,N-dimethylanilin (1.5 mL, $1.2*10^{-2}$ mol) in water (100 mL, pH6). After 2.5 hours, the red precipitate was filtered off. The filtrate was neutralised with a saturated solution of $NaHCO_3$ and the precipitate filtered again. The solids were combined, washed with copious amounts of water and heated under reflux in H_2O:EtOH (1:1, 60 mL) for several hours, before cooling to room temperature and filtration. The yield was 2219 mg or 80%. This procedure was adapted from literature,[6] additionally reporting yield and NMR data.

δH(400 MHz; DMSO-d^6) 8.07 (d, J = 8.6 Hz, 2H; Ph-*H*), 7.83 (d, J = 8.6 Hz, 2H; Ph-*H*), 7.82 (d, J = 9.1 Hz, 2H; Ph-*H*), 6.83 (d, J = 9.4 Hz, 2H; Ph-*H*), 3.07 (s, 6H; $N(Me)_2$).

δC(101 MHz, DMSO-d^6) 167.15 (COOH), 155.30 (Ph), 153.21 (Ph), 142.90 (Ph), 131.10 (Ph), 130.73 (Ph)S, 125.50 (Ph), 121.96 (Ph), 111.81 (Ph), 40.06 ($N(Me)_2$).

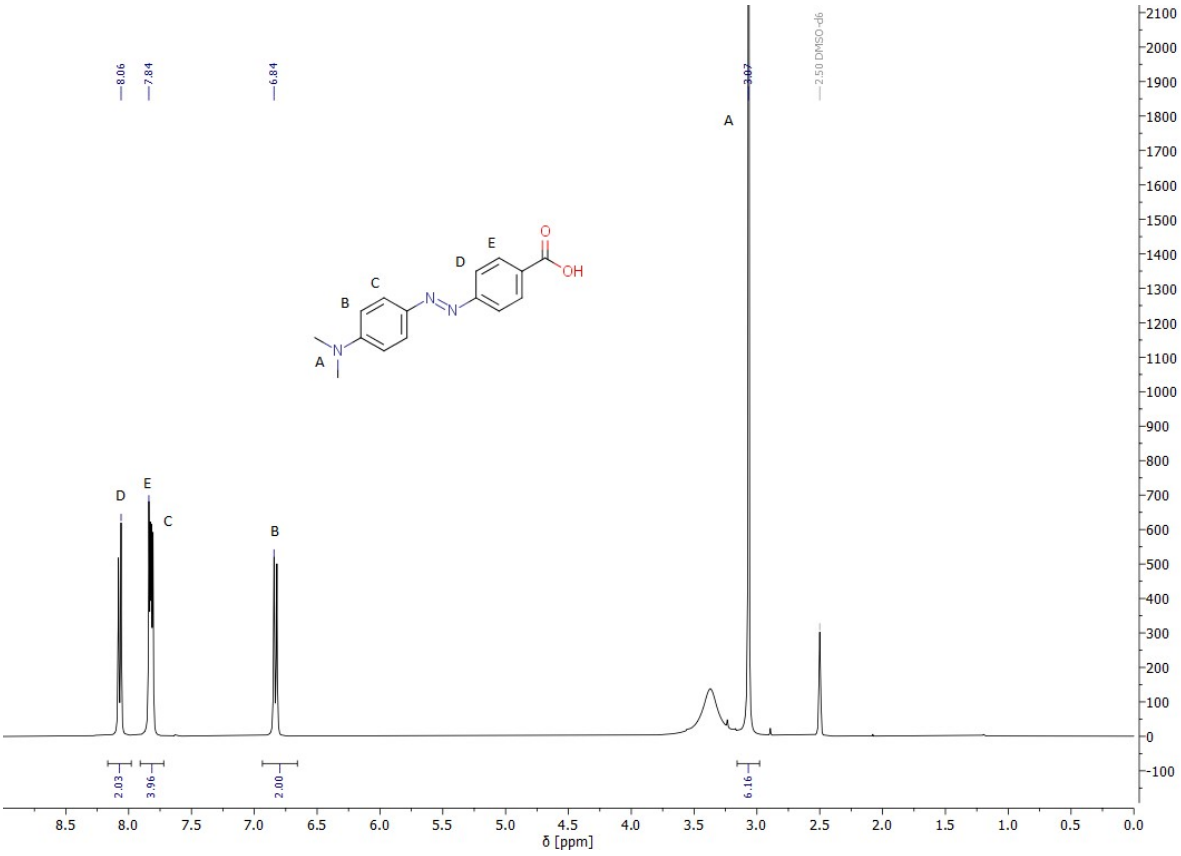

Figure S 3: ^{1}H-NMR spectrum (400 MHz) in DMSO-d^6 of 4-[(1E)-2-[4-(dimethylamino)phenyl]diazen-1-yl]benzoic acid (p-methyl red, p-MR.

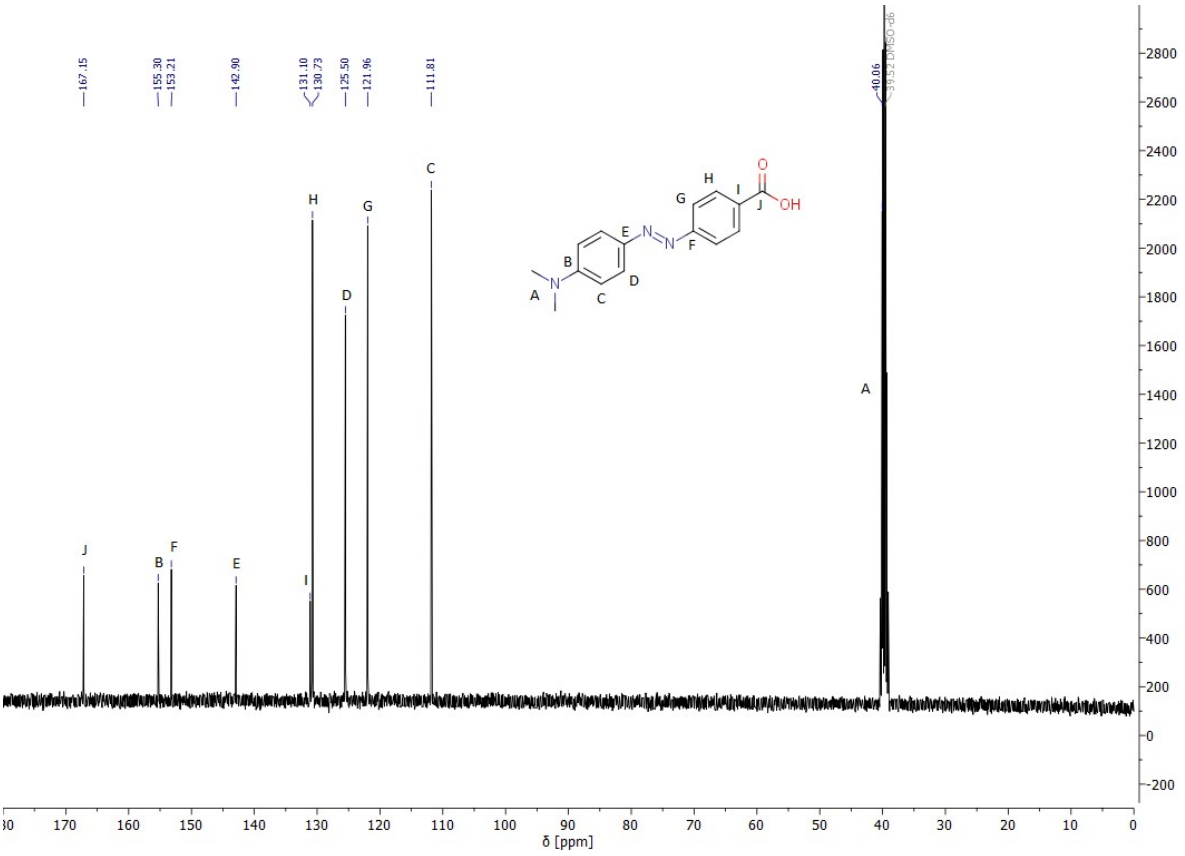

Figure S 4: ^{13}C-NMR spectrum (133 MHz) in DMSO-d^6 of 4-[(1E)-2-[4-(dimethylamino)phenyl]diazen-1-yl]benzoic acid (p-methyl red, p-MR.

Synthesis of 2-(prop-2-enamido)ethyl-4-[(1E)-2-[4-(dimethylamino)phenyl]diazen-1-yl]benzoate (p-methyl red ester of N-(2-hydroxyethyl)acrylamide, p-MREAm):

p-Methyl red (202 mg, 7.5*10^{-4} mol) and carbonyldiimidazole (184 mg, 1.1*10^{-3} mol) were dispersed in tetrahydrofuran (8 mL) and stirred at room temperature for 19 hours. *N*-(2-Hydroxyethyl)acrylamide (0.14 mL, 1.4*10^{-3} mol) and 1,8-diazabicyclo[5.4.0]undec-7-en (0.17 mL, 1.1*10^{-3} mol) were added. The solution was stirred for 1 hour, before the reaction was stopped by addition of acetic acid (5 mL). The organic solvent was removed *in vacuo* and the residue dispersed in water before it was extracted with dichloromethane. The organic phase was washed with brine. The product was purified *via* column chromatography on silica in diethylether. The yield was 252 mg or 92%.

δH(400 MHz; $CDCl_3$) 8.13 (d, J = 8.8 Hz, 2H; Ph-*H*), 7.90 (d, J = 9.2 Hz, 2H; Ph-*H*), 7.86 (d, J = 8.8 Hz, 2H; Ph-*H*), 6.75 (d, J = 9.4 Hz, 2H; Ph-*H*), 6.31 (dd, J = 17.1, 1.5 Hz, 1H; CHC*H*H(trans)), 6.13 (dd, J = 17.1, 10.2 Hz, 1H; C*H*CHH; overlapped 1H;

CON*H*), 5.66 (dd, J = 10.2, 1.5 Hz, 1H; CHCH*H*(cis)), 4.48 (t, J = 5.2 Hz, 2H; COOCH_2), 3.76 (q, J = 5.4 Hz, 2H; CONHCH_2), 3.11 (s, 6H; N(Me)$_2$).

δC(101 MHz, $CDCl_3$) 166.63 (COO), 165.84 (CONH), 156.35 (Ph), 153.09 (Ph), 143.81 (Ph), 130.79 (Ph), 130.71 (CO*C*HCH$_2$), 129.67 (Ph), 127.01 (COCH*C*H$_2$), 125.72 (Ph), 122.18 (Ph), 111.58 (Ph), 63.97 (COO*C*H$_2$), 40.41 (N(Me)$_2$), 39.22 (CONH*C*H$_2$).

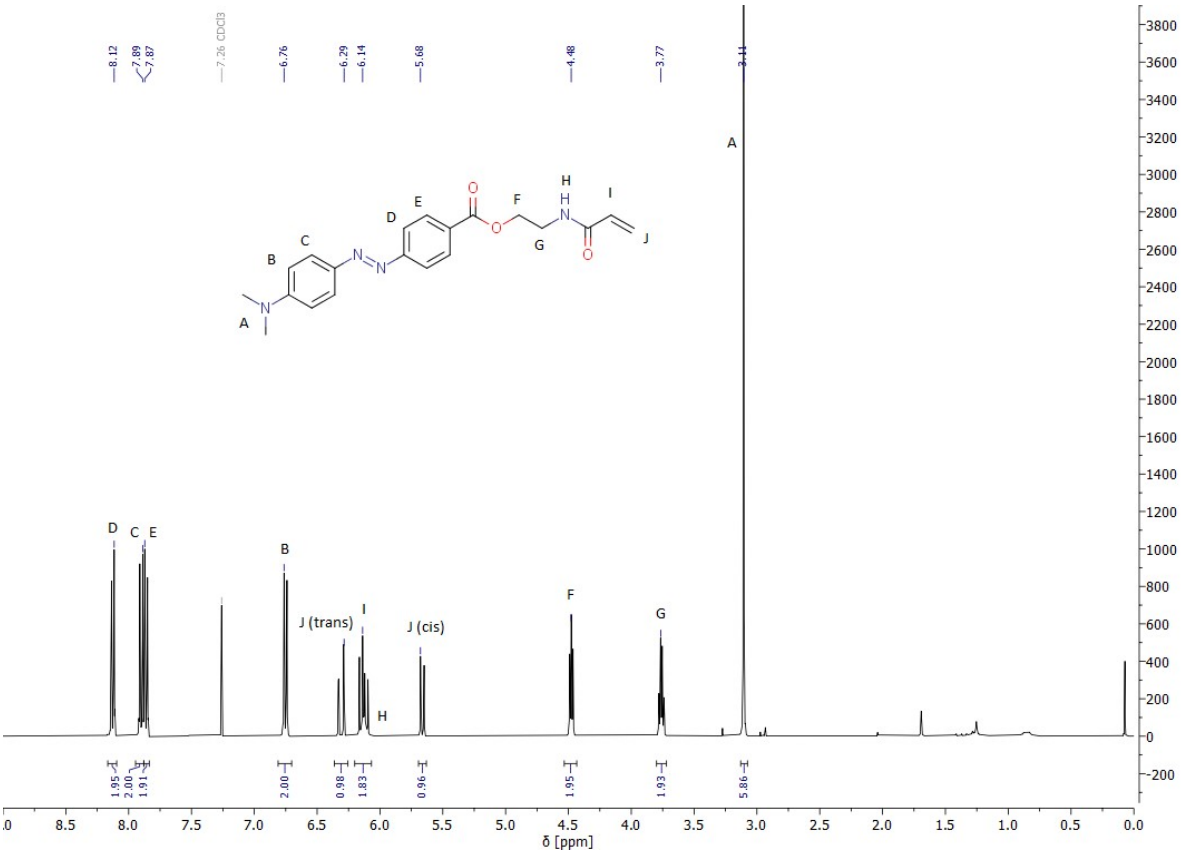

Figure S 5: ^{1}H-NMR spectrum (400 MHz) in $CDCl_3$ of 2-(prop-2-enamido)ethyl-4-[(1E)-2-[4-(dimethylamino)phenyl]diazen-1-yl]benzoate (p-methyl red ester of N-(2-hydroxyethyl)acrylamide, p-MREAm).

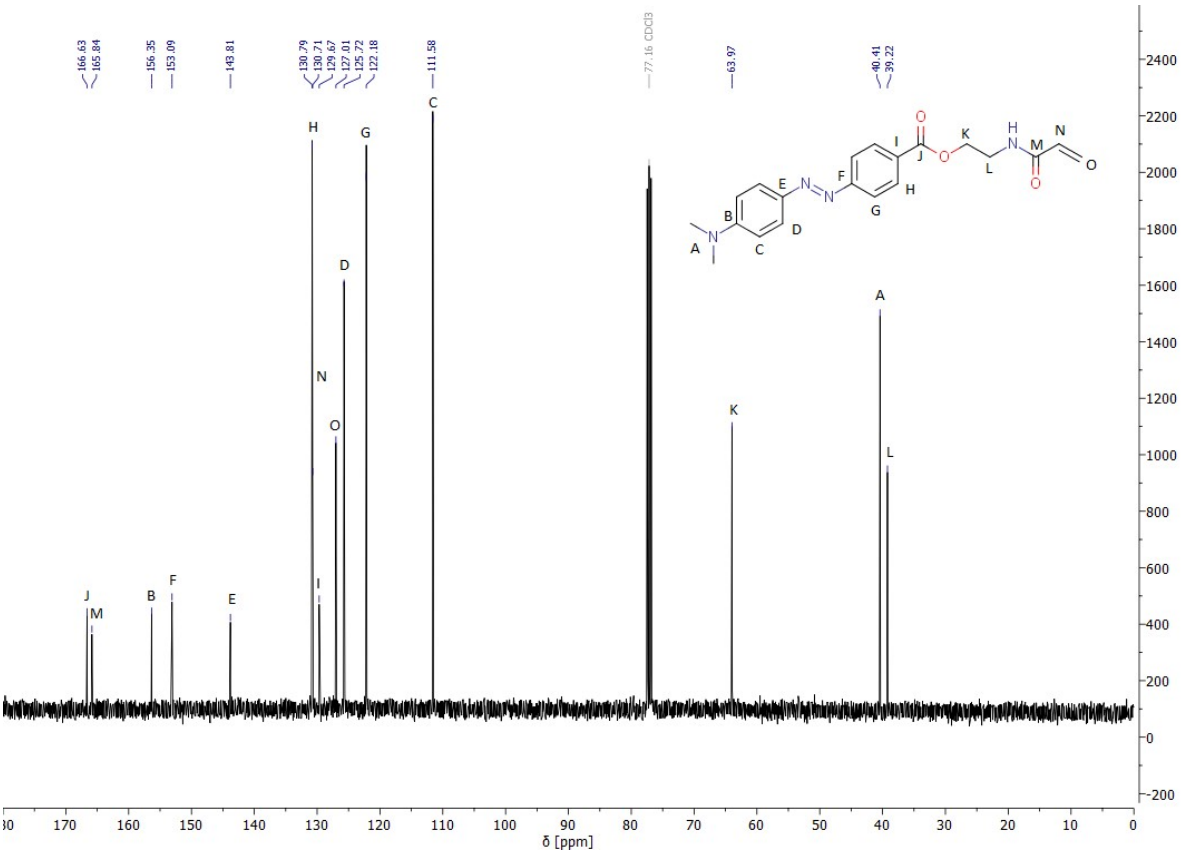

Figure S 6: ^{13}C-NMR spectrum (133 MHz) in $CDCl_3$ of 2-(prop-2-enamido)ethyl-4-[(1E)-2-[4-(dimethylamino)phenyl]diazen-1-yl]benzoate (p-methyl red ester of N-(2-hydroxyethyl)acrylamide, p-MREAm).

Synthesis of 3-[(1E)-2-[4-(dimethylamino)phenyl]diazen-1-yl]benzoic acid (m-methyl red, m-MR):

3-Aminobenzoic acid (141 mg, 1.0*10^{-3} mol) was dispersed in concentrated hydrochloric acid (0.45 mL) and cooled to 0 °C. A cooled aqueous solution of sodium nitrite (71.5 mg, 1.0*10^{-3} mol in 1 mL) was added dropwise to the slurry over the course of 40 minutes. The resulting turbid mixture was stirred at 0 °C for 50 minutes and at room temperature for another 20 minutes. It was added to a solution of *N,N*-dimethylanilin (0.15 mL, 1.2*10^{-3} mol) in water (10 mL, pH5). After 20 hours, the solution was neutralised with aq. NaOH (1M) and then extracted with dichloromethane until the aqueous phase was colourless. The organic phase was dried over magnesium sulfate and the solvent evaporated. The product was purified *via* column chromatography on silica in diethylether. The yield was 136 mg or 49%.

δH(500 MHz; DMSO-d^6) 8.29 (t, J = 1.8 Hz, 2H; Ph-*H*), 8.00 (ddt, J = 10.5, 7.7, 1.2 Hz, 2H; Ph-*H*), 7.83 (d, J = 9.2 Hz, 2H; Ph-*H*), 7.65 (t, J = 7.8 Hz, 1H; Ph-*H*), 6.83 (d, J = 9.3 Hz, 2H; Ph-*H*), 3.06 (s, 6H; $N(Me)_2$).

δC(126 MHz, DMSO-d^6) 166.99 (COO), 152.79 (Ph), 152.48 (Ph), 142.47 (Ph), 131.95 (Ph), 129.90 (Ph), 129.61 (Ph), 126.64 (Ph), 125.02 (Ph), 121.58 (Ph), 111.56 (Ph), 39.82 ($N(Me)_2$).

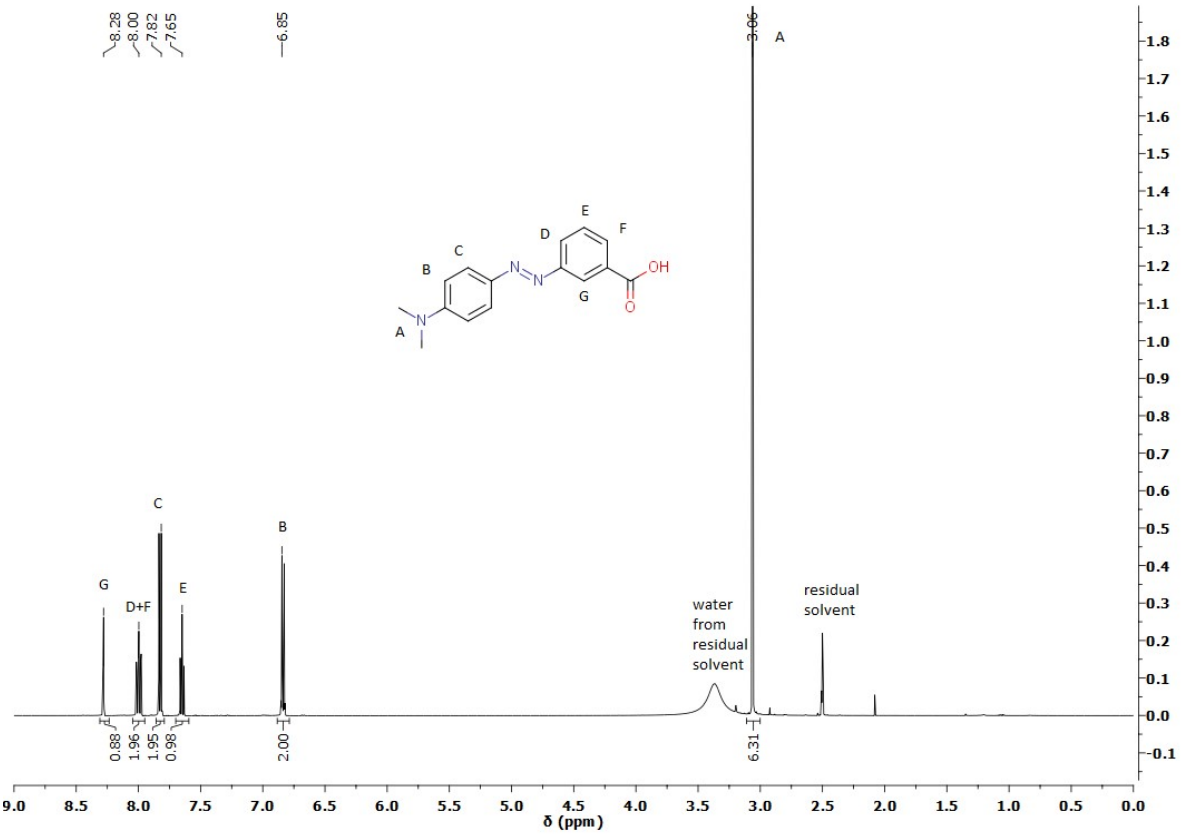

Figure S 7: ^{1}H-NMR spectrum (500 MHz) in DMSO-d^6 of 3-[(1E)-2-[4-(dimethylamino)phenyl]diazen-1-yl]benzoic acid (m-methyl red, m-MR).

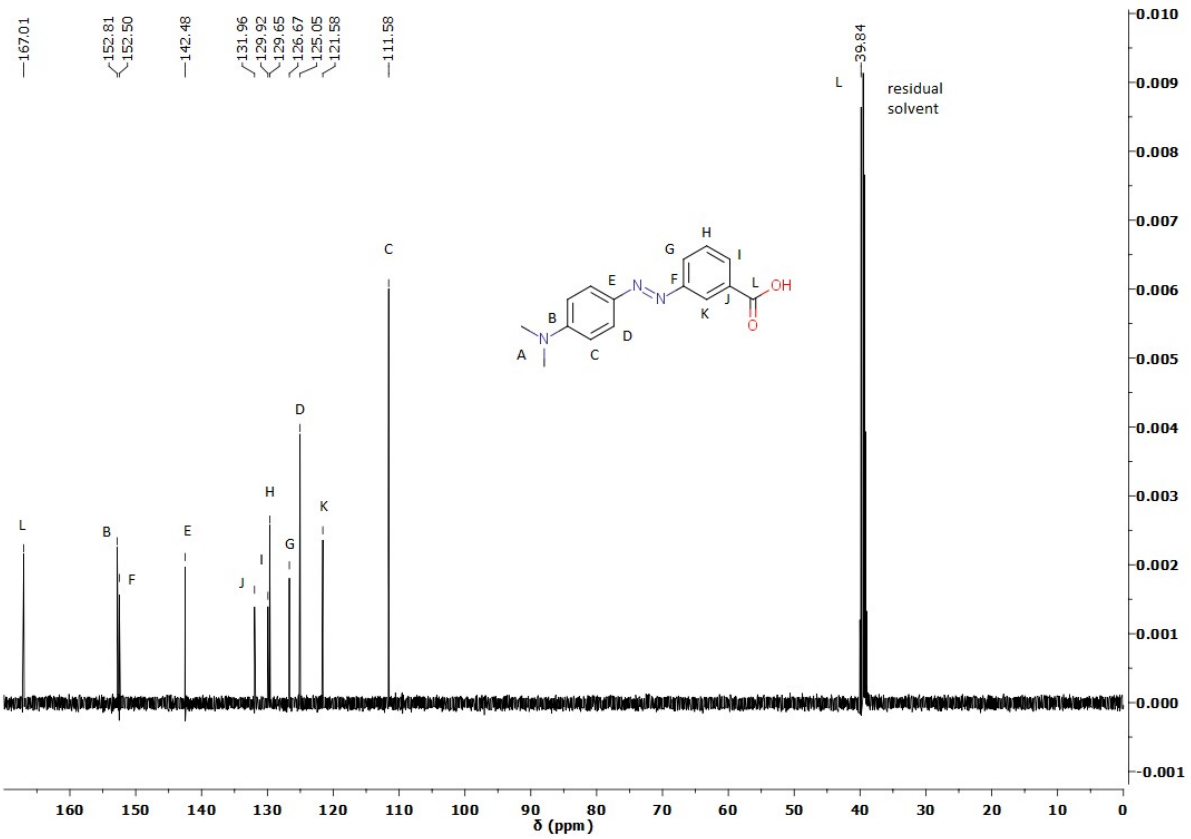

Figure S 8: ^{13}C-NMR spectrum (126 MHz) in DMSO-d^6 of 3-[(1E)-2-[4-(dimethylamino)phenyl]diazen-1-yl]benzoic acid (m-methyl red, m-MR).

Synthesis of 2-(prop-2-enamido)ethyl-3-[(1E)-2-[4-(dimethylamino)phenyl]diazen-1-yl]benzoate (m-methyl red ester of N-(2-hydroxyethyl)acrylamide, m-MREAm):

m-Methyl red (201 mg, 7.5*10^{-4} mol) and carbonyldiimidazole (185 mg, 1.1*10^{-3} mol) were dissolved in tetrahydrofuran (8 mL) and stirred at room temperature for 19 hours. *N*-(2-Hydroxyethyl)acrylamide (0.14 mL, 1.4*10^{-3} mol) and five minutes later 1,8-diazabicyclo[5.4.0]undec-7en (0.17 mL, 1.1*10^{-3} mol) were added. The reaction mixture was stirred for three hours before the reaction was stopped via addition of acetic acid (5 mL).

The solvent was distilled of *in vacuo*, the leftover slurry dissolved in dichloromethane and the organic phase extracted with water. The product was then purified by column chromatography on silica in diethylether. The yield was 247 mg or 90%.

δH(500 MHz, DMSO-d^6) 8.39 (t, J = 5.6 Hz, 1H; Ph-*H*), 8.31 (t, J = 1.6 Hz, 1H; Ph-*H*), 8.03 (ddd, J = 3.6, 1.9, 1.2 Hz, 1H; Ph-*H*), 8.02 (dq, J = 1.9, 1.2 Hz, 1H; Ph-*H*), 7.83 (d, J = 9.3 Hz, 2H; Ph-*H*), 7.67 (t, J = 7.8 Hz, 1H; Ph-*H*), 6.85 (d, J = 9.4 Hz, 2H; Ph-*H*), 6.25 (dd, J = 17.1, 10.2 Hz, 1H; CHC*H*H(trans)), 6.11 (dd, J = 17.1, 2.2 Hz, 1H;

C*H*CHH), 5.60 (dd, J = 10.2, 2.2 Hz, 1H; CHCH*H*(cis)), 4.36 (t, J = 5.5 Hz, 2H; COOCH_2), 3.56 (q, J = 5.8 Hz, 2H; CONHCH_2), 3.07 (s, 6H; N(Me)$_2$).

δC(126 MHz, DMSO-d^6) 165.47 (COO), 165.02 (CONH), 152.88 (Ph), 152.54 (Ph), 142.46 (Ph), 131.57 (CO*C*HCH$_2$), 130.86 (Ph), 129.90 (Ph), 129.76 (Ph), 126.49 (Ph), 125.46 (COCH*C*H$_2$), 125.11 (Ph), 122.15 (Ph), 111.59 (Ph), 63.79 (COO*C*H$_2$), 39. (N(Me)$_2$), 37.79 (CONH*C*H$_2$).

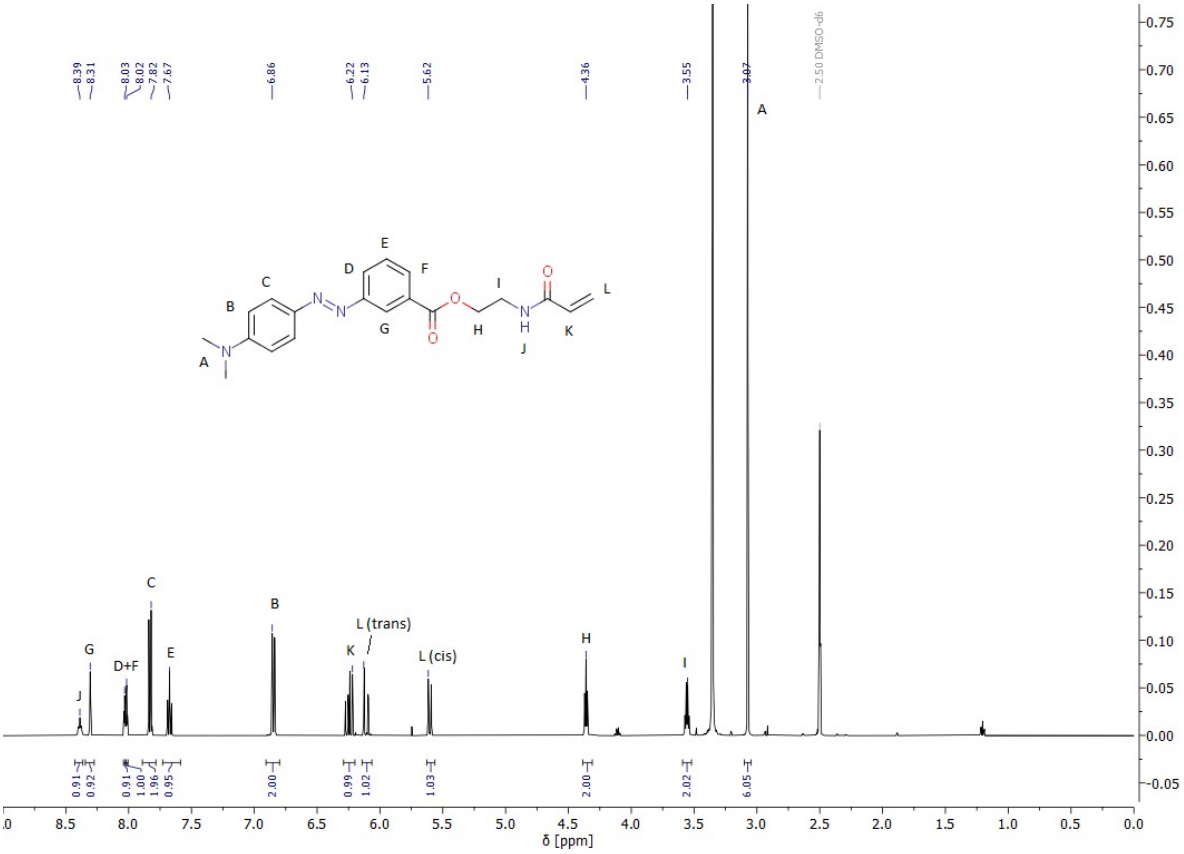

Figure S 9: ^{1}H-NMR spectrum (500 MHz) in DMSO-d^6 of 2-(prop-2-enamido)ethyl-3-[(1E)-2-[4-(dimethylamino)phenyl]diazen-1-yl]benzoate (m-methyl red ester of N-(2-hydroxyethyl)acrylamide, m-MREAm).

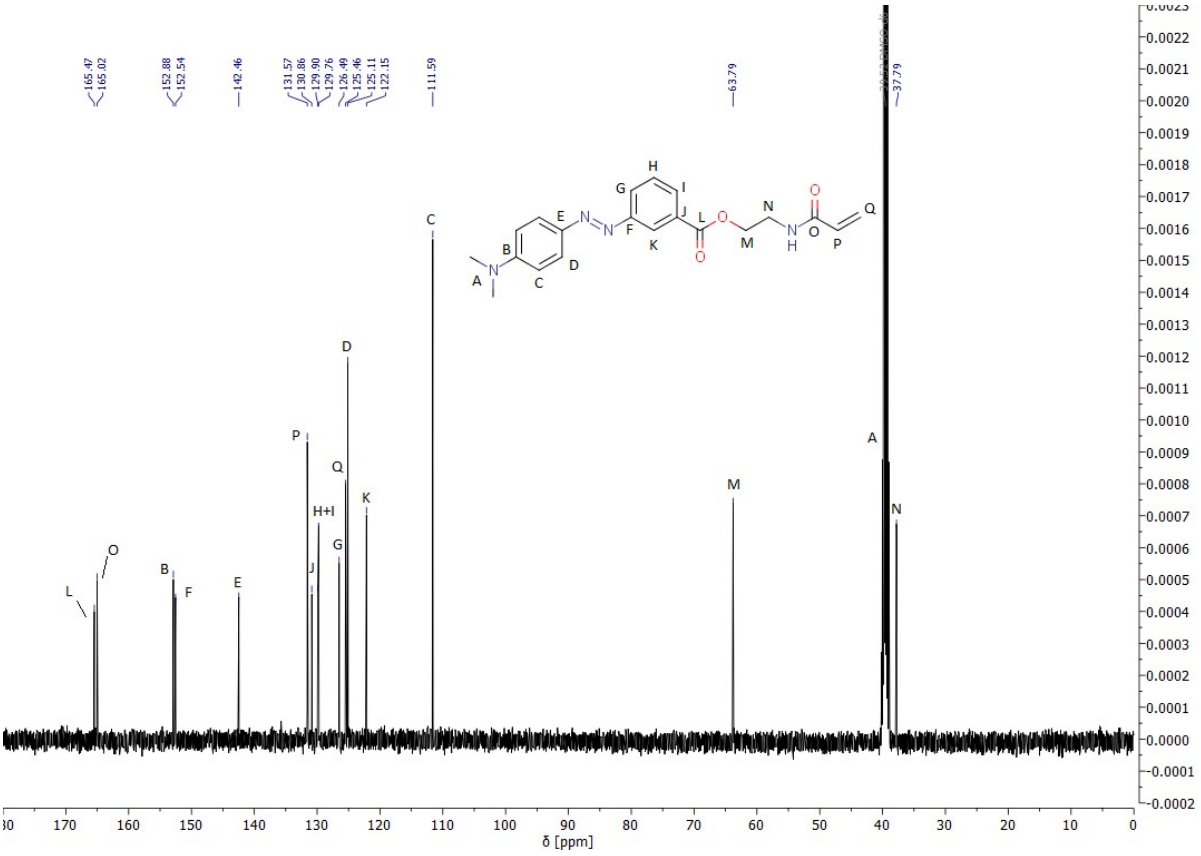

Figure S 10: ^{13}C-NMR spectrum (133 MHz) in DMSO-d^6 of 2-(prop-2-enamido)ethyl-3-[(1E)-2-[4-(dimethylamino)phenyl]diazen-1-yl]benzoate (m-methyl red ester of N-(2-hydroxyethyl)acrylamide, m-MREAm).

Copolymerisations with o-MREAm:

The different copolymers were obtained by radical polymerisation. The monomers (0.6 mol/L) and azobisisobutyronitrile were dissolved in 1,4-dioxane or methanol. The solutions were purged with nitrogen for 30 minutes and heated in an oil bath at 75 °C for 1,4-dioxane or 60 °C for methanol for 24 to 63 hours. The polymers were then precipitated up to three times in a non-solvent. The details are summarised in Table S 1.

P1 (poly(HEAm-co-o-MREAm-co-BPAAm)): δH(500 MHz, MeOD) 8.5-6.5 (br, aromatic H), 4.57 (COOCH_2), 4.38 (Ar-CONHCH_2), 3.66 (CH_2CH_2OH), 3.51-3.12 (CONHCH_2), 2.4-1.25 (backbone)

P2 (poly(NiPAAm-co-HEAm-co-o-MREAm-co-BPAAm)): δH(500 MHz, D_2O) 8.0-6.5 (br, aromatic H), 4.41 (COOCH_2), 3.91 (NHCH(CH_3)$_2$), 3.68 (CH_2CH_2OH), 3.36 (CONHCH_2), 2.3-1.25 (backbone), 1.16 (NHCH(CH_3)$_2$)

P2b (poly(NiPAAm-co-HEAm-co-o-MREAm-co-BPAAm)): δH(400 MHz, MeOD) 8.0-6.75 (br, aromatic H), 4.38 (COOCH_2), 3.96 (NHCH(CH_3)$_2$), 3.65 (CH_2CH_2OH), 3.12 (N(Me)$_2$), 2.3-1.25 (backbone), 1.16 (NHCH(CH_3)$_2$)

P3 (poly(HEAm-co-MAA-co-o-MREAm-co-BPAAm)): δH(400 MHz, D_2O) 8.5-6.5 (br, aromatic H), 4.42 (COOCH_2), 3.66 (CH_2CH_2OH), 3.34 (CONHCH_2), 2.4-1.25 (backbone), 1.00 (backbone-CH_3)

P4 (poly(NiPAAm-co-MAA-co-o-MREAm-co-BPAAm)): δH(500 MHz, MeOD) 8.0-6.5 (br, aromatic H), 4.58 (COOCH_2), 4.38 (Ar-CONHCH_2), 3.91 (NHCH(CH_3)$_2$), 3.12 (N(Me)$_2$), 2.3-1.25 (backbone), 1.16 (NHCH(CH_3)$_2$)

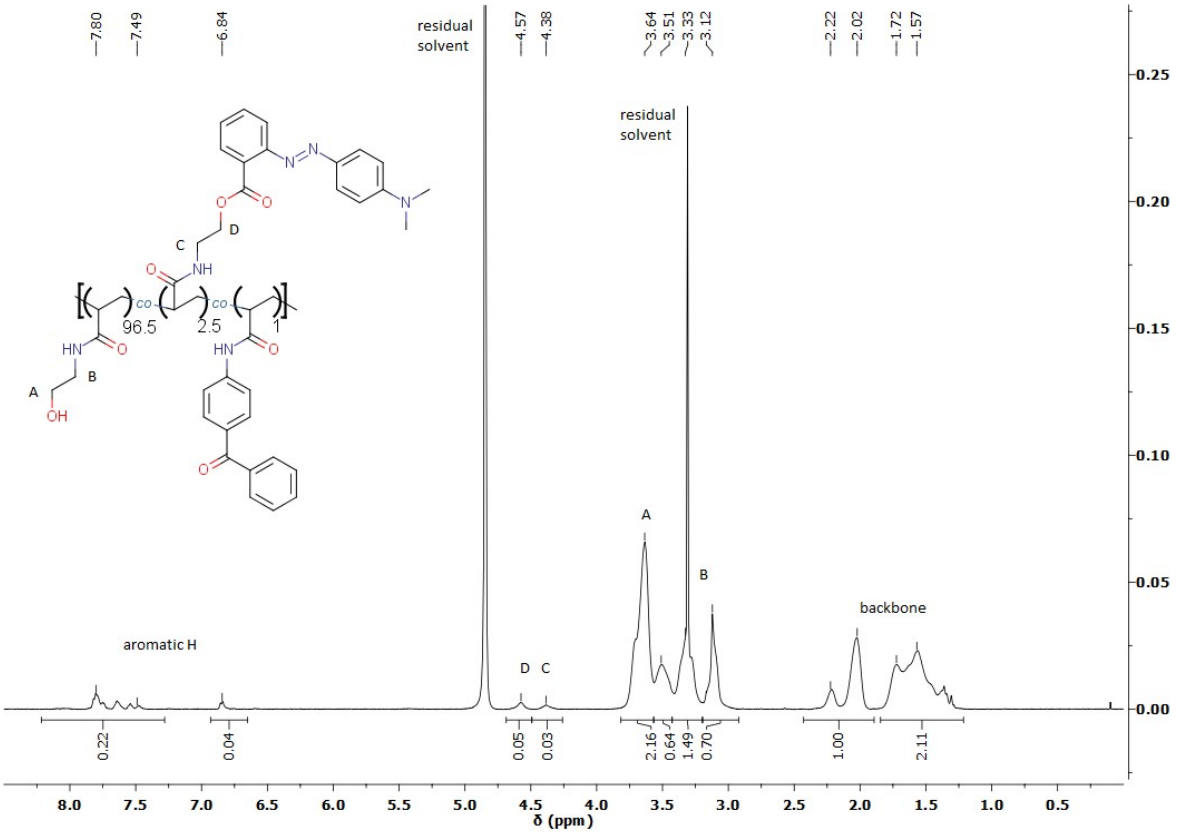

Figure S 11: [1]H-NMR spectrum (500 MHz) in MeOD of a poly(HEAm-co-o-MREAm-co-BPAAm) copolymer (P1) (feed: HEAm:o-MREAm:BPAAm 96.5:2.5:1).

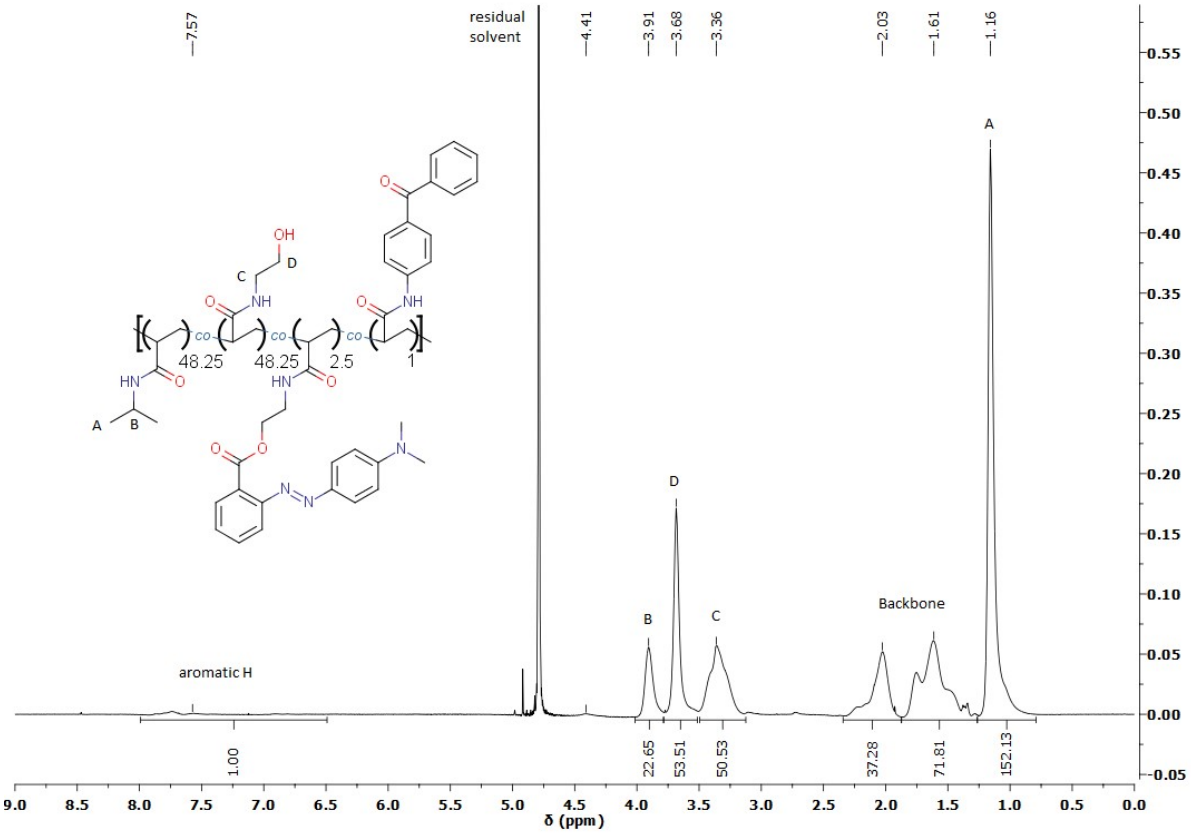

Figure S 12: [1]H-NMR spectrum (500 MHz) in D_2O of a poly(NiPAAm-co-HEAm-co-o-MREAm-co-BPAAm) copolymer (P2) (feed: NiPAAm:HEAm:o-MREAm:BPAAm 48.25:48.25:2.5:1).

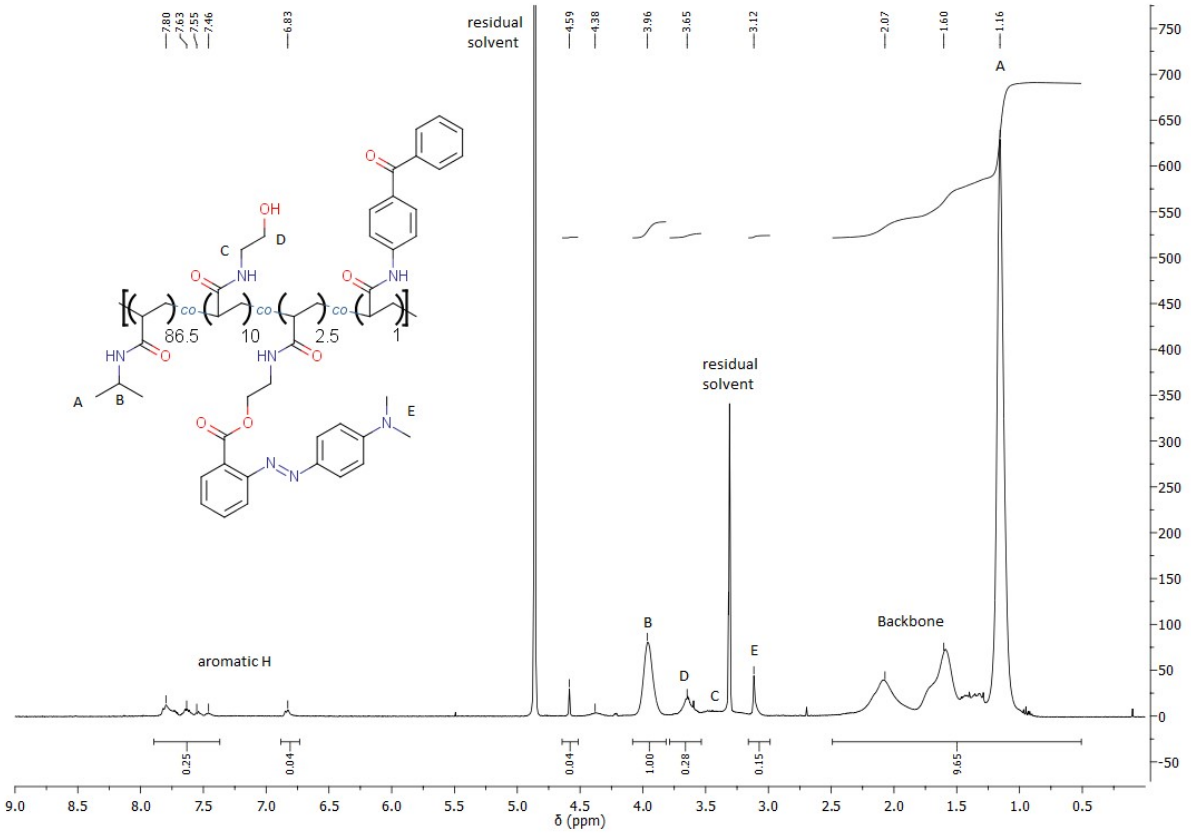

Figure S 13: [1]H-NMR spectrum (400 MHz) in MeOD of a poly(NiPAAm-co-HEAm-co-o-MREAm-co-BPAAm) copolymer (P2b) (feed: NiPAAm:HEAm:o-MREAm:BPAAm 87.2:9.2:2.6:1).

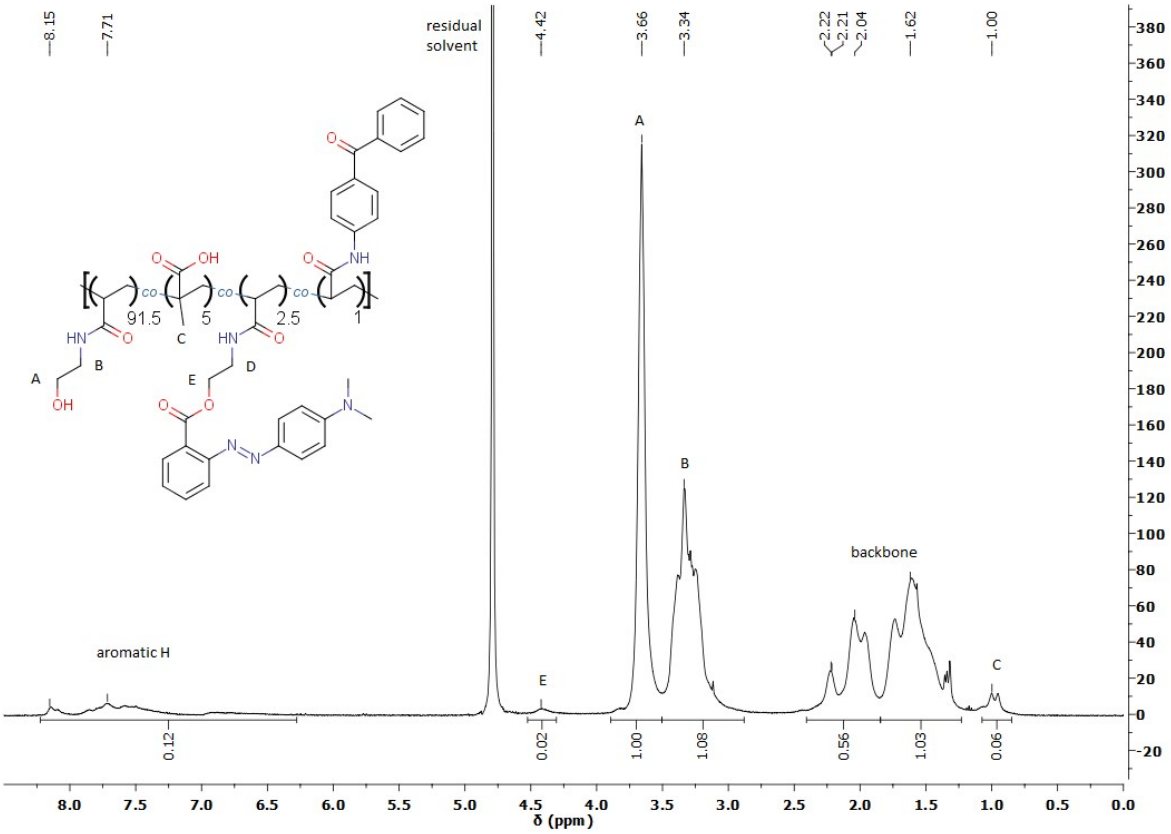

Figure S 14: [1]H-NMR spectrum (400 MHz) in D_2O of a poly(HEAm-co-MAA-co-o-MREAm-co-BPAAm) copolymer (P3) (feed: HEAm:MAA:o-MREAm:BPAAm 91.5:5:2.5:1).

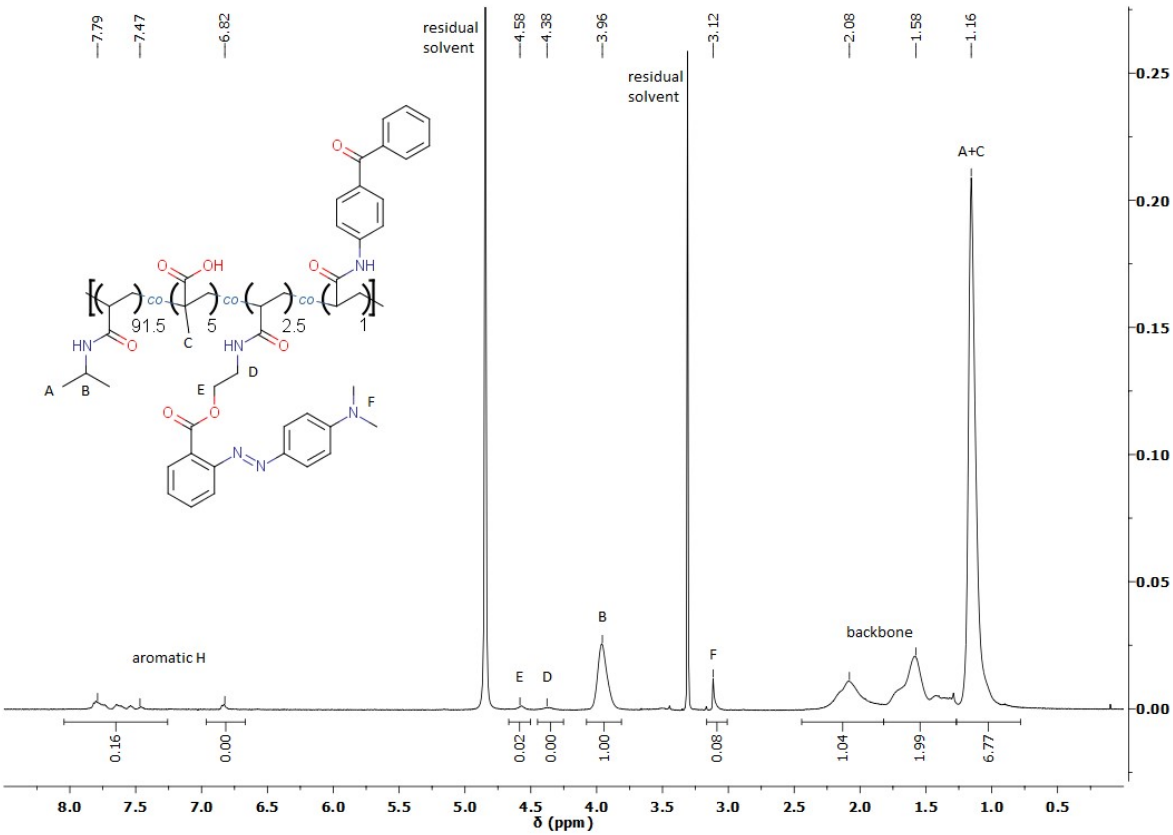

Figure S 15: [1]H-NMR spectrum (500 MHz) in MeOD of a poly(NiPAAm-co-MAA-co-o-MREAm-co-BPAAm) copolymer (P4) (feed: NiPAAm:MAA:o-MREAm:BPAAm 91.8:4.9:2.3:1).

Table S 1: Feed composition in mol% and reaction parameters for the different copolymersations.

Polymer	NiPAAm [%]	HEAm [%]	MAA [%]	MREAm [%]	BPAAm [%]	AIBN [%]	T [°C]	Time [h]	Solvent	Non-solvent
1	0	96.5	0	2.5	1	2	60	24	Methanol	Ethyl acetate
2	48.25	48.25	0	2.5	1	2	60	48	Methanol	Diethylether
2b	87.2	9.2	0	2.6	1	2	60	26	1,4-Dioxane	Diethylether
3	0	91.5	5	2.5	1	2.1	60	63	Methanol	Acetone
4	91.8	0	4.9	2.3	1	1.9	75	24	1,4-Dioxane	Diethylether

Film preparation:

The glass slides used in photocrosslinking experiments were cleaned with fresh Carothers' acid (sulfuric acid:hydrogen peroxide, 3:1) and rinsed thoroughly with water. The slides were dried under a nitrogen stream. They were submerged in an ethanolic solution of benzophenone silane (1 mmol/L) for 24 hours before they were rinsed thrice with absolute ethanol and finally dried under a nitrogen stream.

Polymers were drop-casted on the glass slides from methanolic solution (1 w%, 200 µL on 2.4cmx2.4cm slides). Photocrosslinking was performed at 302 nm with an energy of 20.3 J/cm². The polymer films of P1 and P2 were annealed at 170 °C prior to photocrosslinking. All films were washed with water until the supernatant remained colourless before thermochromicity measurements.

General reference graphs and UV-vis data for thermochromic changes of different systems:

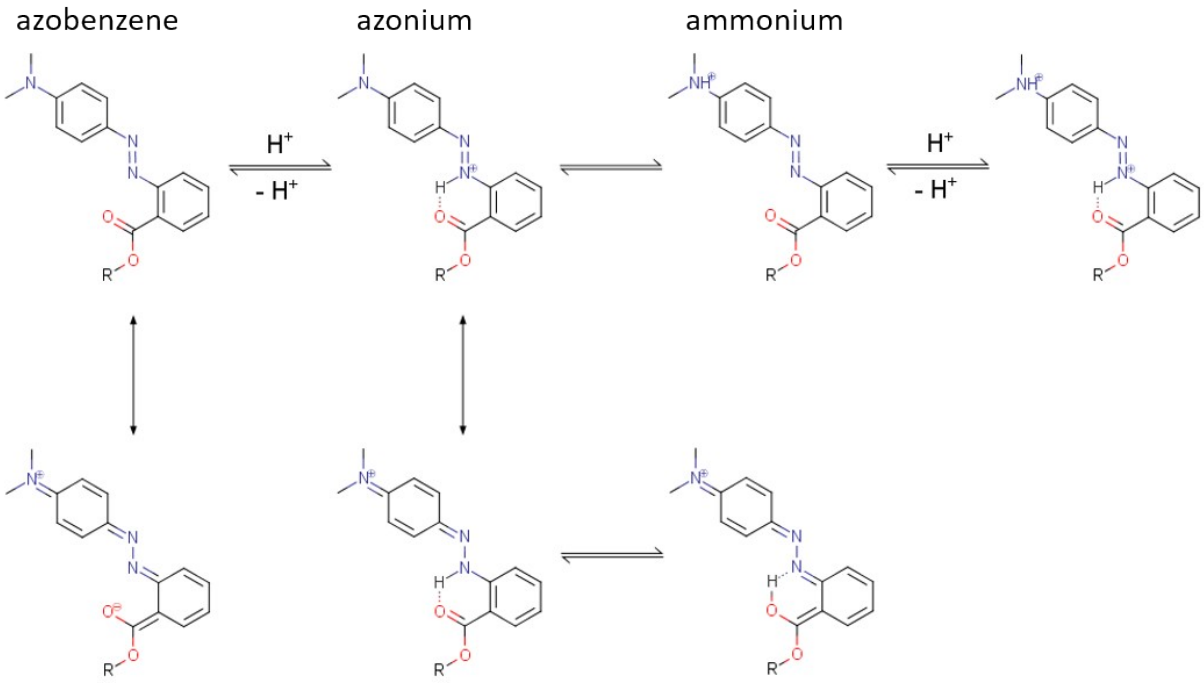

Scheme S 1: Protonation equilibrium of a methyl red derivative showing the azonium, ammonium and diprotonated forms and important mesomeric structures.

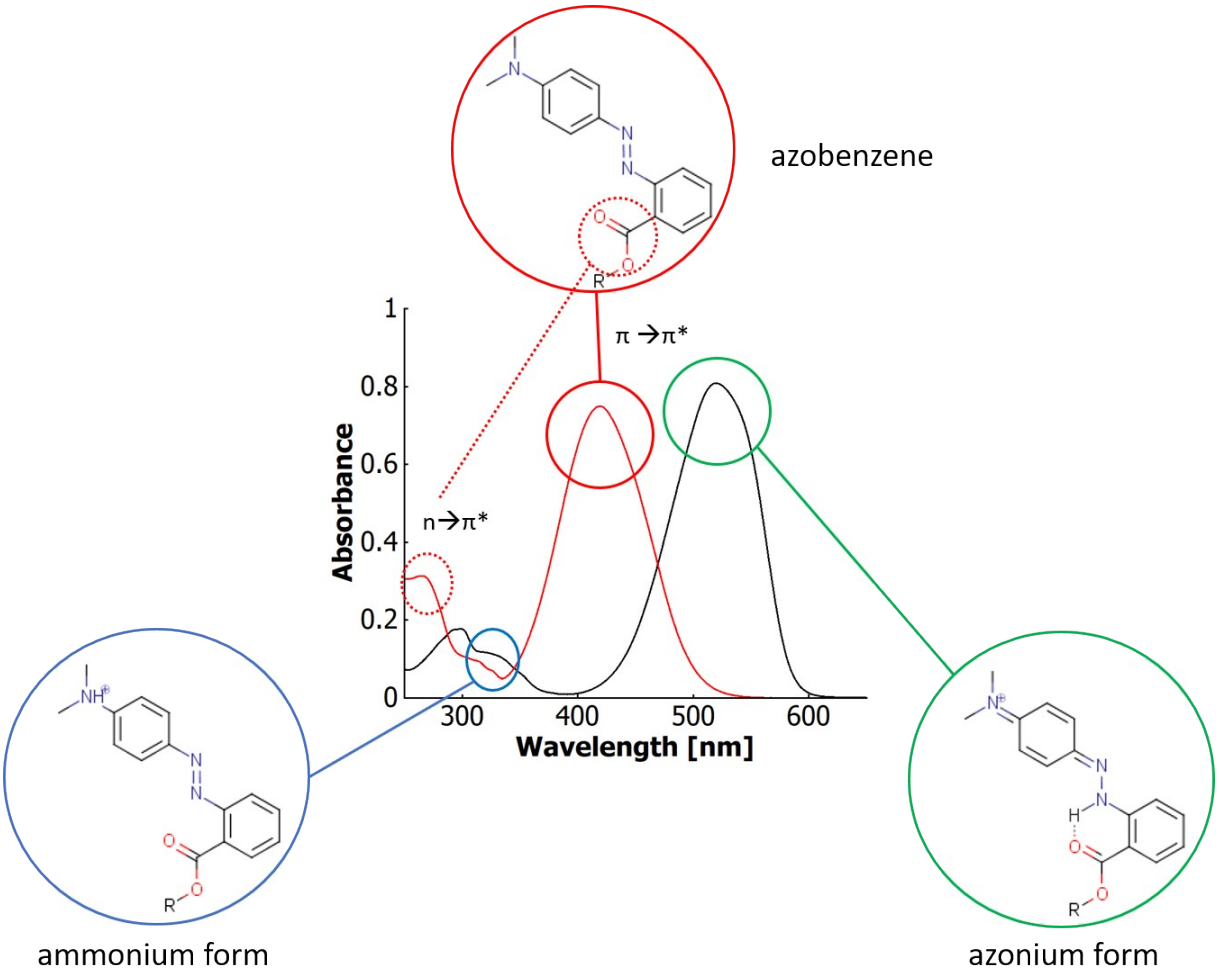

Figure S 16: UV-vis spectra of the neutral and protonated form of a methyl red ester of N-(2-hydroxyethyl)acrylamide with the important absorption bands colour marked with the related structure (bands assigned according to literature [7-9]).

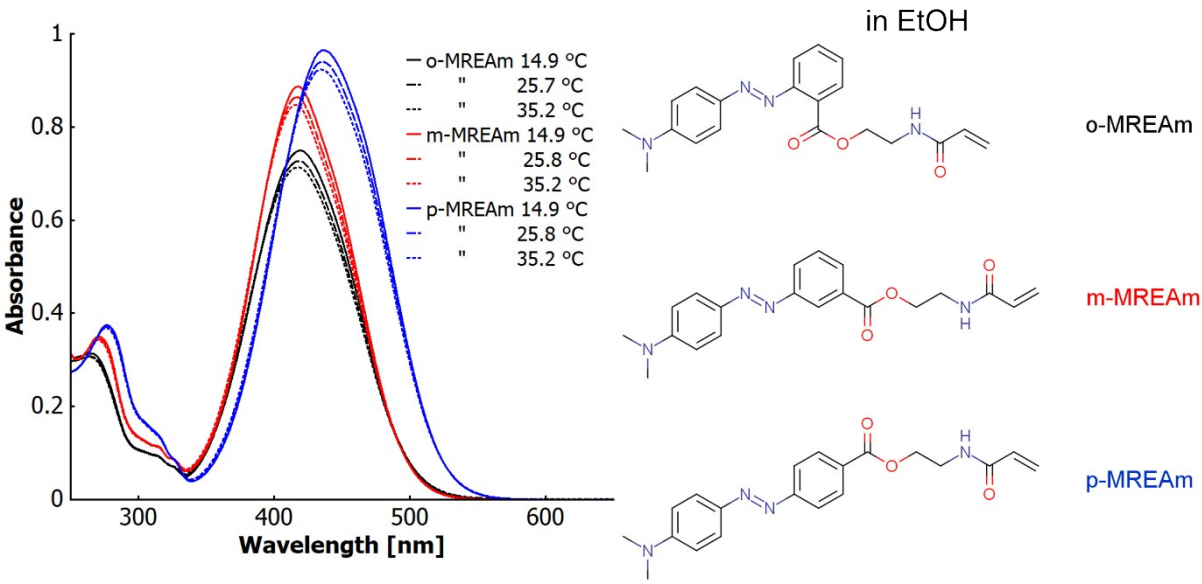

Figure S 17: UV-vis spectra of ortho-, meta- and para-methyl red ester of N-(2-hydroxyethyl)acrylamide ($2.7*10^{-5}$ mol L^{-1}) at different temperatures in neat ethanol with structures.

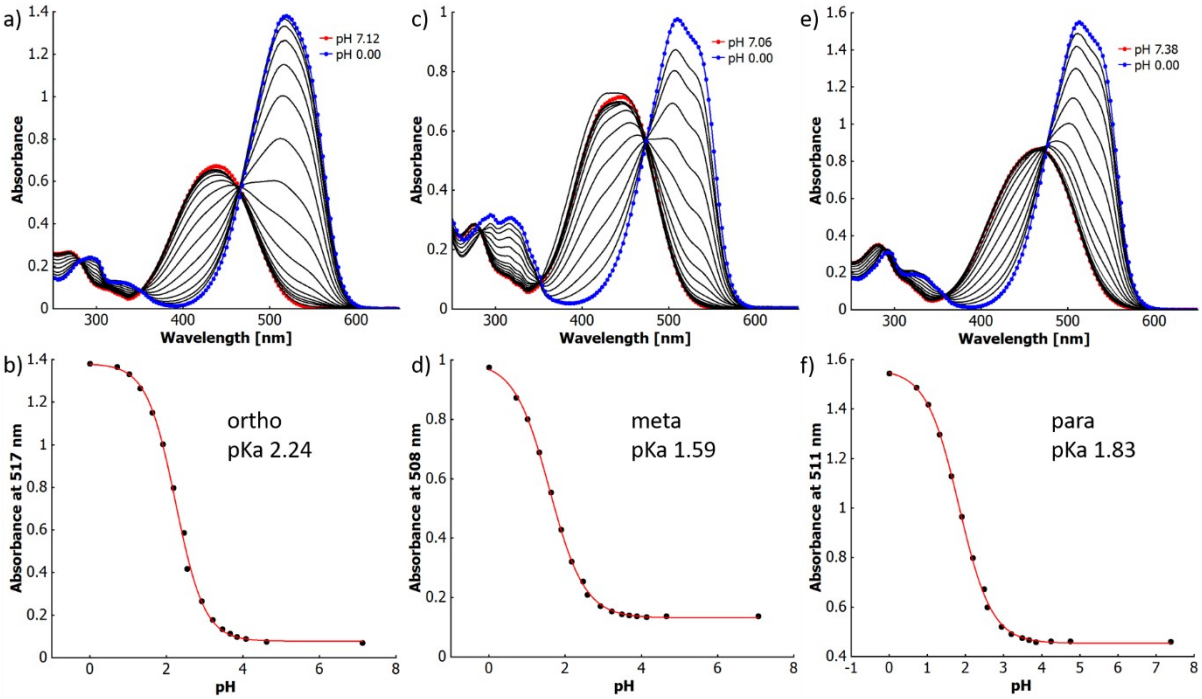

*Figure S 18: UV-vis spectra in H_2O:EtOH (X_{EtOH}=0.31) at different pH values at 20 °C for a) o-MREAm, c) m-MREAm and e) p-MREAm (all 2.7*10^{-5} mol L^{-1}); and absorption at maximum of the azonium vs. pH for b) o-MREAm (517 nm), d) m-MREAm (508 nm) and f) p-MREAm (511 nm).*

Table S 2: pKa values of the constitutional isomers of methyl red and their esters of 2-hydroxylethyl acrylamide.

	o-MR[7]	m-MR[10]	p-MR[11]	o-MREAm	m-MREAm	p-MREAm
pKa free acid	4.85	4.94	4.93	-[a]	-[a]	-[a]
pKa azonium	2.38	1.99	2.08	2.24	1.54	1.83

[a] this value is not available, as the free acid is substituted by an ester functionality

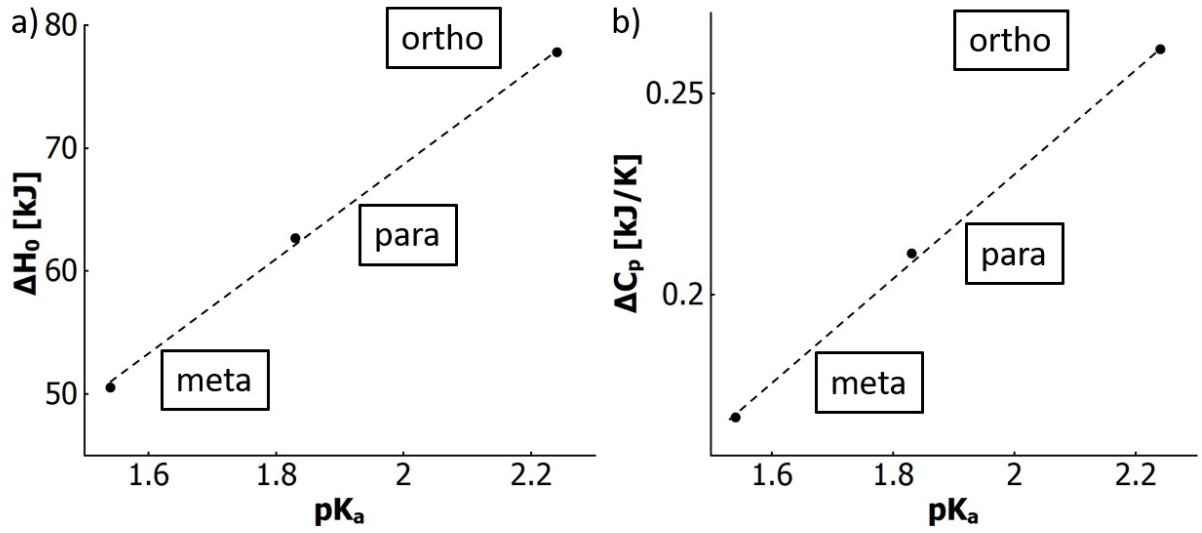

Figure S 19: Correlation of thermochromicity parameters a) H_0 and b) C_p and pK_a for the constitutional isomers of the methyl red ester of N-(2-hydroxyethyl)acrylamide in H_2O:EtOH (X_{EtOH}=0.31). The black line serves as a guide to the eye.

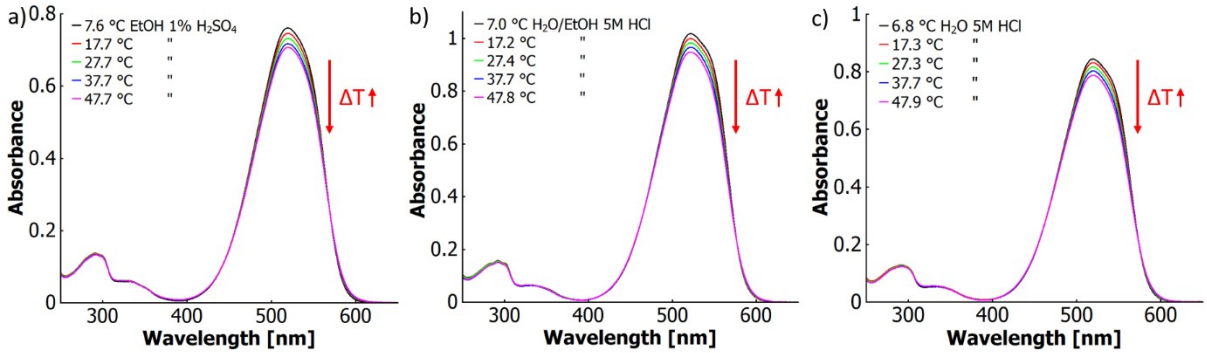

Figure S 20: UV-vis spectra of o-MREAm ($1.4*10^{-5}$ mol) at different temperatures in a) ethanol saturated with HCl; b) H_2O:EtOH (X_{EtOH}=0.31) with 5M HCl and c) H_2O with 5M HCl to determine thermo-solvatochromism of the azonium ion.

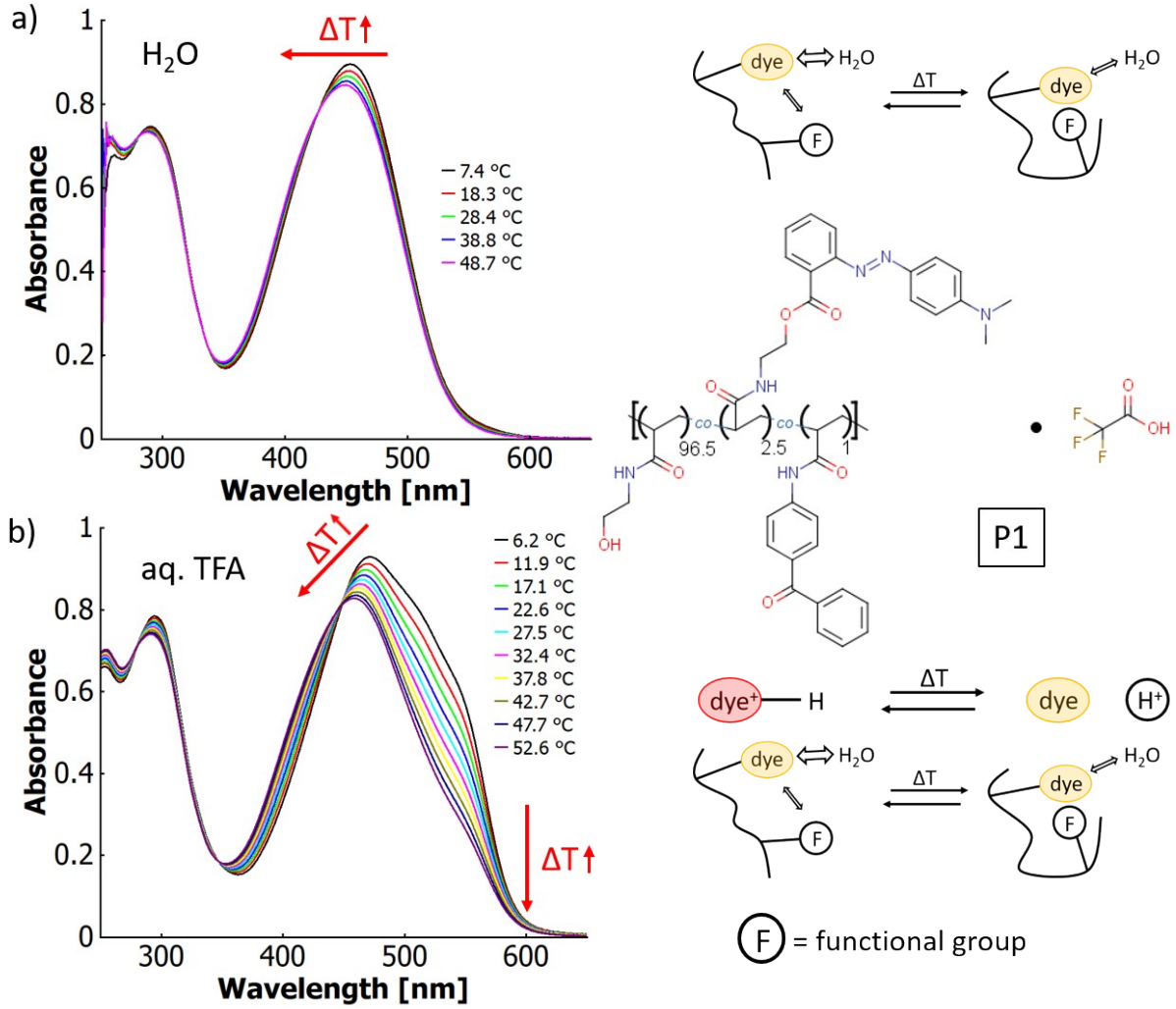

Figure S 21: UV-vis spectra of a poly(HEAm-co-o-MREAm-co-BPAAm) copolymer (P1) at different temperatures with structure of the copolymer a) 0.03 w% in pure water and b) 0.03 w% in aqueous trifluoroacetic acid (0.001 v/v%), with the thermo-peri-halochromic mechanism sketched on the right side.

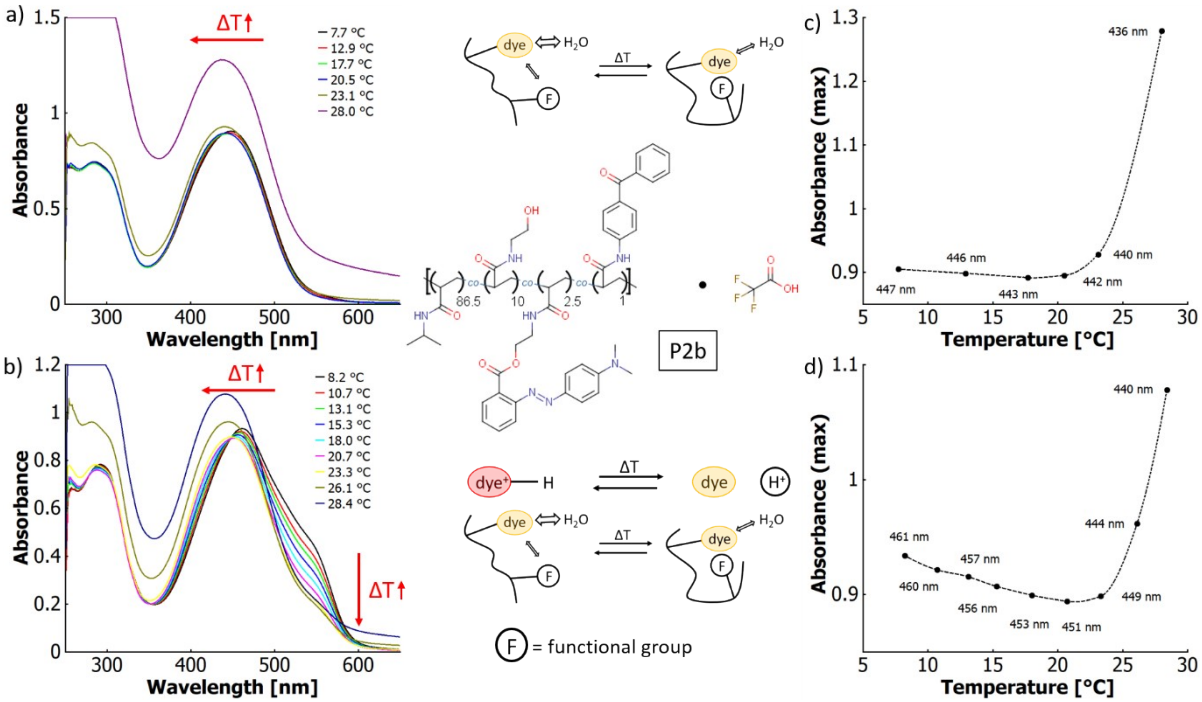

Figure S 22: UV-vis spectra of a poly(NiPAAm-co-HEAm-co-o-MREAm-co-BPAAm) copolymer (P2b) 0.03 w% in a) pure water and b) aqueous trifluoroacetic acid (0.001 v/v%) at different temperatures (direction of shifts in absorbance upon heating marked with red arrows); absorbance at maximum (wavelength indicated in graph) vs temperature for c) pure water and d) aqueous trifluoroacetic acid (0.001 v/v%). The lines are generated by a non-rounded Akima interpolation and only serve as guide to the eye. The structure of the copolymer (acid optional) and cartoons of the ongoing thermochromic processes are shown in the middle section.

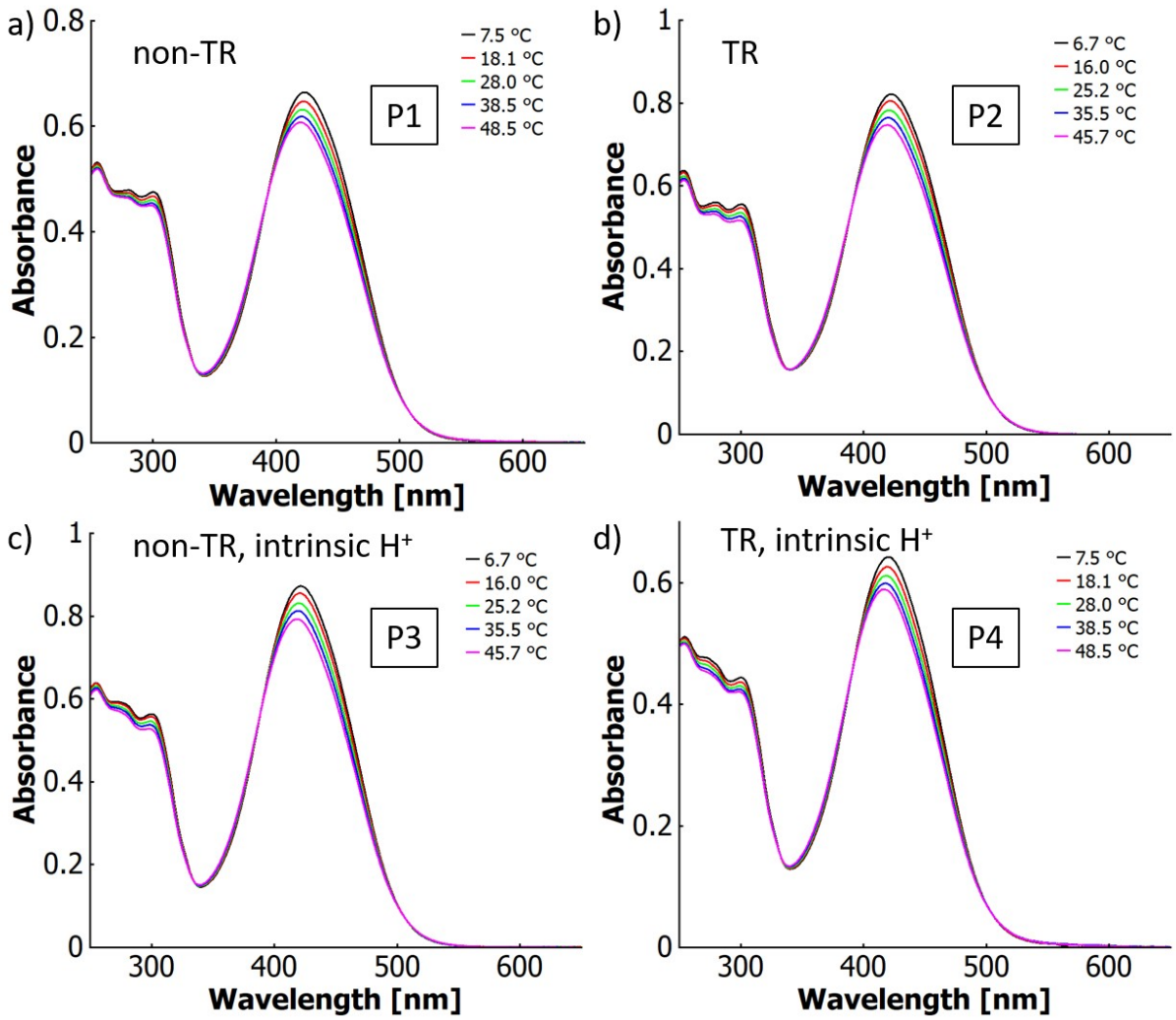

Figure S 23: UV-vis spectra in neat ethanol of four dye-containing copolymers at different temperatures ("TR" = thermoresponsive, "intrinsic H^+" = -COOH substituents in the polymer); a) (P1) poly(HEAm-co-o-MREAm-co-BPAAm); b) (P2) poly(NiPAAm-co-HEAm-co-o-MREAm-co-BPAAm); c) (P3) poly(HEAm-co-MAA-co-o-MREAm-co-BPAAm) and d) (P4) poly(NiPAAm-co-MAA-co-o-MREAm-co-BPAAm) (all 0.2 g/L, TR denotes thermoresponsive).

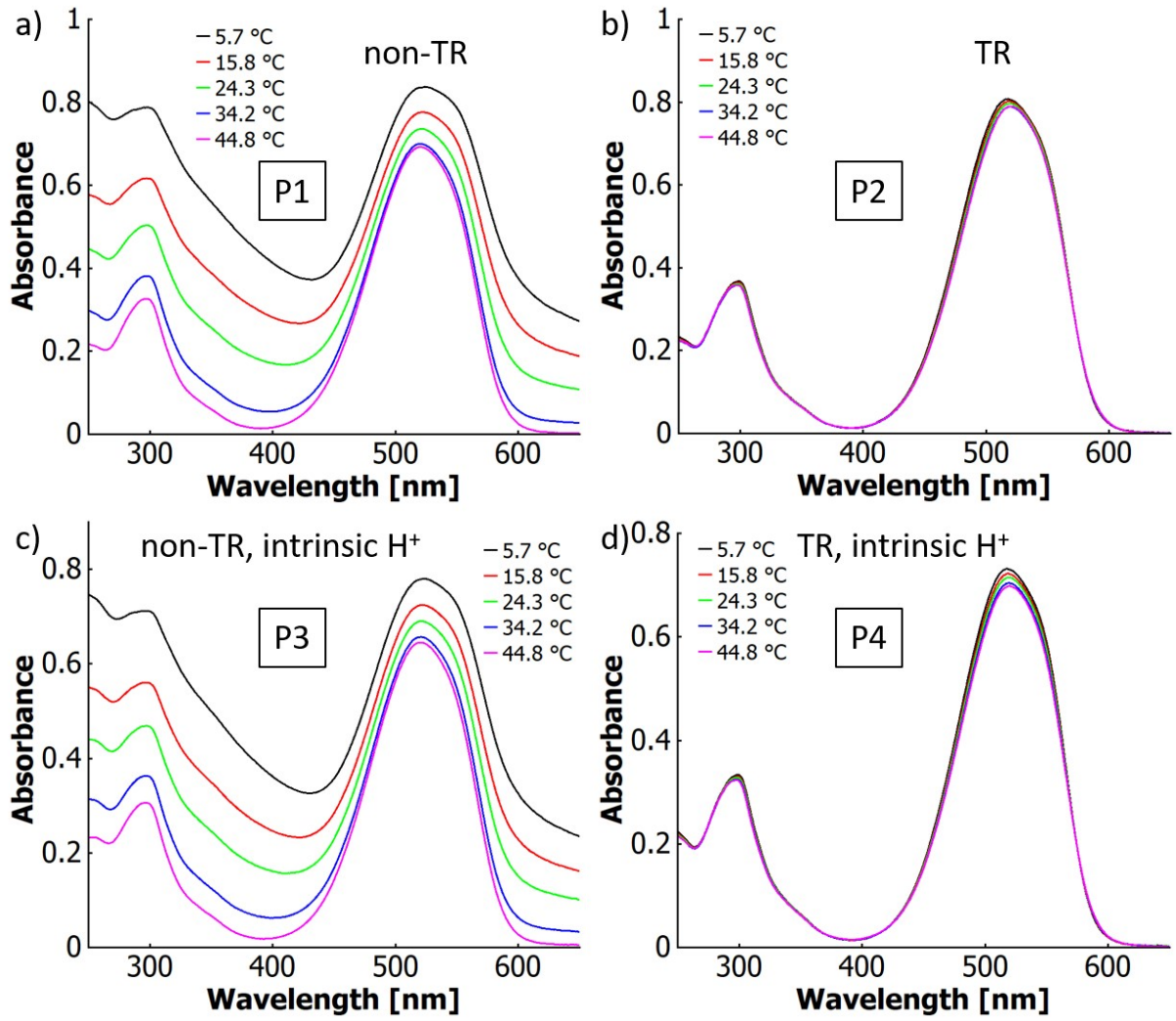

Figure S 24: UV-vis spectra in ethanolic sulfuric acid (1 v/v%) of four dye-containing copolymers at different temperatures ("TR" = thermoresponsive, "intrinsic H^+" = -COOH substituents in the polymer); a) (P1) poly(HEAm-co-o-MREAm-co-BPAAm); b) (P2) poly(NiPAAm-co-HEAm-co-o-MREAm-co-BPAAm); c) (P3) poly(HEAm-co-MAA-co-o-MREAm-co-BPAAm) and d) (P4) poly(NiPAAm-co-MAA-co-o-MREAm-co-BPAAm) (all 0.1 g/L).

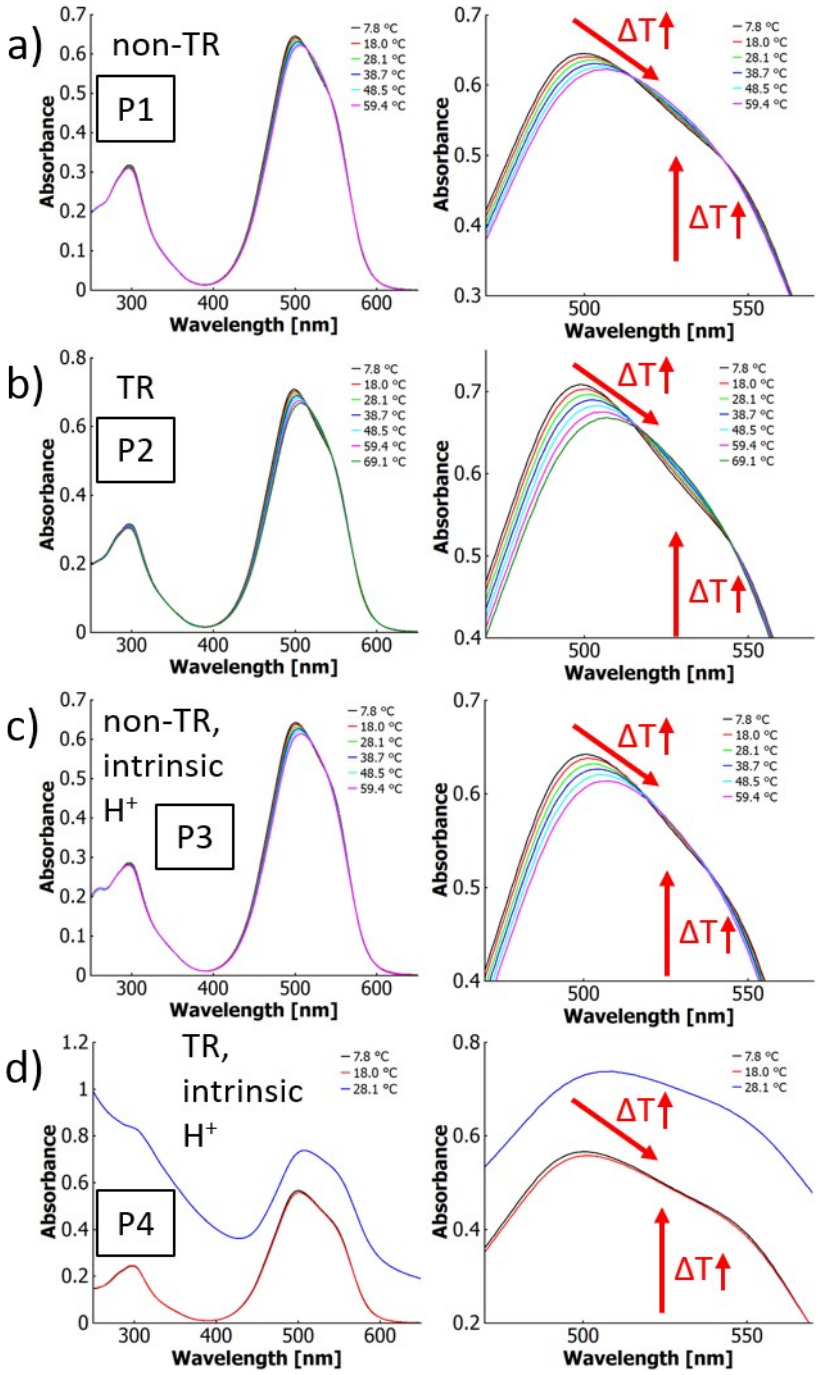

Figure S 25: UV-vis spectra in aqueous hydrochloric acid (1 M) of four dye-containing copolymers at different temperatures ("TR" = thermoresponsive, "intrinsic H^+" = -COOH substituents in the polymer); a) (P1) poly(HEAm-co-o-MREAm-co-BPAAm); b) (P2) poly(NiPAAm-co-HEAm-co-o-MREAm-co-BPAAm); c) (P3) poly(HEAm-co-MAA-co-o-MREAm-co-BPAAm) and d) (P4) poly(NiPAAm-co-MAA-co-o-MREAm-co-BPAAm) (all 0.1 g/L).

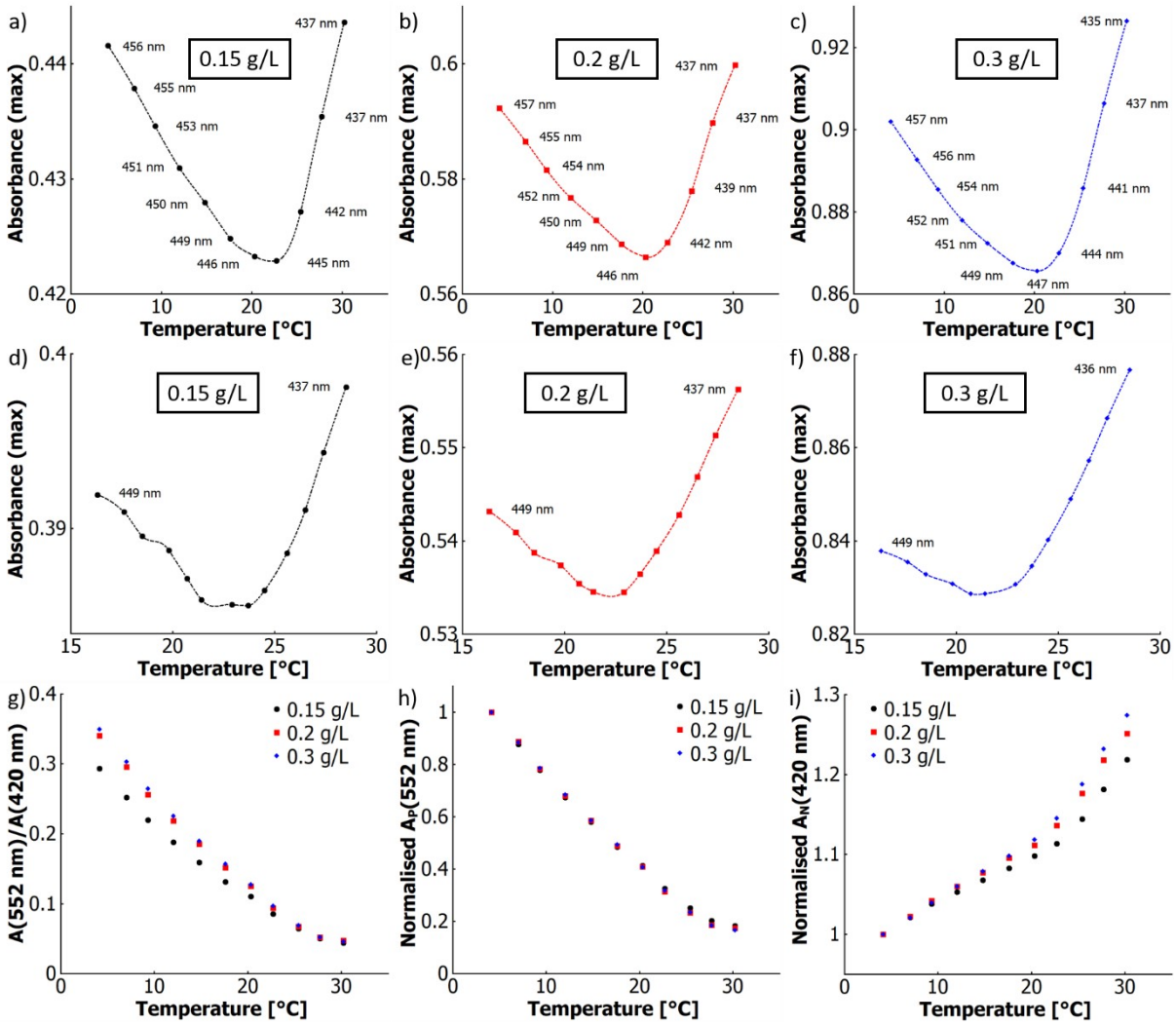

Figure S 26: Absorbance at maximum vs temperature for the poly(NiPAAm-co-MAA-co-o-MREAm-co-BPAAm) copolymer P4 at a) and d) 0.15 g/L, b) and e) 0.2 g/L and c) and f) 0.3 g/L; g) ratio of absorbance at 552 nm and at 420 nm vs temperature, h) normalised absorbance at 552 nm vs temperature (normalised by dividing all values by the value at the lowest temperature) and i) normalised absorbance at 420 nm vs temperature (normalised by dividing all values by the value at the lowest temperature) for the same concentrations. The lines are generated by a non-rounded Akima interpolation and only serve as guide to the eye

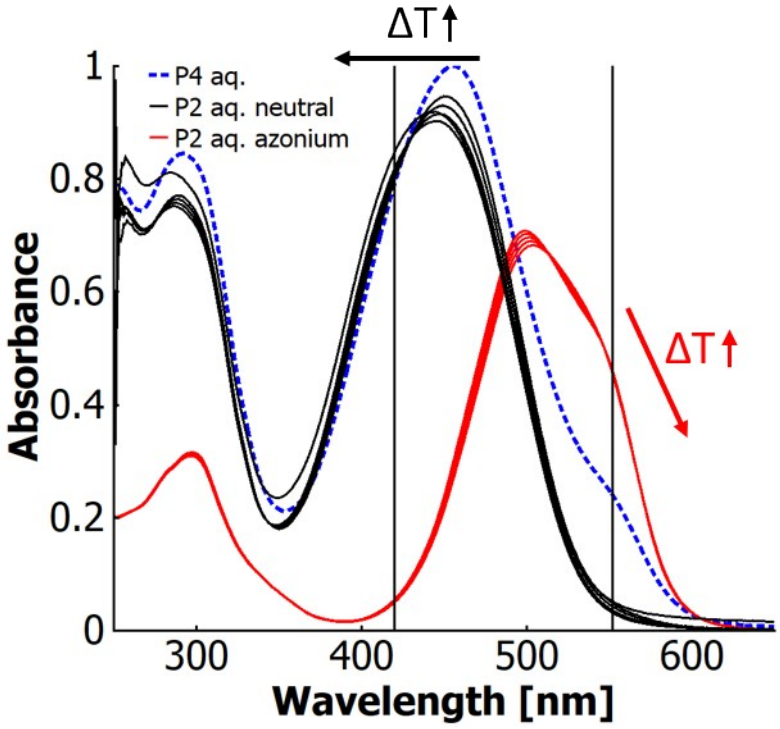

Figure S 27: UV-vis spectra at different temperatures of the poly(NiPAAm-co-HEAm-co-o-MREAm-co-BPAAm) copolymer P2 in water (black) and in aqueous HCl (1M), as well as of the poly(NiPAAm-co-MAA-co-o-MREAm-co-BPAAm) P4 in water (blue). The wavelengths relevant and read were marked by vertical black lines.

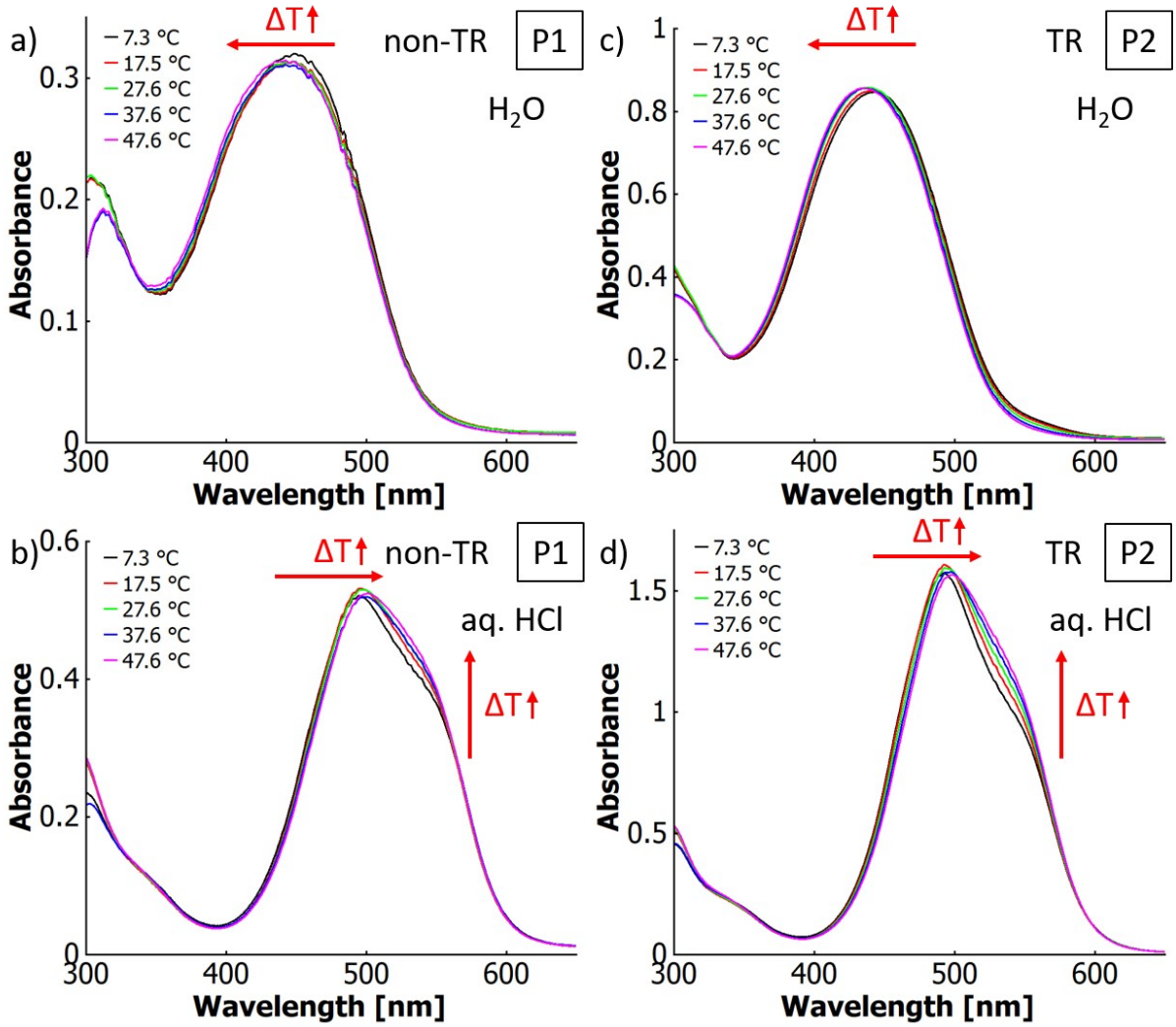

Figure S 28: UV-vis spectra of photocrosslinked, swollen films at different temperatures of poly(HEAm-co-o-MREAm-co-BPAAm) P1 in a) water and b) aqueous HCl (1M), and of poly(NiPAAm-co-HEAm-co-o-MREAm-co-BPAAm) P2 in c) water and d) aqueous HCl (1M) ("TR" = thermoresponsive).

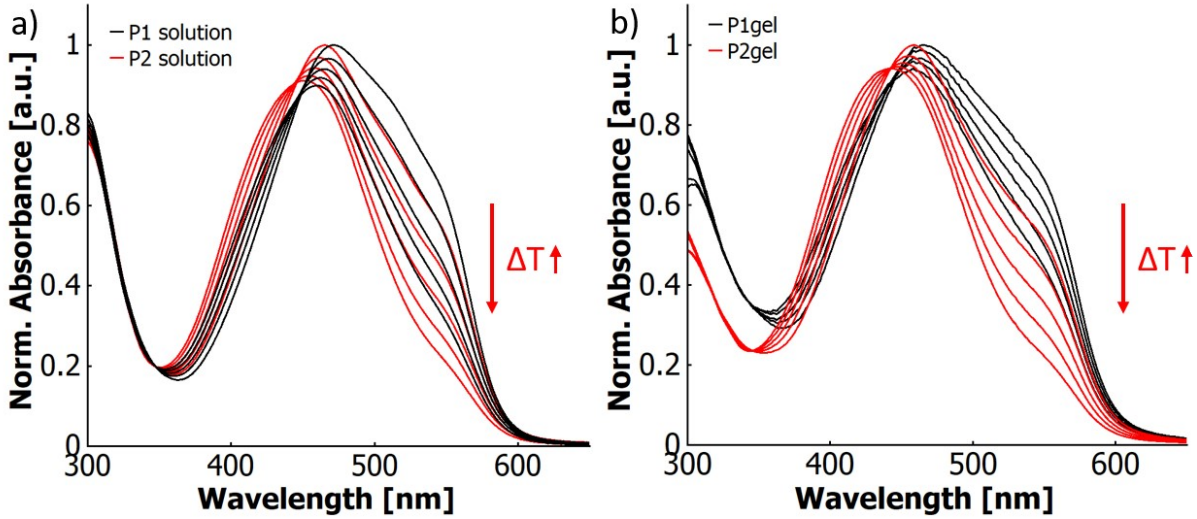

Figure S 29: Normalised UV-vis spectra of poly(HEAm-co-MREAm-co-BPAAm) P1 (black spectra) and poly(NiPAAm-co-HEAm-co-MREAm-co-BPAAm) P2 (red spectra) at different temperatures (ca. 10-50 °C) a) dissolved in aqueous TFA (0.001 v/v%) and b) as a hydrogel film swollen in aqueous TFA (0.01 v/v%). Note the 10x higher acid concentration for the partially protonated films compared to the polymers in solution.

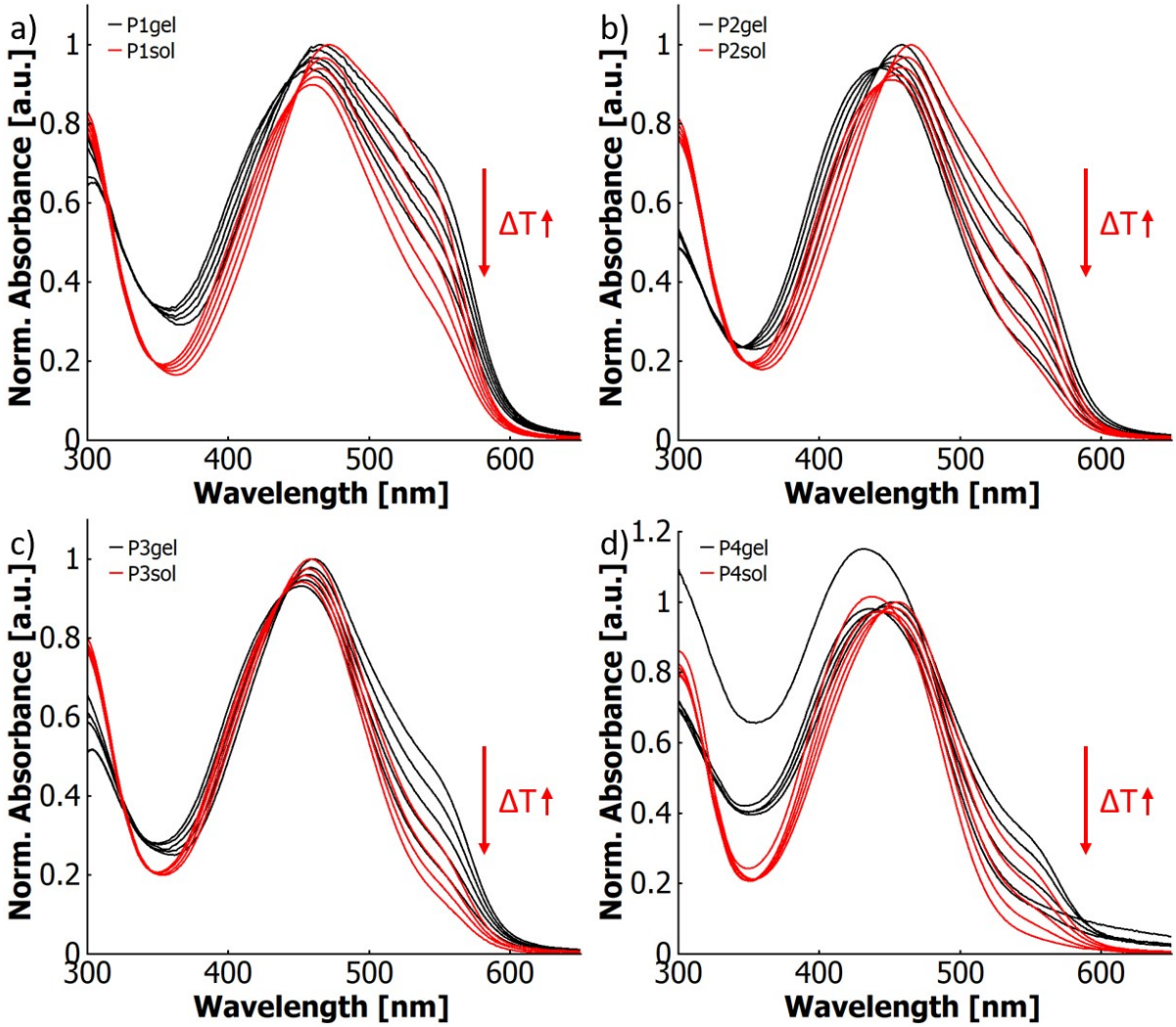

Figure S 30: Normalised UV-vis spectra of a) poly(HEAm-co-MREAm-co-BPAAm) P1, b) poly(NiPAAm-co-HEAm-co-MREAm-co-BPAAm) P2, c) poly(HEAm-co-MAA-co-MREAm-co-BPAAm) P3 and d) poly(NiPAAm-co-MAA-co-MREAm-co-BPAAm) P4 at different temperatures (ca. 10-50 °C). The black spectra show the polymers as a hydrogel film swollen in aqueous TFA (0.01 v/v%) (P1 and P2) or water (P3 and P4), while the red spectra show the polymers dissolved in aqueous TFA (0.001 v/v%, P1 and P2) or water (P3 and P4). Note the 10x higher acid concentration for the partially protonated films compared to the polymers in solution for P1 and P2.

Difference and derivative spectra:

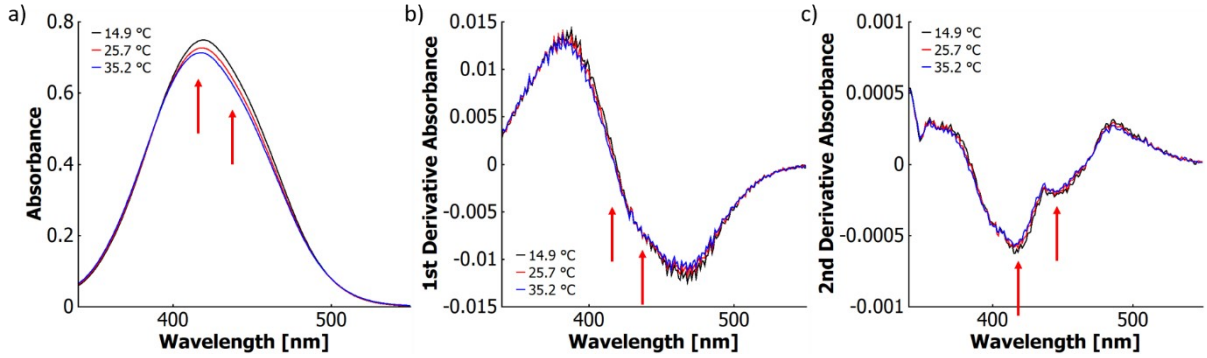

*Figure S 31: a) UV-vis spectra, b) 1st derivative of the UV-vis spectra and c) smoothed (Savitzky-Golay,[12] 25 points) 2nd derivative of the UV-vis spectra of o-MREAm (2.7*10^{-5} mol/L) in ethanol at different temperatures to determine the wavelength of the vibronic sub-band maxima (marked with red arrows).*

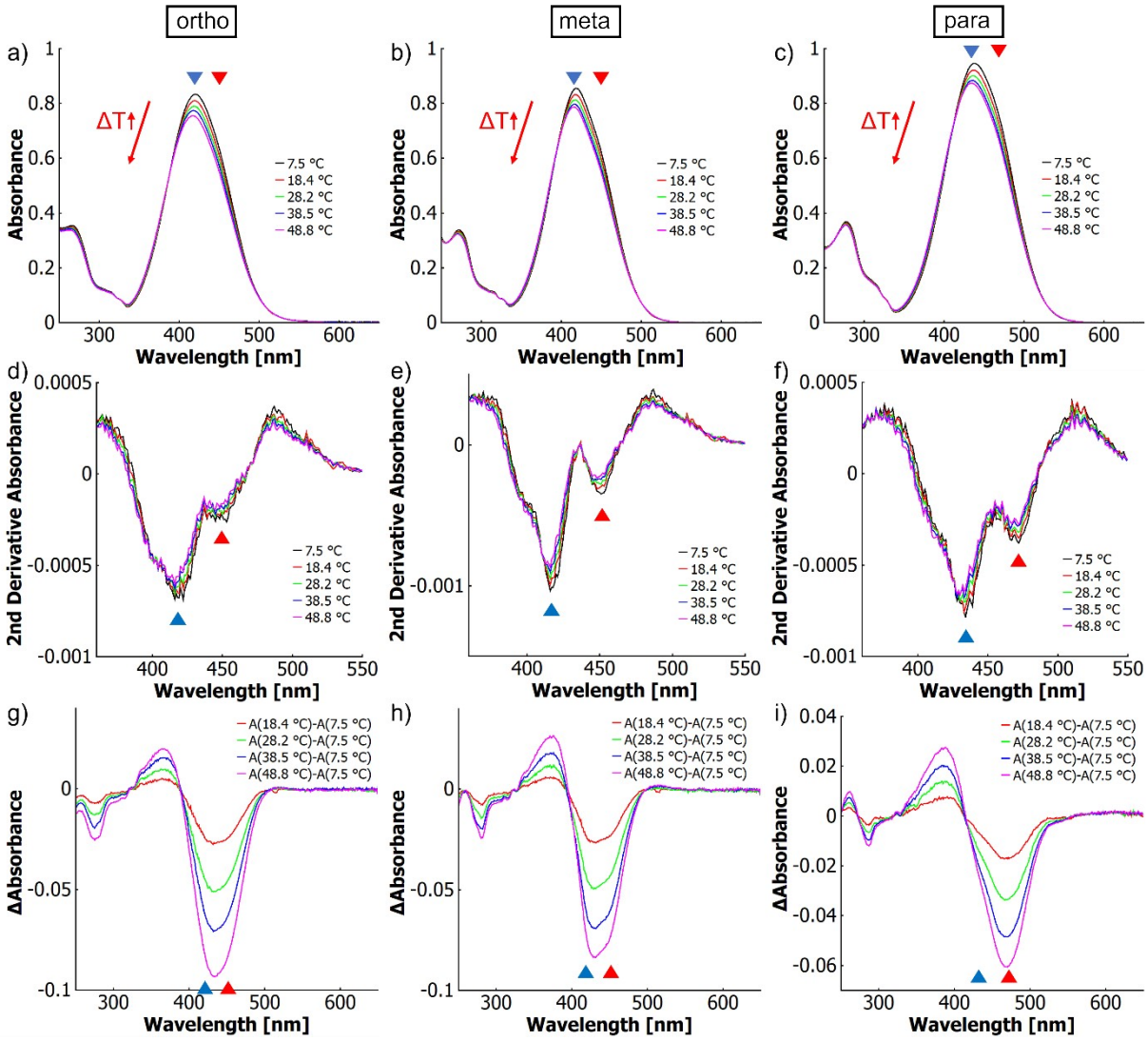

*Figure S 32: a)-c) UV-vis spectra, d)-f) derivative spectra and g)-i) difference spectra showing thermo-solvatochromism of ortho-, meta- and para-methyl red esters of N-(2-hydroxyethyl)acrylamide (2.7*10^{-5} mol L^{-1}) at different temperatures in ethanol. Triangles mark the wavelength positions of vibronic sub-bands in the respective graphs (red: 0-0 transition; blue: 0-1 transition).*

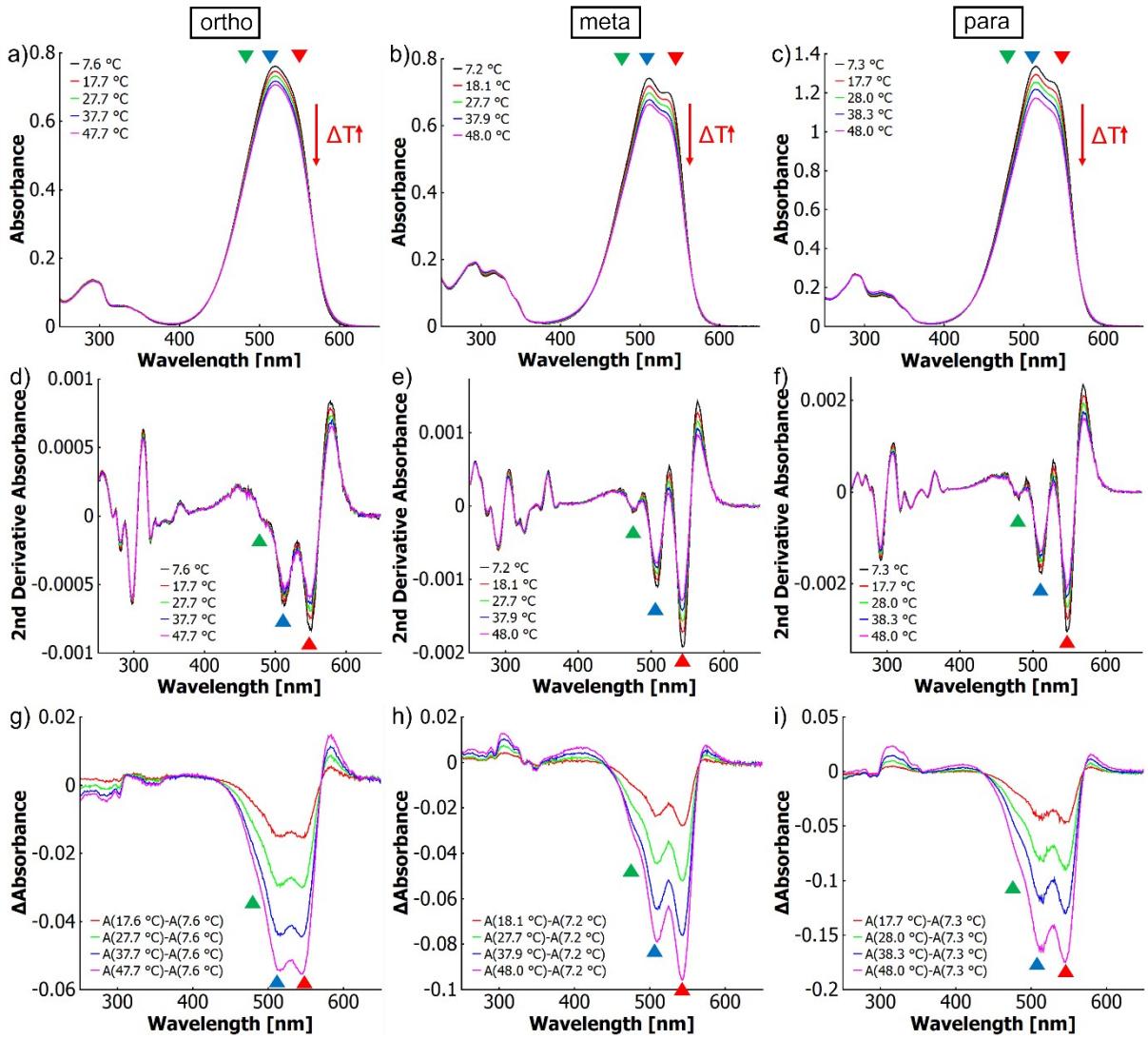

Figure S 33: a)-c) UV-vis spectra, d)-f) derivative spectra and g)-i) difference spectra showing thermo-solvatochromism of completely protonated ortho-, meta- and para-methyl red esters of N-(2-hydroxyethyl)acrylamide ($1.4*10^{-5}$ mol L^{-1}) at different temperatures in ethanolic sulfuric acid (1 v/v%). Triangles mark the wavelength positions of vibronic sub-bands in the respective graphs (red: 0-0 transition; blue: 0-1 transition; green 0-2 transition).

In the derivative spectra corresponding to the azonium ion in ethanolic solution (cf. ESI Figure S 33 d-f), three sub-bands can be identified for all isomers, with the $0\text{-}2_{azonium}$ sub-band being more pronounced for the meta- and para-isomers. The energy differences between the $0\text{-}0_{azonium}$ and the $0\text{-}1_{azonium}$ sub-band is in the energy range of the N-N stretching mode of the parent compound MR.[13,14] The energy difference between the $0\text{-}1_{azonium}$ and the $0\text{-}2_{azonium}$ sub-band is slightly lower, reflecting the anharmonicity of electronic potentials (cf. Table 3).

The vibronic fine structure is also visible in the difference spectra (cf. ESI Figure S 33 g-i), yet with considerable distinctions between the constitutional isomers. While the negative peaks of the ortho-isomer possess equal intensity at the positions of the $0\text{-}0_{azonium}$ and $0\text{-}1_{azonium}$ sub-bands, the negative peak corresponding to the $0\text{-}0_{azonium}$

sub-band is substantially stronger for the meta- and para-isomers. This leads to a significant temperature-induced variation of the band shape in the absorption spectra for the meta- and para-isomers, while the effect is of minor relevance for the ortho-isomer. Positive peaks can be observed at longer wavelengths above the 0-$0_{azonium}$ sub-band as well as around the absorption band of the ammonium ion (~310 nm). Apparently, the tautomeric equilibrium shifts slightly from the azonium ion to the ammonium form with rising temperature. Concomittantly to a reduced dye volume fraction due to the thermal expansion of the solvent, this tautomerism contributes to the observed decrease of the azonium ion absorbance (cf. ESI Figure S 33 a-c).

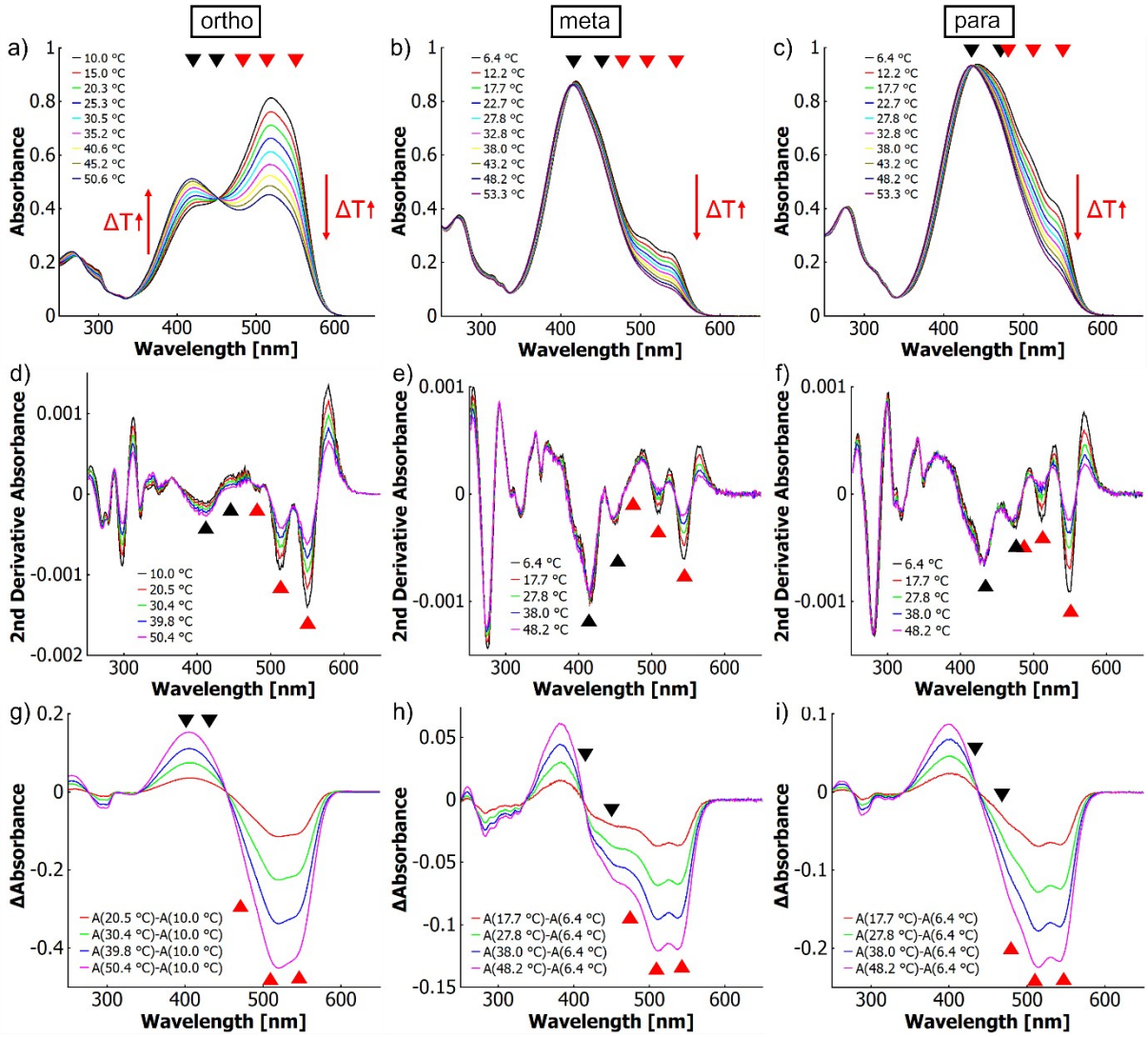

Figure S 34: a)-c) UV-vis spectra, d)-f) derivative spectra and g)-i) difference spectra showing thermo-halochromism of ortho-, meta- and para-methyl red esters of N-(2-hydroxyethyl)acrylamide ($2.7*10^{-5}$ mol L^{-1}) at different temperatures in ethanolic trifluoroacetic acid (1 v/v%). Triangles mark the wavelength positions of vibronic sub-bands in the respective graphs (red: vibronic transitions of the azonium ion; black: vibronic transitions of the neutral species).

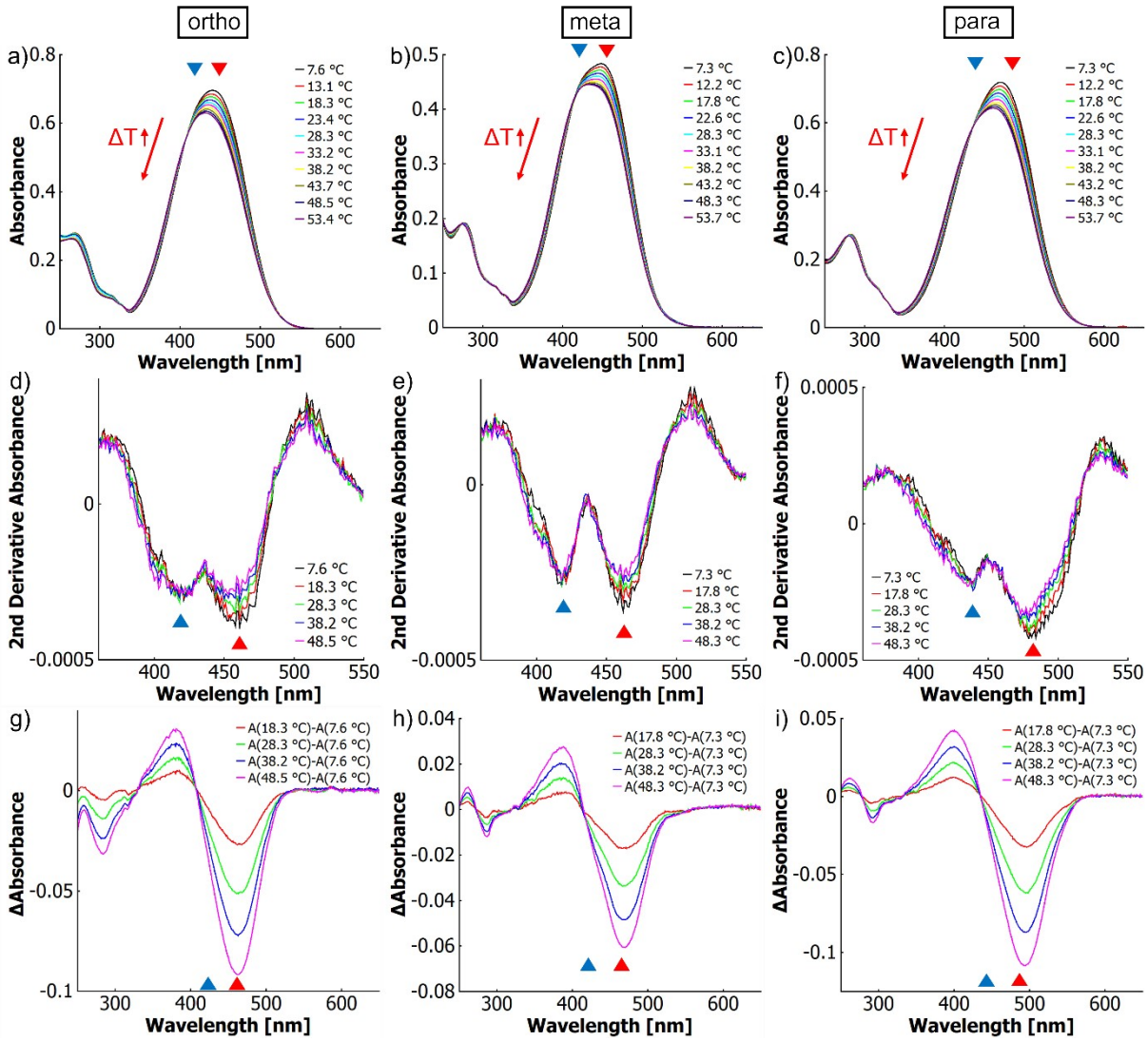

Figure S 35: a)-c) UV-vis spectra, d)-f) derivative spectra and g)-i) difference spectra showing thermo-solvatochromism of ortho-, meta- and para-methyl red esters of N-(2-hydroxyethyl)acrylamide ($2.7*10^{-5}$ mol L^{-1}) at different temperatures in H_2O:EtOH (X_{EtOH}=0.31). Triangles mark the wavelength positions of vibronic sub-bands in the respective graphs (red: 0-0 transition; blue: 0-2 transition).

As performed for the dyes in neat ethanol, derivative and difference spectroscopy were applied to the UV-vis spectra for the binary solvent mixture. As observed with vibronic thermochromism in neat ethanol, a variation of temperature also results in a change of the vibronic structure in the UV-vis spectra for thermo-solvatochromism occurring in the binary solvent mixture. However, the application of both techniques reveals intricate differences between the mechanisms of vibronic thermochromism and thermo-solvatochromism. For thermo-solvatochromism, the sub-bands in the derivative spectra are broadened and their energy difference is by about 450-500 cm^{-1} higher than in the case of vibronic thermochromism (cf. ESI Figure S 32 d-f, Figure S 35 d-f, Table 2). The intensity ratio of the sub-bands is inverse for the two mechanisms. In thermo-solvatochromism, the lower energy sub-band is stronger than the high

energy sub-band, while in vibronic thermochromism the lower energy sub-band is weaker. The larger energy differences of 2100-2300 cm^{-1} between the sub-bands in the binary solvent mixture do not match any specific vibration of the MR dye that would be responsible for the vibronic transition.[1,2] The mismatch between these energy differences and the vibrational modes found in Raman spectra suggests that either a combination of vibrations leads to the observed vibronic transition or that the 0-1 transition is forbidden and only the 0-2 transition is allowed. Assuming a considerable influence of the binary solvent mixture on the energy of the vibrational modes, as follows, the 0-2 transition would roughly agree with the N=N stretching mode in an anharmonic oscillator. In the parent compound MR, the 0-1 stretching mode equals to about 1400 cm^{-1}. This energy would be lower in the 1-2 mode, totaling to around 2600-2700 cm^{-1} for the 0-2 transition, which approaches the range of the observed energy difference in derivative spectroscopy. However, as stated above, vibrational mode mixing[15,16] would be another likely scenario. In the binary solvent mixture, temperature has an unequal influence on the sub-band structure in the derivative spectra. Consequently, for all positional isomers, the higher energy sub-bands do not change in intensity, while the lower energy sub-bands decrease noticeably as signified by an increase in the second derivative. This is in contrast to the behaviour in neat ethanol, where both bands change equally upon temperature increase (cf. ESI Figure S 32 d-f, Figure S 35 d-f).

At the same time, there is only one symmetric negative band without any vibronic structure in the difference spectra for each of the configurational isomers (cf. ESI Figure S 35 g-i). The higher intensity of the 0-0 transition compared to the 0-x (x=1, 2) transition in the derivative spectra and the distinct decrease in only one sub-band are considered here to be features of thermo-solvatochromism. In contrast, the lower intensity of the 0-0 transition compared to the 0-1 transition and a vibronic component in the negative bands in the difference spectra can be considered a feature of vibronic thermochromism.

The azonium ions of all three configurational isomers in binary solvent mixtures of water and ethanol exhibit a vibronic structure in UV-vis, derivative, and difference spectra (cf. ESI Figure S 36). In the derivative spectra, there are three vibronic sub-bands with energy differences between them that correspond to N-N valence modes (assuming a single bond between the nitrogens in the quinoid structure of the azonium form).[1,2] The negative bands in the difference spectra show peaks at the positions of

the vibronic sub-bands as identified by derivative spectroscopy. The absorbance change upon temperature variation is more intense at the 0-0 sub-band than at the higher energy sub-bands in all isomers. The corresponding 0-1 sub-band changes are less intense to varying degrees in the three isomers. While the meta- and para-isomers exhibit similar changes for 0-0 and 0-1, the ortho-isomer shows a distinct difference between the changes of the 0-0 and the 0-1 sub-bands (compare red and blue triangles in ESI Figure S 36 g-i). Consequently, the vibronic structure is in all cases reduced at higher temperatures as the higher energy sub-bands are more populated. A slight increase in absorbance can be observed at the wavelength for the ammonium ion, meaning that the tautomeric equilibrium shifts slightly towards the ammonium ion at higher temperatures. In essence, the obtained results surprisingly reveal that the thermochromic behaviour of the azonium ions are quite similar both in the binary solvent mixture and in neat ethanol (cf. ESI Figure S 33, Figure S 36).

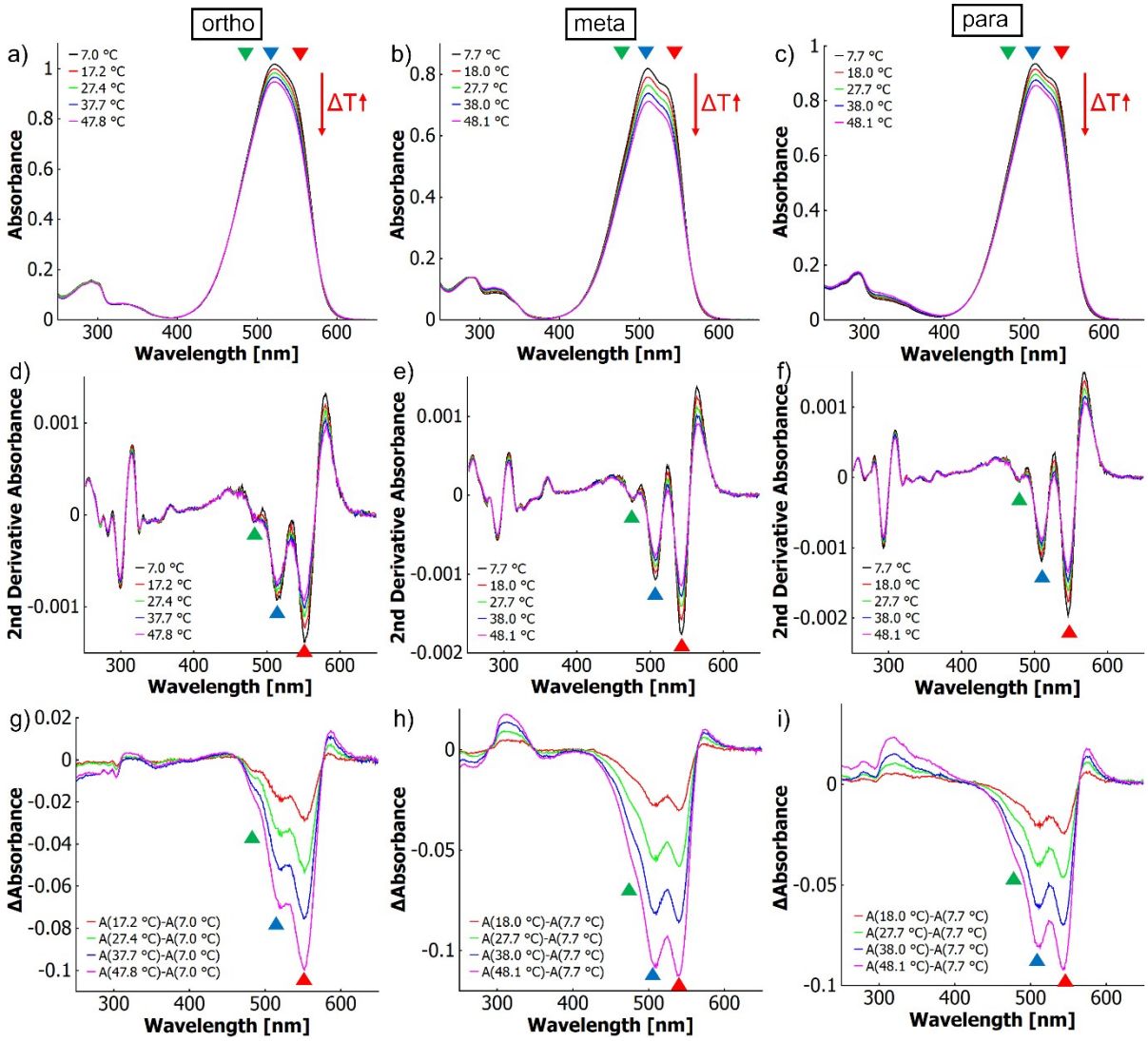

Figure S 36: a)-c) UV-vis spectra, d)-f) derivative spectra and g)-i) difference spectra showing thermo-solvatochromism of completely protonated ortho-, meta- and para-methyl red esters of N-(2-hydroxyethyl)acrylamide ($1.4*10^{-5}$ mol L^{-1}) at different temperatures in H_2O:EtOH (X_{EtOH}=0.31) with hydrochloric acid (5 M). Triangles mark the wavelength positions of vibronic sub-bands in the respective graphs (red: 0-0 transition; blue: 0-1 transition; green 0-2 transition).

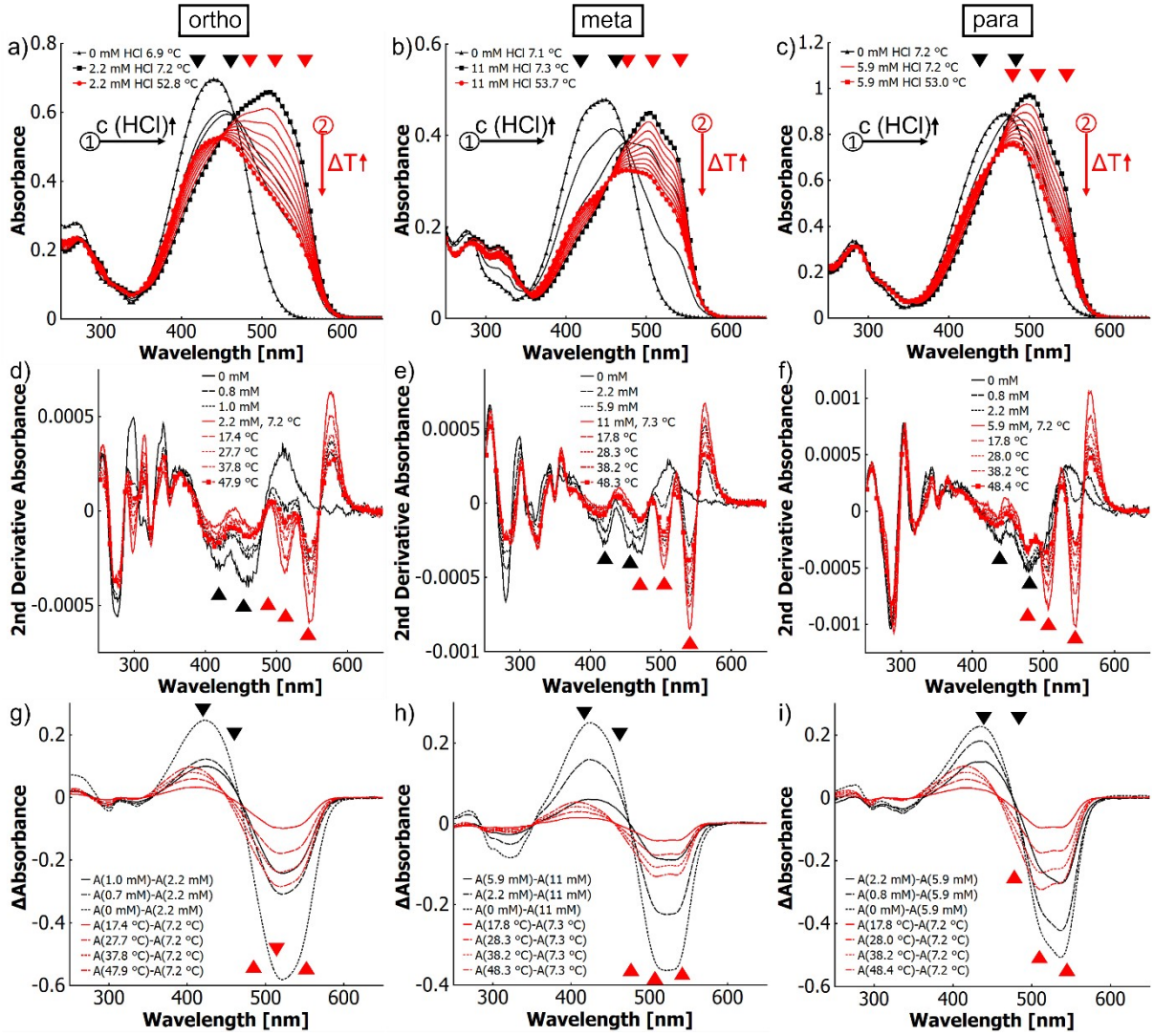

Figure S 37: a)-c) UV-vis spectra, d)-f) derivative spectra and g)-i) difference spectra showing thermo-solvato-halochromism of ortho-, meta- and para-methyl red esters of N-(2-hydroxyethyl)acrylamide ($2.7*10^{-5}$ mol L^{-1}) in H_2O:EtOH (X_{EtOH}=0.31) after titration (black arrow 1) with hydrochloric acid at ~6-7 °C to ~50% protonation and at different temperatures (red arrow 2). The black graphs represent different concentrations of hydrochloric acid (provided as values in brackets in the legends) and the red graphs changes in temperature. Triangles mark the wavelength positions of vibronic sub-bands in the respective graphs (red: vibronic transitions of the azonium ion; black: vibronic transitions of the neutral species).

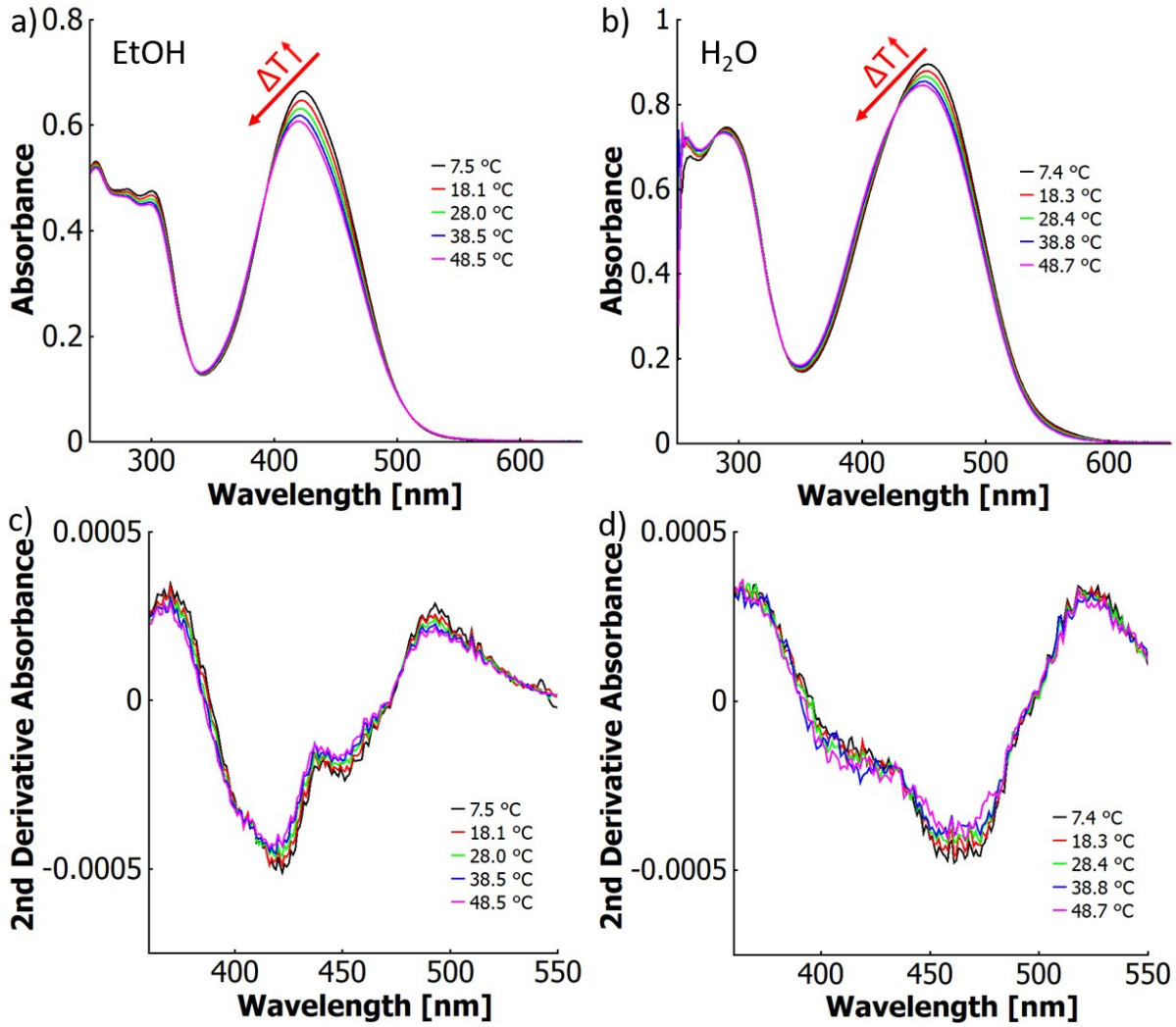

Figure S 38: UV-vis spectra of a poly(HEAm-co-o-MREAm-co-BPAAm) copolymer (P1) a) 0.02 w% in ethanol and b) 0.03 w% in water, as well as their second derivatives in c) ethanol and d) water at different temperatures.

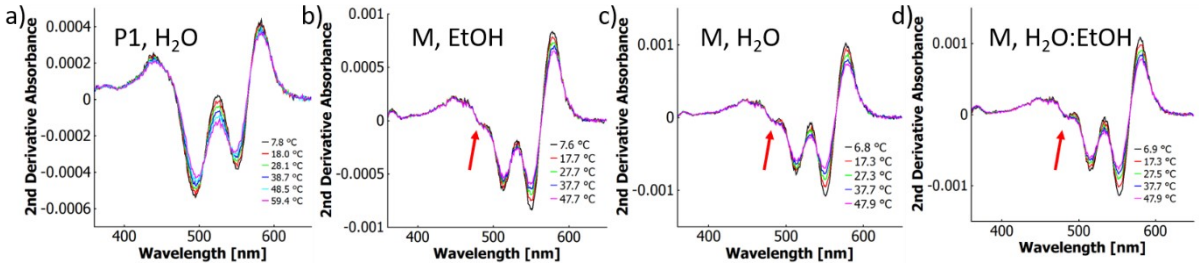

Figure S 39: Smoothed (Savitzky-Golay, 25 points) 2nd derivative of the UV-vis spectra of a) the completely protonated copolymer (P1) poly(HEAm-co-o-MREAm-co-BPAAm) in aqueous HCl (1 M), and of the completely protonated dye monomer M o-MREAm ($1.4*10^{-5}$ mol/L) in b) ethanolic sulfuric acid (1 v/v%), c) aqueous HCl (5 M) and d) in H_2O:EtOH (X_{EtOH}=0.31) with 5M HCl. Red arrows indicate a third vibronic sub-band for the monomer.

Van't Hoff analysis graphs:

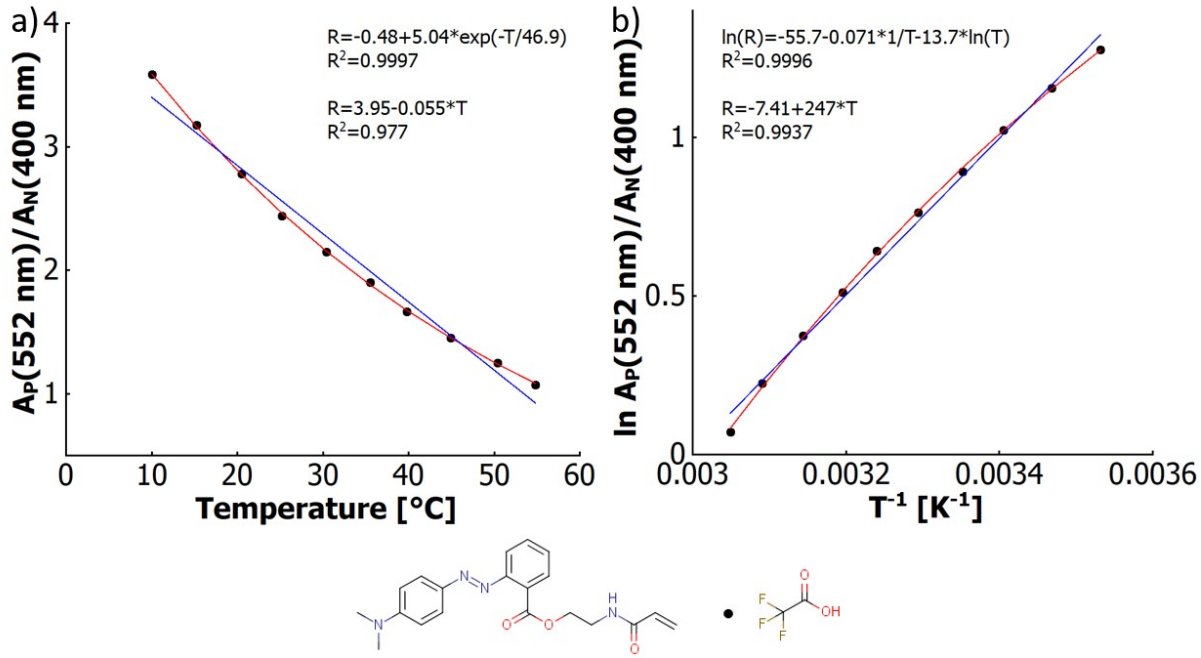

*Figure S 40: a) Ratio of the absorbance of the protonated species (552 nm) and the neutral species (400 nm) (R) vs temperature, analysed with a linear fit in comparison to an exponential decay fit and b) natural logarithm of R vs the inverse absolute temperature, analysed with a linear fit (blue) in comparison to a ln(R)=a-b*1/T+c*ln(T) fit (red) for a solution of ortho-methyl red ethyl acrylamide in EtOH (2.7*10^{-5} mol/L) with trifluoroacetic acid (1v/v%).*

The non-linearity of the decrease in the ratio of absorbances of the protonated and neutral species (R) with temperature, as well as the non-linearity of the van't Hoff plot are shown in ESI Figure S 40. Linear fits and non-linear fits (exponential decay in the case of R and ln(R)=a-b*1/T+c*ln(T) for the van't Hoff plot) are both applied. In both plots, the non-linear fit has a higher coefficient of determination than the linear fit. While the R^2 is high in the linear fit as well, this seems to be a statistical error, as the data points deviate similarly from the fit on both of its sides. This has also been pointed out in the literature for different systems.[17,18]

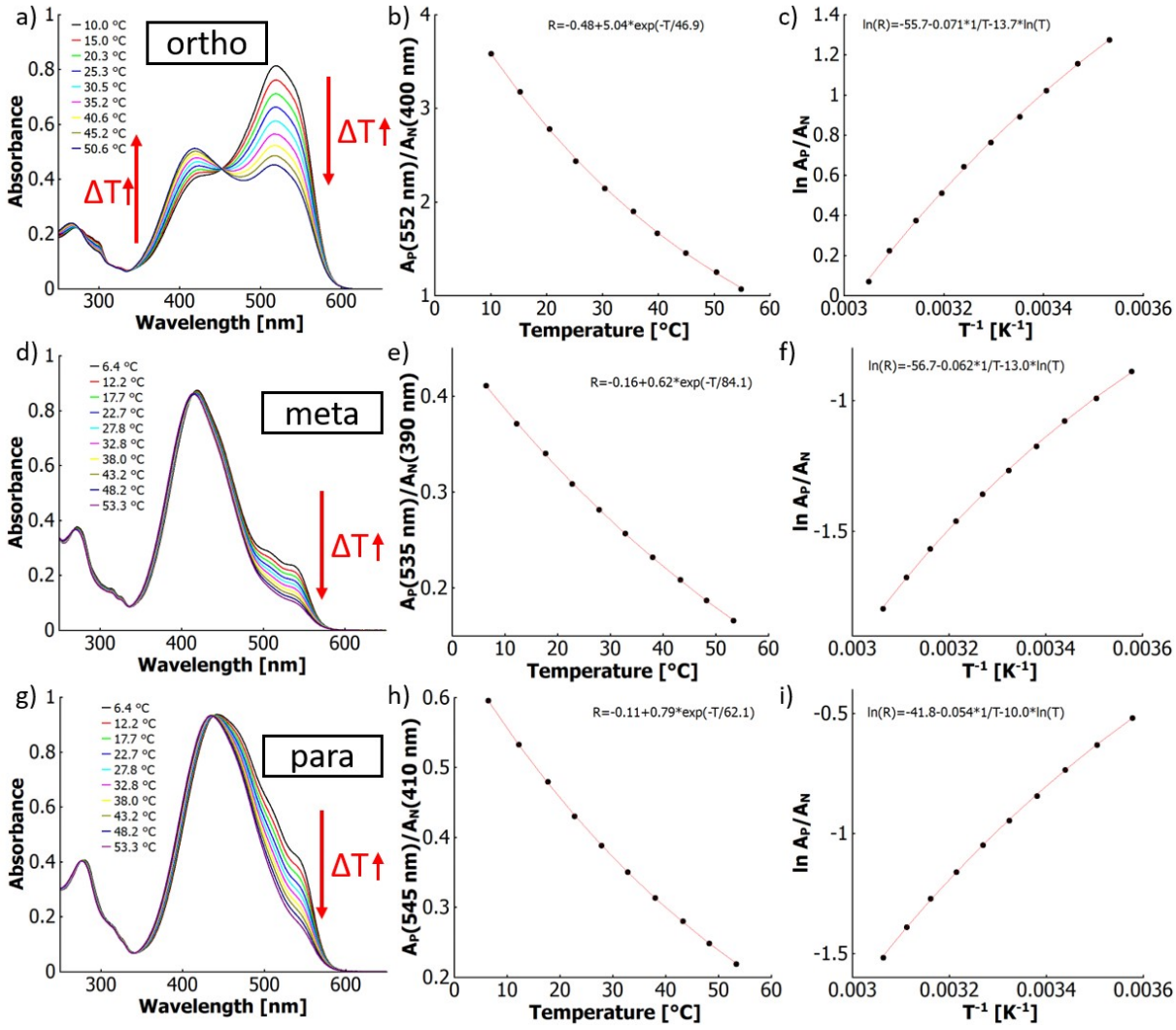

*Figure S 41: UV-vis spectra demonstrating thermo-halochromism of a) o-MREAm, d) m-MREAm and g) p-MREAm (all 2.7*10^{-5} mol/L) in ethanolic trifluoroacetic acid (1 v/v%); ratio of the absorbance of the protonated species and the neutral species ("R" in the equation, wavelengths marked in the axis description) vs temperature, fitted with a first order exponential decay function for b) o-MREAm, e) m-MREAm and h) p-MREAm; natural logarithm of the ratio of the absorbance of the protonated species and the neutral species vs the inverse of the absolute temperature, fitted with a function ln(R)=a-b*1/T+c*ln(T) for c) o-MREAm, f) m-MREAm and i) p-MREAm.*

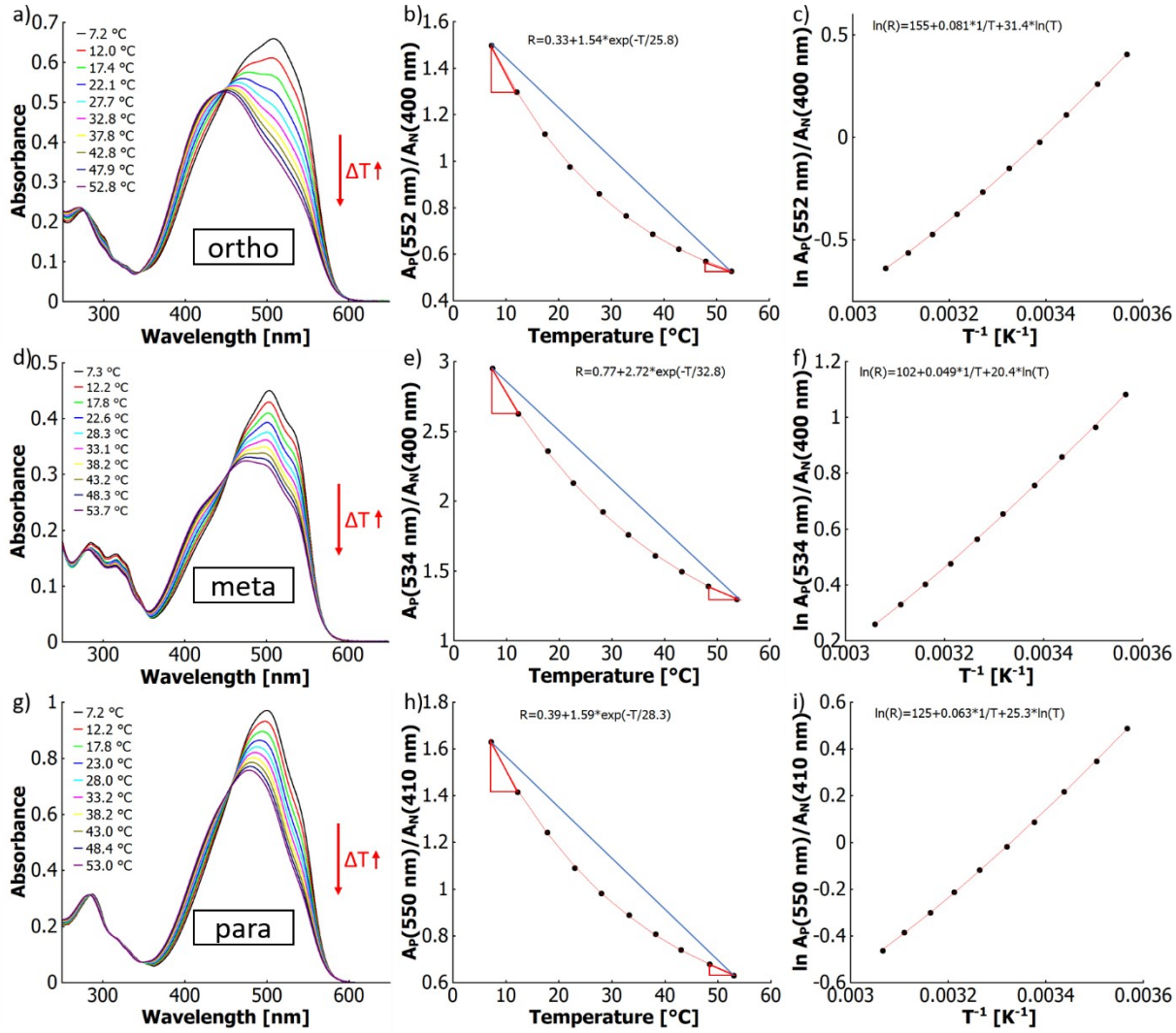

*Figure S 42: UV-vis spectra demonstrating thermo-halochromism of a) o-MREAm, d) m-MREAm and g) p-MREAm (all 2.7*10^{-5} mol/L) in H_2O:EtOH (X_{EtOH}=0.31) with added hydrochloric acid: a) 2.2 mM, d) 11 mM and g) 5.9 mM; Ratio of the absorbance of the protonated species and the neutral species ("R" in the equation, wavelengths marked in the axis description) vs temperature, fitted with a first order exponential decay function for b) o-MREAm, e) m-MREAm and h) p-MREAm. The blue line along with the red slope triangles serve as a reference to display the non-linearity of the graphs; Natural logarithm of the ratio of the absorbance of the protonated species and the neutral species vs the inverse of the absolute temperature, fitted with a function ln(R)=a-b*1/T+c*ln(T) for c) o-MREAm, f) m-MREAm and i) p-MREAm.*

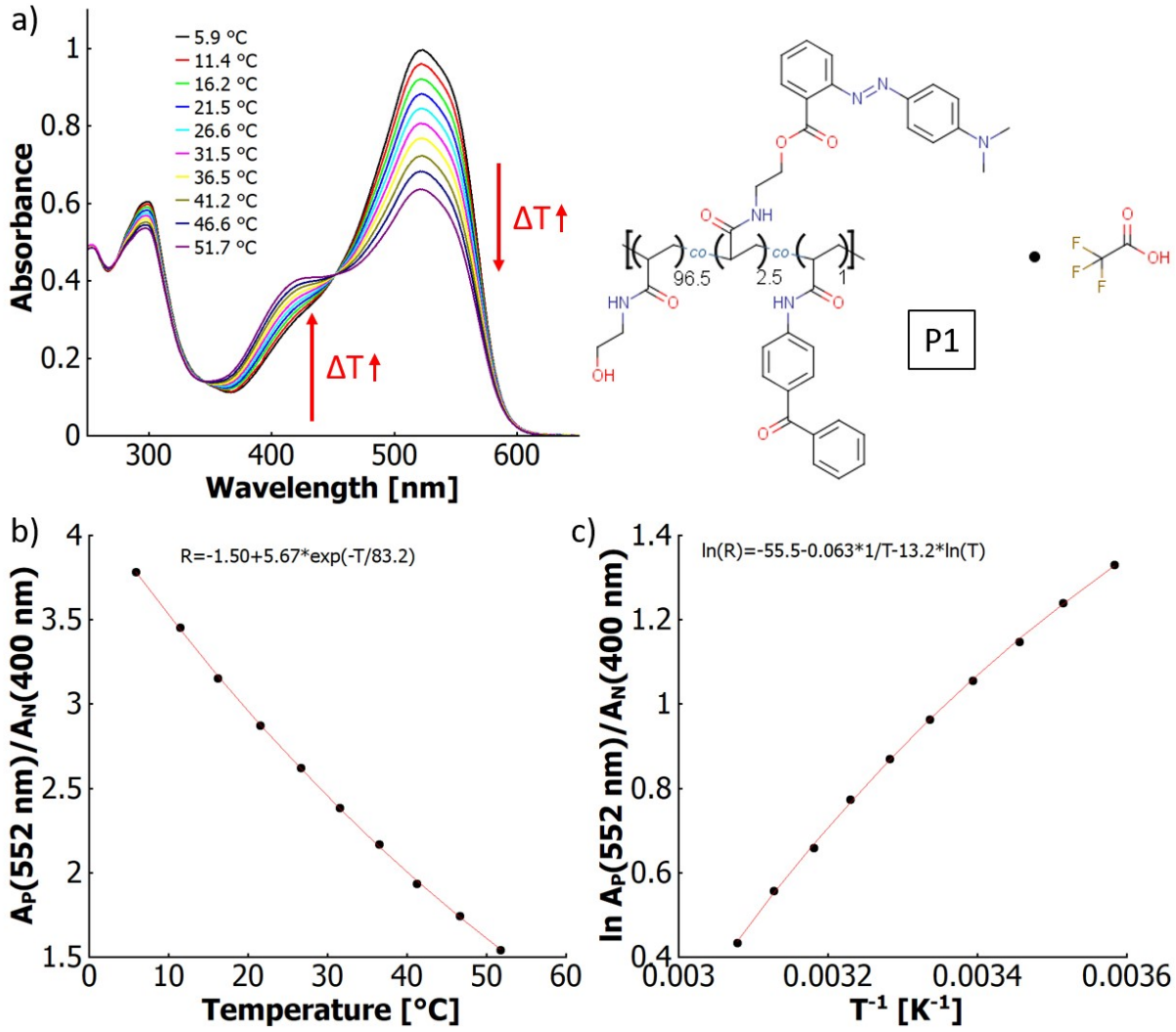

*Figure S 43: a) UV-vis spectra of a poly(HEAm-co-o-MREAm-co-BPAAm) copolymer (P1) 0.02 w% in ethanolic trifluoroacetic acid (1 v/v%) at different temperatures with structure of the copolymer, direction of shifts in absorbance upon heating marked with red arrows; b) absorbance ratio of the protonated (552 nm) and the neutral species (400 nm) vs temperature, fitted with an exponential decay function; c) van't Hoff plot of the logarithmic absorbance ratio vs the inverse temperature, fitted with a function ln(R)=a-b*1/T+c*ln(T).*

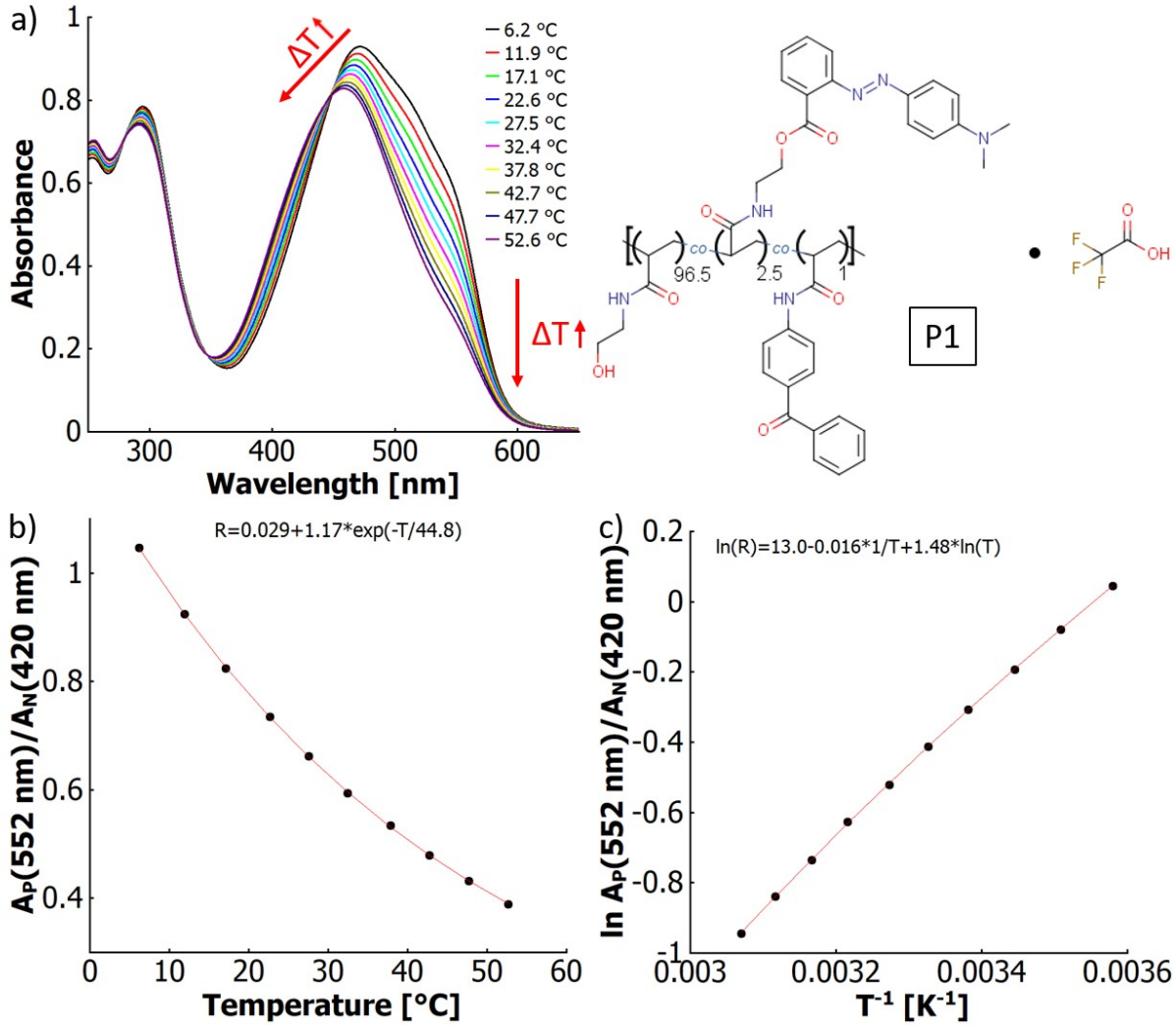

*Figure S 44: a) UV-vis spectra of a poly(HEAm-co-o-MREAm-co-BPAAm) copolymer (P1) 0.03 w% in aqueous trifluoroacetic acid (0.001 v/v%) at different temperatures with structure of the copolymer, direction of shifts in absorbance upon heating marked with red arrows; b) absorbance ratio of the protonated (552 nm) and the neutral species (420 nm) vs temperature, fitted with an exponential decay function; c) van't Hoff plot of the logarithmic absorbance ratio vs the inverse temperature, fitted with a function ln(R)=a-b*1/T+c*ln(T).*

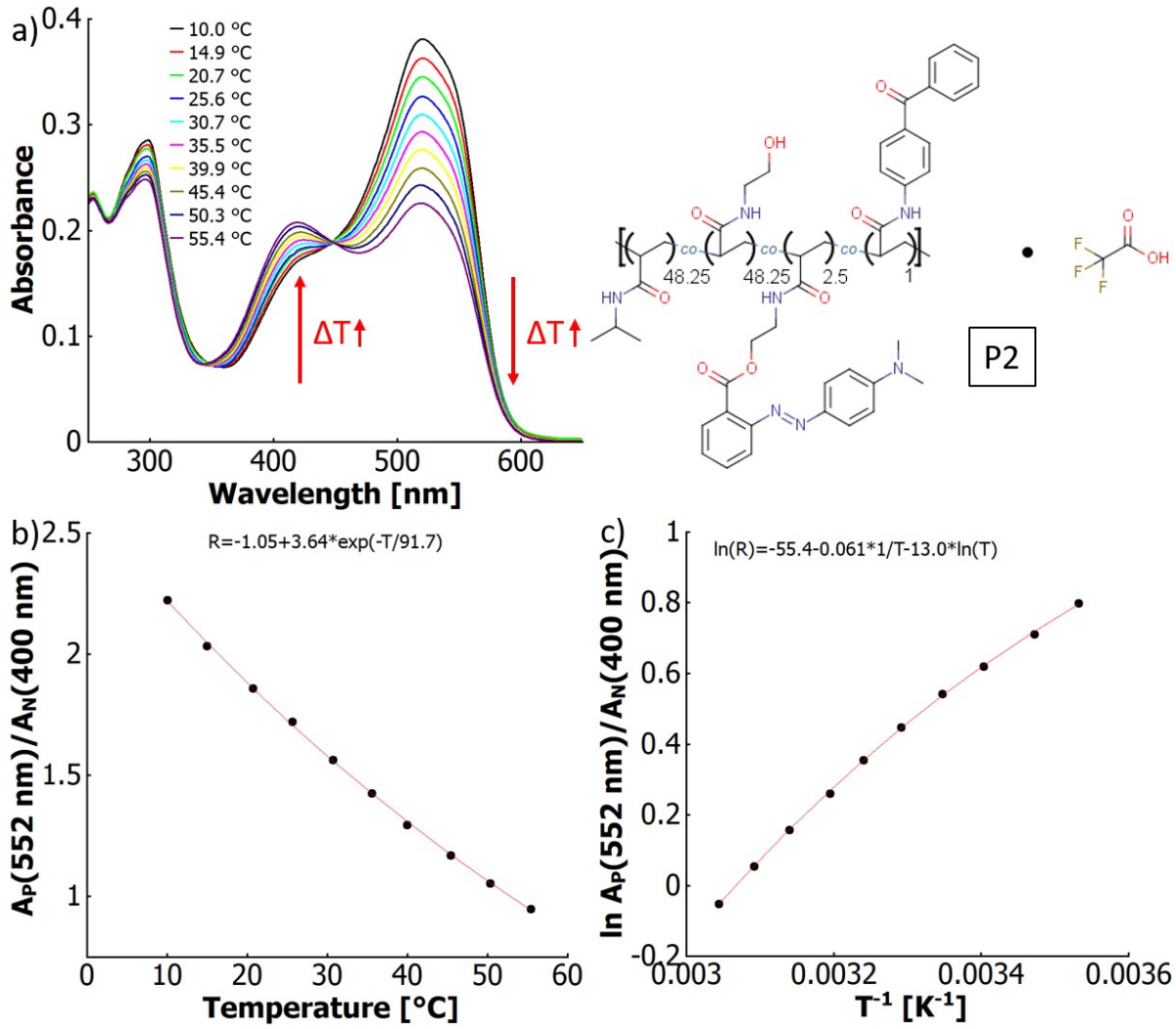

*Figure S 45: a) UV-vis spectra of a poly(NiPAAm-co-HEAm-co-o-MREAm-co-BPAAm) copolymer (P2) 0.02 w% in ethanolic trifluoroacetic acid (1 v/v%) at different temperatures with structure of the copolymer, direction of shifts in absorbance upon heating marked with red arrows; b) absorbance ratio of the protonated (552 nm) and the neutral species (400 nm) vs temperature, fitted with an exponential decay function; c) van't Hoff plot of the logarithmic absorbance ratio vs the inverse temperature, fitted with a function ln(R)=a-b*1/T+c*ln(T).*

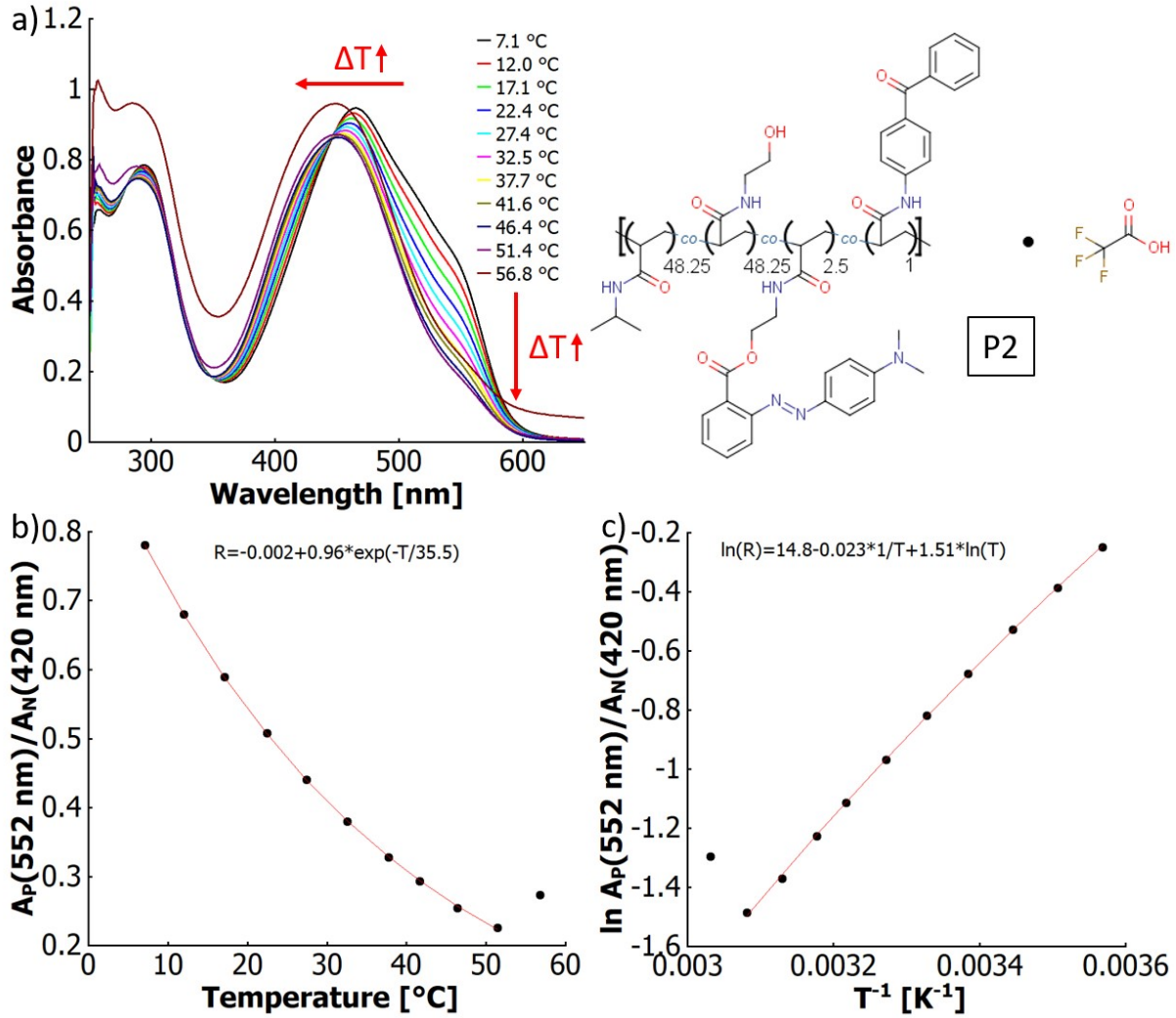

*Figure S 46: a) UV-vis spectra of a poly(NiPAAm-co-HEAm-co-o-MREAm-co-BPAAm) copolymer (P2) 0.03 w% in aqueous trifluoroacetic acid (0.001 v/v%) at different temperatures with structure of the copolymer, direction of shifts in absorbance upon heating marked with red arrows; b) absorbance ratio of the protonated (552 nm) and the neutral species (420 nm) vs temperature, fitted with an exponential decay function; c) van't Hoff plot of the logarithmic absorbance ratio vs the inverse temperature, fitted with a function ln(R)=a-b*1/T+c*ln(T).*

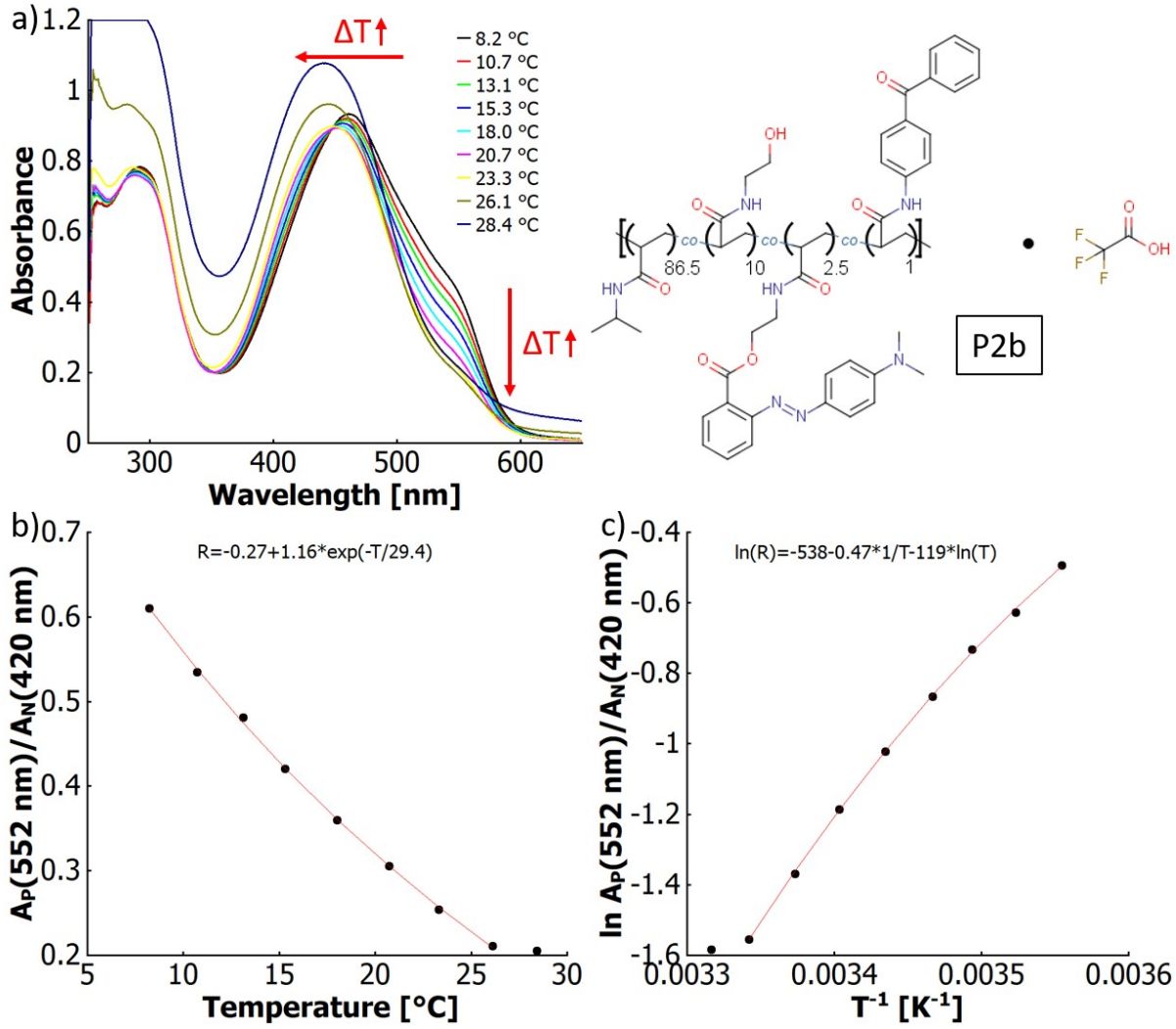

*Figure S 47: a) UV-vis spectra of a poly(NiPAAm-co-HEAm-co-o-MREAm-co-BPAAm) copolymer (P2b) 0.03 w% in aqueous trifluoroacetic acid (0.001 v/v%) at different temperatures with structure of the copolymer, direction of shifts in absorbance upon heating marked with red arrows; b) absorbance ratio of the protonated (552 nm) and the neutral species (420 nm) vs temperature, fitted with an exponential decay function; c) van't Hoff plot of the logarithmic absorbance ratio vs the inverse temperature, fitted with a function ln(R)=a-b*1/T+c*ln(T).*

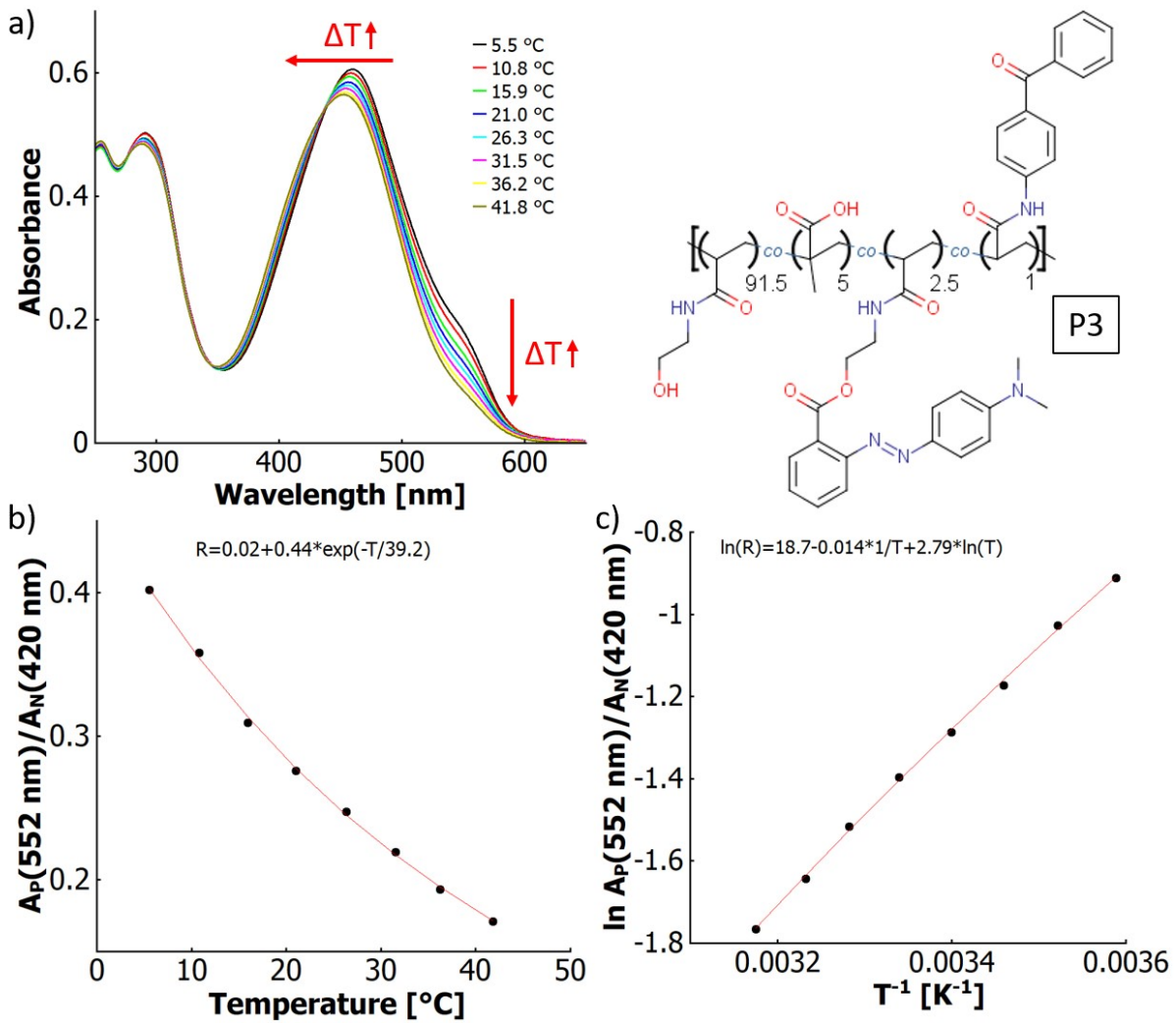

*Figure S 48: a) UV-vis spectra of a poly(HEAm-co-MAA-co-o-MREAm-co-BPAAm) copolymer (P3) 0.02 w% in water at different temperatures with structure of the copolymer, direction of shifts in absorbance upon heating marked with red arrows; b) absorbance ratio of the protonated (552 nm) and the neutral species (420 nm) vs temperature, fitted with an exponential decay function; c) van't Hoff plot of the logarithmic absorbance ratio vs the inverse temperature, fitted with a function ln(R)=a-b*1/T+c*ln(T).*

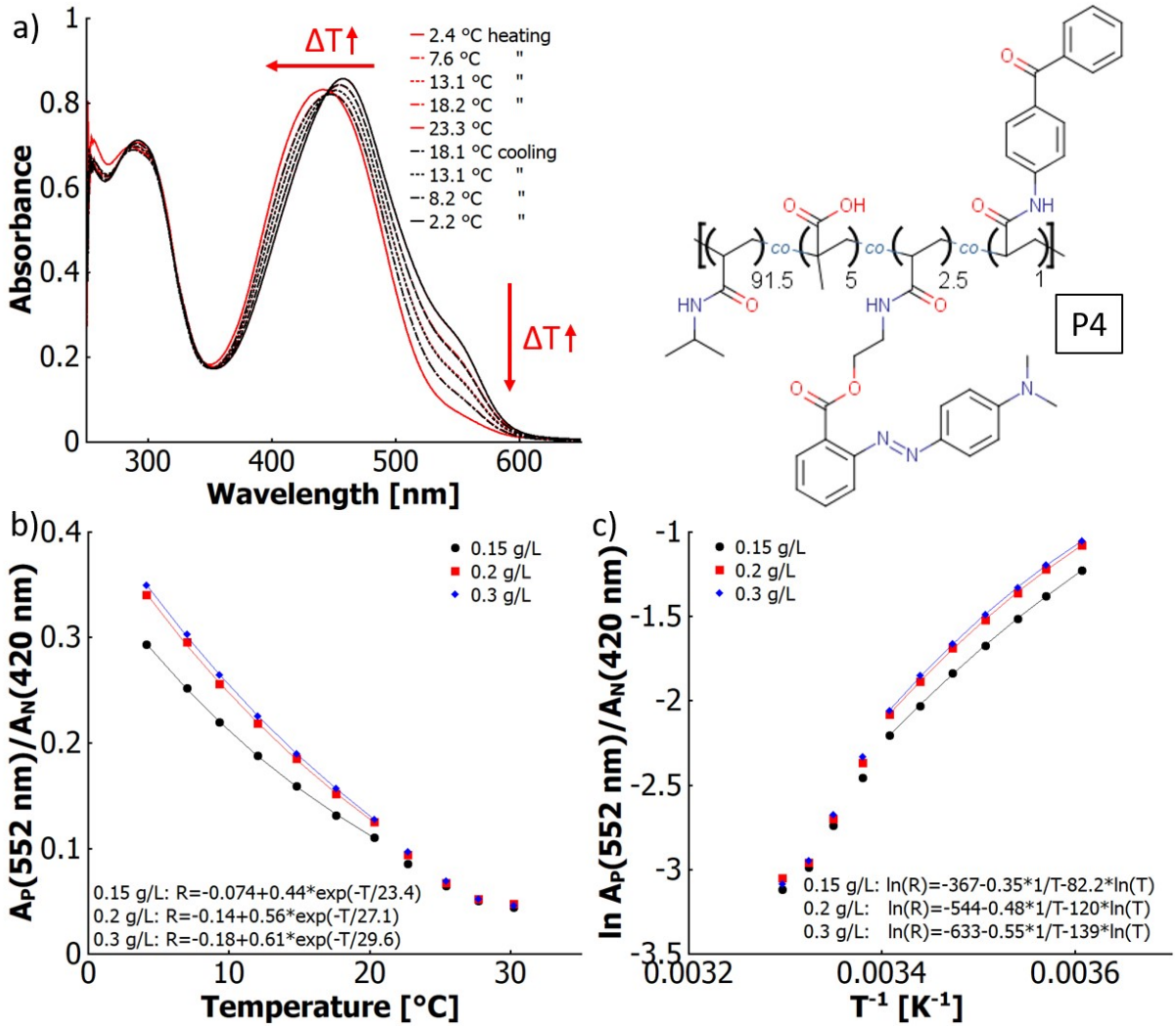

*Figure S 49: a) UV-vis spectra of a poly(NiPAAm-co-MAA-co-o-MREAm-co-BPAAm) copolymer (P4) 0.03 w% in water at different temperatures with structure of the copolymer, direction of shifts in absorbance upon heating marked with red arrows; b) absorbance ratio of the protonated (552 nm) and the neutral species (420 nm) vs temperature, fitted with an exponential decay function; c) van't Hoff plot of the logarithmic absorbance ratio vs the inverse temperature, fitted with a function ln(R)=a-b*1/T+c*ln(T).*

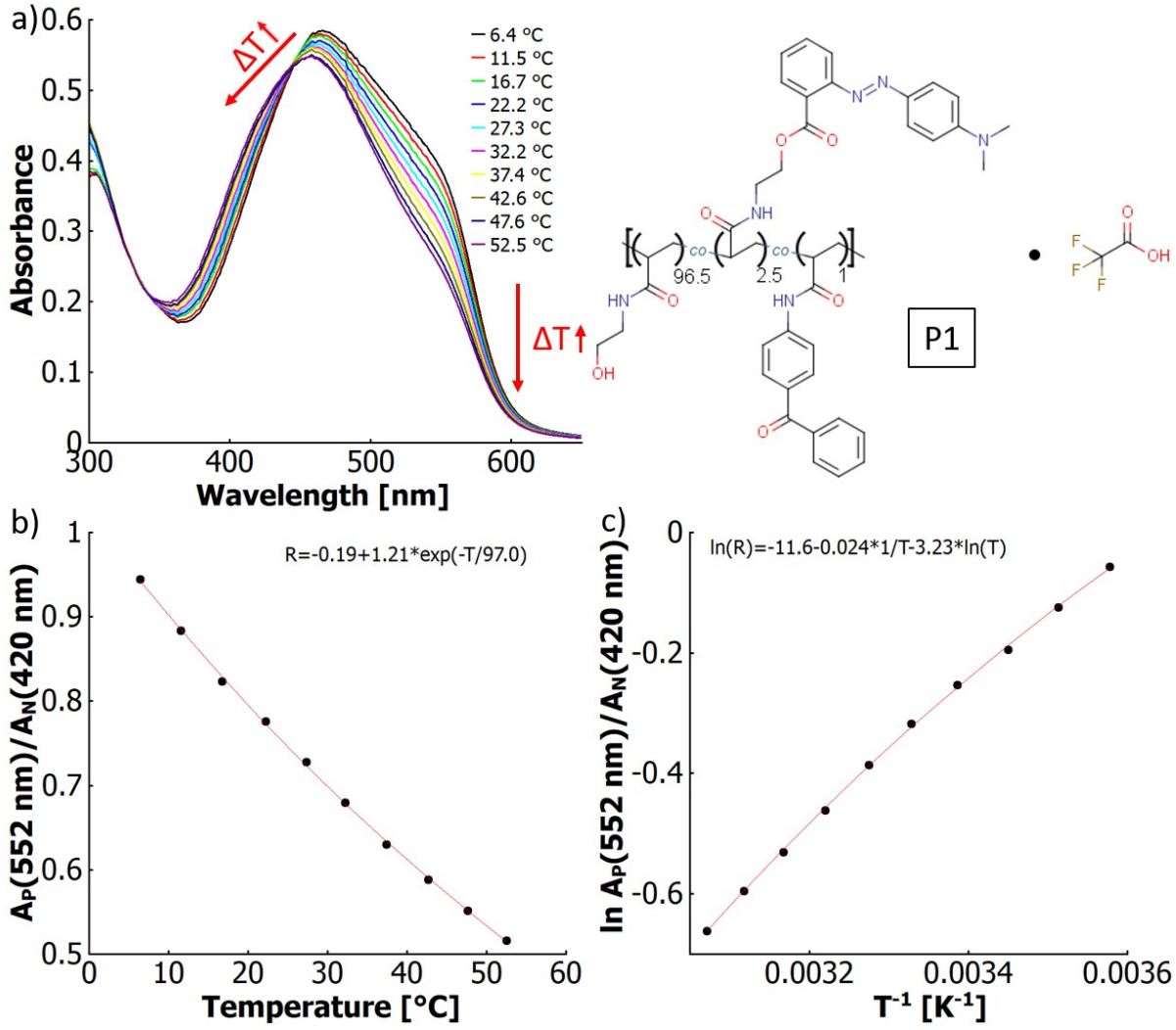

*Figure S 50: a) UV-vis spectra of a photocrosslinked poly(HEAm-co-o-MREAm-co-BPAAm) P1 film swollen in aqueous TFA (0.01 v%), at different temperatures with the structure of the copolymer before crosslinking; b) absorbance ratio R of the protonated (552 nm) and the neutral species (420 nm) vs temperature, fitted with an exponential decay function; c) van't Hoff plot of the logarithmic absorbance ratio vs the inverse temperature, fitted with a function ln(R)=a-b*1/T+c*ln(T). The absorbance was baseline corrected by subtracting the absorbance at 750 nm.*

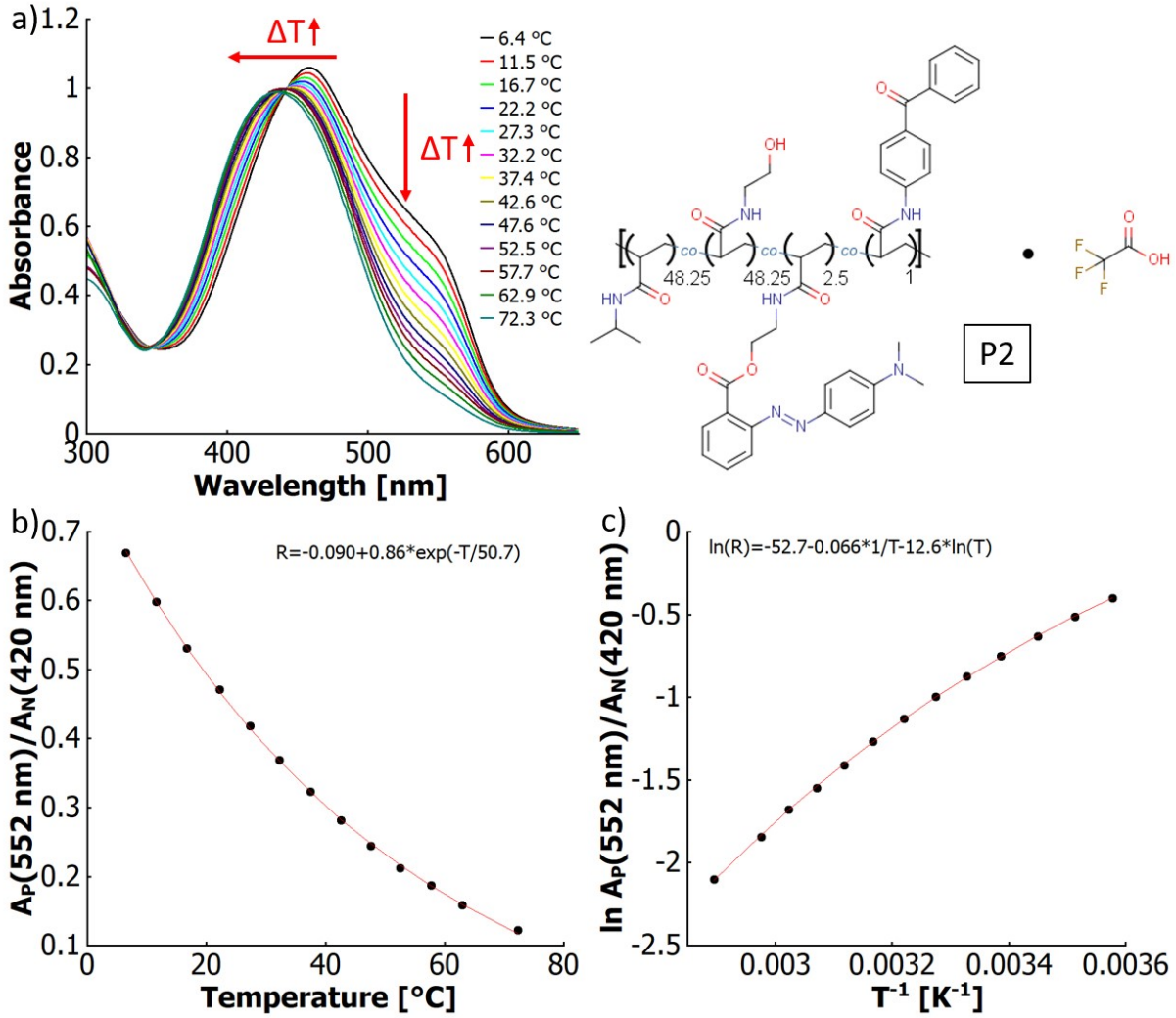

*Figure S 51: a) UV-vis spectra of a photocrosslinked poly(NiPAAm-co-HEAm-co-o-MREAm-co-BPAAm) P2 film swollen in aqueous TFA (0.01 v%), at different temperatures with the structure of the copolymer before crosslinking; b) absorbance ratio R of the protonated (552 nm) and the neutral species (420 nm) vs temperature, fitted with an exponential decay function; c) van't Hoff plot of the logarithmic absorbance ratio vs the inverse temperature, fitted with a function ln(R)=a-b*1/T+c*ln(T). The absorbance was baseline corrected by subtracting the absorbance at 750 nm.*

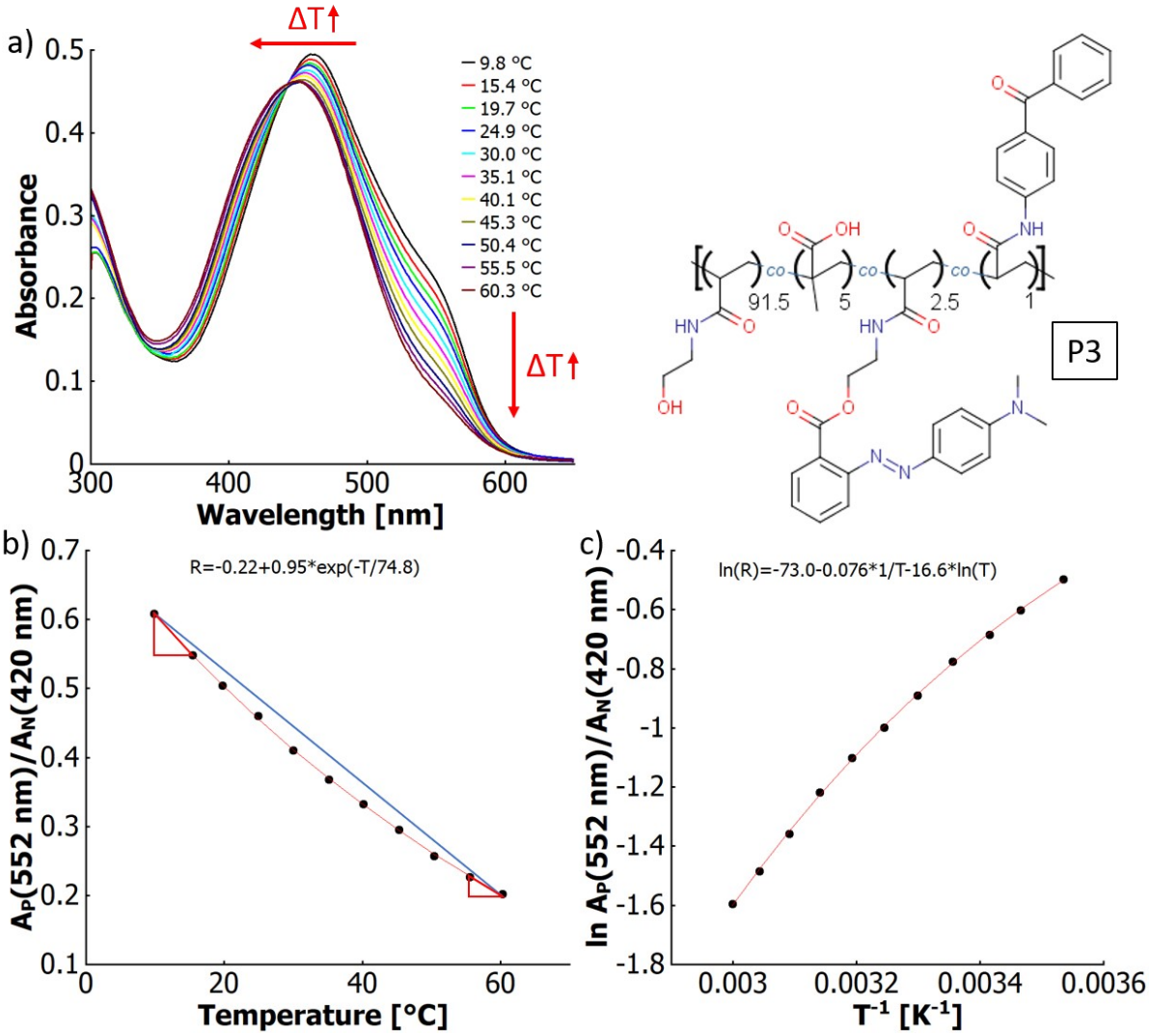

*Figure S 52: a) UV-vis spectra of a photocrosslinked poly(HEAm-co-MAA-co-o-MREAm-co-BPAAm) P3 film swollen in water, at different temperatures with the structure of the copolymer before crosslinking; b) absorbance ratio R of the protonated (552 nm) and the neutral species (420 nm) vs temperature, fitted with an exponential decay function. The blue line along with the red slope triangles serve as a reference to display the non-linearity of the graphs; c) van't Hoff plot of the logarithmic absorbance ratio vs the inverse temperature, fitted with a function ln(R)=a-b*1/T+c*ln(T).*

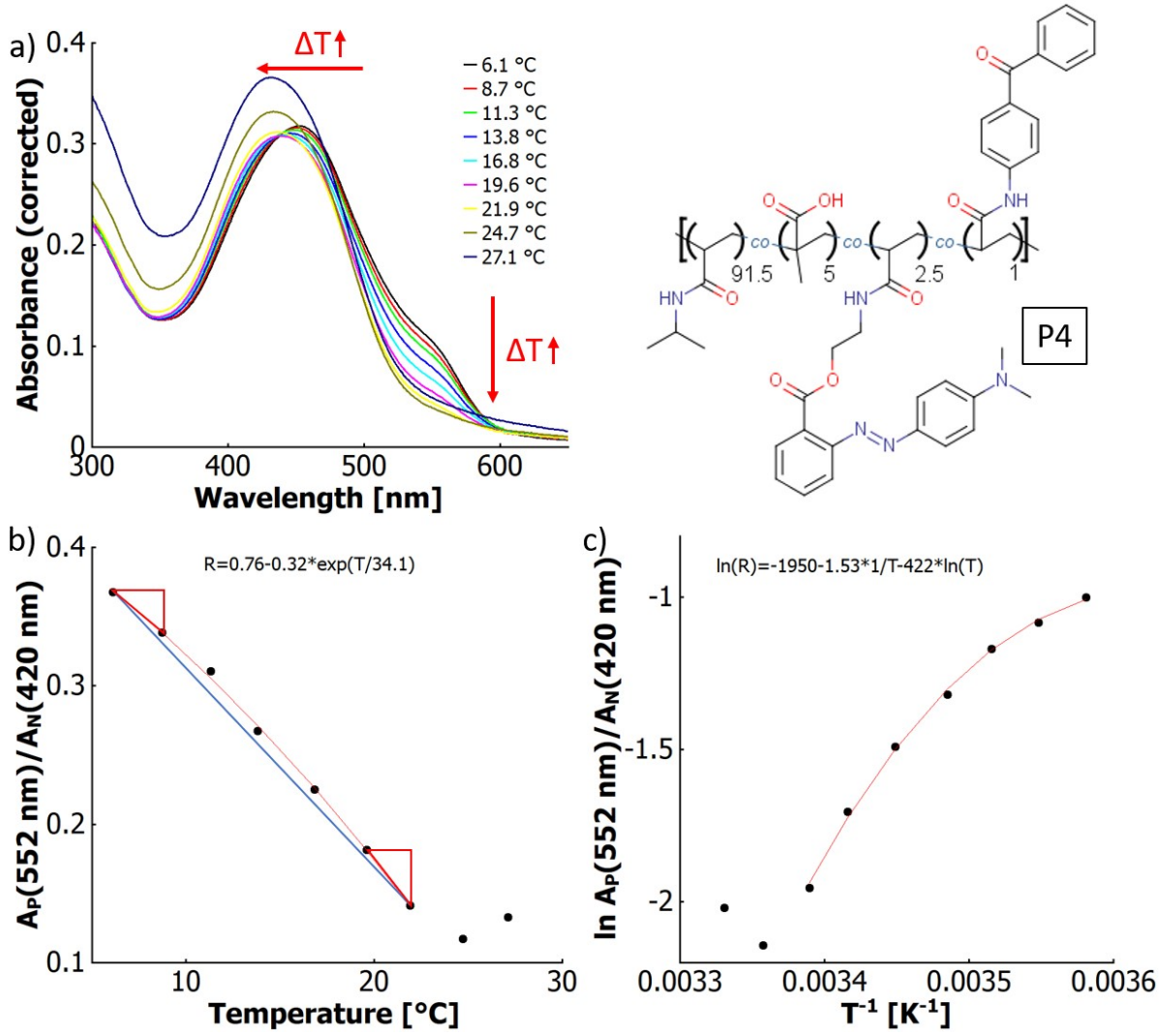

*Figure S 53: a) UV-vis spectra of a photocrosslinked poly(NiPAAm-co-MAA-co-o-MREAm-co-BPAAm) P4 film swollen in water, at different temperatures with the structure of the copolymer before crosslinking; b) absorbance ratio R of the protonated (552 nm) and the neutral species (420 nm) vs temperature, fitted with an exponential decay function. The blue line along with the red slope triangles serve as a reference to display the non-linearity of the graphs; c) van't Hoff plot of the logarithmic absorbance ratio vs the inverse temperature, fitted with a function ln(R)=a-b*1/T+c*ln(T). The absorbance was baseline corrected by subtracting the absorbance at 750 nm.*

Photocrosslinking:

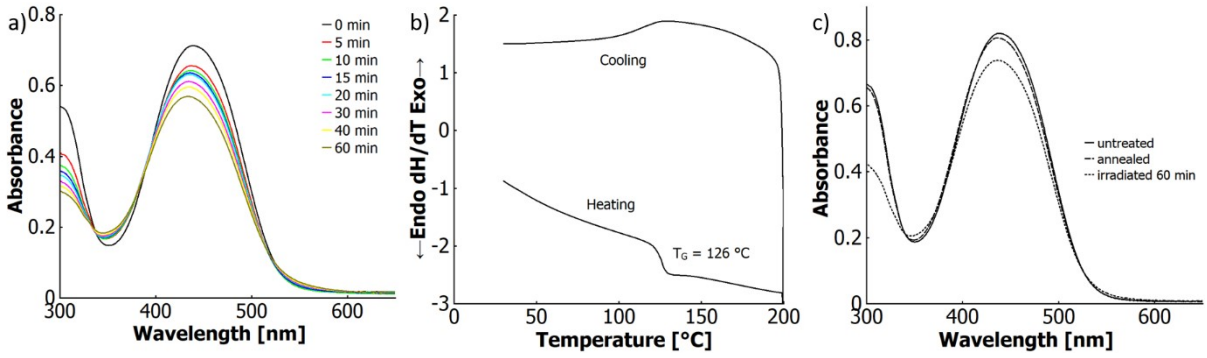

Figure S 54: a) UV-vis spectra of poly(HEAm-co-MREAm-co-BPAAm) P1 after successive irradiation intervals at 302 nm (additive exposure time provided, overall energy dose 20.3 J/cm²); b) DSC curves of P1 with heating and cooling rates of 10 K/min; c) UV-vis spectra of P1 after dropcasting, annealing, and photocrosslinking after annealing.

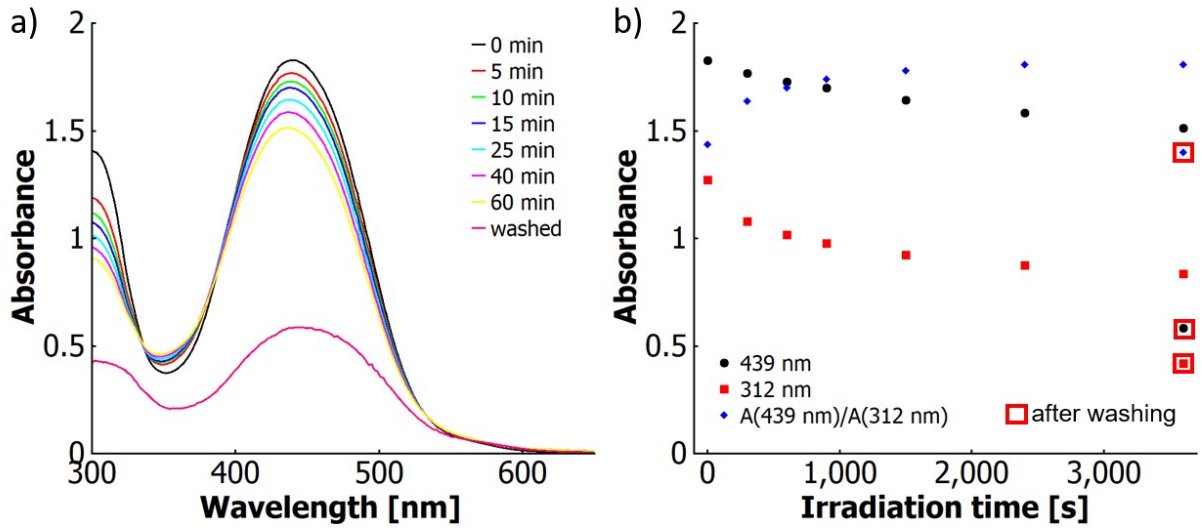

Figure S 55: a) UV-vis spectra of poly(HEAm-co-MAA-co-MREAm-co-BPAAm) P3 after successive irradiation intervals at 302 nm (additive exposure time provided, overall energy dose 20.3 J/cm²); b) absorbances at different wavelengths (characteristic for benzophenone 312 nm, azobenzene 439 nm) and ratio of the absorbances of the azobenzene and benzophenone vs irradiation time at 302 nm.

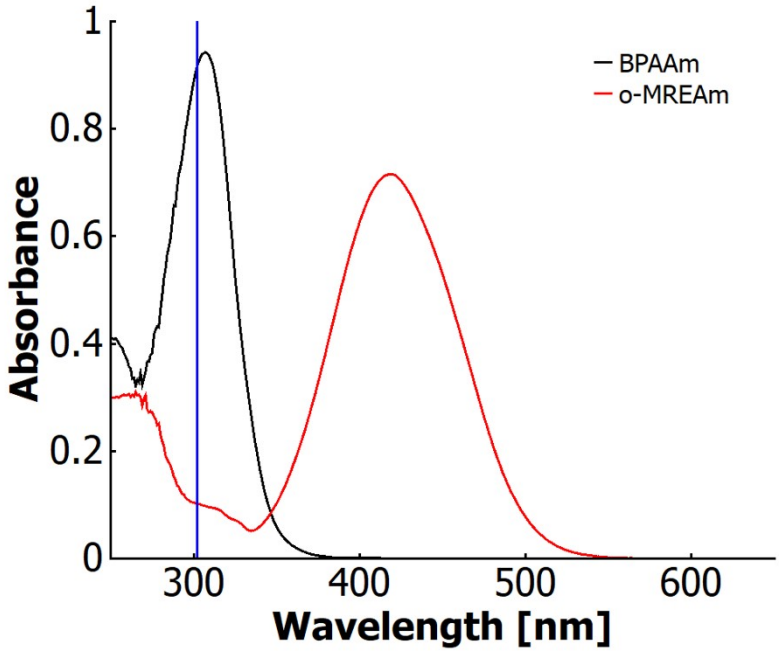

Figure S 56: Absorbance spectra in ethanolic solution at room temperature of an ortho-methyl red ester of N-(2-hydroxyethyl)acrylamide ($2.7*10^{-5}$ mol L^{-1}) (red spectrum) and 4-benzophenone acrylamide ($4.0*10^{-5}$ mol L^{-1}) (black spectrum). The vertical blue line indicates the wavelength at which copolymers containing both units were irradiated at.

References

1 J. Jia, M. Sarker, M. G. Steinmetz, R. Shukla and R. Rathore, Photochemical elimination of leaving groups from zwitterionic intermediates generated via electrocyclic ring closure of alpha,beta-unsaturated anilides, The Journal of organic chemistry, 2008, 73, 8867–8879.

2 M. Gianneli, R. F. Roskamp, U. Jonas, B. Loppinet, G. Fytas and W. Knoll, Dynamics of swollen gel layers anchored to solid surfaces, Soft matter, 2008, 4, 1443–1447.
3 H. A. Staab and A. Mannschreck, Synthese von Carbonsäureestern nach der Imidazolidmethode, Chem. Ber., 1962, 95, 1284–1297.
4 D. E. Bergbreiter, P. L. Osburn and C. Li, Soluble Polymer-Supported Catalysts Containing Azo Dyes, Org. Lett., 2002, 4, 737–740.
5 H. A. Staab, M. Lüking and F. H. Dürr, Darstellung von Imidazoliden. Synthese von Amiden, Hydraziden und Hydroxamsäuren nach der Imidazolidmethode, Chem. Ber., 1962, 95, 1275–1283.
6 J. Gao, Y. He, F. Liu, X. Zhang, Z. Wang and X. Wang, Azobenzene-Containing Supramolecular Side-Chain Polymer Films for Laser-Induced Surface Relief Gratings, Chem. Mater., 2007, 19, 3877–3881.
7 K. M. Tawarah and H. M. Abu-Shamleh, A spectrophotometric study of the acid-base equilibria of o-methyl red in aqueous solutions, Dyes and Pigments, 1991, 17, 203–215.
8 E. Sawicki, Physical Properties of Aminoazobenzene Dyes. V. The C ϵ /A ϵ Ratio, J. Org. Chem., 1957, 22, 621–625.
9 G. Seu, Spectrophotometric study of the prototropic equilibrium of methyl red in organic solvents, Dyes and Pigments, 1995, 29, 227–240.
10 S. J. Khouri, I. A. Abdel-Rahim, E. M. Alshamaileh and A. M. Altwaiq, Equilibrium and Structural Study of m-Methyl Red in Aqueous Solutions: Distribution Diagram Construction, J Solution Chem, 2013, 42, 1844–1853.
11 K. Tawarah, The tautomeric and acid-base equilibria of p-methyl red in aqueous solutions, Dyes and Pigments, 1992, 20, 261–270.
12 A. Savitzky and M. J. E. Golay, Smoothing and Differentiation of Data by Simplified Least Squares Procedures, Anal. Chem., 1964, 36, 1627–1639.
13 S. Bell, A. Bisset and T. J. Dines, Ab initio and density functional study of the resonance Raman spectra of Methyl Red, Ethyl Red and their protonated derivatives, *J. Raman Spectrosc.*, 1998, **29**, 447–462.
14 S.-K. Park, C.-K. Lee, K.-C. Min and N.-S. Lee, Fourier Transform Raman Studies of Methyl Red Adsorbed on γ-Alumina and Silica-Alumina, *Bulletin of the Korean Chemical Society*, 2004, **25**, 1817–1821.

15 A. M. Mebel, M. Hayashi, K. K. Liang and S. H. Lin, Ab Initio Calculations of Vibronic Spectra and Dynamics for Small Polyatomic Molecules: Role of Duschinsky Effect, *J. Phys. Chem. A*, 1999, **103**, 10674–10690.

16 A. Baiardi, J. Bloino and V. Barone, General Time Dependent Approach to Vibronic Spectroscopy Including Franck-Condon, Herzberg-Teller, and Duschinsky Effects, *Journal of chemical theory and computation*, 2013, **9**, 4097–4115.

17 A. Zhukov and R. Karlsson, Statistical aspects of van't Hoff analysis: a simulation study, Journal of molecular recognition:JMR, 2007, 20, 379–385.

18 H. Naghibi, A. Tamura and J. M. Sturtevant, Significant discrepancies between van't Hoff and calorimetric enthalpies, Proceedings of the National Academy of Sciences of the United States of America, 1995, 92, 5597–5599.

Polymer Chemistry

ROYAL SOCIETY OF CHEMISTRY

CORRECTION

View Article Online
View Journal | View Issue

Check for updates

Cite this: *Polym. Chem.*, 2022, **13**, 1282

Correction: Thermal response and thermochromism of methyl red-based copolymer systems – coupled responsiveness in critical solution behaviour and optical absorption properties

Thorben Gwydion Jaik,[a] Betty Ciubini,[b] Francesca Frascella[b] and Ulrich Jonas*[a]

DOI: 10.1039/d2py90024f

rsc.li/polymers

Correction for 'Thermal response and thermochromism of methyl red-based copolymer systems – coupled responsiveness in critical solution behaviour and optical absorption properties' by Thorben Gwydion Jaik *et al.*, *Polym. Chem.*, 2022, DOI: 10.1039/D1PY01361K.

Open Access Article. Published on 16 February 2022. Downloaded on 1/30/2023 11:32:30 AM.
This article is licensed under a Creative Commons Attribution 3.0 Unported Licence.

The Royal Society of Chemistry regrets the incorrect colour scheme applied in Table 7 in the original manuscript. The corrected version of Table 7 of this paper is shown below.

Table 7 Overview of the relevant parameters obtained from van't Hoff analyses of thermochromic solutions of methyl red-based monomers and different polymer systems. "a", "b", and "c term" refer to the raw data from the van't Hoff analyses and the colour code is applied to distinguish categories of thermo-halochromic systems with similar behaviour, both discussed in the main text

System	Solvent	Acid	a term	b term	c term	ΔH_0 [kJ]	ΔC_p [kJ K^{-1}]	Linearity factor [°C]
o-MREAm	EtOH	130 mM TFA	−55.7	0.071	−13.7	−34	−0.11	47
m-MREAm	EtOH	130 mM TFA	−56.7	0.062	−13.0	−32	−0.11	84
p-MREAm	EtOH	130 mM TFA	−41.8	0.054	−10.0	−25	−0.08	62
o-MREAm	H_2O : EtOH	2.2 mM HCl	155	−0.081	31.4	78	0.26	26
m-MREAm	H_2O : EtOH	11 mM HCl	102	−0.049	20.4	51	0.17	33
p-MREAm	H_2O : EtOH	5.9 mM HCl	125	−0.063	25.3	63	0.21	28
P1	EtOH	130 mM TFA	−55.5	0.063	−13.2	−33	−0.11	83
P1	H_2O	0.13 mM TFA	13.0	0.016	1.48	3.7	0.01	45
P1gel	H_2O	1.3 mM TFA	−11.6	0.024	−3.23	−8.0	−0.03	97
P2	EtOH	130 mM TFA	−55.4	0.061	−13.0	−32	−0.11	92
P2	H_2O	0.13 mM TFA	14.8	0.023	1.51	3.7	0.01	36
P2gel	H_2O	1.3 mM TFA	−52.7	0.066	−12.6	−31	−0.11	51
P2b	H_2O	0.13 mM TFA	−538	0.46	−119	−295	−0.99	29
P3	H_2O	MAA	18.7	0.014	2.79	6.9	0.02	39
P3gel	H_2O	MAA	−73	0.076	−16.6	−41	−0.14	75
P4 0.15 g L^{-1}	H_2O	MAA	−367	0.35	−82.2	−204	−0.68	23
P4 0.2 g L^{-1}	H_2O	MAA	−544	0.48	−120	−298	−1.00	27
P4 0.3 g L^{-1}	H_2O	MAA	−633	0.55	−139	−345	−1.2	30
P4gel	H_2O	MAA	−1950	1.53	−422	−1046	−3.51	−34

The Royal Society of Chemistry apologises for these errors and any consequent inconvenience to authors and readers.

[a]*Department of Chemistry and Biology, University of Siegen, Adolf-Reichwein-Strasse 2, D-57076 Siegen, Germany. E-mail: jonas@chemie.uni-siegen.de*
[b]*Department of Applied Science and Technology, Politecnico di Torino, Corso Duca degli Abruzzi 24, IT-10129 Torino, Italy*

This journal is © The Royal Society of Chemistry 2022

4 The "Tethered Solvent" Effect – H-Bonding-Controlled Thermo-Halochromism of a Push-Pull Azo Chromophore via its Secondary Amidoalkyl Acrylamide Side Chain

Thorben Gwydion Jaik, Ulrich Jonas

ChemPhysChem, 2023, **24,** e202200512.
http://dx.doi.org/10.1002/cphc.202200512

Published by *Wiley-VCH* in *ChemPhysChem* as an Open Access article under the terms of the Creative Commons CC BY-NC 4.0 license, which permits distribution, and reproduction in any medium, provided the original work is properly cited (CC BY-NC 4.0, https://creativecommons.org/licenses/by-nc/4.0/).

Contributions of the authors to this project:

- All UV-vis measurements, data analysis, synthesis of monomers, as well as interpretation were done by me.
- The complete draft was written by me and completed, refined, and edited together with Prof. Dr. Jonas.

Corrections:

- In Figure 1 a) of the paper, the vibrational wavefunction of the first vibrationally excited state in the first electronically excited state S1 must be inversed.
- On page 9 of the paper in point ii.), a red-shifting region of intersections is described, but a blue-shifting region of intersections should have been described for MREtAAm in *partially* protonated states in ethanol.
- On page 11 of the paper, red-shifting regions of intersections are described in acidified chloroform, while in actuality, blue-shifting regions of intersections have been observed.

ChemPhysChem

Research Article
doi.org/10.1002/cphc.202200512

Chemistry Europe
European Chemical Societies Publishing

www.chemphyschem.org

Check for updates

The "Tethered Solvent" Effect – H-Bonding-Controlled Thermo-Halochromism of a Push-Pull Azo Chromophore via Its Secondary Amidoalkyl Acrylamide Side Chain

Thorben Gwydion Jaik[a] and Ulrich Jonas*[a]

The fascinating field of thermo-halochromism of azo chromophores still astounds with unexplored facets nourished by the intricate relationship between molecular structure variations and their spectroscopic signatures. In this respect, we investigated the thermally dependent absorption behaviour of acrylamide derivatives of *o*-methyl red, characterised by two secondary amide linkages with hydrogen bonding-active protons in the pendant alkyl substituent. The systems were studied by a combination of UV-vis, derivative, and difference, as well as 2D-NMR (Nuclear Overhauser Effect Spectroscopy, NOESY) spectroscopy. These experiments show that the thermo-halochromism is specifically influenced by hydrogen bonding interaction of the secondary amidoalkyl acrylamide side chain with the azobenzene core in dependence of the spacer length. Apparently, the substituent acts like a solvent, which is directly tethered to the chromophore and where the tether length determines the interaction by conformational freedom. We refer to this novel phenomenon as "H-bonding-controlled thermo-halochromism".

Introduction

Despite the fact that azo dyes have been known and utilised for more than a century,[1] very little is known about their complex thermochromic behaviour. The term "thermochromism" generally refers to a reversible or irreversible colour change with temperature.[2]

A sub-category is thermo-halochromism, which involves a change in interaction and/or reaction with an ion, e.g., a reversible protonation of a molecule. This has been demonstrated for phenolates with metal ions,[3] hydrazones by deprotonation,[4] different pH-indicators in buffer solutions,[5] an azo dye in a micelle containing a chromoionophore,[6] and for this study of particular importance, for the well-known pH indicator (*ortho*-)methyl red (oMR) adsorbed on silica gel.[7]

o-Methyl red changes in aqueous solution from red at pH 4.4, when it is in its protonated, cationic form with an absorption maximum at ca. 525 nm to the yellow, deprotonated state above pH 6.2 with the maximum at ca. 430 nm.[8] The protonated form of *o*-methyl red exists in two different ionic structures. Apart from an ammonium ion expected for a tertiary amine, also an azonium structure is formed in aminoazobenzene-type dyes. In *o*-methyl red, the azonium form is the prevalent structure as it is stabilised *via* a quinoidal resonance structure and intramolecular hydrogen bonding.[9] The different protonation states of *o*-methyl red are summarised in Scheme 1. The thermochromic effect observed when the dye is adsorbed on silica gel, is a colour change from red (acidic) to orange (neutral/basic) when the gel is heated. This thermochromism was attributed to a combination of the thermal response of the dye with an increased basicity of the solvated silica gel at low temperatures owing to release of water.[7]

The same behaviour of a shift in the protonation equilibrium towards the neutral dye has been observed for *N*-hydroxyethyl acrylamide esters of the positional isomers of methyl red. This thermochromism occurs in *partially* protonated systems and is heavily influenced by thermo-solvatochromism in binary solvent mixtures and by incorporation in copolymers as a side group. We were able to identify this mechanism in our recent studies.[10] For these derivatives and also for *trans*-azobenzene,[11] difference spectroscopy was used to demonstrate the temperature-induced vibronic changes. We referred to this mechanism involving a shift in the ratio between vibronic sub-bands as "vibronic thermochromism".

As hydrogen bonding interactions between a chromophore and its surrounding solvent are known to strongly affect the optical absorption behaviour, it is of high relevance to also study the perichromic effect of such H-bonding of a flexible substituent directly attached to the azo chromophore.

In this light, we synthesised secondary amides of *o*-methyl red with different alkyl spacer lengths between the chromophore and an additional secondary amide group in order to evaluate their thermochromism in ethanolic solution under neutral, *partially* protonated, and *completely* protonated conditions. For these systems, a strong influence of the spacer length on the thermo-halochromism was observed despite the minute direct electronic influence of the alkyl chain on the

[a] *T. G. Jaik, Prof. Dr. U. Jonas*
Department Chemistry – Biology,
University of Siegen
Adolf-Reichwein-Strasse 2, 57076 Siegen, Germany
E-mail: jonas@chemie.uni-siegen.de

Supporting information for this article is available on the WWW under https://doi.org/10.1002/cphc.202200512

© 2022 The Authors. ChemPhysChem published by Wiley-VCH GmbH. This is an open access article under the terms of the Creative Commons Attribution Non-Commercial License, which permits use, distribution and reproduction in any medium, provided the original work is properly cited and is not used for commercial purposes.

© 2022 The Authors. ChemPhysChem published by Wiley-VCH GmbH

14397641, 2023, 1, Downloaded from https://chemistry-europe.onlinelibrary.wiley.com/doi/10.1002/cphc.202200512 by Cochrane Germany, Wiley Online Library on [30/01/2023]. See the Terms and Conditions (https://onlinelibrary.wiley.com/terms-and-conditions) on Wiley Online Library for rules of use; OA articles are governed by the applicable Creative Commons License

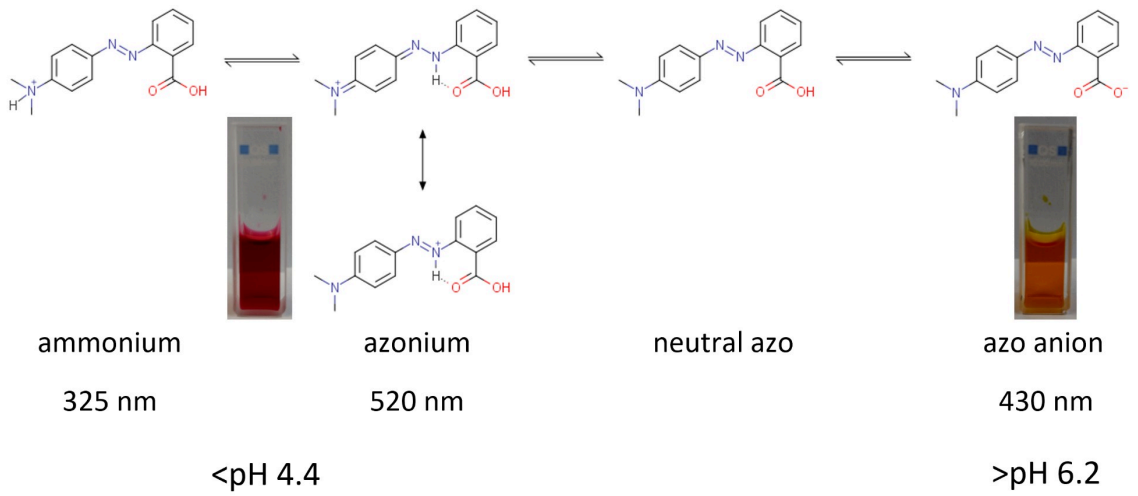

Scheme 1. Prototropic equilibrium of o-methyl red in aqueous solution at different pH with an ammonium, azonium, neutral, and deprotonated form. The pictures are of solutions of the dye in aqueous hydrochloric acid (1.2 M, left, red, product of a tautomer mixture of ammonium and azonium forms) and in aqueous sodium hydroxide solution (0.1 M, right, orange). If the dye is functionalised at the carboxylic acid, the anion cannot be formed.

chromophore. This thermochromic behaviour is ascribed to an intramolecular H-bonding motif acting on the chromophore in dependence on the spacer length, which has implications for the temperature-dependent protonation of azobenzene derivatives in solution. In the following, experimental evidence from UV-vis, derivative, and difference spectroscopy is presented and contrasted with 2D-NMR (NOESY) measurements and solvatochromic data to support this hypothesis.

The findings of this work may be relevant for the understanding of the interdependence between the structure of a molecular scaffold and intramolecular H-bonding motifs, which is a fundamental aspect, for example, in the elucidation of protein functionality and the design of molecular machines.

Results and Discussion

Acrylamides based on *o*-methyl red exhibit characteristic thermochromic behaviours in ethanolic solution. The thermochromisms differ between vibronic thermochromism in the neutral or *completely* protonated dyes, or thermo-halochromism in solutions containing both the neutral and the protonated dye. The thermo-halochromism strongly depends on the spacer length between the acrylamide functionality and the chromophore.

Four different acrylamide derivatives were synthesised in two steps by monoamidation of an alkyldiamine (C2, C3, C6 and C8) with *o*-methyl red employing carbonyldiimdazole and subsequent reaction of the remaining free amine group with acryloyl chloride (cf. Scheme 2). It must be noted that the reported yields of the monoamidation were determined by ^{1}H NMR spectroscopy. The purification of these amines proved to be challenging and they were thus used in the second step with only rudimentary work-up. In the following, the dyes will be referred to as MREtAAm, MRPrAAm, MRHexAAm and MROctAAm for the C2, C3, C6, and C8 derivatives, respectively.

These dyes were studied in ethanolic solution by UV-vis spectroscopy regarding their temperature-dependent absorption behaviour. Specifically, three scenarios were investigated with three different methods.

The spectral characteristics of the dyes were measured in three protonation states at different temperatures: 1. neutral, 2. *completely* protonated, and 3. *partially* protonated. These terms refer to the dye molecules in solution (1.) being all dissolved in pure solvent in the neutral state, or (2.) all being protonated in one site at high acid concentration, or (3.) at low acid concentration, only a certain percentage of the dye molecules being protonated in one site, while the remaining fraction is in the neutral state. In the last case, both species must coexist in significant numbers so that they both clearly contribute to the spectral features.

In addition to the overall protonation state of the system, these substituted, push-pull 4-aminoazobenzenes feature more than one protonation site. Protonation can occur either at the dimethylaniline-group, forming an ammonium ion, or at the β-nitrogen of the azo bridge, forming an azonium ion (cf. ESI Scheme S2). In the parent compound *o*-methyl red, the azonium form is stabilised by internal hydrogen bonding owing to the carbonyl in ortho-position to the azo bridge. This shifts the tautomeric ammonium-azonium equilibrium strongly on the side of the azonium form.[12] The same was found in the secondary amides in this study (cf. Figure 2b).

It was found that the four dye derivatives (MREtAAm, MRPrAAm, MRHexAAm and MROctAAm) differ considerably in their thermochromic behaviour in the *partially* protonated state. In the neutral and *completely* protonated states the four homologues behaved similar to each other.

Apart from standard UV-vis spectroscopy, the spectral changes were analysed *via* derivative spectroscopy and differ-

© 2022 The Authors. ChemPhysChem published by Wiley-VCH GmbH

14397641, 202, 1, Downloaded from https://chemistry-europe.onlinelibrary.wiley.com/doi/10.1002/cphc.202200512 by Cochrane Germany, Wiley Online Library on [30/01/2023]. See the Terms and Conditions (https://onlinelibrary.wiley.com/terms-and-conditions) on Wiley Online Library for rules of use; OA articles are governed by the applicable Creative Commons License

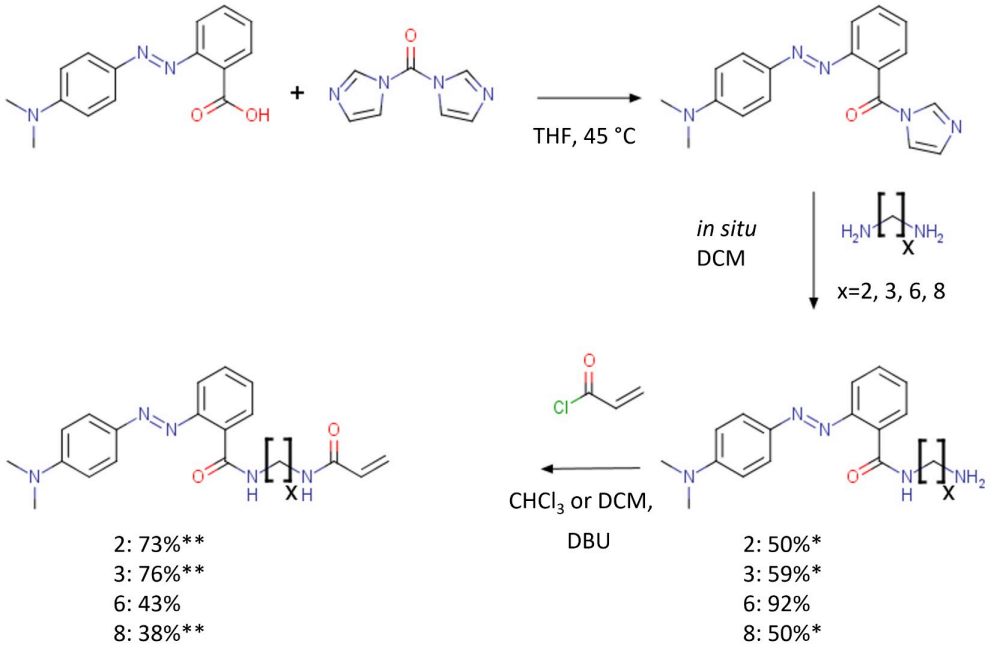

Scheme 2. Synthesis of amidoalkyl acrylamide of o-methyl red with different spacer length by first forming an imidazolide, reacting with the corresponding diamines, and finally reacting the free amine with acryloylchloride. *yield determined by ^{1}H NMR spectroscopy, **yield adjusted to the educt content of the raw product used in this synthesis step.

ence spectroscopy. Derivative spectroscopy can be utilised to identify the position of sub-bands under less resolved absorption bands. Negative peaks in the second or positive peaks in the fourth derivative of the absorbance indicate the position of sub-bands.[13] For the present study, only the second derivatives of the main absorption bands were generated. In addition, difference spectroscopy shows the absolute changes between spectra that were measured under different conditions. Here, the spectra at the lowest temperature were subtracted from those at higher temperatures.

For the interpretation of the data obtained, the Franck-Condon principle was consulted (cf. Figure 1 a).[14] This theory assumes an electronic transition from the ground state S_0 to the first excited state S_1 to take place without changing the position of the nuclei. This is explained by the much larger timescales of vibrational rearrangements compared to the absorption of a photon. However, vibrational levels exist in the S_1 state that may be populated *via* the electronic transition if there is overlap between the vibrational wavefunction in the ground state S_0 and in the excited state S_1. Necessary conditions are that the

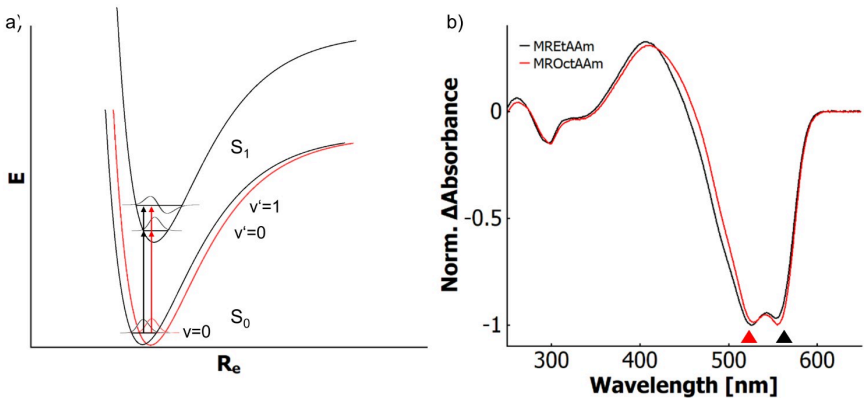

Figure 1. a) Franck-Condon principle with Morse potentials of the electronic ground state in different configurations and the first excited state in a graph of the energy (E) versus the molecule geometry (represented by the generic reaction coordinate R_e); b) difference spectra calculated by subtracting the spectra at low temperature from those at high temperatures (low temperatures: ca. 7 °C; high temperatures: ca. 48 °C), normalised to the curve minimum of MREtAAm and MROctAAm in ethanolic trifluoroacetic acid (1 v/v%). The black triangle denotes the position of the 0–0 sub-band, and the red triangle the position of the 0–1 sub-band.

© 2022 The Authors. ChemPhysChem published by Wiley-VCH GmbH

14397641, 202, 1, Downloaded from https://chemistry-europe.onlinelibrary.wiley.com/doi/10.1002/cphc.202200512 by Cochrane Germany, Wiley Online Library on [30/01/2023]. See the Terms and Conditions (https://onlinelibrary.wiley.com/terms-and-conditions) on Wiley Online Library for rules of use; OA articles are governed by the applicable Creative Commons License

excited vibrational wavefunction has the same symmetry as the ground state vibrational wavefunction and is Raman-active. As the ground state wavefunction is considered as totally symmetric, the vibrational mode to be excited in S_1 must be as well. In azobenzenes, the only strong, totally symmetric vibration is the N=N valence mode (ca. 1400 cm^{-1}).[14] Hence, it can be assumed that this mode is the main origin of vibronic sub-bands in UV-vis spectra of this class of compounds.

1. *Neutral dye*: The absorbance maxima (435–445 nm) of the neutral azobenzene derivatives in ethanol blue-shift upon temperature increase concomitant with a change in the asymmetry of the absorption band. This can be attributed to a change in the ratio between different vibronic sub-bands. We refer to these temperature-dependent spectral changes as "vibronic thermochromism", which we assign to a slight variation in equilibrium conformation. Consequently, the Franck-Condon factors change, which in turn affects the vibronic signature.[15] The following main factors are influenced by temperature and lead to a shift in the conformational populations: (1) reorganisation of the solvation shell, and (2) variation of the population as a consequence from intramolecular hydrogen bonding.

According to the data from derivative spectroscopy, the absorption band of the neutral dye consists mainly of two vibronic sub-bands (cf. Figure 2a, ESI Figure S36e–h). The maxima of the vibronic sub-bands lie at almost the same wavelength for all four derivatives (~475 nm and ~425 nm, cf. Table 1). The long wavelength sub-band corresponds to the 0–0 vibronic transition, while the second sub-band is blue-shifted by about 2360–2500 cm^{-1} in dependence of the alkyl spacer length. On the basis of Resonance Raman data from the literature for the parent compound *o*-methyl red[16] and vibronic analysis of other azobenzene compounds,[11,14,17] this energy difference does not seem to correspond to a specific 0–1 transition, as the only totally symmetric mode is the N=N stretching vibration. This may be explained on the one hand by a large overlap between the 0–1 and the 0–2 transition even in the derivative spectra, making it impossible to differentiate. On the other hand, considerable mode mixing may influence the energy of the mode.[18]

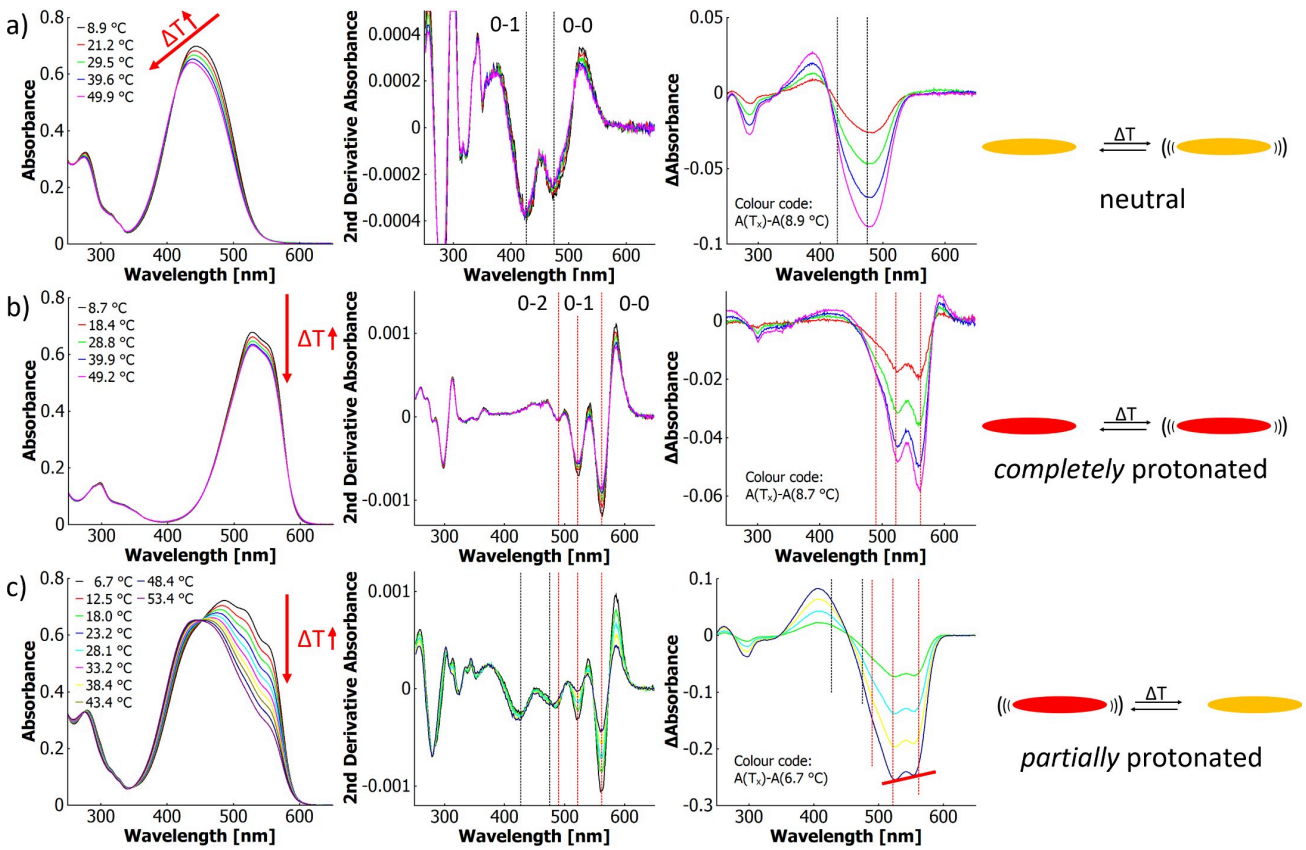

Figure 2. From left to right: UV-vis spectra of MREtAAm (2.7*10^{-5} molL^{-1} for a and c, 1.4*10^{-5} molL^{-1} for b) at different temperatures, the corresponding second derivative spectra, the corresponding difference spectra, and cartoons showing the corresponding thermochromic processes involving a) vibronic effects of the neutral species in pure ethanol, b) vibronic effects of the protonated species (azonium ion) in ethanolic sulfuric acid (1 v/v%), and c) thermohalochromism in ethanolic trifluoroacetic acid (1 v/v%). The positions of the vibronic sub-bands as determined by derivative spectroscopy are marked by dashed lines (black: neutral dye 0–0 and 0–1 vibronic transition; red: protonated dye 0–0, 0–1, and 0–2 vibronic transition). The derivative spectra have the same colour code as the UV-vis spectra. The colour of the difference spectra corresponds to the spectrum from which the spectrum at the respective lowest temperature was subtracted. The pictograms provided on the right-hand side denote a vibrational/thermal excitation of the chromophore compared to the initial temperature (orange colour denotes a neutral molecule, red colour a protonated molecule, stacked round brackets indicate vibrationally excited states).

© 2022 The Authors. ChemPhysChem published by Wiley-VCH GmbH

14397641, 202, 1, Downloaded from https://chemistry-europe.onlinelibrary.wiley.com/doi/10.1002/cphc.202200512 by Cochrane Germany, Wiley Online Library on [30/01/2023]. See the Terms and Conditions (https://onlinelibrary.wiley.com/terms-and-conditions) on Wiley Online Library for rules of use; OA articles are governed by the applicable Creative Commons License

14397641, 202, 1, Downloaded from https://chemistry-europe.onlinelibrary.wiley.com/doi/10.1002/cphc.202200512 by Cochrane Germany, Wiley Online Library on [30/01/2023]. See the Terms and Conditions (https://onlinelibrary.wiley.com/terms-and-conditions) on Wiley Online Library for rules of use; OA articles are governed by the applicable Creative Commons License

Table 1. Absorbance maxima at low temperatures, vibronic sub-bands as determined by derivative spectroscopy and wavelength shifts of the absorbance maxima with temperature increase from around 10 °C to around 50 °C of the neutral dyes in ethanol. λ-shift refers to the shift of the absorbance maxima of the main absorption bands.

Derivative	λ_{max}(neutral) [nm]	$0–0_{max}$ [nm]	$0–1_{max}$ [nm]	$\tilde{\nu}_{01}$ [cm^{-1}]	λ-shift [nm]	λ-shift [cm^{-1}]
MREtAAm	445	475	427	2370	445→437	410
MRPrAAm	434	470	423	2360	434→432	110
MRHexAAm	437	472	423	2450	437→433	210
MROctAAm	436	473	423	2500	436→434	110
o-MREAm	420	450	420	1590	420→417	170

Consequently, the assignment of the transition is rather ambiguous. Assuming that it is indeed a single transition, as literature would suggest,[14,17,19] the energy neither fits a 0–1 transition corresponding to a N=N stretching vibration of around 1400 cm^{-1}, nor to a 0–2 transition for the same stretching mode, which is dominant in azobenzenes.[14,17] For a 0–2 transition, the energy would be higher at around 2700–2800 cm^{-1}. However, similar behaviour has been reported for other azobenzene derivatives in 50% aqueous ethanol solution.[19] In that case it was argued that a strong solvent cage with hydrogen bonding leads to planarization and thus a disturbance of the totally symmetric N=N stretching vibration. On the basis of these reports, mode mixing[18] in the here studied, asymmetric derivatives is highly likely. The combination of the ethanolic solvent cage with hydrogen bonding of the secondary amide proton to the azo bridge, as suggested by NOESY spectra of the compounds (cf. ESI Scheme S1, S28–35), perturbs the symmetry of the N=N stretching mode.

The derivative spectra of the neutral dyes suggest that the 0–1 transition is favoured over the 0–0 transition. In the C2-derivative MREtAAm, the 0–0 sub-band has a higher intensity relative to the 0–1 sub-band compared to the other derivatives (cf. ESI Figure S36). Only MREtAAm shows a noticeable decrease in intensity for the 0–0 sub-band with temperature increase. In all other derivative spectra, the changes with temperature are too small to be visible.

The difference spectra show a negative peak primarily at the wavelength of the 0–0 vibronic sub-band and an increase at wavelengths shorter than the 0–1 transition (cf. Figure 2a). This is reflected in the changes of the wavelength of the absorption maximum and in the asymmetry of the absorption band in the UV-vis spectrum. For MRPrAAm with C3-spacer, the difference spectra deviate from those of the other three derivatives. Here, the decrease in absorbance is at a shorter wavelength (by 13 nm) compared to the wavelength of the 0–0 sub-band as determined by derivative spectroscopy (cf. ESI Figure S36, Figure S39 of the neutral dyes). In these difference spectra, the asymmetry of the negative spectral changes leans towards shorter wavelengths from the centre of the band, while it leans towards longer wavelengths for the other derivatives. This suggests that the proportion of higher vibronic transitions being excited upon temperature increase is higher in MRPrAAm than in the other derivatives. A detailed analysis of the derivative and difference spectra is necessary to identify the subtle deviation of the C3-derivative MRPrAAm, as this is not obvious in the parent UV-vis spectra.

The absorption maximum of the main band in the UV-vis spectra is almost identical for MRPrAAm, MRHexAAm, and MROctAAm (434–437 nm) in ethanol, while only for MREtAAm it is noticeably red-shifted (445 nm, cf. Table 1). As the 0–0 sub-band is more pronounced in MREtAAm, its absorption band must be red-shifted if the vibronic sub-bands of all derivatives lie at the same positions. At the same time, the temperature-induced blueshift is most pronounced in MREtAAm (cf. Figure 2a) with a shift from 445 nm at 8.9 °C to 437 nm at 49.9 °C (ca. 410 cm^{-1}, Table 1). Like mentioned previously, the difference spectra show a negative peak mainly at the wavelength of the 0–0 sub-band. Only for MREtAAm a considerable change in the temperature-dependent derivative spectra can be observed for the same sub-band. It follows that the blueshift of the UV-vis band must be larger in this derivative.

2. *Completely protonated dye:* In contrast to the neutral species, the UV-vis spectra of the *completely* protonated species (azonium ion) in ethanolic sulfuric acid (1 v/v%) are highly similar for all derivatives. All maxima lie in the range of 527–528 nm and the shape of the bands with richer features more clearly suggest an underlying vibronic structure than in the neutral case (cf. Figure 2b, Figure 5b), which is even more apparent in the derivative spectra (cf. Figure 2b, ESI Figure S37). However, while the vibronic structure becomes vaguer upon temperature increase, no shift in the wavelength of the absorption maximum can be observed.

The UV-vis bands of the azonium ion consist of three vibronic sub-bands at 562–563 nm, 522–523 nm, and 489–490 nm. The energy difference between the first sub-band and second sub-band is 1330–1360 cm^{-1}, between the first and third sub-band 2610–2690 cm^{-1}. These findings are summarised in Table 2. The first sub-band is assigned to the 0–0 transition like in the neutral case. The second and third sub-band result from the 0–1 and 0–2 transitions of vibronic coupling with the N–N stretching mode. These assignments are chosen according to reported Raman studies on the parent compound *o*-methyl red.[16,20] In the derivative spectra, the transitions decrease in intensity with increasing order (0–0 > 0–1 > 0–2). A decrease in intensity is visible for both the 0–0 sub-band and the 0–1 sub-band upon temperature increase, while the 0–2 sub-band appears invariant (cf. Figure 2b, ESI Figure S37).

The change in absorbance with temperature is more apparent in the difference spectra, which even show a vibronic sub-structure for the azonium ion in contrast to the neutral species. Such difference spectra show minima at wavelengths

© 2022 The Authors. ChemPhysChem published by Wiley-VCH GmbH

14397641, 2023, 1, Downloaded from https://chemistry-europe.onlinelibrary.wiley.com/doi/10.1002/cphc.202200512 by Cochrane Germany, Wiley Online Library on [30/01/2023]. See the Terms and Conditions (https://onlinelibrary.wiley.com/terms-and-conditions) on Wiley Online Library for rules of use; OA articles are governed by the applicable Creative Commons License

Table 2. Absorbance maxima at low temperatures and vibronic sub-bands as determined by derivative spectroscopy of the protonated dyes in ethanolic sulfuric acid (1 v/v%).

Derivative	λ_{max}(azonium) [nm]	0–0$_{max}$ [nm]	0–1$_{max}$ [nm]	0–2$_{max}$ [nm]	$\tilde{\nu}_{01}$ [cm^{-1}]	$\tilde{\nu}_{12}$ [cm^{-1}]
MREtAAm	527	562	522	490	1360	1250
MRPrAAm	528	562	523	489	1330	1330
MRHexAAm	528	562	523	489	1330	1330
MROctAAm	528	563	523	489	1360	1330
o-MREAm	519	549	513	482	1280	1250

corresponding to the 0–0 and 0–1 vibronic sub-bands identified by derivative spectroscopy. The absorbance decrease with temperature is stronger in the case of the 0–0 transition than for the 0–1 transition (cf. Figure 2, ESI Figure S39). This may be explained by a stronger temperature effect on the configuration of the ground state compared to that of the excited state.

3. *Partially protonated system:* The UV-vis spectra of the *partially* protonated situation exhibit a more complex thermochromic behaviour. The concept of the underlying mechanism, referred to as thermo-halochromism, has been previously introduced for the thermochromism observed for the *N*-hydroxyethyl acrylamide ester of *o*-methyl red (*o*-MREAm) in a *partially* protonated state.[10] In short, the protonation equilibrium between the neutral azobenzene and the ionic azonium is shifted towards the neutral azobenzene upon heating. This is signified by a decrease in absorbance of the azonium ion (~550 nm) and an increase in absorbance of the neutral azobenzene (~450 nm). While for the ester *o*-MREAm an isosbestic point can be observed in ethanolic TFA (1 v/v%), only the C6-derivative of the amides, MRHexAAm, shows an isosbestic point for the temperature-dependent measurements. MREtAAm shows a considerable blueshift of the intersections between spectra of adjacent temperature steps, while these intersections red-shift with about the same magnitude for MRPrAAm and MROctAAm (cf. Figure 3, Table 3). As for a simple equilibrium between two absorbing species with spectral overlap, an isosbestic point would be expected, the observed deviation warrants an explanation. We refer to this phenomenon as "region of intersections".[10]

The derivative spectra (cf. Figure 2c, ESI Figure S38) of these mixtures show only four sub-bands between 400 and 600 nm instead of the expected five (two from the neutral species and three from the azonium ion). The 0–0$_{neutral}$ and 0–2$_{azonium}$ sub-

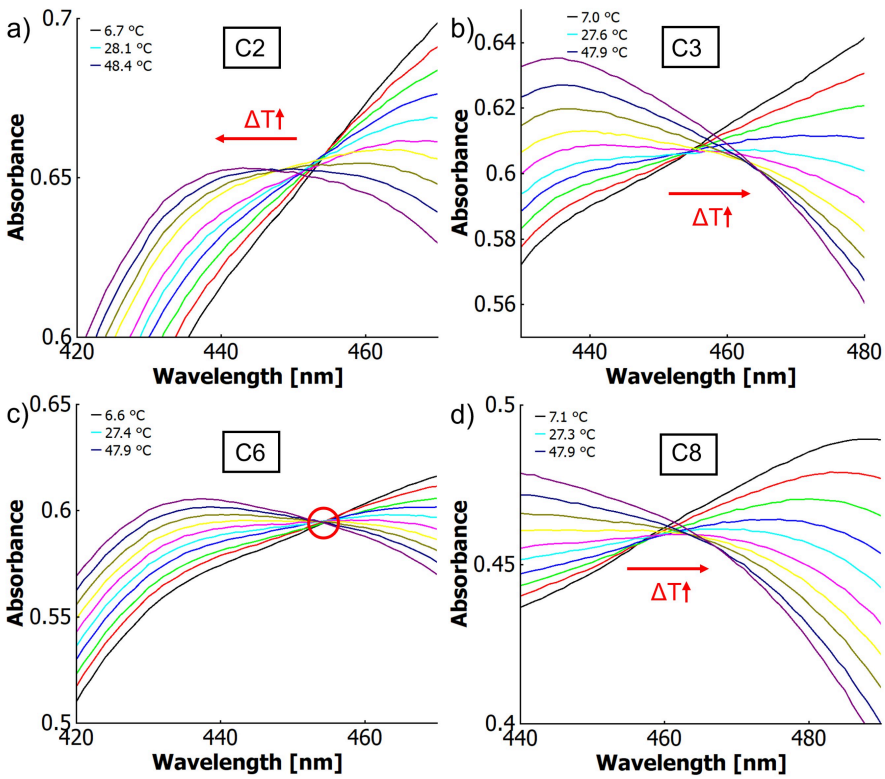

Figure 3. Zoom-in of temperature-dependent UV-vis spectra of different amidoalkyl acrylamide of o-methyl red in ethanolic trifluoroacetic acid (0.01 gL^{-1}, 1 v/v% TFA). a) MREtAAm; b) MRPrAAm; c) MRHexAAm and d) MROctAAm. Shifts upon heating in the intersections between adjacent temperature steps are indicated by red arrows or circles in the case of an isosbestic point.

© 2022 The Authors. ChemPhysChem published by Wiley-VCH GmbH

Table 3. Region of intersections or isosbestic point and thermodynamic data as determined by van't Hoff analysis for the thermo-halochromism of the partially protonated dye mixtures in ethanolic trifluoroacetic acid (1 v/v%) compared to H_2O:EtOH ($\chi_{EtOH} = 0.31$) with HCl (2.2 mM) and isosbestic point found in the corresponding titrations. Data for the ester derivative o-MREAm is taken from literature.[10]

Derivative	Solvent/Acid	Region of intersections [nm] ([cm^{-1}])	ΔH_0 [$kJmol^{-1}$]	ΔC_p [$kJmol^{-1}K^{-1}$]	Isosbestic point Titration [nm]
MREtAAm	EtOH/TFA	455–446 (440)	−31.2	−0.10	475
MRPrAAm	EtOH/TFA	454–465 (−520)	−29.7	−0.10	472
MRHexAAm	EtOH/TFA	454 (0)	−28.3	−0.09	475
MROctAAm	EtOH/TFA	456–467 (−520)	−45.6	−0.15	475
o-MREAm	EtOH/TFA	453 (0)	−38.4	−0.13	460
o-MREAm	H_2O:EtOH/HCl	455–434 (1060)	78	0.26	465

bands overlap, reducing the total number of observable bands by one. The band formed by the overlapping vibronic sub-bands blue-shifts with increasing temperatures, as the sub-bands of the azonium species decrease with the protonation equilibrium shifting towards the neutral azobenzene. The changes upon temperature increase occur primarily in the azonium ion region. The $0–0_{azonium}$ and the $0–1_{azonium}$ sub-bands decrease. The $0–1_{neutral}$ sub-band does not increase considerably, while the $0–0_{neutral}$ does increase, apparent by the blueshift at around 480 nm.

Like in the neutral and the *completely* protonated cases, the difference spectra document the temperature-induced spectral changes more clearly than normal UV-vis spectra or derivative spectra. The positions of the changes in these spectra are roughly the same for all investigated *o*-methyl red amides. The decrease in absorbance takes place mostly above 500 nm with minima at ~555 nm and at ~526 nm, while an increase occurs at ~406 nm (cf. Figure 2, EI Figure S39, Table 4). The minima are slightly shifted compared to the positions of the vibronic sub-bands determined by derivative spectroscopy, indicated by the dashed vertical lines in Figure 5c, and compared to the minima in the difference spectra of the *completely* protonated species. The maximum lies somewhere in the absorption band of the neutral species but not at the position of any specific vibronic sub-band. This stems from a spectral overlap between the neutral and the protonated species (cf. Figure 5). The decrease in absorbance at a given wavelength resulting from a decrease of the azonium ion concentration by thermally activated deprotonation must be compensated by the absorbance of the neutral species concurrently increasing in concentration before the overall absorbance can increase in the overlap region. A positive change then occurs only at wavelengths at which the azonium ion either has no absorption or when that absorbance is overcompensated by the formed neutral species.

Depending on the specific derivative, the ratio between the $0–0_{azonium}$ and the $0–1_{azonium}$ peaks differs. For MREtAAm (blue-shifting region of intersections) the $0–1_{azonium}$ band is more negative, while the bands are equal for MRHexAAm (isosbestic point). In MRPrAAm and MROctAAm (red-shifting region of intersections) the $0–0_{azonium}$ band is more negative.

However, when the degree of protonation is altered by titrating with free acid while keeping the *temperature constant*, a distinct isosbestic point is observed instead of the region of intersections found in the first approach of *ramping the temperature*. This significant difference in spectral behaviour between the two approaches is highly unexpected, as in both experiments the dye is nominally protonated (increase of acid concentration in titration, temperature decrease in thermo-chromism). The isosbestic points are located at significantly longer wavelengths compared to the regions of intersections in the temperature-dependent measurements (cf. Table 3, ESI Figure S40, zoom-ins provided in Figure S41).

Difference spectroscopy provides further insights on the spectral details of the observed deviation between temperature-induced and pH-induced changes in the protonation equilibrium. The corresponding spectra are shown in Figure 4. A striking contrast is that the difference spectra of the titrations (black curves) carry little vibronic information compared to those of thermo-halochromism (red curves). The negative peaks in the titrations are asymmetric, suggesting an underlying sub-band structure, but do not have distinct minima like those observed in thermo-halochromism. This behaviour and the corresponding UV-vis spectra can be reproduced fairly well by simple linear combinations of spectra of the pure neutral azobenzene and azonium ion (cf. ESI Figure S42, Figure S44). This suggests that the neutral species and the azonium ion coexist independently with no apparent influence of one species on the other nor are additional species and long-living

Table 4. Maxima in nm of positive (Pos.) and negative (Neg.) changes in difference spectra subtracting the lowest temperature spectra from higher temperature spectra of the neutral dyes in ethanol, the completely protonated dyes in ethanolic sulfuric acid (1 v/v%) and the partially protonated mixture in ethanolic trifluoroacetic acid (1 v/v%).

Derivative	Pos. neutral	Neg. neutral	Pos. azonium	Neg. 1 azonium	Neg. 2 azonium	Pos. mixture	Neg. 1 mixture	Neg. 2 mixture
MREtAAm	388	479	593	559	525	406	554	526
MRPrAAm	377	457	591	559	525	406	555	527
MRHexAAm	378	472	592	560	525	406	556	526
MROctAAm	378	474	592	560	525	410	555	528
o-MREAm	367	434	584	545	515	405	545	519

© 2022 The Authors. ChemPhysChem published by Wiley-VCH GmbH

14397641, 202, 1, Downloaded from https://chemistry-europe.onlinelibrary.wiley.com/doi/10.1002/cphc.202200512 by Cochrane Germany, Wiley Online Library on [30/01/2023]. See the Terms and Conditions (https://onlinelibrary.wiley.com/terms-and-conditions) on Wiley Online Library for rules of use; OA articles are governed by the applicable Creative Commons License

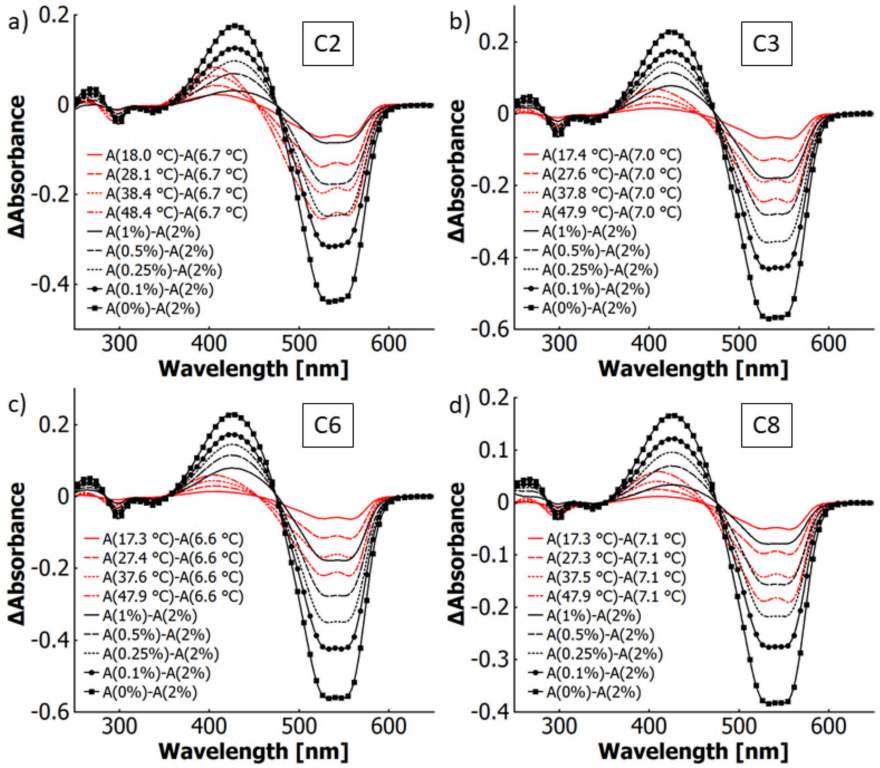

Figure 4. Difference spectra obtained by subtraction of spectra with a higher degree of protonation from those with a lower degree of protonation for different amidoalkyl acrylamides of o-methyl red a) MREtAAm; b) MRPrAAm; c) MRHexAAm; and d) MROctAAm (all 0.01 g/L) in ethanolic trifluoroacetic acid. The black graphs indicate different concentrations of trifluoroacetic acid at 25 °C (v/v% given in the legends), while the red graphs indicate different temperatures at 1 v/v% trifluoroacetic acid in ethanol.

transition states involved when the azonium ion concentration is increased by titration with acid.

Interestingly, the linear combinations of spectra of the neutral dyes and the azonium ions show isosbestic points regardless of the measuring temperature for the original spectra. These simulated isosbestic points lie at approximately the same wavelength (~476 nm, cf. Figure S43). As the spectra of the neutral and the protonated dyes were not measured at the exact same temperature, small differences in the wavelength of the simulated isosbestic points occur.

As mentioned above, the vibronic sub-bands can be identified in the difference spectra for the thermochromic experiment. In direct comparison with the titrations, the negative peaks are significantly broadened in the short wavelength region, suggesting a larger contribution from higher energy transitions of the azonium ion in the thermochromic pathway (cf. Figure 4). The significantly different absorption behaviour upon a shift in the degree of protonation either by titration or by thermochromism strongly suggests that the protonation/deprotonation mechanism differs strongly between thermally induced (thermochromism) and acid-induced (titration) protonation/deprotonation.

H-Bonding-Controlled Thermo-Halochromism

In order to explain the observed stark difference between plain *titration at constant temperature* and *temperature ramping*, we postulate the involvement of a third, metastable species in the protonation equilibrium (cf. Scheme 3). The most probable nature of this species would be a distorted conformer of the azonium species formed immediately upon protonation. To observe this species, the distorted conformer needs to relax within the time frame of the observation window into the stable azonium ion ground state as found in the experiment of *complete* protonation.

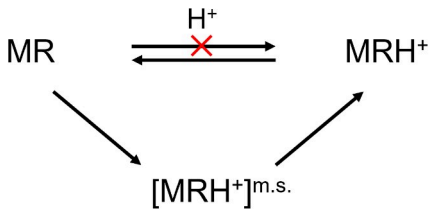

Scheme 3. Postulated protonation equilibrium of secondary amides of o-methyl red involving a metastable conformer directly after protonation. The superscript "m.s." stands for "metastable state".

© 2022 The Authors. ChemPhysChem published by Wiley-VCH GmbH

14397641, 202, 1, Downloaded from https://chemistry-europe.onlinelibrary.wiley.com/doi/10.1002/cphc.202200512 by Cochrane Germany, Wiley Online Library on [30/01/2023]. See the Terms and Conditions (https://onlinelibrary.wiley.com/terms-and-conditions) on Wiley Online Library for rules of use; OA articles are governed by the applicable Creative Commons License

Several questions arise from this postulate: (1) Why is the metastable species an azonium ion? (2) Why are the observed differences between the dye derivatives in this study not simply vibronic effects of the neutral and the relaxed azonium ion species? (3) Why is the metastable species a conformer? And (4) what is the origin of the temperature-dependency of the observed regions of intersections?

Question (1) has a straight answer. The spectral differences between the derivatives with varying spacer lengths occur predominantly in the absorption bands of the azonium ions. Since for the neutral species no lower vibronic transitions exist below the 0–0 transition, which lies at higher energies than the azonium transitions, no red-shift of its absorbance band into this spectral region can occur.

To answer question (2), the temperature-dependent vibronic behaviours of the separate neutral and protonated dyes have to be related to their vibronic changes in thermohalochromism. One crucial factor affecting the ratio between the 0–$0_{azonium}$ and the 0–$1_{azonium}$ minima is the spectral overlap between the neutral and the protonated dye species. There is miniscule overlap at the wavelength of the 0–$0_{azonium}$ but considerable overlap at the wavelength of the 0–$1_{azonium}$ sub-band (cf. Figure 5c). In an ideal scenario, in which the shift of a chemical equilibrium results in a linear combination of the individual absorbances of the involved species, the observed decrease in absorbance in the difference spectra related to the azonium ion would be simply the absorbance value in the UV-vis spectrum of the azonium ion with reversed algebraic sign. An increase in the concentration of the neutral species would contribute with a corresponding absorbance value at that given wavelength and would lead to a lowered absorbance change at the 0–$1_{azonium}$ sub-band owing to the spectral overlap.

Since an additional contribution of vibronic thermochromism of both the azonium ion (reflected in a comparatively lower decrease in 0–$1_{azonium}$) and the neutral azobenzene (strong decrease in 0–0) is expected, the absorbance ratio of the 0–$0_{azonium}$ to the 0–$1_{azonium}$ sub-bands in the difference spectra is difficult to predict for the hypothetical ideal case.

However, the following reasons suggest that the influence of vibronic thermochromism of the separate species may be neglected.

i.) The vibronic changes of the neutral species are small at the wavelength of the 0–$1_{azonium}$ transition (cf. Figure 5d). This is found even for the derivative with the highest spectral overlap between the isolated neutral and protonated species, MREtAAm.

ii.) For the same derivative, a red-shifting region of intersections along with a stronger decrease in the 0–$1_{azonium}$ sub-band is found in the *partially* protonated scenario. However, in an ideal case this highest spectral overlap should lead to the largest compensation of the decrease in absorbance of the azonium species by the increase in

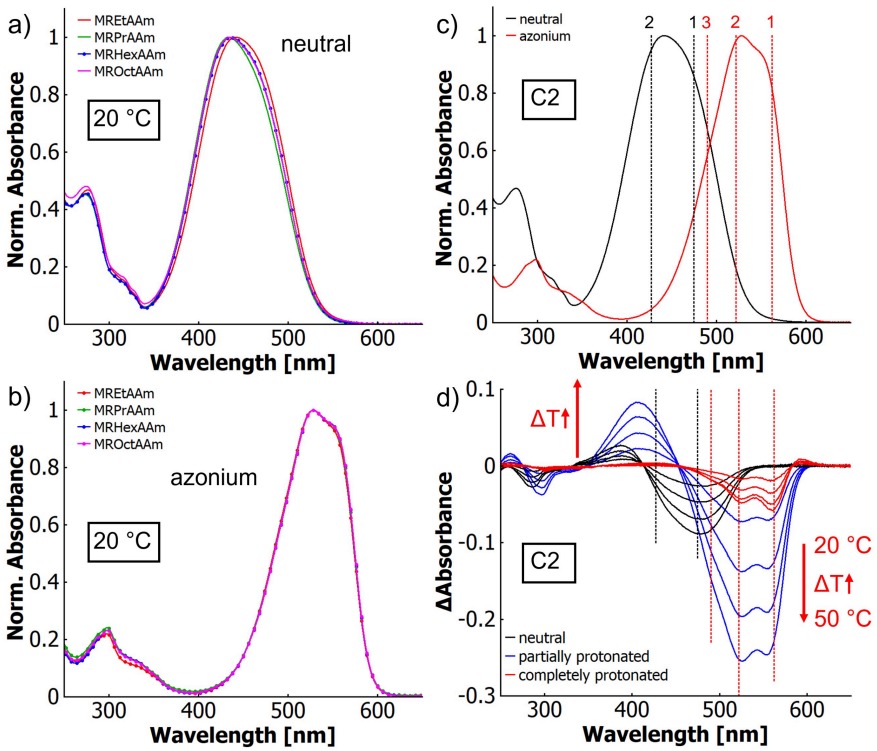

Figure 5. Normalised UV-vis spectra of different amidoalkyl acrylamides of o-methyl red (MREtAAm, MRPrAAm, MRHexAAm, MROctAAm) as a) the neutral dye in ethanol and b) the protonated dye in ethanolic sulfuric acid (1 v/v%); c) normalised UV-vis spectra of MREtAAm as the neutral dye in ethanol and the protonated dye in ethanolic sulfuric acid (1 v/v%) with black and red vertical lines marking the position of vibronic sub-bands of the neutral and protonated dye, respectively, and d) difference spectra of MREtAAm in the neutral, completely protonated, and partially protonated state, where the spectra were generated by substracting spectra at the lowest measured temperature (~10 °C) from those at higher temperatures. The black and red vertical lines again mark the positions of the vibronic sub-bands, 1 denoting the 0–0 sub-bands, 2 the 0–1 sub-bands, and 3 the 0–2 sub-band.

© 2022 The Authors. ChemPhysChem published by Wiley-VCH GmbH

14397641, 202, 1, Downloaded from https://chemistry-europe.onlinelibrary.wiley.com/doi/10.1002/cphc.202200512 by Cochrane Germany, Wiley Online Library on [30/01/2023]. See the Terms and Conditions (https://onlinelibrary.wiley.com/terms-and-conditions) on Wiley Online Library for rules of use; OA articles are governed by the applicable Creative Commons License

absorbance of the neutral species. In turn, this should lead to a smaller decrease in the 0–$1_{azonium}$ sub-band, but the observed stronger decrease of this sub-band suggests that spectral overlap of the separate species does not explain the distinct vibronic characteristics in the *partially* protonated scenario.

iii.) The magnitude of the spectral changes related to thermohalochromism is considerably larger than those of vibronic origin for the separate species.

iv.) MRPrAAm and MROctAAm display the same net effect in the *partially* protonated scenario but have considerable differing vibronic variation in the neutral species (cf. ESI Figure S39b, d). Since the vibronic thermochromism of the azonium ions does not differ between derivatives, a large influence of the vibronic thermochromisms of the pure species can be excluded.

v.) MRHexAAm and MROctAAm show almost identical spectral traces in the neutral and protonated state (cf. Figure 5) and have almost identical temperature-dependent derivative and difference spectra (cf. Table 1, Table 2, Table 4; ESI Figure S36, Figure S37, Figure S39). Yet, MRHexAAm exhibits an isosbestic point while MROctAAm features a red-shifting region of intersections (cf. Figure 3). This corroborates the statements of ii.) and iv.).

According to the line of argument above, the origin of the ratio of the 0–$0_{azonium}$ and 0–$1_{azonium}$ sub-bands in thermohalochromism must lie in the mechanism of protonation and is predominantly related to the azonium ion.

A suitable concept to solve question (3), why the metastable species is a conformer, is the Franck-Condon principle (cf. Figure 1 a).[14] To reiterate, the intensity of a vibronic transition is determined by the overlap integral between the vibrational wavefunctions in S_0 and in S_1. If the potential of S_1 is assumed to be of a relaxed molecule, the overlap integral is highly sensitive to the conformation of the molecule in the electronic ground state S_0. This is illustrated in Figure 1 a. With only small changes of the conformation (in the figure simplified by the reaction coordinate R_e), the ratio of overlap of the vibrational ground state of S_0 with the zeroth and the first vibrationally excited state in S_1 changes considerably. Consequently, the ratio of the 0–0 and higher sub-bands varies. In this way, information about the conformation of the ground state can be extracted.

In Figure 1 b, normalised difference spectra of the two extremes MREtAAm (blue-shifting region of intersections) and MROctAAm (red-shifting region of intersections) are shown to exemplify this behaviour. For MROctAAm, the 0–$0_{azonium}$ sub-band is more negative than the 0–$1_{azonium}$ sub-band and the spectral changes are overall farther in the red compared to MREtAAm. These effects are too small to be a consequence of changes in the electronic structure of the chromophore. Instead, they suggest that the equilibrium conformation of the ground state in the present chemical equilibria is either more similar (MROctAAm) or rather dissimilar (MREtAAm) to the equilibrium conformation in the excited state S_1.

Thus, the visual signature of the deviation from the equilibrium conformation in the UV-vis spectrum of the two dye species results from the combination of two processes. The first process is the protonation equilibrium that constantly leads to protonation and deprotonation of the azo dye. This equilibrium shifts with temperature (thermo-halochromism). The second process is the relaxation of a molecule from a longer-lived, distorted conformation (compared to the time scale of the proton exchange). In the case of the azonium ion, there are two opportunities for a distortion to occur. Either the protonated species is deprotonated in a preferred conformation, which relaxes after deprotonation, or the neutral species is protonated in a conformation which is then unfavourable for the formed azonium ion, leading to a relaxation process immediately after protonation.

The first possibility is excluded here, as the spectral changes would have to occur in the absorption band of the neutral species, but as mentioned above, the spectral variations are assigned to the azonium species.

In the second possibility, protonation of the azo bridge of the neutral species compulsorily leads to a large variation in the conformation. The conformation change is a consequence of the hydrogen bonds between the azo bridge and the secondary amide(s) being disturbed upon protonation.

The NOESY (Nuclear Overhauser Effect SpectroscopY) spectra from 2D-NMR measurements of the neutral and the protonated state as the end points have been measured in chloroform (cf. ESI Figure S28–Figure S35). The NOE signals visible for the proton of the secondary amide attached to the chromophore clearly show that in the neutral state, the nitrogen is turned towards the azo bridge. The aromatic amide proton is in proximity to the second aromatic ring with the dimethylamine substituent (cf. Scheme 4, ESI Scheme S 1, structure I, NOE signals from proton C to proton H). In the protonated state, however, the carbonyl oxygen is turned towards the β-protonated azo bridge. Here, the amide proton is in proximity to the aromatic proton in *ortho*-position to the secondary amide substituent (cf. Scheme 4, ESI Scheme S 1, structure I, NOE signals from proton G to proton H). Thus, the secondary amide substituent at the aromatic ring has to rotate by 180° upon protonation of the azo bridge.

In contrast, the secondary amide substituent attached to the alkyl tether does not show NOE signals to the chromophore.

The last question (4) regarding the temperature-dependence of the regions of intersections necessitates the introduction of another concept, namely a H-bonding-controlled thermochromism that depends on the competition of several hydrogen bonding motifs.

The thermo-halochromism involving regions of intersections is reminiscent of thermo-solvato-halochromism occurring in binary solvent mixtures of water and ethanol for *partially* protonated solutions of the *N*-hydroxyethyl acrylamide ester of *ortho*-MR.[10] In those systems, a blue-shifting region of intersections can be observed and has been explained by a considerable change in the solvent shell with temperature, which affects one of the species in the protonation equilibrium more strongly than the other.

© 2022 The Authors. ChemPhysChem published by Wiley-VCH GmbH

14397641, 202, 1, Downloaded from https://chemistry-europe.onlinelibrary.wiley.com/doi/10.1002/cphc.202200512 by Cochrane Germany, Wiley Online Library on [30/01/2023]. See the Terms and Conditions (https://onlinelibrary.wiley.com/terms-and-conditions) on Wiley Online Library for rules of use; OA articles are governed by the applicable Creative Commons License

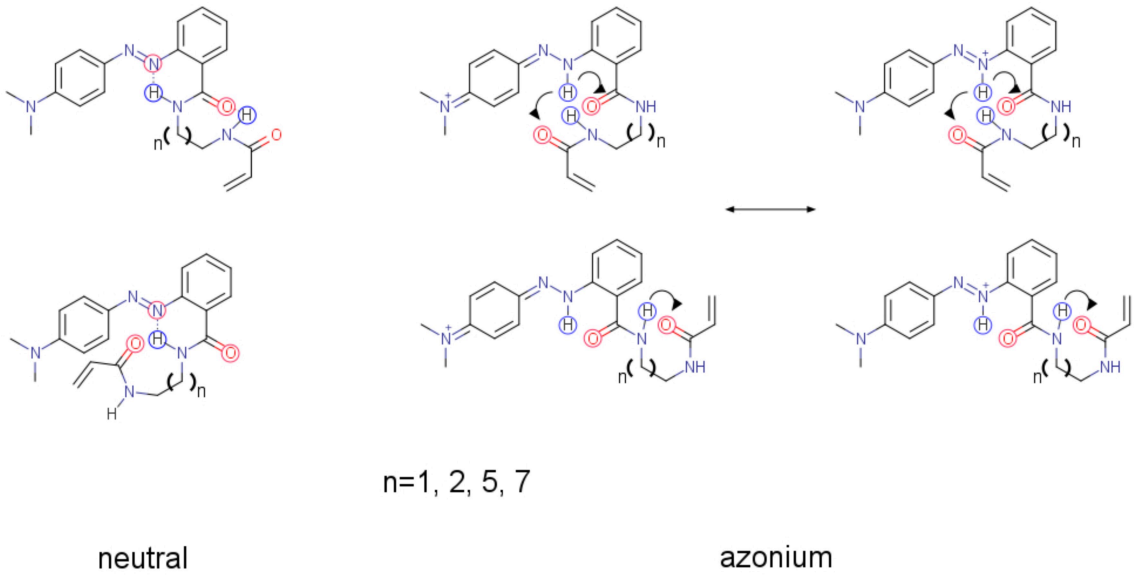

Scheme 4. Different options of intramolecular interaction between hydrogen bond acceptors (marked with a red circle) and donors (marked with a blue circle) for neutral and protonated amidoalkyl acrylamide of o-methyl red.

A similar behaviour can be hypothesised for the derivatives in this study. However, although there is only a single solvent, the three different cases of blue-shifting regions of intersections, red-shifting regions of intersections, or a concrete isosbestic point can be observed. Thus, the influencing factor must be part of the molecules themselves. For this purpose, we consider the alkyl spacer attached to the secondary amide of the chromophore, as well as the second secondary amide on the other end of the alkyl spacer as a "tethered solvent".

The complex relation between the spacer length and the thermochromic response suggests that the effect is not simply related to hydrophobicity of the coupled group. If that was the case, the effects should be in ascending order with spacer length. Yet, with the observed variation of the region of intersections for the different derivatives, we suggest that the intramolecular interaction between the two secondary amides induces a considerable thermo-perichromic effect on the thermo-halochromism of these compounds. The proposed intramolecular hydrogen bonding patterns involving the two secondary amide groups and the azo bridge is characteristically affected by the conformation of the alkyl tether, which in turn depends on the tether length. Several motifs are perceivable, which are depicted in Scheme 4.

In the neutral azobenzenes, hydrogen bonding can in principle occur from the secondary amides as hydrogen bond donor (marked with blue circles in Scheme 4) to the acceptors (marked with red circles) represented by the electron-rich azo bridge and tertiary amine, as well as between the carbonyl oxygen of one amide and the hydrogen of the other amide.

In the azonium ion, the azo bridge is protonated at the β-nitrogen[21] and consequently electron-deficient itself. Hydrogen bonding can then occur between the hydrogen bound to the azo bridge and the carbonyl oxygens of the two amides. At the same time, the hydrogen bonding between the hydrogen of one amide to the carbonyl oxygen of the other and *vice versa* can still take place.

As there are two secondary amides that compete in terms of hydrogen bonding, the ratio of interactions to one or the other affect the conformation of the chromophore. The alkyl spacer length plays a crucial role how or if the terminal amide participates in the overall hydrogen bonding motif.

The particular hydrogen bond arrangement should vary with temperature, which in turn will be reflected in a gradual change of the overall molecular geometry, altering the absorbance, as has been explained by the Franck-Condon principle earlier, and resulting in a region of intersections. We refer to this new thermochromic mechanism as "H-bonding-controlled" thermo-halochromism.

Thermo-halochromism in solvents with increased or decreased intramolecular hydrogen bonding exhibits a completely different behaviour regarding regions of intersections. In acidified chloroform (0.0025 v/v% TFA), which has been shown to lead to almost exclusive intramolecular hydrogen bonding in the parent compound *o*-MR,[22] red-shifting regions of intersections can be observed upon temperature increase for all spacer lengths examined in this study (cf. ESI Figure S45, Figure S46). In acidified methanol (0.025 v/v% TFA), which largely suppresses intramolecular hydrogen bonding,[22] almost ideal isosbestic points occur in temperature-dependent measurements (cf. ESI Figure S47, Figure S48).

These experimental results, combined with the rudimentary structure in solution as determined by NOESY, strongly suggest that the observed spectral effects in ethanolic TFA are indeed a consequence of a balance of intramolecular and intermolecular (to solvent molecules) H-bonding. If intra- or intermolecular H-

© 2022 The Authors. ChemPhysChem published by Wiley-VCH GmbH

14397641, 202, 1, Downloaded from https://chemistry-europe.onlinelibrary.wiley.com/doi/10.1002/cphc.202200512 by Cochrane Germany, Wiley Online Library on [30/01/2023]. See the Terms and Conditions (https://onlinelibrary.wiley.com/terms-and-conditions) on Wiley Online Library for rules of use; OA articles are governed by the applicable Creative Commons License

bonding occur exclusively, the tethered solvent effect vanishes and all derivatives in this study behave the same.

In principle, another reasonable explanation for the regions of intersections would be aggregation behaviours of the dye. However, the aggregation effects described in literature for azo dyes require confinement and water as medium. Such confinement was achieved, for example, by attaching the dye to artificial DNA scaffolds[23] or by increasing surfactant concentration.[24] Yet, for *o*-methyl red as the parent compound of the derivatives in the present study, aggregation was not achieved at the low concentrations as used here. Additionally, aggregation would be accompanied by a characteristic spectral signature, typically with large wavelength shifts, that is not observed in a dilution series of the here investigated molecules (cf. example in ESI Figure S49).

Despite the plethora of experimental evidence collected in this work, a detailed picture for the mechanism of the temperature-induced deprotonation of the dye remains elusive. Determining the exact reaction mechanism would require time-resolved rovibrational spectroscopy supported by high-level computation including solvent, hydrogen bonding, and a large number of atoms in the chromophores.

The experimentally observed stark difference between H-bonding-controlled thermo-halochromism and thermo-solvato-halochromism is their respective thermochromicity. Thermochromicity of a system is defined as the magnitude of thermochromism, i.e., the extent of the shift in a colour change-inducing equilibrium with temperature variation.[5]

Despite the deviating behaviours regarding the regions of intersections for the studied derivatives with different alkyl spacer lengths, the thermochromicity of the H-bonding-controlled thermo-halochromism is in the same order of magnitude for all derivatives, both in the enthalpy of deprotonation ΔH_0 and the heat capacity of ionisation ΔC_p (cf. Table 3, ESI Figure S50, Figure S51, Figure S52, Figure S53). The enthalpy ΔH_0 may be understood as a measure of the ratio of deprotonation at 25 °C. Its sign also tells whether the process is endothermic or exothermic. The heat capacity of ionisation ΔC_p quantifies how strong the temperature-dependence of the enthalpy is. This gives information about whether deprotonation becomes more favourable or disfavourable with increasing temperatures. These two values ΔH_0 and ΔC_p may be exploited as thermochromicity parameters in a modified van't Hoff analysis as previously discussed.[10]

For this purpose, the plot of the natural logarithm of the absorbance ratio of the ionic azonium and neutral azobenzene, *ln* R, versus the inverse absolute temperature T^{-1} was fitted to

$$\ln\left(\frac{R}{R_0}\right) = \frac{\Delta H_0 - T_0 \Delta C_p}{R}\left(\frac{1}{T_0} - \frac{1}{T}\right) + \frac{\Delta C_p}{R}\ln\left(\frac{T}{T_0}\right) \quad (1)$$

This equation may be simplified to ln(R) = a−b*1/T + c*ln(T) for fitting.[25]

In thermo-solvato-halochromism in binary solvent mixtures, the deprotonation behaviour varies considerably with temperature. At low temperatures, significantly more azonium ions are deprotonated per temperature increment than at high temperatures, which has been explained by the differing stability of the neutral and the protonated dyes in those solvent mixtures. This is reflected in a positive value for ΔC_p (cf. Table 3).[10]

Such a behaviour is not observed for H-bonding-controlled thermo-halochromism. Here, the thermochromicity parameters are almost the same as those determined for the ester derivative previously studied in ethanolic trifluoroacetic acid (1 v/v%) (cf. Table 3).[10] It follows that the H-bonding-controlled thermo-halochromism has a negligible influence on the magnitude of thermochromism compared to thermo-solvato-halochromism. However, its underlying mechanism apparently affects the equilibrium conformation of the chromophores.

Conclusion

In conclusion, we synthesised four novel amidoalkyl acrylamide derivatives of the azo dye *o*-methyl red with different alkyl spacer lengths and analysed their thermochromic behaviour in ethanolic solutions. When the dyes are neutral or *completely* protonated, they show vibronic thermochromism. Specifically, lower energy vibronic sub-bands lose intensity, while those of higher energy gain with increasing temperature.

In *partially* protonated systems, the four dye homologues all show thermo-halochromic behaviour of similar magnitudes, where the azonium ion is deprotonated to the benefit of the neutral species upon temperature increase. In dependence of the alkyl spacer length between the chromophore and the acrylamide moiety, the four homologues show a peculiar deviation from an ideal protonation behaviour, which would entail the existence of an isosbestic point in UV-vis spectroscopy. The temperature-dependent UV-vis spectra display either an isosbestic point, a red-shifting, or a blue-shifting region of intersections between spectra of adjacent temperature steps. Surprisingly, this behaviour does not follow a systematic trend with alkyl spacer length.

In contrast, when titrating the dyes with an acid at a fixed temperature, the spectra are characterised by isosbestic points differing in position from the intersections in the temperature-dependent measurements. The observed differences in halochromism (pH-dependency) and thermo-halochromism (temperature-dependency) suggest two independent mechanisms of protonation. The experimental evidence strongly suggests a characteristic influence of various intramolecular hydrogen bonding patterns on thermo-halochromism, assigned here as "H-bonding-controlled thermo-halochromism", which to the best of our knowledge has not been reported previously in the literature.

These results reflect the critical importance of structural variations on the thermochromism of molecular dyes engaging in multiple H-bonding motifs. The informed development of novel thermochromic azobenzene derivatives for potential applications, such as molecular thermometers and sensors, will benefit from further detailed investigation of this structure-property relationship.

© 2022 The Authors. ChemPhysChem published by Wiley-VCH GmbH

14397641, 202, 1, Downloaded from https://chemistry-europe.onlinelibrary.wiley.com/doi/10.1002/cphc.202200512 by Cochrane Germany, Wiley Online Library on [30/01/2023]. See the Terms and Conditions (https://onlinelibrary.wiley.com/terms-and-conditions) on Wiley Online Library for rules of use; OA articles are governed by the applicable Creative Commons License

Experimental Section

Materials and Equipment

All solvents used were of Milli-Q®, spectroscopic or HPLC-grade. Absolute ethanol was purchased from VWR Chemicals. Tetrahydrofurane was dried and distilled over potassium. Trifluoroacetic acid was purchased from Carl Roth (Germany) in PEPTIPURE® ≥99,9% quality. Sulfuric acid (≥95%, Fisher Chemical), hydrochloric acid (37%, Anal. Reag. Gr., Fisher Chemical), acetic acid (Anal. Reag. Gr., ChemSolute), methyl red (Alfa Aesar), carbonyldiimidazole (97%, Alfa Aesar), 1,3-diaminopropane (for synth., Merck), 1,6-diaminohexane (98%+, Alfa Aesar) and 1,8-diaminooctane (98%, Alfa Aesar) were used as received. 1,8-Diazabicyclo[5.4.0]undec-7-ene was dried over calciumchloride (anhydrous, technical, Bernd Kraft) and distilled *in vacuo*. 1,2-Diaminoethane was distilled *in vacuo*.

UV-vis measurements were performed on a Thermo Scientific™ Evolution™ 220 UV-Vis-spectrophotometer. If not stated otherwise, the measurements were done with 100 nm/min and a resolution of 1 nm.

NMR-measurements were performed on a Jeol EZC 500. ^{1}H-^{1}H-NOESY NMR spectra were measured with a mixing time of 500 ms. 1D-Spectra were analysed with MestreNova 9. 2D-Spectra were analysed with Delta 5.3 by JEOL. NMR spectra can be found in the ESI.

Synthesis of Methyl Red Imidazolide

Methyl red (1 mol eq.) was dissolved in tetrahydrofuran (0.1 mmol/L), carbonyldiimidazole (1.8 mol eq.) was added and the solution was stirred until no more gas evolution occurred, typically overnight or for three hours at 45 °C. The solution was used without purification for further syntheses. (Adapted from literature[26])

Synthesis of N-(x-aminoalkyl)-2-[(1E)-2-[4-(dimethylamino)phenyl]diazen-1-yl]benzamide (x–aminoalkyl-o–methyl red amide, AminoalkylMR)

A solution of methyl red imidazolide (500.1 mg, $1.9*10^{-3}$ mol methyl red) in tetrahydrofuran (12.5 mL) was added dropwise to a solution of a diamine (C2, C3, C6, C8) in 2–7 molar excess in dichloromethane (25 mL). The reaction mixture was stirred overnight, the solvent removed *in vacuo* and the residue redissolved in dichloromethane. The organic phase was washed with water and dried *in vacuo*. The crude product was subjected to column chromatography on silica in acetone→acetone:triethylamine 10:1. It was then dried *in vacuo*. These products were not pure but used in the next synthesis step. For NMR spectroscopy, small portions were purified further by column chromatography on basic alumina in methanol→methanol:acetic acid 9:1 and then lyophilised from 1,4-dioxane. The yields of raw products and determined by ^{1}H NMR spectroscopy are reported in Scheme 2. In the following, only the yield determined by ^{1}H NMR spectroscopy will be reported.

C2: Yield: 50%

δH(500 MHz, $CDCl_3$:MeOD 9:1) 9.41 (s, 1H; CO–N*H*), 8.15 (d, J= 7.6 Hz, 1H; Ph–*H*), 7.71 (dd, J=8.4, 3.1 Hz, 3H; Ph–*H*), 7.46 (t, J= 7.1 Hz, 1H; Ph–*H*), 7.39 (t, J=7.5 Hz, 1H; Ph–*H*), 6.72 (d, J=9.3 Hz, 2H; Ph–*H*), 3.06 (s, 6H; $N(Me)_2$), 3.01 (s, 2H; CONH–CH_2), 1.87 (s, 2H; NH_2–CH_2).

δC NMR (126 MHz, $CDCl_3$:MeOD 9:1) 168.19 (CONH), 153.36 (Ph), 150.53 (Ph), 143.31 (Ph), 132.09 (Ph), 130.80 (Ph), 129.41 (Ph), 129.00 (Ph), 125.79 (Ph), 116.25 (Ph), 111.72 (Ph), 40.46 (CONH–CH_2), 40.20 (NH_2–CH_2), 40.18 ($N(Me)_2$).

C3: Yield: 59%

δH(500 MHz, $CDCl_3$) 9.11 (s, 1H; CO–N*H*), 8.34 (m, 1H; Ph–*H*), 7.77 (d, J=9.2 Hz, 2H; Ph–*H*), 7.73 (m, 1H; Ph–*H*), 7.51–7.41 (m, 2H; Ph–*H*), 6.76 (d, J=9.2 Hz, 2H; Ph–*H*), 3.61 (dd, J=12.6, 6.8 Hz, 2H; CONH–CH_2), 3.11 (s, 6H; $N(Me)_2$), 2.79 (t, J=6.7 Hz, 2H; NH_2–CH_2), 1.79 (p, J=6.8 Hz, 2H; CH_2–CH_2–CH_2).

δC NMR (126 MHz, $CDCl_3$) 166.54 (CONH), 153.22 (Ph), 150.57 (Ph), 143.51 (Ph), 131.67 (Ph), 131.40 (Ph), 129.74 (Ph), 129.60 (Ph), 125.79 (Ph), 116.05 (Ph), 111.71 (Ph), 40.37 (CONH–CH_2), 39.66 (NH_2–CH_2), 37.45 ($N(Me)_2$), 33.47 (CH_2–CH_2–CH_2).

C6: Yield: 92%

δH(500 MHz, $CDCl_3$ + 1dr. MeOD) 9.14 (t, J=5.4 Hz, 1H; CO–N*H*), 8.23 (dd, J=7.7, 1.6 Hz, 1H; Ph–*H*), 7.71 (d, J=9.2 Hz, 2H; Ph–*H*), 7.70 (m, 1H; Ph–*H*), 7.43 (dtd, J=21.1, 7.3, 1.5 Hz, 2H; Ph–*H*), 6.71 (d, J=9.2 Hz, 2H; Ph–*H*), 3.44 (m, 2H; CONH–CH_2), 3.07 (s, 6H; $N(Me)_2$), 2.72 (t, J=7.4 Hz, 2H; NH_2–CH_2), 1.60 (p, J=7.0 Hz, 2H; CONH–CH_2–CH_2), 1.52 (p, J=6.9 Hz, 2H; NH_2–CH_2–CH_2), 1.35 (m, 4H; CH_2–CH_2–CH_2–CH_2–CH_2–CH_2).

δC(126 MHz, $CDCl_3$ + 1dr. MeOD) 166.71 (CONH), 153.26 (Ph), 150.55 (Ph), 143.35 (Ph), 131.81 (Ph), 131.04 (Ph), 129.52 (Ph), 129.24 (Ph), 129.22 (Ph), 125.73 (Ph), 116.10 (Ph), 111.62 (Ph), 40.24 ($N(Me)_2$), 39.69 (CONH–CH_2), 39.56 (NH_2–CH_2), 29.45 (CONH–CH_2–CH_2), 29.43 (NH_2–CH_2–CH_2), 28.69 (CONH–CH_2–CH_2–CH_2), 26.41 (alkyl), 25.96 (alkyl), 23.90 (alkyl).

C8: Yield: 50%

δH(500 MHz, $CDCl_3$:MeOD 9:1) 9.09 (s, 1H; CO–N*H*), 8.16 (d, J= 7.5 Hz, 1H; Ph–*H*), 7.65 (dd, J=12.5, 8.7 Hz, 3H; Ph–*H*), 7.39 (dt, J= 23.2, 7.1 Hz, 2H; Ph–*H*), 6.66 (d, J=8.9 Hz, 2H; Ph–*H*), 3.39 (t, J= 6.5 Hz, 2H; CONH–CH_2), 3.03 (s, 6H; $N(Me)_2$), 2.72 (m, 2H; NH_2–CH_2), 1.62–1.40 (m, 4H; CONH–CH_2–CH_2 + NH_2–CH_2–CH_2), 1.36–1.04 (m, 8H, alkyl).

δC(126 MHz, $CDCl_3$:MeOD 9:1) 166.74 (CONH), 166.65 (Ph), 153.20 (Ph), 150.47 (Ph), 143.26 (Ph), 131.73 (Ph), 130.85 (Ph), 129.39 (Ph), 129.10 (Ph), 125.66 (Ph), 116.03 (Ph), 111.51 (Ph), 40.09 ($N(Me)_2$), 39.87 (CONH–CH_2), 39.74 (NH_2–CH_2), 39.34 (NH_2–CH_2–CH_2), 29.38 (CONH–CH_2–CH_2), 28.83 (alkyl), 28.80 (alkyl), 27.59 (alkyl), 26.80 (alkyl), 26.23 (alkyl).

Synthesis of N-[x-({2-[(1E)-2-[4-(dimethylamino)phenyl]diazen-1-yl]phenyl} formamido)alkyl]prop-2-enamide (1-o–methyl red amide of alkyl-6-acrylamide, MRAlkAm)

Aminoalkyl-o-methyl red and 1,8-diazabicyclo[5.4.0]undec-7-ene (2 mol. eq.) were dissolved in chloroform (C2, C3, C8) or dichloromethane (C6). The mixture was cooled to 0 °C and acryloyl chloride (1.5–2 mol. eq.) added. After 45 minutes, the ice bath was removed. After 24 hours, the organic phase was extracted with water. The product was purified *via* column chromatography on neutral aluminium oxide in ethyl acetate (C2, C3, C8) or on silica in diethylether (C6). The reported yields are adjusted for the purity of the educt.

© 2022 The Authors. ChemPhysChem published by Wiley-VCH GmbH

14397641, 2023, 1, Downloaded from https://chemistry-europe.onlinelibrary.wiley.com/doi/10.1002/cphc.202200512 by Cochrane Germany, Wiley Online Library on [30/01/2023]. See the Terms and Conditions (https://onlinelibrary.wiley.com/terms-and-conditions) on Wiley Online Library for rules of use; OA articles are governed by the applicable Creative Commons License

C2: Yield: 73 %

δH(500 MHz; $CDCl_3$) 9.49 (t, J = 5.7 Hz, 1H; Ar–CO–N*H*), 8.31 (dd, J = 7.7, 1.7 Hz, 1H; Ph–*H*), 7.77 (dd, J = 8.1, 1.3 Hz, 1H; Ph–*H*), 7.74 (d, J = 9.2 Hz, 2H; Ph–*H*), 7.51 (ddd, J = 8.1, 7.2, 1.7 Hz, 1H; Ph–*H*), 7.45 (ddd, J = 7.7, 7.2, 1.3 Hz, 1H; Ph–*H*), 6.89 (s, 1H; DB–CO–N*H*), 6.76 (d, J = 9.3 Hz, 2H; Ph–*H*), 6.23 (dd, J = 17.0, 1.5 Hz, 1H; CHC*H*H(trans)), 6.07 (dd, J = 17.1, 10.3 Hz, 1H; C*H*CHH), 5.56 (dd, J = 10.3, 1.5 Hz, 1H; CHCH*H*(cis)), 3.71 (dd, J = 11.5, 5.8 Hz, 2H; Ar–CONH–CH_2), 3.59 (dd, J = 11.1, 5.3 Hz, 2H; DB–CONH–CH_2), 3.12 (s, 6H; $N(Me)_2$).

δC(126 MHz; $CDCl_3$) 168.10 (Ar–CONH), 166.12 (DB–CONH), 153.40 (Ph), 150.57 (Ph), 143.47 (Ph), 132.12 (Ph), 131.29 (CO*C*HCH$_2$), 131.26 (Ph), 129.60 (Ph), 129.05 (Ph), 126.01 (COCH*C*H$_2$), 125.84 (Ph), 116.17 (Ph), 111.96 (Ph), 41.48 (Ar–CONH*C*H$_2$), 40.40 ($N(Me)_2$), 39.50 (DB–CONH*C*H$_2$).

C3: Yield: 76 %

δH(500 MHz; $CDCl_3$) 9.17 (t, J = 6.0 Hz, 1H; Ar–CO–N*H*), 8.30 (dd, J = 7.6, 1.8 Hz, 1H; Ph–*H*), 7.76 (dd, J = 7.3, 1.3 Hz, 1H; Ph–*H*), 7.75 (d, J = 9.2 Hz, 2H; Ph–*H*), 7.51 (ddd, J = 8.0, 7.2, 1.7 Hz, 1H; Ph–*H*), 7.46 (ddd, J = 7.3, 7.2, 1.3 Hz, 1H; Ph–*H*), 7.03 (t, J = 5.0 Hz, 1H; DB–CO–N*H*), 6.76 (d, J = 9.3 Hz, 2H; Ph–H), 6.27 (dd, J = 17.1, 1.7 Hz, 1H; CHC*H*H(trans)), 6.17 (dd, J = 17.1, 10.1 Hz, 1H; C*H*CHH), 5.60 (dd, J = 10.1, 1.7 Hz, 1H; CHCH*H*(cis)), 3.61 (dd, J = 12.5, 6.3 Hz, 2H; Ar–CONH–CH_2), 3.39 (dd, J = 12.3, 6.2 Hz, 2H; DB–CONH–CH_2), 3.12 (s, 6H; $N(Me)_2$), 1.81 (t, J = 6.2 Hz, 2H; CH_2–CH_2–CH_2).

δC(126 MHz; $CDCl_3$) 167.67 (Ar–CONH), 165.85 (DB–CONH), 153.36 (Ph), 150.59 (Ph), 143.51 (Ph), 131.99 (CO*C*HCH$_2$), 131.65 (Ph), 131.26 (Ph), 129.65 (Ph), 129.43 (Ph), 125.84 (Ph), 125.81 (COCH*C*H$_2$), 116.19 (Ph), 111.84 (Ph), 40.42 ($N(Me)_2$), 36.72 (Ar–CONH*C*H$_2$), 35.99 (DB–CONH*C*H$_2$), 30.13 (CH_2–CH_2–CH_2).

C6: Yield: 43 %

δH(500 MHz; $CDCl_3$) 9.08 (t, J = 5.3 Hz, 1H; Ar–CO–N*H*), 8.34 (dd, J = 7.7, 1.7 Hz, 1H; Ph–*H*), 7.76 (d, J = 9.2 Hz, 2H; Ph–*H*), 7.73 (dd, J = 7.9, 1.4 Hz, 1H; Ph–*H*), 7.47 (dqd, J = 14.7, 7.2, 1.6 Hz, 2H; Ph–*H*), 6.76 (d, J = 9.2 Hz, 2H; Ph–*H*), 6.25 (dd, J = 17.0, 1.6 Hz, 1H; CHC*H*H(trans)), 6.13 (dd, J = 17.0, 10.2 Hz, 1H; C*H*CHH), 6.09 (s, 1H; DB–CO–N*H*), 5.59 (dd, J = 10.2, 1.6 Hz, 1H; CHCH*H*(cis)), 3.52 (dd, J = 12.6, 6.9 Hz, 2H; Ar–CONH–CH_2), 3.26 (dd, J = 12.9, 6.9 Hz, 2H; DB–CONH–CH_2), 3.12 (s, 6H; $N(Me)_2$), 1.64 (p, J = 7.0 Hz, 2H; Ar–CONH–CH_2–CH_2), 1.48 (p, J = 6.9 Hz, 2H; DB–CONH–CH_2–CH_2), 1.43–1.31 (m, 4H; CH_2–CH_2–CH_2–CH_2–CH_2–CH_2).

δC(126 MHz; $CDCl_3$) 166.43 (Ar–CONH), 165.73 (DB–CONH), 153.28 (Ph), 150.64 (Ph), 143.53 (Ph), 131.74 (Ph), 131.41 (CO*C*HCH$_2$), 131.25 (Ph), 129.64 (Ph), 129.61 (Ph), 126.05 (COCH*C*H$_2$), 125.83 (Ph), 116.11 (Ph), 111.72 (Ph), 40.42 ($N(Me)_2$), 39.66 (Ar–CONH*C*H$_2$), 39.27 (DB–CONH*C*H$_2$), 29.77 (Ar–CONHCH$_2$CH$_2$), 29.36 (DB–CONHCH$_2$CH$_2$), 26.53 (Ar–CONHCH$_2$CH$_2$CH$_2$), 26.32 (DB–CONHCH$_2$CH$_2$CH$_2$).

C8: Yield: 38 %

δH(500 MHz; $CDCl_3$) 9.05 (t, J = 5.0 Hz, 1H; Ar–CO–N*H*), 8.37 (dd, J = 7.2, 2.2 Hz, 1H; Ph–*H*), 7.78 (d, J = 9.2 Hz, 2H; Ph–*H*), 7.74 (dd, J = 7.4, 1.9 Hz, 1H; Ph–*H*), 7.48 (dqd, J = 14.6, 7.2, 1.7 Hz, 2H; Ph–*H*), 6.76 (d, J = 9.3 Hz, 2H; Ph–*H*), 6.25 (dd, J = 17.0, 1.5 Hz, 1H; CHC*H*H(trans)), 6.08 (dd, J = 17.0, 10.3 Hz, 1H; C*H*CHH), 5.76 (s, 1H; DB–CO–N*H*), 5.60 (dd, J = 10.3, 1.5 Hz, 1H; CHCH*H*(cis)), 3.52 (td, J = 7.0, 5.6 Hz, 2H; Ar–CONH–CH_2), 3.27 (td, J = 7.1, 6.0 Hz, 2H; DB–CONH–CH_2), 3.13 (s, 6H; $N(Me)_2$), 1.64 (p, J = 7.2, 2H; Ar–CONH–CH_2–CH_2), 1.47 (p, J = 7.2, 2H; DB–CONH–CH_2–CH_2), 1.37 (td, J = 13.9, 7.0 Hz, 2H; Ar–CONH–CH_2–CH_2–CH_2), 1.33–1.09 (m, 6H; CH_2–CH_2–CH_2–CH_2–CH_2–CH_2–CH_2–CH_2).

δC(126 MHz; $CDCl_3$) 166.26 (Ar–CONH), 165.62 (DB–CONH), 153.25 (Ph), 150.66 (Ph), 143.58 (Ph), 131.67 (Ph), 131.49 (CO*C*HCH$_2$), 131.18 (Ph), 129.76 (Ph), 129.66 (Ph), 126.17 (COCH*C*H$_2$), 125.85 (Ph), 116.08 (Ph), 111.70 (Ph), 40.43 ($N(Me)_2$), 40.11 (Ar–CONH*C*H$_2$), 39.67 (DB–CONH*C*H$_2$), 29.74 (Ar–CONHCH$_2$CH$_2$), 29.61 (DB–CONHCH$_2$CH$_2$), 29.25 (Ar–CONHCH$_2$CH$_2$CH$_2$), 29.21 (DB–CONHCH$_2$CH$_2$*C*H$_2$), 27.18 (AR–CONHCH$_2$CH$_2$CH$_2$CH$_2$), 26.91 (DB–CONHCH$_2$CH$_2$CH$_2$CH$_2$).

Acknowledgements

We thank the Faculty IV of the University of Siegen for funding, and Dr. Thomas Paululat for NMR measurements. Open Access funding enabled and organized by Projekt DEAL.

Conflict of Interest

The authors declare no conflict of interest.

Data Availability Statement

The data that support the findings of this study are available in the supplementary material of this article.

Keywords: Azobenzene · hydrogen bonding · NOESY · thermochromism · vibronic transitions

[1] P. Grieß, *Ann. Phys. Chem.* **1858**, *106*, 12.
[2] a) A. Seeboth, D. Lötzsch, R. Ruhmann, O. Muehling, *Chem. Rev.* **2014**, *114*, 3037–3068; b) W. Theilacker, G. Kortüm, G. Friedheim, *Chem. Ber.* **1950**, *83*, 508–519; c) J. H. Day, *Chem. Rev.* **1963**, *63*, 65–80.
[3] L. Hermosilla, M. C. Rezende, V. G. Machado, R. I. Stock, *Spectrochim. Acta Part A* **2017**, *173*, 556–561.
[4] a) T. A. Khattab, B. D. B. Tiu, S. Adas, S. d. Bunge, R. C. Advincula, *RSC Adv.* **2016**, *6*, 102296–102305; b) M. S. Abdelrahman, T. A. Khattab, S. Kamel, *New J. Chem.* **2021**, *45*, 5382–5390.
[5] D. G. Hafeman, K. L. Crawford, L. J. Bousse, *J. Phys. Chem.* **1993**, *97*, 3058–3066.
[6] X. Du, C. Zhu, X. Xie, *Langmuir* **2017**, *33*, 5910–5914.
[7] M. Tajima, M. Sugai, K. Matsunaga, T. Yamashita, H. Inoue, M. Hida, *Dyes Pigm.* **1998**, *39*, 97–109.
[8] a) J. A. Dean, N. A. Lange, in *Lange's handbook of chemistry*, 15th ed. ed., McGraw-Hill; [Distributed by] Knovel, New York, [Norwich, N. Y.], **1999**; b) K. M. Tawarah, H. M. Abu-Shamleh, *Dyes Pigm.* **1991**, *17*, 203–215.
[9] T. Kuwabara, A. Nakamura, A. Ueno, F. Toda, *J. Phys. Chem.* **1994**, *98*, 6297–6303.
[10] T. G. Jaik, B. Ciubini, F. Frascella, U. Jonas, *Polym. Chem.* **2022**, *13*, 1186–1214.
[11] Š. Sršeň, J. Sita, P. Slavíček, V. Ladányi, D. Heger, *J. Chem. Theory Comput.* **2020**, *16*, 6428–6438.
[12] E. Sawicki, *J. Org. Chem.* **1957**, *22*, 365–367.
[13] L. Antonov, D. Nedeltcheva, *Chem. Soc. Rev.* **2000**, *29*, 217–227.
[14] H. Mustroph, S. Ernst, B. Senns, A. D. Towns, *Color. Technol.* **2015**, *131*, 9–26.
[15] J. M. Hollas, in *Modern spectroscopy*, 4. ed., Wiley, Chichester, **2004**.
[16] S. Bell, A. Bisset, T. J. Dines, *J. Raman Spectrosc.* **1998**, *29*, 447–462.
[17] a) S. Lunák, M. Nepraš, R. Hrdina, H. Mustroph, *Chem. Phys.* **1994**, *184*, 255–260; b) H. Mustroph, *Dyes Pigm.* **1991**, *15*, 129–137.

© 2022 The Authors. ChemPhysChem published by Wiley-VCH GmbH

14397641, 202, 1, Downloaded from https://chemistry-europe.onlinelibrary.wiley.com/doi/10.1002/cphc.202200512 by Cochrane Germany, Wiley Online Library on [30/01/2023]. See the Terms and Conditions (https://onlinelibrary.wiley.com/terms-and-conditions) on Wiley Online Library for rules of use; OA articles are governed by the applicable Creative Commons License

[18] a) A. M. Mebel, M. Hayashi, K. K. Liang, S. H. Lin, *J. Phys. Chem. A* **1999**, *103*, 10674–10690; b) A. Baiardi, J. Bloino, V. Barone, *J. Chem. Theory Comput.* **2013**, *9*, 4097–4115.
[19] T. Stoyanova, S. Stoyanov, L. Antonov, V. Petrova, *Dyes Pigm.* **1996**, *31*, 1–12.
[20] S.-K. Park, C.-K. Lee, K.-C. Min, N.-S. Lee, *Bull. Korean Chem. Soc.* **2004**, *25*, 1817–1821.
[21] a) E. Sawicki, *J. Org. Chem.* **1957**, *22*, 621–625; b) G. E. Lewis, *Tetrahedron* **1960**, *10*, 129–134.
[22] G. Seu, *Dyes Pigm.* **1995**, *29*, 227–240.
[23] H. Asanuma, K. Shirasuka, T. Takarada, H. Kashida, M. Komiyama, *J. Am. Chem. Soc.* **2003**, *125*, 2217–2223.
[24] R. T. Buwalda, J. M. Jonker, J. B. F. N. Engberts, *Langmuir* **1999**, *15*, 1083–1089.
[25] a) H. Naghibi, A. Tamura, J. M. Sturtevant, *Proc. Natl. Acad. Sci. USA* **1995**, *92*, 5597–5599; b) Y. Liu, J. M. Sturtevant, *Protein Sci.* **1995**, *4*, 2559–2561; c) A. Zhukov, R. Karlsson, *J. Mol. Recognit.* **2007**, *20*, 379–385; d) L. S. Mizoue, J. Tellinghuisen, *Biophys. Chem.* **2004**, *110*, 15–24.
[26] a) H. A. Staab, A. Mannschreck, *Chem. Ber.* **1962**, *95*, 1284–1297; b) D. E. Bergbreiter, P. L. Osburn, C. Li, *Org. Lett.* **2002**, *4*, 737–740; c) H. A. Staab, M. Lüking, F. H. Dürr, *Chem. Ber.* **1962**, *95*, 1275–1283.

Manuscript received: July 15, 2022
Revised manuscript received: September 2, 2022
Accepted manuscript online: September 6, 2022
Version of record online: October 18, 2022

© 2022 The Authors. ChemPhysChem published by Wiley-VCH GmbH

14397641, 202, 1, Downloaded from https://chemistry-europe.onlinelibrary.wiley.com/doi/10.1002/cphc.202200512 by Cochrane Germany, Wiley Online Library on [30/01/2023]. See the Terms and Conditions (https://onlinelibrary.wiley.com/terms-and-conditions) on Wiley Online Library for rules of use; OA articles are governed by the applicable Creative Commons License

ChemPhysChem

Supporting Information

The "Tethered Solvent" Effect – H-Bonding-Controlled Thermo-Halochromism of a Push-Pull Azo Chromophore via Its Secondary Amidoalkyl Acrylamide Side Chain

Thorben Gwydion Jaik and Ulrich Jonas*

This document contains experimental details like syntheses and sample preparations, additional optical analysis data, graphs from the van't Hoff analyses, NMR data, etc.

Experimentals

Materials and equipment:

All solvents used were of Milli-Q®, spectroscopic or HPLC-grade. Absolute ethanol was purchased from VWR Chemicals. Tetrahydrofurane was dried and distilled over potassium. Trifluoroacetic acid was purchased from Carl Roth (Germany) in PEPTIPURE® ≥99,9% quality. Sulfuric acid (≥95%, Fisher Chemical), hydrochloric acid (37%, Anal. Reag. Gr., Fisher Chemical), acetic acid (Anal. Reag. Gr., ChemSolute), methyl red (Alfa Aesar), carbonyldiimidazole (97%, Alfa Aesar), 1,3-diaminopropane (for synth., Merck), 1,6-diaminohexane (98%+, Alfa Aesar) and 1,8-diaminooctane (98%, Alfa Aesar) were used as received. 1,8-Diazabicyclo[5.4.0]undec-7-ene was dried over calciumchloride (anhydrous, technical, Bernd Kraft) and distilled *in vacuo*. 1,2-Diaminoethane was distilled *in vacuo*.

UV-vis measurements were performed on a Thermo Scientific™ Evolution™ 220 UV-Vis-spectrophotometer. If not stated otherwise, the measurements were done with 100 nm/min and a resolution of 1 nm.

In cases of excessive evaporation during long time periods for temperature equilibration, spectra were normalised to account for the systematic variation in concentration.

NMR-measurements were performed on a Jeol EZC 500. ^{1}H-^{1}H-NOESY NMR spectra were measured with a mixing time of 500 ms. 1D-Spectra were analysed with MestreNova 9. 2D-Spectra were analysed with Delta 5.3 by JEOL.

Synthesis of methyl red imidazolide:

Methyl red (1 mol eq.) was dissolved in tetrahydrofuran (0.1 mmol/L), carbonyldiimidazole (1.8 mol eq.) was added and the solution was stirred until no more gas evolution occurred, typically overnight or for three hours at 45 °C. The solution was used without purification for further syntheses. (Adapted from literature[1–3])

Synthesis of N-(x-aminoalkyl)-2-[(1E)-2-[4-(dimethylamino)phenyl]diazen-1-yl]benzamide (x-aminoalkyl-o-methyl red amide, AminoalkylMR):

A solution of methyl red imidazolide (500.1 mg, $1.9*10^{-3}$ mol methyl red) in tetrahydrofuran (12.5 mL) was added dropwise to a solution of a diamine (summarised in Table S 1) in dichloromethane (25 mL). The reaction mixture was stirred overnight, the solvent removed *in vacuo* and the residue redissolved in dichloromethane. The organic phase was washed with water. It was then dried *in vacuo*. The crude product was subjected to column chromatography on silica in acetone → acetone:triethylamine 10:1. It was then dried *in vacuo*. However, these products were not pure. The yields of raw product are summarised in Table S 1. For NMR spectroscopy, small portions were purified further by column chromatography on basic alumina in methanol → methanol:acetic acid 9:1 and then lyophilised from 1,4-dioxane.

Table S 1: Reaction parameters of amidation reactions of methyl red including educt ratios, and yield.

Derivative	MR feed [mg]	Diamine feed [mg]/mol eq.	Raw yield [mg]/%	^{1}H-NMR yield [%]
AminoEtMR	500.1	225 (2)	483.4 (83)	50
AminoPrMR	500.1	365 (2.6)	631.3 (104)	59
AminoHexMR	2002	5977 (6.9)	2404 (92)	92
AminoOctMR	500.1	541 (2)	455.2 (62)	50

C2: δH(500 MHz, $CDCl_3$:MeOD 9:1) 9.41 (s, 1H; CO-N*H*), 8.15 (d, J = 7.6 Hz, 1H; Ph-*H*), 7.71 (dd, J = 8.4, 3.1 Hz, 3H; Ph-*H*), 7.46 (t, J = 7.1 Hz, 1H; Ph-*H*), 7.39 (t, J = 7.5 Hz, 1H; Ph-*H*), 6.72 (d, J = 9.3 Hz, 2H; Ph-*H*), 3.06 (s, 6H; $N(Me)_2$), 3.01 (s, 2H; CONH-CH_2), 1.87 (s, 2H; NH_2-CH_2).

δC NMR (126 MHz, $CDCl_3$:MeOD 9:1) 168.19 (CONH), 153.36 (Ph), 150.53 (Ph), 143.31 (Ph), 132.09 (Ph), 130.80 (Ph), 129.41 (Ph), 129.00 (Ph), 125.79 (Ph), 116.25 (Ph), 111.72 (Ph), 40.46 (CONH-*C*H_2), 40.20 (NH_2-*C*H_2), 40.18 ($N(Me)_2$).

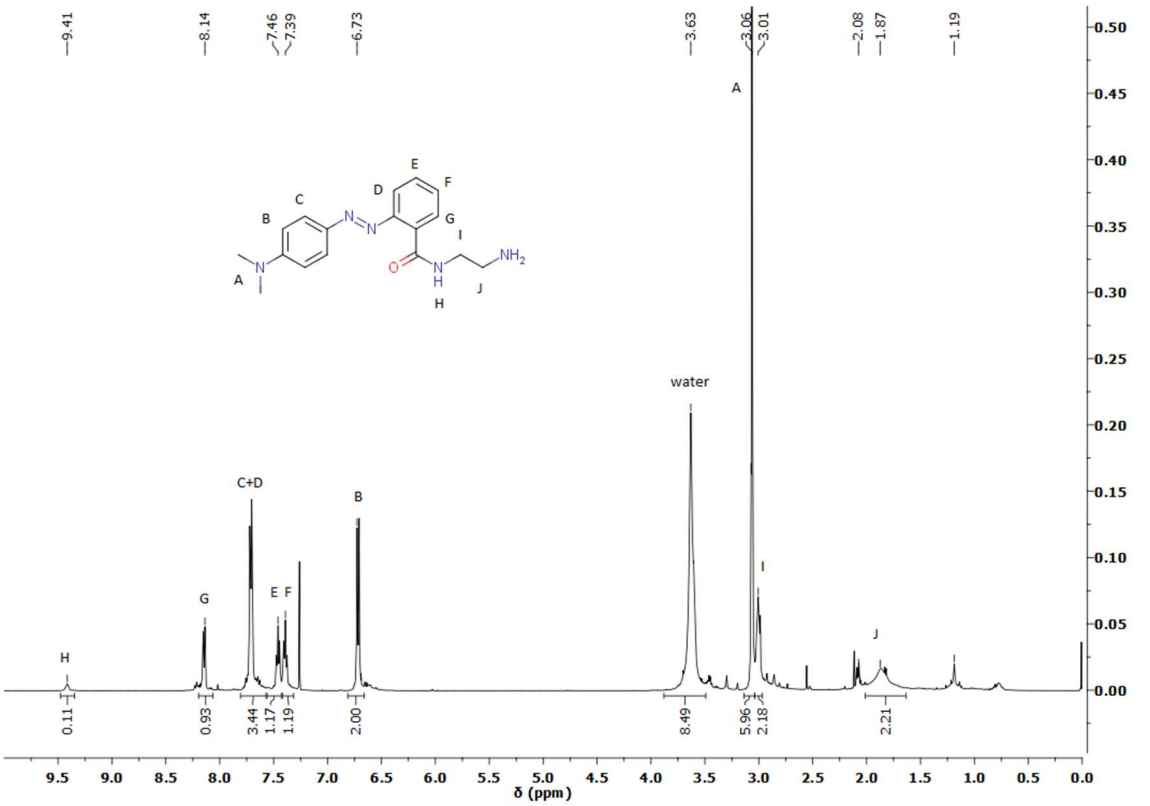

Figure S 1: ^{1}H NMR spectrum (500 MHz) in $CDCl_3$:MeOD 9:1 of N-(2-aminoethyl)-2-[(1E)-2-[4-(dimethylamino)phenyl]diazen-1-yl]benzamide (2-aminoethyl-o-methyl red amide, AminoEtMR). The peak at 1.87 ppm is attributed to associated acetic acid.

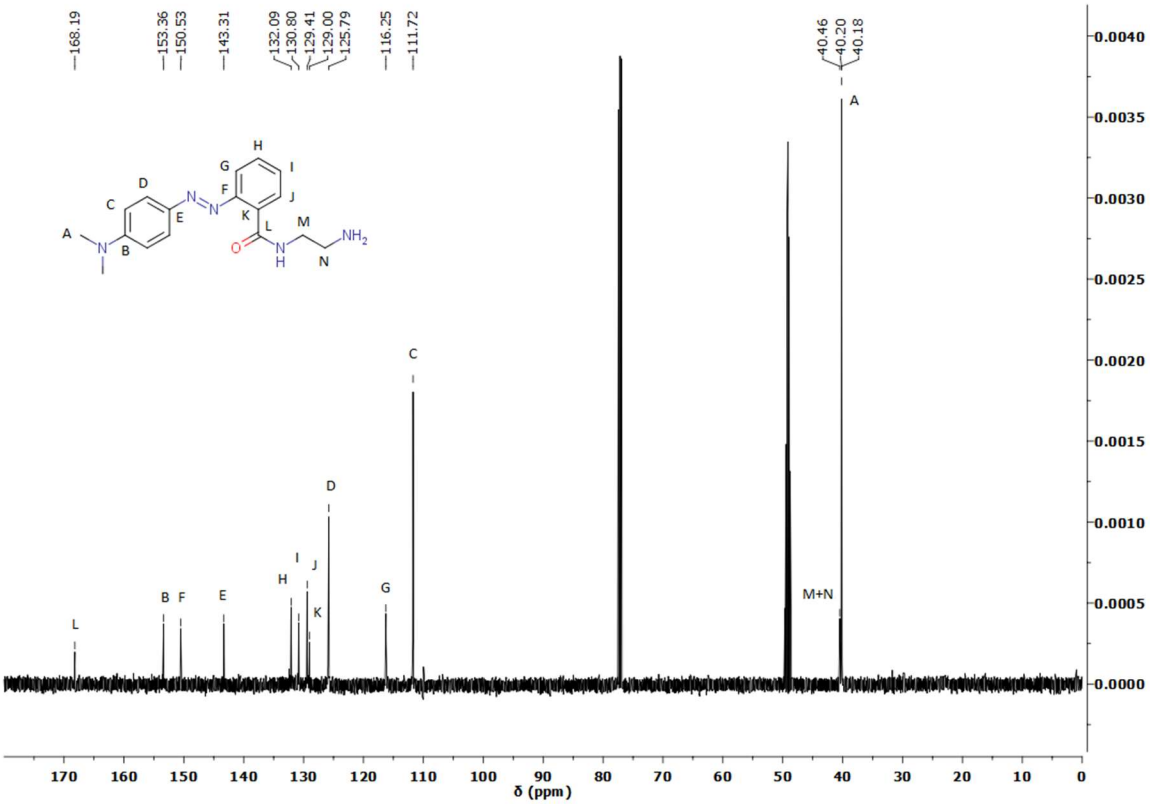

Figure S 2: ^{13}C NMR spectrum (126 MHz) in $CDCl_3$:MeOD 9:1 of N-(2-aminoethyl)-2-[(1E)-2-[4-(dimethylamino)phenyl]diazen-1-yl]benzamide (2-aminoethyl-o-methyl red amide, AminoEtMR).

C3: δH(500 MHz, $CDCl_3$) 9.11 (s, 1H; CO-N*H*), 8.34 (m, 1H; Ph-*H*), 7.77 (d, J = 9.2 Hz, 2H; Ph-*H*), 7.73 (m, 1H; Ph-*H*), 7.51 – 7.41 (m, 2H; Ph-*H*), 6.76 (d, J = 9.2 Hz, 2H; Ph-*H*), 3.61 (dd, J = 12.6, 6.8 Hz, 2H; CONH-CH_2), 3.11 (s, 6H; $N(Me)_2$), 2.79 (t, J = 6.7 Hz, 2H; NH_2-CH_2), 1.79 (p, J = 6.8 Hz, 2H; CH_2-CH_2-CH_2).

δC NMR (126 MHz, $CDCl_3$) 166.54 (CONH), 153.22 (Ph), 150.57 (Ph), 143.51 (Ph), 131.67 (Ph), 131.40 (Ph), 129.74 (Ph), 129.60 (Ph), 125.79 (Ph), 116.05 (Ph), 111.71 (Ph), 40.37 (CONH-*C*H_2), 39.66 (NH_2-*C*H_2), 37.45 ($N(Me)_2$), 33.47 (CH_2-*C*H_2-CH_2).

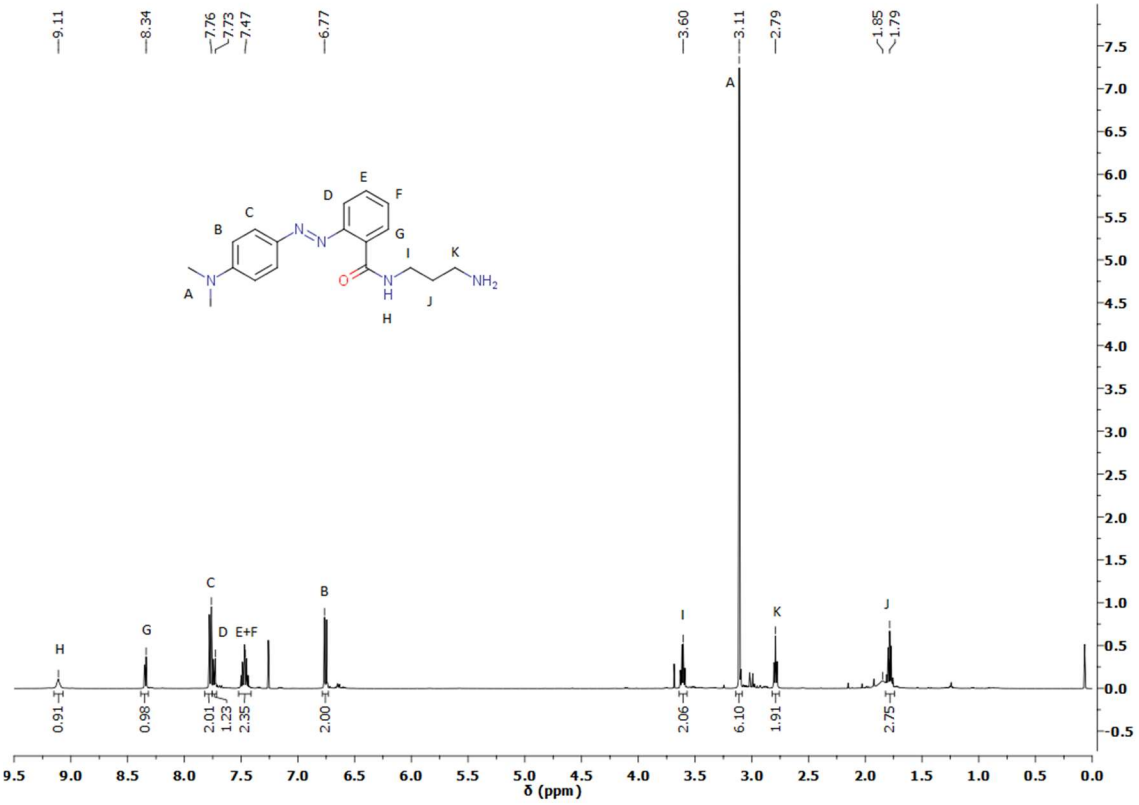

Figure S 3: ^{1}H NMR spectrum (500 MHz) in $CDCl_3$ of N-(2-aminopropyl)-2-[(1E)-2-[4-(dimethylamino)phenyl]diazen-1-yl]benzamide (2-aminopropyl-o-methyl red amide, AminoPrMR).

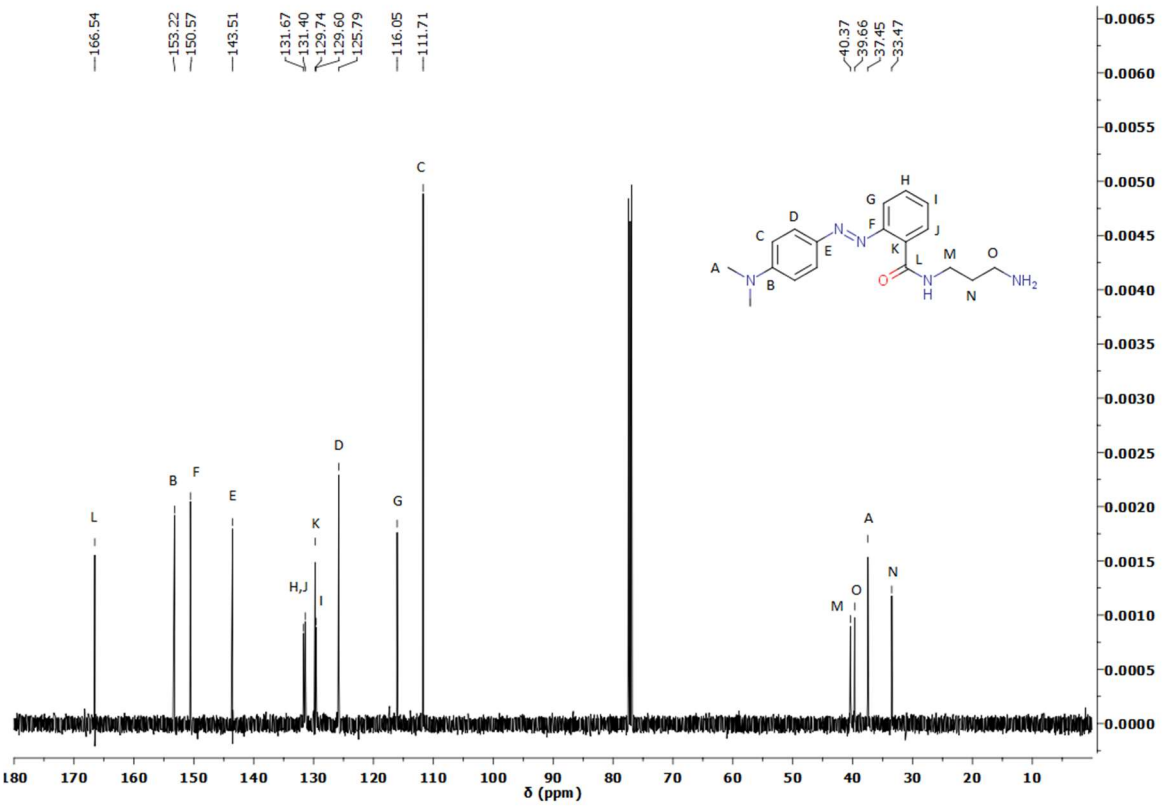

Figure S 4: ^{13}C NMR spectrum (126 MHz) in $CDCl_3$ of N-(2-aminopropyl)-2-[(1E)-2-[4-(dimethylamino)phenyl]diazen-1-yl]benzamide (2-aminopropyl-o-methyl red amide, AminoPrMR).

C6: δH(500 MHz, $CDCl_3$+1dr. MeOD) 9.14 (t, J = 5.4 Hz, , 1H; CO-N*H*), 8.23 (dd, J = 7.7, 1.6 Hz, 1H; Ph-*H*), 7.71 (d, J = 9.2 Hz, 2H; Ph-*H*), 7.70 (m, 1H; Ph-*H*), 7.43 (dtd, J = 21.1, 7.3, 1.5 Hz, 2H; Ph-*H*), 6.71 (d, J = 9.2 Hz, 2H; Ph-*H*), 3.44 (m, 2H; CONH-C*H*$_2$), 3.07 (s, 6H; N(Me)$_2$), 2.72 (t, J = 7.4 Hz, 2H; NH_2-C*H*$_2$), 1.60 (p, J = 7.0 Hz, 2H; CONH-CH_2-C*H*$_2$), 1.52 (p, J = 6.9 Hz, 2H; NH_2-CH_2-C*H*$_2$), 1.35 (m, 4H; CH_2-CH_2-C*H*$_2$-C*H*$_2$-CH_2-CH_2).

δC(126 MHz, $CDCl_3$+1dr. MeOD) 166.71 (CONH), 153.26 (Ph), 150.55 (Ph), 143.35 (Ph), 131.81 (Ph), 131.04 (Ph), 129.52 (Ph), 129.24 (Ph), 129.22 (Ph), 125.73 (Ph), 116.10 (Ph), 111.62 (Ph), 40.24 (N(Me)$_2$), 39.69 (CONH-*C*H$_2$), 39.56 (NH_2-*C*H$_2$), 29.45 (CONH-CH_2-*C*H$_2$), 29.43 (NH_2-CH_2-*C*H$_2$), 28.69 (CONH-CH_2-CH_2-*C*H$_2$), 26.41 (alkyl), 25.96 (alkyl), 23.90 (alkyl).

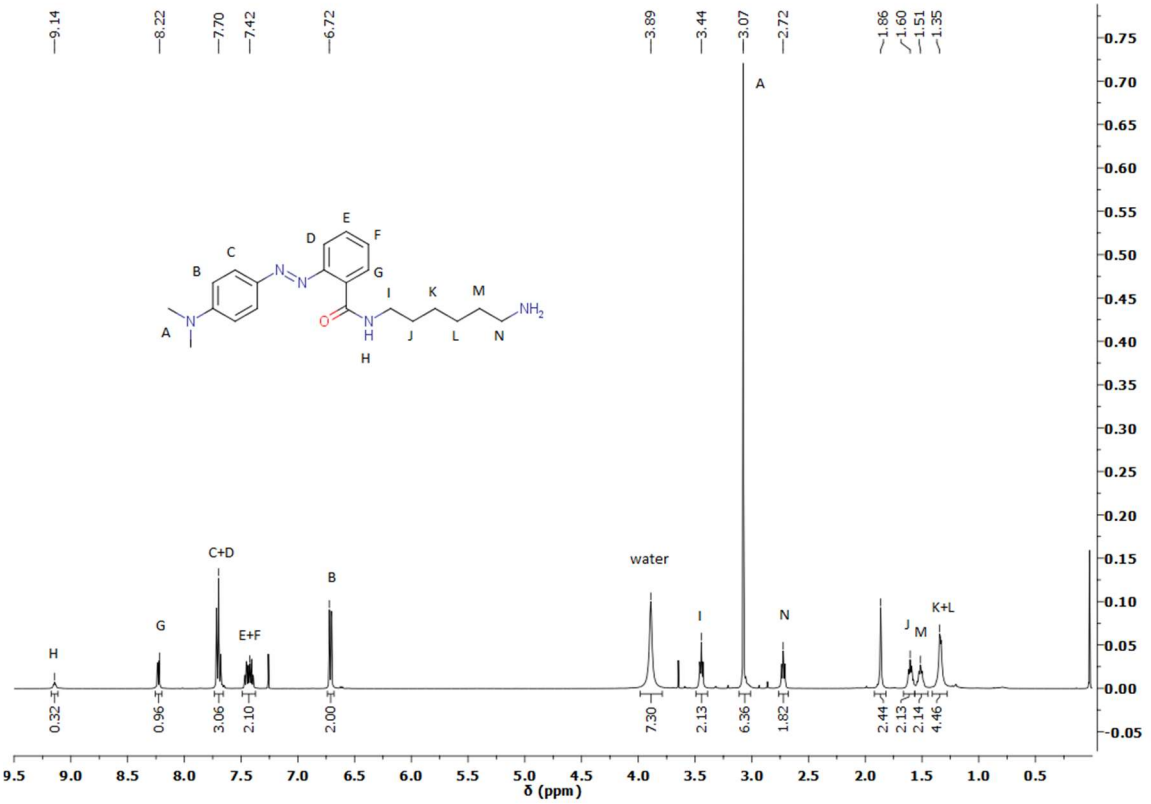

Figure S 5: ^{1}H NMR spectrum (500 MHz) in $CDCl_3$ + 1 drop MeOD of N-(2-aminohexyl)-2-[(1E)-2-[4-(dimethylamino)phenyl]diazen-1-yl]benzamide (2-aminohexyl-o-methyl red amide, AminoHexMR). The peak at 1.86 ppm is attributed to associated acetic acid.

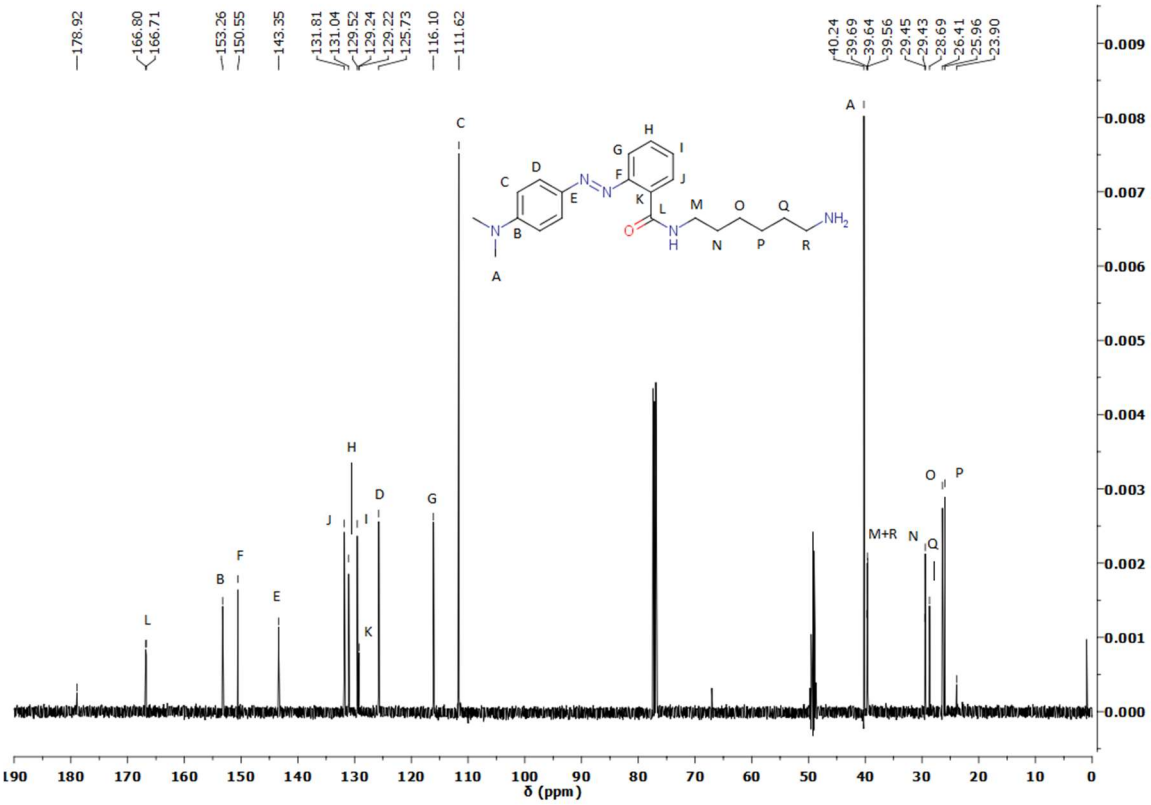

Figure S 6: ^{13}C NMR spectrum (126 MHz) in $CDCl_3$ + 1 drop MeOD of N-(2-aminohexyl)-2-[(1E)-2-[4-(dimethylamino)phenyl]diazen-1-yl]benzamide (2-aminohexyl-o-methyl red amide, AminoHexMR). The peak at 173 ppm is attributed to associated acetic acid.

C8: δH(500 MHz, $CDCl_3$:MeOD 9:1) 9.09 (s, 1H; CO-N*H*), 8.16 (d, J = 7.5 Hz, 1H; Ph-*H*), 7.65 (dd, J = 12.5, 8.7 Hz, 3H; Ph-*H*), 7.39 (dt, J = 23.2, 7.1 Hz, 2H; Ph-*H*), 6.66 (d, J = 8.9 Hz, 2H; Ph-*H*), 3.39 (t, J = 6.5 Hz, 2H; CONH-C*H*$_2$), 3.03 (s, 6H; N(Me)$_2$), 2.72 (m, 2H; NH_2-C*H*$_2$), 1.62 – 1.40 (m, 4H; CONH-CH_2-C*H*$_2$ + NH_2-CH_2-C*H*$_2$), 1.36 – 1.04 (m, 8H, alkyl).

δC(126 MHz, $CDCl_3$:MeOD 9:1) 166.74 (CONH), 166.65 (Ph), 153.20 (Ph), 150.47 (Ph), 143.26 (Ph), 131.73 (Ph), 130.85 (Ph), 129.39 (Ph), 129.10 (Ph), 125.66 (Ph), 116.03 (Ph), 111.51 (Ph), 40.09 (N(Me)$_2$), 39.87 (CONH-*C*H_2), 39.74 (NH_2-*C*H_2), 39.34 (NH_2-CH_2-*C*H_2), 29.38 (CONH-CH_2-*C*H_2), 28.83 (alkyl), 28.80 (alkyl), 27.59 (alkyl), 26.80 (alkyl), 26.23 (alkyl).

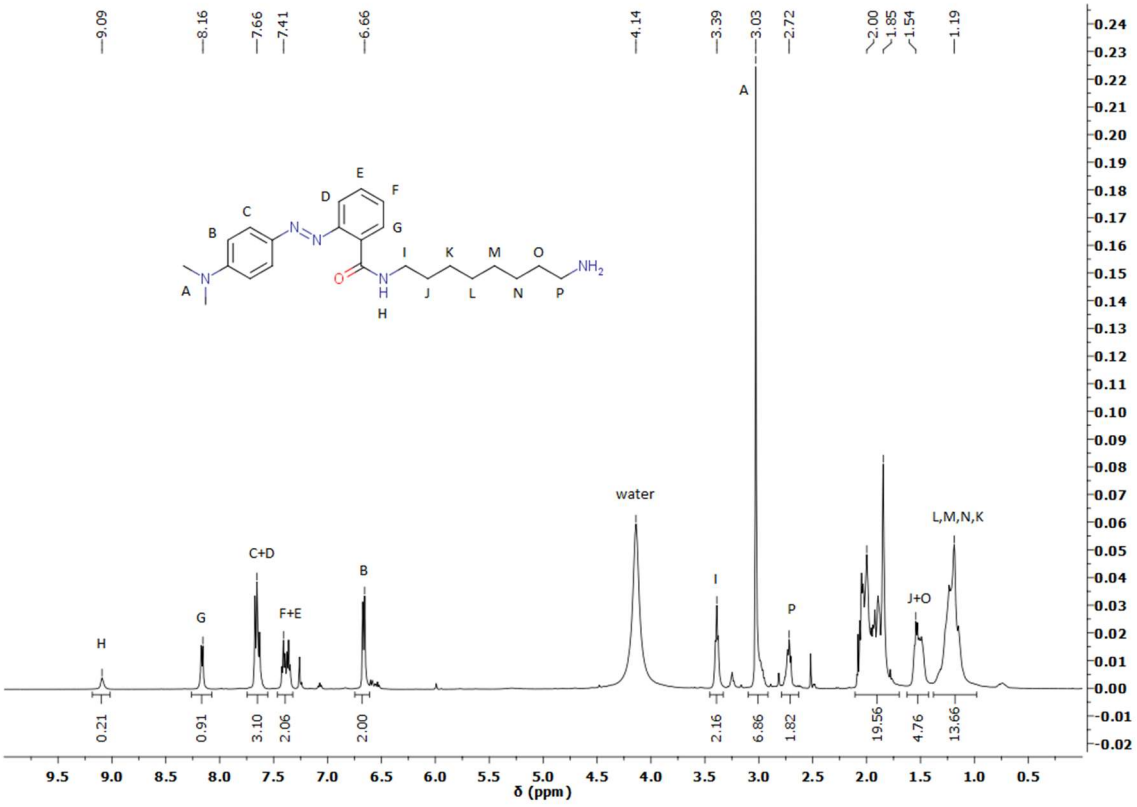

Figure S 7: ^{1}H NMR spectrum (500 MHz) in $CDCl_3$:MeOD 9:1 of N-(2-aminooctyl)-2-[(1E)-2-[4-(dimethylamino)phenyl]diazen-1-yl]benzamide (2-aminooctyl-o-methyl red amide, AminoOctMR). The peak at ca. 2 ppm is attributed to associated acetic acid.

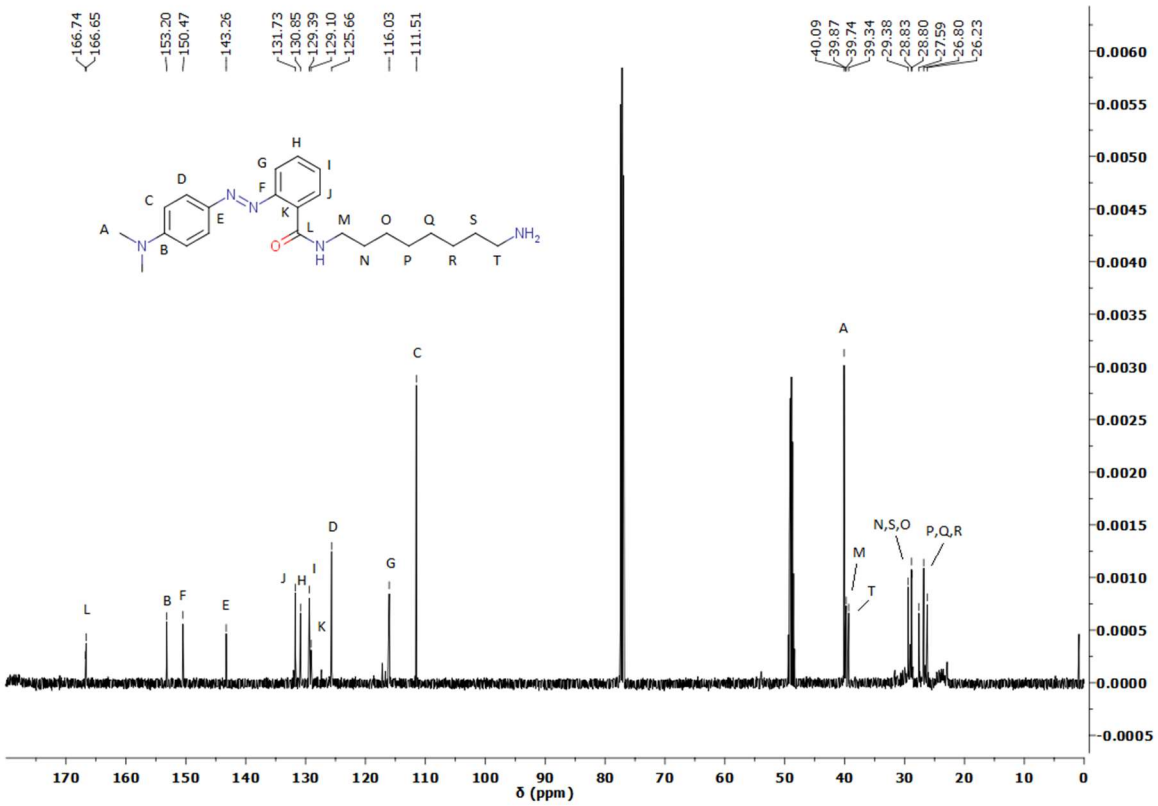

Figure S 8: ^{13}C NMR spectrum (126 MHz) in $CDCl_3$:MeOD 9:1 of N-(2-aminooctyl)-2-[(1E)-2-[4-(dimethylamino)phenyl]diazen-1-yl]benzamide (2-aminooctyl-o-methyl red amide, AminoOctMR).

Synthesis of N-[x-({2-[(1E)-2-[4-(dimethylamino)phenyl]diazen-1-yl]phenyl}formamido)alkyl]prop-2-enamide (1-o-methyl red amide of alkyl-6-acrylamide, MRAlkAm):

Aminoalkyl-o-methyl red and 1,8-diazabicyclo[5.4.0]undec-7-ene were dissolved in chloroform (C2, C3, C8) or dichloromethane (C6). The mixture was cooled to 0 °C and acryloyl chloride added. After 45 minutes, the ice bath was removed. After 24 hours, the organic phase was extracted with water. The product was purified *via* column chromatography on neutral aluminium oxide in ethyl acetate (C2, C3, C8) or on silica in diethylether (C6). The amounts of educts and yields are summarised in Table S2.

C2: δH(500 MHz; $CDCl_3$) 9.49 (t, J = 5.7 Hz, 1H; Ar-CO-N*H*), 8.31 (dd, J = 7.7, 1.7 Hz, 1H; Ph-*H*), 7.77 (dd, J = 8.1, 1.3 Hz, 1H; Ph-*H*), 7.74 (d, J = 9.2 Hz, 2H; Ph-*H*), 7.51 (ddd, J = 8.1, 7.2, 1.7 Hz, 1H; Ph-*H*), 7.45 (ddd, J = 7.7, 7.2, 1.3 Hz, 1H; Ph-*H*), 6.89 (s, 1H; DB-CO-N*H*), 6.76 (d, J = 9.3 Hz, 2H; Ph-*H*), 6.23 (dd, J = 17.0, 1.5 Hz, 1H; CHC*H*H(trans)), 6.07 (dd, J = 17.1, 10.3 Hz, 1H; C*H*CHH), 5.56 (dd, J = 10.3, 1.5 Hz,

1H; CHCH*H*(cis)), 3.71 (dd, J = 11.5, 5.8 Hz, 2H; Ar-CONH-CH_2), 3.59 (dd, J = 11.1, 5.3 Hz, 2H; DB-CONH-CH_2), 3.12 (s, 6H; N(Me)$_2$).

δC(126 MHz; $CDCl_3$) 168.10 (Ar-CONH), 166.12 (DB-CONH), 153.40 (Ph), 150.57 (Ph), 143.47 (Ph), 132.12 (Ph), 131.29 (CO*C*HCH$_2$), 131.26 (Ph), 129.60 (Ph), 129.05 (Ph), 126.01 (COCH*C*H$_2$), 125.84 (Ph), 116.17 (Ph), 111.96 (Ph), 41.48 (Ar-CONH*C*H$_2$), 40.40 (N(Me)$_2$), 39.50 (DB-CONH*C*H$_2$).

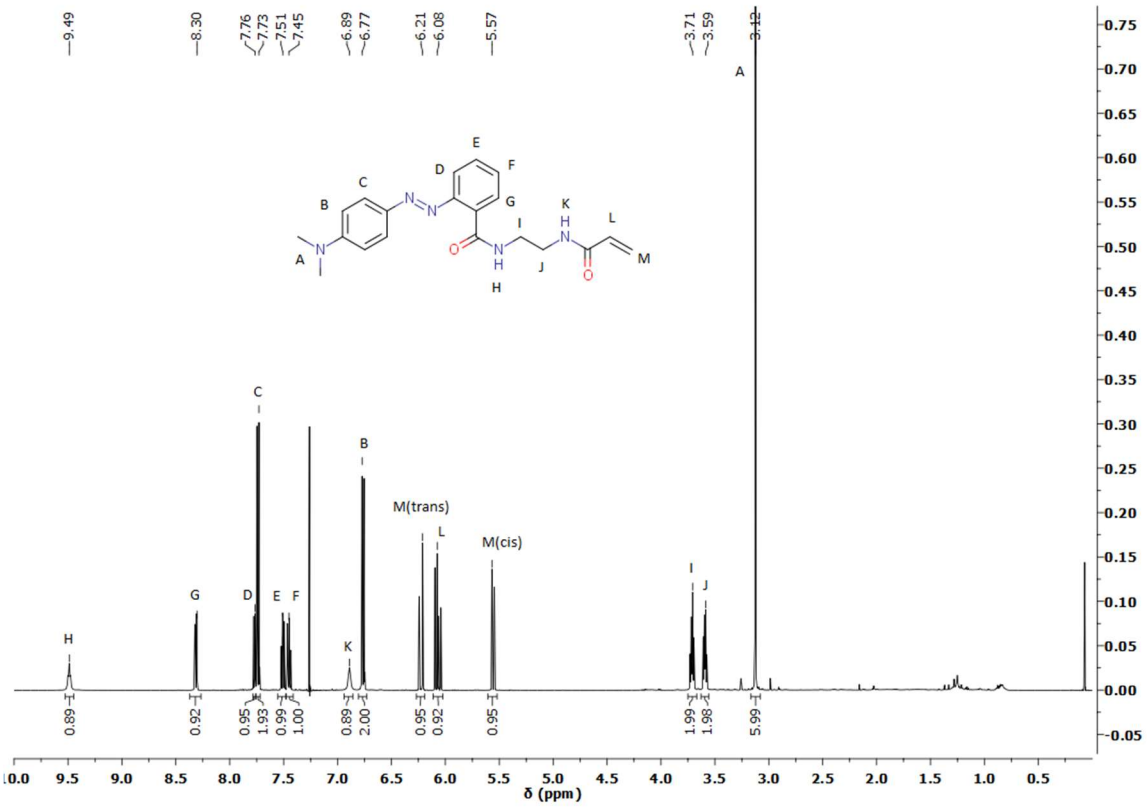

Figure S 9: ^{1}H NMR spectrum (500 MHz) in $CDCl_3$ of N-[6-({2-[(1E)-2-[4-(dimethylamino)phenyl]diazen-1-yl]phenyl}formamido)ethyl]prop-2-enamide (1-o-methyl red amide of ethyl-6-acrylamide, MREtAAm).

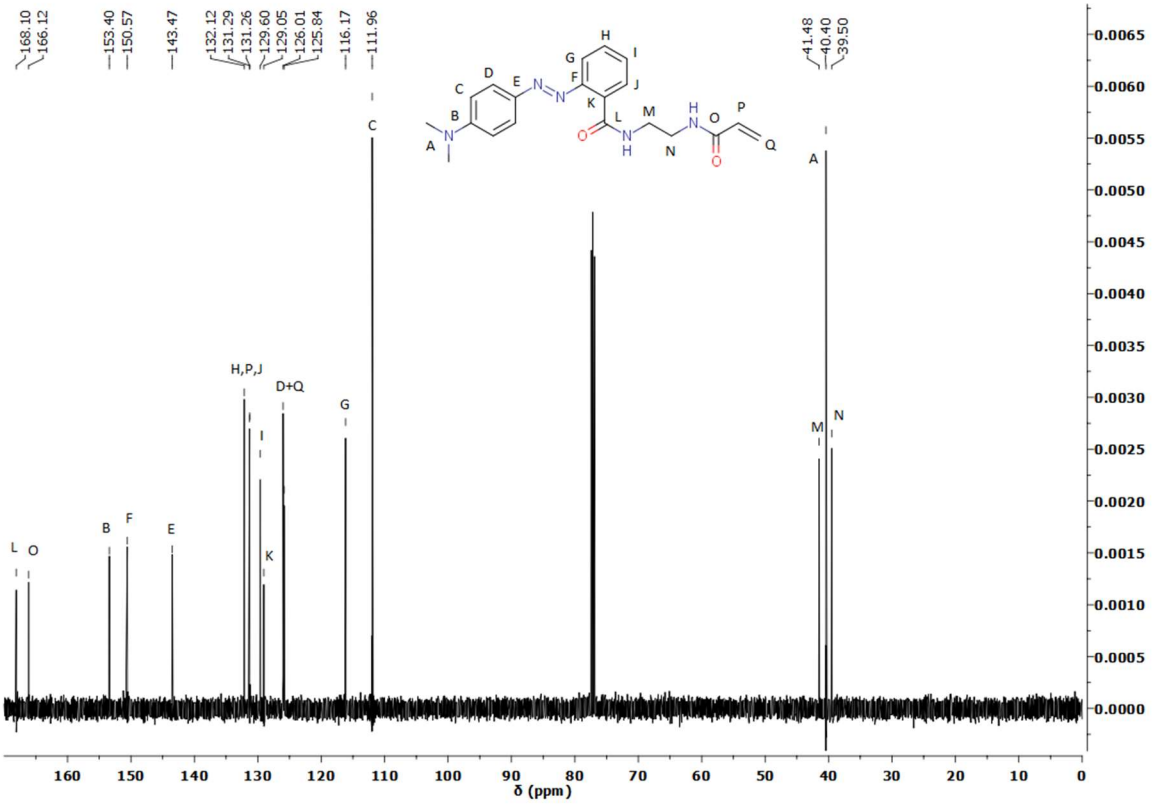

Figure S 10: ^{13}C NMR spectrum (126 MHz) in $CDCl_3$ of N-[6-({2-[(1E)-2-[4-(dimethylamino)phenyl]diazen-1-yl]phenyl}formamido)ethyl]prop-2-enamide (1-o-methyl red amide of ethyl-6-acrylamide, MREtAAm).

C3: δH(500 MHz; $CDCl_3$) 9.17 (t, J = 6.0 Hz, 1H; Ar-CO-N*H*), 8.30 (dd, J = 7.6, 1.8 Hz, 1H; Ph-*H*), 7.76 (dd, J = 7.3, 1.3 Hz, 1H; Ph-*H*), 7.75 (d, J = 9.2 Hz, 2H; Ph-*H*), 7.51 (ddd, J = 8.0, 7.2, 1.7 Hz, 1H; Ph-*H*), 7.46 (ddd, J = 7.3, 7.2, 1.3 Hz, 1H; Ph-*H*), 7.03 (t, J = 5.0 Hz, 1H; DB-CO-N*H*), 6.76 (d, J = 9.3 Hz, 2H; Ph-H), 6.27 (dd, J = 17.1, 1.7 Hz, 1H; CHC*H*H(trans)), 6.17 (dd, J = 17.1, 10.1 Hz, 1H; C*H*CHH), 5.60 (dd, J = 10.1, 1.7 Hz, 1H; CHCH*H*(cis)), 3.61 (dd, J = 12.5, 6.3 Hz, 2H; Ar-CONH-CH_2), 3.39 (dd, J = 12.3, 6.2 Hz, 2H; DB-CONH-CH_2), 3.12 (s, 6H; $N(Me)_2$), 1.81 (t, J = 6.2 Hz, 2H; CH_2-CH_2-CH_2).

δC(126 MHz; $CDCl_3$) 167.67 (Ar-CONH), 165.85 (DB-CONH), 153.36 (Ph), 150.59 (Ph), 143.51 (Ph), 131.99 (CO*C*HCH_2), 131.65 (Ph), 131.26 (Ph), 129.65 (Ph), 129.43 (Ph), 125.84 (Ph), 125.81 (COCH*C*H_2), 116.19 (Ph), 111.84 (Ph), 40.42 ($N(Me)_2$), 36.72 (Ar-CONH*C*H_2), 35.99 (DB-CONH*C*H_2), 30.13 (CH_2-*C*H_2-CH_2).

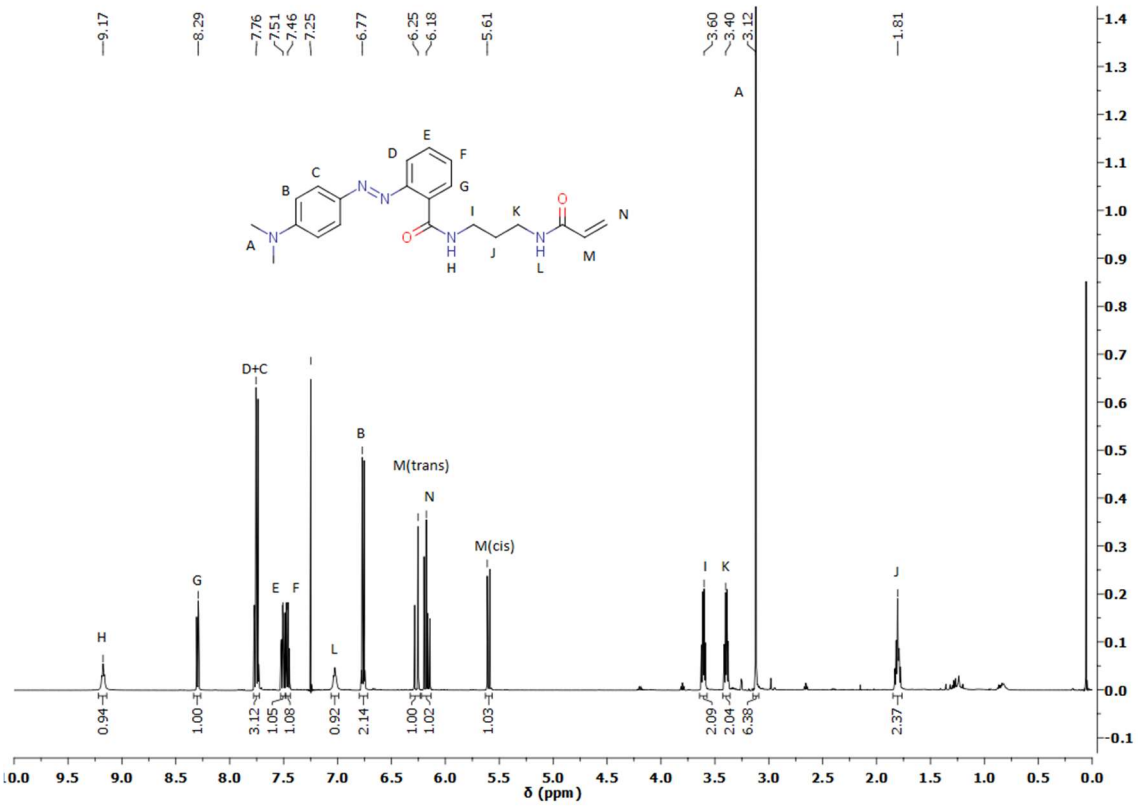

Figure S 11: ^{1}H NMR spectrum (500 MHz) in $CDCl_3$ of N-[6-({2-[(1E)-2-[4-(dimethylamino)phenyl]diazen-1-yl]phenyl}formamido)propyl]prop-2-enamide (1-o-methyl red amide of propyl-6-acrylamide, MRPrAAm).

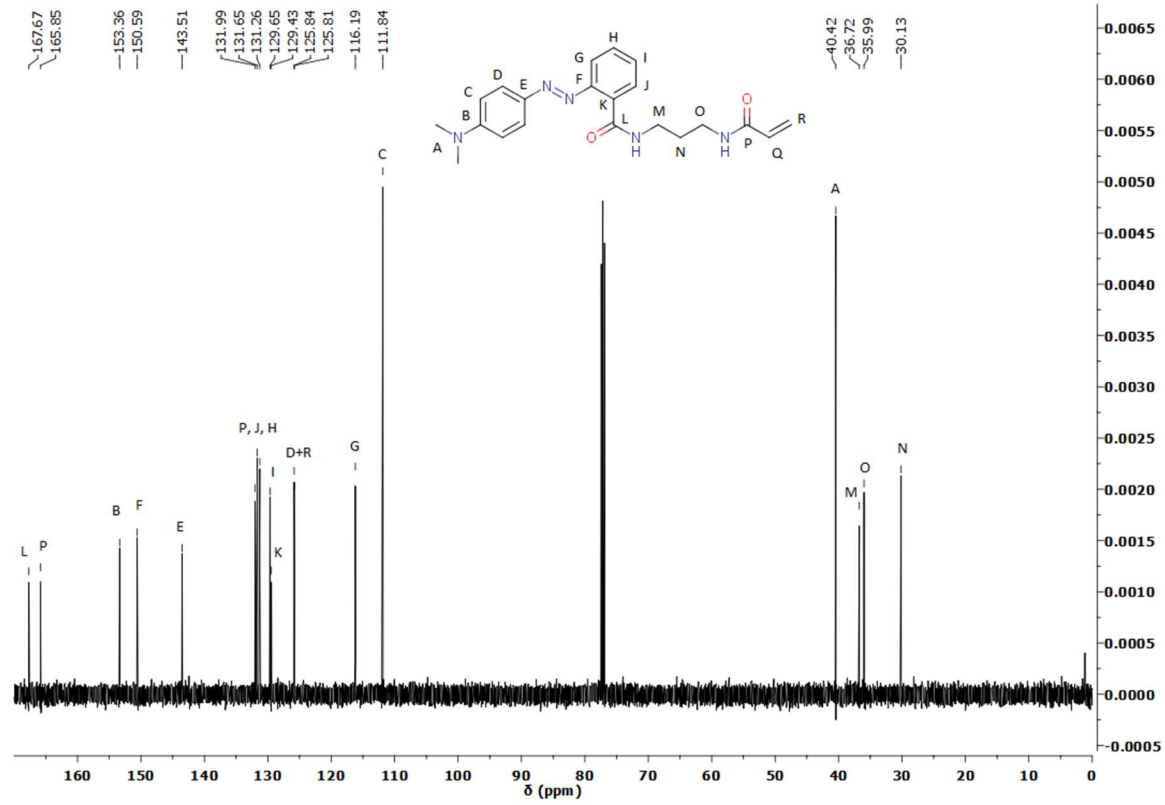

Figure S 12: ^{13}C NMR spectrum (126 MHz) in $CDCl_3$ of N-[6-({2-[(1E)-2-[4-(dimethylamino)phenyl]diazen-1-yl]phenyl}formamido)propyl]prop-2-enamide (1-o-methyl red amide of propyl-6-acrylamide, MRPrAAm).

C6: δH(500 MHz; $CDCl_3$) 9.08 (t, J = 5.3 Hz, 1H; Ar-CO-N*H*), 8.34 (dd, J = 7.7, 1.7 Hz, 1H; Ph-*H*), 7.76 (d, J = 9.2 Hz, 2H; Ph-*H*), 7.73 (dd, J = 7.9, 1.4 Hz, 1H; Ph-*H*), 7.47 (dqd, J = 14.7, 7.2, 1.6 Hz, 2H; Ph-*H*), 6.76 (d, J = 9.2 Hz, 2H; Ph-*H*), 6.25 (dd, J = 17.0, 1.6 Hz, 1H; CHC*H*H(trans)), 6.13 (dd, J = 17.0, 10.2 Hz, 1H; C*H*CHH), 6.09 (s, 1H; DB-CO-N*H*), 5.59 (dd, J = 10.2, 1.6 Hz, 1H; CHCH*H*(cis)), 3.52 (dd, J = 12.6, 6.9 Hz, 2H; Ar-CONH-CH_2), 3.26 (dd, J = 12.9, 6.9 Hz, 2H; DB-CONH-CH_2), 3.12 (s, 6H; $N(Me)_2$), 1.64 (p, J = 7.0 Hz, 2H; Ar-CONH-CH_2-CH_2), 1.48 (p, J = 6.9 Hz, 2H; DB-CONH-CH_2-CH_2), 1.43 – 1.31 (m, 4H; CH_2-CH_2-CH_2-CH_2-CH_2-CH_2).

δC(126 MHz; $CDCl_3$) 166.43 (Ar-CONH), 165.73 (DB-CONH), 153.28 (Ph), 150.64 (Ph), 143.53 (Ph), 131.74 (Ph), 131.41 (CO*C*HCH_2), 131.25 (Ph), 129.64 (Ph), 129.61 (Ph), 126.05 (COCH*C*H_2), 125.83 (Ph), 116.11 (Ph), 111.72 (Ph), 40.42 ($N(Me)_2$), 39.66 (Ar-CONH*C*H_2), 39.27 (DB-CONH*C*H_2), 29.77 (Ar-CONHCH_2*C*H_2), 29.36 (DB-CONHCH_2*C*H_2), 26.53 (Ar-CONHCH_2CH_2*C*H_2), 26.32 (DB-CONHCH_2CH_2*C*H_2).

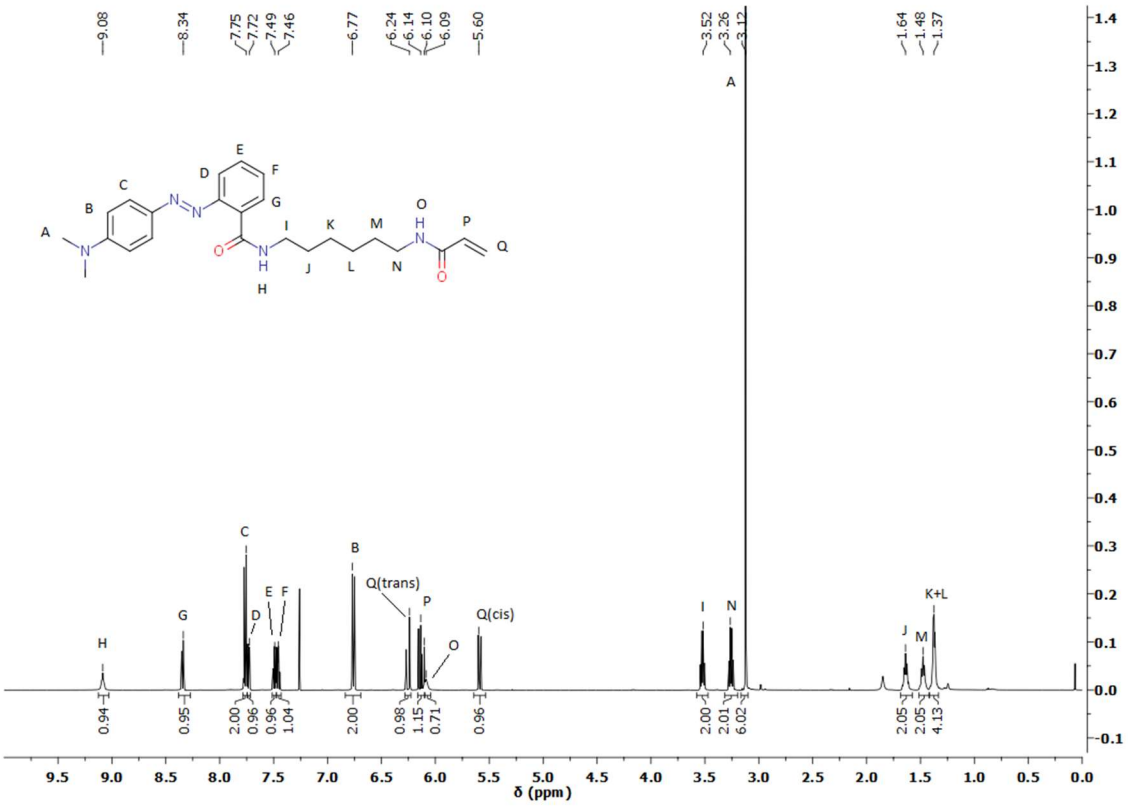

Figure S 13: ^1H NMR spectrum (500 MHz) in $CDCl_3$ of N-[6-({2-[(1E)-2-[4-(dimethylamino)phenyl]diazen-1-yl]phenyl}formamido)hexyl]prop-2-enamide (1-o-methyl red amide of hexyl-6-acrylamide, MRHexAAm).

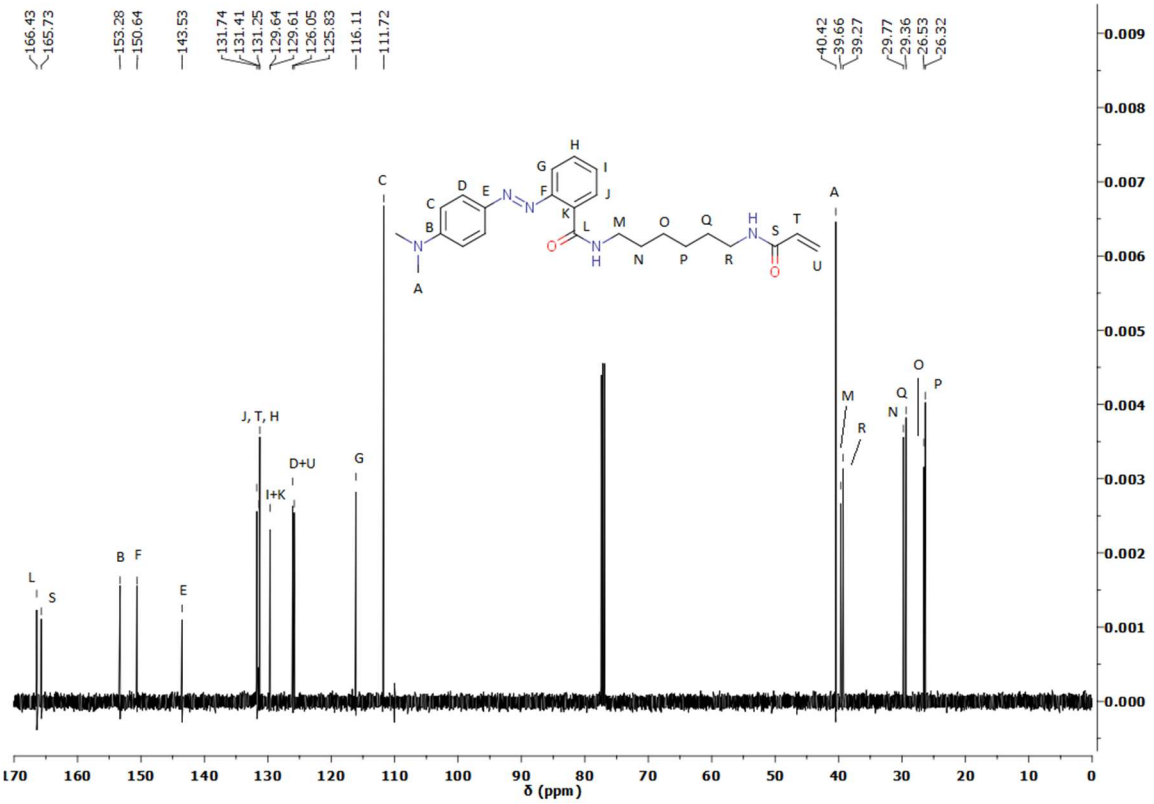

Figure S 14: ^{13}C NMR spectrum (126 MHz) in $CDCl_3$ of N-[6-({2-[(1E)-2-[4-(dimethylamino)phenyl]diazen-1-yl]phenyl}formamido)hexyl]prop-2-enamide (1-o-methyl red amide of hexyl-6-acrylamide, MRHexAAm).

C8: δH(500 MHz; $CDCl_3$) 9.05 (t, J = 5.0 Hz, 1H; Ar-CO-N*H*), 8.37 (dd, J = 7.2, 2.2 Hz, 1H; Ph-*H*), 7.78 (d, J = 9.2 Hz, 2H; Ph-*H*), 7.74 (dd, J = 7.4, 1.9 Hz, 1H; Ph-*H*), 7.48 (dqd, J = 14.6, 7.2, 1.7 Hz, 2H; Ph-*H*), 6.76 (d, J = 9.3 Hz, 2H; Ph-*H*), 6.25 (dd, J = 17.0, 1.5 Hz, 1H; CHC*H*H(trans)), 6.08 (dd, J = 17.0, 10.3 Hz, 1H; C*H*CHH), 5.76 (s, 1H; DB-CO-N*H*), 5.60 (dd, J = 10.3, 1.5 Hz, 1H; CHCH*H*(cis)), 3.52 (td, J = 7.0, 5.6 Hz, 2H; Ar-CONH-CH_2), 3.27 (td, J = 7.1, 6.0 Hz, 2H; DB-CONH-CH_2), 3.13 (s, 6H; N(Me)$_2$), 1.64 (p, J = 7.2, 2H; Ar-CONH-CH$_2$-CH_2), 1.47 (p, J = 7.2, 2H; DB-CONH-CH$_2$-CH_2), 1.37 (td, J = 13.9, 7.0 Hz, 2H; Ar-CONH-CH$_2$-CH$_2$-CH_2), 1.33 – 1.09 (m, 6H; CH$_2$-CH$_2$-CH$_2$-CH_2-CH_2-CH_2-CH$_2$-CH$_2$).

δC(126 MHz; $CDCl_3$) 166.26 (Ar-CONH), 165.62 (DB-CONH), 153.25 (Ph), 150.66 (Ph), 143.58 (Ph), 131.67 (Ph), 131.49 (CO*C*HCH$_2$), 131.18 (Ph), 129.76 (Ph), 129.66 (Ph), 126.17 (COCH*C*H$_2$), 125.85 (Ph), 116.08 (Ph), 111.70 (Ph), 40.43 (N(Me)$_2$), 40.11 (Ar-CONH*C*H$_2$), 39.67 (DB-CONH*C*H$_2$), 29.74 (Ar-CONHCH$_2$*C*H$_2$), 29.61 (DB-CONHCH$_2$*C*H$_2$), 29.25 (Ar-CONHCH$_2$CH$_2$*C*H$_2$), 29.21 (DB-CONHCH$_2$CH$_2$*C*H$_2$), 27.18 (AR-CONHCH$_2$CH$_2$CH$_2$*C*H$_2$), 26.91 (DB-CONHCH$_2$CH$_2$CH$_2$*C*H$_2$).

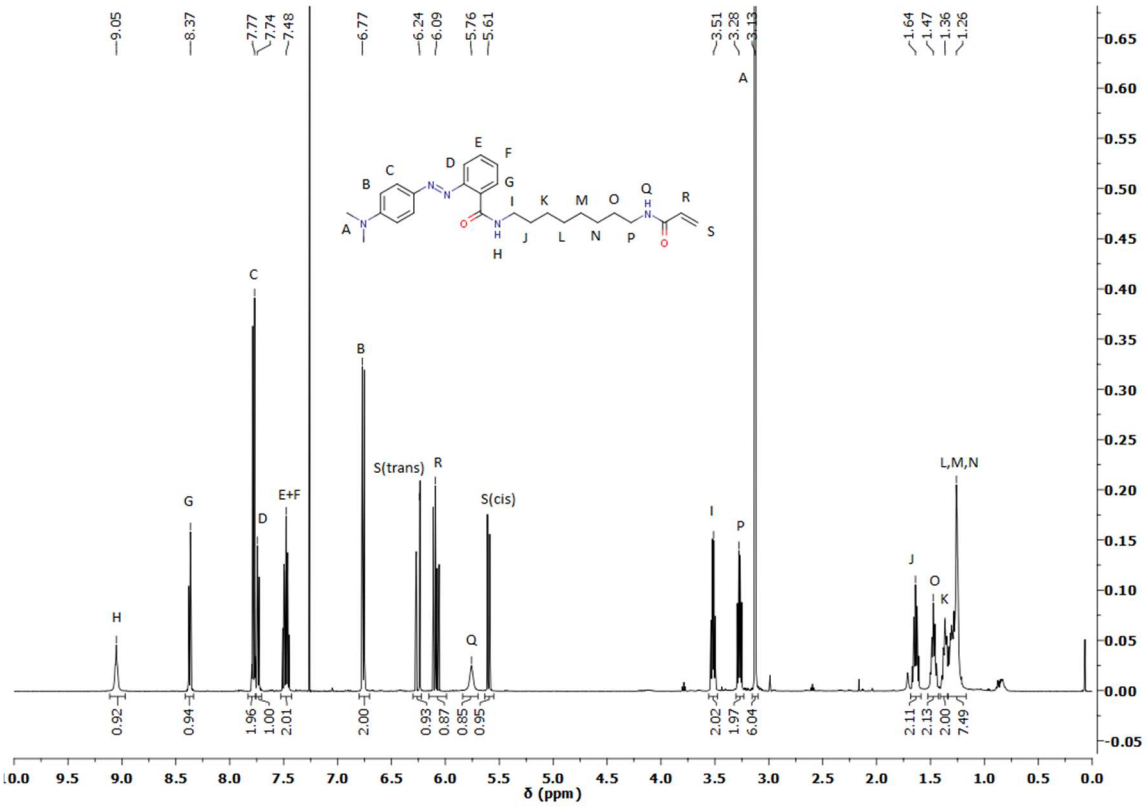

Figure S 15: ^{1}H NMR spectrum (500 MHz) in $CDCl_3$ of N-[6-({2-[(1E)-2-[4-(dimethylamino)phenyl]diazen-1-yl]phenyl}formamido)octyl]prop-2-enamide (1-o-methyl red amide of octyl-6-acrylamide, MROctAAm).

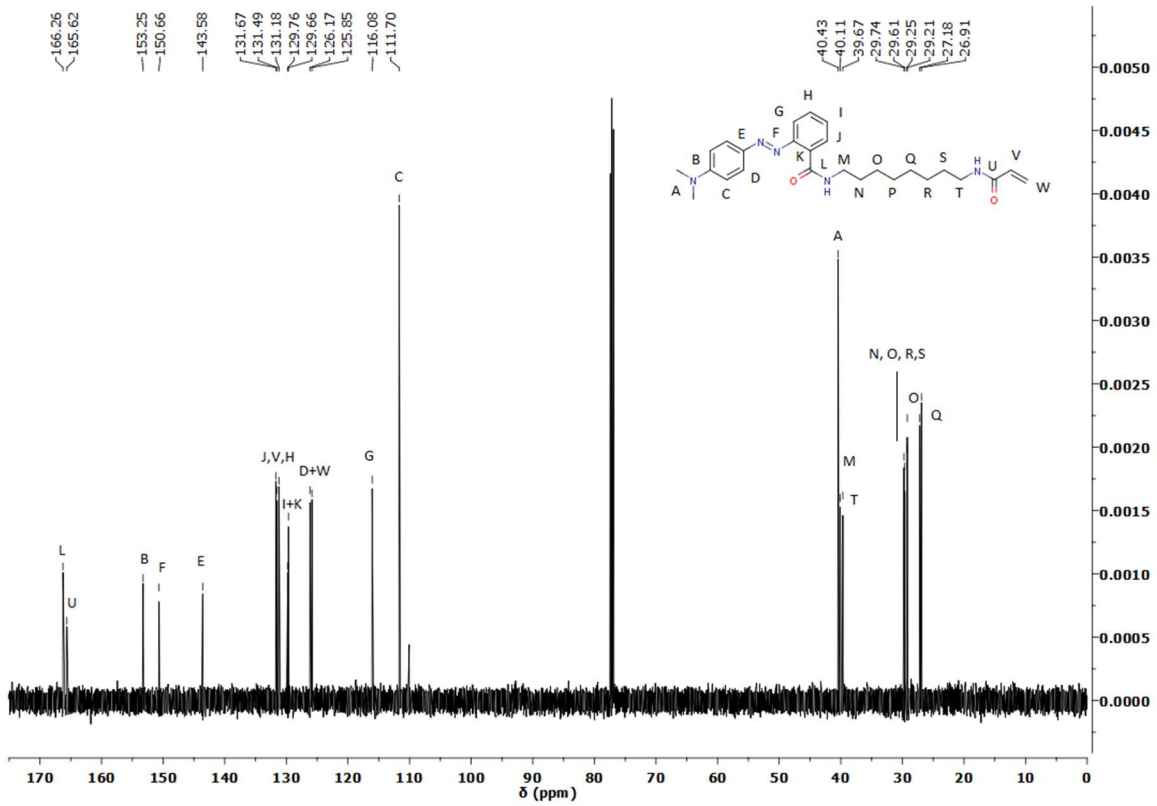

Figure S 16: ^{13}C NMR spectrum (126 MHz) in $CDCl_3$ of N-[6-({2-[(1E)-2-[4-(dimethylamino)phenyl]diazen-1-yl]phenyl}formamido)octyl]prop-2-enamide (1-o-methyl red amide of octyl-6-acrylamide, MROctAAm).

Table S 2: Reaction parameters of acylation reactions of aminoalkylmetyl red including educt ratios, base, and yield.

Derivative	MRimidazolid [mg]	Acryloyl chloride [mL]/mol eq.	DBU [mL]/mol eq.	Yield [mg]/%
MREtAAm	100.8	0.04 (1.5)	0.1 (2.2)	52.8 (44)
MRPrAAm	100.2	0.04 (1.6)	0.09 (2)	49.7 (43)
MRHexAAm	203.8	0.09 (2)	0.16 (1.9)	101.5 (43)
MROctAAm	100.4	0.04 (1.9)	0.08 (2.1)	35.7 (31)

Further NMR Experiments on Amidoalkyl Acrylamides of *o*-Methyl Red:

2D-NMR Data of N-[6-({2-[(1E)-2-[4-(dimethylamino)phenyl]diazen-1-yl]phenyl}formamido)hexyl]prop-2-enamide (1-o-methyl red amide of hexyl-6-acrylamide, MRHexAAm):

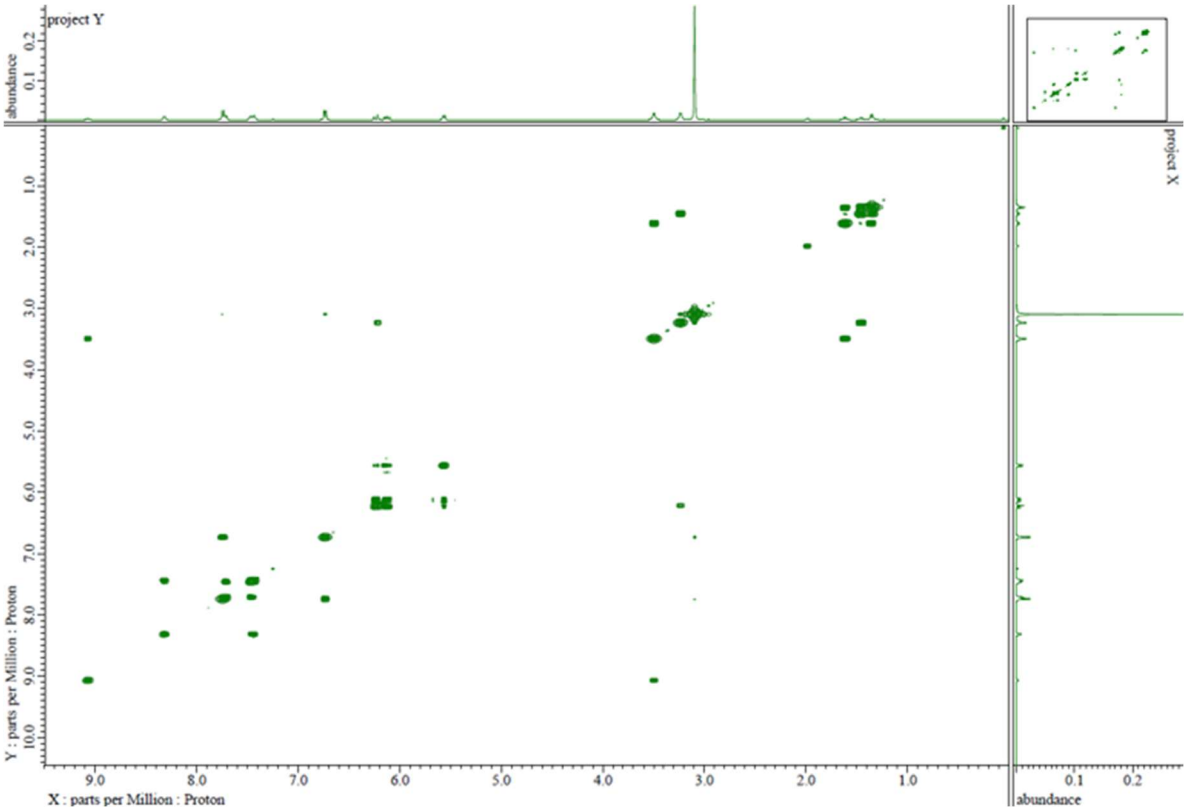

Figure S 17: ^{1}H-^{1}H-COSY spectrum (500 MHz) in $CDCl_3$ of N-[6-({2-[(1E)-2-[4-(dimethylamino)phenyl]diazen-1-yl]phenyl}formamido)hexyl]prop-2-enamide (1-o-methyl red amide of hexyl-6-acrylamide, MRHexAAm).

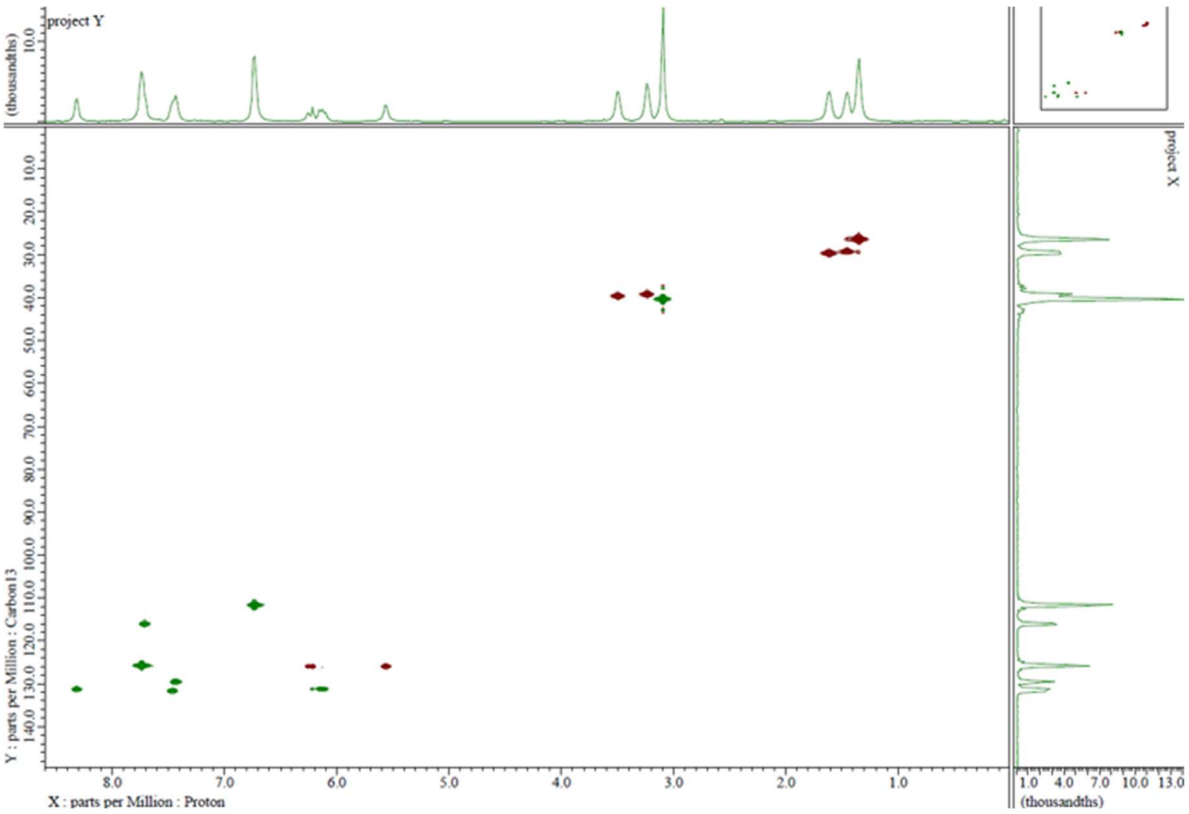

Figure S 18: ^{1}H-^{13}C-HSQC spectrum (500 MHz; 126 MHz) in $CDCl_3$ of N-[6-({2-[(1E)-2-[4-(dimethylamino)phenyl]diazen-1-yl]phenyl}formamido)hexyl]prop-2-enamide (1-o-methyl red amide of hexyl-6-acrylamide, MRHexAAm).

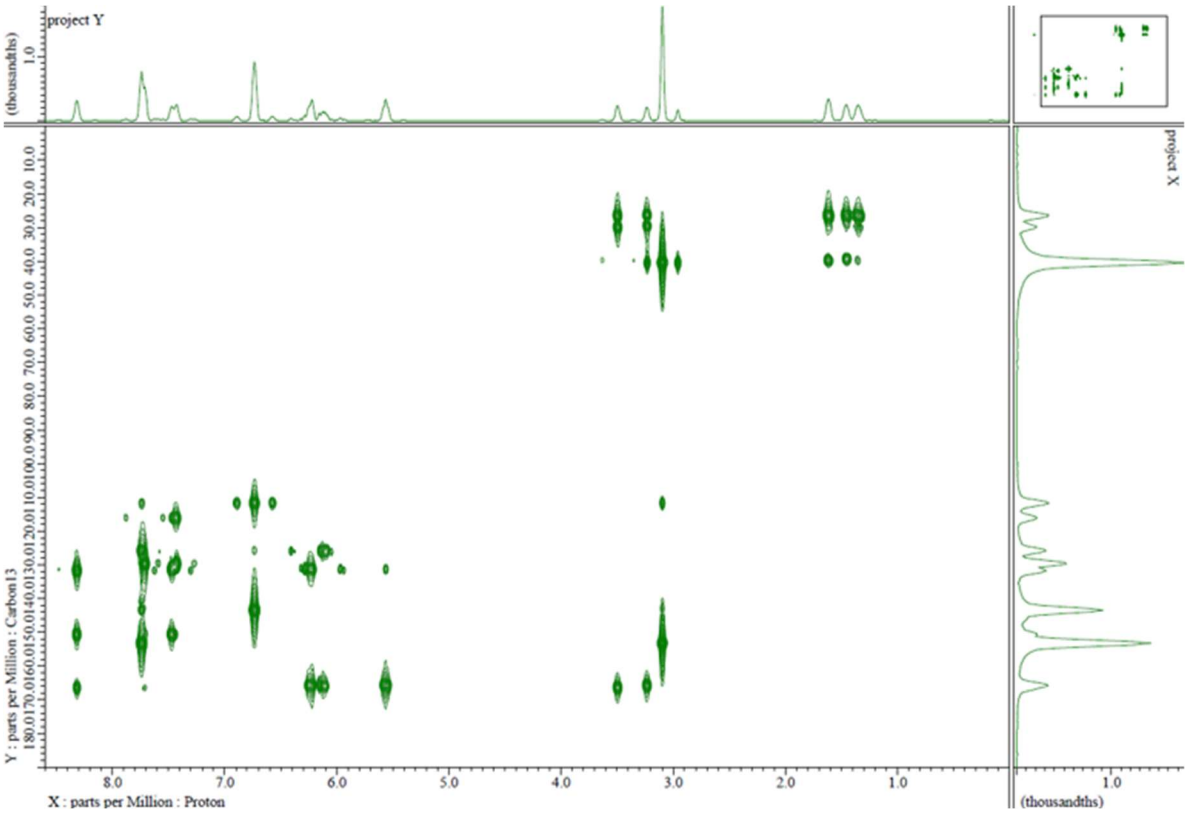

Figure S 19: ^{1}H-^{13}C-HMBC spectrum (500 MHz; 126 MHz) in $CDCl_3$ of N-[6-({2-[(1E)-2-[4-(dimethylamino)phenyl]diazen-1-yl]phenyl}formamido)hexyl]prop-2-enamide (1-o-methyl red amide of hexyl-6-acrylamide, MRHexAAm).

NMR Data of Protonated Amidoalkyl Acrylamides of o-Methyl Red:

For these NMR-experiments, the different derivatives were dissolved in deuterated chloroform with 10 v/v% trifluoroacetic acid. The solvent and acid were removed under reduced pressure. The resulting solids were redissolved in deuterated chloroform and then measured.

C2: δH(500 MHz; $CDCl_3$) 14.01 (s, associated TFA), 9.10 (s, 1H; Ar-CO-N*H*), 7.98 (ddd, J = 15.1, 8.2, 0.9 Hz, 2H; Ph-*H* and DB-CO-N*H*), 7.79 (d, J = 9.6 Hz, 2H; Ph-*H*), 7.66 – 7.51 (m, 1H; Ph-*H*), 7.48 – 7.34 (m, 1H; Ph-*H*), 7.00 (d, J = 9.6 Hz, 2H; Ph-*H*), 6.29 – 6.16 (m, 2H; CHC*H*H(trans) and C*H*CHH), 5.64 (dd, J = 6.7, 4.9 Hz, 1H; CHCH*H*(cis)), 3.76 – 3.59 (m, 4H; Ar-CONH-CH_2 and DB-CONH-CH_2), 3.42 (s, 6H; $N(Me)_2$).

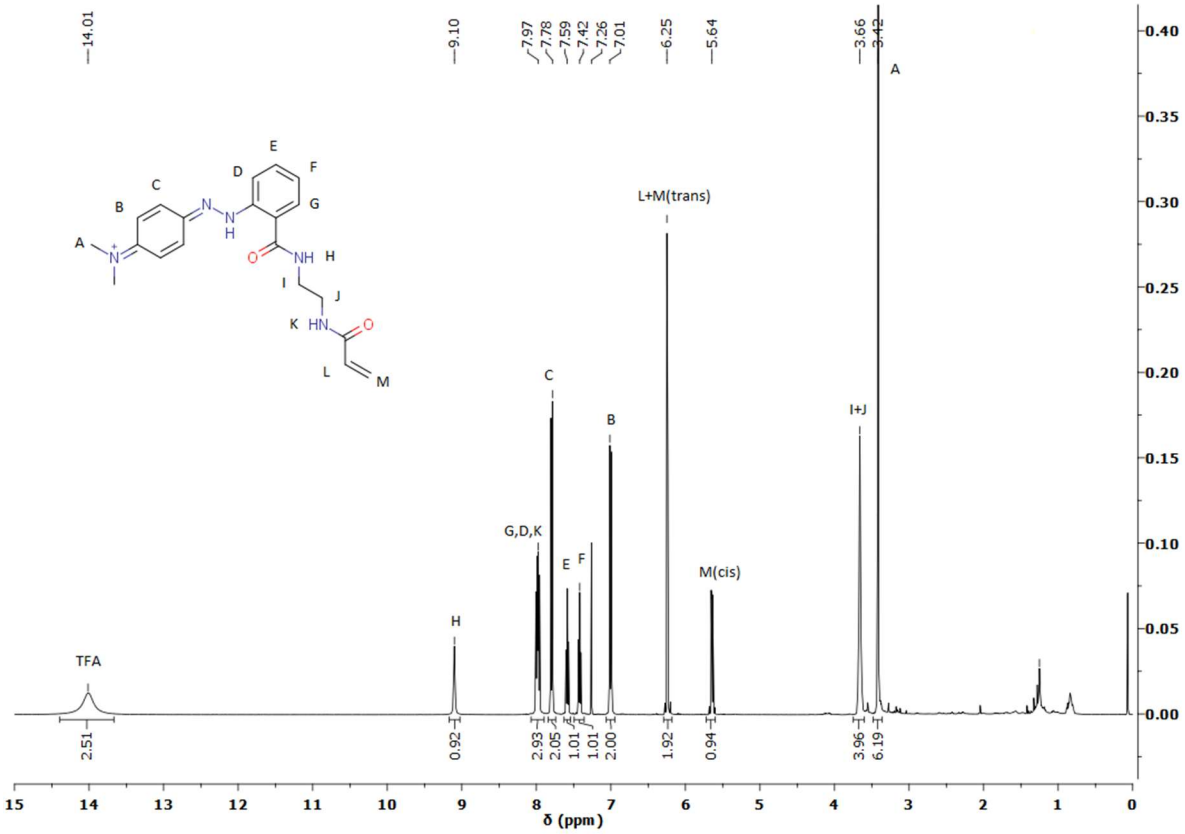

Figure S 20: ^{1}H NMR spectrum (500 MHz) in $CDCl_3$ of protonated N-[6-({2-[(1E)-2-[4-(dimethylamino)phenyl]diazen-1-yl]phenyl}formamido)ethyl]prop-2-enamide (1-o-methyl red amide of ethyl-6-acrylamide, MREtAAm) with trifluoroacetate as counter-ion.

C3: δH(500 MHz; $CDCl_3$) 14.16 (s, associated TFA), 9.03 (t, J = 5.9 Hz, 1H; Ar-CO-N*H*), 8.07 (dd, J = 8.0, 1.0 Hz, 1H; Ph-*H*), 7.99 (dd, J = 8.3, 0.9 Hz, 1H; Ph-*H*), 7.81 (d, J = 9.6 Hz, 2H; Ph-*H*), 7.71 (t, J = 5.8 Hz, 1H; DB-CO-N*H*), 7.67 – 7.54 (m, 1H; Ph-*H*), 7.50 – 7.40 (m, 1H; Ph-*H*), 7.01 (d, J = 9.6 Hz, 2H; Ph-*H*), 6.37 – 6.14 (m, 2H; CHC*H*H(trans) and C*H*CHH), 5.66 (dd, J = 6.3, 5.2 Hz, 1H; CHCH*H*(cis)), 3.54 (dd, J = 12.2, 6.1 Hz, 2H; Ar-CONH-CH_2), 3.46 (dd, J = 12.1, 6.1 Hz, 2H; DB-CONH-CH_2), 3.42 (s, 6H; $N(Me)_2$), 1.90 (p, J = 6.0 Hz, 2H; Ar-CONH-CH_2-CH_2).

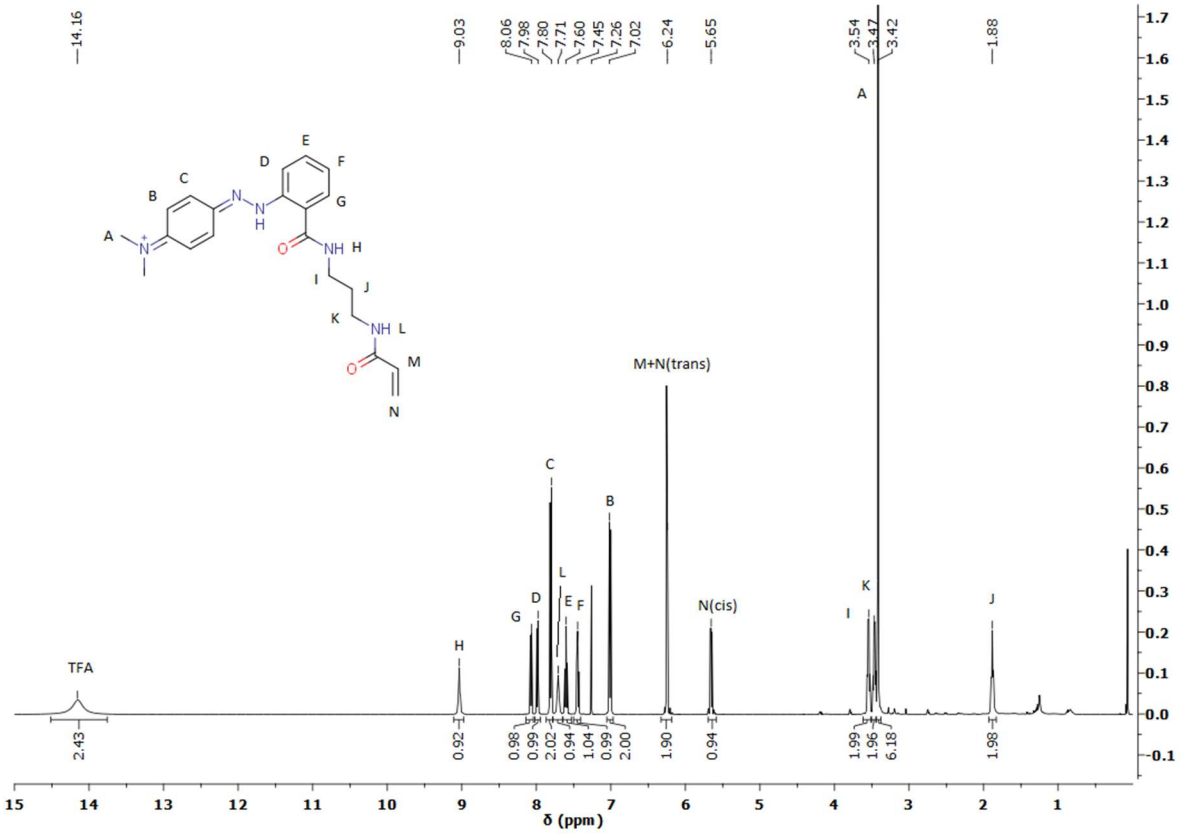

Figure S 21: ^{1}H NMR spectrum (500 MHz) in $CDCl_3$ of protonated N-[6-({2-[(1E)-2-[4-(dimethylamino)phenyl]diazen-1-yl]phenyl}formamido)propyl]prop-2-enamide (1-o-methyl red amide of propyl-6-acrylamide, MRPrAAm) with trifluoroacetate as counter-ion.

C6: δH(500 MHz; $CDCl_3$) 14.19 (s, associated TFA), 8.62 (s, 1H; Ar-CO-N*H*), 8.08 (dd, J = 8.0, 1.0 Hz, 1H; Ph-*H*), 7.95 (dd, J = 8.3, 0.9 Hz, 1H; Ph-*H*), 7.79 (d, J = 9.6 Hz, 2H; Ph-*H*), 7.63 – 7.50 (m, 1H; Ph-*H*), 7.46 – 7.34 (m, 1H; Ph-*H*), 6.99 (d, J = 9.6 Hz, 2H; Ph-*H*), 6.27 – 6.15 (m, 2H; CHC*H*H(trans) and C*H*CHH), 5.65 (dd, J = 7.8, 3.8 Hz, 1H; CHCH*H*(cis)), 3.46 (dd, J = 12.9, 6.8 Hz, 2H; Ar-CONH-CH_2), 3.38 (s, 6H; N(Me)$_2$), 3.30 (dd, J = 12.9, 6.8 Hz, 2H; DB-CONH-CH_2), 1.64 (p, J = 7.0 Hz, 2H; Ar-CONH-CH$_2$-CH_2), 1.53 (p, J = 7.0 Hz, 2H; DB-CONH-CH$_2$-CH_2), 1.45 – 1.32 (m, 4H; Ar-CONH-CH$_2$-CH$_2$-CH_2).

δC(126 MHz; $CDCl_3$) 168.21 (Ar-CONH), 167.42 (DB-CONH), [160.54, 160.23, 159.92, 159.61] (TFA), 157.25 (Ph), 144.49 (Ph), 139.55 (Ph), 133.24 (Ph), 130.38 (CO*C*HCH$_2$), 129.17 (Ph), 129.06 (Ph), 127.29 (COCH*C*H$_2$), 122.62 (Ph), 116.69 (Ph), 115.28 (Ph), 114.51 (Ph), 41.74(N(Me)$_2$), 40.17 (Ar-CONH*C*H$_2$), 39.71 (DB-CONH*C*H$_2$), 28.84 (alkyl), 26.13 (alkyl), 25.98 (alkyl).

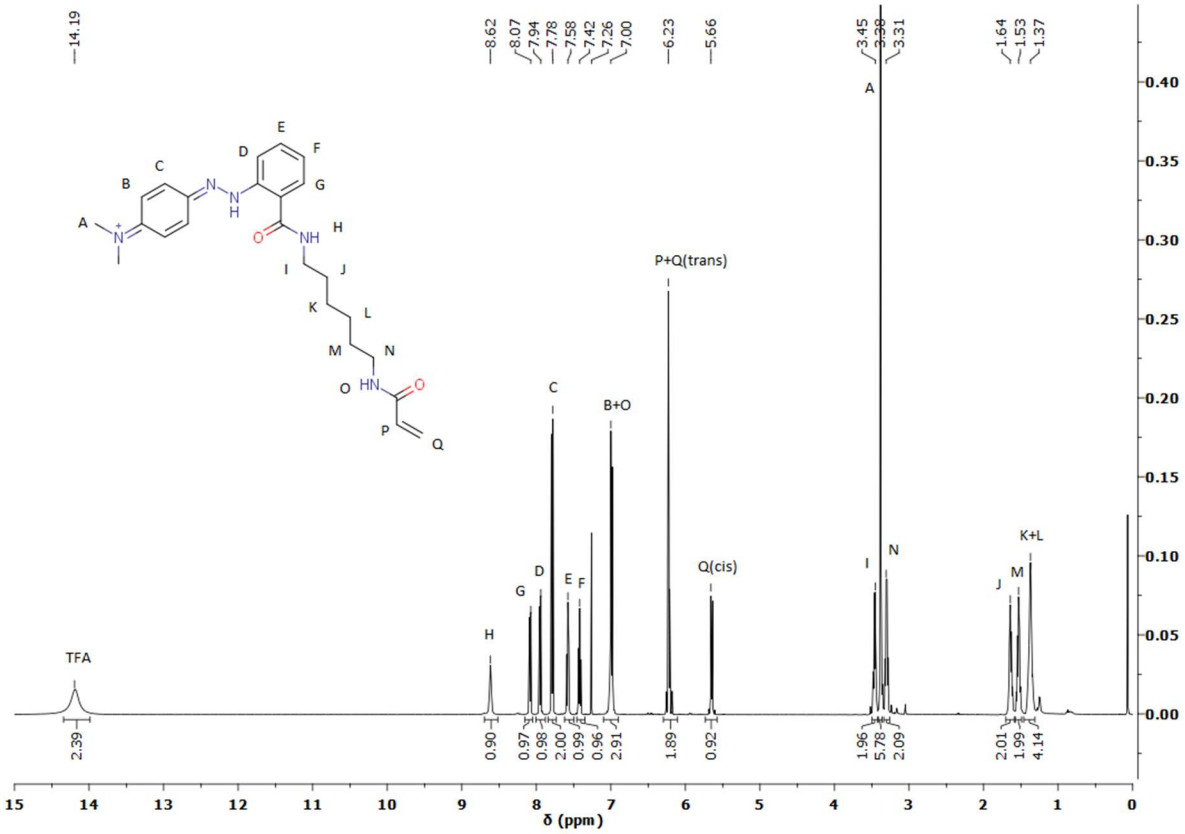

Figure S 22: ^{1}H NMR spectrum (500 MHz) in $CDCl_3$ of protonated N-[6-({2-[(1E)-2-[4-(dimethylamino)phenyl]diazen-1-yl]phenyl}formamido)hexyl]prop-2-enamide (1-o-methyl red amide of hexyl-6-acrylamide, MRHexAAm) with trifluoroacetate as counter-ion.

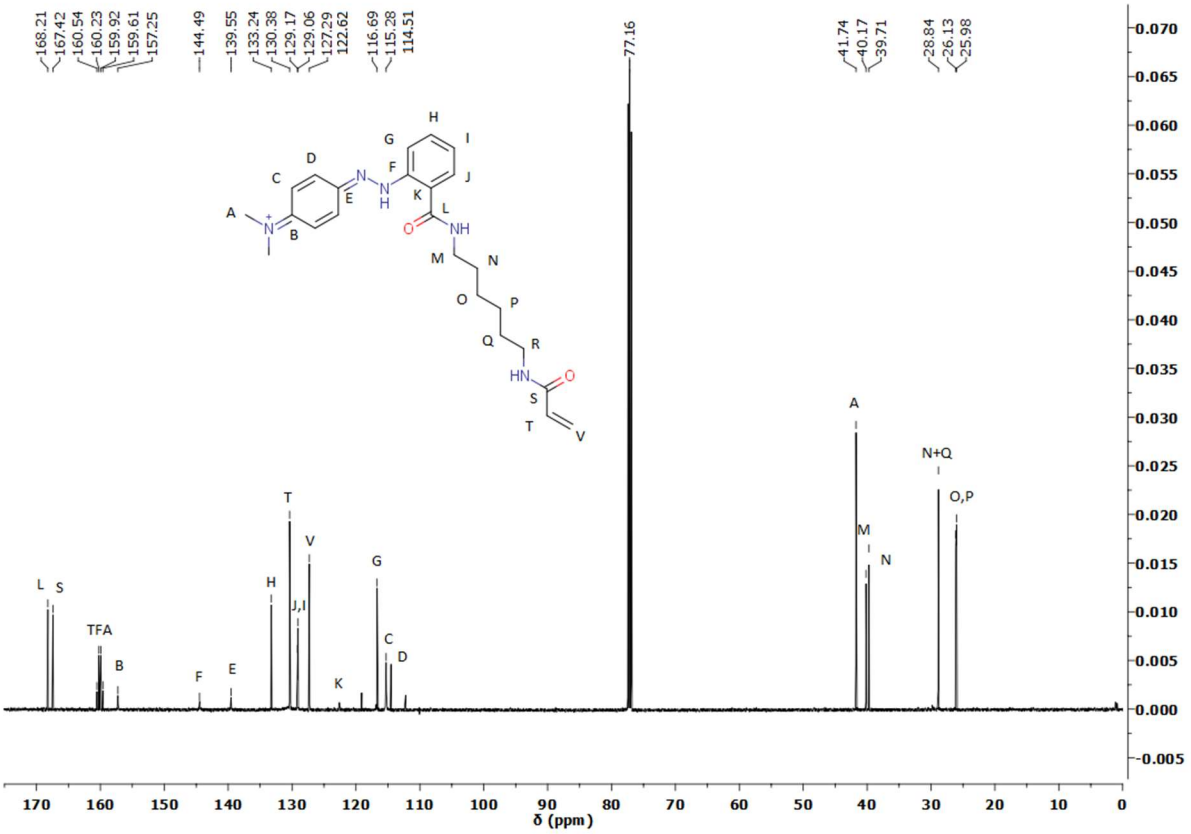

Figure S 23: ^{13}C NMR spectrum (126 MHz) in $CDCl_3$ of protonated N-[6-({2-[(1E)-2-[4-(dimethylamino)phenyl]diazen-1-yl]phenyl}formamido)hexyl]prop-2-enamide (1-o-methyl red amide of hexyl-6-acrylamide, MRHexAAm) with trifluoroacetate as counter-ion.

C8: δH(500 MHz; $CDCl_3$) 14.15 (s, associated TFA), 8.61 (s, 1H; Ar-CO-N*H*), 8.08 (dd, J = 7.8, 0.6 Hz, 1H; Ph-*H*), 7.93 (dd, J = 8.2, 0.6 Hz, 1H; Ph-*H*), 7.79 (d, J = 9.5 Hz, 1H; Ph-*H*), 7.62 – 7.50 (m, 1H; Ph-*H*), 7.51 – 7.35 (m, 1H; Ph-*H*), 6.97 (d, J = 9.5 Hz, 1H; Ph-*H*), 6.72 (s, 1H; DB-CO-N*H*), 6.25 (dd, J = 17.1, 1.8 Hz, 1H; CHC*H*H(trans)), 6.18 (dd, J = 17.1, 9.8 Hz, 1H; C*H*CHH), 5.66 (dd, J = 9.8, 1.7 Hz, 1H; CHCH*H*(cis)), 3.47 (dd, J = 12.9, 6.9 Hz, 2H; Ar-CONH-CH_2), 3.36 (s, 6H; $N(Me)_2$), 3.29 (dd, J = 13.1, 6.9 Hz, 2H; DB-CONH-CH_2), 1.63 (p, J = 7.1 Hz, 2H; Ar-CONH-CH_2-CH_2), 1.50 (p, J = 7.0 Hz, 2H; DB-CONH-CH_2-CH_2), 1.40 – 1.22 (m, 8H, alkyl).

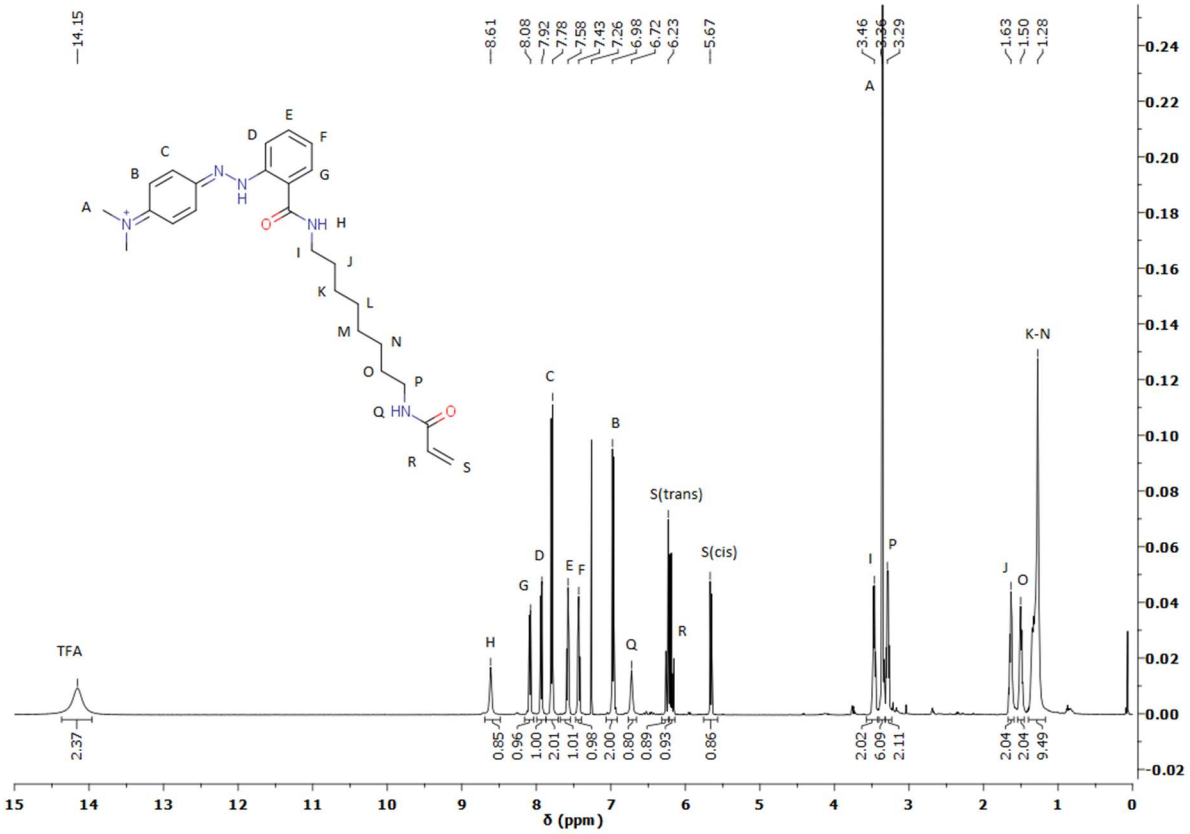

Figure S 24: ^{1}H NMR spectrum (500 MHz) in $CDCl_3$ of protonated N-[6-({2-[(1E)-2-[4-(dimethylamino)phenyl]diazen-1-yl]phenyl}formamido)octyl]prop-2-enamide (1-o-methyl red amide of octyl-6-acrylamide, MROctAAm) with trifluoroacetate as counter-ion.

2D-NMR Data of protonated N-[6-({2-[(1E)-2-[4-(dimethylamino)phenyl]diazen-1-yl]phenyl}formamido)hexyl]prop-2-enamide (1-o-methyl red amide of hexyl-6-acrylamide, MRHexAAm) with trifluoroacetate as counter-ion:

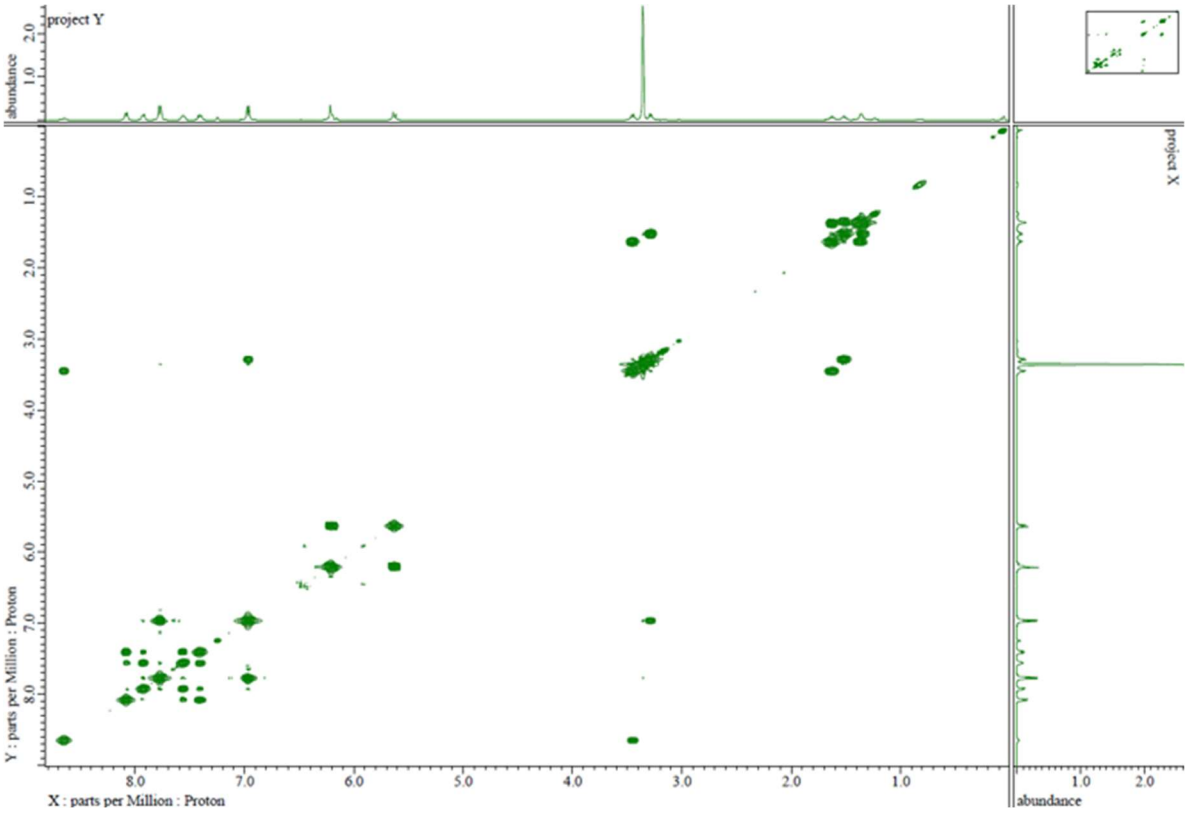

Figure S 25: ^{1}H-^{1}H-COSY spectrum (500 MHz) in $CDCl_3$ of protonated N-[6-({2-[(1E)-2-[4-(dimethylamino)phenyl]diazen-1-yl]phenyl}formamido)hexyl]prop-2-enamide (1-o-methyl red amide of hexyl-6-acrylamide, MRHexAAm) with trifluoroacetate as counter-ion.

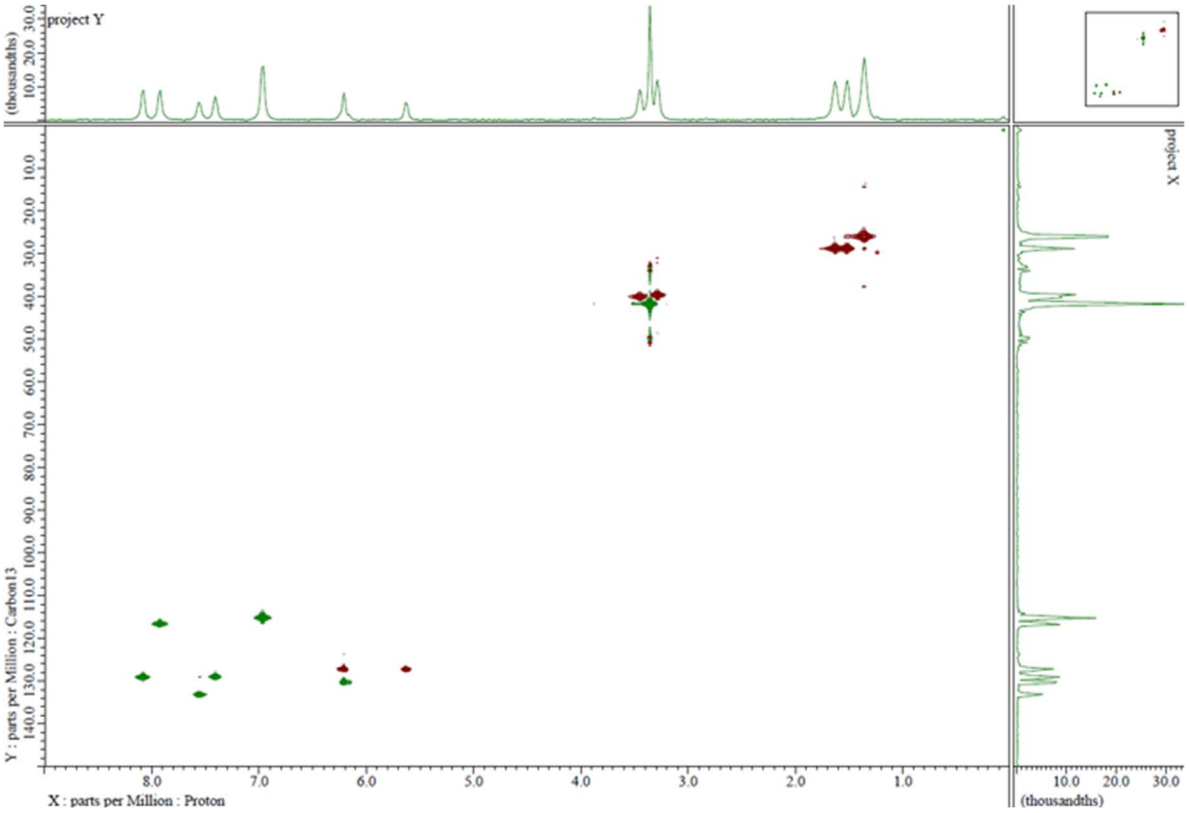

Figure S 26: ^{1}H-^{13}C-HSQC spectrum (500 MHz) in $CDCl_3$ of protonated N-[6-({2-[(1E)-2-[4-(dimethylamino)phenyl]diazen-1-yl]phenyl}formamido)hexyl]prop-2-enamide (1-o-methyl red amide of hexyl-6-acrylamide, MRHexAAm) with trifluoroacetate as counter-ion.

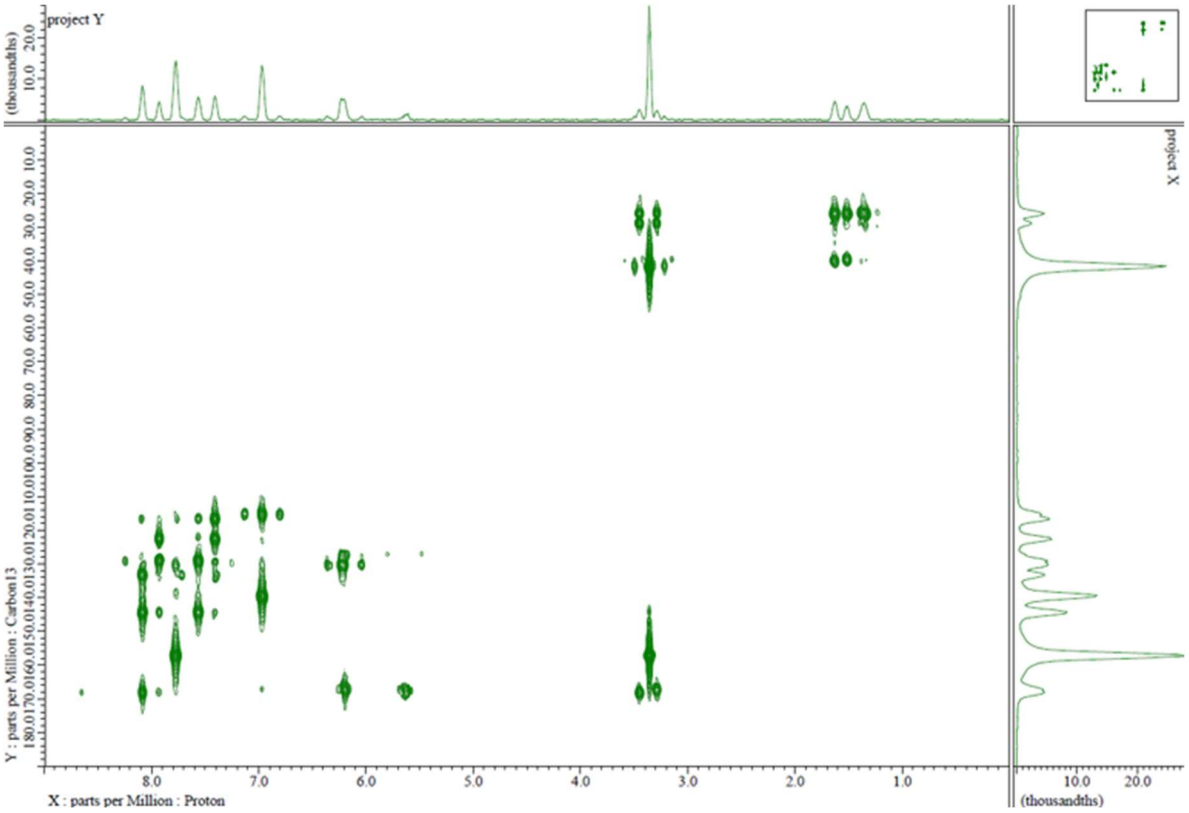

Figure S 27: ^{1}H-^{13}C-HMBC spectrum (500 MHz) in $CDCl_3$ of protonated N-[6-({2-[(1E)-2-[4-(dimethylamino)phenyl]diazen-1-yl]phenyl}formamido)hexyl]prop-2-enamide (1-o-methyl red amide of hexyl-6-acrylamide, MRHexAAm) with trifluoroacetate as counter-ion.

^{1}H-^{1}H-NOESY Spectra of Neutral and Protonated Amidoalkyl Acrylamides of o-Methyl Red:

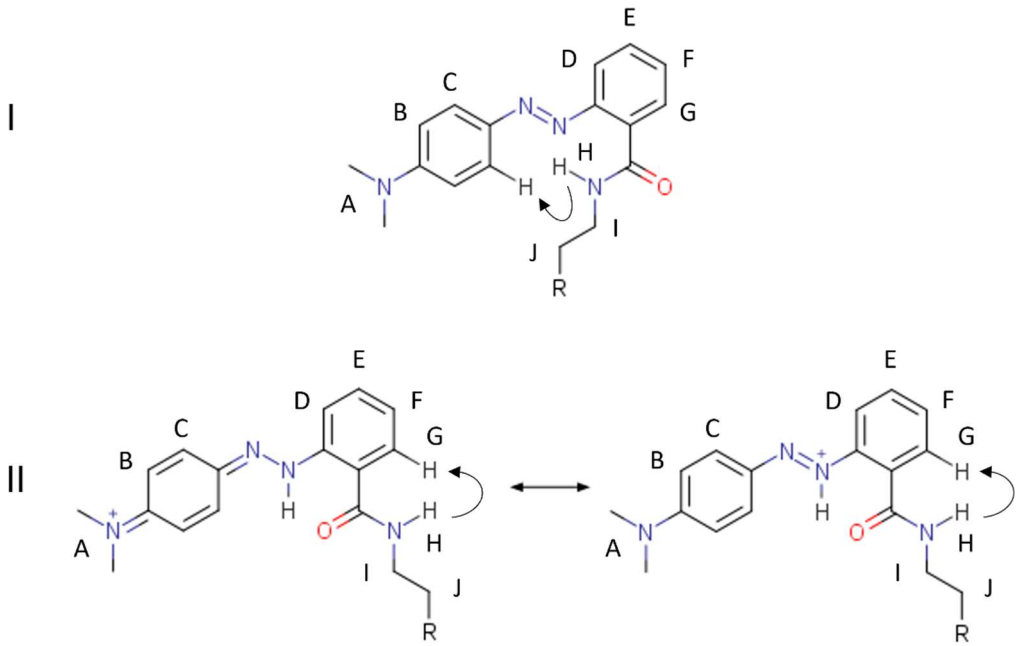

Scheme S 1: Neutral (I) and protonated (II, azonium ion) generic amidoalkyl acrylamide of o-methyl red with primary configuration according to the orientation of the secondary amide linkage as determined by NOESY.

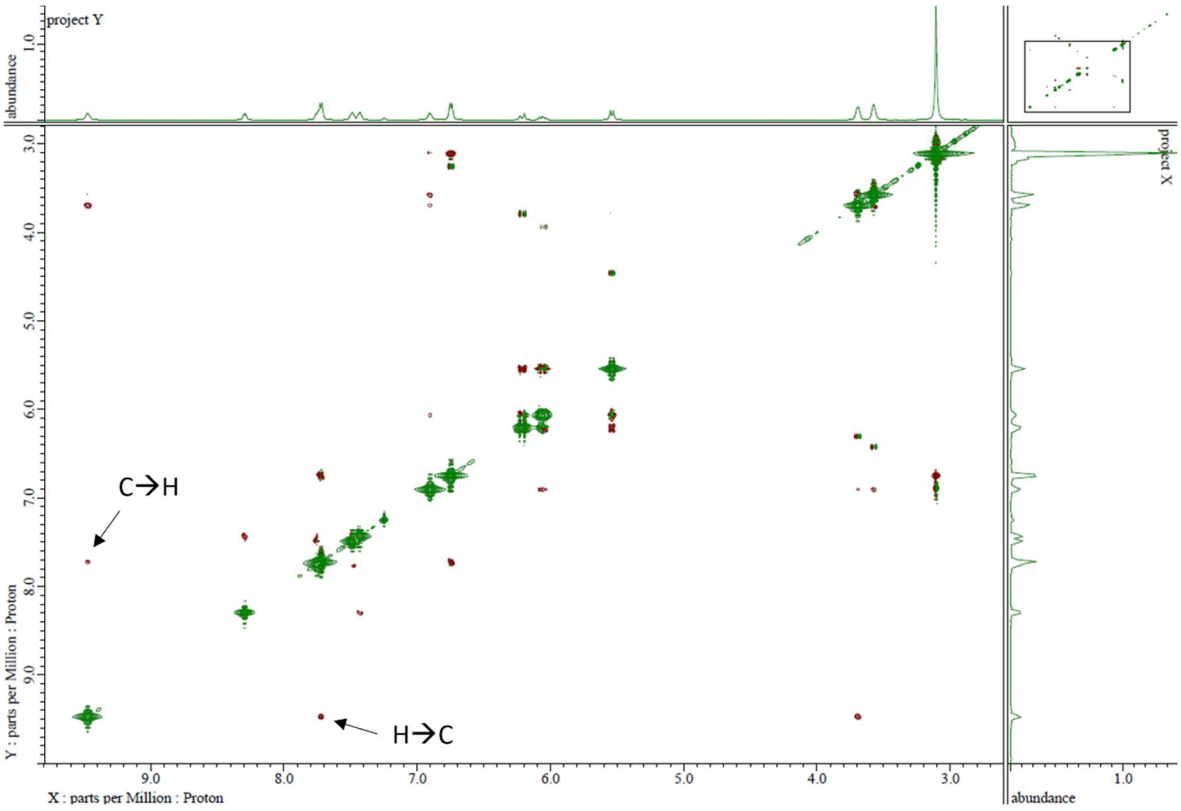

Figure S 28: ^{1}H-^{1}H-NOESY spectrum (500 MHz) in $CDCl_3$ of N-[6-({2-[(1E)-2-[4-(dimethylamino)phenyl]diazen-1-yl]phenyl}formamido)ethyl]prop-2-enamide (1-o-methyl red amide of ethyl-6-acrylamide, MREtAAm).

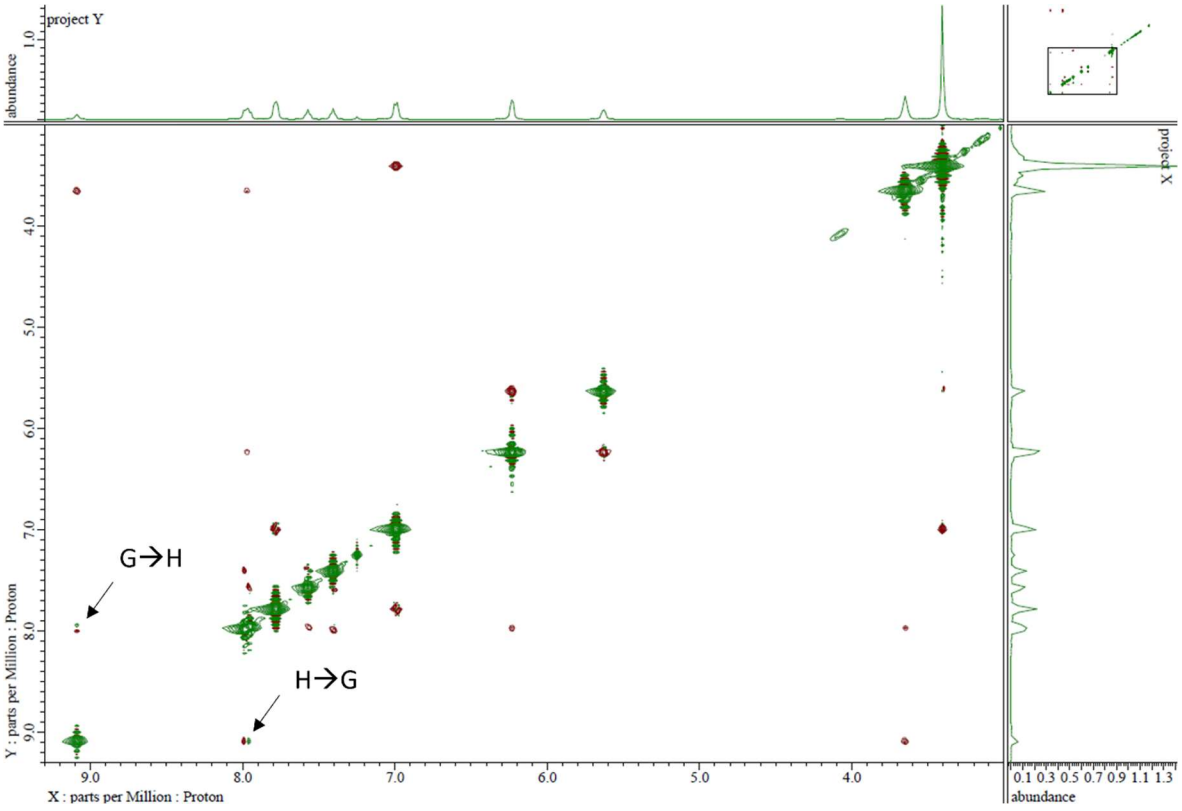

Figure S 29: ^{1}H-^{1}H-NOESY spectrum (500 MHz) in $CDCl_3$ of protonated N-[6-({2-[(1E)-2-[4-(dimethylamino)phenyl]diazen-1-yl]phenyl}formamido)ethyl]prop-2-enamide (1-o-methyl red amide of ethyl-6-acrylamide, MREtAAm) with trifluoroacetate as counter-ion.

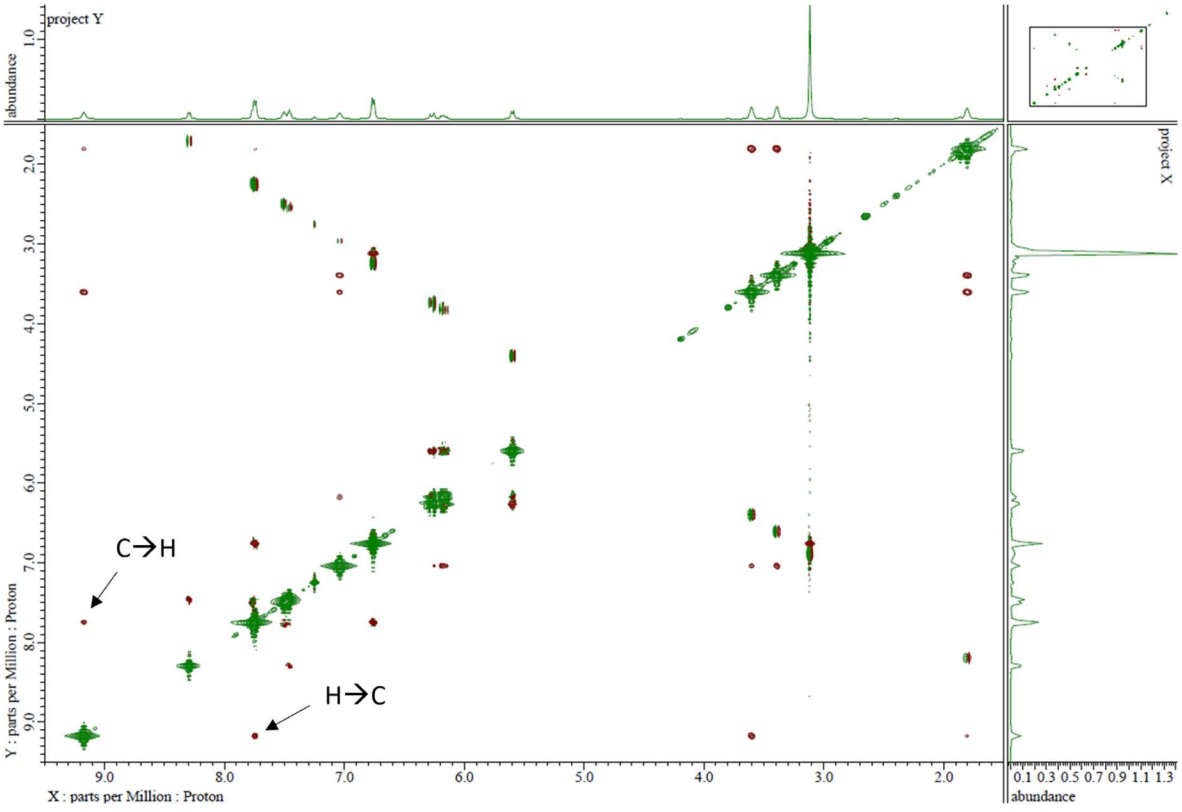

Figure S 30: ^{1}H-^{1}H-NOESY spectrum (500 MHz) in $CDCl_3$ of N-[6-({2-[(1E)-2-[4-(dimethylamino)phenyl]diazen-1-yl]phenyl}formamido)propyl]prop-2-enamide (1-o-methyl red amide of propyl-6-acrylamide, MRPrAAm).

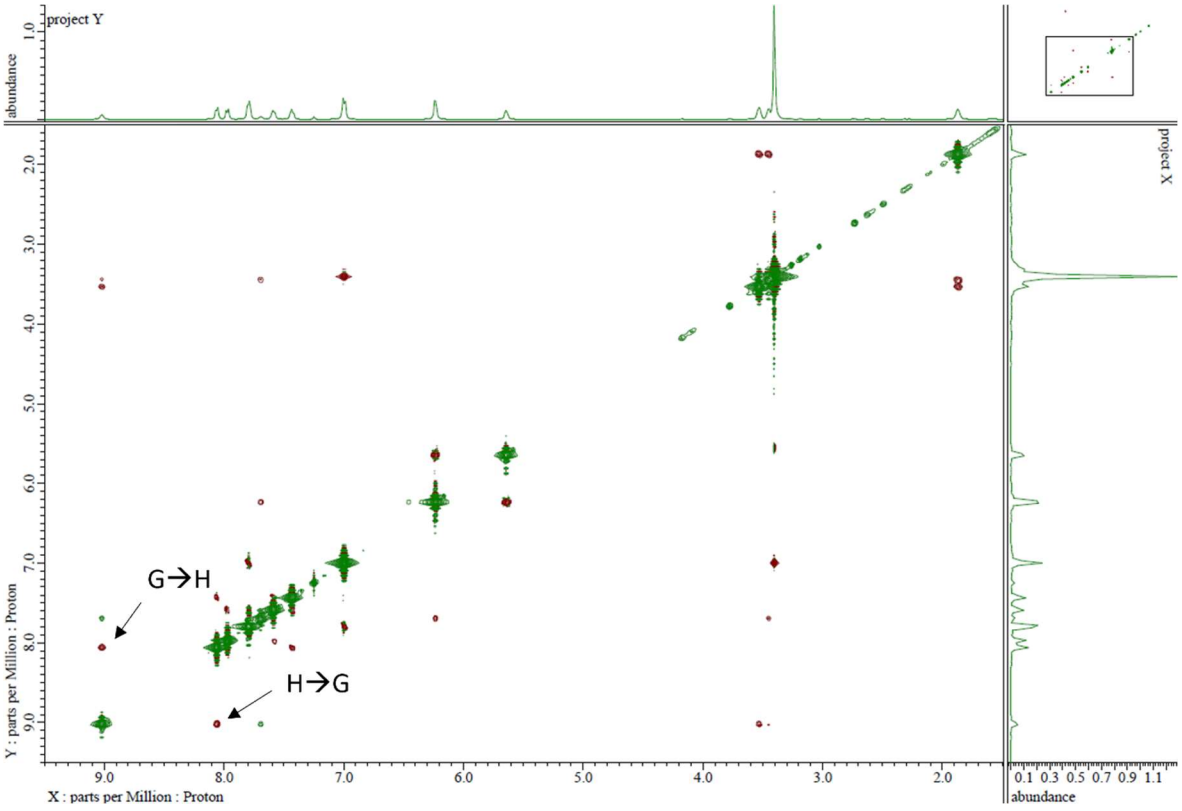

Figure S 31: ^{1}H-^{1}H-NOESY spectrum (500 MHz) in $CDCl_3$ of protonated N-[6-({2-[(1E)-2-[4-(dimethylamino)phenyl]diazen-1-yl]phenyl}formamido)propyl]prop-2-enamide (1-o-methyl red amide of propyl-6-acrylamide, MRPrAAm) with trifluoroacetate as counter-ion.

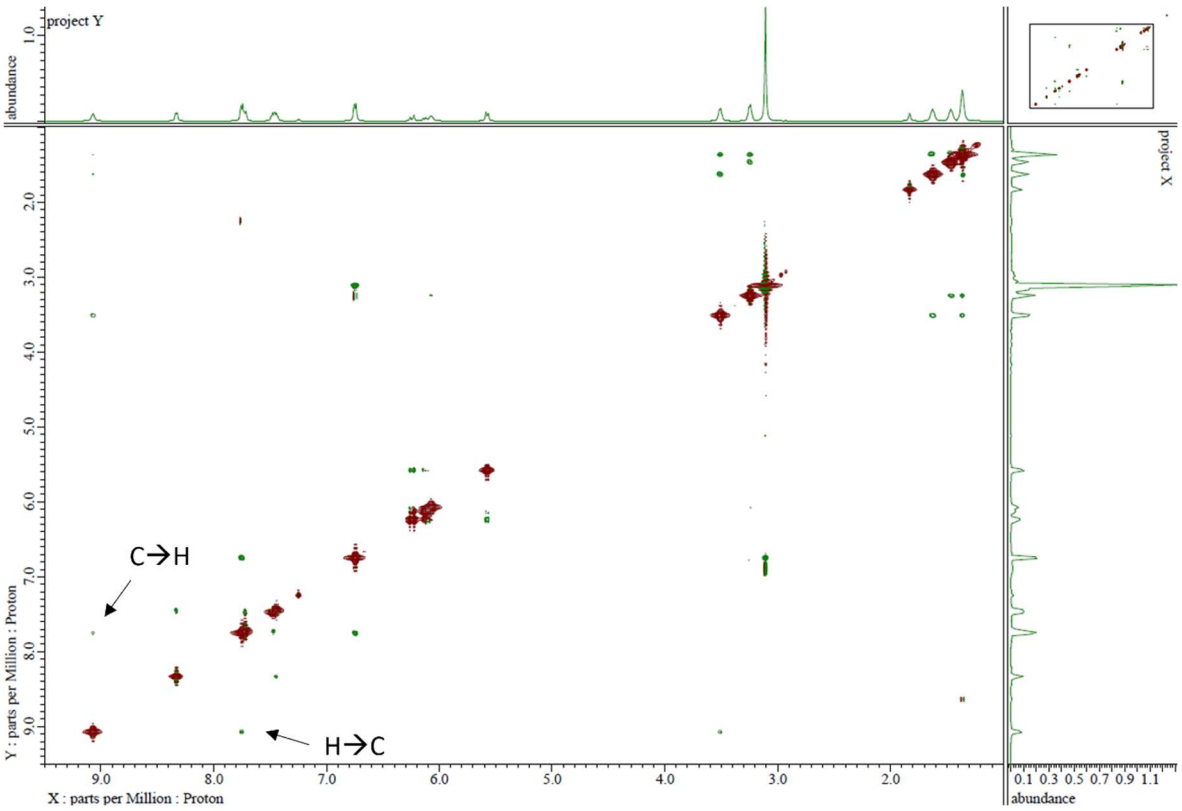

Figure S 32: ^{1}H-^{1}H-NOESY spectrum (500 MHz) in $CDCl_3$ of N-[6-({2-[(1E)-2-[4-(dimethylamino)phenyl]diazen-1-yl]phenyl}formamido)hexyl]prop-2-enamide (1-o-methyl red amide of hexyl-6-acrylamide, MRHexAAm).

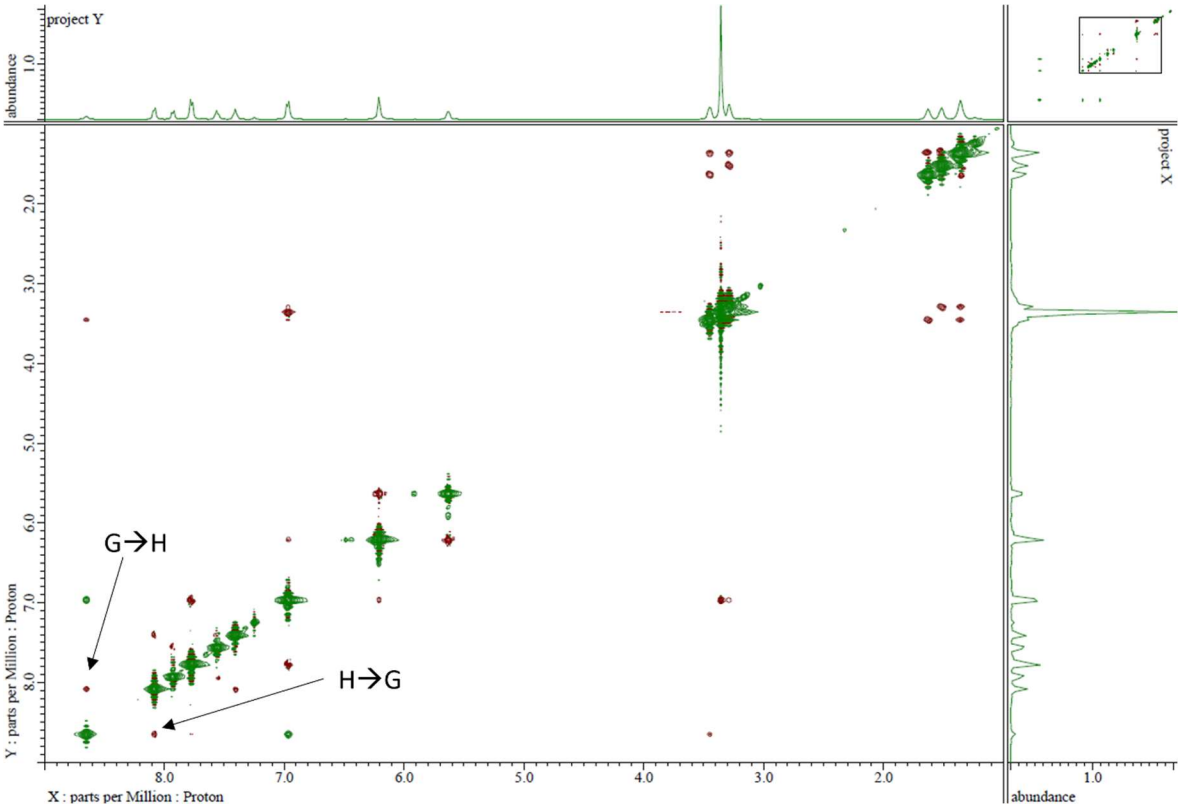

Figure S 33: ^{1}H-^{1}H-NOESY spectrum (500 MHz) in $CDCl_3$ of protonated N-[6-({2-[(1E)-2-[4-(dimethylamino)phenyl]diazen-1-yl]phenyl}formamido)hexyl]prop-2-enamide (1-o-methyl red amide of hexyl-6-acrylamide, MRHexAAm) with trifluoroacetate as counter-ion.

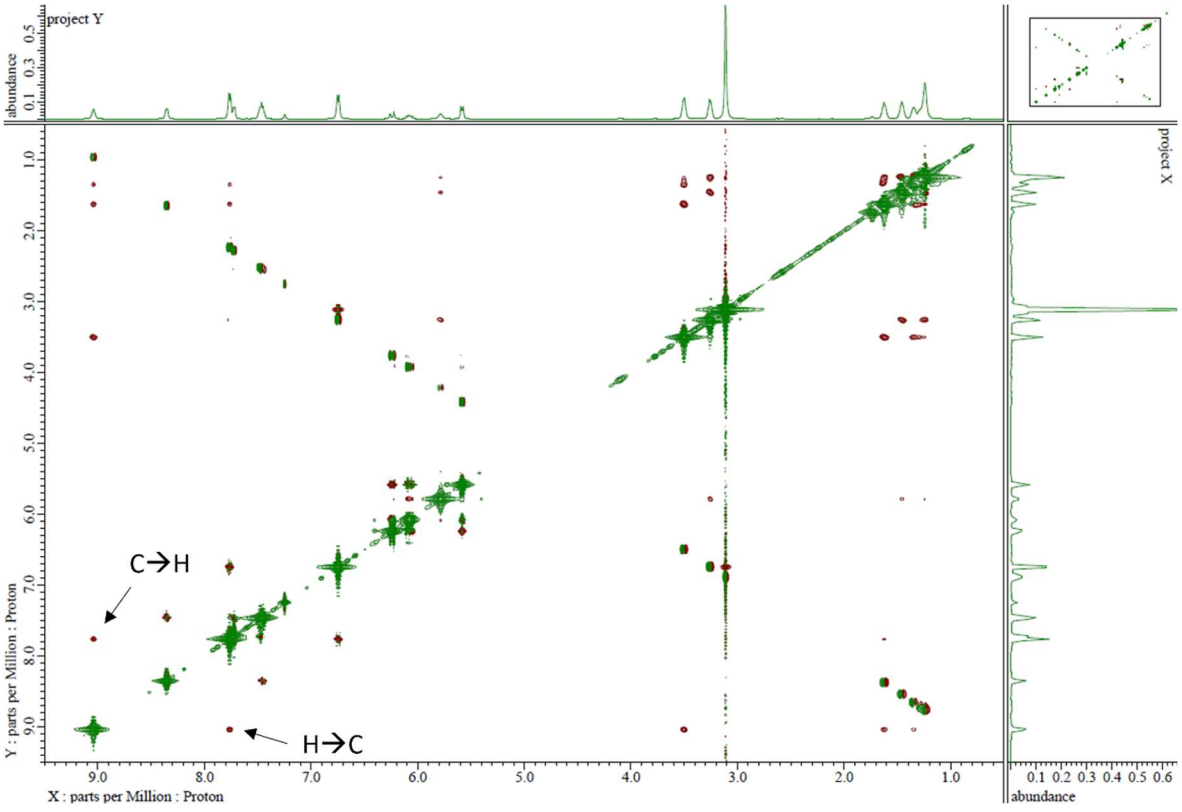

Figure S 34: ^{1}H-^{1}H-NOESY spectrum (500 MHz) in $CDCl_3$ of N-[6-({2-[(1E)-2-[4-(dimethylamino)phenyl]diazen-1-yl]phenyl}formamido)octyl]prop-2-enamide (1-o-methyl red amide of octyl-6-acrylamide, MROctAAm).

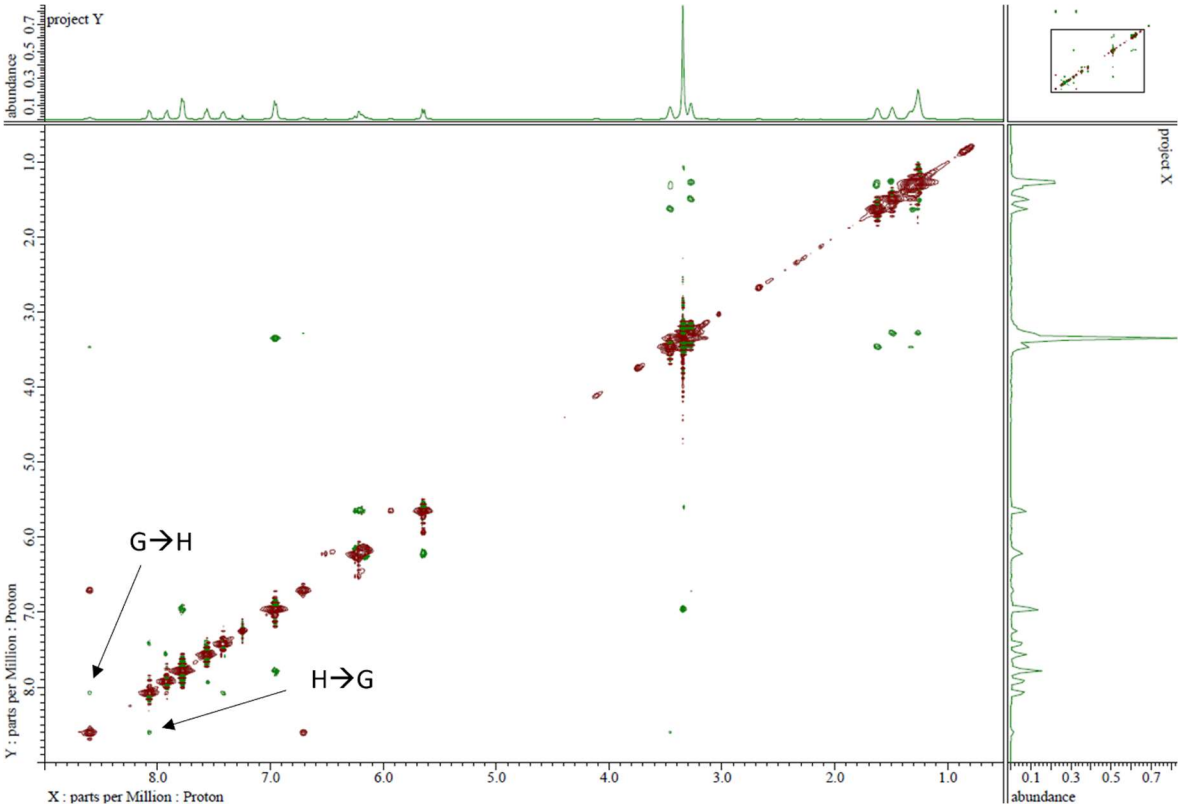

Figure S 35: ^{1}H-^{1}H-NOESY spectrum (500 MHz) in $CDCl_3$ of protonated N-[6-({2-[(1E)-2-[4-(dimethylamino)phenyl]diazen-1-yl]phenyl}formamido)octyl]prop-2-enamide (1-o-methyl red amide of octyl-6-acrylamide, MROctAAm) with trifluoroacetate as counter-ion.

Miscelleaneous and Optical Data:

Protonation Equilibrium of Secondary Amidoalkyl Acrylamides of o-Methyl Red and Tautomerism of the Protonated Species:

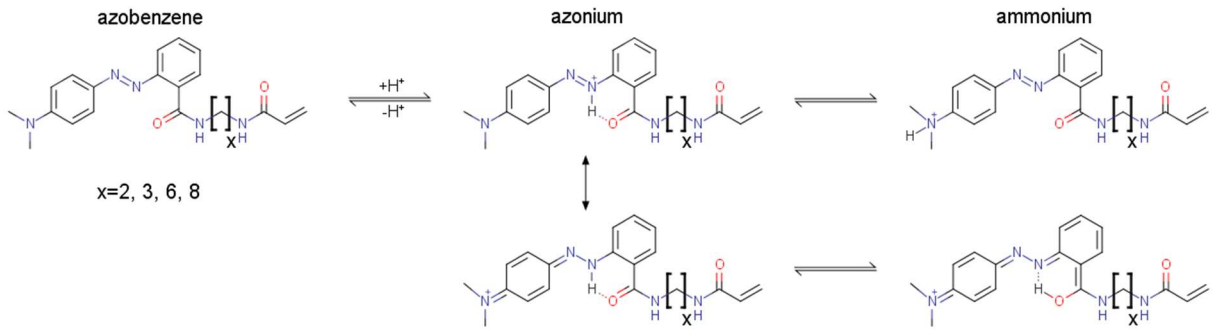

Scheme S 2: Structure and protonation equilbrium of amidoalkyl acrylamides of methyl red with different spacer lengths.

Scheme S2 shows the different possible protonation states of amidoalkyl acrylamides of methyl red, including the neutral azobenzene, the azonium ion with its resonance

structures, and the ammonium ion. The neutral azobenzene absorbs in ethanol around 440 nm, the azonium ion around 540 nm, and the ammonium ion at around 320 nm.

Temperature-dependent UV-vis Spectra of amidoalkyl acrylamides with different spacer lengths under various conditions:

Table S 3: Approximate extinction coefficients [L mol^{-1} cm^{-1}] at ~20 °C of the neutral dye species and the azonium ion at maximum in ethanol and ethanolic sulfuric acid (1 v/v%), respectively.

Derivative	ε (neutral dye)	ε (azonium ion)	ε (azonium ion)/ ε (neutral dye)
MREtAAm	24900	48300	1.95
MRPrAAm	28100	55200	1.95
MRHexAAm	30600	60400	2.00
MROctAAm	27500	51900	1.90
o-MREAm	29700	54900	1.85

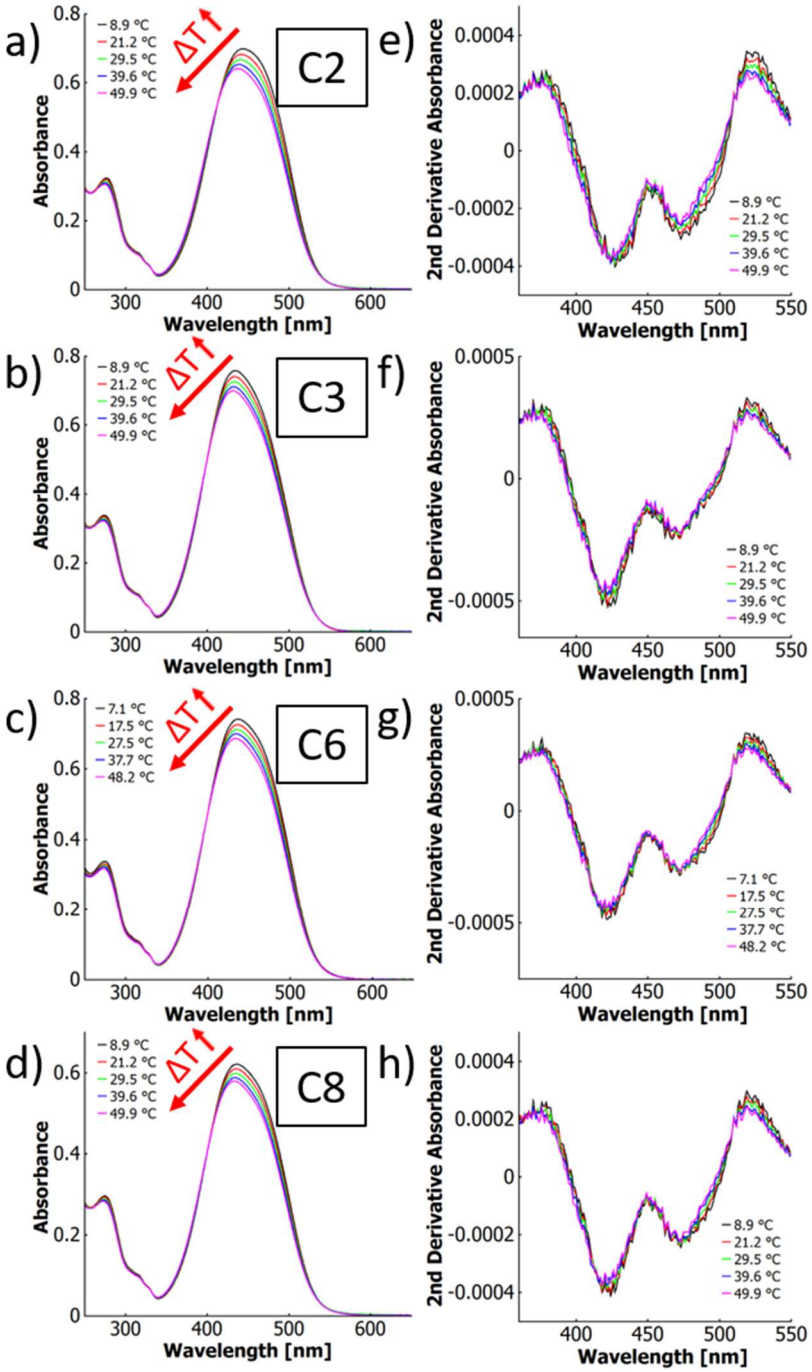

Figure S 36: Temperature-dependent UV-vis spectra (left) and second derivative spectra (right) of different alkylacrylamides amides of methyl red in ethanol (0.01 g/L). a), e) MREtAAm; b), f) MRPrAAm; c), g) MRHexAAm and d), h) MROctAAm.

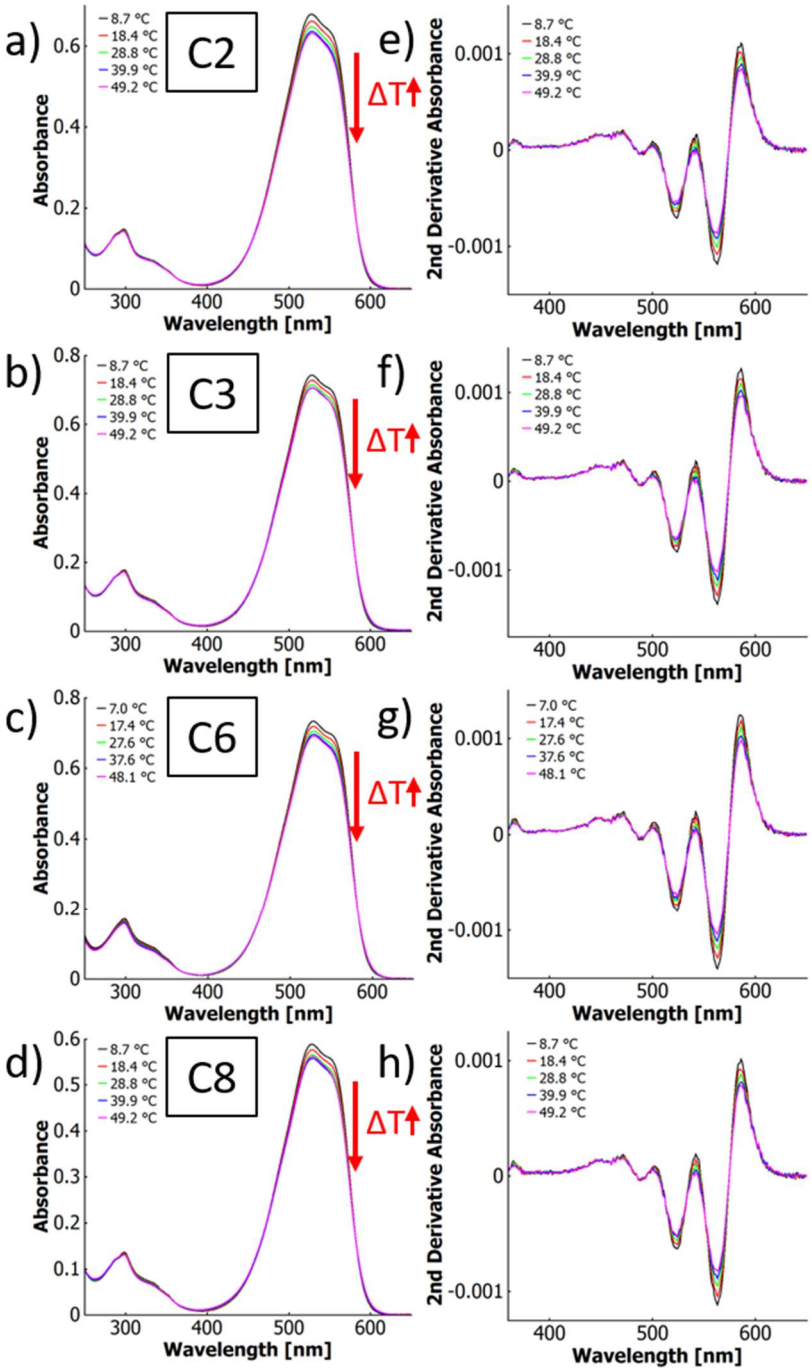

Figure S 37: Temperature-dependent UV-vis spectra (left) and second derivative spectra (right) of different alkylacrylamides amides of methyl red in ethanolic sulfuric acid (1 v/v%, 0.005 g/L). a), e) MREtAAm; b), f) MRPrAAm; c), g) MRHexAAm and d), h) MROctAAm.

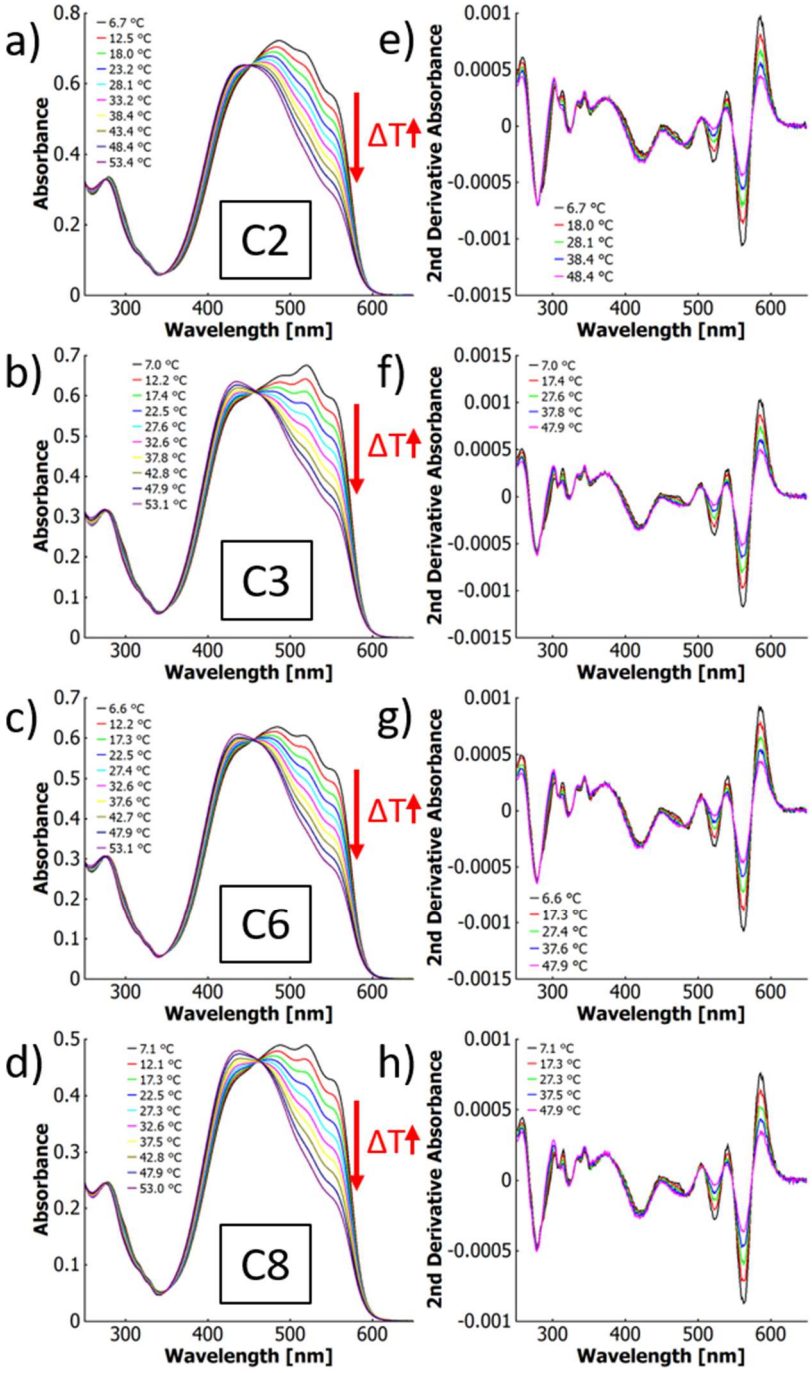

Figure S 38: Temperature-dependent UV-vis spectra (left) and second derivative spectra (right) of different alkylacrylamides amides of methyl red in ethanolic trifluoroacetic acid (1 v/v%, 0.01 g/L). a), e) MREtAAm; b), f) MRPrAAm; c), g) MRHexAAm and d), h) MROctAAm.

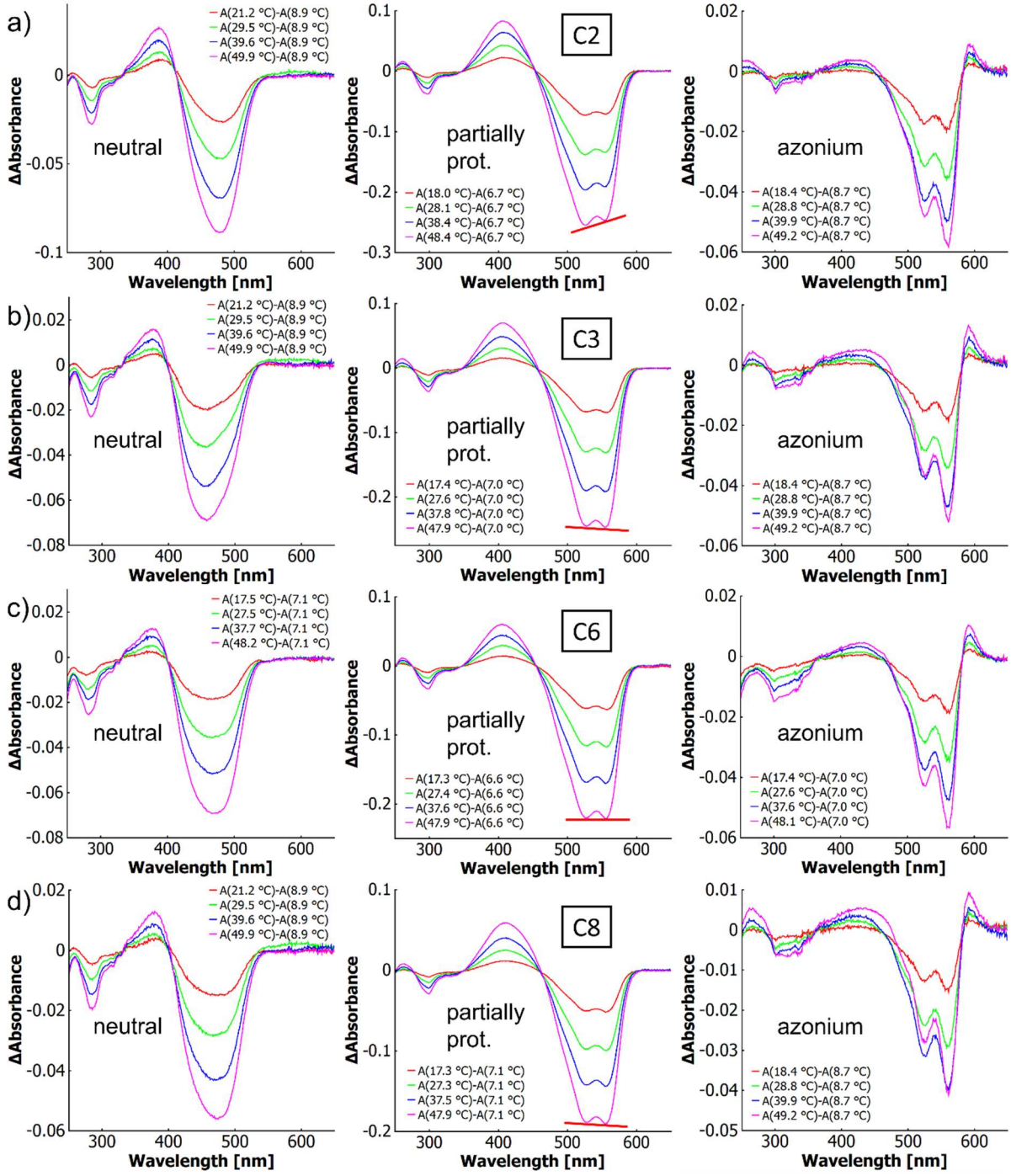

Figure S 39: Difference spectra subtracting the lowest temperature spectrum from higher temperature spectra in (left) ethanol (neutral dye), (middle) ethanolic trifluoroacetic acid (1 v/v%, partially protonated) and (right) ethanolic sulfuric acid (1 v/v%, completely protonated) of different alkylacrylamides amides of methyl red a) MREtAAm; b) MRPrAAm; c) MRHexAAm; and d) MROctAAm. In the partially protonated case (middle), the apparent ratio of the changes in the vibronic sub-bands is marked with a red line.

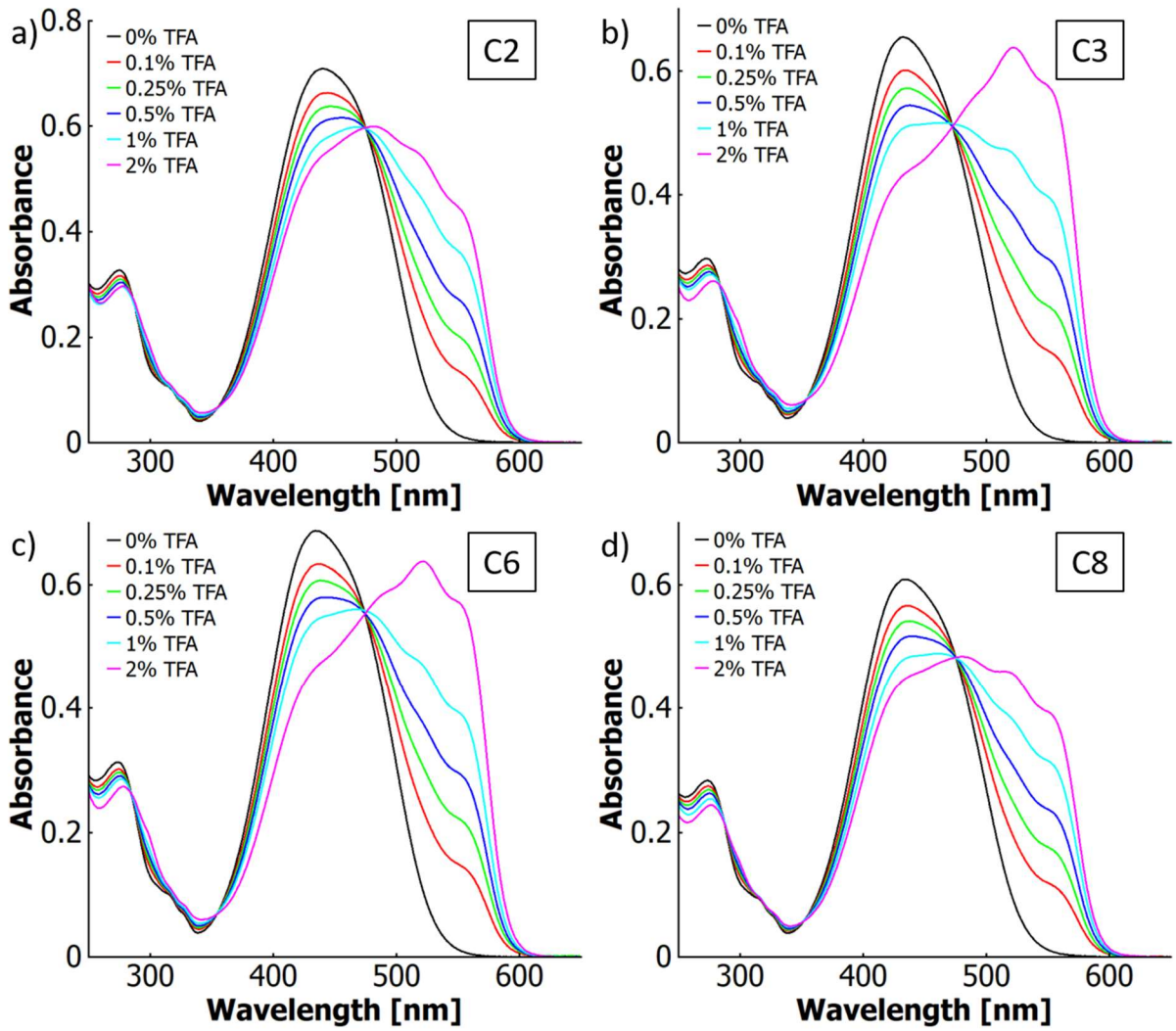

Figure S 40: UV-vis spectra of titrations in ethanol with trifluoroacetic acid (v/v% given in the spectra) of different alkylacrylamides amides of methyl red a) MREtAAm; b) MRPrAAm; c) MRHexAAm; and d) MROctAAm (all 0.01 g/L) at 25 °C.

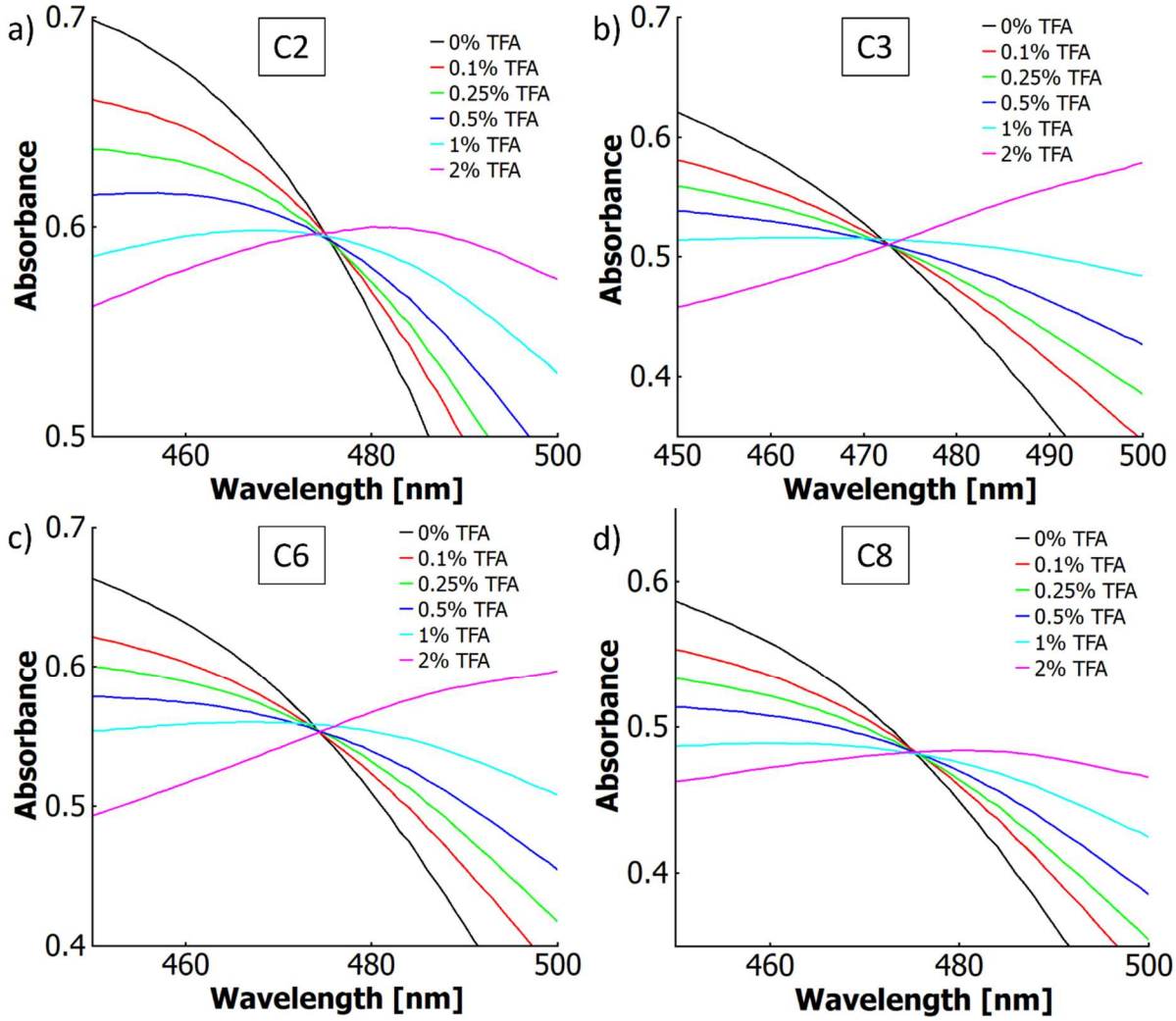

Figure S 41: Zoom-in on the isosbestic points of UV-vis spectra of titrations in ethanol with trifluoroacetic acid (v/v% given in the spectra) of different alkylacrylamides amides of methyl red a) MREtAAm; b) MRPrAAm; c) MRHexAAm; and d) MROctAAm (all 0.01 g/L) at 25 °C.

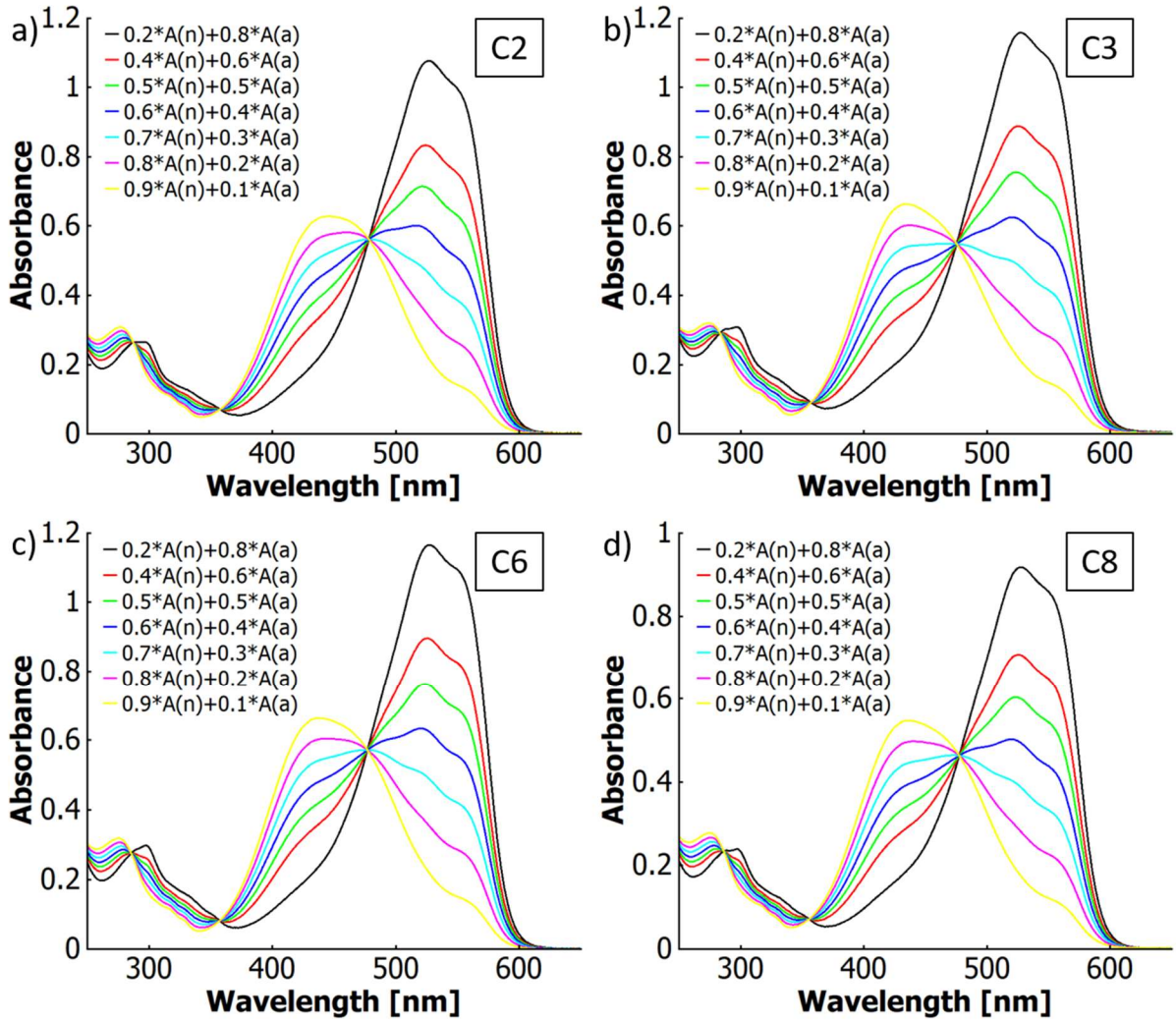

Figure S 42: Calculated UV-vis spectra of different mixtures of the neutral dye and the azonium ion in ethanol for a) MREtAAm; b) MRPrAAm; c) MRHexAAm; and d) MROctAAm (all 0.01 g/L). The spectra were generated by linear combination of the spectra of the neutral azobenzene in ethanol and the completely protonated dye in ethanolic sulfuric acid (2 v/v%), assuming $\varepsilon_{azobenzene}=0.5*\varepsilon_{azonium}$.

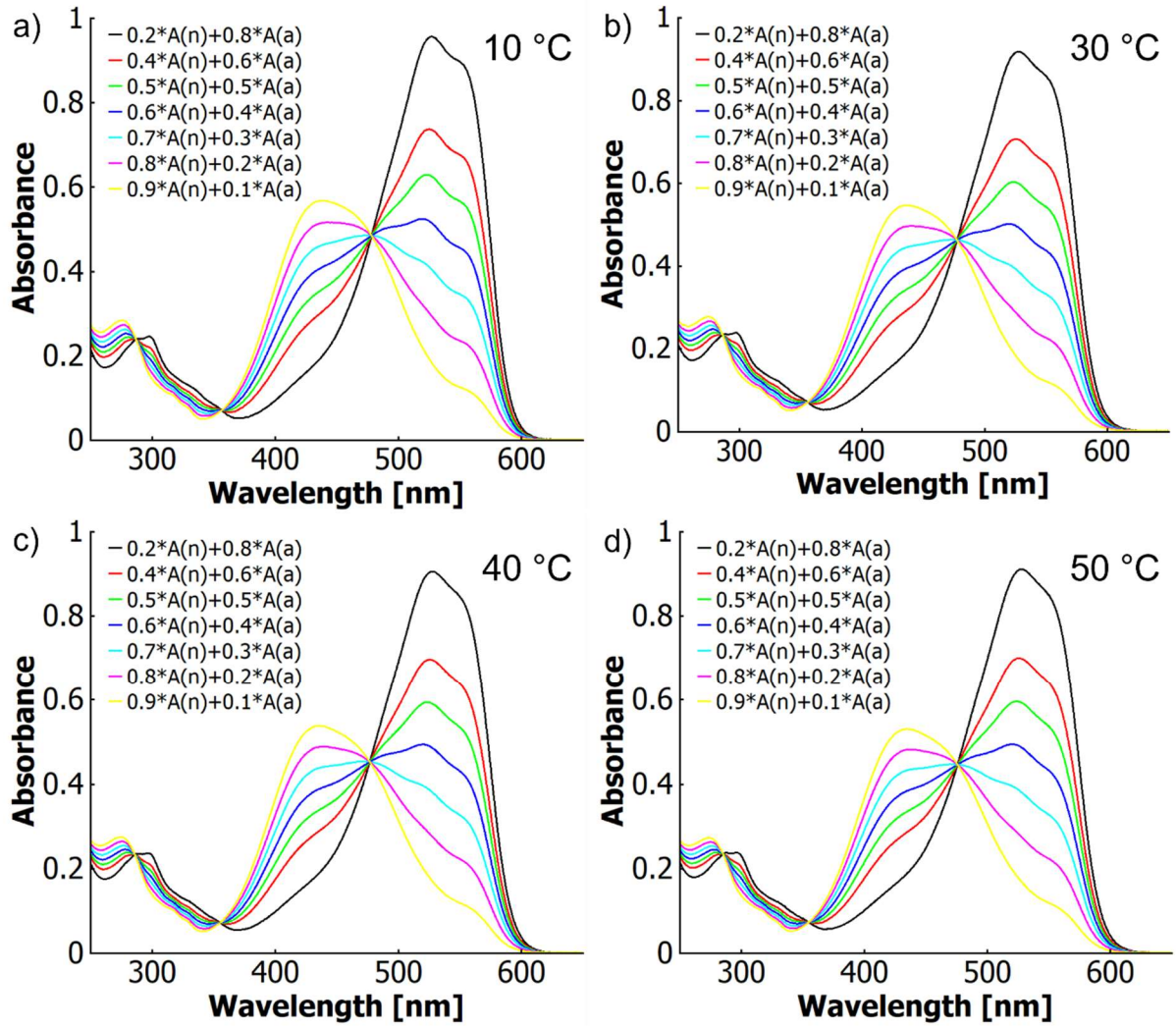

Figure S 43: Calculated UV-vis spectra of different mixtures of the neutral dye and the azonium ion in ethanol for MROctAAm (all 0.01 g/L) at different temperatures. The spectra were generated by linear combination of the spectra of the neutral azobenzene in ethanol and the completely protonated dye in ethanolic sulfuric acid (2 v/v%), assuming $\varepsilon_{azobenzene}=0.5*\varepsilon_{azonium}$.

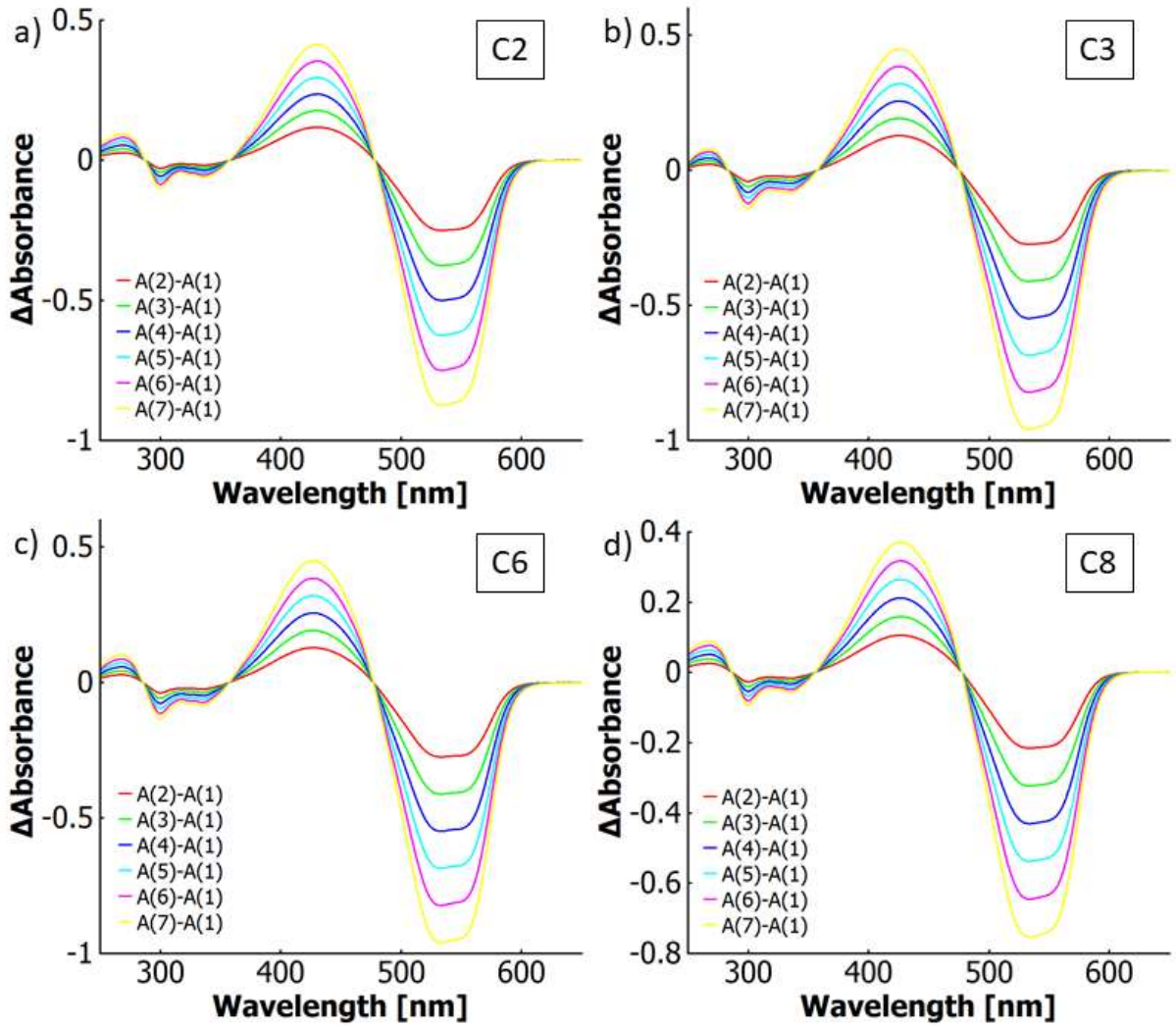

Figure S 44: Difference spectra of calculated UV-vis spectra of different mixtures of the neutral dye and the azonium ion in ethanol for a) MREtAAm; b) MRPrAAm; c) MRHexAAm; and d) MROctAAm (all 0.01 g/L). The UV-vis spectra were generated by linear combination of the spectra of the neutral azobenzene in ethanol and the completely protonated dye in ethanolic sulfuric acid (2 v/v%), assuming $\varepsilon_{azobenzene}=0.5*\varepsilon_{azonium}$. The difference spectra were generated by subtracting the spectrum with the highest degreee of protonation from those with a lower degree of protonation.

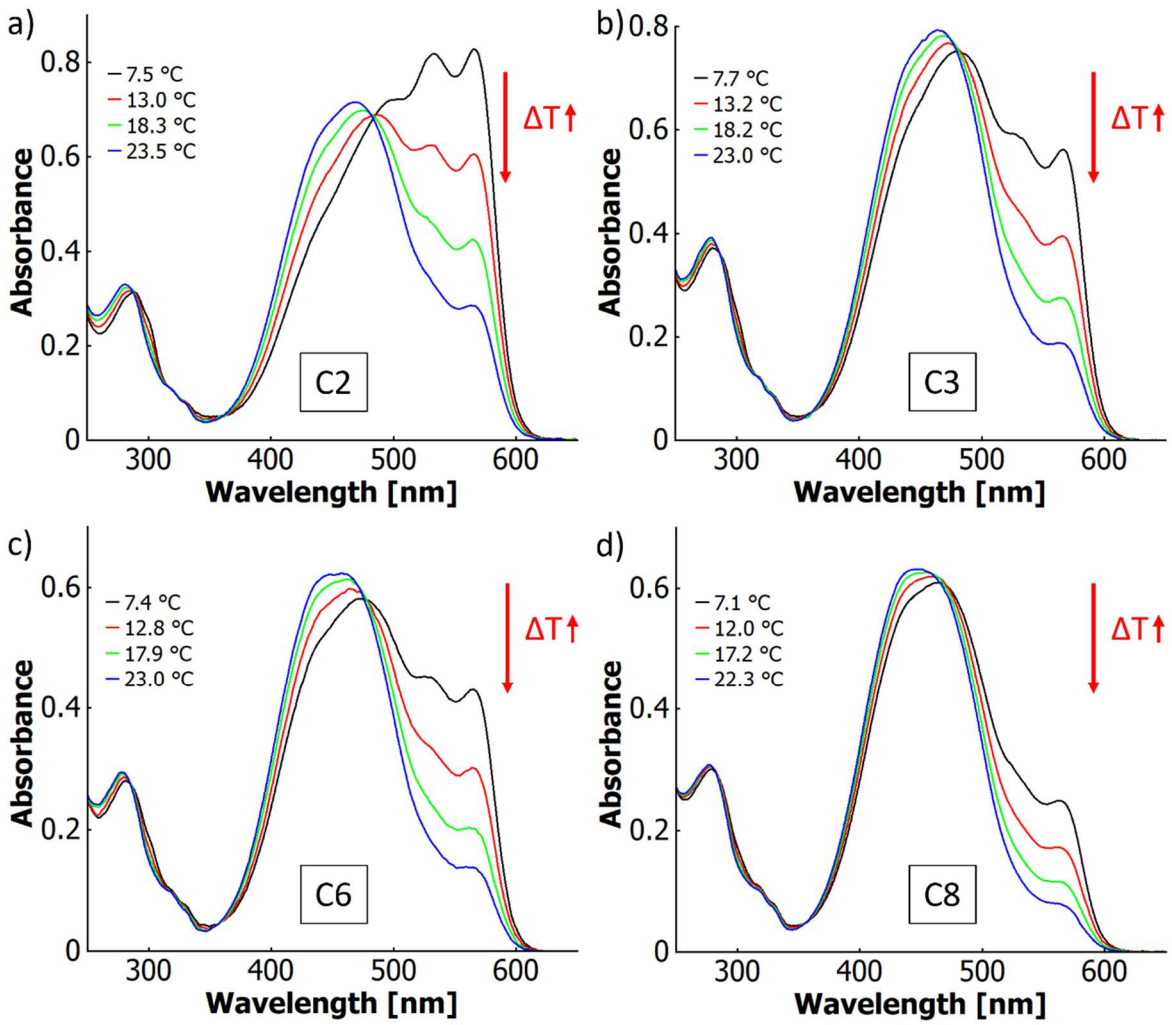

Figure S 45: Temperature-dependent UV-vis spectra of different amidoalkyl acrylamide of methyl red in chloroform acidified with trifluoroacetic acid (0.01 gL^{-1}, 0.0025 v/v% TFA). a) MREtAAm; b) MRPrAAm; c) MRHexAAm and d) MROctAAm.

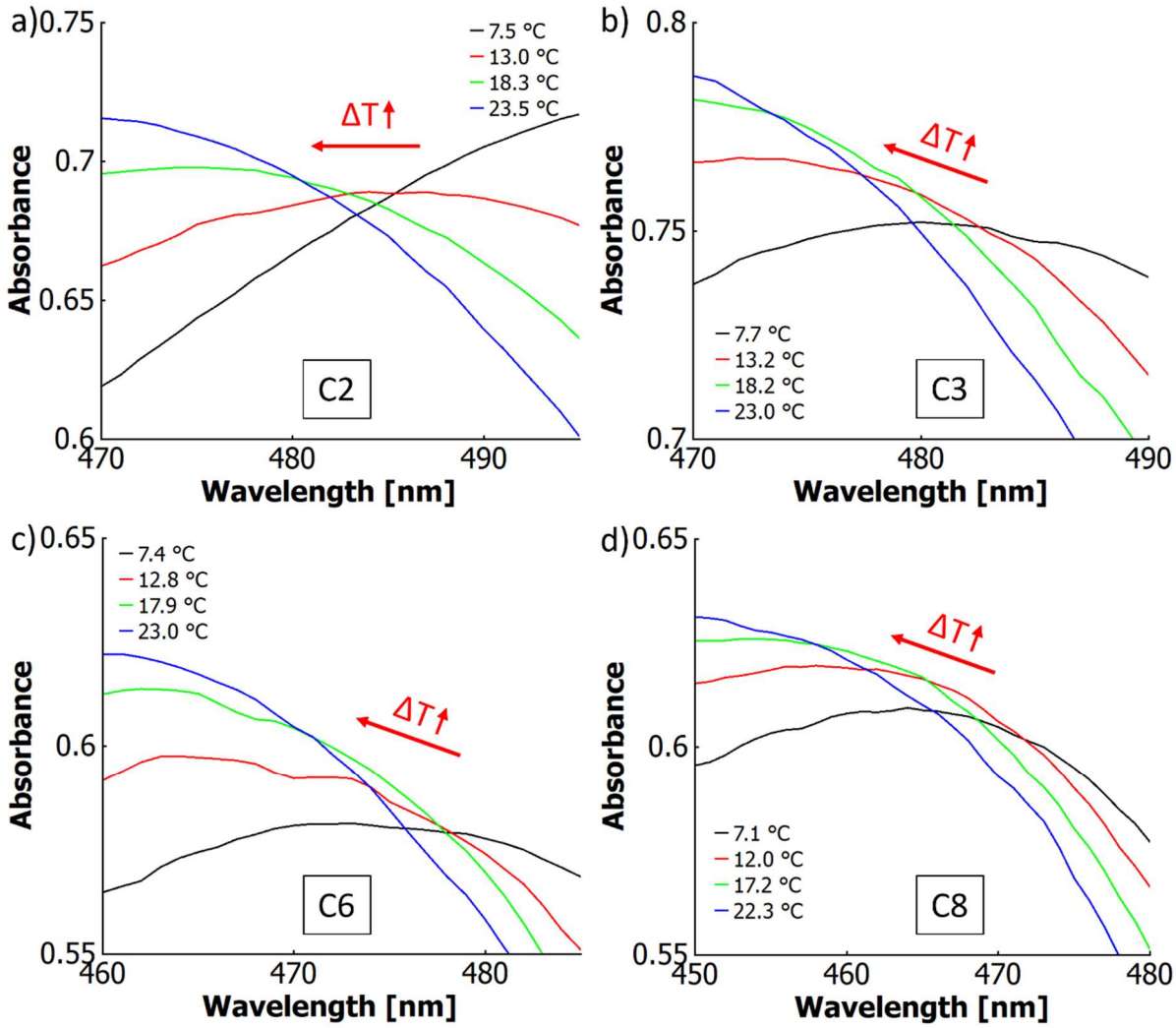

Figure S 46: Zoom-in of temperature-dependent UV-vis spectra of different amidoalkyl acrylamide of methyl red in chloroform acidified with trifluoroacetic acid (0.01 gL^{-1}, 0.0025 v/v% TFA). a) MREtAAm; b) MRPrAAm; c) MRHexAAm and d) MROctAAm. Shifts upon heating in the intersections between adjacent temperature steps are indicated by red arrows.

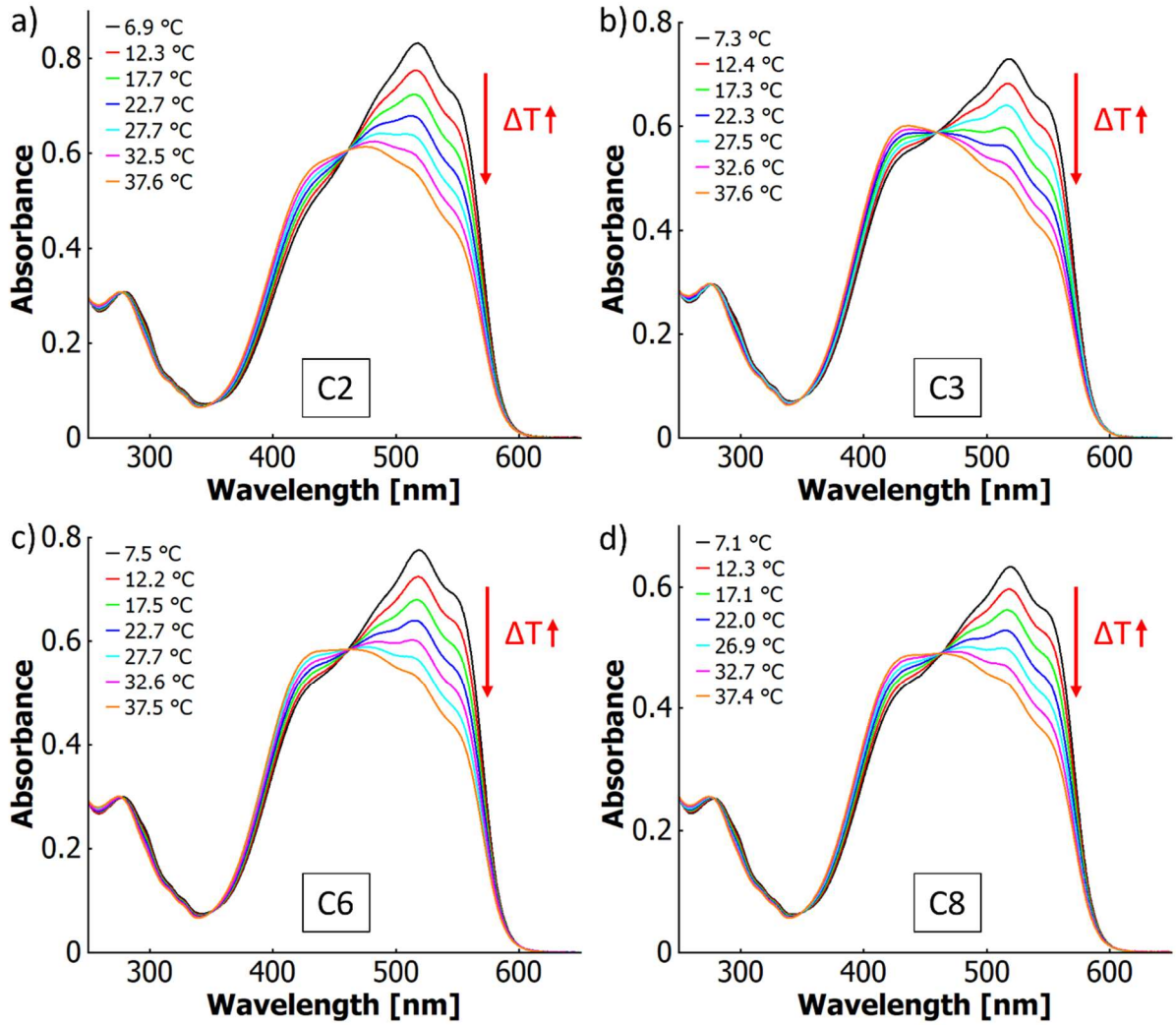

Figure S 47: Temperature-dependent UV-vis spectra of different amidoalkyl acrylamide of methyl red in methanolic trifluoroacetic acid (0.01 gL^{-1}, 0.025 v/v% TFA). a) MREtAAm; b) MRPrAAm; c) MRHexAAm and d) MROctAAm.

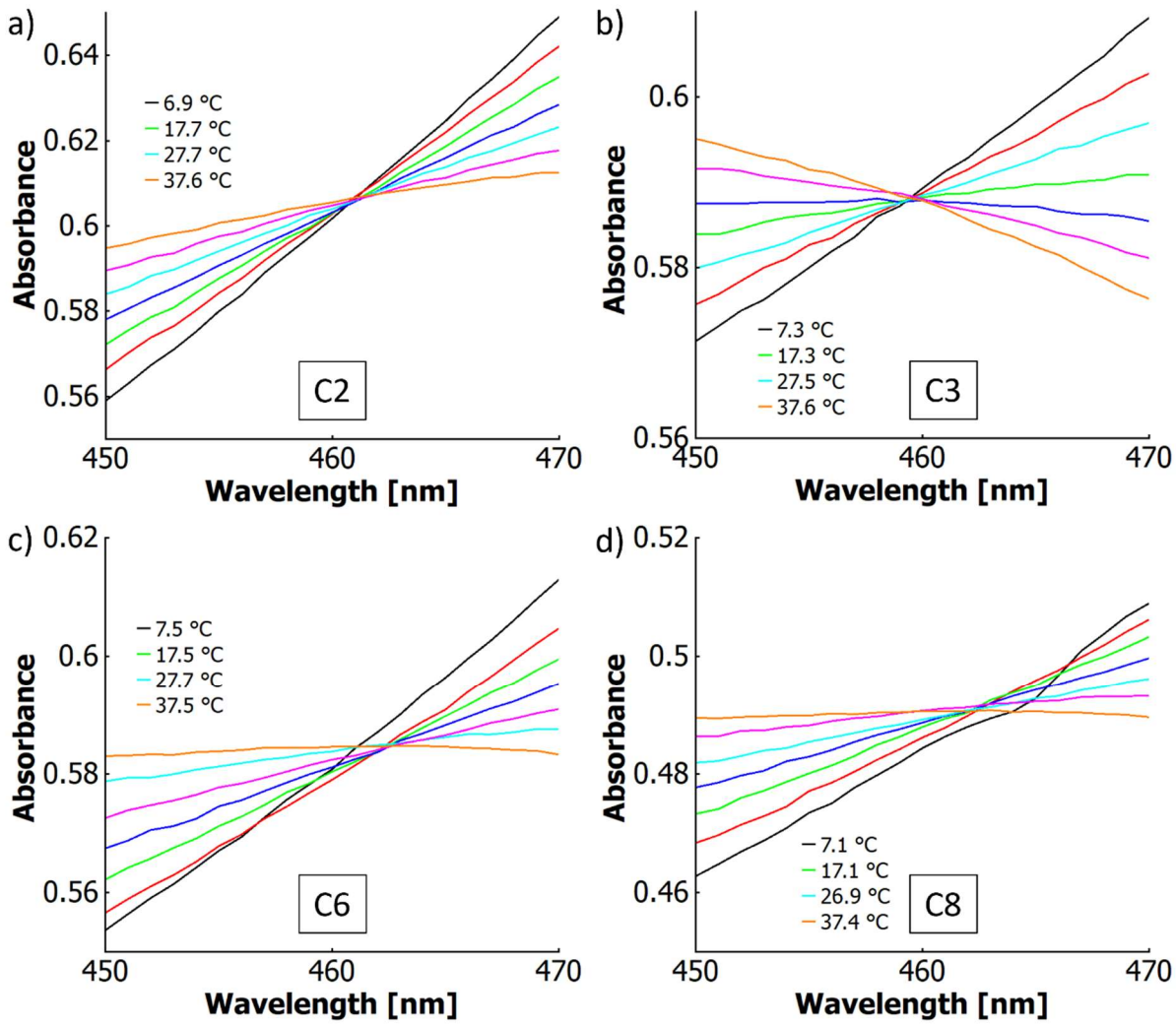

Figure S 48: Zoom-in of temperature-dependent UV-vis spectra of different amidoalkyl acrylamide of methyl red in methanolic trifluoroacetic acid (0.01 gL^{-1}, 0.025 v/v% TFA). a) MREtAAm; b) MRPrAAm; c) MRHexAAm and d) MROctAAm.

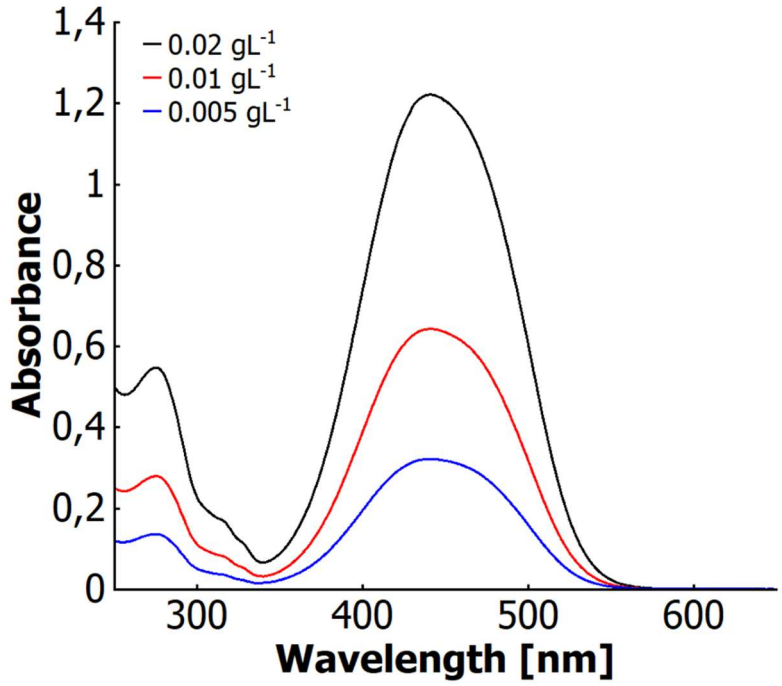

Figure S 49: UV-vis spectra of MREtAAm in ethanol at different concentrations at 22.5 °C.

Van't Hoff Plots for Amidoalkyl Acrylamides with Different Spacer Lengths in Ethanolic Trifluoroacetic Acid:

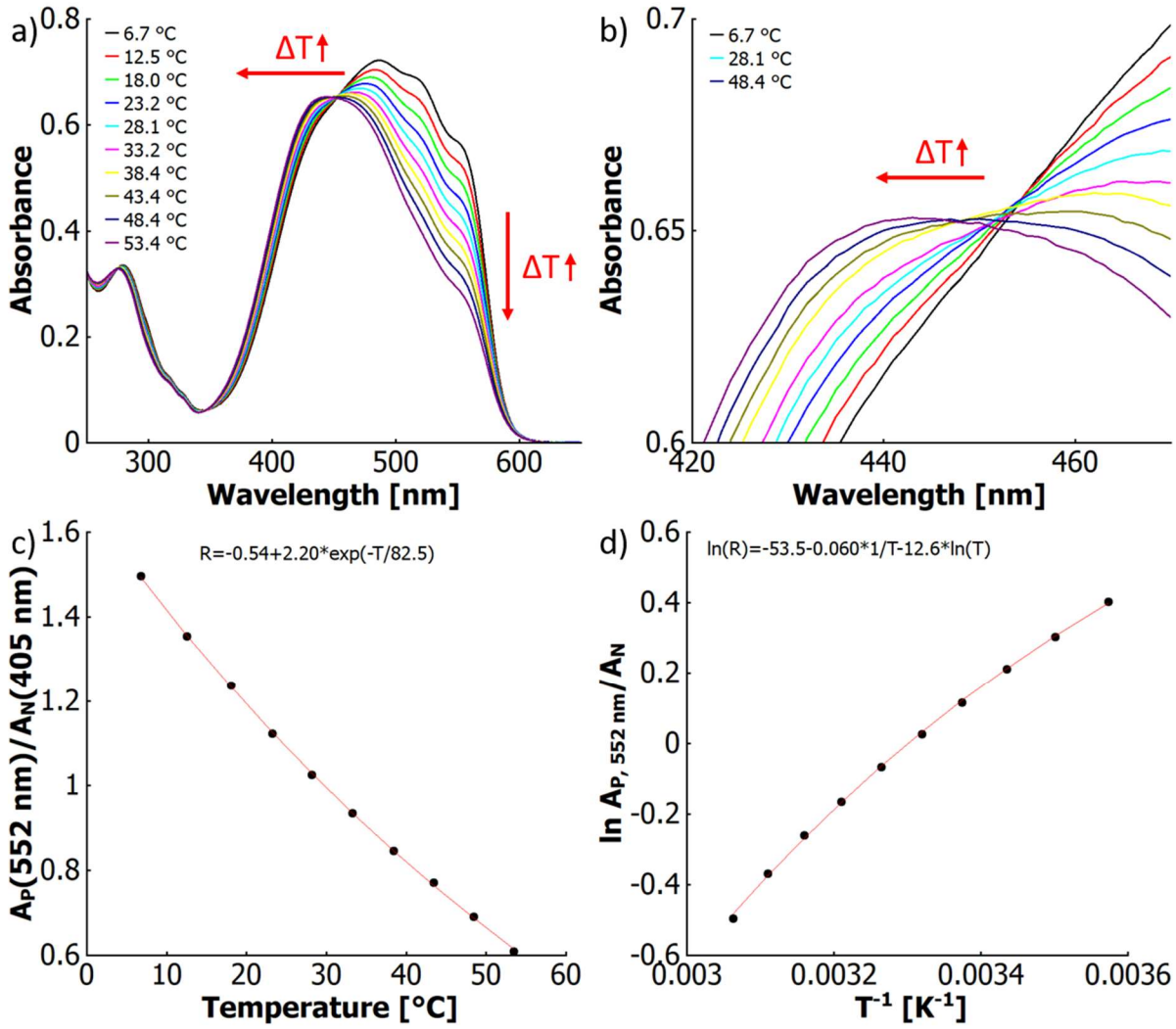

*Figure S 50: a) UV-vis spectra of MREtAAm (0.01 g/L) in ethanolic trifluoroacetic acid (1 v/v%) at different temperatures, direction of shifts in absorbance upon heating marked with red arrows; b) zoom-in of the spectra shown in a) to demonstrate the region of intersections, a red arrow showing the shift of the intersections upon heating; c) absorbance ratio of the protonated (552 nm) and the neutral species (405 nm) vs temperature, fitted with an exponential decay function; d) van't Hoff plot of the logarithmic absorbance ratio vs the inverse temperature, fitted with a function ln(R)=a-b*1/T+c*ln(T).*

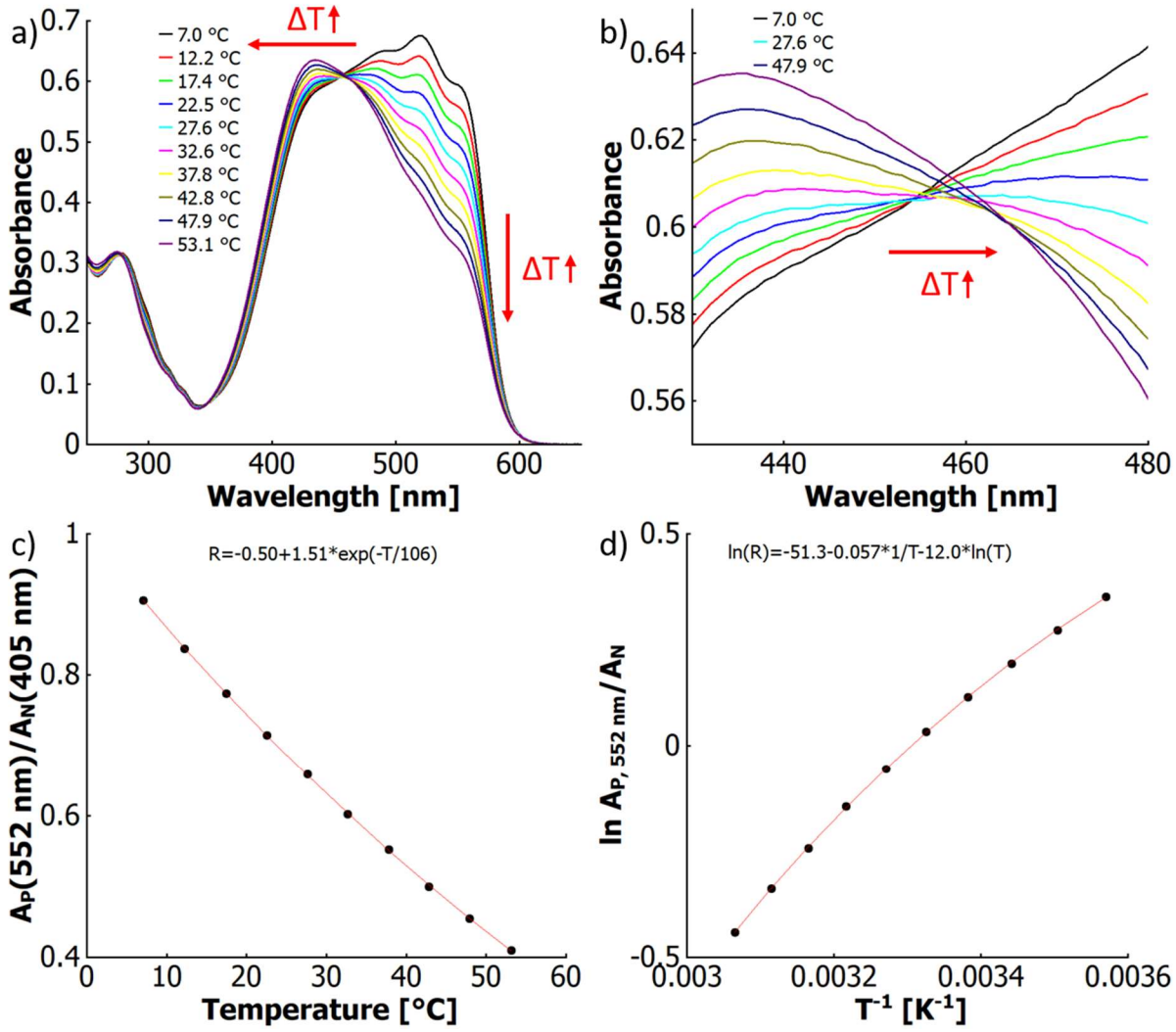

*Figure S 51: a) UV-vis spectra of MRPrAAm (0.01 g/L) in ethanolic trifluoroacetic acid (1 v/v%) at different temperatures, direction of shifts in absorbance upon heating marked with red arrows; b) zoom-in of the spectra shown in a) to demonstrate the region of intersections, a red arrow showing the shift of the intersections upon heating; c) absorbance ratio of the protonated (552 nm) and the neutral species (405 nm) vs temperature, fitted with an exponential decay function; d) van't Hoff plot of the logarithmic absorbance ratio vs the inverse temperature, fitted with a function ln(R)=a-b*1/T+c*ln(T).*

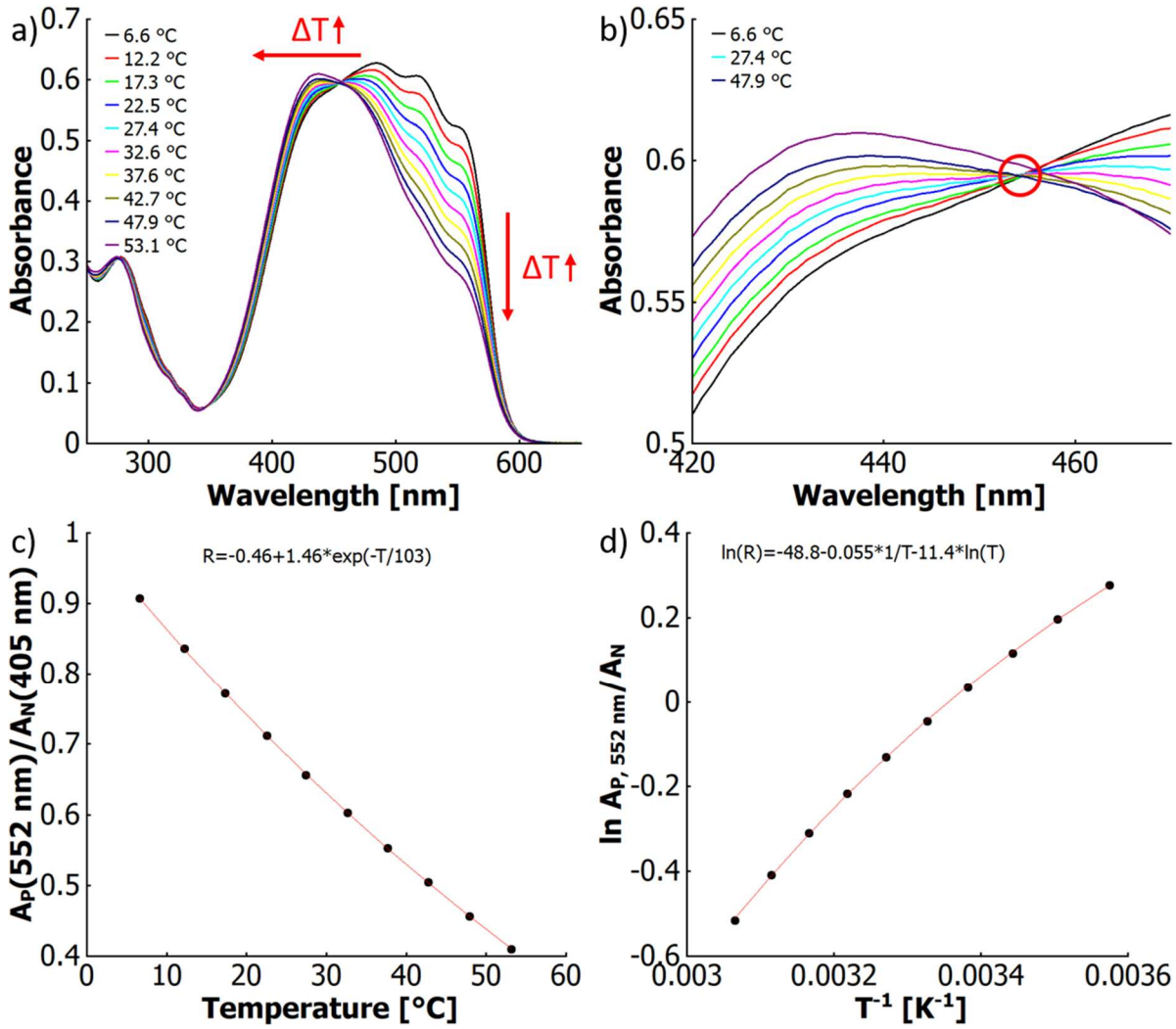

*Figure S 52: a) UV-vis spectra of MRHexAAm (0.01 g/L) in ethanolic trifluoroacetic acid (1 v/v%) at different temperatures, direction of shifts in absorbance upon heating marked with red arrows; b) zoom-in of the spectra shown in a) to demonstrate the isosbestic point; c) absorbance ratio of the protonated (552 nm) and the neutral species (405 nm) vs temperature, fitted with an exponential decay function; d) van't Hoff plot of the logarithmic absorbance ratio vs the inverse temperature, fitted with a function ln(R)=a-b*1/T+c*ln(T).*

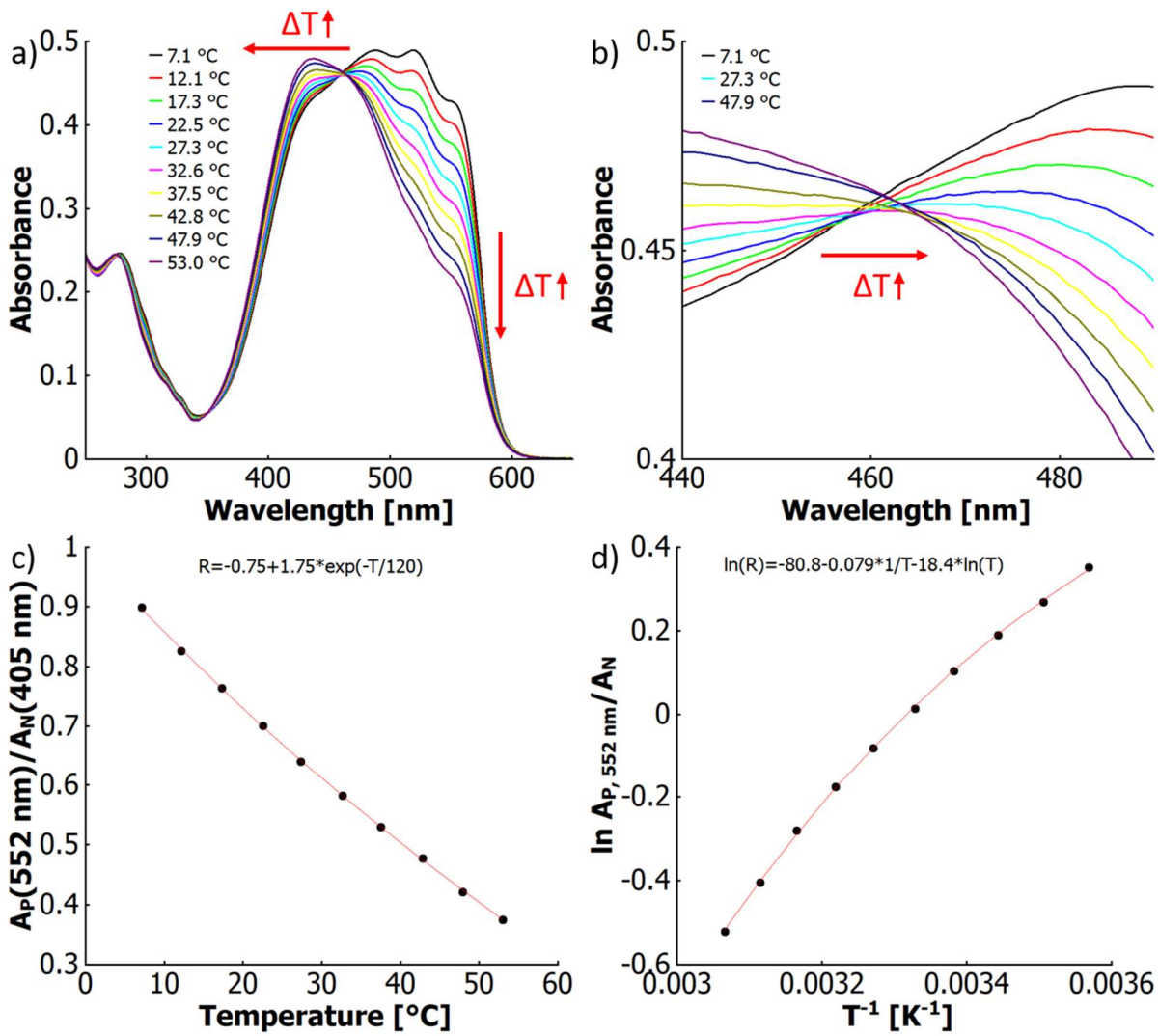

*Figure S 53: a) UV-vis spectra of MROctAAm (0.01 g/L) in ethanolic trifluoroacetic acid (1 v/v%) at different temperatures, direction of shifts in absorbance upon heating marked with red arrows; b) zoom-in of the spectra shown in a) to demonstrate the region of intersections, a red arrow showing the shift of the intersections upon heating; c) absorbance ratio of the protonated (552 nm) and the neutral species (405 nm) vs temperature, fitted with an exponential decay function; d) van't Hoff plot of the logarithmic absorbance ratio vs the inverse temperature, fitted with a function ln(R)=a-b*1/T+c*ln(T).*

References

(1) Staab, H. A.; Mannschreck, A. Synthese von Carbonsäureestern nach der Imidazolidmethode. *Chem. Ber.* **1962**, *95* (5), 1284–1297. DOI: 10.1002/cber.19620950527.

(2) Bergbreiter, D. E.; Osburn, P. L.; Li, C. Soluble Polymer-Supported Catalysts Containing Azo Dyes. *Org. Lett.* **2002**, *4* (5), 737–740. DOI: 10.1021/ol017198s.

(3) Staab, H. A.; Lüking, M.; Dürr, F. H. Darstellung von Imidazoliden. Synthese von Amiden, Hydraziden und Hydroxamsäuren nach der Imidazolidmethode. *Chem. Ber.* **1962**, *95* (5), 1275–1283. DOI: 10.1002/cber.19620950526.

5 Thermo-Tautochromic Polymer Architectures from Tertiary Methyl Red Amides

Thorben Gwydion Jaik, Ulrich Jonas

Macromol. Chem. Phys., 2022, **223**, 2200201.
https://doi.org/10.1002/macp.202200201

Published by *Wiley-VCH* in *Macromolecular Chemistry and Physics* as an Open Access article under the terms of the Creative Commons CC BY-NC 4.0 license, which permits distribution, and reproduction in any medium, provided the original work is properly cited (CC BY-NC 4.0, https://creativecommons.org/licenses/by-nc/4.0/).

Contributions of the authors to this project:

- All UV-vis measurements, data analysis, synthesis of monomers and polymers, specimen preparation and method design, as well as interpretation were done by me.
- The project was mainly initiated by me. The complete draft was written by me and completed, refined, and edited together with Prof. Dr. Jonas.

Macromolecular Chemistry and Physics
www.mcp-journal.de

Check for updates

Thermo-Tautochromic Polymer Architectures from Tertiary Methyl Red Amides

Thorben G. Jaik and Ulrich Jonas**

The ammonium-azonium tautomerism of protonated push–pull- or dialkylaminoazobenzenes has been subject of research for single molecular dyes but not for the interesting architectures of polymers or gels. To address this gap in knowledge, two different types of polymer systems are devised. First, a 2-oxazoline of *o*-methyl red is developed for cationic ring-opening copolymerization with 2-methyl-2-oxazoline. Second, a piperazine acrylamide of *o*-methyl red is synthesized for free radical copolymerization with *N*-hydroxyethyl acrylamide and a benzophenone acrylamide. The resulting copolymer can be photocrosslinked and swollen in water to form a hydrogel. Investigation of the optical properties of these systems in response to temperature variation reveals unusual phenomena related to the stability and dynamics of the ammonium-azonium tautomerism in aqueous media. Reversible and irreversible thermochromic phenomena are found for completely protonated, partially protonated, and neutral states of the systems. Reversible thermochromism is linked to an ammonium-azonium tautomerism, while irreversible thermochromism is a consequence of hydrolysis at unusually low temperatures, apparently catalyzed by intramolecular hydrogen bonding motifs between the tertiary amide in *ortho*-position to the protonated azo bridge. Hydrolysis is strongly affected by the particular molecular structure of the copolymer. In the hydrogel, hydrolysis rates decrease by a reduced degree of conformational freedom.

1. Introduction

Detailed knowledge of the optical characteristics of dye molecules, particularly in dependence of environmental influences like pH and temperature, is of paramount relevance for the application of dyes as colorants or as molecular probes in sensing, to mention only a few examples. Protonation processes in azobenzenes have been an early focus of azo dye research. In particular, the two possible protonation sites in aminoazobenzenes were topic of discussion over many years.[1,2] The conceivable two protonated tautomers are the ammonium form absorbing light at wavelengths around 320 nm and the azonium form with an absorption band around 520 nm. In the ammonium ion, the aromatic amino group is protonated, while protonation of the azonium ion occurs at the β-nitrogen of the azo group. The longer absorption wavelength of the azonium ion has been explained by the partial quinoid character of this tautomer.[2]

Quantification of the tautomeric equilibrium in dependence of the particular molecular structure of the dye was established by the ratio of the absorption bands of the azonium and the ammonium ions, C_ϵ/A_ϵ.[2] An example with an especially high C_ϵ/A_ϵ ratio is the push-pull-type azo dye *o*-methyl red. Here, the azonium ion is stabilized by internal hydrogen bonding of the carbonyl group in *ortho*-position to the β-protonated azo bridge, shifting the tautomeric equilibrium toward the azonium form.[2] The C_ϵ/A_ϵ ratio does not solely depend on the molecular structure of the dye but is also characteristically influenced by the pH of the liquid medium. Most notably, the C_ϵ/A_ϵ ratio shifts toward the azonium ion with increasing acid concentration.[2,3] However, a factor that has not been widely considered is temperature, which may influence the tautomeric equilibrium and with that the spectral features.

Such a shift in the equilibrium would result in thermochromism, which refers to color changes of a system upon temperature variation that may be either reversible or irreversible.[4,5] Thermochromic behavior specifically of azobenzenes has not been widely investigated and only a few examples are reported in the literature that relate temperature-induced color changes to the chromophore itself. The mechanism that is closest to the ammonium-azonium tautomerism discussed above was described for hydroxyazobenzenes and tricyanofuran hydrazone dyes entailing a temperature-sensitive azo-hydrazone tautomerism. In these dyes, the protonated azo group of the hydrazone is deprotonated at elevated temperatures, forming either a neutral azo form[6] or a hydrazone anion with an extended π-system.[7]

T. G. Jaik, U. Jonas
Department Chemistry – Biology
University of Siegen
Adolf-Reichwein-Strasse 2, D-57076 Siegen, Germany
E-mail: thorben@jaik.de; jonas@chemie.uni-siegen.de

The ORCID identification number(s) for the author(s) of this article can be found under https://doi.org/10.1002/macp.202200201

© 2022 The Authors. Macromolecular Chemistry and Physics published by Wiley-VCH GmbH. This is an open access article under the terms of the Creative Commons Attribution-NonCommercial License, which permits use, distribution and reproduction in any medium, provided the original work is properly cited and is not used for commercial purposes.

DOI: 10.1002/macp.202200201

15213935, 2022, 21, Downloaded from https://onlinelibrary.wiley.com/doi/10.1002/macp.202200201 by Cochrane Germany, Wiley Online Library on [30/01/2023]. See the Terms and Conditions (https://onlinelibrary.wiley.com/terms-and-conditions) on Wiley Online Library for rules of use; OA articles are governed by the applicable Creative Commons License

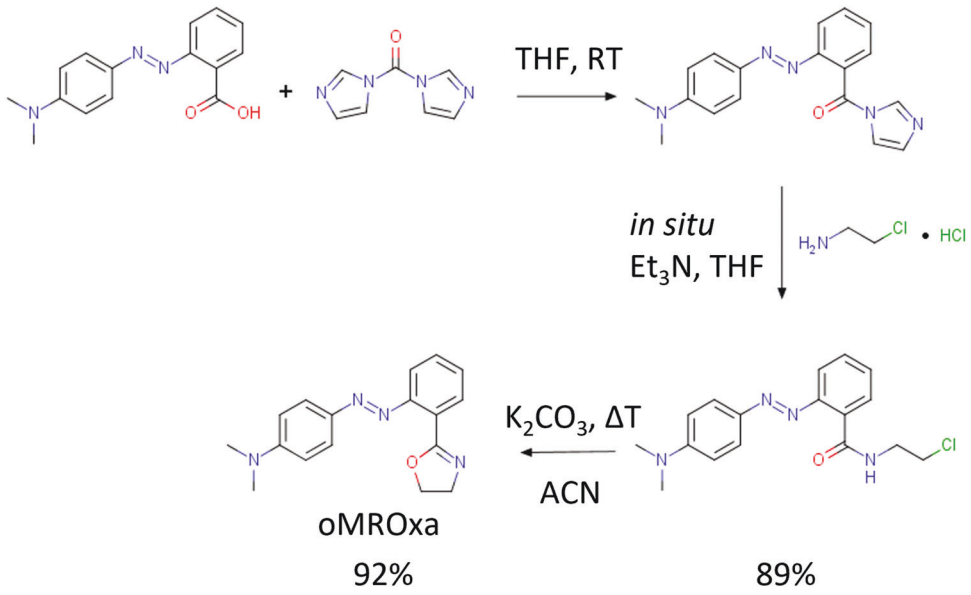

Scheme 1. Reaction scheme for the synthesis of 2-*o*-methyl red-2-oxazoline (oMROxa) via carbonyldiimidazole-mediated coupling of *o*-methyl red with 2-chloroethylamine and subsequent ring closure.

In polymers with characteristic spectral features, especially water-soluble polymers and gels, the study of temperature-dependent color change is a rather recent topic.[5] In such studies, the polymer matrix has been demonstrated to have manifold effects influencing different mechanisms of thermochromism. Yet, none of the described mechanisms relate to the observed behavior of the *o*-methyl red-modified polymers that are currently under investigation.

In this context, we could establish new mechanisms of thermochromism in polyacrylamides with the azo dye *o*-methyl red connected via an ester linkage to the polymer backbone.[8] Of special interest in this study is thermo-halochromism of *o*-methyl red-derivatives that occurs in *partially* protonated systems. A temperature-dependent equilibrium between the azonium ion and the neutral azobenzene was demonstrated, which is influenced by the microenvironment of the dyes. For all investigated systems, the general trend shows deprotonation of the azonium ion with increasing temperature, resulting in the formation of the neutral azobenzene. This process is reversible.

With the present study, we want to expand to *o*-methyl red-containing polymers, in which the chromophore is connected via a tertiary amide linkage to the polymer backbone and elaborate on the influence of this specific amide linkage on the thermochromic behavior. The corresponding polymer systems were prepared by two routes. On the one hand, a 2-oxazoline unit was introduced to the dye that led to the tertiary amide linkage upon cationic ring-opening polymerization (CROP). On the other hand, *o*-methyl red was functionalized with piperazine to yield a tertiary amide, which was converted to an acrylamide derivative that can be polymerized by free radical polymerization (FRP). When copolymerized with benzophenone acrylamide, the resulting polymer can be photocrosslinked to form a hydrogel after swelling with water. The monomers and the resulting polymers were analyzed with temperature-dependent UV–vis spectroscopy in neutral, slightly, and strongly acidic solution.

Table 1. Polymer characteristics including dye and crosslinker contents determined via UV–vis spectroscopy, as well as molecular weights determined by gel permeation chromatography, and yields.

Copolymer	Dye [mol%][a)]	BPAAm [mol%][a)]	M_n [kDa]	M_w [kDa]	$Đ$	Yield [%]
POxa	3.6 (72%)	–	20.5	34.6	1.69	96
PAAm	4.3 (88%)	–	19.6	52.1	2.65	94
PAAmBP	1.8 (72%)	0.82 (82%)	25.8	59.7	2.32	79

[a)] The %-value in parentheses indicates the amount of the monomer integrated into the polymer backbone in comparison to the feed.

2. Results and Discussion

First, the synthesis of monomers yielding tertiary amides of *o*-methyl red after their copolymerization with 2-oxazolines or acrylamides is discussed before the thermochromic behavior in solution and in a hydrogel is analyzed and put into context.

2.1. Synthesis of Monomers and Copolymers

2-o-Methyl red-2-oxazoline (oMROxa) was synthesized in two steps by carbonyldiimidazole (CDI)-mediated coupling of 2-chloroethylamine to the acid group of the azo dye *o*-methyl red and subsequent base-assisted ring closure (cf. **Scheme 1**), following established 2-oxazoline synthesis procedures.[9] The oMROxa synthesis resulted in a good overall yield of 82% over the two-step synthesis. It was then copolymerized with 2-methyl-2-oxazoline by CROP utilizing microwave heating, yielding a hydrophilic polymer that renders the hydrophobic dye soluble in water.

The copolymerization featured an excellent yield (>95%, cf. **Table 1**), yet the resulting copolymer had an atypically high dispersity for CROP (>1.6). Experimental details and characterization results are provided in the Supporting Information. Potentially,

© 2022 The Authors. Macromolecular Chemistry and Physics published by Wiley-VCH GmbH

15213935, 2022, 21, Downloaded from https://onlinelibrary.wiley.com/doi/10.1002/macp.202200201 by Cochrane Germany, Wiley Online Library on [30/01/2023]. See the Terms and Conditions (https://onlinelibrary.wiley.com/terms-and-conditions) on Wiley Online Library for rules of use; OA articles are governed by the applicable Creative Commons License

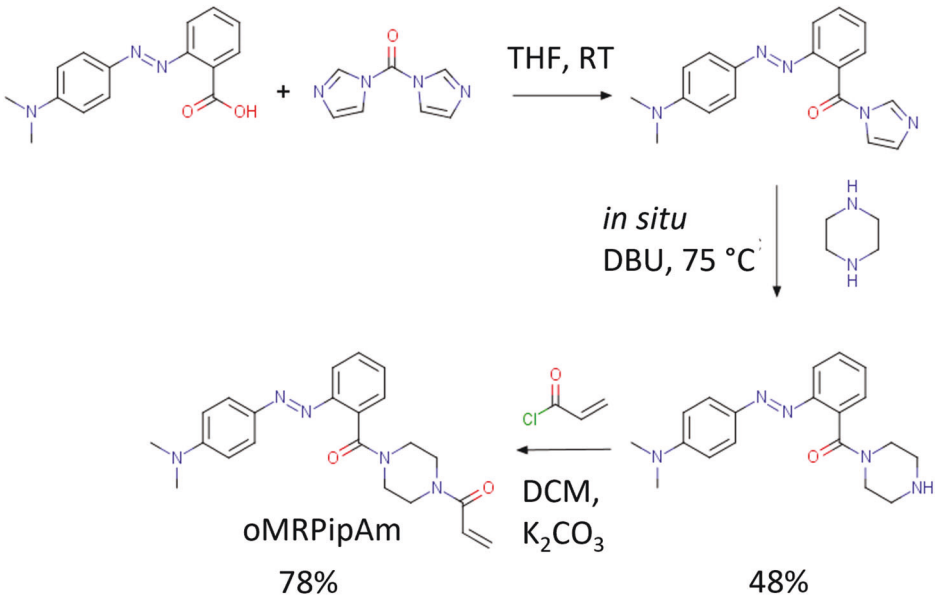

Scheme 2. Reaction scheme for the synthesis of *o*-methyl red piperazine acrylamide (oMRPipAm) via the carbonyldiimidazole-mediated amidation of piperazine with *o*-methyl red and subsequent acrylation.

this broader distribution may be a consequence of the initiator species, methenium, or the active chain ends reversibly interacting with the azo groups, in a similar fashion as free radicals[10–14] or protons. This would also explain why we were unable to prepare homopolymers of the dye monomers, as only oligomers could be isolated.

o-Methyl red piperazine acrylamide (oMRPipAm) was obtained in two steps by monofunctionalization of piperazine with *o*-methyl red and CDI as coupling agent, followed by functionalization of the remaining secondary amine with acryloylchloride (cf. **Scheme 2**). The piperazine acrylamide of the *para*-isomer of methyl red (pMRPipAm) was prepared in the same manner.

It is worthwhile to note that the synthesis yields varied significantly between these positional isomers. While pMRPipAm was obtained in an overall yield of 76%, the synthesis of oMRPipAm showed a considerably lower overall yield of 37%. While the reaction of the *para*-isomer occurred readily at room temperature throughout all reaction steps, amidation of the *ortho*-isomer with piperazine required harsher conditions with longer reaction times at higher temperatures. This is likely a consequence of considerable steric hindrance between the bulky piperazine and the azo bridge in *ortho*-position to the imidazole-activated carboxy group.

Two different types of copolymers were obtained from oMRPipAm by FRP, a binary copolymer with *N*-hydroxyethyl acrylamide (HEAm) as hydrophilic comonomer, and a terpolymer with HEAm and 4-benzophenone acrylamide (BPAAm) as photocrosslinker. Both copolymers were hydrophilic enough to allow solubilization of the hydrophobic *o*-methyl red moieties in water, as described above for the poly-2-oxazoline system. The copolymerizations featured reasonable to high yields and dispersities above 2.3 (cf. Table 1). Indeed, increasing dispersities and decreasing molecular weights with a higher feed of dye monomers in FRP are to be expected, as azobenzenes act as a retarder in radical polymerizations.[10–14]

The 2-oxazoline-based copolymer is in the following referred to as "POxa," while "PAAm" is used for the HEAm-based copolymers without the photocrosslinker, and "PAAmBP" for the copolymer containing benzophenone.

Both the 2-oxazoline-based monomer and the piperazine acrylamide dye yield copolymers with tertiary amides linkages in conjugation to the π-system of the chromophore with similar electronic structure. This structural similarity allows for comparison and evaluation of the effect of the two different copolymer types on the spectral characteristics of the dye substituents. Of note is that POxa and PAAm were polymerized with 5% of the respective dye monomers in the feed, while the PAAmBP feed contained only 2.5% of the dye monomer. The lower amount of dye monomer in the copolymerization of PAAmBP was chosen as we experienced difficulties with photocrosslinking for higher amounts of azo dyes in copolymers.

Synthetical details, materials, methods, and NMR-data can be found in the electronic supporting information.

2.2. Thermochromism of Azo Monomers in Solution

The thermochromism of the three monomers oMROxa, oMRPipAm, and pMRPipAm was investigated by temperature-dependent UV–vis spectroscopy in solution. These measurements were performed for the dyes in the *neutral* state in ethanolic solution and in the *completely* protonated form in 1.2 M aqueous hydrochloric acid. The solubility of the uncharged dye monomers in water was too low to perform similar measurements in neutral aqueous solution.

The UV–vis data was analyzed by derivative spectroscopy and difference spectroscopy. In the former method, the second and fourth derivatives of UV–vis spectra can be used to identify the positions of overlapping absorption bands.[15] Difference spectroscopy can be employed to monitor absolute

© 2022 The Authors. Macromolecular Chemistry and Physics published by Wiley-VCH GmbH

15213935, 2022, 21, Downloaded from https://onlinelibrary.wiley.com/doi/10.1002/macp.202200201 by Cochrane Germany, Wiley Online Library on [30/01/2023]. See the Terms and Conditions (https://onlinelibrary.wiley.com/terms-and-conditions) on Wiley Online Library for rules of use; OA articles are governed by the applicable Creative Commons License

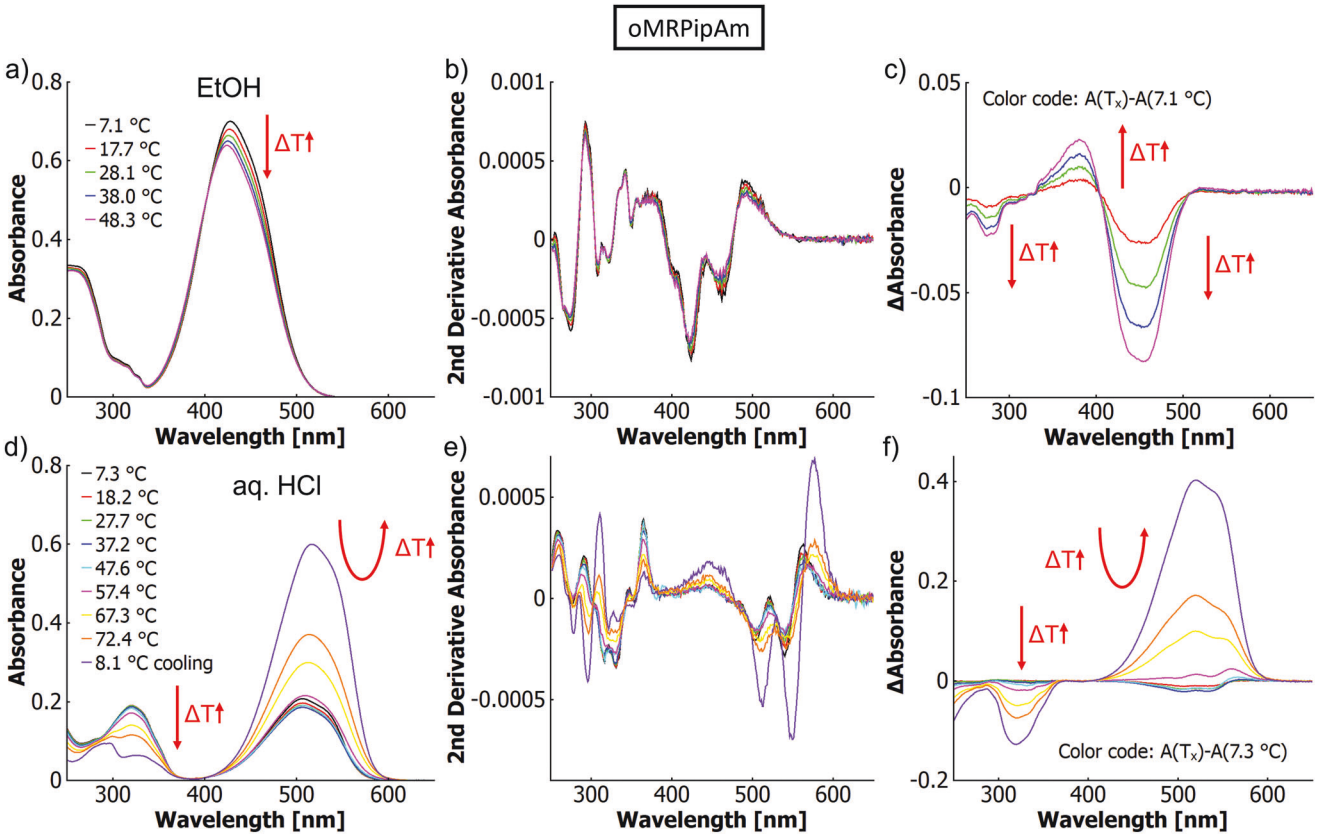

Figure 1. UV–vis spectra of *o*-methyl red piperazine acrylamide (oMRPipAm) at different temperatures a) in ethanol (0.01 g L^{-1}), and d) in aq. HCl (1.2 M, 0.005 g L^{-1}), b,e) the corresponding second derivative spectra, and c,f) the corresponding difference spectra. The legends provided in the UV–vis spectra (a, d) also apply to the derivative spectra (b, e). For the difference spectra (c, f), the spectrum at the lowest temperature was subtracted from each at a higher temperature, with the line color from a) and d) depicting the higher temperature, indicated by "Color code: $A(T_x) - A(T_{min})$."

changes in the optical spectra upon variation of the experimental parameters, and was recently applied to determine vibronic changes in temperature-dependent UV–vis spectroscopy of *trans*-azobenzene.[16]

2.2.1. Neutral State

In the neutral state, all three dye monomers, oMROxa, oMRPipAm, and pMRPipAm, show the same general thermochromic behavior in ethanolic solution. A small blueshift of the absorption maximum can be observed for all dyes upon temperature increase (cf. **Figure 1**a, Figures S20a and S25a, Supporting Information). The maxima shift for oMROxa from 420 nm at 7.8 °C to 417 nm at 48.8 °C, for oMRPipAm from 428 nm at 7.1 °C to 424 nm at 48.3 °C, and for pMRPipAm from 427 nm at 8.0 °C to 422 nm at 48.5 °C.

These shifts are in the same order of magnitude for all three derivatives (cf. **Table 2**) and they arise from the sub-band structure of the corresponding absorption bands, which is likely of vibronic origin.[8] Details of the sub-band structure were scrutinized by derivative spectroscopy (cf. Figure 1b, Figures S20b and S25b, Supporting Information), however, the second derivatives of the parent UV–vis spectra showed considerable overlap so that the band positions can only be estimated. While three sub-bands could be identified by this approach, the shortest wavelength sub-band is only visible as a small shoulder and was thus not included in Table 2. The lowest energy sub-band, which is assumed to correspond to the 0-0 transition, and the sub-band at second lowest energy, assigned to the 0-1 transition, have an energy difference of 1590 cm^{-1} for oMROxa, 1990 cm^{-1} for oMRPipAm, and 1790 cm^{-1} for pMRPipAm, respectively. These energies are all higher than the most probable Raman-active vibration for vibronic transition in the parent compound *o*-methyl red.[17,18] The energy of the N=N valence mode is ≈1400 cm^{-1}.

In all cases, the shortest wavelength bands are estimated to lie around 400 nm, which would result in a smaller energy differ-

Table 2. Absorbance maxima at low temperatures (λ_{max}), wavelength shifts (λ-shift) of the absorbance maxima with temperature increase from around 10 °C to around 50 °C, vibronic sub-bands as determined by derivative spectroscopy ($0\text{–}0_{max}$, $0\text{–}1_{max}$), and energy difference between the sub-bands ($\tilde{\nu}_{01}$) for the azo dyes oMROxa, oMRPipAm, and pMRPipAm in ethanol.

Derivative	λ_{max} [nm]	λ-shift [nm]	$0\text{–}0_{max}$ [nm]	$0\text{–}1_{max}$ [nm]	$\tilde{\nu}_{01}$ [cm^{-1}]
oMROxa	420	420→417	450	420	1590
oMRPipAm	428	428→424	463	424	1990
pMRPipAm	427	427→422	458	424	1790

© 2022 The Authors. Macromolecular Chemistry and Physics published by Wiley-VCH GmbH

15213935, 2022, 21, Downloaded from https://onlinelibrary.wiley.com/doi/10.1002/macp.202200201 by Cochrane Germany, Wiley Online Library on [30/01/2023]. See the Terms and Conditions (https://onlinelibrary.wiley.com/terms-and-conditions) on Wiley Online Library for rules of use; OA articles are governed by the applicable Creative Commons License

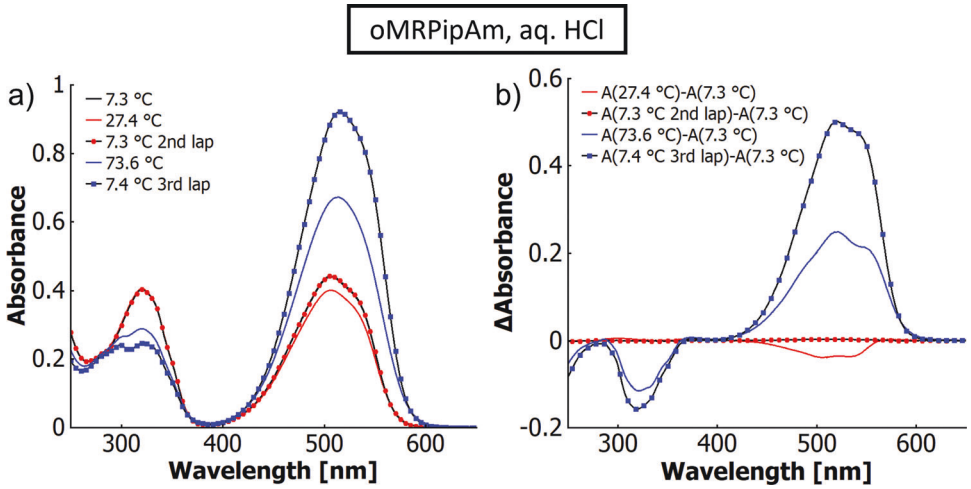

Figure 2. a) UV–vis spectra of oMRPipAm (0.01 g L^{-1}) in aq. HCl (1.2 M) from a temperature series starting at 7.3 °C, heating to 27.4 °C, cooling to 7.3 °C, ramping to 73.6 °C and holding for 20 min, before cooling back to 7.4 °C. b) The corresponding difference spectra, subtracting the first spectrum at low temperature from all following spectra.

ence between this 0-2 transition and 0-1 compared to the energy difference between the 0-1 and 0-0 sub-bands. Based on the rather poor resolution of the derivative spectra it is not possible to assign specific effects to the high energy differences between the 0-0 and 0-1 transitions.

The difference spectra reveal the spectral changes to occur at wavelengths corresponding to the 0-0 and 0-1 transitions (cf. Figure 1c, Figures S20c and S25c, Supporting Information).

2.2.2. Completely Protonated State

In the *completely* protonated state in aqueous hydrochloric acid, the thermochromic behavior differs considerably between the three dye monomers oMROxa, oMRPipAm, and pMRPipAm.

For the 2-oxazoline monomer oMROxa, the short-wavelength band at 330 nm of the ammonium ion and the long-wavelength band at 507 nm of the quinoid azonium ion have similar magnitudes of absorbance at low temperatures. Upon raising the temperature, the short-wavelength band loses intensity, while the long-wavelength band increases and red-shifts (cf. Figure S20, Supporting Information). These absorbance changes are irreversible, which is a consequence of hydrolytic ring-opening of the 2-oxazoline unit, catalyzed by the present acid. The hydrolysis product is protonated by the acidic medium, preferentially at the β-nitrogen of the azo bridge,[2,19] forming an azonium ion with quinoid character (cf. Scheme S1, Supporting Information). As a consequence of this hydrolytic instability, the thermochromic behavior of the 2-oxazoline monomer cannot be unambiguously evaluated.

The *completely* protonated tertiary amide oMRPipAm in acidic aqueous solution shows a complex thermochromic behavior, which can be divided into a low- and a high-temperature regime (cf. Figure 1d). Starting from low temperatures, the magnitude of the ammonium ion absorption band at 320 nm slightly increases with temperature, while concurrently the azonium ion absorption band at 507 nm loses intensity. Upon exceeding a threshold temperature (≈35 °C), the intensity of the short-wavelength band is strongly reduced and the long-wavelength band red-shifts, accompanied by a significant absorbance gain.

In order to assess if these two characteristic thermochromic features at low and high temperature are reversible, a solution of the monomer in aqueous acid was measured with a temperature cycle program (cf. **Figure 2**).

When cycling the temperature between 7.5 and 27.5 °C, the variations of the spectral features are reversible. In contrast, the optical characteristics change irreversibly when heating and cooling above 27.5 up to 74 °C. Difference spectra were calculated by subtracting the initial spectrum from all following spectra to analyze such spectral changes (cf. Figure 2b).

The difference spectrum of a comparison of the initial, low (7.5 °C) to the medium temperature spectrum at 27.5 °C reveals a negative band with two minima at 507 and 533 nm, and a slight increase at 302 nm (red spectrum in Figure 2b). The negative long-wavelength band corresponds to a decrease of the azonium ion concentration, while the positive short-wavelength band results from an increase of the ammonium ion concentration. When comparing the low-temperature spectra before and after thermal cycling, the difference spectra result in a flat line, which corroborates the reversibility of thermochromic processes in this temperature regime (black spectrum with red dots in Figure 2b). As such, this thermochromism is a consequence of an ammonium-azonium equilibrium that shifts from the intensely pink-colored azonium ion toward the colorless ammonium ion upon temperature increase, meaning that the solution discolors reversibly with increasing temperatures. We refer to this process as "thermo-tautochromism," following the terminology applied to solvent-dependent absorption behavior of phenazines.[20]

Conversely, difference spectra obtained from measurements in the high-temperature regime at 74 °C show a positive band with maxima at 518 and 547 nm, and a strong negative band at 321 nm (blue line in Figure 2b). At the same time, a shift of the band at 506 nm in the initial spectrum at 7.5 °C to 513 nm at high temperatures occurs. When cooling back to 7.5 °C, the long-wavelength band possesses a significantly higher absorbance compared to the sample before heating, while the

© 2022 The Authors. Macromolecular Chemistry and Physics published by Wiley-VCH GmbH

15213935, 2022, 21, Downloaded from https://onlinelibrary.wiley.com/doi/10.1002/macp.202200201 by Cochrane Germany, Wiley Online Library on [30/01/2023]. See the Terms and Conditions (https://onlinelibrary.wiley.com/terms-and-conditions) on Wiley Online Library for rules of use; OA articles are governed by the applicable Creative Commons License

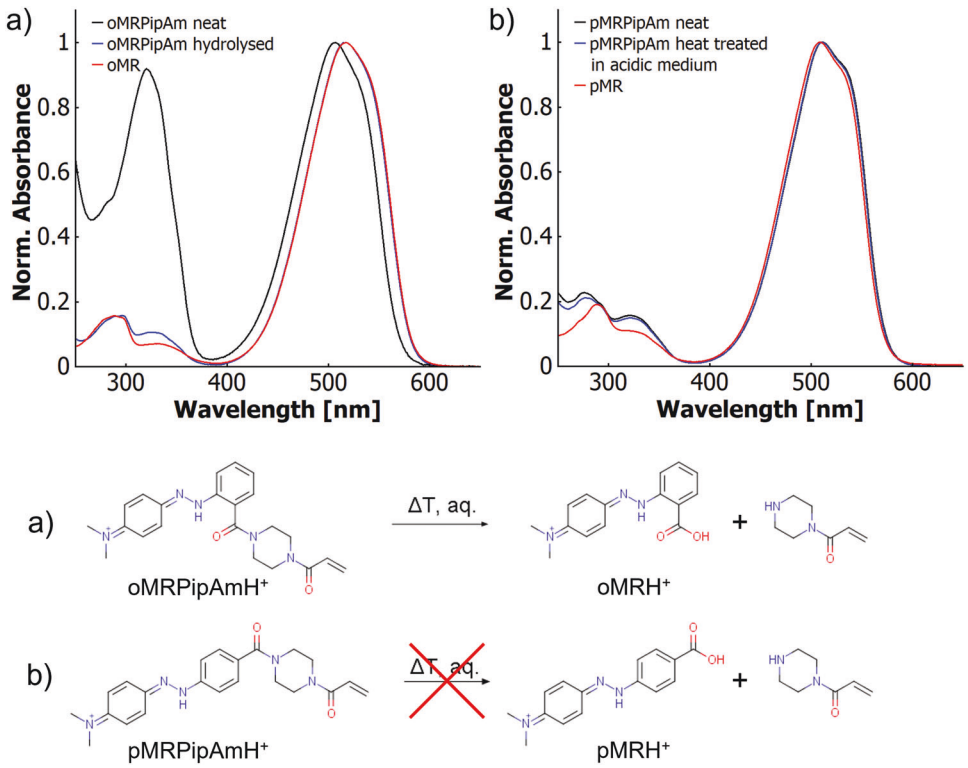

Figure 3. a) Normalized UV–vis spectra of neat *o*-methyl red piperazine acrylamide, oMRPipAm, in aq. HCl (1.2 M), hydrolyzed after heat treatment (7.5 °C → 72.5 °C over the course of 5 h), and *o*-methyl red, oMR. b) Normalized UV–vis spectra of neat p-methyl red piperazine acrylamide, pMRPipAm, in aq. HCl (1.2 M), after heat treatment (7.5 °C → 79 °C over the course of 5 h), and p-methyl red, pMR. The corresponding hydrolysis reactions are sketched below.

short-wavelength band decreased (black line with blue squares in Figure 2b).

These observations reflect an irreversible increase in the concentration of an azonium species at the expense of an ammonium species, which is as such an unexpected experimental result. To explain the substantial increase of the azonium ion concentration after heating to the high-temperature regime, a chemical reaction is postulated that does not degrade the azo dye chromophore itself but influences its electronic structure. The only plausible reaction is an acid-catalyzed hydrolysis of the tertiary amide linkage between the chromophore and the piperazine ring, yielding the parent dye *o*-methyl red. Under these conditions, the liberated dye is protonated but exhibits a significantly stronger absorbance in the red compared to the tertiary amide oMRPipAm. Consequently, the solution becomes intensely colored.

The hypothesis of hydrolysis as the underlying mechanism for the irreversible thermochromism can be verified by two approaches. The first approach is UV–vis and derivative spectroscopy to proof that the effects are not of vibronic nature in contrast to the neutral state. The UV–vis spectra of the hydrolysis product and of protonated *o*-methyl red are identical in the azonium ion band region, yet with a slight difference in the ammonium ion band at around 320 nm (cf. **Figure 3**a). This difference is likely a consequence of the presence of piperazine acrylamide as the second hydrolysis product. The derivative spectra show a substantial and irreversible shift of the sub-band pattern between low and high temperatures (cf. Figure 1e), instead of a reversible change in their ratio expected for vibronic thermochromism (as demonstrated for the *para*-isomer pMRPipAm in aq. HCl, cf. Figure S25e, Supporting Information). The sub-bands of oMRPipAm in aq. HCl lie at 540 nm for the 0-0 transition and at 493 nm for the 0-1 transition. After heating, those sub-bands shift to 549 and 510 nm, respectively, which are the sub-band positions for the parent compound *o*-methyl red (cf. Figure S22, Supporting Information).

^{1}H NMR spectroscopy serves as the second method to probe the hydrolysis reaction. For this purpose, oMRPipAm was dissolved in deuterium oxide with trifluoroacetic acid (1 v/v%), with the first measurement taken at room temperature, heated to 60 °C for 20 h, and then measured again at room temperature (cf. Figure S23, Supporting Information). After the heating cycle, an insoluble precipitate with dark red color formed and the ^{1}H NMR spectra revealed piperazine acrylamide as soluble hydrolysis product.

Surprisingly and in contrast to reported hydrolysis reactions for tertiary amides of aromatic acids,[21,22] the rather mild conditions found for oMRPipAm suggest a catalytic influence of the molecular environment on the amide linkage via polar and hydrogen bonding groups in close proximity, as known for the specific interaction of a substrate with the binding pocket in enzymes. For our azo dye, the protonated azo bridge in *ortho*-position presents such a catalytic motif in direct neighborhood to the carbonyl group (cf. **Figure 4**, structure (II)).

© 2022 The Authors. Macromolecular Chemistry and Physics published by Wiley-VCH GmbH

15213935, 2022, 21, Downloaded from https://onlinelibrary.wiley.com/doi/10.1002/macp.202200201 by Cochrane Germany, Wiley Online Library on [30/01/2023]. See the Terms and Conditions (https://onlinelibrary.wiley.com/terms-and-conditions) on Wiley Online Library for rules of use; OA articles are governed by the applicable Creative Commons License

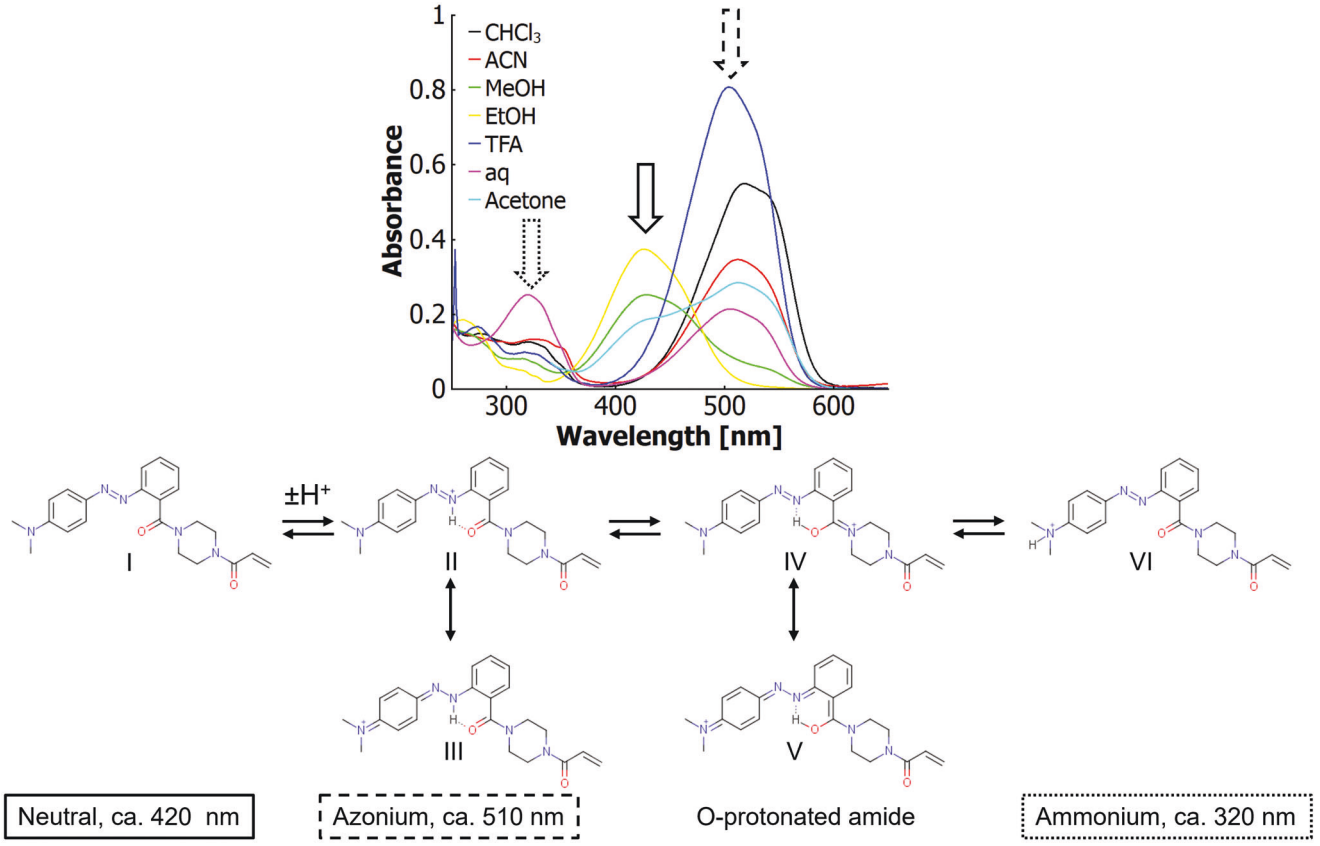

Figure 4. Top: UV–vis spectra of oMRPipAm (either 2.7×10^{-5} mol L^{-1} or normalized to this concentration) at 22.5 °C in several solvents with 1 v/v% trifluoroacetic acid. Bottom: Protonation states and corresponding resonance structures for oMRPipAm. The absorption bands are assigned to the absorbing species by marking with arrows of matching character (solid line neutral dye, dashed line azonium ion, dotted line ammonium ion).

This hypothesis was tested with the *para*-isomer pMRPipAm, which is not able to form an intramolecular hydrogen bond between the protonated azo bridge and the tertiary amide group in *para*-position. Indeed, the observed thermochromic behavior of pMRPipAm is in stark contrast to that of the *ortho*-isomer.

The temperature-dependent UV–vis spectra of the *para*-isomer pMRPipAm do not show the substantial irreversible spectral changes associated with an effective hydrolysis reaction (cf. Figure 3b, Figure S25d–f, Supporting Information). The minute variation found in the difference spectra around 500 nm after heating to 78 °C and again cooling the solution to 8.4 °C may be associated with a very slow hydrolysis reaction or simply solvent evaporation, but the overall thermochromic behavior is essentially reversible (cf. Figure S25f, Supporting Information).

As such, the absorbance decreases of the long-wavelength band at 511 nm of the azonium ion and the increase in absorbance at 320 nm of the ammonium ion upon temperature increase follow the behavior of the *ortho*-isomer oMRPipAm in the low-temperature regime. However, the ratio of the azonium and ammonium absorption bands differs between the *ortho*- and the *para*-isomers. For the *ortho*-isomer, this ratio is close to one, with a slight emphasis on the azonium absorption (cf. Figure 1d). On the other hand, the absorption band of the azonium ion of the *para*-isomer is considerably stronger than its ammonium band. The experimental data of the *para*-isomer pMRPipAm fully reflect the expected spectral characteristics of common push-pull azo dyes with protonation predominantly occurring at the *β*-nitrogen of the azo bridge.[2,19] This preference of the tautomeric equilibrium favoring protonation of the azo bridge over the ammonium form is especially apparent in *o*-methyl red.[2] The more striking is the fact that the tertiary amide of the *ortho*-isomer oMRPipAm, derived from *o*-methyl red, shows a conspicuously contrary spectral behavior.

The study of solvatochromism of the parent compound neutral *o*-methyl red in comparison to the protonated form of oMRPipAm represents a valuable tool to investigate this anomaly (cf. Figure 4).

The parent compound *o*-methyl red shows intense solvatochromism based on the tautomeric equilibrium between the neutral carboxylic acid form and the azonium form of the dye.[23] This equilibrium is controlled by several solvent parameters that influence the balance between intramolecular hydrogen bonding, favoring the azonium form, and intermolecular hydrogen bonding, favoring the neutral carboxylic acid. This balance cannot be described clear-cut with solely a single solvent parameter related to polarity, polarizability, and hydrogen bonding features, but a detailed picture demands correlation of several parameters, like the Kamlet–Taft parameters, Reichardt scale, and Gutmann donor and acceptor numbers.[23] These studies evaluating the interplay of the various solvent parameters indicate a

© 2022 The Authors. Macromolecular Chemistry and Physics published by Wiley-VCH GmbH

15213935, 2022, 21, Downloaded from https://onlinelibrary.wiley.com/doi/10.1002/macp.202200201 by Cochrane Germany, Wiley Online Library on [30/01/2023]. See the Terms and Conditions (https://onlinelibrary.wiley.com/terms-and-conditions) on Wiley Online Library for rules of use; OA articles are governed by the applicable Creative Commons License

clear distinction between three different classes of non-hydrogen bonding, hydrogen bond accepting (HBA) or hydrogen bond donating (HBD) solvents.

Following this rationale, the absorbance spectra of oMRPipAm were measured in representative examples from each of these solvent classes in the presence of 1 v/v% trifluoroacetic acid. Three protonation sites can be identified in the molecular structure of oMRPipAm as depicted in Figure 4: The azonium form with protonation at the *β*-nitrogen (II/III), the *O*-protonated amide (IV/V), and the ammonium form with protonation at the aromatic tertiary amine (VI). In the first two forms (II/III and IV/V), intramolecular hydrogen bonding can occur between the azo bridge and the carbonyl function of the aromatic tertiary amide (cf. Figure 4). The exact structure of the azonium ion present in solution lies between the resonance structures (II)–(V), as a consequence of the tautomeric and mesomeric equilibria that depend on the environmental conditions (i.e., the nature of the liquid medium).

Furthermore, a second tautomeric equilibrium exists between the resulting azonium form and the ammonium form (VI), which depends on the stability of the intramolecular hydrogen bonding motif and is thus strongly affected by the particular solvent competing via intermolecular hydrogen bonding. An additional factor on solvation is the localization of charges in the tautomers. While the charge of the ammonium ion is essentially localized at the nitrogen atom, the positive charge of the azonium ion is delocalized over the whole chromophore.

As described previously, in water (magenta spectrum in Figure 4) the ammonium form is favored over the azonium ion. This is apparent by the stronger ammonium absorbance at ≈320 nm, marked with a dotted-line arrow, in relation to the azonium absorbance at around 510 nm, indicated by the dotted-line arrow. Water as a strong hydrogen bond donor can form strong intermolecular hydrogen bonds with the dye, thus perturbing the intramolecular H-bonding motif of the azonium ion, which results in an increased ammonium concentration.

Such a relative increase in the ammonium concentration is not observed for the two other hydrogen bond donors methanol (green spectrum) and ethanol (yellow spectrum) at the same acid concentration. Notably, in methanol an additional absorption band at ≈420 nm dominates the spectrum, relating to the neutral form (solid-line arrow). Yet, partial protonation still occurs, manifested in a long-wavelength shoulder in the main absorption band and a weak absorption at 320 nm related to the ammonium form. In ethanol, only negligible protonation takes place as only the absorption band of the neutral form is visible. The spectrum in ethanolic trifluoroacetic acid (TFA) is almost identical to the one in neat ethanol, with only slight increases in absorbance around 320 and 550 nm in ethanolic TFA (cf. Figure S24, Supporting Information). This protonation behavior is in stark contrast to the recently reported, analogous ester-based monomer of *o*-methyl red, where about 50% of the dye is protonated at the same acid concentration in ethanol as used above for oMRPipAm.[8] This means that the basicity of the *ortho*-substituted chromophore is drastically decreased in the tertiary amide compared to the ester.

This can also be shown indirectly by comparing the *para*-isomer pMRPipAm in ethanolic TFA with its ester analogue.[8] Both *para*-isomers are partially protonated in ethanolic TFA and exhibit similar thermo-halochromism upon temperature variation. The protonation equilibrium is shifted from the azonium ion toward the neutral species with increasing temperatures. The ammonium ion is only minimally involved in this process, as the tautomerism between the ammonium and azonium lies heavily on the side of the azonium in both *para*-derivatives (cf. Figure S26, Supporting Information and ref. [8]). Thus, the lower basicity of oMRPipAm does not originate from the tertiary amide functionality itself but from the specific interaction between the amide linkage in *ortho*-position and the azo bridge.

Similar effects observed for hydrogen bond donating solvents are found in the hydrogen bond accepting solvents acetonitrile (red spectrum) and acetone (turquoise spectrum). In acetonitrile, the azonium ion is preferred compared to the ammonium ion, and no neutral azo dye can be detected. This is different in acetone as less polar solvent, where all three forms, the neutral azo dye, the azonium ion, and the ammonium ion are observed. Here, the lower degree of protonation is likely a consequence of a weaker dissociation of the dissolved acid in this less polar solvent. Yet, the degree of protonation in acidified acetone is considerably higher than in the more polar solvents methanol and ethanol with added acid. From this observation and the comparison between the tautomeric equilibria in acetonitrile and in water above follows that hydrogen bond accepting solvents disturb intramolecular hydrogen bonding less than hydrogen bond donating solvents.

In the non-hydrogen bonding solvent chloroform (black spectrum), the tautomeric equilibrium lies strongly on the side of the azonium form. Therefore, a lack of hydrogen bonds with the solvent leads to preference of intramolecular hydrogen bonding between the aromatic amide and the azo bridge.

Lastly, in neat trifluoroacetic acid (blue spectrum) the azonium ion is observed almost exclusively. This matches the reported behavior of other azobenzenes, where the tautomerism is shifted toward the azonium ion at higher acid concentrations.[2]

As a consequence of these experimental results, the role of the intramolecular hydrogen bond between the tertiary amide linkage and the azo bridge in the hydrolysis reaction of oMRPipAm may be inferred from the solvatochromic behavior of the dye in acidic media discussed above.

While it can be assumed that the *para*-isomer would hydrolyze eventually as well, no considerable spectral changes can be observed under the experimental conditions (cf. Figure 3b), which suggests very slow hydrolysis kinetics in absence of the intramolecular hydrogen bonding motif. On the other hand, the *ortho*-isomer exhibits a significantly higher reaction rate with its hydrolysis being observable even at temperatures well below 40 °C, corroborating the catalytic role of the intramolecular hydrogen bond.

In summary, HBD solvents interfere with the intramolecular hydrogen bonding motif in oMRPipAm, as evidenced by the solvatochromic behavior of the dye in acidified solvents (cf. Figure 4). In acidified water as very effective HBD, the ammonium-azonium tautomerism lies on the side of the ammonium ion. In contrast, the tautomeric equilibrium lies on the side of the azonium form in acidified chloroform, which exhibits only weak hydrogen bonding interactions and thus is classified as non-hydrogen bonding solvent.[23] In methanol and ethanol, the degree of protonation is considerably lower. This is likely a conse-

© 2022 The Authors. Macromolecular Chemistry and Physics published by Wiley-VCH GmbH

15213935, 2022, 21, Downloaded from https://onlinelibrary.wiley.com/doi/10.1002/macp.202200201 by Cochrane Germany, Wiley Online Library on [30/01/2023]. See the Terms and Conditions (https://onlinelibrary.wiley.com/terms-and-conditions) on Wiley Online Library for rules of use; OA articles are governed by the applicable Creative Commons License

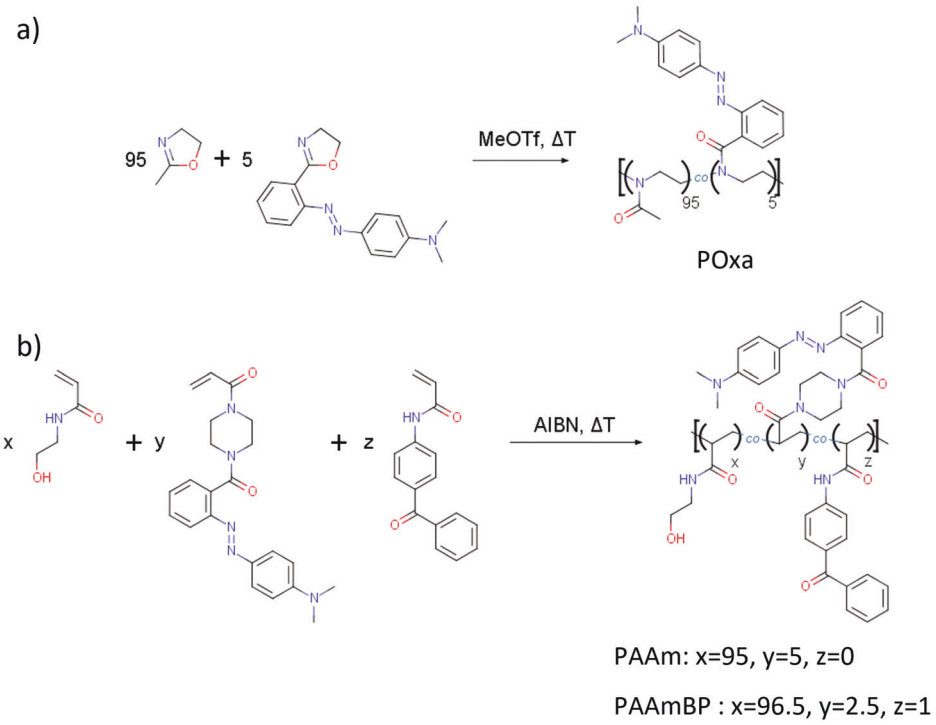

Scheme 3. a) Methyl triflate-initiated, microwave-assisted cationic ring-opening polymerization of 2-methyl-2-oxazoline with 2-*o*-methyl red-2-oxazoline. b) Azobisisobutyronitrile-initiated free radical polymerization of *N*-hydroxyethyl acrylamide with benzophenone acrylamide and o-methyl red piperazine acrylamide.

quence of stronger intermolecular hydrogen bonds between the HBD solvents and the dye, leading to a solvent cage that increases the steric demand, in turn interfering with the intramolecular H-bond and restricting protonation of the azo bridge. As a consequence, the overall basicity of the *ortho*-derivative oMRPipAm is reduced in comparison to the *para*-isomer pMRPipAm and of the ester published earlier.[8] In this context, we define Brønsted basicity as the macroscopic property of susceptibility to protonation in dependence of acid concentration, thus being a net effect from the combination of sterics, electron density at the protonation site, and the effective proton concentration in a specific solvent.

Despite the interference of the solvent cage with the intramolecular hydrogen bonding motif a substantial amount of the azonium form coexists with the ammonium form in aqueous acid. Consequently, the intramolecular hydrogen bond of the protonated azo bridge leads to proximity of a proton to the considerably less basic aromatic tertiary amide in *ortho*-position.[2,8,22,24a,b] This arrangement facilitates the catalytic effect of the azo bridge and reduces the activation energy for hydrolysis. This catalytic effect mediated by intramolecular hydrogen bonding cannot occur in the *para*-isomer, which hydrolyses at much lower rates.

2.3. Thermochromism of Copolymers Bearing Tertiary Amides of Methyl Red in Solution

The copolymers POxa, PAAmBP, and PAAm (structures shown in **Scheme 3**) were studied with UV–vis spectroscopy in water, aqueous hydrochloric acid (*completely* protonated at 1.2 M HCl), and in aqueous trifluoroacetic acid (*partially* protonated at 49 mM/0.3 v/v% TFA for the oxazoline copolymer and 13 mM/0.1 v/v% TFA for the HEAm copolymers). PAAm was additionally measured in ethanolic solution.

2.3.1. Neutral

In the neutral state, all dye-containing polymers in solution (ethanol and water) show small blueshifts of the absorption maximum with increasing temperatures that are related to a shift in sub-bands and likely of vibronic origin.[8] This thermochromic behavior is similar to the one of the dye monomers in ethanolic solution. While the neutral monomers are not soluble in water, the polar polymer backbones provide sufficient hydrophilicity to dissolve the dye substituents in aqueous media.

In ethanol, the UV–vis spectra, as well as the derivative spectra of the polymer PAAm, are almost identical to those of the oMRPipAm monomer (cf. Figure 1, Figure S28, Supporting Information). This similarity indicates that incorporation into copolymers does not considerably influence the vibronic thermochromism of this dye.

In aqueous solution, distinct differences are observed in comparison to the ethanolic solution. Only two sub-bands are visible in the vibronic fine-structure of all polymers with a considerably larger energy difference than a single N=N stretching mode (cf. **Table 3**, Figures S28–S31, Supporting Information).[17,18] As described for the monomers in ethanol, resolution of the fine-structure is poor even in the derivative spectra as a consequence of considerable overlap of sub-bands, possibly being influenced by mode mixing.[25]

© 2022 The Authors. Macromolecular Chemistry and Physics published by Wiley-VCH GmbH

15213935, 2022, 21, Downloaded from https://onlinelibrary.wiley.com/doi/10.1002/macp.202200201 by Cochrane Germany, Wiley Online Library on [30/01/2023]. See the Terms and Conditions (https://onlinelibrary.wiley.com/terms-and-conditions) on Wiley Online Library for rules of use; OA articles are governed by the applicable Creative Commons License

Table 3. Absorbance maxima at low temperatures (λ_{max}), wavelength shifts (λ-shift) of the absorbance maxima with temperature increase from around 10 °C to around 50 °C, vibronic sub-bands as determined by derivative spectroscopy ($0–0_{max}$, $0–1_{max}$), and energy difference between the sub-bands ($\tilde{\nu}_{01}$) for the POxa, PAAm, and PAAmBP copolymers in water and the copolymer PAAm in ethanol.

Copolymer	λ_{max} [nm]	λ-shift [nm]	$0–0_{max}$ [nm]	$0–1_{max}$ [nm]	$\tilde{\nu}_{01}$ [cm^{-1}]
POxa	459	459→454	475	423	2590
PAAm aq	448	448→442	477	411	3370
PAAm EtOH	430	430→424	464	424	2030
PAAmBP	458	458→454	473	420	2670

The UV–vis spectra of the two copolymers POxa and PAAmBP in aqueous solution are very similar. In POxa, the absorption maximum blue-shifts from 459 nm at 7.3 °C to 454 nm at 54 °C, while in PAAmBP it shifts from 458 nm at 7.2 °C to 454 nm at 48.3 °C (cf. Table 3, Figures S29a and S36a, Supporting Information). Apart from the wavelength shift of the maximum, the asymmetry of the absorption bands decreases.

The copolymer PAAm with a higher dye substitution (4.3 mol% dye content) than PAAmBP (1.8 mol% dye content) shows some deviation in the UV–vis spectra in aqueous solution compared to PAAmBP. The absorption maximum of PAAm at 7.0 °C lies with 448 nm at shorter wavelengths compared to PAAmBP ($\Delta\lambda = 10$ nm) and blue-shifts upon temperature increase to 442 nm at 48.8 °C.

This may be attributed to the influence of the different degree of dye substitution on the equilibrium conformation of the two polymer types in aqueous solution, which would result in a perichromic effect. The higher dye content in PAAm supports an increased hydrophobic dye–dye interaction. As the core of the polymer coil is more hydrophobic than its periphery in contact with the surrounding aqueous phase the apolar dye side groups would preferably be localized inside the coil. In turn, the amplified hydrophobic environment in the coil core induces a blue shift of the absorption maximum, in agreement with the positive solvatochromism typically observed for push-pull azobenzenes.[26]

2.3.2. Completely Protonated

The completely protonated copolymers in aqueous hydrochloric acid exhibit the same kind of thermochromism as the dye monomer oMRPipAm in aqueous hydrochloric acid (cf. **Figure 5** vs Figure 2). A reversible thermo-tautochromism can be observed in a low-temperature regime, with the absorbance of the ammonium ion at ≈320 nm increasing or stagnating, while the absorbance of the azonium ion at ≈510 nm decreases upon temperature increase. Above a threshold temperature, irreversible changes owing to hydrolysis occur, releasing protonated *o*-methyl red.

While PAAm and PAAmBP exhibit similar threshold temperatures to oMRPipAm, with irreversible changes becoming apparent at temperatures between 35 and 40 °C, the 2-oxazoline copolymer POxa shows noticeable hydrolysis only at around 60 °C.

Another striking difference between the three *completely* protonated systems PAAm, POxa, as well as oMRPipAm is the ratio of the ammonium ions and the azonium ions in aqueous hydrochloric acid at room temperature. For POxa, the absorbance of the ammonium ion is stronger than that of the azonium ion, while for PAAm the absorption band of the azonium ion is more intense. For the monomer oMRPipAm, the absorption bands are about equal under these conditions (cf. Figure S34, Supporting Information). As the electronic structure of the chromophore is essentially the same for the polyacrylamides, the polyoxazoline, and the monomer, and since the liquid medium is composed of water as solvent and HCl as acid (1.2 M) in all cases, the different behaviors must result from other influences.

The only factor differing between the systems is the local environment provided by the substituents. Thus, in the macromolecular systems, a perichromic effect originates from the polymer chains, which strongly affects the ammonium-azonium tautomerism. This perichromic effect is most likely a consequence of different possibilities of hydrogen bonding with the chromophore in the two types of copolymers. While the polyacrylamides contain secondary amide, as well as alcohol groups and thus exhibit characteristics of both hydrogen bond donors and hydrogen bond acceptors, the polyoxazoline contains only tertiary amides, which can only act as hydrogen bond acceptors.

Consequently, these tertiary amide groups may interact with the hydrogen of the ammonium group, thus stabilizing this tautomer. The azonium ion is already engaged in an intramolecular hydrogen bonding motif with considerable steric requirements (cf. Figure 4, structures II–V), and therefore hydrogen bonding with the polyoxazoline backbone is less favorable. The stabilization via the POxa backbone leads to a higher population of the ammonium tautomer and decreases susceptibility of the tertiary amide linkage of the chromophore to hydrolysis. By this perichromic effect, the proton concentration at the amide linkage is reduced and the charge more localized, leading to a reduction in the hydrolysis rate with the associated irreversible changes only becoming apparent at higher temperatures.

The reasoning for the higher ratio of azonium to ammonium ions in PAAm is also based on perichromism. The secondary amide and alcohol hydrogen bond donors of the PAAm chain are weaker than water. Therefore, less interference with the intramolecular hydrogen bonding of the azonium form is expected, shifting the tautomeric equilibrium slightly toward the azonium ion compared to the case of the monomer in aqueous HCl.

For the POxa copolymer, not only hydrolysis of the dye but also of the ethyl amide side groups may occur, as especially poly(2-methyl-2-oxazoline), which is the main constituent of the copolymer, is prone to acidic hydrolysis at higher temperatures.[27] To determine the susceptibility to acidic hydrolysis of either comonomer, the copolymer was heated in aqueous hydrochloric acid (1.2 M, 60 °C) for 20 h. The acid treatment resulted in about half of the ethyl amides being hydrolyzed, while only a negligible part of the dye side groups was hydrolyzed (cf. Figures S13 and S14, Supporting Information), as determined by ^{1}H NMR spectroscopy. Yet, it becomes apparent that the ethyl amides are considerably more susceptible to hydrolysis than the dye side groups. This may be exploited as a route to linear polyethylenimine with a controllable degree of substitution with dye molecules.

A van't Hoff analysis (cf. **Table 4** and detailed discussion in Supporting Information) shows that the polyacrylamides have similar thermochromicity parameters (enthalpy of proton

 © 2022 The Authors. Macromolecular Chemistry and Physics published by Wiley-VCH GmbH

15213935, 2022, 21, Downloaded from https://onlinelibrary.wiley.com/doi/10.1002/macp.202200201 by Cochrane Germany, Wiley Online Library on [30/01/2023]. See the Terms and Conditions (https://onlinelibrary.wiley.com/terms-and-conditions) on Wiley Online Library for rules of use; OA articles are governed by the applicable Creative Commons License

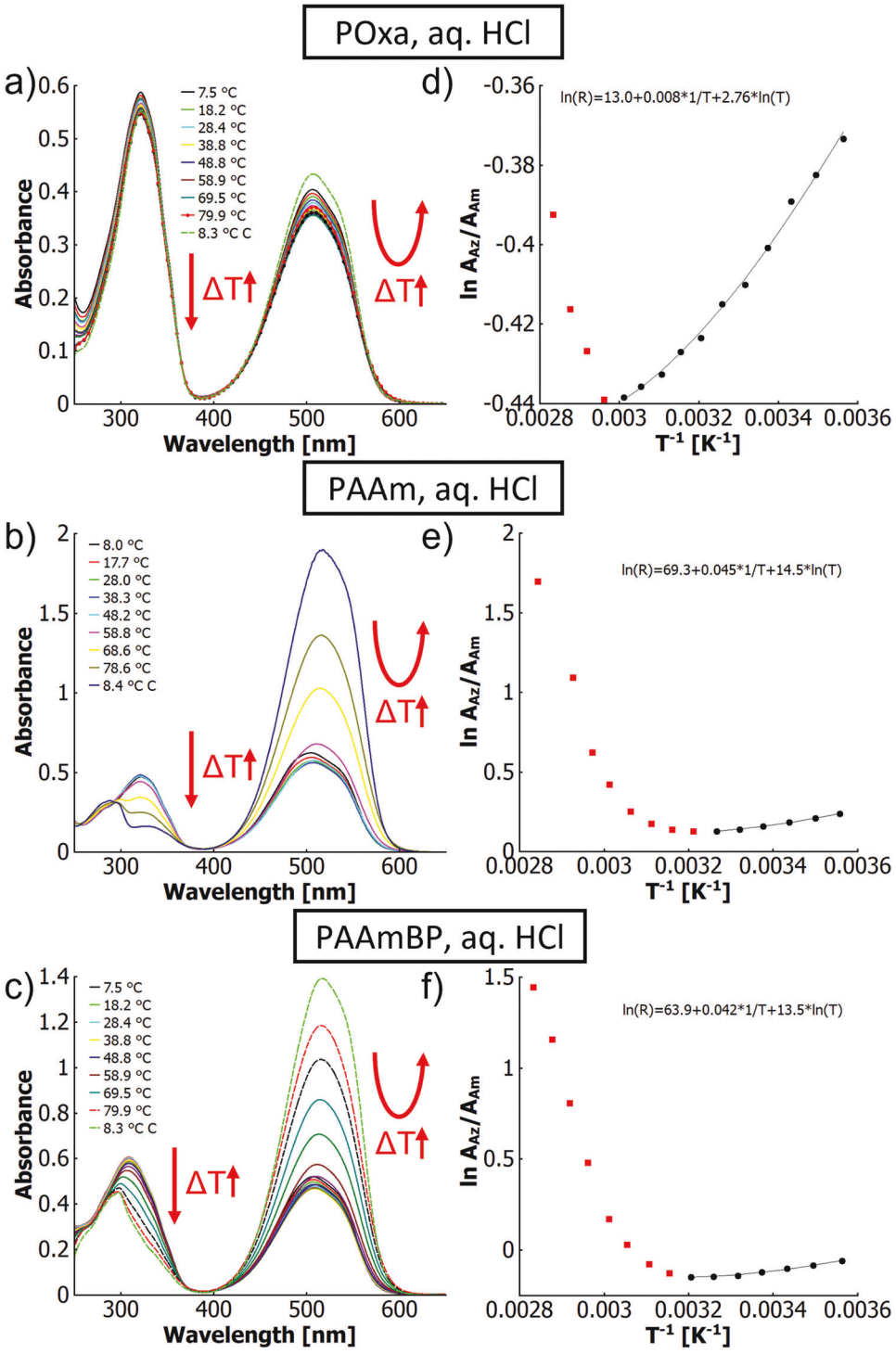

Figure 5. Temperature-dependent UV–vis spectra in aqueous HCl (1.2 M) of a) poly(MeOxa-co-oMROxa) (POxa, 0.1 g L^{-1}), b) poly(HEAm-co-oMRPipAm) (PAAm, 0.1 g L^{-1}), and c) poly(HEAm-co-oMRPipAm-co-BPAAm (PAAmBP, 0.2 g L^{-1}), as well as corresponding van't Hoff plots of the natural logarithm of absorbance ratios R of the azonium ion and the ammonium ion versus the inverse absolute temperature for d) POxa, e) PAAm, and f) PAAmBP, the reversible regimes fitted with a function $\ln(R) = a - b*1/T + c*\ln(T)$.

© 2022 The Authors. Macromolecular Chemistry and Physics published by Wiley-VCH GmbH

15213935, 2022, 21, Downloaded from https://onlinelibrary.wiley.com/doi/10.1002/macp.202200201 by Cochrane Germany, Wiley Online Library on [30/01/2023]. See the Terms and Conditions (https://onlinelibrary.wiley.com/terms-and-conditions) on Wiley Online Library for rules of use; OA articles are governed by the applicable Creative Commons License

Table 4. Overview of the relevant parameters obtained from van't Hoff analyses of thermochromic solutions of copolymers bearing tertiary amides of *o*-methyl red and fully protonated oMRPipAm.

Copolymer	Protonation	Abs. Ratio [nm]	ΔH_0 [kJ mol^{-1}]	ΔC_p [kJ mol^{-1} K^{-1}]	Linearity factor [°C]
POxa	Partial	319/430	15	0.05	62
POxa	Partial	542/430	34	0.11	40
POxa	Partial	542/319	11	0.04	15
PAAm	Partial	319/415	24	0.08	37
PAAm	Partial	539/415	35	0.12	39
PAAm	Partial	539/319	18	0.06	45
PAAmBP	Partial	305/415	24	0.08	43
PAAmBP	Partial	542/415	48	0.16	32
PAAmBP	Partial	542/305	27	0.09	34
oMRPipAm	Complete	516/323	38	0.13	18
POxa	Complete	506/321	7	0.02	44
PAAm	Complete	516/323	36	0.12	24
PAAmBP	Complete	516/323	33	0.11	20

transfer ΔH_0 and heat capacity of tautomerization ΔC_p) as the dye monomer in aqueous hydrochloric acid and that larger values indicate a higher tendency for hydrolysis.

2.3.3. Partially Protonated

Partial protonation of the *ortho*-monomer was not achieved as the neutral form is insoluble in water. Yet, as stated above, the polymeric versions are soluble in aqueous media as the backbones are hydrophilic enough to allow solubilization of even the hydrophobic, neutral form.

For the *partially* protonated copolymers, the thermochromic behavior becomes more complex with hydrolysis taking place concurrently with thermo-halochromism. In addition, thermotautochromism exists but is superimposed by the thermo-halochromic phenomena and thus cannot be distinguished. In the temperature-dependent ammonium-azonium tautomerism, azonium ions are transformed into ammonium ions, while in thermo-halochromism the protonated species are deprotonated to the benefit of the neutral species. Consequently, both processes deplete the azonium ion content at low temperatures, while thermo-halochromism depletes both the ammonium and the azonium species.

The UV–vis spectra and the corresponding difference spectra show for all three copolymers POxa, PAAm, and PAAmBP below their threshold temperatures that the absorbance of the ammonium ion (≈320 nm) and the azonium ion (≈510 nm) decrease upon temperature increase (cf. **Figure 6**). At the same time, the absorbance corresponding to the neutral species (≈400 nm) increases. The polyacrylamides show a stronger reduction in the azonium absorbance in the difference spectra, while the polyoxazoline shows a stronger decrease in the ammonium absorbance (cf. Figure 6d–f).

From a ratiometric approach involving the three components of the equilibrium (ammonium ion, azonium ion, neutral dye), two main conclusions can be drawn: 1) The equilibrium between the protonated and neutral species in thermo-halochromism is not shifted by hydrolysis, only the overall concentration of the tertiary amides is reduced. This follows from the graph of the ratio of ammonium ions to neutral species against temperature, which varies continuously with temperature for all three copolymers even above the threshold temperature of hydrolysis (cf. Figures S38a, S40a, and S41a, Supporting Information). If hydrolysis would have an effect on the equilibrium, a discontinuous curve progression would be expected. In the molecular picture, this is explained by the hydrolysis product, *o*-methyl red, not taking part in the thermo-halochromic equilibrium.

2) The hydrolysis occurs at lower temperatures in the *partially* protonated state than in the *fully* protonated state. This can be concluded from the graphs of the azonium-ammonium absorbance ratio (cf. Figures S38c, S40c, and S41c, Supporting Information), which show a 5 K lower threshold temperature in the *partially* protonated state compared to the *fully* protonated form for the polyacrylamides and a drop by about 20 K for the polyoxazoline. Based on the existing literature, this may be explained by the hydrolysis mechanisms differing slightly between high and low acid concentrations.[21,22,28,29]

A more detailed discussion of the ratiometric graphs and van't Hoff analysis of the *partially* protonated case is provided in the Supporting Information.

The reversibility of thermo-halochromism in *partially* protonated systems was investigated in the same manner as for the *completely* protonated monomer oMRPipAm (cf. Figures 2 and **7**). Solutions of POxa and PAAmBP were heated to 28.5 °C, which is below the threshold temperature and cooled to 7.5 °C to analyze the reversible part of thermochromism in these systems. Subsequently, they were heated well above the threshold temperature and cooled to 7.5 °C again to visualize the irreversible features. The measurements show that thermo-halochromism for POxa and PAAmBP is fully reversible below the threshold temperature. Yet above this temperature, reversibility is affected by the concurrent hydrolysis reducing the overall tertiary amide concentration, as stated above.

Hydrolysis of PAAmBP proceeds quantitatively in both *completely* and *partially* protonated cases for PAAmBP when heating

© 2022 The Authors. Macromolecular Chemistry and Physics published by Wiley-VCH GmbH

15213935, 2022, 21, Downloaded from https://onlinelibrary.wiley.com/doi/10.1002/macp.202200201 by Cochrane Germany, Wiley Online Library on [30/01/2023]. See the Terms and Conditions (https://onlinelibrary.wiley.com/terms-and-conditions) on Wiley Online Library for rules of use; OA articles are governed by the applicable Creative Commons License

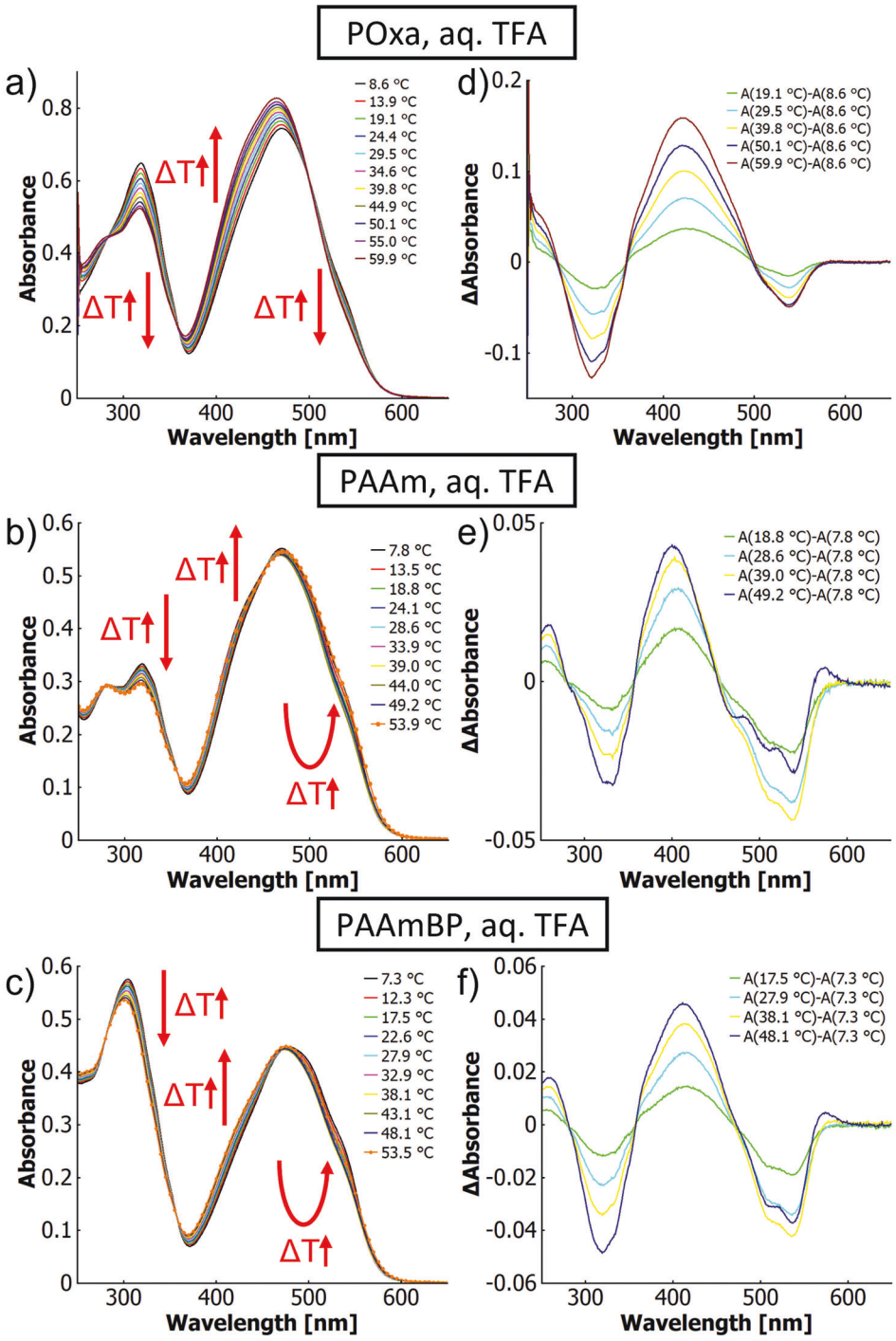

Figure 6. Temperature-dependent UV–vis spectra in aqueous trifluoroacetic acid of a) poly(MeOxa-co-oMROxa) (POxa, 0.1 g L^{-1}, 0.3 v/v% TFA), b) poly(HEAm-co-oMRPipAm) (PAAm, 0.1 g L^{-1}, 0.1 v/v% TFA), and c) poly(HEAm-co-oMRPipAm-co-BPAAm (PAAmBP, 0.2 g L^{-1}, 0.1 v/v% TFA), as well as corresponding difference spectra calculated by subtracting the spectrum at the lowest temperature from those at higher temperatures for d) POxa, e) PAAm, and f) PAAmBP.

for 18 h to 60 °C and only protonated *o*-methyl red remains (cf. **Figure 8**). In the experiment, this hydrolysis is observed as an irreversible color switch of both the dark orange solution of the *partially* protonated system and of the weakly pink solution of the *completely* protonated system changing into intensely colored pink solutions. Photographic evidence for the color changes is provided in the Supporting Information (cf. Figures S32 and S33, Supporting Information).

© 2022 The Authors. Macromolecular Chemistry and Physics published by Wiley-VCH GmbH

15213935, 2022, 21, Downloaded from https://onlinelibrary.wiley.com/doi/10.1002/macp.202200201 by Cochrane Germany, Wiley Online Library on [30/01/2023]. See the Terms and Conditions (https://onlinelibrary.wiley.com/terms-and-conditions) on Wiley Online Library for rules of use; OA articles are governed by the applicable Creative Commons License

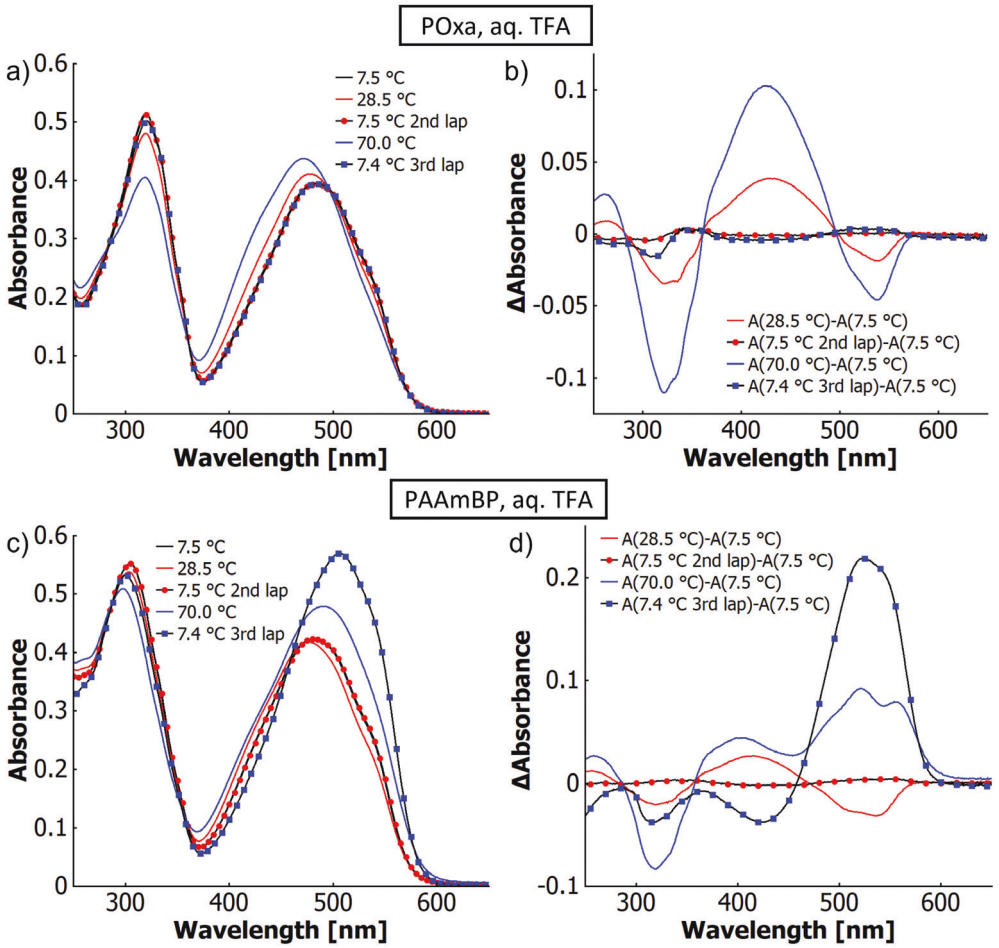

Figure 7. UV–vis spectra in aqueous TFA of a) poly(MeOxa-co-oMROxa) (0.1 g L^{-1}, 0.3 v/v% TFA), and b) poly(HEAm-co-oMRPipAm-co-BPAAm) (0.2 g L^{-1}, 0.1 v/v% TFA) from a temperature series starting at 7.5 °C, heating to 28.5 °C, cooling to 7.5 °C, ramping to 70.0 °C and holding for 20 min, before cooling back to 7.4 °C. The corresponding difference spectra were generated by subtracting a spectrum at low temperatures without heat treatment from the other spectra in the measurement series of c) poly(MeOxa-co-oMROxa) and d) poly(HEAm-co-oMRPipAm-co-BPAAm).

2.4. Thermochromism in Photocrosslinked, Swollen Gels of PAAmBP

Hydrogels of crosslinked PAAmBP exhibit the same thermochromic mechanisms as the corresponding solutions of the non-crosslinked polymer in the neutral and *completely* protonated state but show distinct differences in the specific thermochromic behaviors. They were obtained by photocrosslinking the PAAmBP copolymer at 254 nm (8.6 J cm^{-2}) and subsequent swelling in water. Attachment of the gels to a surface proved to be challenging. Ultimately, plates of tissue-culture grade polystyrene were treated with a Corona discharge to increase the surface hydrophilicity followed by drop-casting of the copolymer solution, drying, and finally UV-irradiation. Of note is that photocrosslinking at 254 nm led to attachment of the polymer film, while photocrosslinking at 302 nm yielded a hydrogel that delaminated from the surface upon swelling with water.

Some general differences between the UV–vis spectra of gels and of solutions exist. Owing to the fixation of the dyes in the gels, thermal expansion does not affect the number of dye molecules in the irradiated volume dramatically, in contrast to solutions. However, slight movement of the rather inhomogeneous films may lead to drastic changes in the absorbance. Also, the spectra are affected by the generally poorer optical quality of the hydrogels, as they scatter light to a certain degree even when swollen. In an attempt to counteract the scattering effect, all spectra were subjected to a basic baseline correction by subtracting the absorbance value at 650 nm from all data points.

The water-swollen, neutral PAAmBP gel shows features of vibronic thermochromism, with the wavelength at maximum shifting from 451 nm at 8.8 °C to 444 nm at 48.7 °C (cf. Figure S42, Supporting Information). This maximum is blue-shifted compared to the aqueous copolymer solution with a maximum at 458 nm at low temperatures and is closer in wavelength to the maximum of PAAm at 448 nm in aqueous solution. The blueshift is likely a consequence of the local environment of the dye becoming more hydrophobic owing to a substantially larger polymer volume fraction in the hydrogel than in solution.

When the *completely* protonated gels in aqueous hydrochloric acid are heated, the absorbance corresponding to the azonium ion at ≈500 nm decreases, while that of the ammonium ion at ≈320 nm increases below a certain threshold temperature. When

© 2022 The Authors. Macromolecular Chemistry and Physics published by Wiley-VCH GmbH

15213935, 2022, 21, Downloaded from https://onlinelibrary.wiley.com/doi/10.1002/macp.202200201 by Cochrane Germany, Wiley Online Library on [30/01/2023]. See the Terms and Conditions (https://onlinelibrary.wiley.com/terms-and-conditions) on Wiley Online Library for rules of use; OA articles are governed by the applicable Creative Commons License

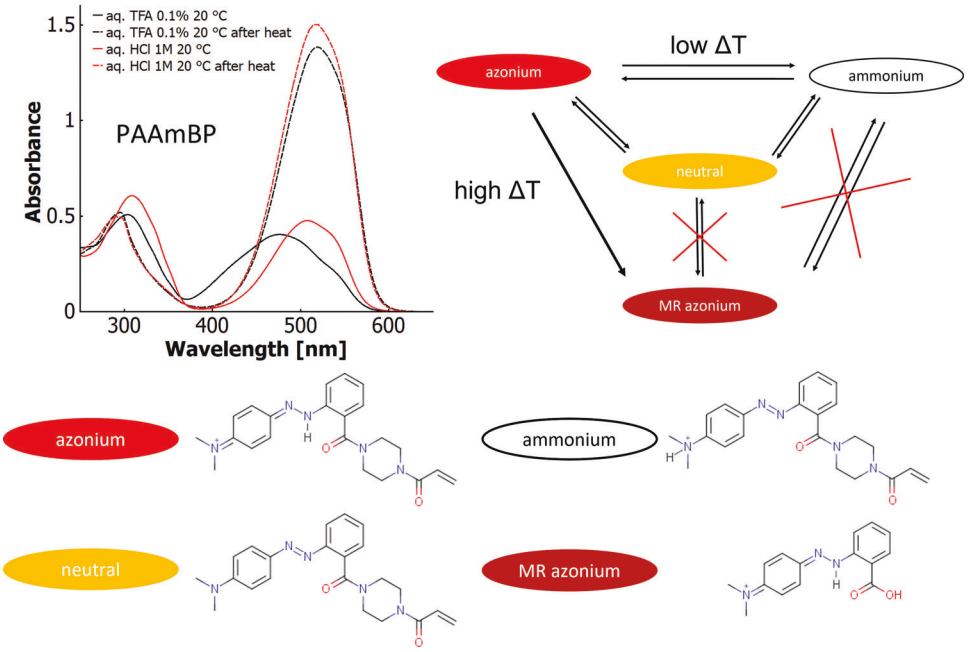

Figure 8. Left: UV–vis spectra of poly(HEAm-co-oMRPipAm-co-BPAAm) (PAAmBP, 0.2 g L^{-1}) in aqueous trifluoroacetic acid (partially protonated, black, 0.1 v/v%) and in aqueous hydrochloric acid (fully protonated, red, 1 M) at 20 °C of the fresh solution (solid line) and after heating the solution to 60 °C for 18 h (dashed line). Right: Sketch of the protonation equilibria involved in the thermochromic processes of these tertiary *o*-methyl red amides.

this threshold temperature is exceeded, an irreversible increase in absorbance at 516 nm, along with a decrease in absorbance at 320 nm, occurs. The thermochromic behavior of the ammonium-azonium tautomerism below the threshold temperature and the hydrolysis of the dye follows that of the copolymer in solution (cf. **Figure 9**a,c).

However, there are two distinct differences. First, the slide with the gel can simply be removed from the solvent, leaving only the protonated hydrolysis product *o*-methyl red in solution, allowing convenient tracking of released dye (cf. Figure S44, Supporting Information). Photographs of this process are provided in the Supporting Information (cf. Figure S45, Supporting Information). Second, the threshold temperature for irreversible change is considerably higher in the gel. The limited optical quality of the gels renders a ratiometric approach challenging. Consequently, to determine the threshold temperature the absorbance at the maximum corresponding to the azonium ion was plotted against the temperature (cf. Figure 9b,d). While the minimum of this plot is around 40 °C for the dissolved copolymer PAAmBP, for the corresponding gel a minimum is only reached well above 60 °C. This may be a consequence of the more hydrophobic and considerably more crowded environment in the polymer network, impeding mobility of the attached dye and in turn reducing the reaction rate.

3. Summary and Conclusion

In summary, we developed novel azo dye monomers based on *o*-methyl red featuring an acrylamide or a 2-oxazoline moiety as polymerizable units with the aim of constructing polymer architectures, which feature a tertiary amide linkage with the chromophore.

Acrylamide copolymers were successfully obtained by free radical copolymerization of the tertiary amide *o*-methyl red piperazine acrylamide with *N*-hydroxyethyl acrylamide. Additionally, 4-benzophenone acrylamide could be integrated in these polymers as photocrosslinking unit to allow the preparation of polymer networks by irradiation with UV-light, which yielded hydrogels upon subsequent swelling with water. Cationic ring-opening copolymerization of 2-methyl-2-oxazoline with 2-*o*-methyl red-2-oxazoline provided the corresponding azo dye poly-2-oxazoline.

The thermochromic behavior was studied for all monomers, the copolymers, and the hydrogel under neutral and acidic conditions in order to learn about the specific effect of the characteristic structural motif with tertiary amide linkage in *ortho*-position on the optical response of the chromophore. In acidic aqueous environment, all protonated tertiary amide systems (thus, excluding the 2-oxazoline monomer) with the *ortho*-derivative of methyl red show an unusually strong preference for the colorless ammonium form in the ammonium-azonium equilibrium, owing to intramolecular hydrogen bonding motifs involving the protonated azo bridge and the tertiary amide functionality in *ortho*-position.

In these systems, two peculiar manifestations of thermochromic behavior were observed. First, upon heating, the ammonium-azonium tautomerism reversibly shifts further toward the ammonium ion up to a threshold temperature. We termed this reversible shift "thermo-tautochromism." Second, owing to hydrolysis, irreversible changes become apparent by liberation of the parent dye *o*-methyl red above this threshold temperature. This hydrolysis dominates at unusually low temperatures (below 40 °C for the monomer oMRPipAm and its copolymers) and results in a strong and irreversible color change originating from the liberated *o*-methyl red, whose

 © 2022 The Authors. Macromolecular Chemistry and Physics published by Wiley-VCH GmbH

15213935, 2022, 21, Downloaded from https://onlinelibrary.wiley.com/doi/10.1002/macp.202200201 by Cochrane Germany, Wiley Online Library on [30/01/2023]. See the Terms and Conditions (https://onlinelibrary.wiley.com/terms-and-conditions) on Wiley Online Library for rules of use; OA articles are governed by the applicable Creative Commons License

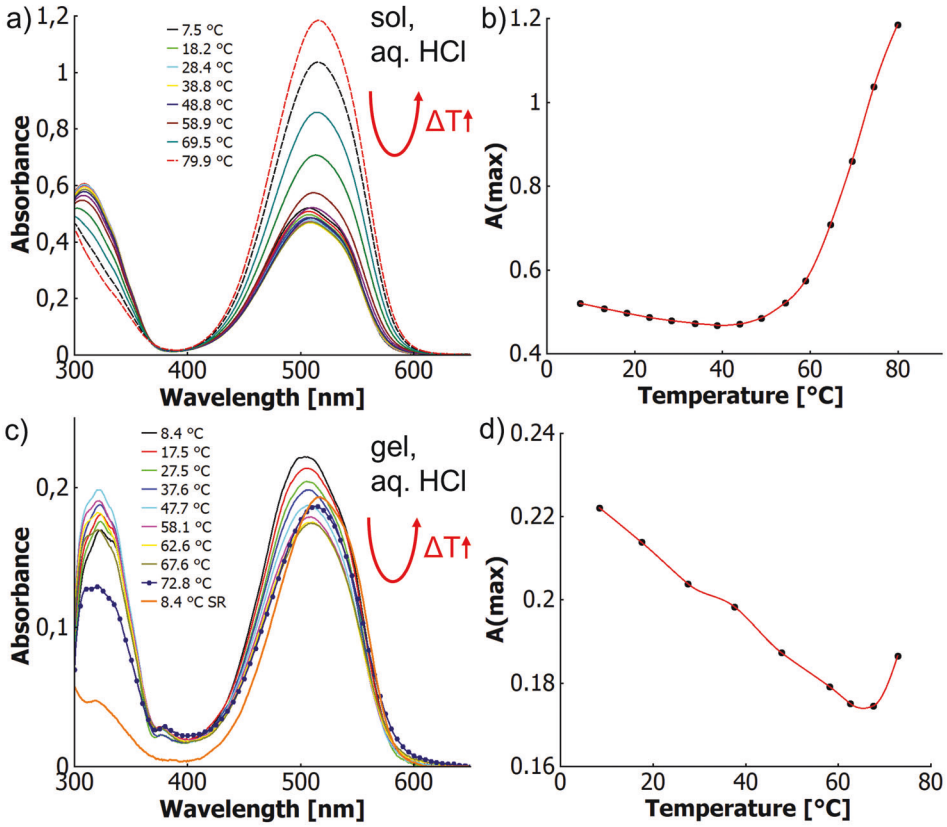

Figure 9. UV–vis spectra of poly(HEAm-co-oMRPipAm-co-BPAAm) in aqueous HCl (1.2 M) as a) solution (0.2 g L^{-1}) and c) a photocrosslinked, swollen gel, as well as corresponding graphs of the absorbance at maximum versus the temperature for b) the polymer in solution and d) the photocrosslinked, swollen gel. The red lines in (b,d) were generated by non-rounded Akima extrapolation and serve only as guide to the eye. "SR" ("slide removed") in the legend of (c) refers to the slide being removed, which is colorless at this point, leaving only the liberated dye.

ammonium-azonium tautomerism lies strongly on the side of the red azonium form.

The nature of the copolymer architecture has a profound influence on the onset of hydrolysis, with the polyoxazoline showing a considerably higher threshold temperature than the polyacrylamides. This is attributed to favorable hydrogen bonding between the dye and the polyoxazoline backbone, stabilizing the ammonium tautomer. In the polyacrylamide hydrogel, a higher threshold temperature than in the corresponding polymer solution is observed. Here, it is likely a consequence of the conformationally restrictive environment of the polymer network.

Partially protonated systems show overlap of the ammonium-azonium tautomerism and the more dominant thermohalochromism that is a consequence of the protonation equilibrium shifting toward the neutral azo dye upon temperature increase. However, even at these lower acid concentrations hydrolysis becomes dominant above a threshold temperature.

Here, we found a strong influence of the dye structure and environment via characteristic hydrogen bonding motifs on thermochromism and hydrolysis under mild conditions. These findings bear great potential for various fields, for example, in organic chemistry for novel protecting groups for secondary amines, which can be cleaved under fairly mild conditions mediated by specific hydrogen bonding motifs. The relevance for physical chemistry lies in the description of a new thermochromic mechanism based on thermo-tautochromism. The new dye monomers are of great interest for polymer chemistry, specifically for CROP to obtain dye-substituted PEI. The dye substituents serve as optical reporter to study spectroscopically the influence of the polymer architecture on reactions occurring at the side groups. The irreversibility of the observed thermochromism may be further explored in polymeric temperature-time-tags for potential application in food or drug storage and transport.

Supporting Information

Supporting Information is available from the Wiley Online Library or from the author.

Acknowledgements

The authors thank the Faculty IV of the University of Siegen for funding and Dr. Thomas Paululat for NMR-measurements.

Open access funding enabled and organized by Projekt DEAL.

Conflict of Interest

The authors declare no conflict of interest.

 © 2022 The Authors. Macromolecular Chemistry and Physics published by Wiley-VCH GmbH

15213935, 2022, 21, Downloaded from https://onlinelibrary.wiley.com/doi/10.1002/macp.202200201 by Cochrane Germany, Wiley Online Library on [30/01/2023]. See the Terms and Conditions (https://onlinelibrary.wiley.com/terms-and-conditions) on Wiley Online Library for rules of use; OA articles are governed by the applicable Creative Commons License

Data Availability Statement

The data that support the findings of this study are available in the Supporting Information of this article.

Keywords

azobenzene, hydrolysis, methyl red, tautochromism, tertiary amide, thermochromism

Received: June 22, 2022
Revised: August 5, 2022
Published online: September 14, 2022

[1] a) E. Sawicki, *J. Org. Chem.* **1957**, *22*, 365; b) H. H. Jaffé, S.-J. Yeh, R. W. Gardner, *J. Mol. Spectrosc.* **1958**, *2*, 120; c) S.-J. Yeh, H. H. Jaffé, *J. Am. Chem. Soc.* **1959**, *81*, 3283; d) S. Yamamoto, N. Nishimura, S. Hasegawa, *Bull. Chem. Soc. Jpn.* **1973**, *46*, 194.
[2] E. Sawicki, *J. Org. Chem.* **1957**, *22*, 621.
[3] T. Stoyanova, S. Stoyanov, L. Antonov, V. Petrova, *Dyes Pigm.* **1996**, *31*, 1.
[4] J. H. Day, *Chem. Rev.* **1963**, *63*, 65.
[5] A. Seeboth, D. Lötzsch, R. Ruhmann, O. Muehling, *Chem. Rev.* **2014**, *114*, 3037.
[6] a) I. Y. Bershtein, O. F. Ginzburg, *Russ. Chem. Rev.* **1972**, *41*, 97; b) M. Nepraš, M. Titz, M. Nečas, S. Luňák, R. Hrdina, A. Lyčka, *Collect. Czech. Chem. Commun.* **1988**, *53*, 213; c) E. Fischer, Y. F. Frei, *J. Chem. Soc.* **1959**, 3159; d) H. Joshi, F. S. Kamounah, G. van der Zwan, C. Gooijer, L. Antonov, *J. Chem. Soc., Perkin Trans. 2* **2001**, *12*, 2303.
[7] a) T. A. Khattab, B. D. B. Tiu, S. Adas, S. D. Bunge, R. C. Advincula, *RSC Adv.* **2016**, *6*, 102296; b) M. S. Abdelrahman, T. A. Khattab, S. Kamel, *New J. Chem.* **2021**, *45*, 5382; c) T. A. Khattab, M. E. El-Naggar, M. S. Abdelrahman, A. Aldalbahi, M. R. Hatshan, *Chemosensors* **2020**, *8*, 132.
[8] T. G. Jaik, B. Ciubini, F. Frascella, U. Jonas, *Polym. Chem.* **2022**, *13*, 1186.
[9] a) M. T. Zarka, O. Nuyken, R. Weberskirch, *Chemistry* **2003**, *9*, 3228; b) M. N. Holerca, V. Percec, *Justus Liebigs Ann. Chem.* **2000**, *12*, 2257.
[10] V. O. F. Olaj, J. W. Breitenbach, I. Hofreiter, *Makromol. Chem.* **1967**, *110*, 72.
[11] O. F. Olaj, J. W. Breitenbach, I. Hofreiter, *Monatsh. Chem.* **1967**, *98*, 997.
[12] V. O. F. Olaj, J. W. Breitenbach, I. Hofreiter, *Makromol. Chem.* **1966**, *91*, 264.
[13] V. D. Braun, G. Arcache, R. J. Faust, W. Neumann, *Makromol. Chem.* **1968**, *114*, 51.
[14] D. Braun, G. Arcache, *Makromol. Chem.* **1971**, *148*, 119.
[15] L. Antonov, D. Nedeltcheva, *Chem. Soc. Rev.* **2000**, *29*, 217.
[16] Š. Sršeň, J. Sita, P. Slavíček, V. Ladányi, D. Heger, *J. Chem. Theory Comput.* **2020**, *16*, 6428.
[17] S.-K. Park, C.-K. Lee, K.-C. Min, N.-S. Lee, *Bull. Korean Chem. Soc.* **2004**, *25*, 1817.
[18] S. Bell, A. Bisset, T. J. Dines, *J. Raman Spectrosc.* **1998**, *29*, 447.
[19] G. E. Lewis, *Tetrahedron* **1960**, *10*, 129.
[20] a) W. John, *Angew. Chem.* **1947**, *59*, 188; b) C. Reichardt, *J. Org. Chem.* **2022**, *87*, 1616.
[21] R. A. Cox, *Can. J. Chem.* **2008**, *86*, 290.
[22] C. R. Smith, K. Yates, *J. Am. Chem. Soc.* **1971**, *93*, 6578.
[23] G. Seu, *Dyes Pigm.* **1995**, *29*, 227.
[24] a) J. T. Edward, H. S. Chang, K. Yates, R. Stewart, *Can. J. Chem.* **1960**, *38*, 1518; b) K. M. Tawarah, H. M. Abu-Shamleh, *Dyes Pigm.* **1991**, *17*, 203.
[25] a) A. M. Mebel, M. Hayashi, K. K. Liang, S. H. Lin, *J. Phys. Chem. A* **1999**, *103*, 10674; b) A. Baiardi, J. Bloino, V. Barone, *J. Chem. Theory Comput.* **2013**, *9*, 4097.
[26] a) C. Reichardt, *Solvents and Solvent Effects in Organic Chemistry*, 3rd ed., Wiley-VCH, Weinheim **2003**; b) M. G. Hutchings, P. Gregory, J. S. Campbell, A. Strong, J.-P. Zamy, A. Lepre, A. Mills, *Chemistry* **1997**, *3*, 1719.
[27] a) H. M. L. Lambermont-Thijs, F. S. Van Der Woerdt, A. Baumgaertel, L. Bonami, F. E. Du Prez, U. S. Schubert, R. Hoogenboom, *Macromolecules* **2010**, *43*, 927; b) M. H. Litt, C. S. Lin, *J. Polym. Sci., Part A: Polym. Chem.* **1992**, *30*, 779.
[28] A. Williams, *J. Am. Chem. Soc.* **1976**, *98*, 5645.
[29] C. R. Smith, K. Yates, *J. Am. Chem. Soc.* **1972**, *94*, 8811.

 © 2022 The Authors. Macromolecular Chemistry and Physics published by Wiley-VCH GmbH

15213935, 2022, 21, Downloaded from https://onlinelibrary.wiley.com/doi/10.1002/macp.202200201 by Cochrane Germany, Wiley Online Library on [30/01/2023]. See the Terms and Conditions (https://onlinelibrary.wiley.com/terms-and-conditions) on Wiley Online Library for rules of use; OA articles are governed by the applicable Creative Commons License

Macromolecular Chemistry and Physics

Supporting Information

for *Macromol. Chem. Phys.*, DOI 10.1002/macp.202200201

Thermo-Tautochromic Polymer Architectures from Tertiary Methyl Red Amides

Thorben G. Jaik and Ulrich Jonas**

Electronic Supporting Information (ESI)

Thermo-Tautochromic Polymer Architectures from Tertiary Methyl Red Amides

Thorben Jaik; Ulrich Jonas*

[1] Department Chemistry - Biology, University of Siegen, Adolf-Reichwein-Strasse 2, D-57076, Siegen, Germany

*Corresponding author: Prof. Dr. Ulrich Jonas, jonas@chemie.uni-siegen.de

This document contains experimental details like syntheses and sample preparations, additional optical analysis data, graphs from the van't Hoff analyses, etc.

Experimentals

Materials and equipment:

All solvents used were of Milli-Q®, spectroscopic or HPLC-grade. Absolute ethanol and anhydrous acetonitrile were purchased from VWR Chemicals. Tetrahydrofurane was dried and distilled over potassium. Trifluoroacetic acid was purchased from Carl Roth (Germany) in PEPTIPURE® ≥99,9% quality. Hydrochloric acid (37%, Anal. Reag. Gr., Fisher Chemical), o-methyl red (Alfa Aesar), carbonyldiimidazole (97%, Alfa Aesar), *N*-hydroxyethyl acrylamide (97%, Sigma Aldrich), 2-chloroethylamine hydrochloride (Alfa Aesar, 98+%), piperazine (Alfa Aesar, anhydrous, 99%, stored in glove box), and acryloylchloride (Alfa Aesar, 96%) were used as received. 1,8-Diazabicyclo[5.4.0]undec-7-ene was dried over calciumchloride (anhydrous, technical, Bernd Kraft) and distilled *in vacuo*. 2-Methyl-2-oxazoline and methyl triflate were distilled *in vacuo*. Potassium carbonate (reinst, Bernd Kraft) was stored in a drying oven (130 °C). Triethylamine was used as received (ChemSolute, puriss) for column chromatography or distilled *in vacuo* for synthesis. Azobisisobutyronitrile was recrystallised from methanol. 4-Benzophenoneacrylamide was synthesized according to literature.[1] *para*-Methyl red was synthesized according to a procedure we published recently.[2]

UV-vis measurements were performed on a Thermo Scientific™ Evolution™ 220 UV-Vis-spectrophotometer. If not stated otherwise, the measurements were done with 100 nm/min and a resolution of 1 nm.
NMR-measurements were performed on either a Bruker AV 400 or a Jeol EZC 500. Detailed assignments of peaks are given in the ESI in the corresponding spectra.
GPC/SEC was measured on a PSS GRAM linM column (Polymer Standards Service GmbH, Mainz, Germany) in dimethylacetamide with LiBr (0.1 g L^{-1}) at 60 °C with PMMA-standards as reference.

Synthesis of o-methyl red imidazolide:
Methyl red (1 mol eq.) was dissolved in tetrahydrofuran (0.1 mmol L^{-1}), carbonyldiimidazole (1.8 mol eq.) was added and the solution was stirred until no more gas evolution occurred, typically overnight or for three hours at 45 °C. The solution was used without purification for further syntheses. (Adapted from literature[3])

Synthesis of N-(2-chloroethyl)-2-[(1E)-2-[4-(dimethylamino)phenyl]diazen-1-yl]benzamide (o-methyl red chloroethylamide, MREtCl):
To a solution of o-methyl red imidazolide (5020 mg, $1.9*10^{-2}$ mol o-methyl red) in tetrahydrofuran (140 mL), chloroethylamine hydrochloride (3424 mg, $3.0*10^{-2}$ mol) and triethylamine (5 mL, $3.6*10^{-2}$ mol) were added and the reaction mixture was stirred for 46 hours. The organic solvent was removed *in vacuo* and the resulting solid was extracted with water overnight. The residual solid was purified *via* a short silica column in dichloromethane.
The yield was 5402 mg or 88%.

δH(500 MHz, $CDCl_3$) 9.64 (s, 1H, CO-N*H*), 8.39 (dd, J = 7.8, 1.6 Hz, 1H, Ph-*H*), 7.87 (d, J = 9.2 Hz, 2H, Ph-*H*), 7.80 (dd, J = 8.1, 1.3 Hz, 1H, Ph-*H*), 7.52 (ddt, J = 8.6, 3.1, 1.5 Hz, 1H, Ph-*H*), 7.47 (ddt, J = 8.6, 2.8, 1.4 Hz, 1H, Ph-*H*), 6.76 (d, J = 9.2 Hz, 2H, Ph-*H*), 3.91 (q, J = 5.6 Hz, 2H, CO-NH-CH_2), 3.77 (t, J = 5.6 Hz, 2H, Cl-CH_2), 3.12 (s, 6H, $N(Me)_2$).
δC(126 MHz, $CDCl_3$) 166.56 (*C*ONH), 153.31 (Ph), 150.70 (Ph), 143.43 (Ph), 132.01 (Ph), 131.49 (Ph), 129.51 (Ph), 128.94 (Ph), 126.13 (Ph), 116.15 (Ph), 111.66 (Ph), 44.48 (Cl-CH_2), 42.11 (CONH-*C*H_2), 40.36 ($N(Me)_2$).

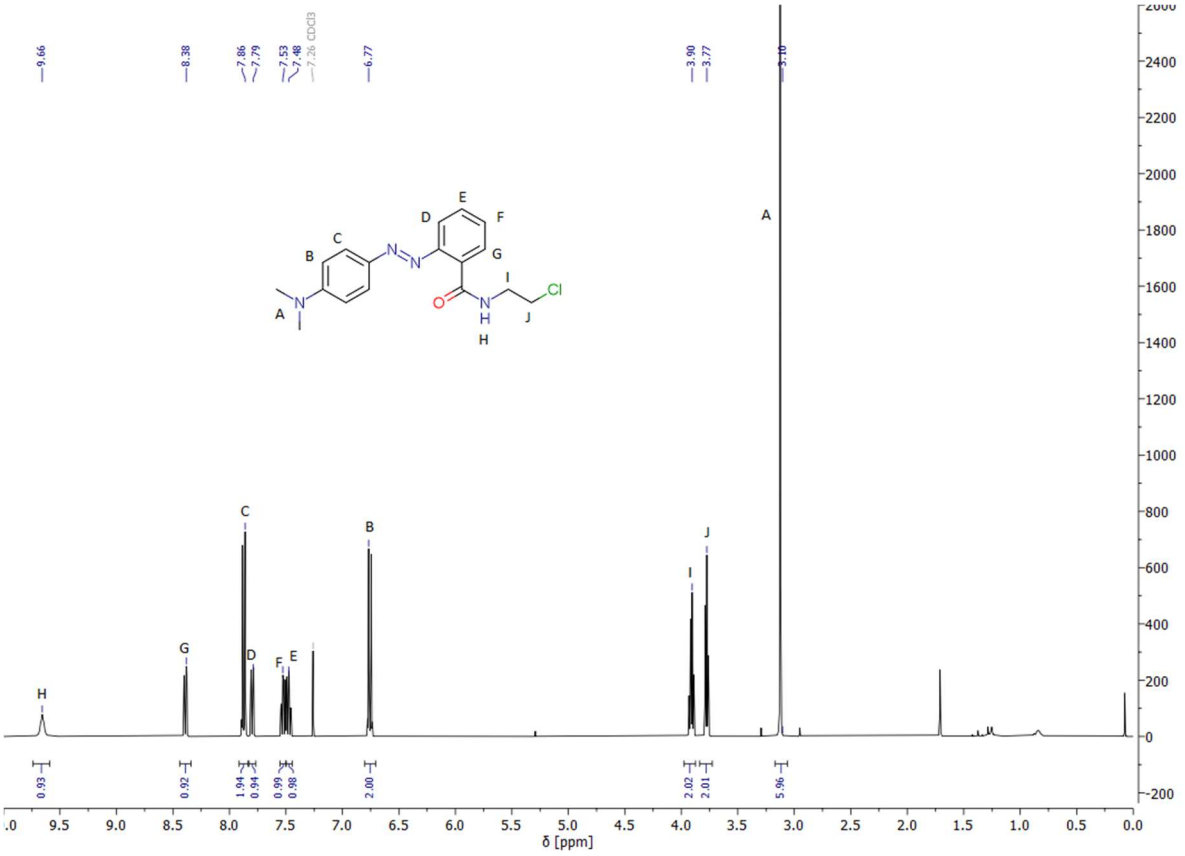

Figure S 1: ^{1}H NMR spectrum (500 MHz) in $CDCl_3$ of N-(2-chloroethyl)-2-[(1E)-2-[4-(dimethylamino)phenyl]diazen-1-yl]benzamide (o-methyl red chloroethylamide, MREtCl)).

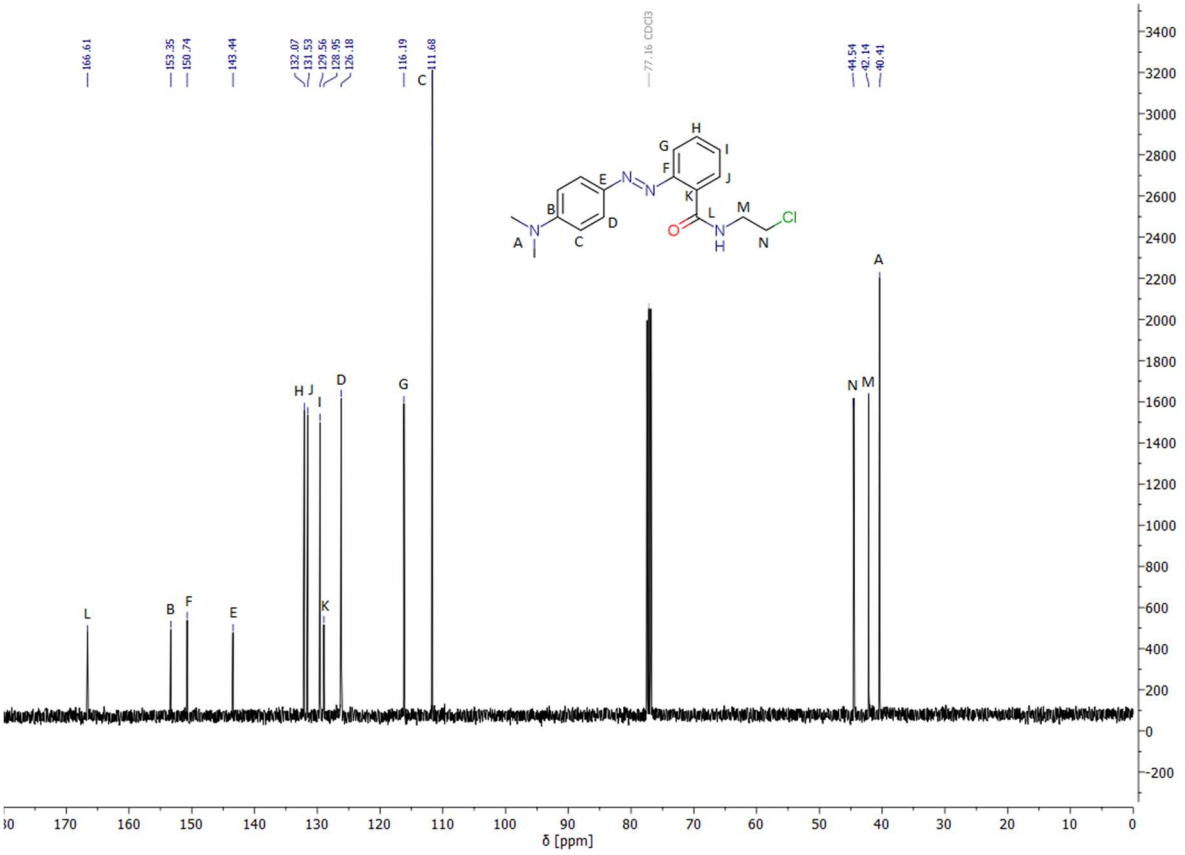

Figure S 2: ^{13}C NMR spectrum (126 MHz) in $CDCl_3$ of N-(2-chloroethyl)-2-[(1E)-2-[4-(dimethylamino)phenyl]diazen-1-yl]benzamide (o-methyl red chloroethylamide, MREtCl).

Synthesis of 2-o-methyl red-2-oxazoline:

o-Methyl red-chloroethylamide (2500.3 mg, $7.56*10^{-3}$ mol) and potassium carbonate (1762.2 mg, $1.28*10^{-2}$ mol) were dissolved/dispersed in acetonitrile (100 mL) and heated to 70 °C for twenty-four hours.

The organic solvent was removed, the residue was redissolved in dichloromethane and filtered via a syringe filter (PTFE, 450 nm). The product was purified *via* a short aluminiumoxide (neutral) column in ethanol twice.

The yield was 2.0356 g or 92%.

δH(400 MHz, $CDCl_3$) 7.87 (d, J = 9.2 Hz, 2H, Ph-*H*), 7.82 (dd, J = 7.7, 1.3 Hz, 1H, Ph-*H*), 7.63 (dd, J = 8.1, 0.9 Hz, 1H, Ph-*H*), 7.51 (td, J = 8.2, 1.5 Hz, 1H, Ph-*H*), 7.38 (td, J = 7.5, 1.3 Hz, 1H, Ph-*H*), 6.74 (d, J = 9.2 Hz, 2H, Ph-*H*), 4.43 (t, J = 9.8 Hz, 2H, C=N-C*H*$_2$), 4.10 (t, J = 9.7 Hz, 2H, C-O-C*H*$_2$), 3.07 (s, 6H, 6H, N(Me)$_2$).

δC(101 MHz, $CDCl_3$) 165.08 (O-*C*=N), 152.66 (Ph), 152.46 (Ph), 144.10 (Ph), 131.29 (Ph), 130.38 (Ph), 128.51 (Ph), 125.54 (Ph), 117.59 (Ph), 111.52 (Ph), 67.94 (C-O-*C*H$_2$), 55.46 (C=N-*C*H$_2$), 40.38 (N(Me)$_2$).

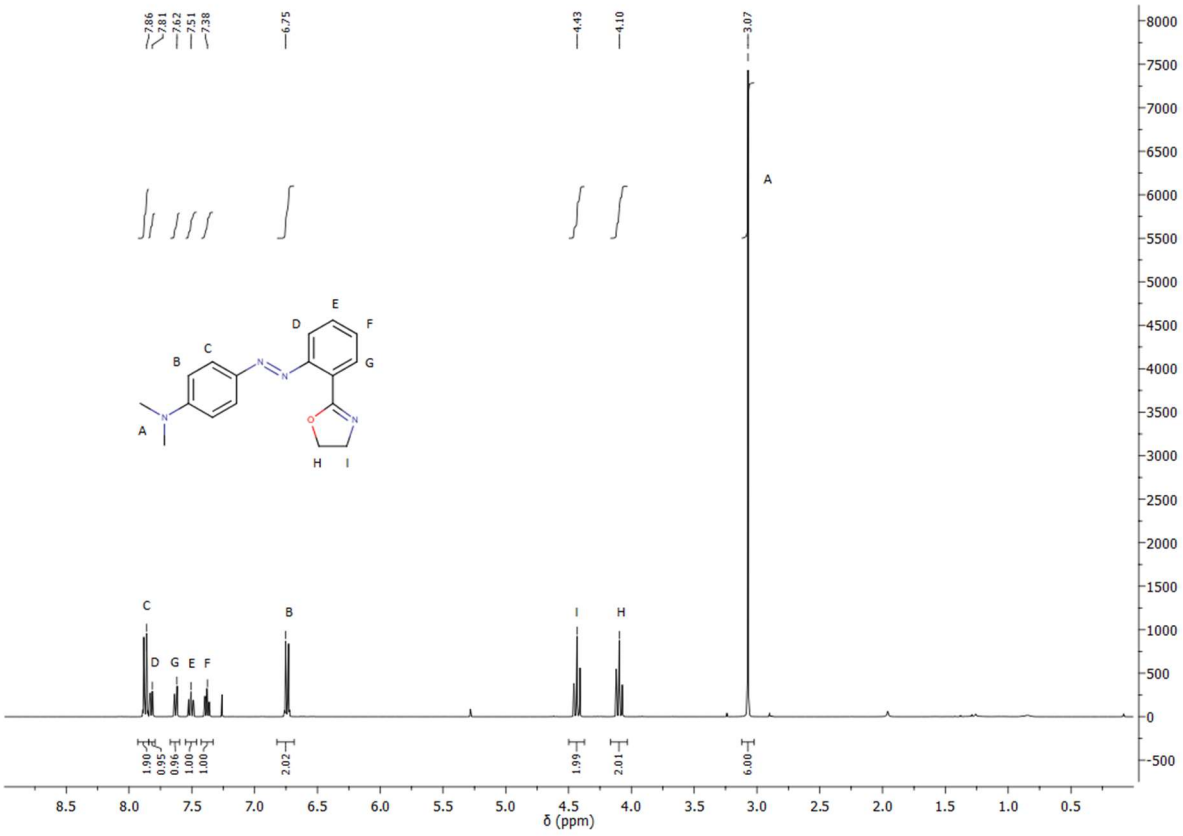

Figure S 3: ^{1}H NMR spectrum (400 MHz) in $CDCl_3$ of 2-o-methyl red-2-oxazoline.

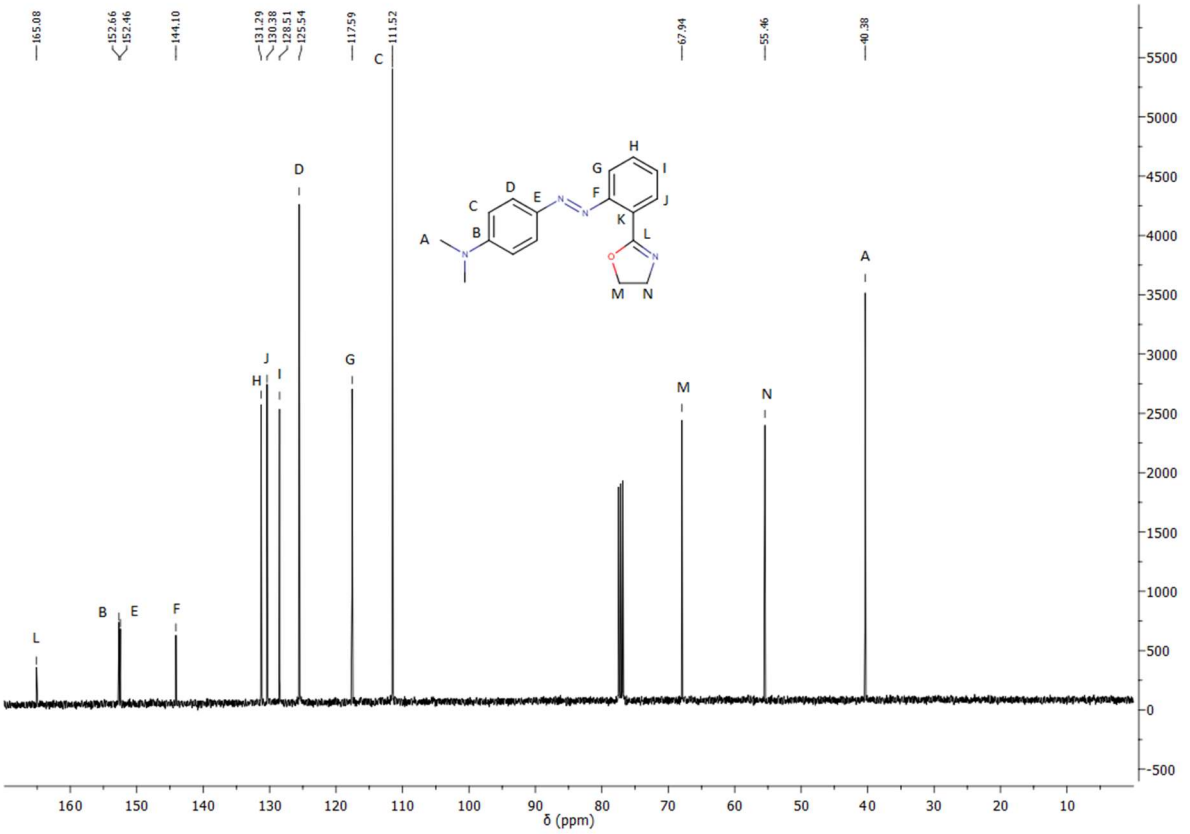

Figure S 4: ^{13}C NMR spectrum (100 MHz) in $CDCl_3$ of 2-o-methyl red-2-oxazoline.

Synthesis of N,N-dimethyl-4-[(1E)-2-[2-(piperazine-1-carbonyl)phenyl]-diazen-1-yl]aniline (o-methyl red piperazine, MRPip):

Piperazine (1320 mg, $1.5*10^{-2}$ mol) was added to a solution of o-methyl red imidazolide (2008 mg, $7.5*10^{-3}$ mol o-methyl red) in tetrahydrofuran (160 mL), followed by 1,8-diazabicyclo[5.4.0]undec-7-ene (1.7 mL, $1.1*10^{-2}$ mol) two hours later. The reaction mixture was heated to 75 °C for 48 hours. After cooling to room temperature, tetrahydrofurane was removed *in vacuo*, the residue dissolved in ethyl acetate, and the organic phase was extracted with water. The product was isolated *via* column chromatography on silica in acetone, followed by acetone:triethylamine (6:1). The yield was 1205 mg or 48%.

δH(500 MHz, $CDCl_3$) 7.83 (d, J = 9.2 Hz, 2H, Ph-*H*), 7.76 (d, J = 7.9 Hz, 1H, Ph-*H*), 7.44 (ddd, J = 8.0, 6.9, 3.9 Hz, 1H, Ph-*H*), 7.39 (qd, J = 3.5, 1.9 Hz, 2H, Ph-*H*), 6.71 (d, J = 9.2 Hz, 2H, Ph-*H*), 3.82 (t, J = 4.8 Hz, 2H, Ar-CO-N-(CH_2)$_2$, axial), 3.12 (dd, J = 10.2, 5.8 Hz, 2H, NH-(CH_2)$_2$, equatorial), 3.07 (s, 6H, N(Me)$_2$), 2.93 (m, 2H, NH-(CH_2)$_2$, axial), 2.61 (dd, J = 11.0, 6.1 Hz, 2H, Ar-CO-N-(CH_2)$_2$, equatorial), 1.75 (s, 1H, N*H*).

δC(126 MHz, $CDCl_3$) 169.31 (Ph-*C*ON), 152.79 (Ph), 149.11 (Ph), 143.68 (Ph), 134.66 (Ph), 129.66 (Ph), 129.62 (Ph), 127.43 (Ph), 125.51 (Ph), 117.22 (Ph), 111.53 (Ph), 48.29 (piperazine), 46.06 (piperazine), 46.02 (piperazine), 42.81 (piperazine), 40.36 ($N(Me)_2$).

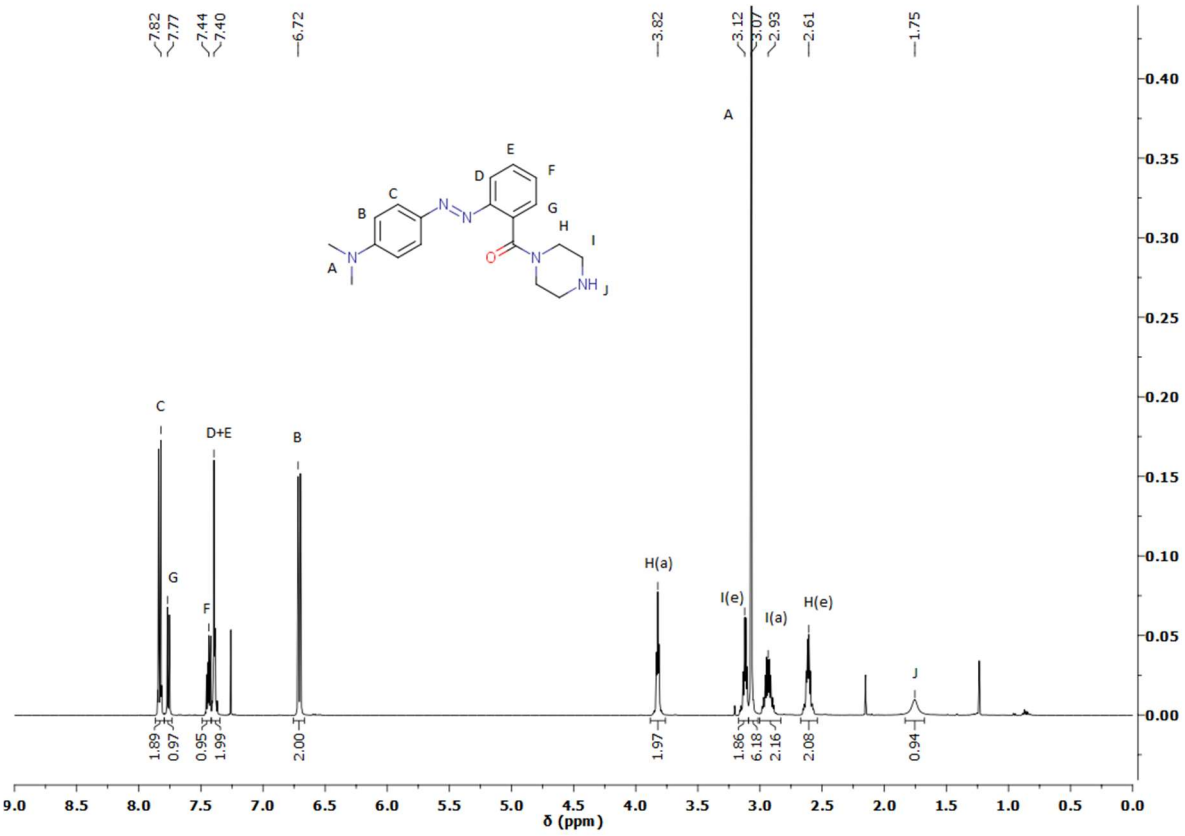

Figure S 5: ^1H NMR spectrum (500 MHz) in $CDCl_3$ of N,N-dimethyl-4-[(1E)-2-[2-(piperazine-1-carbonyl)phenyl]-diazen-1-yl]aniline (o-methyl red piperazine, MRPip).

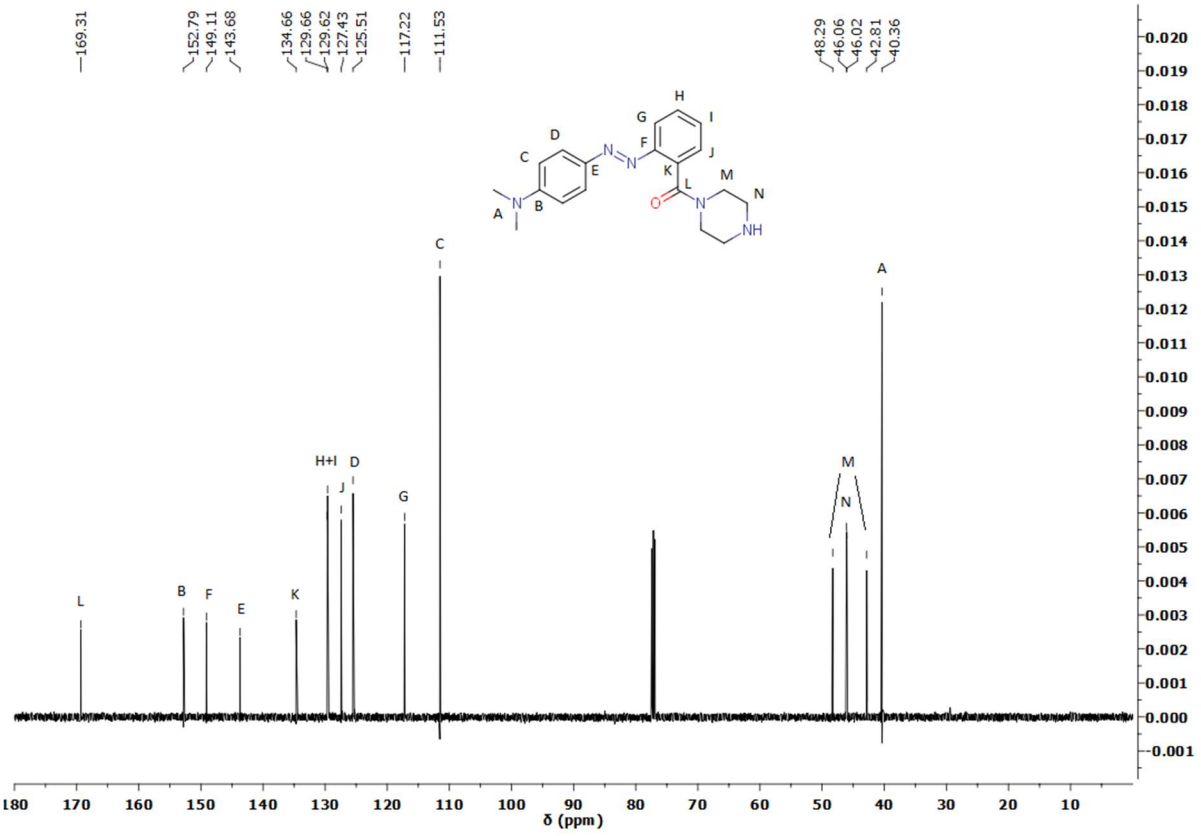

Figure S 6: ^{13}C NMR spectrum (126 MHz) in $CDCl_3$ of N,N-dimethyl-4-[(1E)-2-[2-(piperazine-1-carbonyl)phenyl]-diazen-1-yl]aniline (o-methyl red piperazine, MRPip).

Synthesis of 1-(4-{2-[(1E)-2-[4-(dimethylamino)phenyl]-diazen-1-yl]benzoyl}piperazin-1-yl)prop-2-en-1-one (o-methyl red amide of piperazine acrylamide, oMRPipAm):

o-Methyl red piperazine (103 mg, $3.1*10^{-4}$ mol) and potassium carbonate (145 mg, $1.1*10^{-3}$ mol) were added to dichloromethane (5 mL), followed by acryloyl chloride (0.05 mL, $6.1*10^{-4}$ mol) and the reaction mixture stirred for six hours. The organic phase was extracted with water and hydrochloric acid (1 M). The product was isolated *via* column chromatography on silica in ethyl acetate. The yield was 94 mg or 78%.

δH(500 MHz, DMSO-d^6) 7.72 (d, J = 9.2 Hz, 2H, Ph-*H*), 7.72 (m, 1H, Ph-*H*), 7.54 (td, J = 7.7, 1.5 Hz, 1H, Ph-*H*), 7.49 (td, J = 7.4, 1.3 Hz, 1H, Ph-*H*), 7.41 (dd, J = 7.4, 1.2 Hz, 1H, Ph-*H*), 6.83 (d, J = 9.1 Hz, 2H, Ph-*H*), 6.66 (dd, J = 16.0, 10.9 Hz, 1H, CHC*H*H(trans)), 6.11 (d, J = 16.4 Hz, 1H, C*H*CHH), 5.68 (dd, J = 36.5, 9.9 Hz, 1H, CHCH*H*(cis)), 3.71 (br, 4H, piperazine), 3.44 (br, 1H, piperazine), 3.30 (br, 1H, piperazine), 3.15 (br, 1H, piperazine), 3.05 (s, 6H, $N(Me)_2$), 3.04 (br, 1H, piperazine).

δC(126 MHz, DMSO-d^6) 168.46 (Ph-*C*ON), 164.87 (piperazine-*C*ON), 153.35 (Ph), 148.91 (Ph), 143.03 (Ph), 134.54 (Ph), 130.22 (Ph), 130.19 (Ph), 128.59 ($COCHCH_2$), 128.27 ($COCHCH_2$), 127.91 (Ph), 125.48 (Ph), 117.47 (Ph), 112.18 (Ph), 47.35

(piperazine), 46.71 (piperazine), 45.38 (piperazine), 41.82 (piperazine), 40.34 ($N(Me)_2$).

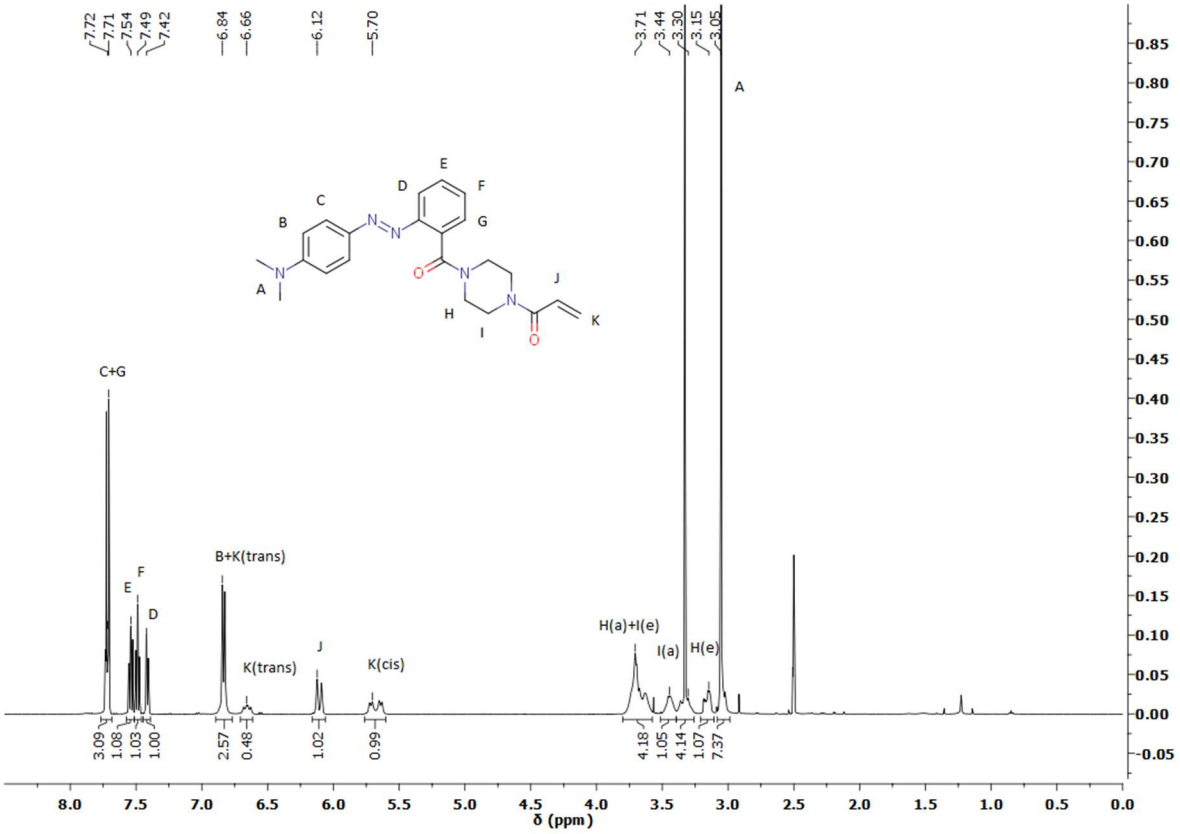

Figure S 7: ^1H NMR spectrum (500 MHz) in DMSO-d^6 of 1-(4-{2-[(1E)-2-[4-(dimethylamino)phenyl]-diazen-1-yl]benzoyl}piperazin-1-yl)prop-2-en-1-one (o-methyl red amide of piperazine acrylamide, oMRPipAm).

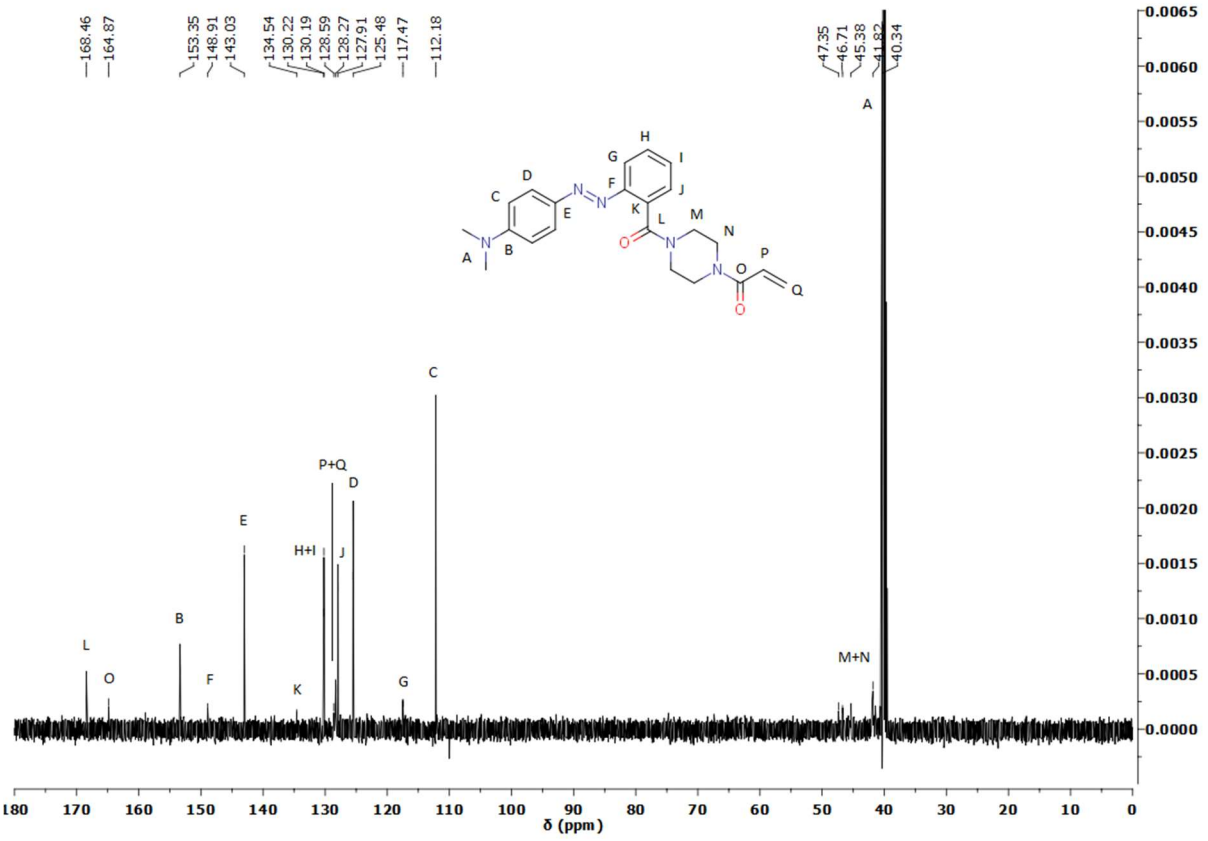

Figure S 8: ^{13}C NMR spectrum (126 MHz) in DMSO-d^6 of 1-(4-{2-[(1E)-2-[4-(dimethylamino)phenyl]-diazen-1-yl]benzoyl}piperazin-1-yl)prop-2-en-1-one (o-methyl red amide of piperazine acrylamide, oMRPipAm).

Synthesis of N,N-dimethyl-4-[(1E)-2-[2-(piperazine-1-carbonyl)phenyl]-diazen-1-yl]aniline(p-methyl red piperazine, pMRPip):

para-Methyl red (501 mg, 1.9*10^{-3} mol) was dispersed in tetrahydrofurane (25 mL) before carbonyldiimidazole (434 mg, 2.7*10^{-3} mol) was added and the mixture stirred for 90 minutes. Piperazine (600 mg, 7.0*10^{-3} mol) and 1,8-diazabicyclo[5.4.0]undec-7-ene (0.43 mL, 2.9*10^{-3} mol) were added and the reaction mixture was stirred for 4.5 hours. The solvent was removed *in vacuo* and the solid washed with heptane. It was then dissolved in chloroform:methanol 3:1, silica was added and the solvent slowly removed *in vacuo*. The product was purified *via* column chromatography in acetone, followed by methanol.

The yield was 525 mg or 84%.

δH(500 MHz, $CDCl_3$) 7.87 (d, J = 9.1 Hz, 2H, Ph-*H*), 7.84 (d, J = 8.5 Hz, 2H, Ph-*H*), 7.50 (d, J = 8.5 Hz, 2H, Ph-*H*), 6.74 (d, J = 9.2 Hz, 2H, Ph-*H*), 3.75 (br, 2H, Ar-CO-N-(C*H*$_2$)$_2$, axial), 3.42 (br, 2H, NH-(C*H*$_2$)$_2$, equatorial), 3.08 (s, 6H, N(Me)$_2$), 2.93 (br, 2H, NH-(C*H*$_2$)$_2$, axial), 2.80 (br, 2H, Ar-CO-N-(C*H*$_2$)$_2$, equatorial), 1.77 (br, 1H, N*H*).

δC(126 MHz, $CDCl_3$) 170.13 (Ph-*C*ON), 153.91 (Ph), 152.79 (Ph), 143.68 (Ph), 136.30 (Ph), 128.02 (Ph), 125.34 (Ph), 122.29 (Ph), 111.54 (Ph), 49.17 (piperazine), 46.44 (piperazine), 46.12 (piperazine), 43.47 (piperazine), 40.35 ($N(Me)_2$).

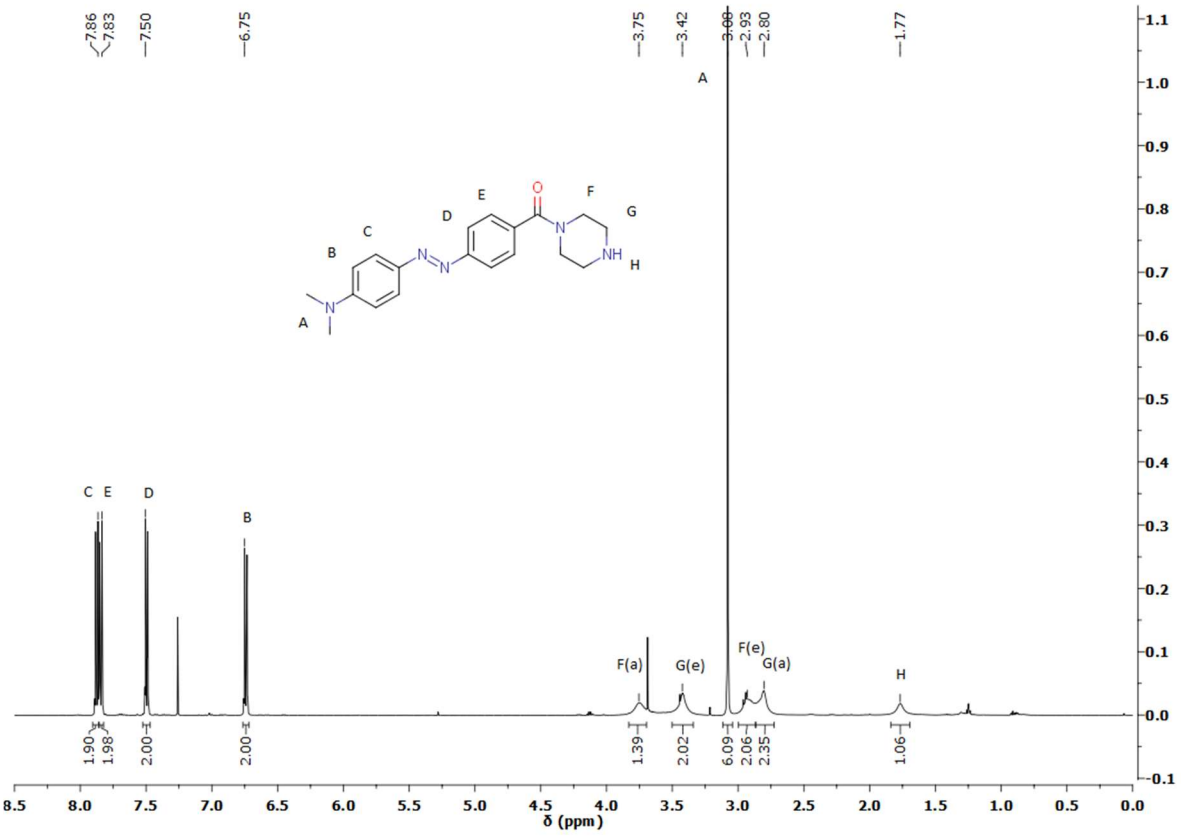

Figure S 9: ^1H NMR spectrum (500 MHz) in $CDCl_3$ of N,N-dimethyl-4-[(1E)-2-[2-(piperazine-1-carbonyl)phenyl]-diazen-1-yl]aniline(p-methyl red piperazine, pMRPip).

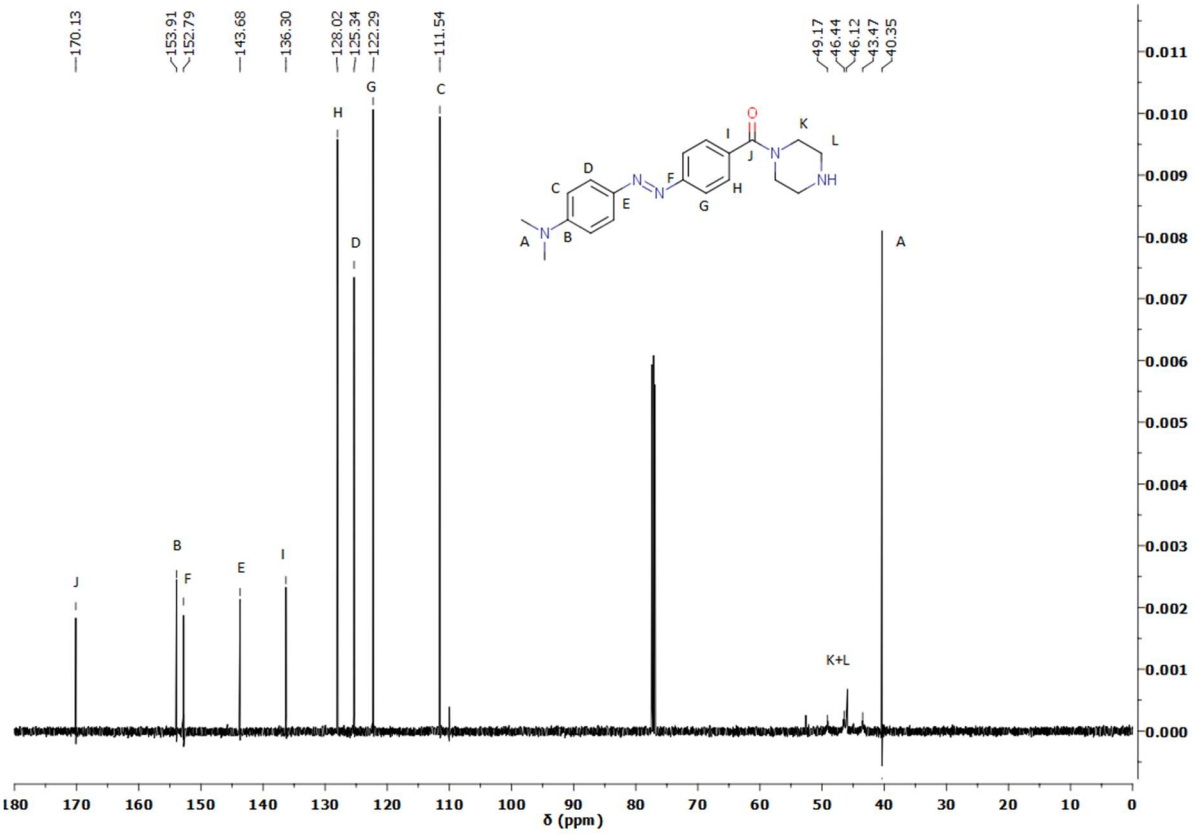

Figure S 10: ^{13}C NMR spectrum (126 MHz) in $CDCl_3$ of N,N-dimethyl-4-[(1E)-2-[2-(piperazine-1-carbonyl)phenyl]-diazen-1-yl]aniline(p-methyl red piperazine, pMRPip).

Synthesis of 1-(4-{2-[(1E)-2-[4-(dimethylamino)phenyl]-diazen-1-yl]benzoyl}piperazin-1-yl)prop-2-en-1-one (p-methyl red amide of piperazine acrylamide, pMRPipAm):

para-Methyl red piperazine (200 mg, $5.9*10^{-4}$ mol) and potassium carbonate (160 mg, $1.2*10^{-3}$ mol) were dispersed in chloroform (10 mL), followed by dropwise addition of acryloyl chloride (0.1 mL, $1.2*10^{-3}$ mol). The reaction mixture stirred for eighteen hours. The organic phase was extracted with water and saturated aqueous sodium hydrogencarbonate solution. The product was isolated *via* column chromatography on silica in ethyl acetate, followed by ethyl acetate:acetone 1:1. The yield was 210 mg or 91%.

δH(500 MHz, $CDCl_3$) 7.87 (m, 4H, Ph-*H*), 7.52 (d, J = 8.6 Hz, 2H, Ph-*H*), 6.75 (d, J = 9.2 Hz, 2H, Ph-*H*), 6.55 (br, 1H, C*H*CHH), 6.32 (dd, J = 16.8, 1.8 Hz, 1H, CHC*H*H(trans)), 5.74 (d, J = 11.4 Hz, 1H, CHCH*H*(cis)), 3.66 (br, piperazine), 3.09 (s, 6H, $N(Me)_2$).

δC(126 MHz, $CDCl_3$) 170.42 (Ph-*C*ON), 165.70 (piperazine-*C*ON), 154.28 (Ph), 152.91 (Ph), 143.69 (Ph), 135.36 (Ph), 128.81 (CO*C*HCH$_2$), 128.18 (Ph), 127.15

(COCHCH$_2$), 125.47 (Ph), 122.44 (Ph), 111.57 (Ph), 45.80 (piperazine), 42.16 (piperazine), 40.39 (N(Me)$_2$).

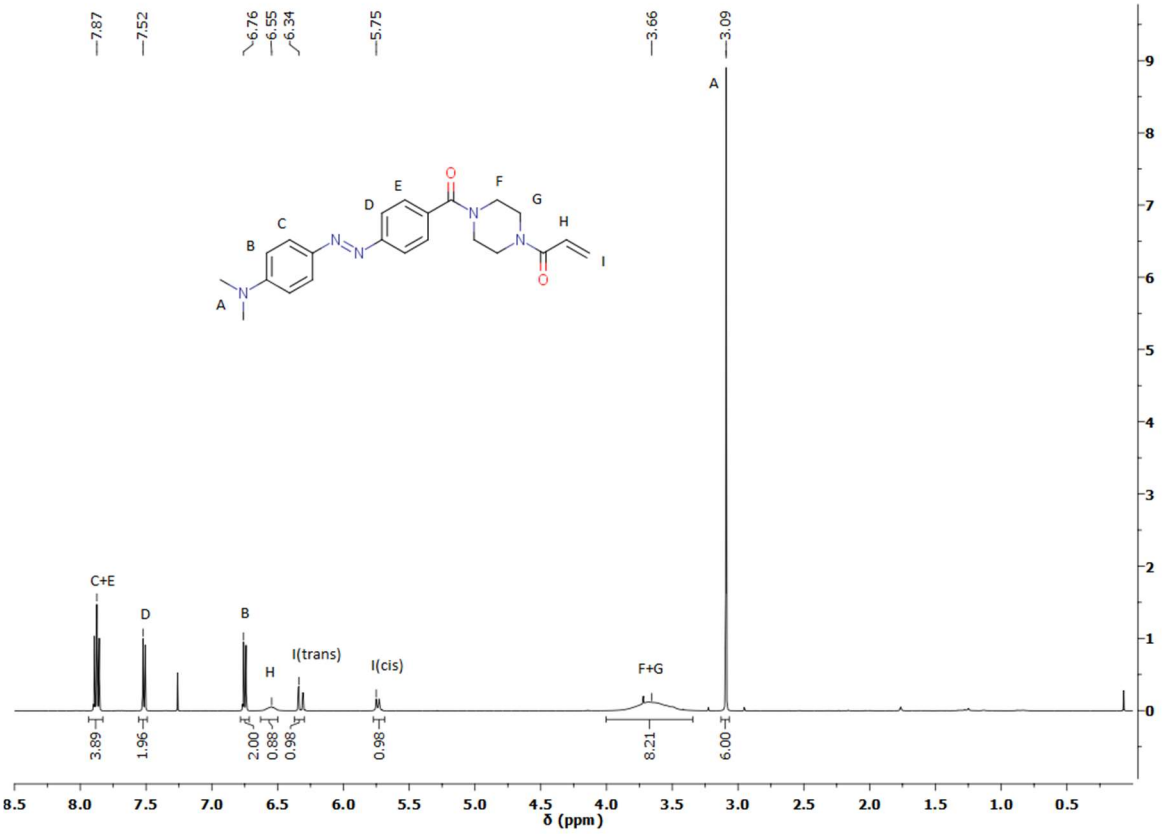

Figure S 11: ^{1}H NMR spectrum (500 MHz) in $CDCl_3$ of 1-(4-{2-[(1E)-2-[4-(dimethylamino)phenyl]-diazen-1-yl]benzoyl}piperazin-1-yl)prop-2-en-1-one (p-methyl red amide of piperazine acrylamide, pMRPipAm).

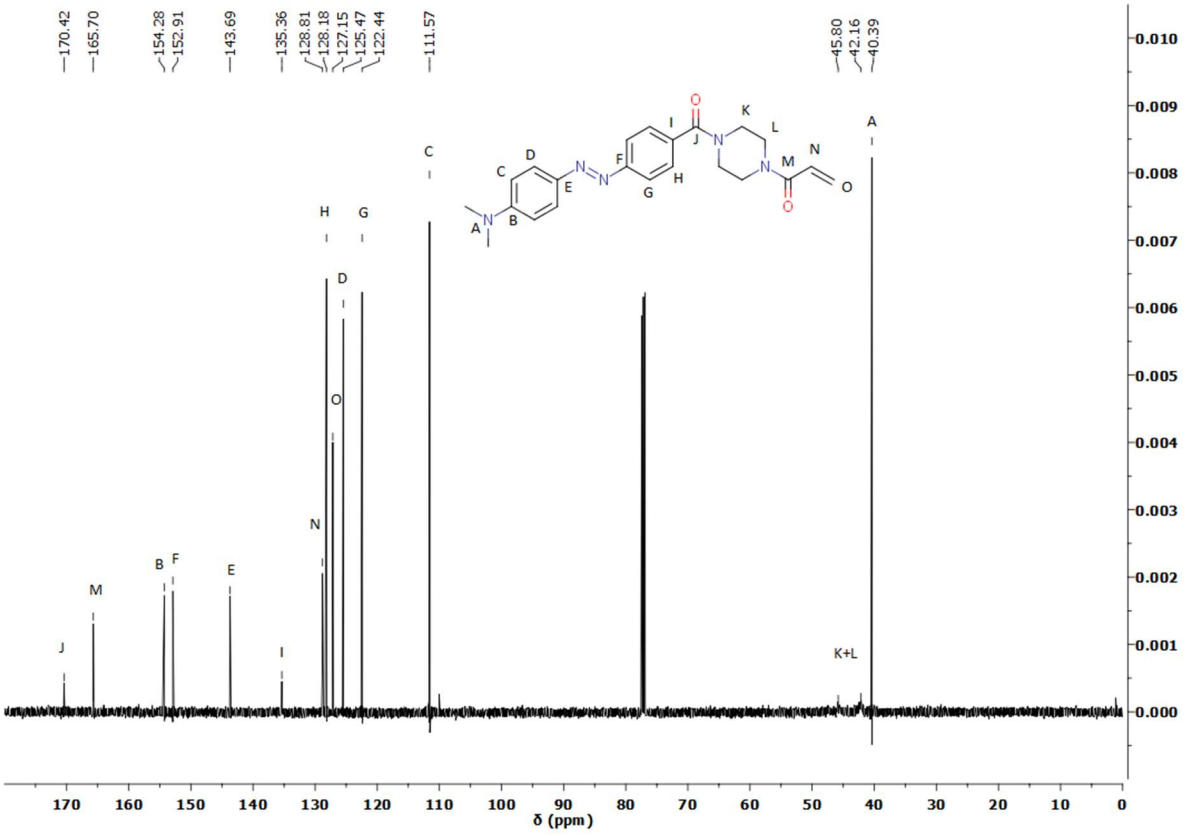

Figure S 12: ^{13}C NMR spectrum (126 MHz) in $CDCl_3$ of 1-(4-{2-[(1E)-2-[4-(dimethylamino)phenyl]-diazen-1-yl]benzoyl}piperazin-1-yl)prop-2-en-1-one (p-methyl red amide of piperazine acrylamide, pMRPipAm).

Microwave-assisted cationic-ring opening copolymerization of 2-methyl-2-oxazoline and 2-o-methyl red-2-oxazoline:

2-Methyl-2-oxazoline (627 mg, $7.4*10^{-3}$ mol), 2-o-methyl red-2-oxazoline (108 mg, $3.7*10^{-4}$ mol) and methyltriflate (6.8 mg, $4.1*10^{-5}$ mol) (MeOxa:oMROxa; 95:5 MeOTf 0.5%) were dissolved in anhydrous acetonitrile (3.1 mL) and sealed in a reaction flask. The solution was heated in a microwave oven with the following program: Power 140 W, Ramp time 2 min, Hold time 90 min at a temperature of 120 °C.

The polymer was precipitated in diethylether and stirred overnight before it was filtered. The yield was 706 mg or 96%.

For partial hydrolysis, POxa was dissolved in aqueous hydrochloric acid (1.2 M) and heated to 75 °C for 20 hours. After cooling, the reaction solution was neutralised with aqueous sodium hydroxide (1 M) before it was dialysed against water, ethanol, and finally water again und subsequently lyophilised.

Copolymer POxa: δH(500 MHz, CDCl3) 7.9-6.6 (aromatic H), 3.7-3.3 (backbone), 3.09 ($N(Me)_2$), 2.3-1.8 (N-CO-C*H*$_3$).

Partially hydrolyzed Copolymer POxa: δH(500 MHz, D_2O) 8.2-6.7 (aromatic H), 4.1-3.7, 3.7-3.3 (2-oxazoline backbone), 3.3-2.7 (polyethyleneimine), 2.4-1.7 (N-CO-C*H*$_3$).

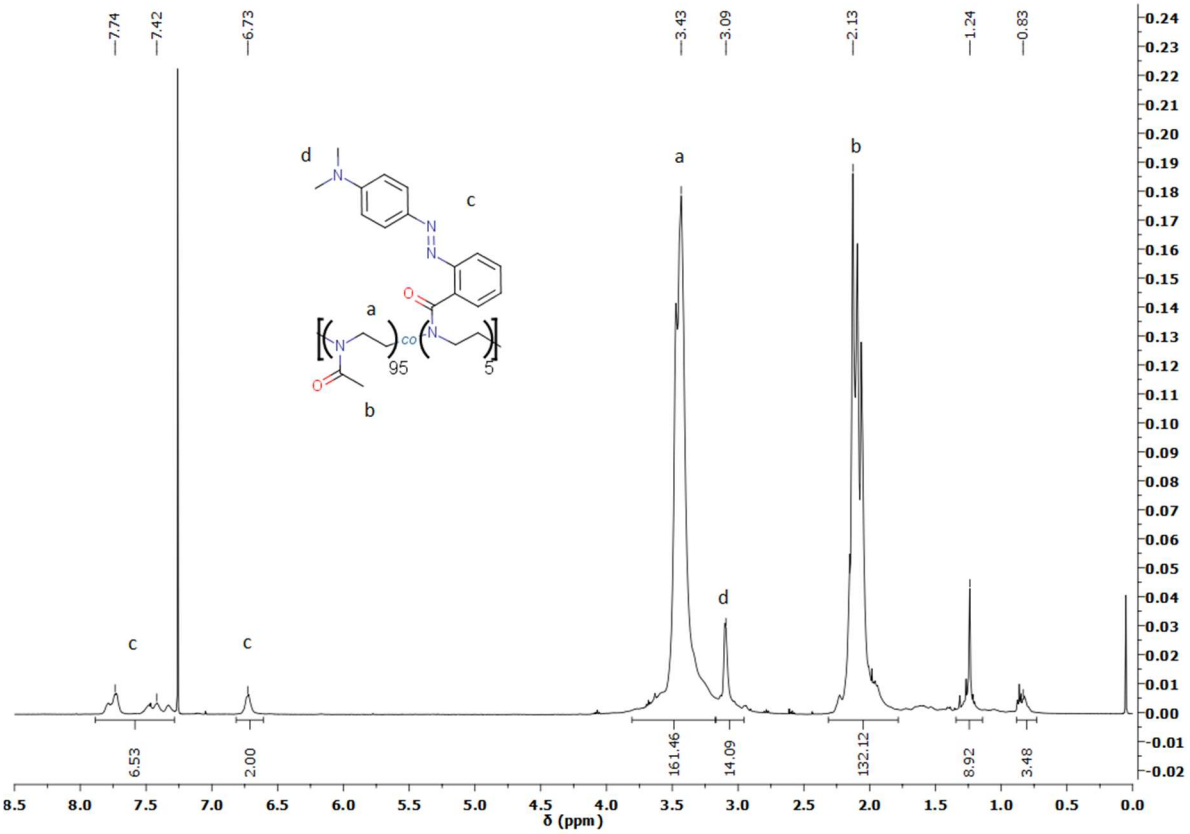

Figure S 13: ^{1}H NMR spectrum (500 MHz) in $CDCl_3$ of poly(2-methyl-2-oxaozline-co-2-o-methyl red-2-oxazoline) (POxa).

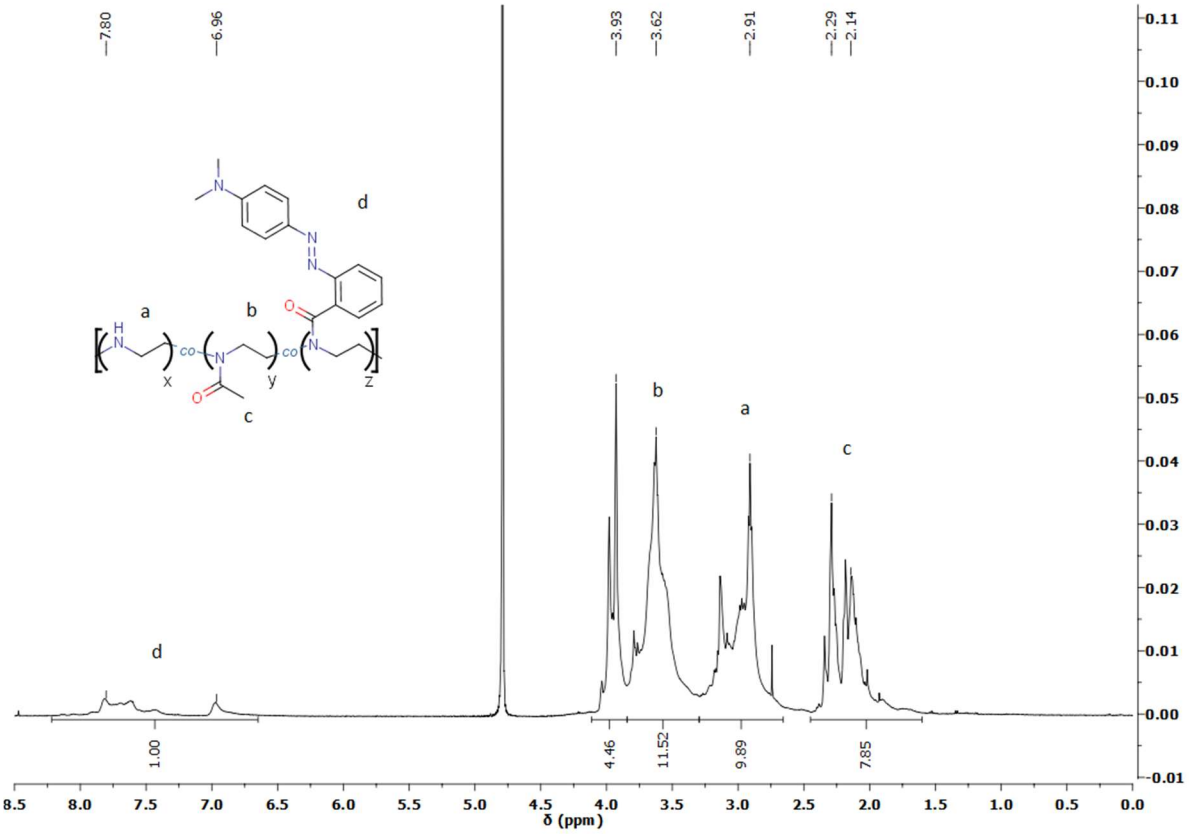

Figure S 14: ^{1}H NMR spectrum (500 MHz) in $CDCl_3$ of poly(2-methyl-2-oxaozline-co-ethyleneimine-co-2-o-methyl red-2-oxazoline) (hydrolyzed POxa).

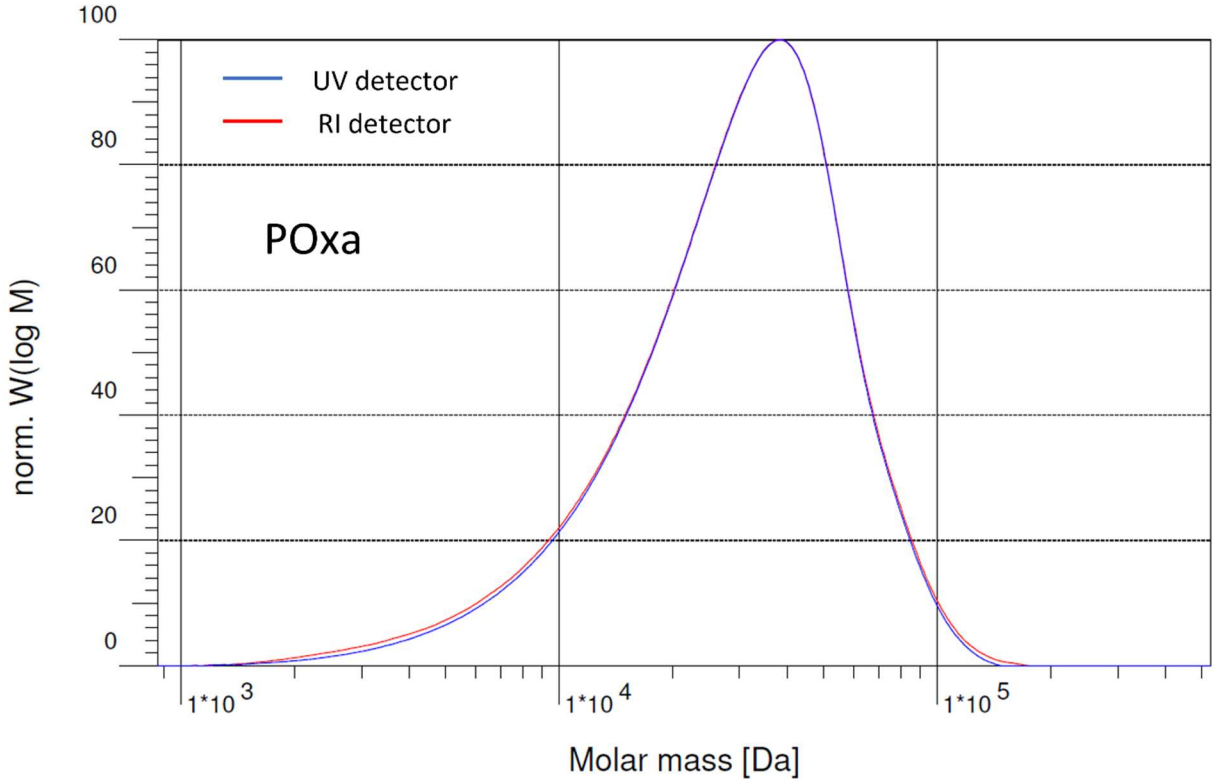

Figure S 15: Gel permeation chromatography chromatograms of of poly(2-methyl-2-oxaozline-co-2-o-methyl red-2-oxazoline) (POxa), measured on a PSS GRAM linM column (Polymer Standards Service GmbH, Mainz, Germany) in dimethylacetamide with LiBr (0.1 g L^{-1}) at 60 °C with PMMA-standards as reference.

Free radical copolymerization of HEAm, oMRPipAm and BPAAm:

The monomers *N*-hydroxyethyl acrylamide (202 mg, $1.8*10^{-3}$ mol), o-methyl red amide of piperazine acrylamide (17.2 mg, $4.4*10^{-5}$ mol) and 4-benzophenone acrylamide (4.6 mg, $1.8*10^{-5}$ mol) were dissolved in methanol (4 mL). Azobisisobutyronitrile (144 µL of a 40.9 mg mL^{-1} solution in 1,4-dioxane, 5.9 mg, $3.6*10^{-5}$ mol) was added and the solution purged with argon for 30 minutes (HEAm:oMRPipAm:BPAAm 96.5:2.5:1, 2% AIBN). The reaction mixture was heated to 60 °C for 24 hours, before it was cooled in an ice bath. The polymer was precipitated once in diethylether and twice in acetone. The yield was 177 mg or 79%.

δH(500 MHz, DMSO) 7.8-6.7 (aromatic H), 5.25-4.6 (piperazine), 3.42 (CONH-CH_2), 3.3-2.8 (OH-CH_2), 2.2-0.9 (backbone).

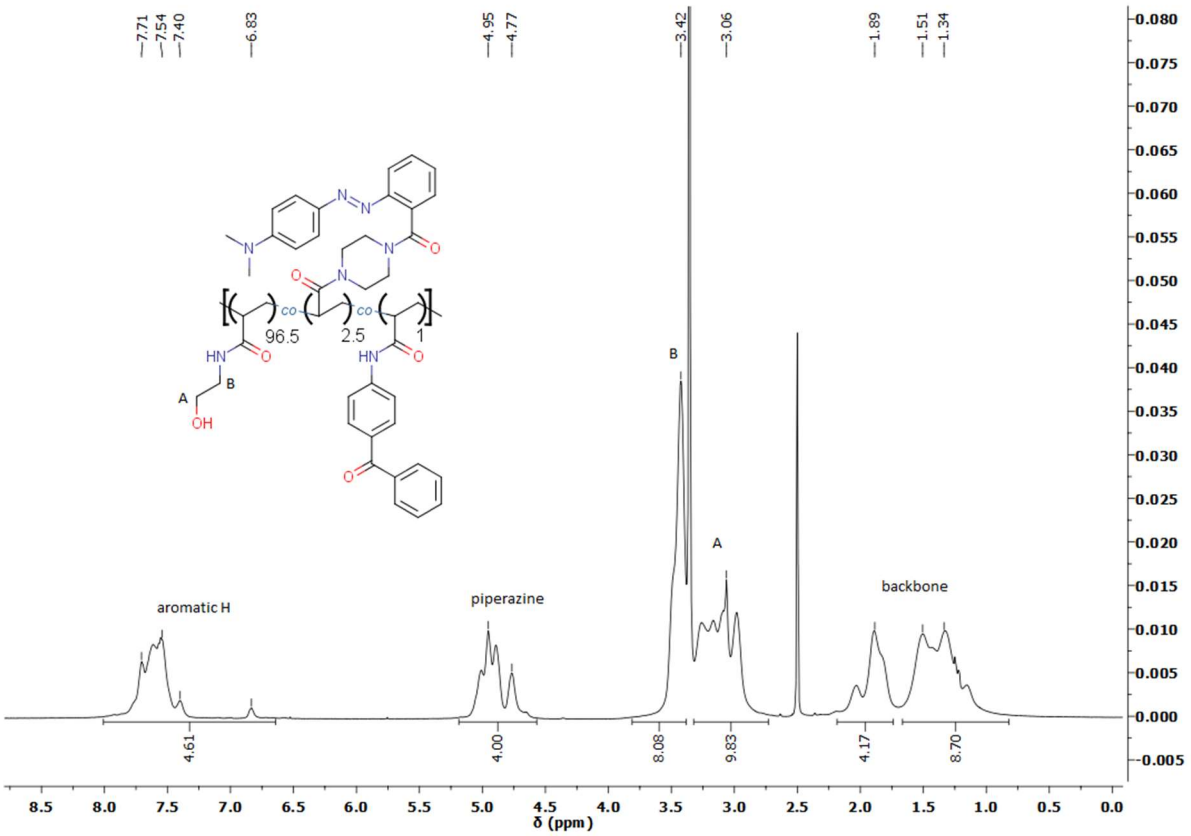

Figure S 16: ^{1}H NMR spectrum (500 MHz) in $CDCl_3$ of poly(N-hydroxyethyl acrylamide-co-o-methyl red piperazine acrylamide-co-benzophenone acrylamide) (PAAmBP).

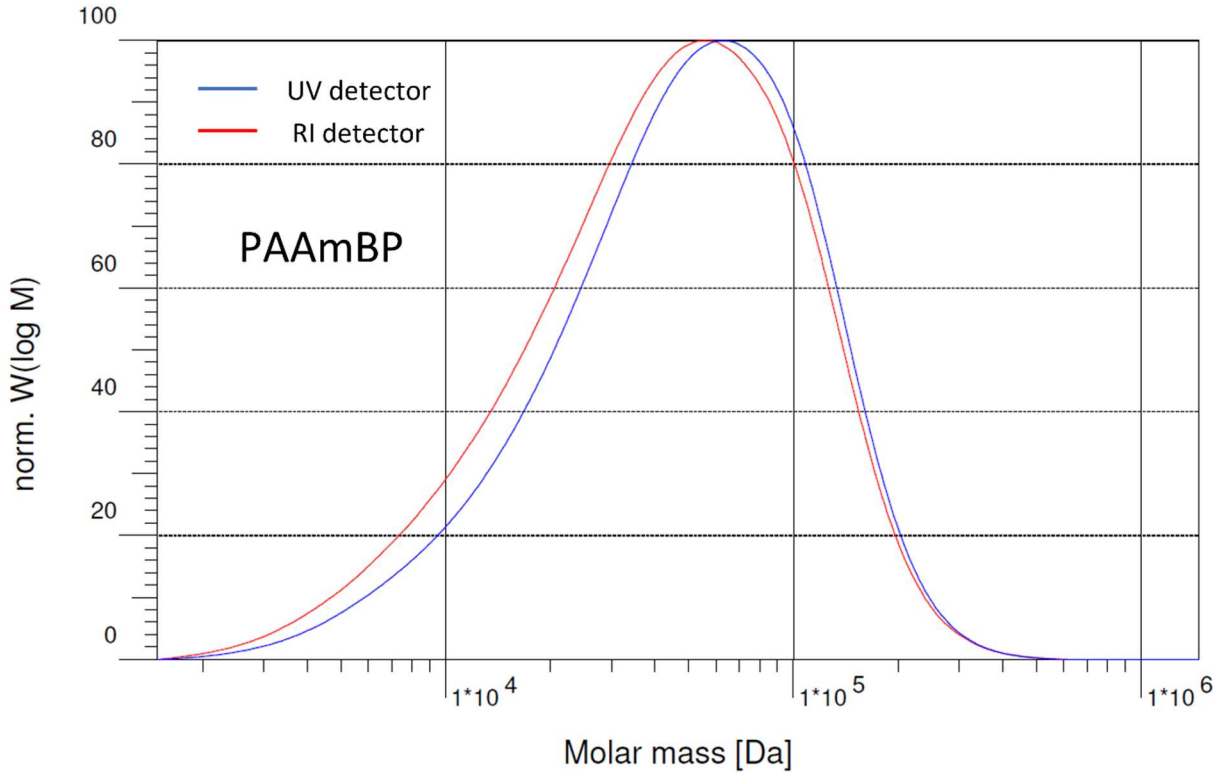

Figure S 17: Gel permeation chromatography chromatograms of poly(N-hydroxyethyl acrylamide-co-o-methyl red piperazine acrylamide-co-benzophenone acrylamide) (PAAmBP), measured on a PSS GRAM linM column (Polymer Standards Service GmbH, Mainz, Germany) in dimethylacetamide with LiBr (0.1 g L^{-1}) at 60 °C with PMMA-standards as reference.

Free radical copolymerization of HEAm and oMRPipAm:

The monomers *N*-hydroxyethyl acrylamide (202 mg, $1.8*10^{-3}$ mol) and the o-methyl red amide of piperazine acrylamide (34.5 mg, $8.8*10^{-5}$ mol) were dissolved in dimethylsulfoxide (4 mL). Azobisisobutyronitrile (6.0 mg, $3.6*10^{-5}$ mol) was added and the solution purged with argon for 30 minutes (HEAm:oMRPipAm 95.1:4.9, 2% AIBN). The reaction mixture was heated to 70 °C for 48 hours, before it was cooled in liquid nitrogen. The polymer was precipitated once in diethylether, before it was dialysed against ethanol until colorless, followed by dialysis against water (molecular weight cut-off: 2000 g mol^{-1}). The yield was 223 mg or 94%.

δH(500 MHz, DMSO) 7.8-6.7 (aromatic H), 5.25-4.6 (piperazine), 3.42 (CONH-CH_2), 3.3-2.8 (OH-CH_2), 2.2-0.9 (backbone).

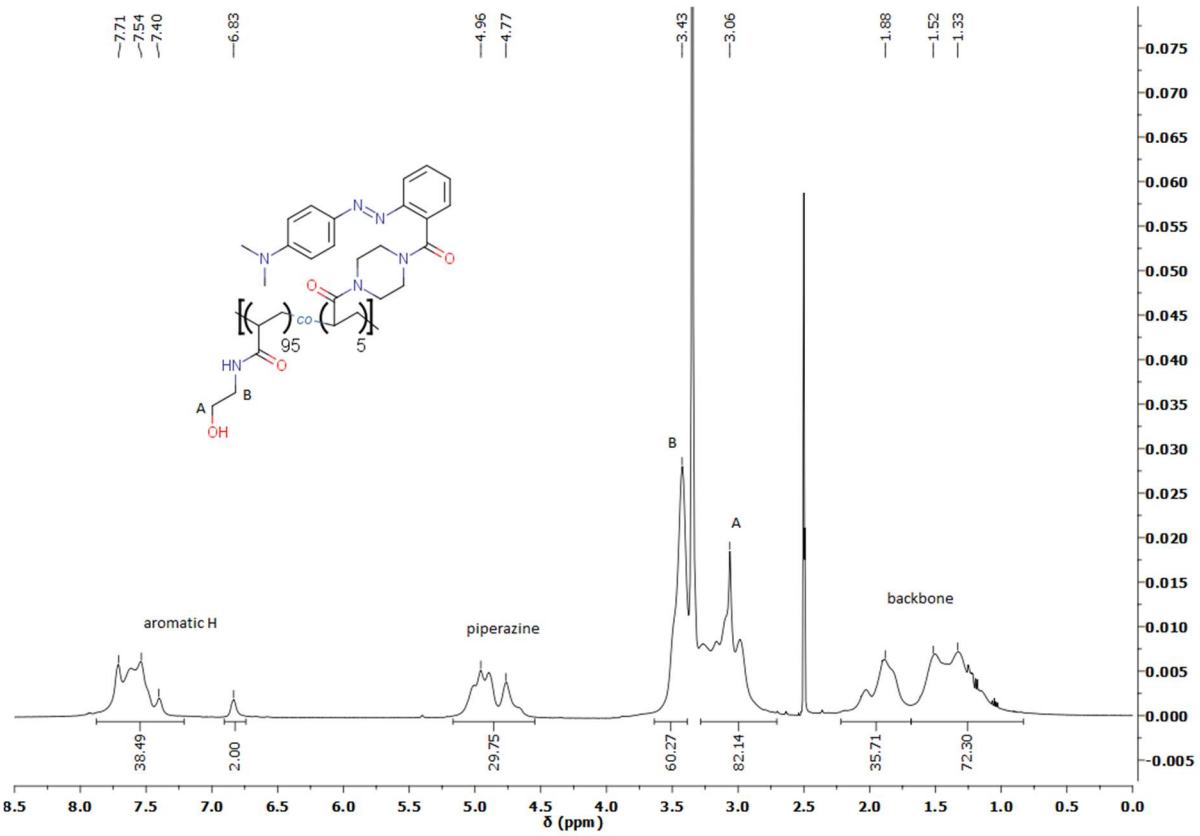

Figure S 18: ^{1}H NMR spectrum (500 MHz) in $CDCl_3$ of poly(N-hydroxyethyl acrylamide-co-o-methyl red piperazine acrylamide) (PAAm).

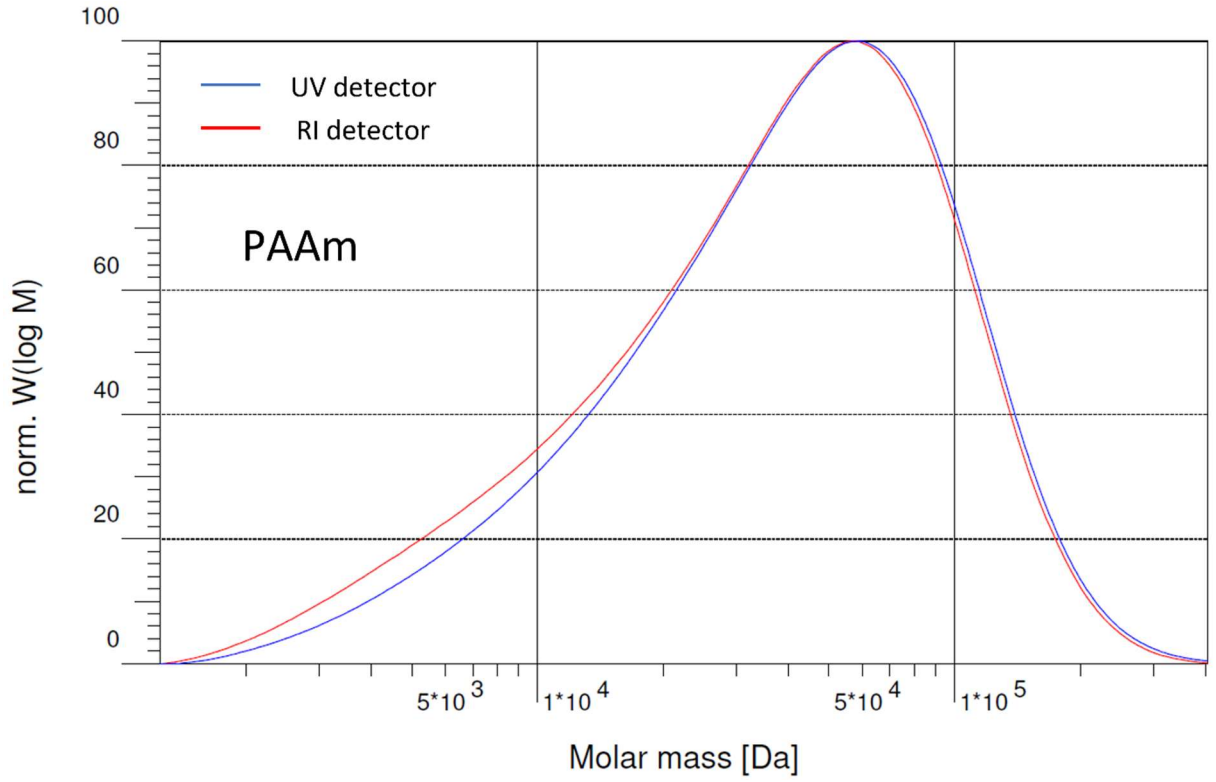

Figure S 19: Gel permeation chromatography chromatograms of poly(N-hydroxyethyl acrylamide-co-o-methyl red piperazine acrylamide) (PAAm), measured on a PSS GRAM linM column (Polymer Standards Service GmbH, Mainz, Germany) in dimethylacetamide with LiBr (0.1 g L^{-1}) at 60 °C with PMMA-standards as reference.

Film preparation and photocrosslinking:

Films of poly(*N*-hydroxyethyl acrylamide-co-o-methyl red piperazine acrylamide-co-benzophenone acrylamide) (PAAmBP) were drop-casted from methanolic solution (200 µL, 1 w%) on prepared slides of tissue culture-grade polystyrene (2.4x2.4 cm). The polystyrene was hydrophilised by Corona-discharge treatment (Sicatech Corona Generator by UNI-SYSTEMS LF1) for fifteen seconds. Photocrosslinking was performed in a UV-chamber (LTF Labortechnik) at 254 nm with 8.6 J cm^{-2}. Prior to measurements, the films were swollen in water and uncrosslinked material was washed out of the films.

Thermochromic Behaviour of 2-Oxazoline and Piperazine Acrylamide Monomers in Solution:

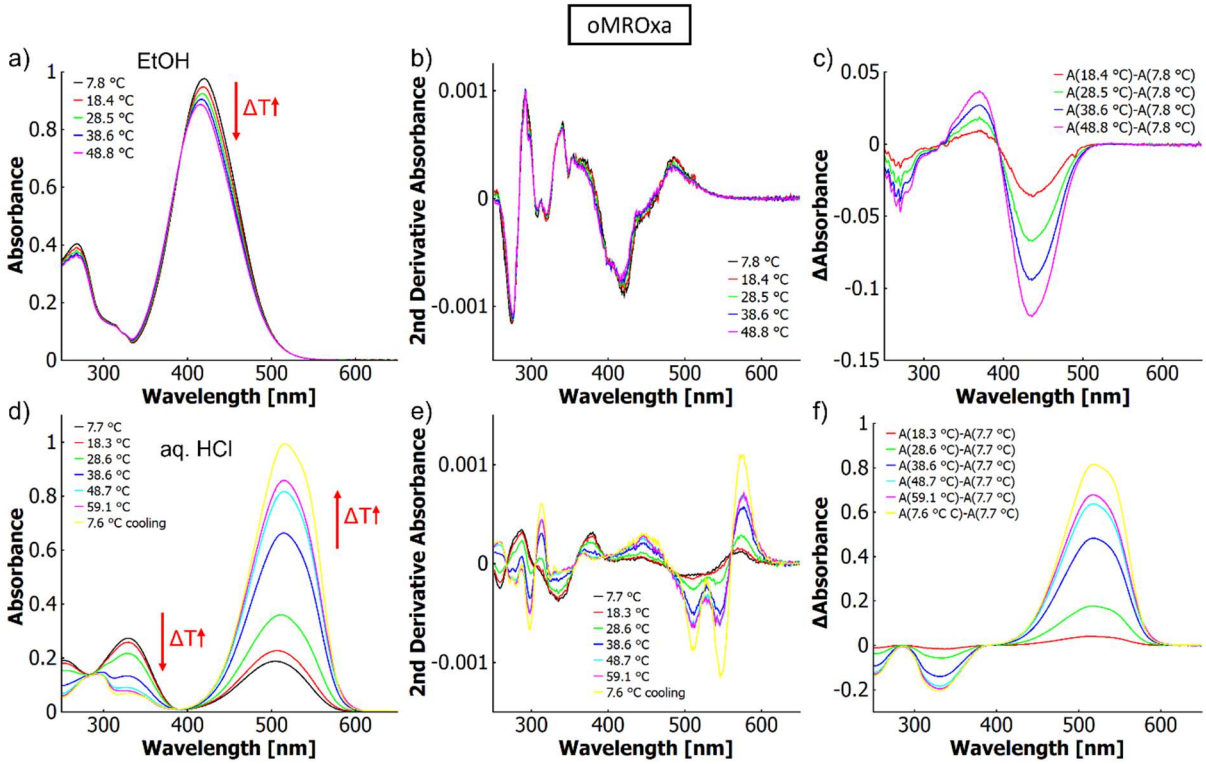

Figure S 20: UV-vis spectra of o-methyl red-2-oxazoline (0.01 g L^{-1}) at different temperatures a) in ethanol, and d) in aq. HCl (1.2 M), b) and e) the corresponding second derivative spectra, and c) and f) the corresponding difference spectra.

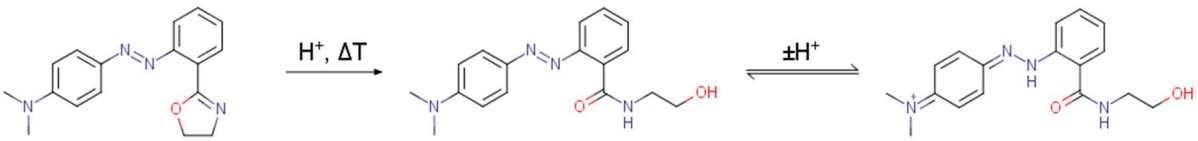

Scheme S 1: Acidic hydrolysis of o-methyl red-2-oxazoline with corresponding protonation equilibrium in acidic medium.

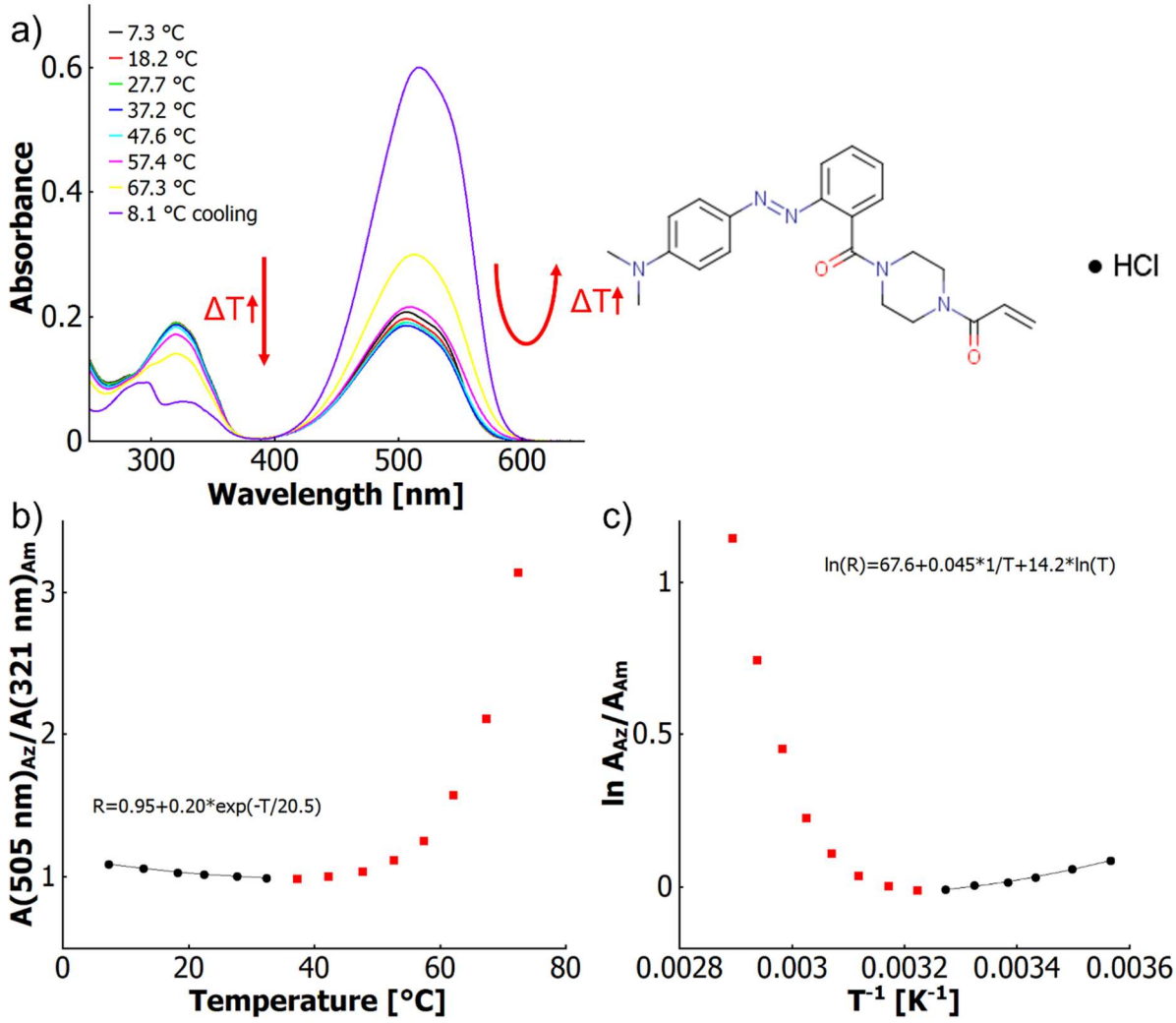

*Figure S 21: Temperature-dependent UV-vis spectra of aqueous solutions of o-methyl red piperazine acrylamide (oMRPipAm, 0.01 g L^{-1}, 1.2 M HCl) a) heating above the threshold temperature of irreversible change, b) shows a plot of the absorbance ratio of the azonium ion absorption band by the ammonium ion absorption band vs temperature. The reversible part in black is fitted with an exponential decay function, the irreversible change is marked in red; c) shows the natural logarithm of the absorbance ratio vs the inverse of the absolute temperature. The reversible part in black is fitted with a function R=a-b*1/T+c*ln(T), the irreversible part marked in red.*

Van't Hoff analysis:

The thermochromic behavior between the different systems up to the threshold temperature of irreversible change can be compared by van't Hoff analysis. A non-linear van't Hoff plot of ln K vs T^{-1}, the equilibrium constant K in this case being replaced by the absorbance ratio R of the azonium ion to the ammonium ion, can be fitted by the following equation:[2, 4]

$$ln\left(\frac{R}{R_0}\right) = \frac{\Delta H_0 - T_0 \Delta C_p}{R}\left(\frac{1}{T_0} - \frac{1}{T}\right) + \frac{\Delta C_p}{R} ln\left(\frac{T}{T_0}\right) \quad (1)$$

Or in a more compact form

$$ln(R) = a - b * \frac{1}{T} + c * ln\,(T) \qquad (2)^{[5]}$$

The parameters ΔH_0 represents the enthalpy of the proton transfer and ΔC_p its temperature dependence in form of the heat capacity of the tautomerization. Thus, these values are considered as parameters to describe the thermochromicity, i.e., the magnitude of thermochromism, of a system.[6]

Owing to the irreversible changes introduced by the hydrolysis of the dye, only the reversible part of the thermochromism can be fitted. The temperature at which the fit is unsuccessful is considered as the threshold temperature.

While the non-linear van't Hoff analysis yields a positive value for ΔH_0 at 298.15 K (cf. Figure 5, Table 4), indicating an endothermic process, the formation of the azonium ion is exothermic, as the equilibrium shifts towards the ammonium form upon temperature increase. As such those values obtained by the van't Hoff analysis must be taken with caution, yet they allow a qualitative comparison between the different systems. The absolute values of both ΔC_p and ΔH_0 give an idea about how dynamic the system is, and how strongly the shift of the tautomerism is affected by temperature. From this analysis it can be concluded that at lower temperatures more of the azonium form is converted to the ammonium form per temperature increment than at higher temperatures for all systems.

The acrylamide copolymers have similar thermochomicity parameters to the monomer in aqueous hydrochloric acid for the ammonium-azonium-tautomerism (in the reversible part of thermochromism). On the other hand, the polyoxazoline-based copolymer POxa shows about five times smaller values for both ΔH_0 and ΔC_p, meaning that fewer azonium ions are converted to ammonium ions per temperature increment, and that this shift is less affected by temperature as well. This indicates a higher barrier between the two tautomers in this copolymer.

It is also notable that higher values in the thermochromicity parameters correlate with a lower threshold temperature for irreversible changes, indicating a higher tendency for hydrolysis.

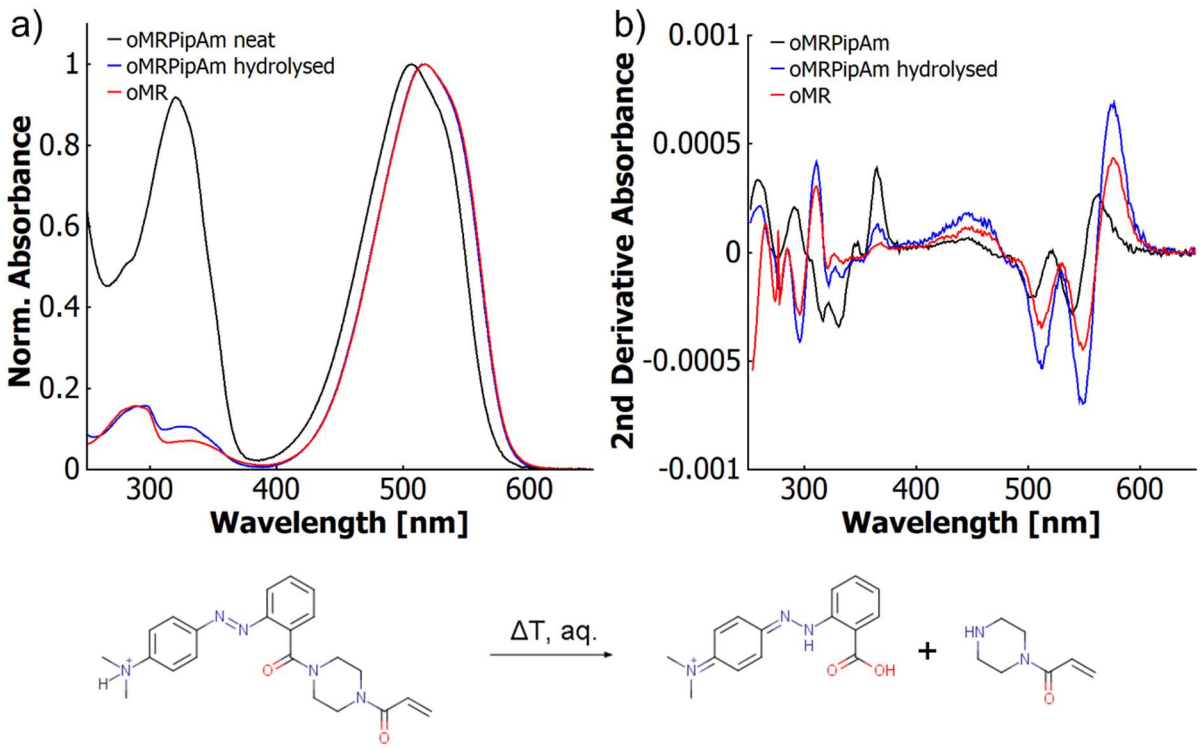

Figure S 22: a) Normalized UV-vis spectra of the hydrolysation product of o-methyl red piperazine acrylamide, oMRPipAm and o-methyl red, oMR, b) corresponding second derivative spectra. At the bottom, the hydrolysis reaction is outlined.

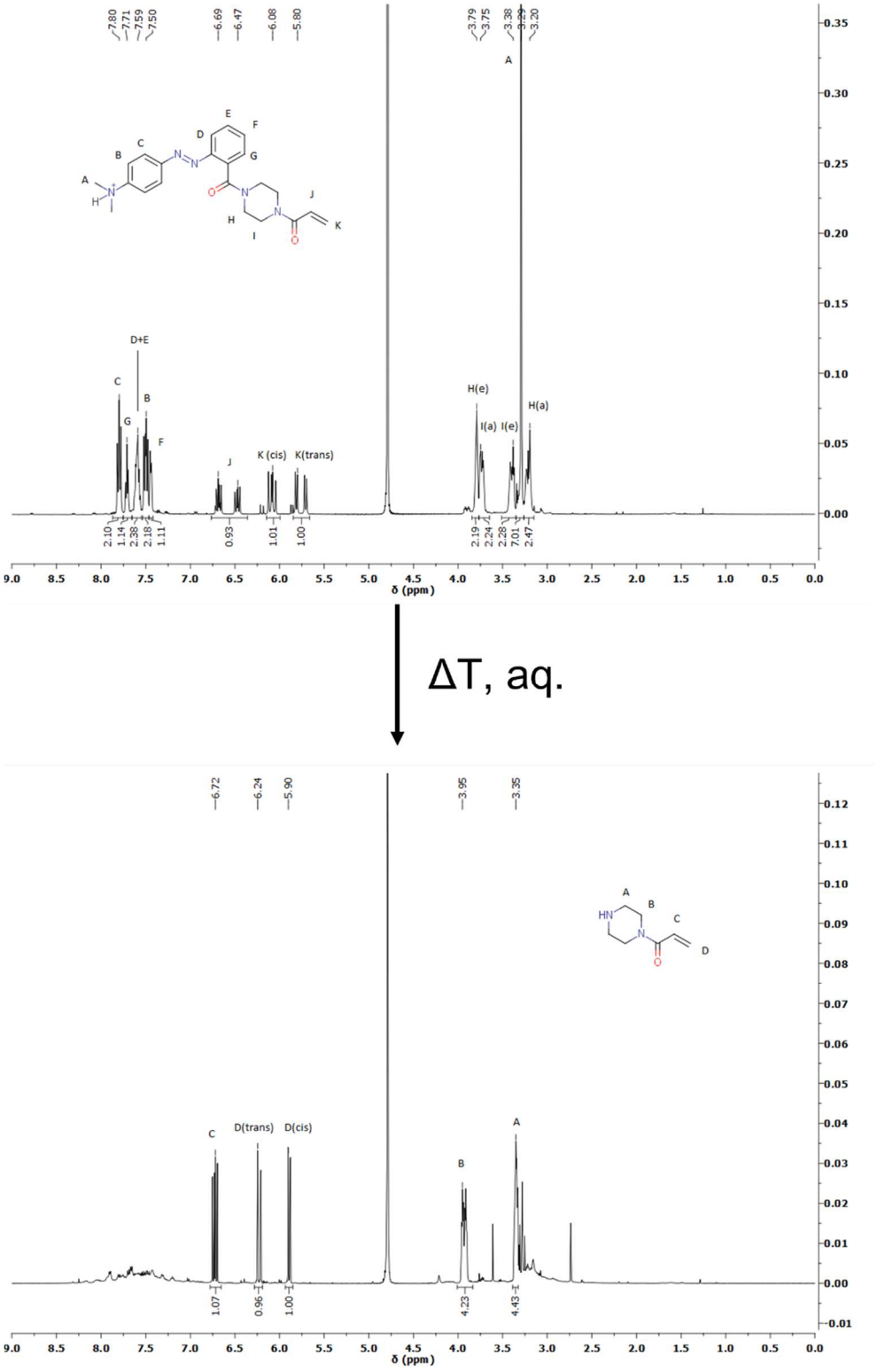

Figure S 23: ^{1}H NMR spectra (500 MHz) in D_2O with trifluoroacetic acid of protonated o-methyl red piperazine acrylamide, oMRPipAm, before (top) and after (bottom) heating to 60 °C for twenty hours.

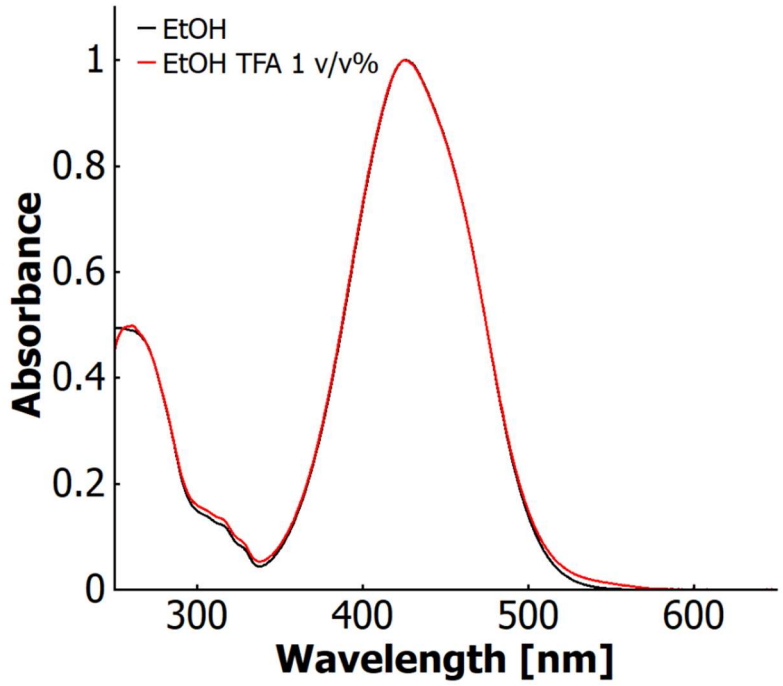

Figure S 24: Normalized UV-vis spectra of o-methyl red piperazine acrylamide (oMRPipAm) in ethanol and in ethanolic trifluoroacetic acid (1 v/v% TFA) at 27.5 °C.

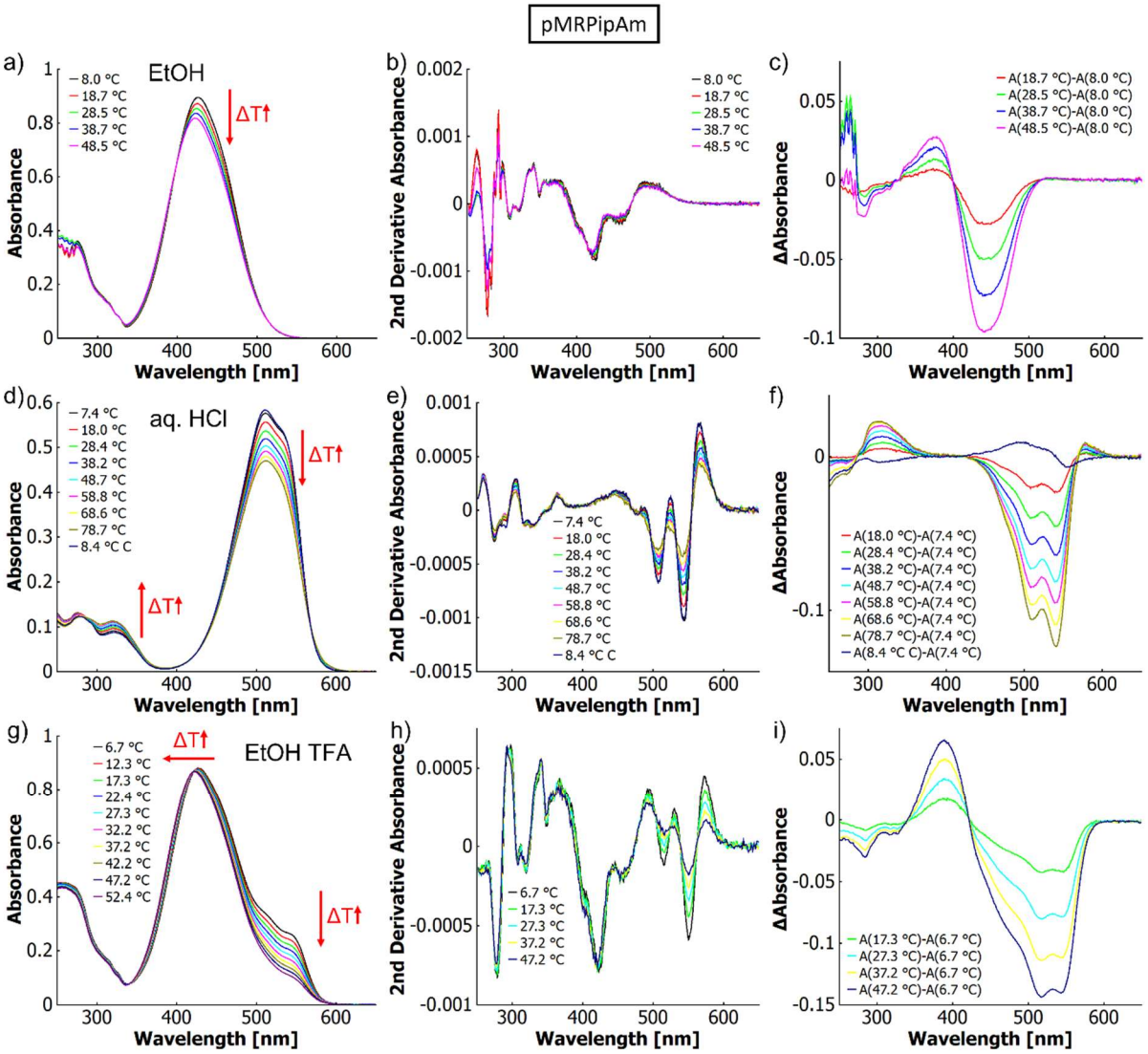

Figure S 25: UV-vis spectra of p-methyl red piperazine acrylamide at different temperatures a) in ethanol (0.01 g L^{-1}), d) in aq. HCl (0.005 g L^{-1}, 1.2 M HCl), and g) in ethanolic trifluoroacetic acid (1 v/v%), b), e) and h) the corresponding second derivative spectra, and c), f) and i) the corresponding difference spectra.

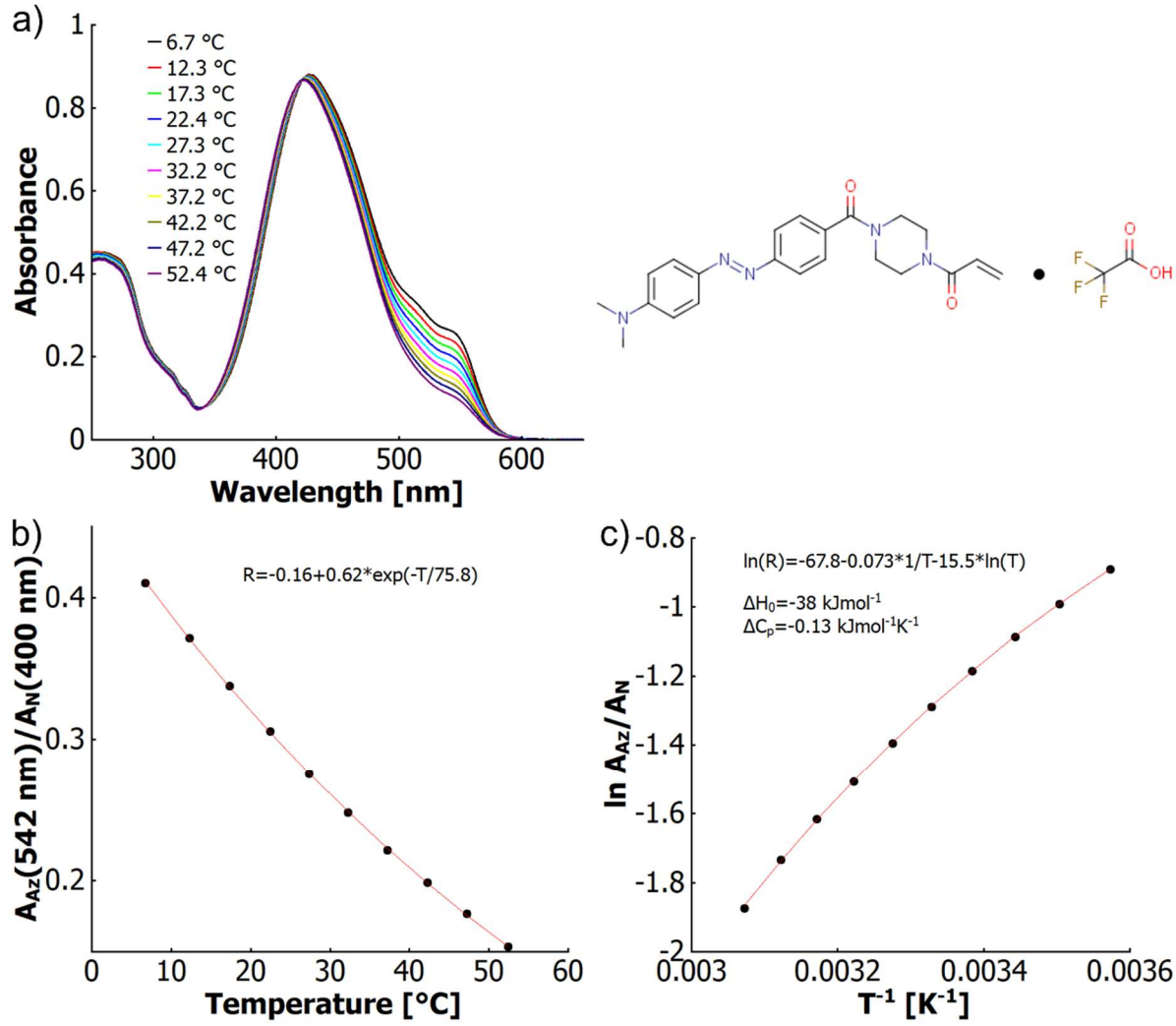

*Figure S 26: a) Temperature-dependent UV-vis spectra in ethanolic trifluoroacetic acid of p-methyl red piperazine acrylamide (pMRPipAm, 0.01 g L^{-1}, 1 v/v% TFA); b) shows a plot of the absorbance ratio of the azonium ion absorption band by the neutral dye absorption band vs temperature. It is fitted with a simple exponential decay function; c) shows the natural logarithm of the absorbance ratio vs the inverse of the absolute temperature. It is fitted with a function R=a-b*1/T+c*ln(T).*

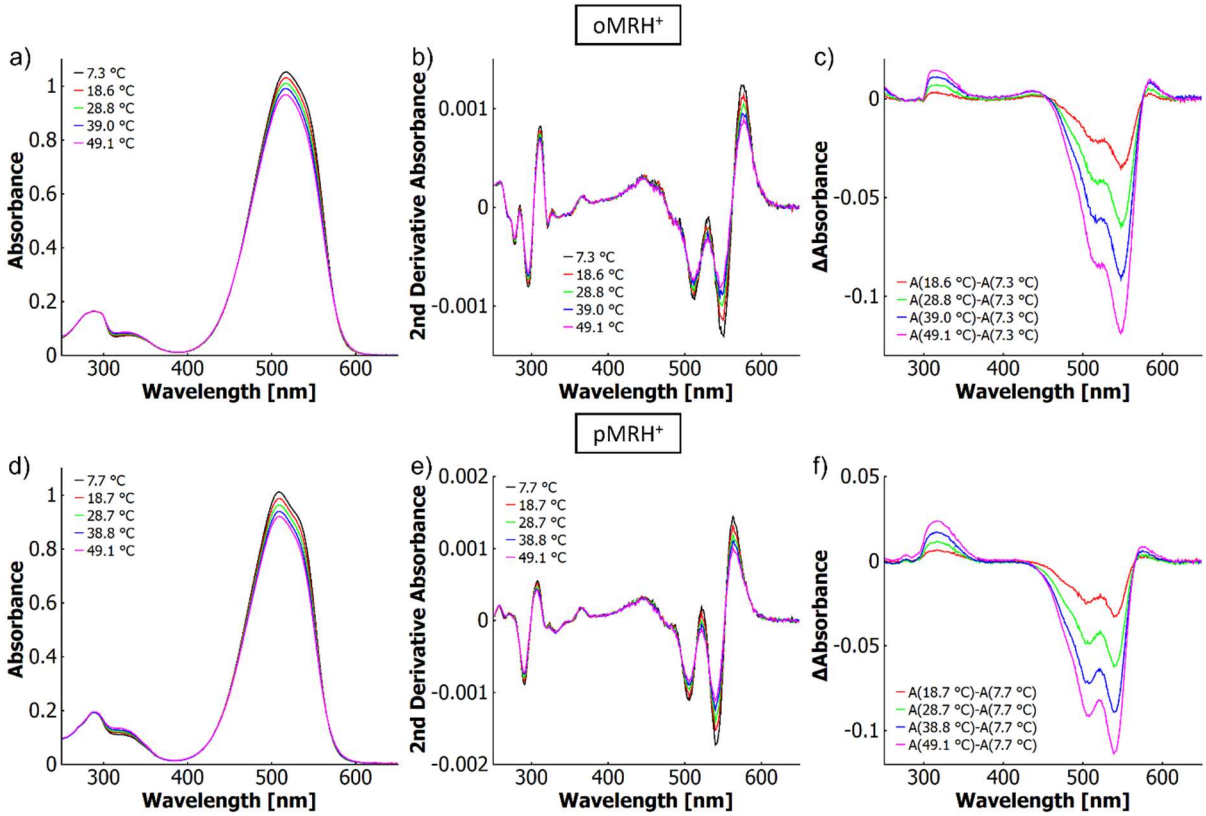

Figure S 27: UV-vis spectra in aq. HCl (1.2 M) at different temperatures a) of o-methyl red (0.005 g L^{-1}), and d) p-methyl red (20 times dilution of a saturated solution), b) and e) the corresponding second derivative spectra, and c) and f) the corresponding difference spectra. Both dyes were completely protonated.

Thermochromic Behaviour of Hydrophilic Copolymers Bearing Tertiary Amides of Methyl Red, as well as Van't Hoff Analysis:

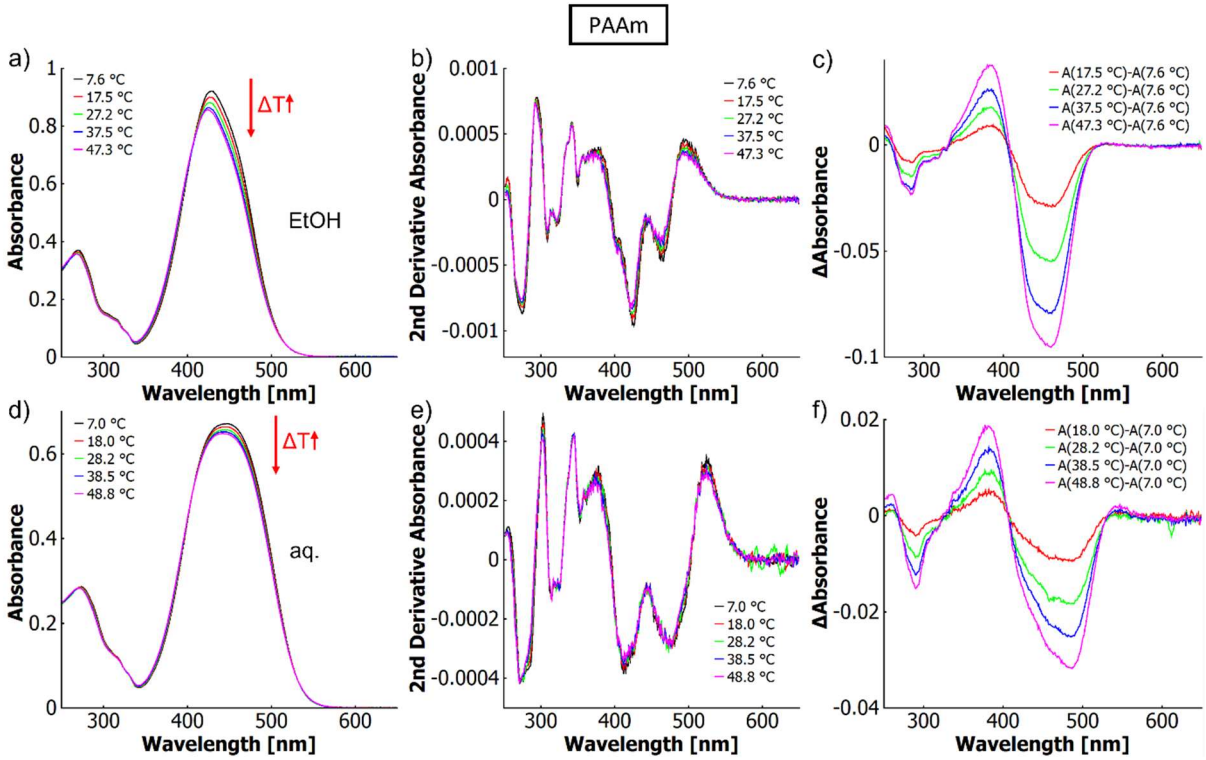

Figure S 28: Temperature-dependent UV-vis spectra, derivative spectra, and difference spectra of poly(HEAm-co-oMRPipAm) (0.1 g L^{-1}) in ethanolic (a), b), c), respectively) and in aqueous solution (d), e), f), respectively).

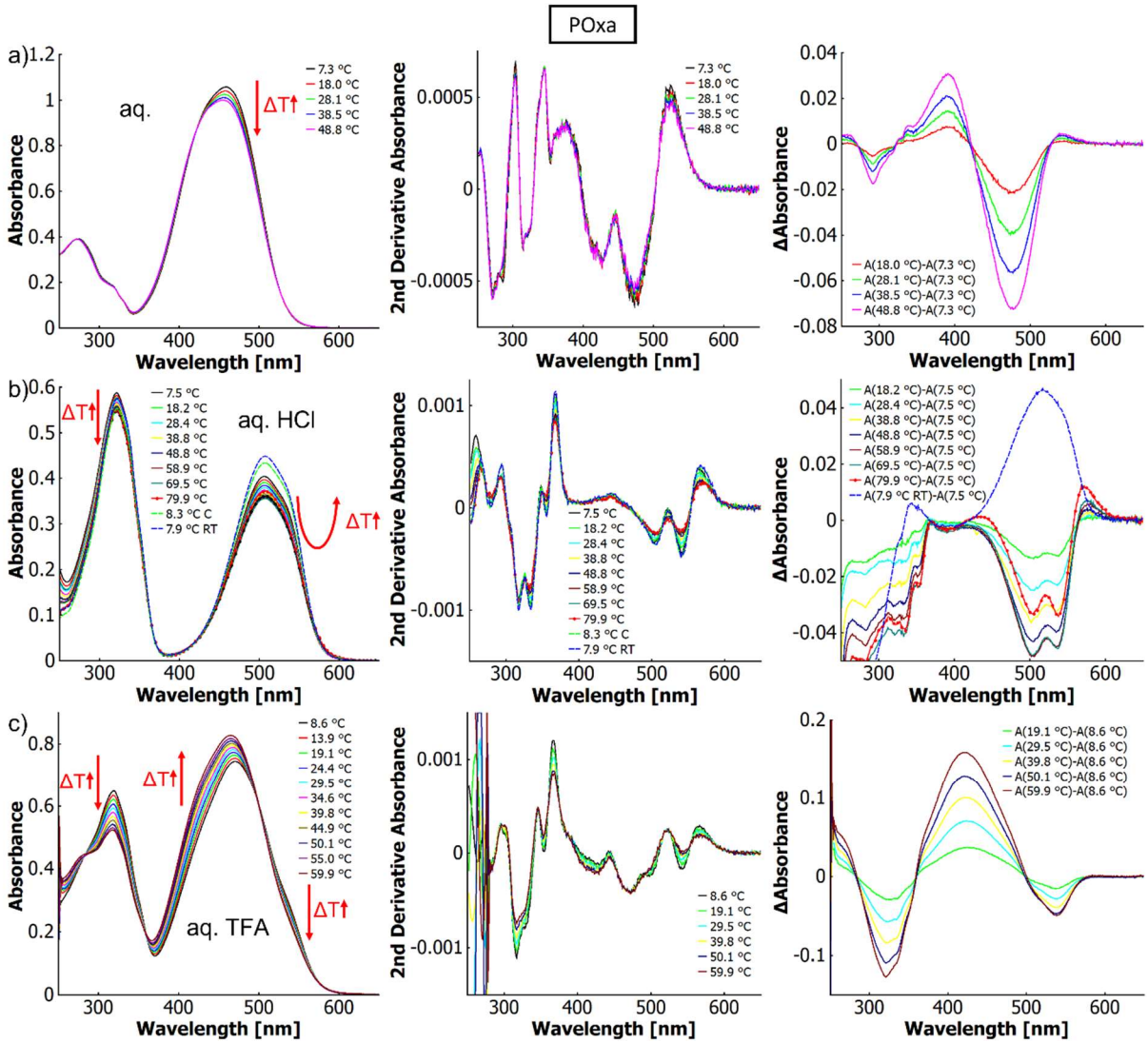

Figure S 29: From left to right: UV-vis spectra of poly(MeOxa-co-oMROxa) (POxa, 0.1 g L^{-1}) at different temperatures, the corresponding second derivative spectra, and the corresponding difference spectra a) in pure water; b) in aq. HCl (1.2 M), and c) in aq. trifluoroacetic acid (0.3 v/v%). The notation "C" in the legend describes that the spectrum was measured upon cooling from high temperatures and "RT" describes, that the same polymer solution was kept at room temperature for 18 hours before it was measured at the noted temperature.

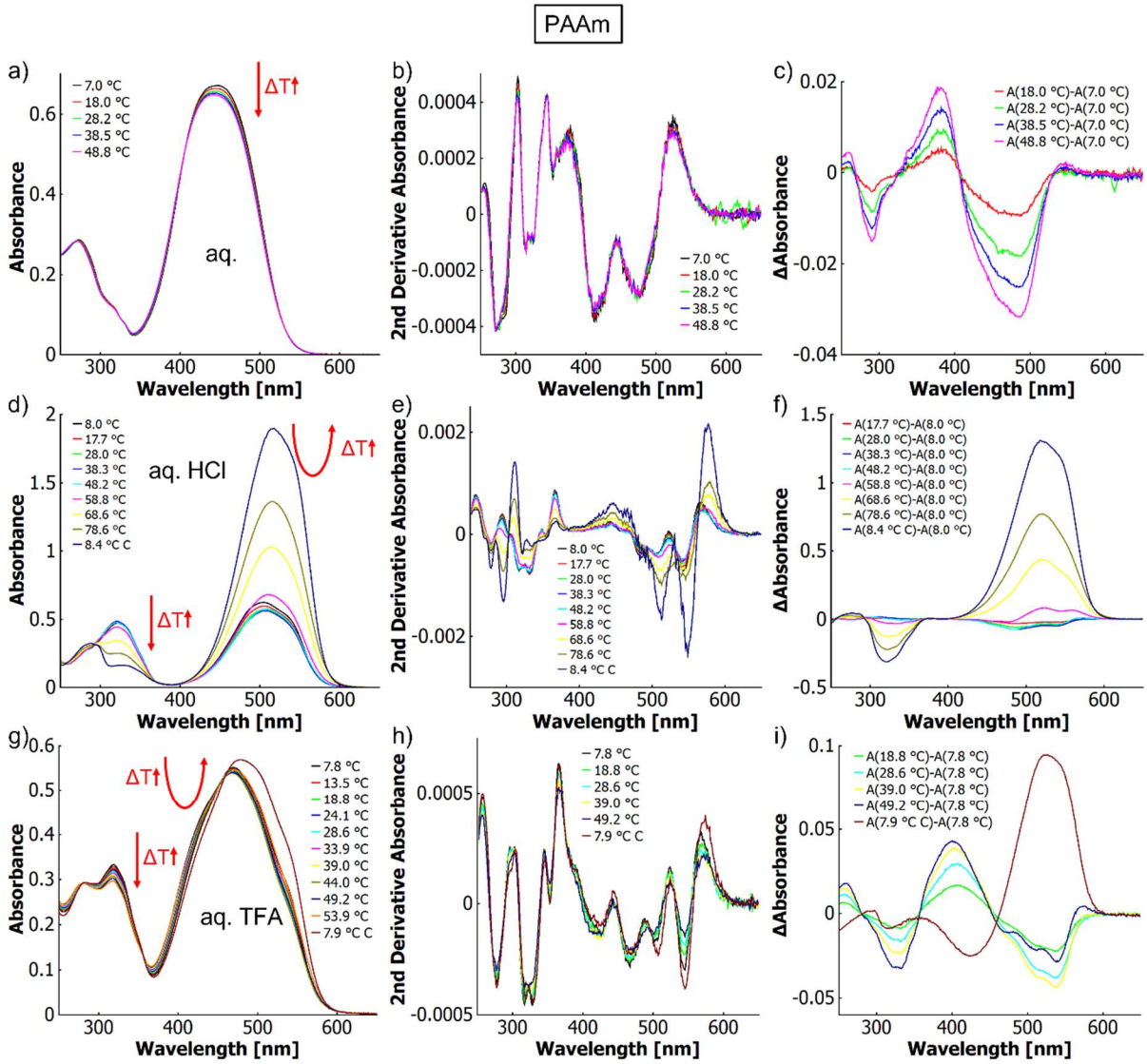

Figure S 30: From left to right: UV-vis spectra of poly(HEAm-co-oMRPipAm) (PAAm, 0.1 g L^{-1}) at different temperatures, the corresponding second derivative spectra, and the corresponding difference spectra a) in pure water; b) in aq. HCl (1.2 M), and c) in aq. trifluoroacetic acid (0.1 v/v%). The notation "C" in the legend describes that the spectrum was measured upon cooling from high temperatures.

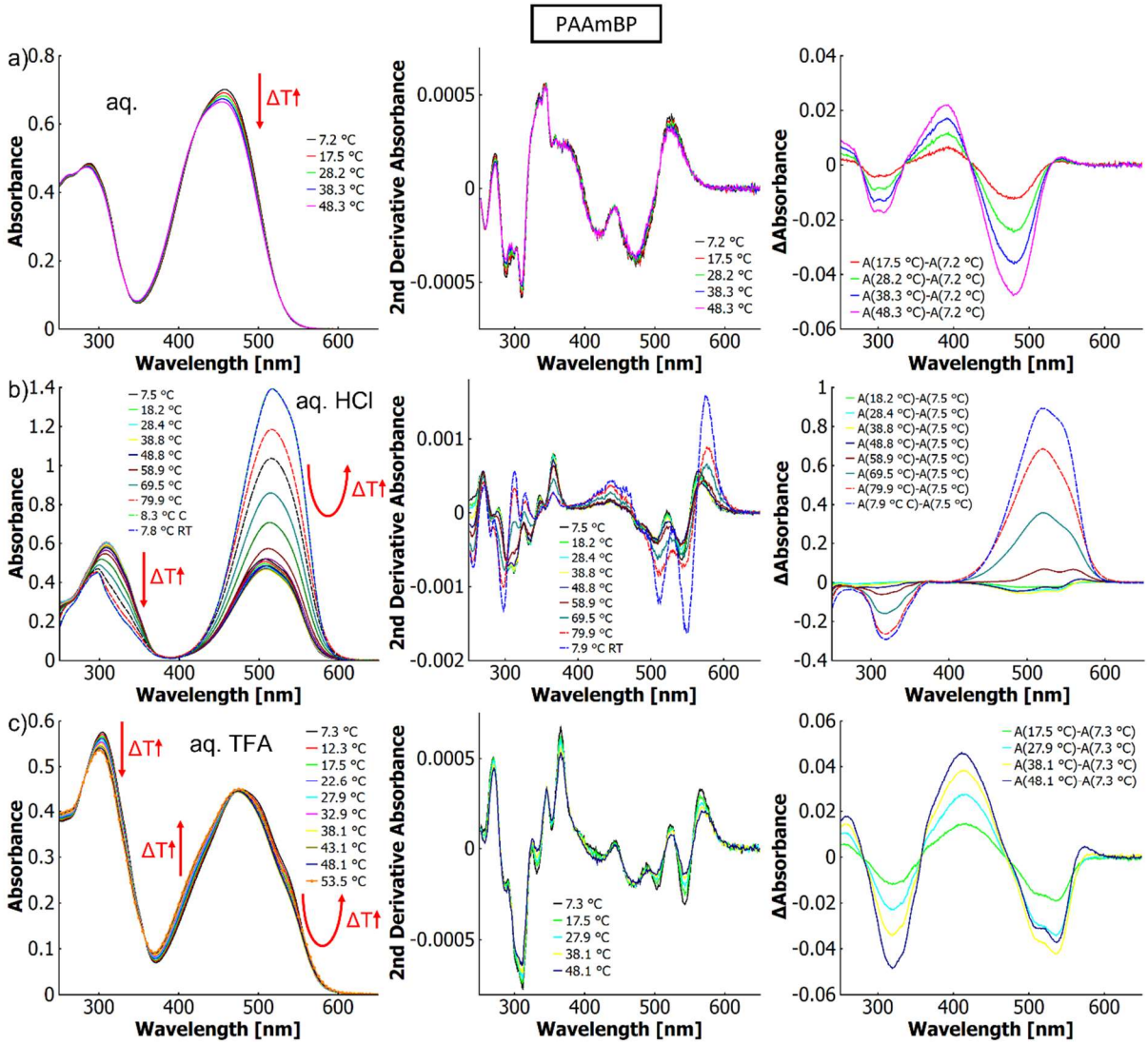

Figure S 31: From left to right: UV-vis spectra of poly(HEAm-co-oMRPipAm-co-BPAAm) (PAAmBP, 0.2 g L^{-1}) at different temperatures, the corresponding second derivative spectra zoomed into the relevant regions and the corresponding difference spectra a) in pure water; b) in aq. HCl (1.2 M), and c) in aq. trifluoroacetic acid (0.1 v/v%). The notation "C" in the legend describes that the spectrum was measured upon cooling from high temperatures and "RT" describes, that the same polymer solution was kept at room temperature for 18 hours before it was measured at the noted temperature.

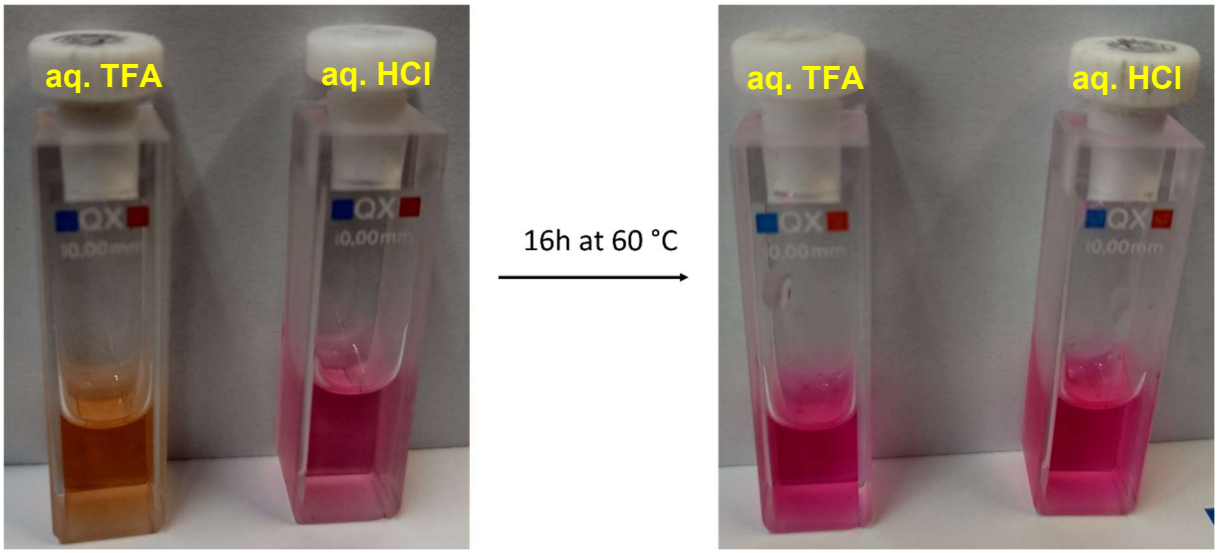

Figure S 32: Photographs of solutions at room temperature in aq. trifluoroacetic acid (cuvettes on the left of each picture, 0.1 v/v%) and in aq. HCl (cuvettes on the right of each picture, 1.2 M) of poly(HEAm-co-oMRPipAm-co-BPAAm) (PAAmBP, 0.2 g L^{-1}). Left picture: Fresh solutions before heat treatment; right picture: after 16 hours at 60 °C.

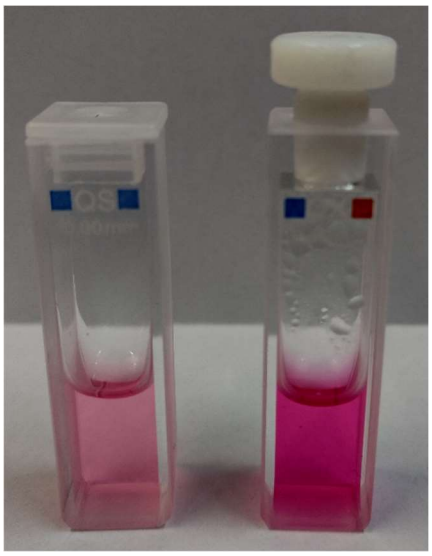

Figure S 33: Photograph of a solution in aq. HCl (1.2 M) of poly(HEAm-co-oMRPipAm-co-BPAAm) (PAAmBP, 0.2 g L^{-1}). The solution on the left is freshly prepared, the solution on the right after 3 hours at 75 °C.

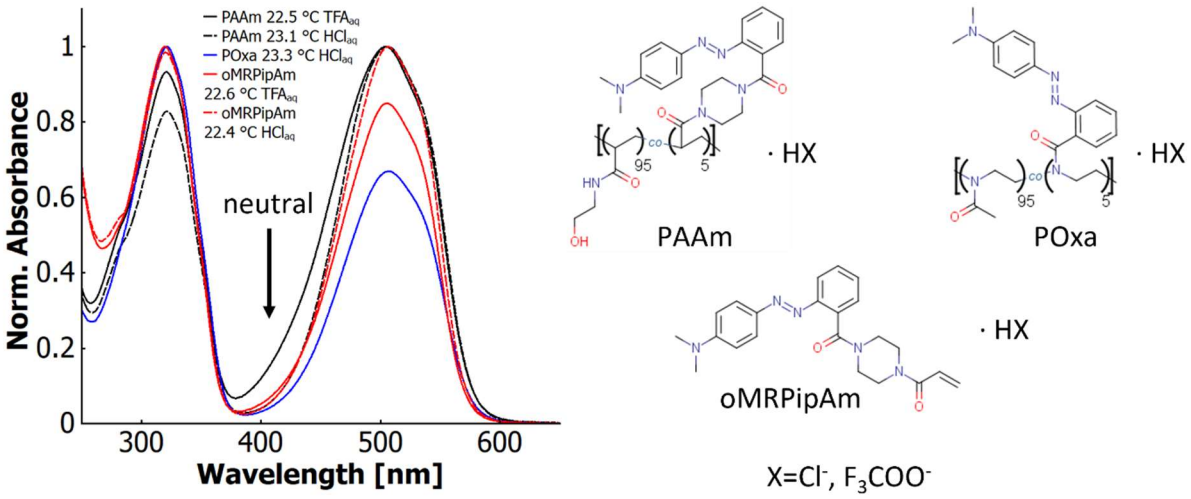

Figure S 34: Normalized UV-vis spectra of poly(HEAm-co-oMRPipAm) (PAAm), poly(MeOxa-co-oMROxa) (POxa), and oMRPipAm in aqueous HCl (1.2 M) or aqueous TFA (130 mM) at room temperature.

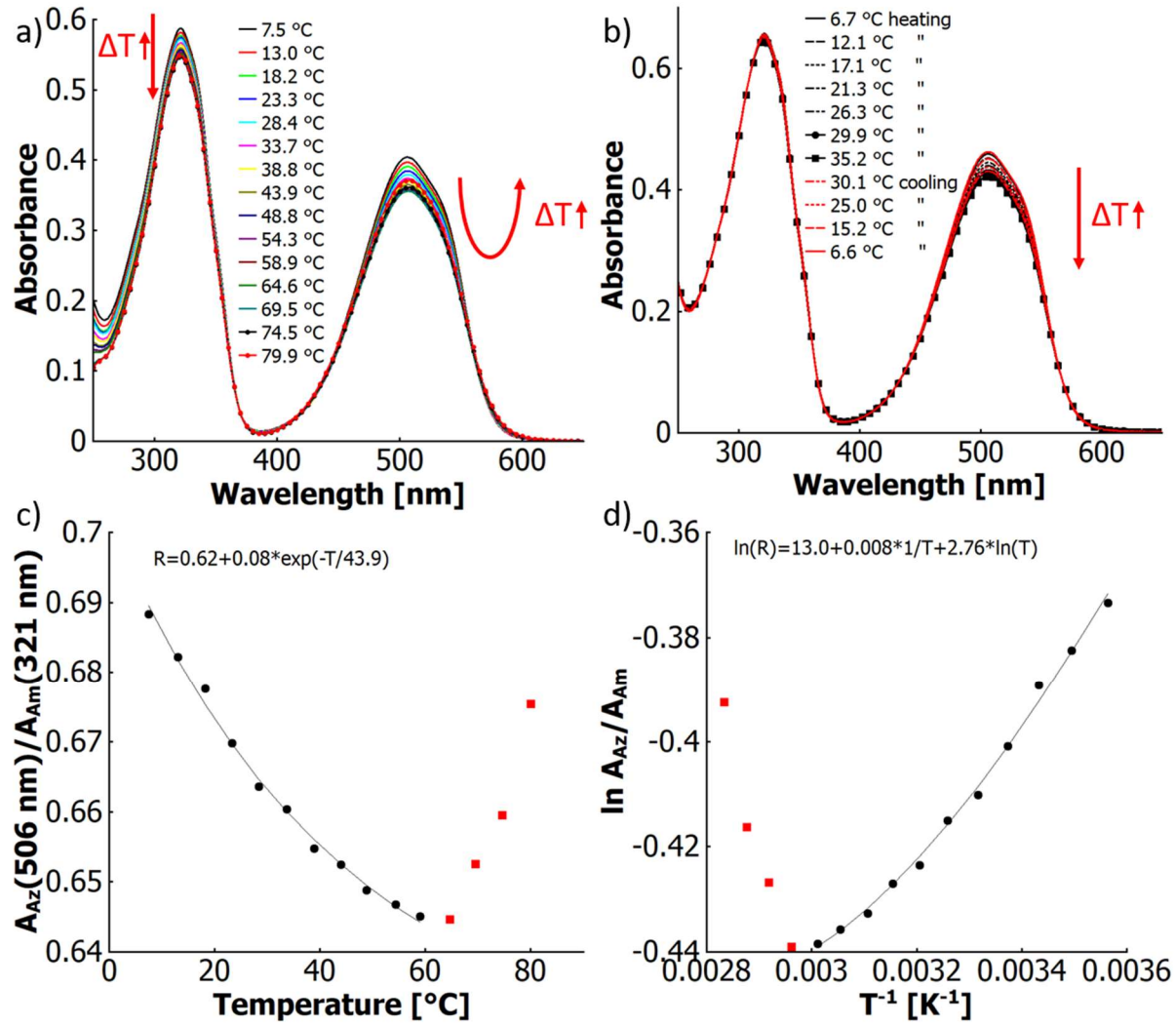

*Figure S 35: Temperature-dependent UV-vis spectra of aqueous solutions of poly(MeOxa-co-oMROxa) (POxa, 0.1 g L^{-1}, 1.2 M HCl) a) heating above the threshold temperature of irreversible change, and b) heating and cooling well below the threshold temperature of irreversible change; c) shows a plot of the absorbance ratio of the azonium ion absorption band by the ammonium ion absorption band vs temperature. The reversible part in black is fitted with an exponential decay function, the irreversible change is marked in red; d) shows the natural logarithm of the absorbance ratio vs the inverse of the absolute temperature. The reversible part in black is fitted with a function R=a-b*1/T+c*ln(T), the irreversible part marked in red.*

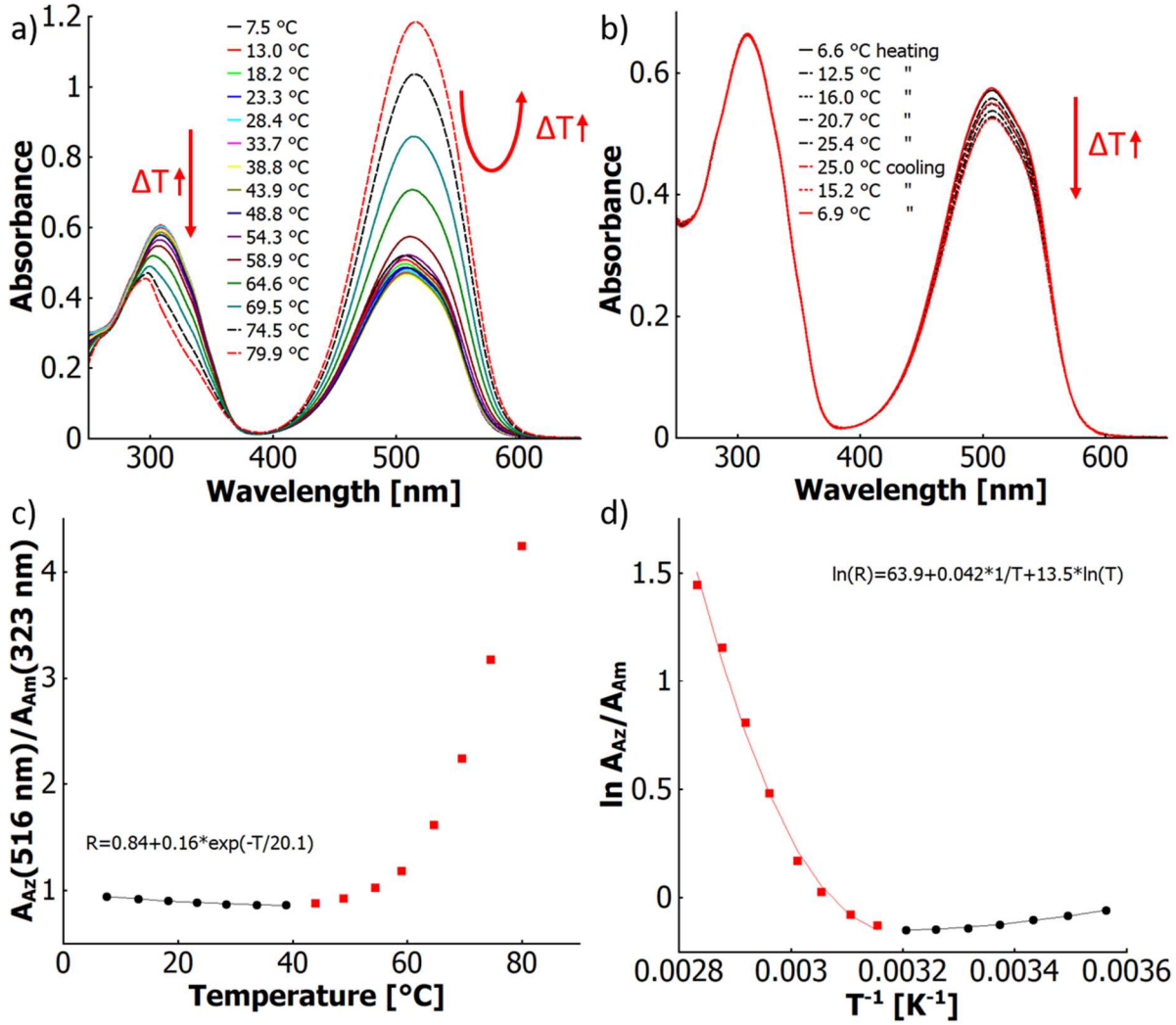

*Figure S 36: Temperature-dependent UV-vis spectra of aqueous solutions of poly(HEAm-co-oMRPipAm-co-BPAAm) (PAAmBP, 0.2 g L^{-1}, 1.2 M HCl) a) heating above the threshold temperature of irreversible change, and b) heating and cooling well below the threshold temperature of irreversible change; c) shows a plot of the absorbance ratio of the azonium ion absorption band by the ammonium ion absorption band vs temperature. The reversible part in black is fitted with an exponential decay function, the irreversible change is marked in red; d) shows the natural logarithm of the absorbance ratio vs the inverse of the absolute temperature. The reversible part in black is fitted with a function R=a-b*1/T+c*ln(T), the irreversible part marked in red.*

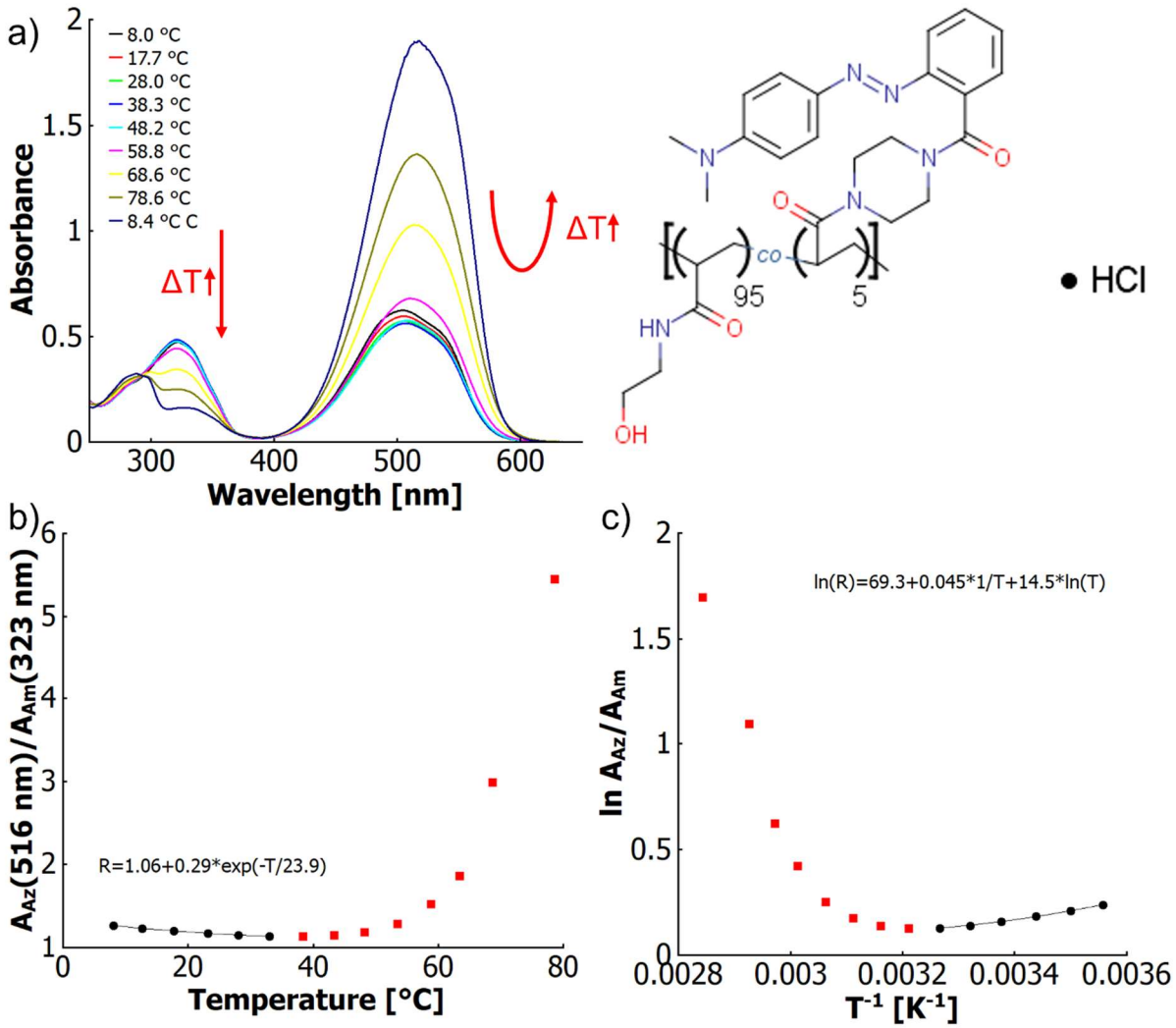

*Figure S 37: Temperature-dependent UV-vis spectra of aqueous solutions of poly(HEAm-co-oMRPipAm) (PAAm, 0.2 g L^{-1}, 1.2 M HCl) a) heating above the threshold temperature of irreversible change, b) shows a plot of the absorbance ratio of the azonium ion absorption band by the ammonium ion absorption band vs temperature. The reversible part in black is fitted with an exponential decay function, the irreversible change is marked in red; c) shows the natural logarithm of the absorbance ratio vs the inverse of the absolute temperature. The reversible part in black is fitted with a function R=a-b*1/T+c*ln(T), the irreversible part marked in red.*

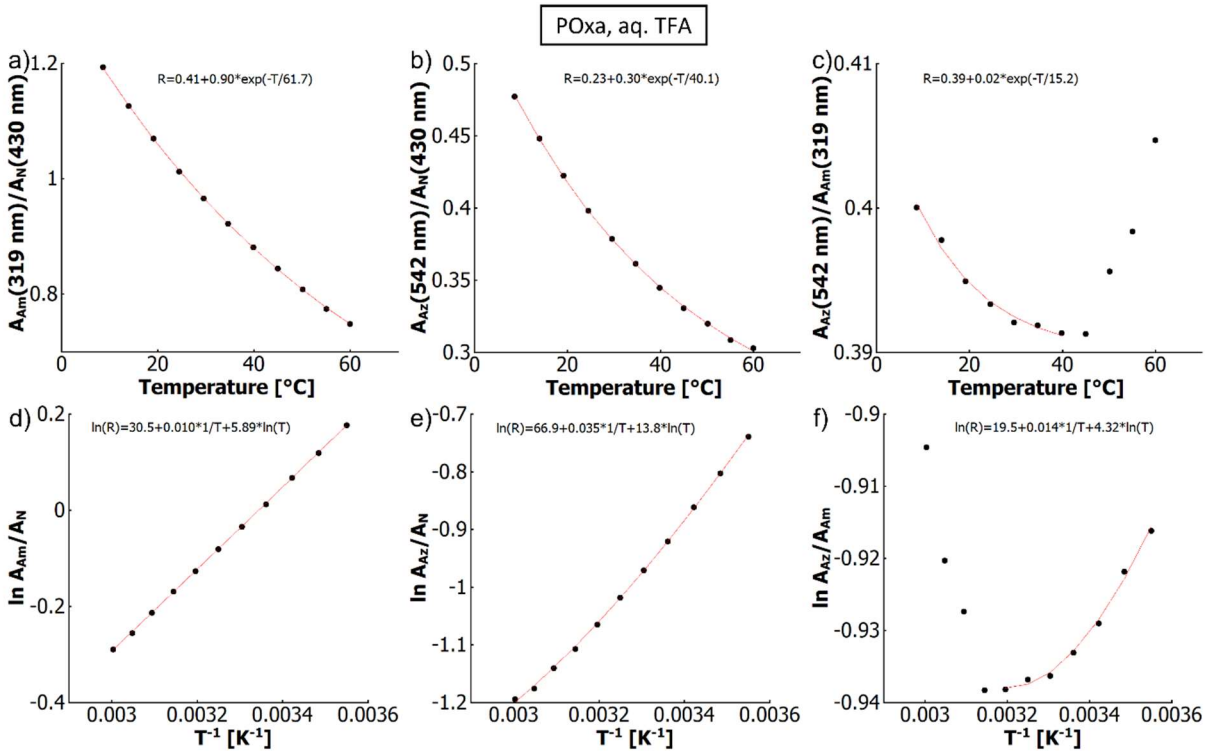

*Figure S 38: Graphs of the absorbance ratio of two species vs temperature for poly(MeOxa-co-oMROxa) (POxa, 0.2 g L^{-1}, 0.3 v/v% TFA) of a) ammonium ion vs neutral dye, b) azonium ion vs neutral dye and c) azonium ion vs ammonium ion, fitted with an exponential decay function, and of the natural logarithm of these ratios vs the inverse absolute temperature of d) ammonium ion vs neutral dye, e) azonium ion vs neutral dye and f) azonium ion vs ammonium ion, fitted with a function ln(R)=a-b*1/T+c*ln(T). The wavelengths of the absorbances were chosen to reduce overlap between the absorption bands of different species.*

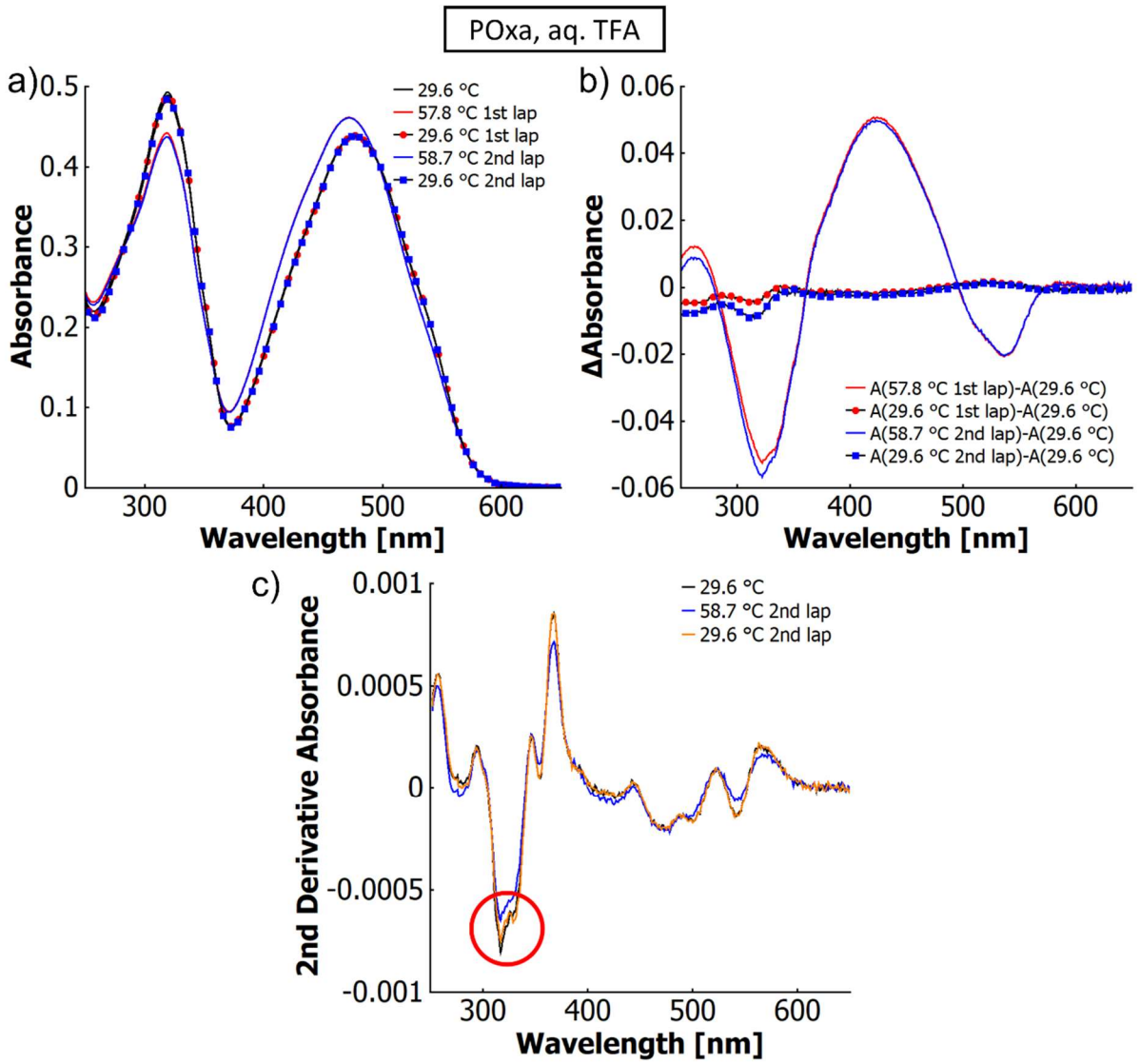

Figure S 39: a) UV-vis spectra of poly(MeOxa-co-oMROxa) (POxa) in aqueous TFA (0.1 g L^{-1}, 0.3 v/v% TFA) following a temperature program (29.6 °C→57.8 °C→29.6 °C→58.7 °C→29.6 °C), b) the corresponding difference spectra that were generated by subtracting the first spectrum from all following spectra, and c) the second derivative spectra of the first spectrum, and the second heating and cooling cycle. The region of interest in marked with a red circle.

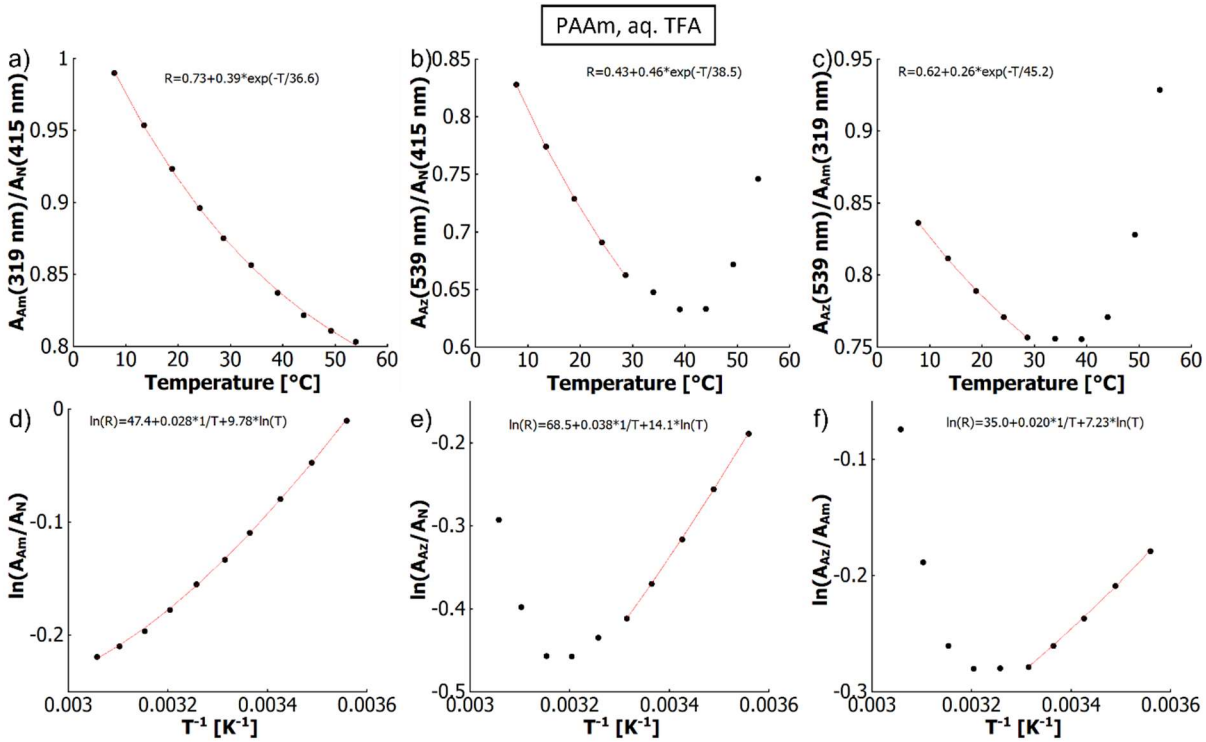

*Figure S 40: Graphs of the absorbance ratio of two species vs temperature for poly(HEAm-co-oMRPipAm) (PAAm, 0.1 g L^{-1}, 0.1 v/v% TFA) of a) ammonium ion vs neutral dye, b) azonium ion vs neutral dye and c) azonium ion vs ammonium ion, fitted with an exponential decay function, and of the natural logarithm of these ratios vs the inverse absolute temperature of d) ammonium ion vs neutral dye, e) azonium ion vs neutral dye and f) azonium ion vs ammonium ion, fitted with a function ln(R)=a-b*1/T+c*ln(T). The wavelengths of the absorbances were chosen to reduce overlap between the absorption bands of different species.*

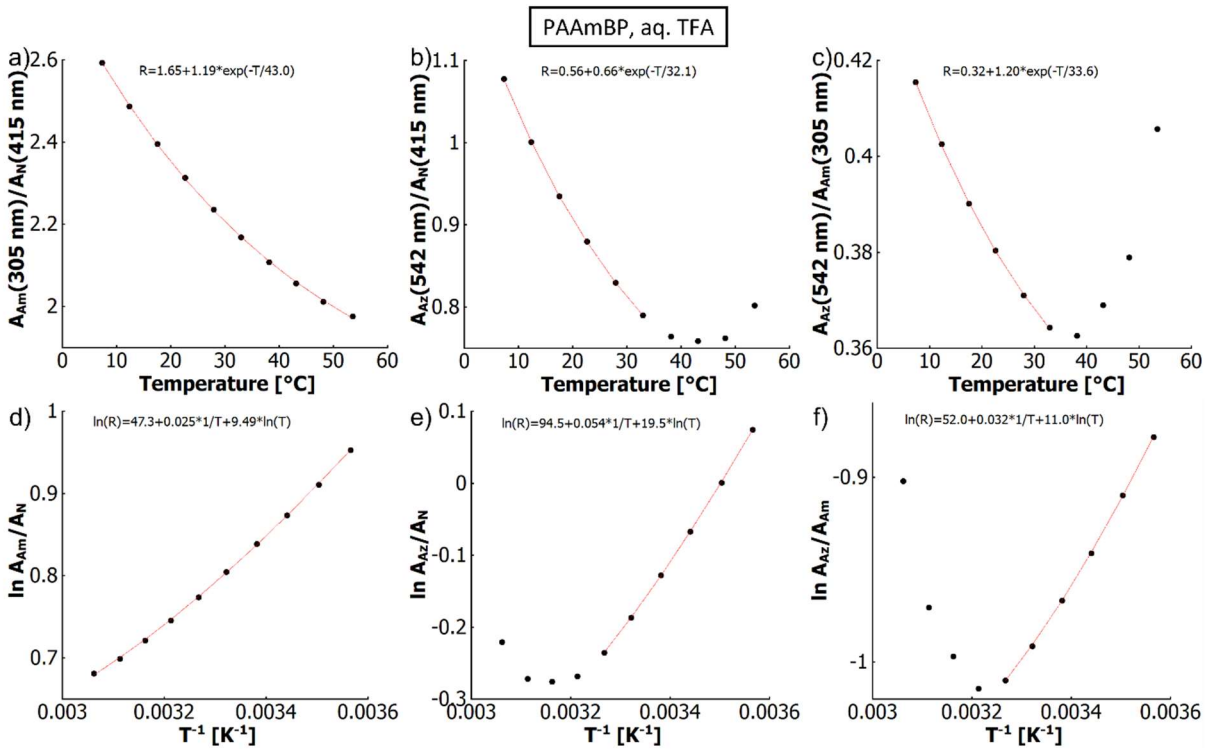

*Figure S 41: Graphs of the absorbance ratio of two species vs temperature for poly(HEAm-co-oMRPipAm-co-BPAAm) (PAAmBP, 0.2 g L^{-1}, 0.1 v/v% TFA) of a) ammonium ion vs neutral dye, b) azonium ion vs neutral dye and c) azonium ion vs ammonium ion, fitted with an exponential decay function, and of the natural logarithm of these ratios vs the inverse absolute temperature of d) ammonium ion vs neutral dye, e) azonium ion vs neutral dye and f) azonium ion vs ammonium ion, fitted with a function ln(R)=a-b*1/T+c*ln(T). The wavelengths of the absorbances were chosen to reduce overlap between the absorption bands of different species.*

Van't Hoff analysis:

In order to analyze the equilibria occurring in *partially* protonated systems, a ratiometric approach for the different possible combinations of the ammonium ion, the azonium ion, and the neutral species was employed. While van't Hoff analysis was applied to these data as well and can be fitted well in the reversible parts of the temperature dependence, the results are only comparative in nature as the equilibrium is rather complex. Some results are repeated from the main text to avoid fragmenting.

Interestingly, the absorbance ratio of the ammonium ion to the neutral dye (A(Am)/A(neutral)) is continuously varying with temperature in all three copolymers, even after irreversible changes owing to hydrolysis (cf. ESI Figure S 38, Figure S 40, Figure S 41). This suggests that thermo-halochromism is not affected by the depletion of the tertiary amide dye side groups and the increase of the hydrolysis product. The reason for this is the solubility of the hydrolysis product, the parent compound *o*-methyl red. Neutral *o*-methyl red is insoluble in water. Thus, only the protonated form exists in aqueous solution and is unable to participate or influence any (thermo-halochromic) protonation equilibrium between another neutral dye and its protonated counterpart. Additionally, the spectral changes of protonated *o*-methyl red at the wavelength corresponding to ammonium ions is miniscule, as the tautomerism lies heavily on the side of the azonium ion in this compound (cf. Figure S 27 a).

Both in PAAm and PAAmBP, the irreversible changes can be observed in the ratiometric plots and corresponding van't Hoff plots of the azonium ion to the neutral species (A(Az)/A(neutral)), as well as of the azonium ion to the ammonium ion (A(Az)/A(Am)) at the same temperature. The threshold temperature is lower in these *partially* protonated systems than it is in the completely protonated system. This was mentioned in the main text and may be a consequence of a difference in the hydrolysis mechanism.[7]

In stark contrast to the behavior of the polyacrylamides, in POxa the ratios of A(Az)/A(neutral) and A(Az)/A(Am) differ in their behavior. While A(Az)/A(neutral) is continuous over the whole temperature range and can be fitted, the plots for A(Az)/A(Am) are discontinuous, with the continuity being disturbed around 40 °C. At this temperature, the ratio of azonium to ammonium ions increases, meaning that more azonium ions are present in the system. This discrepancy is curious for two reasons.

1. In *completely* protonated solutions of the copolymer, the continuity is only disturbed

20 K higher. 2. It would be expected that when one of the plots is discontinuous, the other must be as well, as is the case for the copolymers PAAm and PAAmBP.
The discrepancy suggests that a process affecting only the ammonium-azonium tautomerism but not thermo-halochromism occurs.
Examining the reversibility of that process by alternating the temperature between just below the increase in A(Az)/A(Am) (30 °C) and well above it (60 °C) shows that the process is indeed not reversible (cf. ESI Figure S 39). Interestingly, the absorbance of the ammonium ion (ca. 320 nm) decreases significantly more than the absorbance of the neutral species (ca. 420 nm) decreases and the absorbance of the azonium ion (ca. 510 nm) increases. In the latter two, there is barely any change in the absorbance. However, as the extinction coefficient of the ammonium species is smaller than that of the azonium species, hydrolysis of the dye linker should lead to a considerably higher increase in absorbance corresponding to the azonium ion than the decrease in absorbance corresponding to the ammonium ion.
Two possible reasons for this phenomenon can be hypothesised. 1. The dye is hydrolyzed but stays in solution in the neutral state owing to hydrogen bonding between the carboxylic acid of the dye and the formed polyethyleneimine backbone. This constellation has been shown in dry polymer films before, so it is at least worthy to mention.[8] However, as protonation of the dye would certainly lead to better solubility and hydrogen bonding with water would be stronger than of the neutral dye with the backbone, this option is not very likely.
2. As we were able to show that hydrolysis of the 2-methyl-2-oxazoline groups proceeds at considerably higher rates than that of the dye in the *completely* protonated system at even higher temperatures, a change in the hydrogen bonding patterns stabilizing the ammonium ion may be the cause for the observed shift in the ammonium-azonium tautomerism.
Experimentally, only a slight change in the sub-band pattern of the ammonium ion can be observed at 330 nm in the second derivative spectra before and after heating the copolymer in aqueous TFA (cf. Figure S 39 c). The peaks corresponding to the neutral dye and the azonium ion are completely unaffected, again indicating that not the dye itself is hydrolyzed. It is also reasonable that a change in the hydrogen bonding patterns does affect the sub-band structure, leading to a decrease in absorbance, without considerably affecting the protonation equilibrium. The spectral variation is small enough to be visible in the sensitive ammonium-azonium tautomerism, yet not in

the protonation equilibrium that shows significantly larger spectral changes per temperature increment.

The values of the thermochromicity parameters (cf. Table 4) for these partially protonated solutions are in the same order of magnitude for all three copolymers, thus the curve progression is of more importance than the values themselves. However, it should be noted that the wavelength pair corresponding to the ammonium-azonium tautomerism yields smaller thermochromicity parameters for PAAm and PAAmBP and larger ones for POxa. Still, the values corresponding to thermo-halochromism are considerably higher than those corresponding to the ammonium-azonium tautomerism, meaning that the tautomerism is a secondary effect in *partially* protonated systems.

Because of the limited quality owing to scattering, the spectra of the gel of PAAmBP were not subjected to van't Hoff analysis.

Reversibility of Thermo-halochromism in Partially Protonated Copolymer Solutions Bearing oMRPipAm:

To analyze the temperature-dependent reversibility of the thermochromism, the *partially* protonated systems were measured with a temperature program. The reversible portion of the equilibrium was tested by measuring UV-vis spectra at several temperatures. The solutions were measured at each temperature step, first at low temperatures, then heated to below the threshold temperature, and cooled to the initial, low temperature again. The irreversible part of the equilibrium was examined by heating to 70 °C for twenty minutes, then measuring a spectrum (approx. 5 minutes) and cooled to the initial temperature again. The chosen temperature is well above the threshold temperature of PAAm and slightly above that of POxa, as determined in the *completely* protonated systems. These results are compiled as UV-vis spectra and difference spectra in Figure 7 (main text).

The difference spectra of the temperature series for POxa show that the thermochromic changes are mostly reversible even at high temperatures. Only a small positive irreversible peak above 500 nm, a broad negative corresponding to neutral species (390-480 nm) and a comparatively strong negative peak corresponding to the ammonium ion (~320 nm) can be observed (blue dotted black line in Figure 7 b, main text). Even the stronger band of the ammonium species is small compared to the

reversible thermo-halochromism at the highest temperatures (blue line in Figure 7 b, main text). Thus, the thermochromism of this copolymer in acidified aqueous solution is dominated by reversible thermo-halochromism, owing to its higher threshold temperature.

In the case of PAAm, the spectra below the threshold temperature show the already described, reversible thermo-halochromic behavior (red line in Figure 7 d, main text), with the spectrum upon cooling being virtually the same as the initial one (red dotted line in Figure 7 d, main text). After the heat treatment, the high-temperature spectrum shows features of both thermo-halochromism as well as of hydrolysis (blue line in Figure 7 d). More precisely, a positive band with vibronic features at 557 nm and 521 nm can be observed that shows the formation of *o*-methyl red azonium, as well as a broad positive band with a maximum at 405 nm that shows deprotonation of protonated species at higher temperatures. The only negative band here is at 319 nm, showing the conversion of the ammonium species to either *o*-methyl red azonium or the neutral dye.

When this solution is cooled again, the absolute changes compared to the initial solution become obvious (blue dotted line in Figure 7 d, main text). Both the reversible part, meaning the difference to the solution at 70 °C and the irreversible part, which are the changes compared to the initial solution, can be determined. After cooling, one positive band and two negative bands appear in the difference spectra. The positive band in the red has its maximum at 523 nm, with a shoulder around 560 nm. This fits the formation of the *o*-methyl red azonium by hydrolysis of the tertiary amide. The negative bands at 423 nm and at 317 nm demonstrate the decrease in concentration of the neutral and the ammonium species, respectively.

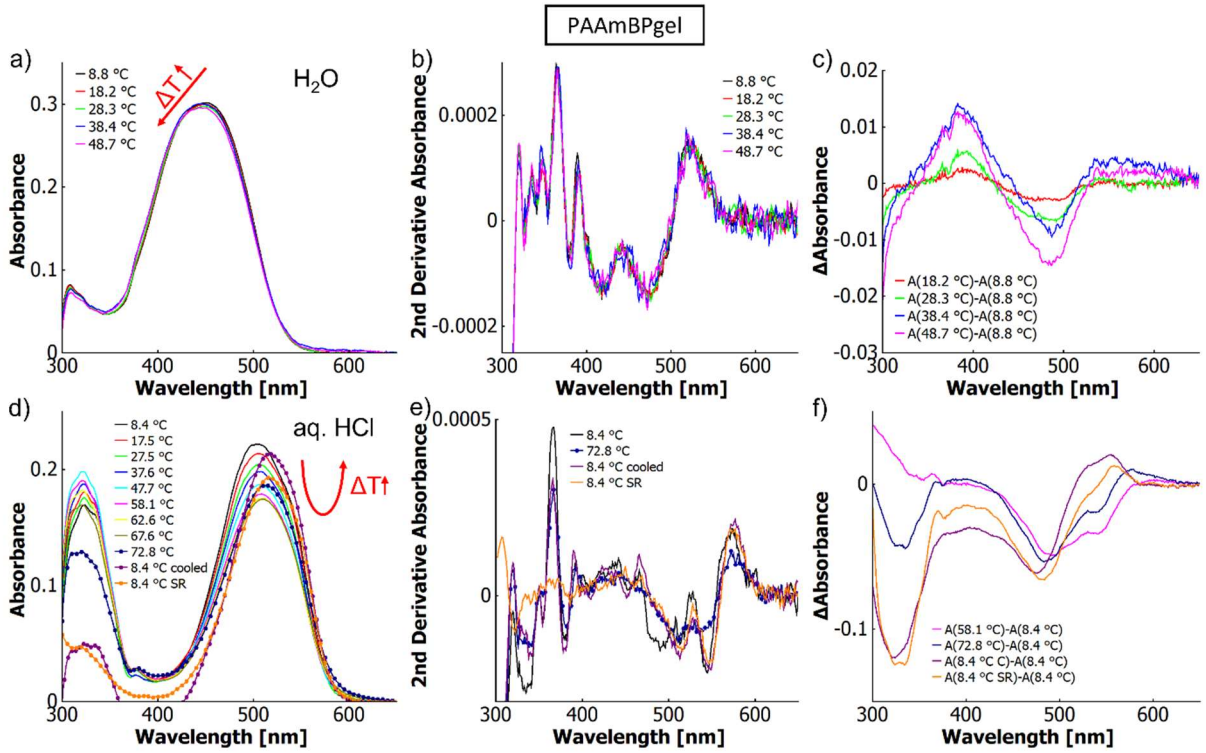

Figure S 42: UV-vis spectra of photocrosslinked, swollen films of poly(HEAm-co-oMRPipAm-co-BPAAm) (PAAmBP) at different temperatures in a) water, and d) aqueous HCl (1.2 M), the corresponding second derivative spectra for b) water, and e) aqueous HCl (1.2 M), and the corresponding difference spectra for c) water, and f) aqueous HCl (1.2 M). The notation "SR" in the legend of d) describes that the spectrum was measured after the slide with the polymer film was removed.

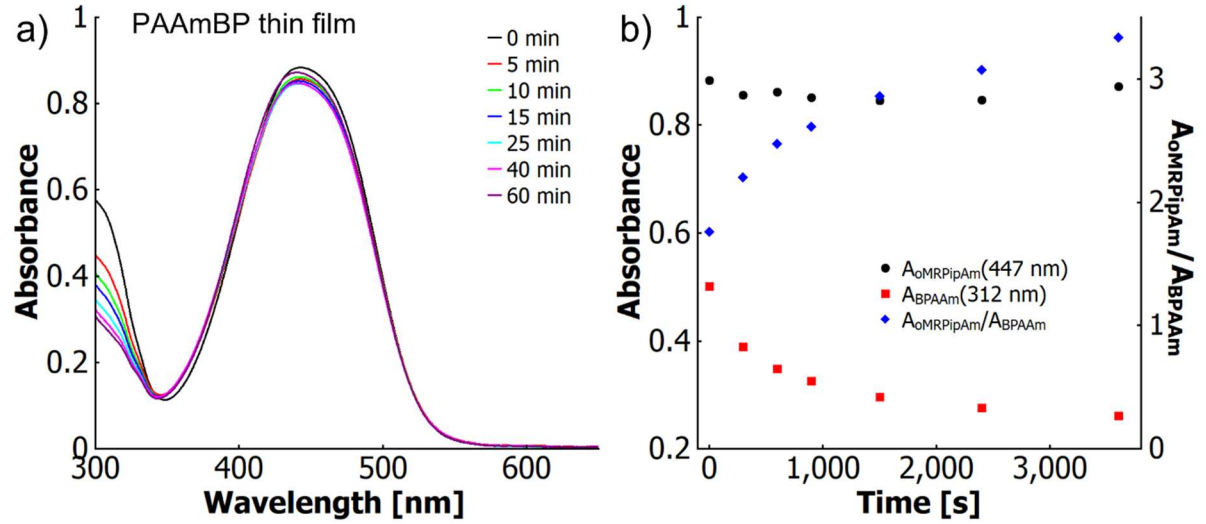

Figure S 43: a) UV-vis spectra of a dry thin film of poly(HEAm-co-oMRPipAm-co-BPAAm) (PAAmBP) on glass after different irradiation times at 302 nm for an overall dose of 28.4 J cm^{-2}; b) progression of the absorbances of the main absorption band of the dye (black filled circles) and of the photocrosslinker (red squares), as well as of their ratio (blue diamonds).

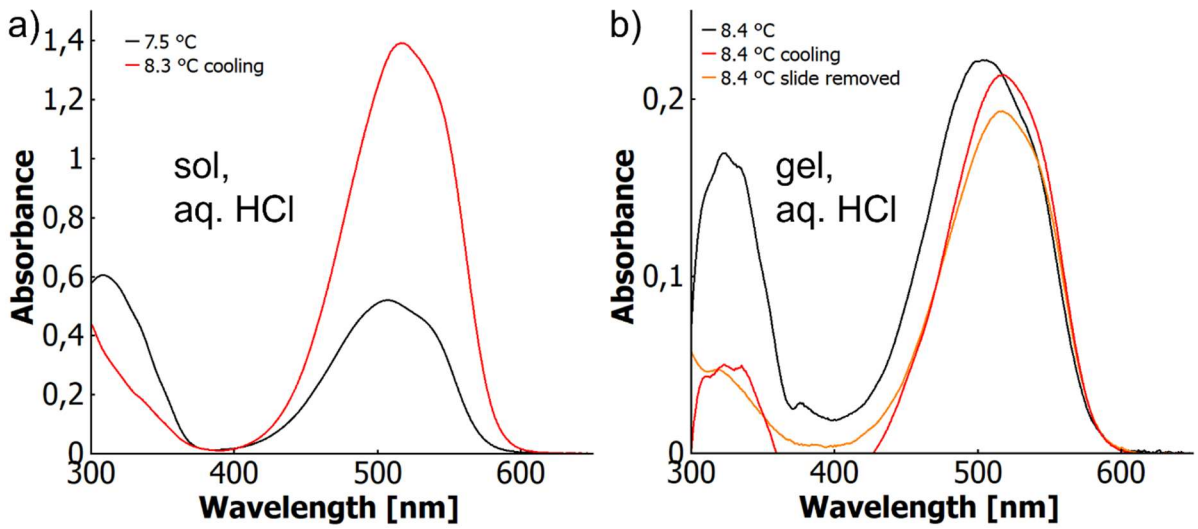

Figure S 44: UV-vis spectra of a) poly(HEAm-co-oMRPipAm-co-BPAAm) (PAAmBP) in aqueous HCl (1.2 M) and b) photocrosslinked, swollen film of PAAmBP in aqueous HCl (1.2 M) at low temperatures before heating, after heating and cooling to initial temperatures again ("cooling") and after the gel films were removed, where applicable ("slide removed").

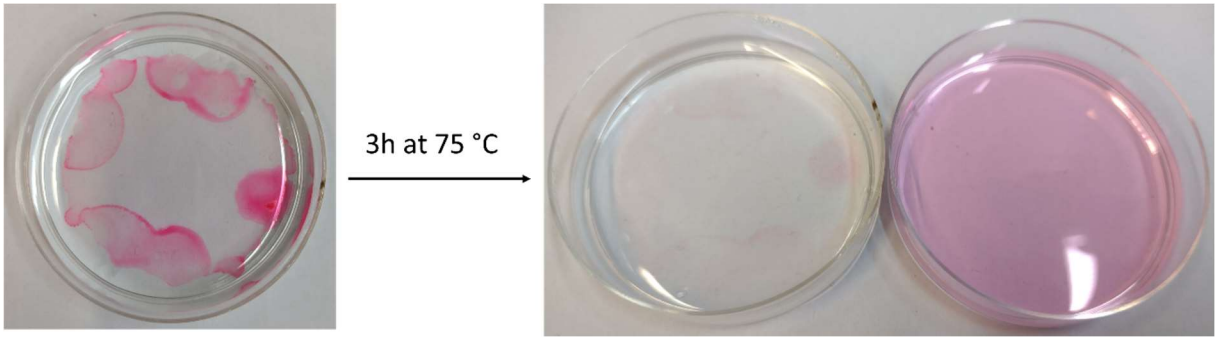

Figure S 45: Photographs of: left picture) patches (pink spots) of a freshly prepared, photocrosslinked gel of poly(HEAm-co-oMRPipAm-co-BPAAm) (PAAmBP) swollen in aqueous HCl (1.2 M), and of right picture) the same gel after 3 hours at 75 °C (petri dish on the left, swollen in water to retain swollen gel structure) and the removed supernatant (right picture).

References

[1] J. Jia, M. Sarker, M. G. Steinmetz, R. Shukla, R. Rathore, J. Org. Chem. 2008, 73, 8867.

[2] T. G. Jaik, B. Ciubini, F. Frascella, U. Jonas, Polym. Chem. 2022, 13, 1186.

[3] a) H. A. Staab, A. Mannschreck, Chem. Ber. 1962, 95, 1284; b) D. E. Bergbreiter, P. L. Osburn, C. Li, Org. Lett. 2002, 4, 737; c) H. A. Staab, M. Lüking, F. H. Dürr, Chem. Ber. 1962, 95, 1275.

[4] a) H. Naghibi, A. Tamura, J. M. Sturtevant, Proc. Natl. Acad. Sci. U.S.A. 1995, 92, 5597; b) Y. Liu, J. M. Sturtevant, Protein Sci. 1995, 4, 2559.

[5] D. Grant, M. Mehdizadeh, A.-L. Chow, J. E. Fairbrother, Int. J. Pharm. 1984, 18, 25.

[6] D. G. Hafeman, K. L. Crawford, L. J. Bousse, J. Phys. Chem. 1993, 97, 3058.
[7] a) R. A. Cox, Can. J. Chem. 2008, 86, 290; b) A. Williams, J. Am. Chem. Soc. 1976, 98, 5645; c) C. R. Smith, K. Yates, J. Am. Chem. Soc. 1971, 93, 6578; d) C. R. Smith, K. Yates, J. Am. Chem. Soc. 1972, 94, 8811.
[8] O. Kulikovska, L. M. Goldenberg, J. Stumpe, Chem. Mater. 2007, 19, 3343.

6 Photomotion of Hydrogels with Covalently Attached Azo Dye Moieties – Thermoresponsive and Non-Thermoresponsive Gels

Thorben Gwydion Jaik, Assegid M. Flatae, Navid Soltani, Philipp Reuschel, Mario Agio, Emiliano Descrovi, Ulrich Jonas

Gels, 2022, **8**, 541-552
https://doi.org/10.3390/gels8090541

Published by *Multidisciplinary Digital Publishing Institute (MDPI)* in the special issue *Advances in Stimuli-Responsive Polymer Gels* in the journal *Gels* as an Open Access article under the terms of the Creative Commons CC BY 4.0 license, which permits distribution, and reproduction in any medium, provided the original work is properly cited (CC BY 4.0, https://creativecommons.org/licenses/by/4.0/).
The electronic supporting information of this publication can be found under https://doi.org/10.3390/gels8090541 and contains apart from the data in the following also three movies (Movie S1, Movie S2, Movie S3).

Contributions of the authors to this project:

- Synthesis of monomers and polymers, sample preparation, active measurements, data analysis, as well as interpretation were done by me.
- The optical setups used in the optical experiments were designed and built by Prof. Dr. Agio, A. M. Flatae, N. Soltani, and P. Reuschel. The optical experiments were supervised by A. M. Flatae and P. Reuschel.
- The project was initiated by Prof. Dr. Descrovi and Prof. Dr. Jonas. The complete draft was written by me and refined and edited together with Prof. Dr. Jonas. The final version was further edited by all authors.

Corrections:

- In Figure 2 of the paper, parts (c) and (d) were mistakenly exchanged with parts (e) and (f), respectively. Thus, the figure caption does not match the content. The correct figure appears below.

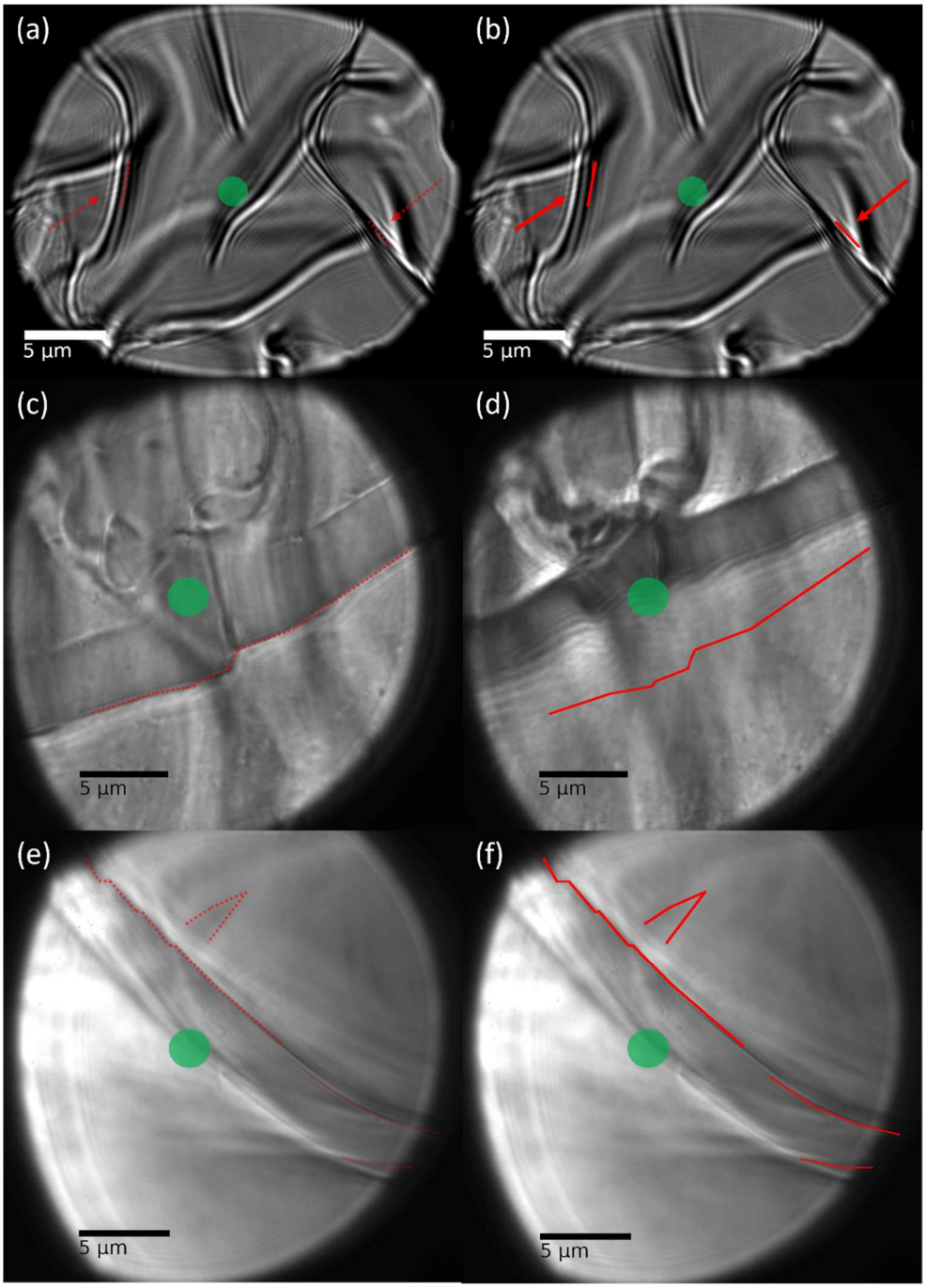

gels

MDPI

Communication

Photomotion of Hydrogels with Covalently Attached Azo Dye Moieties—Thermoresponsive and Non-Thermoresponsive Gels

Thorben G. Jaik [1], Assegid M. Flatae [2], Navid Soltani [2], Philipp Reuschel [2], Mario Agio [2,3], Emiliano Descrovi [4] and Ulrich Jonas [1,*]

[1] Department Chemistry—Biology, University of Siegen, Adolf-Reichwein-Strasse 2, 57076 Siegen, Germany
[2] Department Physics, University of Siegen, Walter-Flex-Str. 3, 57072 Siegen, Germany
[3] National Institute of Optics (INO), National Research Council (CNR), Via Nello Carrara 1, 50019 Sesto Fiorentino, Italy
[4] Department of Applied Science of Technology (DISAT), Politecnico di Torino, Corso Duca degli Abruzzi 24, 10129 Torino, Italy
* Correspondence: jonas@chemie.uni-siegen.de

Abstract: The unique photomotion of azo materials under irradiation has been in the focus of research for decades and has been expanded to different classes of solids such as polymeric glasses, liquid crystalline materials, and elastomers. In this communication, azo dye-containing gels are obtained by photocrosslinking of non-thermoresponsive and lower critical solution temperature type thermoresponsive copolymers. These are analysed with light microscopy regarding their actuation behaviour under laser irradiation. The influences of the cloud-point temperature and of the laser power are investigated in a series of comparative experiments. The thermoresponsive hydrogels show more intense photoactuation when the cloud-point temperature of the non-crosslinked polymer is above, but closer to, room temperature, while higher laser powers lead to stronger motion, indicating a photothermal mechanism. In non-thermoresponsive gels, considerably weaker photoactuation occurs, signifying a secondary mechanism that is a direct consequence of the optical field-azo dye interaction.

Keywords: photoactuation; azo hydrogels; LCST

check for updates

Citation: Jaik, T.G.; Flatae, A.M.; Soltani, N.; Reuschel, P.; Agio, M.; Descrovi, E.; Jonas, U. Photomotion of Hydrogels with Covalently Attached Azo Dye Moieties—Thermoresponsive and Non-Thermoresponsive Gels. *Gels* **2022**, *8*, 541. https://doi.org/10.3390/gels8090541

Academic Editors: Hailei Zhang and Yonggang Wu

Received: 5 August 2022
Accepted: 26 August 2022
Published: 28 August 2022

Publisher's Note: MDPI stays neutral with regard to jurisdictional claims in published maps and institutional affiliations.

Copyright: © 2022 by the authors. Licensee MDPI, Basel, Switzerland. This article is an open access article distributed under the terms and conditions of the Creative Commons Attribution (CC BY) license (https://creativecommons.org/licenses/by/4.0/).

1. Introduction

Photoactuated polymer-based hydrogels are water-swollen networks with macromolecular chain segments that experience mechanical deformation under light irradiation. The photoactuation of these systems can be traced to essentially two mechanisms: A photothermal mechanism, in which, e.g., embedded nanoscaled materials serving as absorbers are heated by light and act on either elastomers or thermoresponsive polymers [1–3], or a photochemical mechanism, in which dyes such as spiropyranes, hexaarylbiimidazoles, and azobenzenes lead to deformation upon light-induced changes in their molecular structure [4,5].

Photothermal effects can be observed in azo dye-containing systems as well. Under irradiation with light of appropriate wavelength according to the dye absorption and high intensity (100–400 mW cm^{-2}), the temperature of films of polymer-dye blends [6], azopolymers [7], and liquid-crystalline elastomers containing azobenzene moieties [8] can increase by up to 80 K temperature difference. However, the temperature rise depends specifically on the characteristics of the system, as an increase of only a few Kelvins has been observed in glassy polymers [9] and thick films of nematic liquid-crystalline elastomers [10].

An application of azobenzene-containing copolymers was reported for artificial extracellular matrices (ECM) that can be switched in stiffness and swelling states by irradiation with light [11]. In these examples, lower critical solution temperature (LCST)-type thermoresponsive polymers in solution and hydrogels containing (hydroxy-) azobenzene units

were alternatingly irradiated with UV- and visible light to switch between the *trans*- and *cis*-state of the dye. In the *trans*-state, the systems are more hydrophobic compared to the *cis*-state, and thus, lowered in their cloud point and swelling ratio. Consequently, both the cloud point of the polymers in solution, as well as the swelling ratio of the corresponding gels can be switched by irradiation with light. It must be noted that the thermal relaxation from the *cis*- to the *trans*-isomer is slow in the specific azobenzene derivatives used.

A widely explored photoresponsive gel system is the combination of cyclodextrin and azobenzene-containing compounds or polymers. In these systems, the azobenzene derivatives can be complexated by cyclodextrin in the *trans*-state but not in the *cis*-state. Therefore, the dye and cyclodextrin form crosslinks that are reversible under irradiation with light of suitable wavelength. As a consequence, it is possible to switch between the sol- and the gel-state [12–26].

In the present study, we aim to expand the range of photoactive soft materials containing azo dyes. For this purpose, we synthesised photocrosslinkable, hydrophilic copolymers by free radical polymerisation with *o*-methyl red attached to the backbone as push-pull azo dye. By photocrosslinking and swelling with water, azo dye-containing hydrogels are obtained. Two classes of gels were prepared for which photoactuation was investigated. The first one is a non-thermoresponsive gel based on *N*-hydroxyethyl acrylamide (HEAm). The second system comprises a hydrogel with LCST-behaviour, prepared from *N*-isopropylacrylamide (NiPAAm). The obtained hydrogels were irradiated with a focussed laser and photoactuation was tracked by light microscopy. A comparison of the systems allows researchers to separate photochemical and photothermal effects.

2. Results and Discussion

Thermoresponsive and non-thermoresponsive copolymers were synthesised by free radical polymerisation from the hydrophilic monomers NiPAAm and HEAm, a *N*-hydroxyethyl acrylamide ester of *o*-methyl red (oMREAm), and the photocrosslinker 4-benzophenone acrylamide (BPAAm). From these copolymers, hydrogels were obtained by photocrosslinking, and subsequent swelling in water. While NiPAAm introduces LCST-type thermoresponsiveness in aqueous copolymer solution, the cloud-point temperature may be tuned by varying the ratio of NiPAAm to HEAm, which is a highly polar monomer and, by itself, does not show thermoresponsiveness. A higher amount of HEAm in a PNiPAAm-copolymer increases the cloud-point temperature, as more hydrophilic comonomers lead to a decrease in cloud-point temperature in LCST-type copolymers. [27] HEAm was chosen as oMREAm is a pH indicator and additional factors such as protonation from a monomer such as methacrylic acid had to be avoided to reduce complexity of the systems.

Thus, four copolymers, which either do not respond to temperature or show LCST-behaviour over a range close to and above room temperature, were synthesised to investigate their photoactuation capacities in comparative optical experiments. P_{NR} does not show thermoresponsive behaviour. A 1 w% aqueous solution of $P_{22°C}$ features a cloud-point temperature at 22 °C, $P_{35°C}$ at 35 °C, and $P_{45°C}$ at 45 °C (cf. Figure 1, ESI Figure S5b). A similar dye content was targeted during the polymer synthesis for these copolymers with an oMREAm monomer feed of 2.5%. The BPAAm feed was set to 1% for P_{NR}, $P_{22°C}$, and $P_{35°C}$, but to 2.5% for $P_{45°C}$, as photocrosslinking and attachment to a surface proved challenging at 1% BPAAm for $P_{45°C}$ due to the increased hydrophilicity and the corresponding higher swelling ratio of this particular polymer.

The copolymers were drop-cast on benzophenone-functionalised glass surfaces and subsequently photocrosslinked with UV-light (302 nm, 28.4 J cm^{-2}). The glass slides were treated prior with 4-(3-triethoxysilyl) propoxybenzophenone to allow for covalent attachment of the polymer network to the glass.

The films were swollen in water before they were fixed in a home-built optical setup. The sample is illuminated from the bottom with a focussed green laser (532 nm wavelength) and from the top with a red LED in a widefield configuration. Scattered light from the sample is collected via the focussing objective (50×, 0.95 NA) and the green light is spectrally

blocked via a dichroic beamsplitter and a longpass filter. A lens focusses the scattered light onto a high-resolution charge-coupled device (CCD) camera, which monitors the sample's mechanical response (cf. Figure 1).

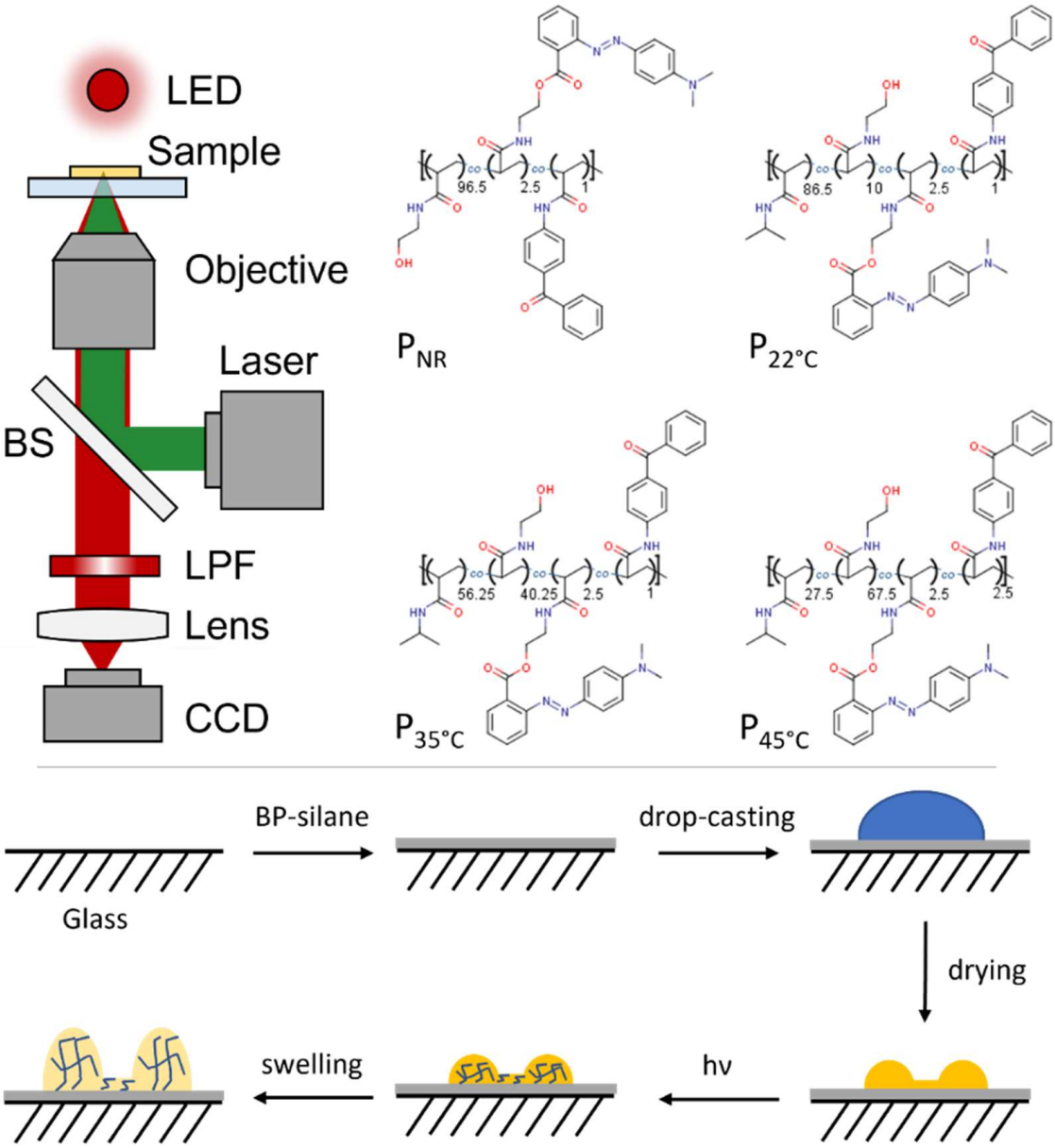

Figure 1. Top left: Sketch of the optical setup used in photoactuation experiments including laser, light-emitting diode (LED), objective, sample, dichroic beamsplitter (BS), longpass filter (LPF), lens, and charge-coupled device (CCD) camera; **Top right**: Structures and monomer feed composition of the different non-thermoresponsive (P_{NR}) and thermoresponsive copolymers ($P_{22°C}$, $P_{35°C}$, $P_{45°C}$) employed in this study; **Bottom**: Sample preparation process of o-methyl red-containing hydrogels for photoactuation experiments, involving functionalisation of the glass surface with a silane of the photocrosslinker benzophenone, drop-casting a solution of the respective copolymer, drying, photocrosslinking, and subsequent swelling.

Three different sets of experiments were performed:

1. The ability for photoactuation was compared between a gel of the non-thermoresponsive P_{NR} and a gel of the thermoresponsive $P_{22°C}$. The LCST-behaviour of $P_{22°C}$ was

then turned off by changing the liquid medium to isopropanol, to study the effect of thermoresponsiveness on photoactuation.
2. Hydrogels of copolymers with different cloud points were photoactuated at high laser powers (in the range of 3.75 mW) to further elucidate photothermal effects.
3. A gel of $P_{22^\circ C}$ was illuminated at different laser powers (from 85 µW to 3.75 mW) to correlate the degree of photoactuation with the light intensity.

A common prerequisite for all experiments was a minimal thickness of the gels (several tens of µm) to allow significant mechanical deformation that is observable in optical microscopy. In order to achieve this thickness, the gels were prepared by drop-casting from water-methanol mixtures on hydrophobic surfaces instead of spin-coating. This procedure leads to a coffee-stain effect, which results in a thicker polymer layer at the edge of the initial droplet. The thicker part of the gel layer (between 25 and 50 µm in the swollen state with swelling ratios of about 2.5) was probed in the photoactuation experiments. Defect structures in the hydrogel films were exploited to follow photoactuation in the optical microscope. These imperfections are usually folds of hydrogel that are formed at high swelling ratios, where the gel partially detaches from the surface. The wavelength of the laser (532 nm) was chosen to match the absorption band of the employed azo dye (cf. ESI Figure S5a).

2.1. Effect of Thermoresponsiveness

When irradiating the non-thermoresponsive gel of P_{NR}, the only interaction of light with the system is expected to be with the azo moieties, which undergo *trans-cis*-isomerisation attaining a photostationary equilibrium. Based on the reported photomotion of other azo dye-containing polymer systems, photoactuation is expected.

Indeed, in the investigated hydrogel system, photoactuation is observed, but in the water-swollen gel, only minute mechanical deformation is visible in the optical microscopy images in Figure 2a,b (cf. ESI Movie S1). The motion is in the sub-µm range, but effective over areas as large as 10 µm away from the illumination centre. In Figure 2, the pristine gel without illumination on the left is compared with the illuminated sample on the right. The images of the irradiated gels were taken three to five seconds after the start of laser exposure.

To better illustrate this minute photoactuation, which is barely visible in the microscopic still pictures, short films of repeated actuation cycles are provided online as supplementary material (cf. ESI Movies S1–S3). These films show the reversibility of the process and the time scales over which they occur as well.

Very much in contrast, the hydrogel of the thermoresponsive $P_{22^\circ C}$ shows an impressively strong and fast response to irradiation. The photoactuation yields mechanical deformation more than 10 µm away from the laser (cf. Figure 2c,d, ESI Movie S2). Apparently, this substantial deformation is caused by a local collapse of the gel. Such a collapse behaviour is known for the NiPAAm-based, thermoresponsive polymers, which show lower critical solution transitions, when exceeding the temperature of the cloud point.

In order to validate the thermal nature of the volume transition, the liquid medium is exchanged from water to isopropanol, thus eliminating the LCST-behaviour. Consequently, in isopropanol the mechanical response of the gel is strongly diminished. Now, only a miniscule movement of features over short distances well below 1 µm are observed (cf. Figure 2e,f, ESI Movie S3), similar to the non-thermoresponsive hydrogel of P_{NR}. Again, the distance from the laser spot at which motion occurs is above 10 µm.

All three samples have in common that motion occurs towards the centre of the laser spot. In the $P_{22^\circ C}$ hydrogel, response to the incident laser beam is immediate, but five seconds pass until the gel is fully collapsed. The system requires about the same timeframe to recover its initial conformation. In both cases, 90% of the collapse or restoring motion occur within 2 s (cf. ESI Movie S2). In the two non-thermoresponsive scenarios, the timeframes are considerably shorter. In less than two frames or 0.47 s, the photoactuation is complete and the gels return to their initial conformation as quickly (cf. ESI Movies S1–S3).

Comparing these results to previous observations of collapse and swelling behaviour of these photocrosslinked PNiPAAm hydrogel layer systems, which show similar volume transitions and kinetics upon thermal stimulation [28], it follows that thermoresponsiveness is a crucial factor in photoactuation of these azobenzene-containing gels. While non-thermoresponsive gels demonstrate a lower degree of motion upon irradiation, the effect in the thermoresponsive gel is magnitudes stronger. Apparently, a photothermal effect, in which the impinging light is converted into thermal energy within the hydrogel, presents the underlying mechanism to trigger thermoresponsiveness, resulting in photoactuation of the gel.

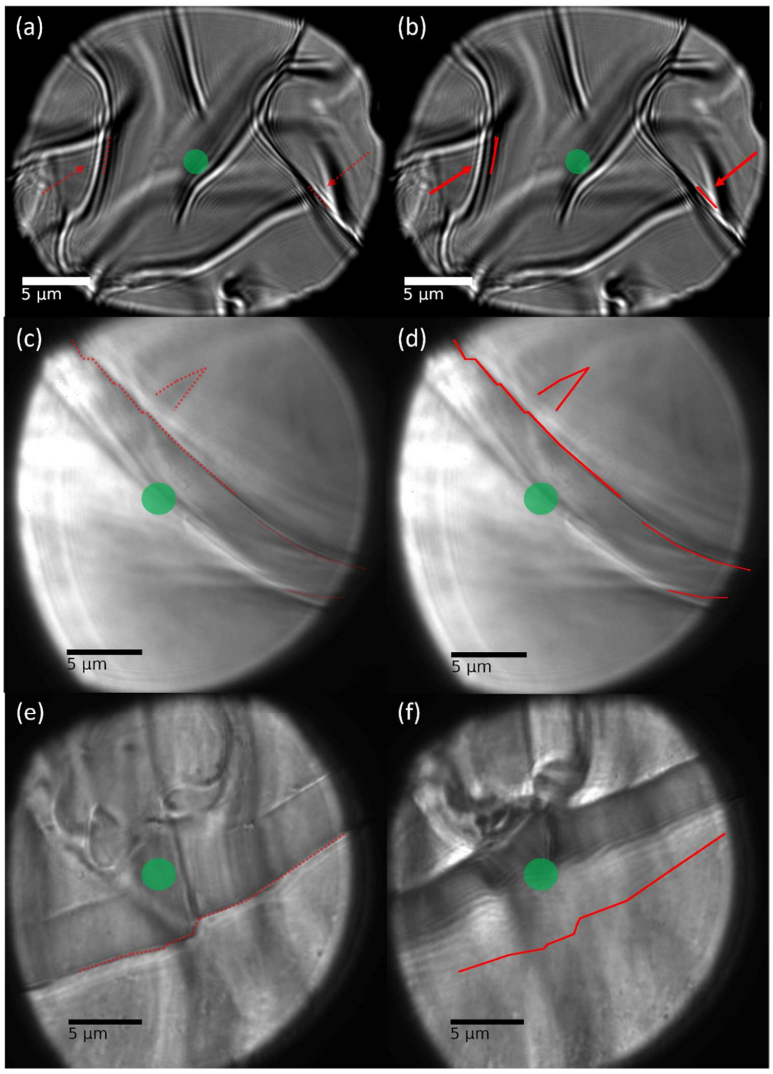

Figure 2. Light microscopy images of pristine (left panels) and photoactuated regions (right panels) of gel layers prepared from (**a**,**b**) poly(HEAm$_{96.5\%}$-co-o-MREAm$_{2.5\%}$-co-BPAAm$_{1\%}$) P$_{NR}$, swollen in water, (**c**,**d**) poly(NipAAm$_{86.5\%}$-HEAm$_{10\%}$-co-o-MREAm$_{2.5\%}$-co-BPAAm$_{1\%}$) P$_{22°C}$, swollen in water, (**e**,**f**) the same polymer in isopropanol. Photoactuation was performed with a laser at λ = 532 nm and 2600 µW (irradiation region marked by a green spot). Red lines and arrows indicate notable gel features that were photoactuated. Videos of the photomotion are provided in the download section of the supporting information.

Generally, photothermal effects in molecules are a consequence of vibrational modes being excited by light. As azobenzenes show optically induced *trans-cis* isomerisation and radiationless decay of the *cis*-state is prominent; such dyes are prominent examples for photothermally active molecules [6,8,9,29,30]. The overlap of the absorption bands of the

trans- and the *cis*-states occurring in push-pull-azobenzenes [31] apparently enhance these effects [6].

2.2. Cloud-Point Temperature Dependence

In the second set of experiments, a dependence of the photoactuation on the cloud point can be identified. A lower cloud point closer to the observation temperature (room temperature) yields a stronger response of the hydrogel towards laser stimulation.

As discussed above, the low cloud-point temperature copolymer $P_{22°C}$ collapses locally in a matter of seconds when irradiated, pulling material over a large area towards the collapsed region (cf. Figure 3a,b). The hydrogels with medium and higher cloud-point temperature from $P_{35°C}$ and $P_{45°C}$ do not exhibit such intense photomotion, but only show a weakened movement towards the laser spot (cf. Figure 3c–f).

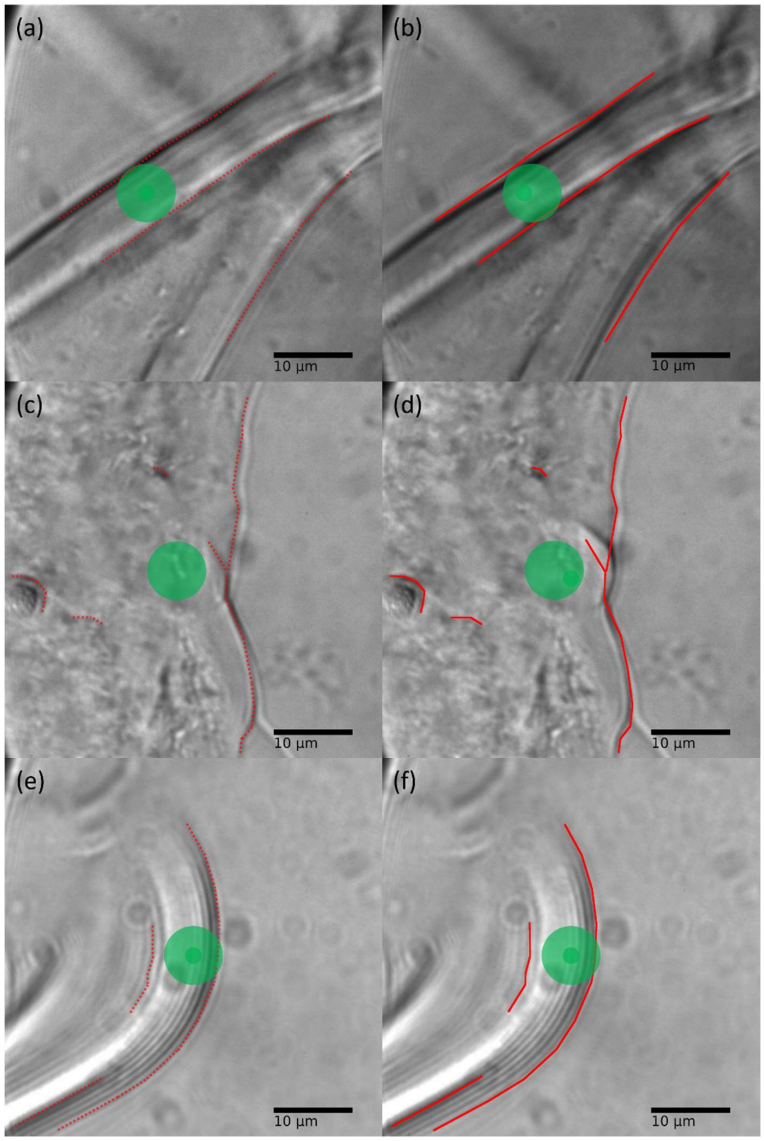

Figure 3. Light microscopy images of pristine (left panels) and photoactuated regions (right panels) of hydrogel layers prepared from (**a**,**b**) poly(NipAAm$_{86.5\%}$-HEAm$_{10\%}$-co-o-MREAm$_{2.5\%}$-co-BPAAm$_{1\%}$) $P_{22°C}$, (**c**,**d**) poly(NipAAm$_{56.25\%}$-HEAm$_{40.25\%}$-co-o-MREAm$_{2.5\%}$-co-BPAAm$_{1\%}$) $P_{35°C}$, and (**e**,**f**) poly(NipAAm$_{27.5\%}$-HEAm$_{67.5\%}$-co-o-MREAm$_{2.5\%}$-co-BPAAm$_{2.5\%}$) $P_{45°C}$. Photoactuation was performed with a laser at λ = 532 nm and 3750 µW (irradiation region marked by a green spot). Red lines indicate notable gel features that were photoactuated.

It should be noted that the photomotion in these experiments is not fully reversible and permanent deformations in the morphology of the gels remain, in particular, close to the laser spot. This can be visualised by subtracting one picture from the other, revealing changes either in the pristine gel to the irradiated gel (photoactuation) or in the pristine gel to the gel after exposure (irreversible change) (cf. ESI Figures S6, S7, S9 and S10). The nature of the irreversible change is ambiguous. In $P_{35°C}$ and $P_{45°C}$, the dimensions after irradiation are larger than prior to contracting it via irradiation, meaning that a higher degree of swelling is attained (cf. ESI Figures S9 and S10). In $P_{22°C}$, on the other hand, the gel is less swollen after irradiation (cf. ESI Figure S7).

Another result of repeated or prolonged exposure to laser light is a diminished response to irradiation. With a higher number of irradiation cycles, the collapse of the gel becomes less pronounced (cf. ESI Figure S8).

To understand the nature of the irreversible changes, further research would be required. Several possible explanations are perceivable, such as photodissociation of the azo dye, photoionization, or breaking of crosslinks, which would all lead to an increased degree of swelling. However, formation of new crosslinks would decrease swelling. Based on the limited experimental evidence from light microscopy, the role of each of these different options cannot be assigned in more details.

The conclusion from this set of experiments is that the local temperature increase is obviously limited and, consequently, the photothermal effect, leading to a local collapse of the $P_{22°C}$ gel, is not intense enough to increase the temperature to a point where also the $P_{35°C}$ or the $P_{45°C}$ gel collapse under otherwise identical conditions.

2.3. Power Dependence

In the last set of experiments, the hydrogel of $P_{22°C}$ was exposed to laser light at different power levels. The hydrogel showed small responses to the incident laser even at low powers of around 400 μW, but considerable motion and collapse of the gel occurred only above a power of 1.2 mW, increasing with higher powers (cf. ESI Figure S6). The magnitude of the photoactuation, discussed above in Section 1, was induced at high power levels (above 2.6 mW) for this gel.

An increase in photoactuation with increasing laser power is expected when considering photothermal effects as the driving force behind the collapse and the concurrent motion of the gel. As is typical for LCST-type thermoresponsive polymers, a certain temperature must be exceeded for the phase transition to occur. Consequently, under irradiation, the local temperature has to increase past this cloud-point temperature to induce the collapse. Assuming the photothermal effect scales proportionally with the energy input, the number of collapsing network segments per volume element increases with the energy input as well, resulting in enhanced photoactuation.

The thermoreponsive gels of $P_{35°C}$ and $P_{45°C}$ have higher cloud-point transition temperatures, thus irradiation leads to smaller motion.

2.4. Reversibility of Photomotion:

The reversibility of photoactuation is linked to the network structure of the swollen gel. In thermoresponsive hydrogels, a laser-induced local collapse results in a strain acting on the circumjacent material. In this situation, two factors contribute to the restoring force: (1) The swollen gel in the surroundings of the collapse shows rubber elasticity [32] and exerts a restoring force of entropic origin on the deformed parts. (2) When laser irradiation is stopped, the local heat dissipates, allowing the temperature in the irradiation spot to drop back below the cloud-point temperature. At this point, the gel reswells and releases the strain.

In photomotion involving a non-thermoresponsive system, the deformation force results from chromophore alignment in the irradiation spot. The strain generated by the stretched polymer network ensures restoring the original shape of the gel after the optical stimulus is removed.

2.5. Photoactuation Models:

From the three sets of experiments, two different pathways of photoactuation can be postulated in these *o*-methyl red-containing hydrogels. The first pathway involves an LCST-type thermoresponse triggered by photothermal effects, induced by repeated *cis-trans* photoisomerisations of the azo dye molecules under irradiation with a focussed laser beam. This pathway is summarised in Scheme 1.

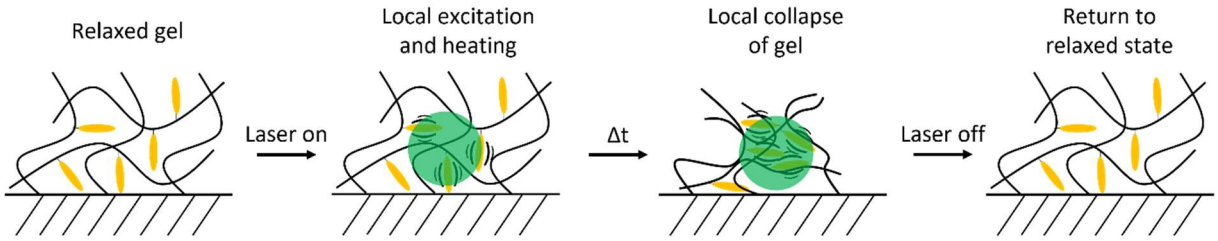

Scheme 1. Cartoon of the photoactuation process of thermoresponsive o-methyl red-containing hydrogels. Local excitation of dye side chains by laser irradiation induces heating, which leads to a local collapse and deformation of the gel. The gel returns to its original conformation when the laser is shut off and the heat is dissipated to the environment.

The second pathway is more intricate, as in the absence of thermoresponsive behaviour, photomotion towards the irradiated area still occurs, although smaller in scale. This is the case in the non-thermoresponsive gels of P_{NR} and of $P_{22^{\circ}C}$ in isopropanol. However, if photo-induced heating was the underlying cause for photoactuation by volume expansion in these systems, the gels should swell slightly, resulting in a motion away from the incident beam.

In the photoactuation experiments for non-thermoresponsive systems, the opposite motion towards the illuminated region is observed. Apparently, additional mechanisms of photoactuation must be considered to explain these experimental findings. Such an explanation may be drawn from the models that attempt to explain the formation of surface relief gratings (SRGs), which are introduced below.

SRG formation, which has been described for glassy, amorphous, and liquid crystalline polymers and materials, usually requires high concentrations of azo dyes. Under these conditions, the dyes are in proximity to each other and can perform collective motions. In the polymer systems here, the degree of substitution along the backbone is low (<2.5 mol%) and the volume fraction in the swollen gel is even lower, because of dilution with the swelling solvent. In contrast, the mobility of the chromophores is considerably higher in these visco-elastic solids compared to the more rigid matrixes in SRG-formation.

Under these conditions, only a few reported models may be suitable as reference. These are the orientation model [33–35], the gradient force model [8,36–40], and the mean field model [41,42]. These models have in common that they assume reorientation of the chromophore during irradiation in the material by *trans-cis-trans* isomerisation cycles and alignment of the chromophores in the optically induced electric field. This reported mechanism may also serve as explanation for the here observed photomotion in the gels. Forced alignment of the chromophores by dipolar interactions in the irradiation field would lead to contraction of the gel, as the chromophores pull the attached segments of the network along with them. However, this motion is limited, as only a comparably weak force can be generated by a single chromophore.

3. Conclusions

The above results demonstrate that the combination of thermoresponsive, water swollen polymer networks with the unique photoresponse of azo dyes provide novel materials with extended photomotion, which may be particularly applicable in the context of living organisms owing to the aqueous medium of the hydrogels. Potentially, such systems could be used for mechanical stimulation of cells with the remote, non-invasive

trigger light, or as optically driven actuators for soft robotics in biological environments. For this future field of application, tests in cell cultures to investigate biocompatibility are a necessary next step. In such environments, also thin films, structured materials, as well as macroscopic gels need to be investigated.

Supplementary Materials: The following supporting information can be downloaded at: https://www.mdpi.com/article/10.3390/gels8090541/s1, Table S1: Feed composition in mol% and reaction parameters for the different free radical copolymersations.; Table S2: Copolymer characteristics as determined by UV-vis spectroscopy and GPC. The built-in ratios for o-MREAm and BPAAm are given in weight percentages and the percentage of the monomer built-in compared to the feed composition. The HEAm:NiPAAm ratio was determined by ^{1}H NMR spectroscopy.; Figure S1: ^{1}H NMR spectrum (500 MHz) in MeOD of a poly(HEAm-co-o-MREAm-co-BPAAm) copolymer (P_{NR}) (feed: HEAm:o-MREAm:BPAAm 96.5:2.5:1).; Figure S2:^{1}H NMR spectrum (400 MHz) in MeOD of a poly(NiPAAm-co-HEAm-co-o-MREAm-co-BPAAm) copolymer ($P_{22°C}$) (feed: NiPAAm:HEAm:o-MREAm:BPAAm 87.2:9.2:2.6:1).; Figure S3:^{1}H NMR spectrum (500 MHz) in D2O of a poly(NiPAAm-co-HEAm-co-o-MREAm-co-BPAAm) copolymer ($P_{35°C}$) (feed: NiPAAm:HEAm:o-MREAm:BPAAm 55.9:40.4:2.7:1).; Figure S4:^{1}H NMR spectrum (500 MHz) in D2O of poly(NiPAAm-co-HEAm-co-o-MREAm-co-BPAAm) copolymer ($P_{45°C}$) (feed: NiPAAm:HEAm:o-MREAm:BPAAm 27.7:67.3:2.5:2.5).; Figure S5: (a) UV-vis spectrum of a photocrosslinked film of poly($HEAm_{96.5\%}$-co-o-$MREAm_{2.5\%}$-co-$BPAAm_{1\%}$) P_{NR} swollen in water at 26 °C, with the wavelength of the green laser used in this marked with a green vertical line at 532 nm. b) Turbidity measurements at 780 nm of aqueous 1 w% solutions of poly($NipAAm_{86.5\%}$-$HEAm_{10\%}$-co-o-$MREAm_{2.5\%}$-co-$BPAAm_{1\%}$) $P_{22°C}$, poly($NipAAm_{56.25\%}$-$HEAm_{40.25\%}$-co-o-$MREAm_{2.5\%}$-co-$BPAAm_{1\%}$) $P_{35°C}$, and poly($NipAAm_{27.5\%}$-$HEAm_{67.5\%}$-co-o-$MREAm_{2.5\%}$-co-$BPAAm_{2.5\%}$) $P_{45°C}$. On the right: structures of the copolymers used in this study with the feed ratios of monomers in the synthesis.; Figure S6:A series of light microscopy images of a hydrogel of poly($NipAAm_{86.5\%}$-$HEAm_{10\%}$-co-o-$MREAm_{2.5\%}$-co-$BPAAm_{1\%}$) $P_{22°C}$ showing left: non-irradiated gel with accumulative irreversible change of irradiations at previous stages of power; middle: difference pictures between the non-irradiated and the irradiated gel with inverted colour scheme (laser at λ = 532 nm); right: irradiated gel after 3 s at (a) 85 μW, (b) 376 μW, (c) 1210 μW, and (d) 3750 μW. The green shaded area shows the approximate dimensions of the laser spot.; Figure S7: Light microscopy images of a hydrogel of poly($NipAAm_{86.5\%}$-$HEAm_{10\%}$-co-o-$MREAm_{2.5\%}$-co-$BPAAm_{1\%}$) $P_{22°C}$ showing (a) the pristine hydrogel, (b) the hydrogel when irradiated with a laser (λ = 532 nm, 3750 μW), (c) after 3 s of exposure, and (d) after 60 s of exposure; Figure S8: Light microscopy images of a hydrogel of poly($NipAAm_{86.5\%}$-$HEAm_{10\%}$-co-o-$MREAm_{2.5\%}$-co-$BPAAm_{1\%}$) $P_{22°C}$ irradiated with laser (λ = 532 nm) at 3750 μW (a) for the first time, (b) after cycling five times between 3 s irradiation intervals and relaxation, (c) after cycling twenty times between 3 s irradiation intervals and relaxation. The red lines in (b) and (c) show the positions of the notable dark features in (a); Figure S9: Light microscopy images of a hydrogel of poly($NipAAm_{56.25\%}$-$HEAm_{40.25\%}$-co-o-$MREAm_{2.5\%}$-co-$BPAAm_{1\%}$) $P_{35°C}$ showing (a) left to right: the pristine gel, a difference picture between the non-irradiated and the irradiated gel, the irradiated gel (laser at λ = 532 nm, 3750 μW), and (b) left to right: the pristine gel, a difference picture between the non-irradiated gel before and after exposure to laser light, the gel after exposure to laser light. The green shaded area shows the approximate dimensions of the laser spot. The difference pictures are shown with inverted colour scheme.; Figure S10: Light microscopy images of a hydrogel of poly($NipAAm_{27.5\%}$-$HEAm_{67.5\%}$-co-o-$MREAm_{2.5\%}$-co-$BPAAm_{2.5\%}$) $P_{45°C}$ showing (a) left to right: the pristine gel, a difference picture between the non-irradiated and the irradiated gel, the irradiated gel (laser at λ=532 nm, 3750 μW), and (b) left to right: the pristine gel, a difference picture between the non-irradiated gel before and after exposure to laser light, the gel after exposure to laser light. The green shaded area shows the approximate dimensions of the laser spot. The difference pictures are shown with inverted colour scheme.; Video S1: MovieS1_PNR_aqueous; Video S2: MovieS2_P22C_aqueous; Video S3: MovieS3_P22C_Isopropanol [43–45].

Author Contributions: T.G.J., E.D. and U.J. conceived and designed the experiments; T.G.J. did the synthetical and preparatory work, analysed the data, and wrote the original draft; T.G.J. and U.J. did the interpretation of the results; A.M.F., N.S., P.R. and M.A. designed, build, and maintained the experimental setup, and provided related data and schemes; T.G.J., A.M.F., N.S. and P.R. performed the optical measurements, T.G.J. and U.J. wrote the final manuscript; All authors proofread and improved the manuscript. All authors have read and agreed to the published version of the manuscript.

Funding: This research was funded by the University of Siegen and Faculty IV of the University of Siegen.

Institutional Review Board Statement: Not applicable.

Informed Consent Statement: Not applicable.

Data Availability Statement: All data is available either in this article or in the Supplementary Materials.

Acknowledgments: We thank Thomas Paululat for NMR measurements.

Conflicts of Interest: The authors declare no conflict of interests.

References

1. Chen, Y.; Yang, J.; Zhang, X.; Feng, Y.; Zeng, H.; Wang, L.; Feng, W. Light-driven bimorph soft actuators: Design, fabrication, and properties. *Mater. Horiz.* **2021**, *8*, 728–757. [CrossRef]
2. Shi, K.; Liu, Z.; Wei, Y.-Y.; Wang, W.; Ju, X.-J.; Xie, R.; Chu, L.-Y. Near-Infrared Light-Responsive Poly(N-isopropylacrylamide)/Graphene Oxide Nanocomposite Hydrogels with Ultrahigh Tensibility. *ACS Appl. Mater. Interfaces* **2015**, *7*, 27289–27298. [CrossRef]
3. He, Y.; Liang, H.; Chen, M.; Jiang, L.; Zhang, Z.; Heng, X.; Yang, L.; Hao, Y.; Gan, J.; Yang, Z. Optical Fiber Waveguiding Soft Photoactuators Exhibiting Giant Reversible Shape Change. *Adv. Optical Mater.* **2021**, *9*, 2101132. [CrossRef]
4. Luo, P.-F.; Xiang, S.-L.; Li, C.; Zhu, M.-Q. Photomechanical polymer hydrogels based on molecular photoswitches. *J. Polym. Sci.* **2021**, *59*, 2246–2264. [CrossRef]
5. Peng, X.; Wang, H. Shape changing hydrogels and their applications as soft actuators. *J. Polym. Sci. Part B Polym. Phys.* **2018**, *56*, 1314–1324. [CrossRef]
6. Chen, Y.; Yu, H.; Quan, M.; Zhang, L.; Yang, H.; Lu, Y. Photothermal effect of azopyridine compounds and their applications. *RSC Adv* **2015**, *5*, 4675–4680. [CrossRef]
7. Wang, J.; Zheng, Y.; Li, L.; Liu, E.; Zong, C.; Zhao, J.; Xie, J.; Xu, F.; König, T.A.F.; Grenzer Saphiannikova, M.; et al. All-Optical Reversible Azo-Based Wrinkling Patterns with High Aspect Ratio and Polarization-Independent Orientation for Light-Responsive Soft Photonics. *ACS Appl. Mater. Interfaces* **2019**, *11*, 25595–25604. [CrossRef]
8. Lee, K.M.; White, T.J. Photochemical Mechanism and Photothermal Considerations in the Mechanical Response of Monodomain, Azobenzene-Functionalized Liquid Crystal Polymer Networks. *Macromolecules* **2012**, *45*, 7163–7170. [CrossRef]
9. Gelebart, A.H.; Vantomme, G.; Meijer, E.W.; Broer, D.J. Mastering the Photothermal Effect in Liquid Crystal Networks: A General Approach for Self-Sustained Mechanical Oscillators. *Adv. Mater. Weinheim.* **2017**, *29*, 1606712. [CrossRef]
10. Hogan, P.M.; Tajbakhsh, A.R.; Terentjev, E.M. UV manipulation of order and macroscopic shape in nematic elastomers. *Phys. Rev. E Stat. Nonlin. Soft Matter Phys.* **2002**, *65*, 41720. [CrossRef]
11. Homma, K.; Chang, A.C.; Yamamoto, S.; Tamate, R.; Ueki, T.; Nakanishi, J. Design of azobenzene-bearing hydrogel with photoswitchable mechanics driven by photo-induced phase transition for in vitro disease modeling. *Acta Biomater.* **2021**, *132*, 103–113. [CrossRef]
12. Zhao, W.; Li, Y.; Zhang, X.; Zhang, R.; Hu, Y.; Boyer, C.; Xu, F.-J. Photo-responsive supramolecular hyaluronic acid hydrogels for accelerated wound healing. *J. Control. Release* **2020**, *323*, 24–35. [CrossRef]
13. Kuwabara, T.; Aoyagi, T.; Takamura, M.; Matsushita, A.; Nakamura, A.; Ueno, A. Heterodimerization of Dye-Modified Cyclodextrins with Native Cyclodextrins. *J. Org. Chem.* **2002**, *67*, 720–725. [CrossRef]
14. Liu, G.; Yuan, Q.; Hollett, G.; Zhao, W.; Kang, Y.; Wu, J. Cyclodextrin-based host–guest supramolecular hydrogel and its application in biomedical fields. *Polym. Chem.* **2018**, *9*, 3436–3449. [CrossRef]
15. Maatz, G.; Maciollek, A.; Ritter, H. Cyclodextrin-induced host-guest effects of classically prepared poly(NIPAM) bearing azo-dye end groups. *Beilstein J. Org. Chem.* **2012**, *8*, 1929–1935. [CrossRef]
16. Guan, Y.; Zhao, H.-B.; Yu, L.-X.; Chen, S.-C.; Wang, Y.-Z. Multi-stimuli sensitive supramolecular hydrogel formed by host–guest interaction between PNIPAM-Azo and cyclodextrin dimers. *RSC Adv.* **2014**, *4*, 4955. [CrossRef]
17. Takashima, Y.; Nakayama, T.; Miyauchi, M.; Kawaguchi, Y.; Yamaguchi, H.; Harada, A. Complex Formation and Gelation between Copolymers Containing Pendant Azobenzene Groups and Cyclodextrin Polymers. *Chem. Lett.* **2004**, *33*, 890–891. [CrossRef]
18. Takashima, Y.; Hatanaka, S.; Otsubo, M.; Nakahata, M.; Kakuta, T.; Hashidzume, A.; Yamaguchi, H.; Harada, A. Expansion-contraction of photoresponsive artificial muscle regulated by host-guest interactions. *Nat. Commun.* **2012**, *3*, 1270. [CrossRef]
19. Iwaso, K.; Takashima, Y.; Harada, A. Fast response dry-type artificial molecular muscles with c2daisy chains. *Nat. Chem.* **2016**, *8*, 625–632. [CrossRef]

20. Tamesue, S.; Takashima, Y.; Yamaguchi, H.; Shinkai, S.; Harada, A. Photoswitchable supramolecular hydrogels formed by cyclodextrins and azobenzene polymers. *Angew. Chem. Int. Ed Engl.* **2010**, *49*, 7461–7464. [CrossRef]
21. Yamaguchi, H.; Kobayashi, Y.; Kobayashi, R.; Takashima, Y.; Hashidzume, A.; Harada, A. Photoswitchable gel assembly based on molecular recognition. *Nat. Commun.* **2012**, *3*, 603. [CrossRef]
22. Tomatsu, I.; Hashidzume, A.; Harada, A. Cyclodextrin-Based Side-Chain Polyrotaxane with Unidirectional Inclusion in Aqueous Media. *Angew. Chem.* **2006**, *118*, 4721–4724. [CrossRef]
23. Wang, J.; Li, Q.; Yi, S.; Chen, X. Visible-light/temperature dual-responsive hydrogel constructed by α-cyclodextrin and an azobenzene linked surfactant. *Soft Matter* **2017**, *13*, 6490–6498. [CrossRef]
24. Wang, M.; Zhang, X.; Li, L.; Wang, J.; Wang, J.; Ma, J.; Yuan, Z.; Lincoln, S.F.; Guo, X. Photo-Reversible Supramolecular Hydrogels Assembled by α-Cyclodextrin and Azobenzene Substituted Poly(acrylic acid)s: Effect of Substitution Degree, Concentration, and Tethered Chain Length. *Macromol. Mater. Eng.* **2016**, *301*, 191–198. [CrossRef]
25. Yuan, W.; Shen, J.; Guo, W. Thermoresponse and light-induced reversible self-assembly/disassembly of supra-amphiphiles from azobenzene- and β-cyclodextrin-containing copolymers. *Mater. Lett.* **2014**, *134*, 259–262. [CrossRef]
26. Yang, M.; Hu, J.; Meng, J.; Shan, X. A thermo and photoresponsive dual performing hydrogel for multiple controlled release mechanisms. *Iran Polym. J.* **2020**, *29*, 891–900. [CrossRef]
27. Zhang, Q.; Weber, C.; Schubert, U.S.; Hoogenboom, R. Thermoresponsive polymers with lower critical solution temperature: From fundamental aspects and measuring techniques to recommended turbidimetry conditions. *Mater. Horiz.* **2017**, *4*, 109–116. [CrossRef]
28. Auer, S.K.; Fossati, S.; Morozov, Y.; Mor, D.C.; Jonas, U.; Dostalek, J. Rapid Actuation of Thermo-Responsive Polymer Networks: Investigation of the Transition Kinetics. *J. Phys. Chem. B* **2022**, *126*, 3170–3179. [CrossRef]
29. Da Pilz Cunha, M.; van Thoor, E.A.J.; Debije, M.G.; Broer, D.J.; Schenning, A.P.H.J. Unravelling the photothermal and photomechanical contributions to actuation of azobenzene-doped liquid crystal polymers in air and water. *J. Mater. Chem. C* **2019**, *7*, 13502–13509. [CrossRef]
30. Gelebart, A.H.; Jan Mulder, D.; Varga, M.; Konya, A.; Vantomme, G.; Meijer, E.W.; Selinger, R.L.B.; Broer, D.J. Making waves in a photoactive polymer film. *Nature* **2017**, *546*, 632–636. [CrossRef]
31. Bandara, H.M.D.; Burdette, S.C. Photoisomerization in different classes of azobenzene. *Chem. Soc. Rev.* **2012**, *41*, 1809–1825. [CrossRef]
32. Anseth, K.S.; Bowman, C.N.; Brannon-Peppas, L. Mechanical properties of hydrogels and their experimental determination. *Biomaterials* **1996**, *17*, 1647–1657. [CrossRef]
33. Loebner, S.; Yadav, B.; Lomadze, N.; Tverdokhleb, N.; Donner, H.; Saphiannikova, M.; Santer, S. Local Direction of Optomechanical Stress in Azobenzene Containing Polymers During Surface Relief Grating Formation. *Macromol. Mater. Eng.* **2022**, 2100990. [CrossRef]
34. Yadav, B.; Domurath, J.; Kim, K.; Lee, S.; Saphiannikova, M. Orientation Approach to Directional Photodeformations in Glassy Side-Chain Azopolymers. *J. Phys. Chem. B* **2019**, *123*, 3337–3347. [CrossRef]
35. Yadav, B.; Domurath, J.; Saphiannikova, M. Modeling of Stripe Patterns in Photosensitive Azopolymers. *Polymers* **2020**, *12*, 735. [CrossRef]
36. Lee, S.; Kang, H.S.; Park, J.-K. Directional photofluidization lithography: Micro/nanostructural evolution by photofluidic motions of azobenzene materials. *Adv. Mater. Weinheim.* **2012**, *24*, 2069–2103. [CrossRef]
37. Viswanathan, N.K.; Kim, D.Y.; Bian, S.; Williams, J.; Liu, W.; Li, L.; Samuelson, L.; Kumar, J.; Tripathy, S.K. Surface relief structures on azo polymer films. *J. Mater. Chem.* **1999**, *9*, 1941–1955. [CrossRef]
38. Natansohn, A.; Rochon, P. Photoinduced Motions in Azo-Containing Polymers. *Chem. Rev.* **2002**, *102*, 4139–4176. [CrossRef]
39. Kumar, J.; Li, L.; Jiang, X.L.; Kim, D.-Y.; Lee, T.S.; Tripathy, S. Gradient force: The mechanism for surface relief grating formation in azobenzene functionalized polymers. *Appl. Phys. Lett.* **1998**, *72*, 2096–2098. [CrossRef]
40. Bian, S.; Liu, W.; Williams, J.; Samuelson, L.; Kumar, J.; Tripathy, S. Photoinduced Surface Relief Grating on Amorphous Poly(4-phenylazophenol) Films. *Chem. Mater.* **2000**, *12*, 1585–1590. [CrossRef]
41. Pedersen, T.G.; Johansen, P.M.; Holme, N.C.R.; Ramanujam, P.S.; Hvilsted, S. Mean-Field Theory of Photoinduced Formation of Surface Reliefs in Side-Chain Azobenzene Polymers. *Phys. Rev. Lett.* **1998**, *80*, 89–92. [CrossRef]
42. Pedersen, T.G.; Johansen, P.M. Mean-Field Theory of Photoinduced Molecular Reorientation in Azobenzene Liquid Crystalline Side-Chain Polymers. *Phys. Rev. Lett.* **1997**, *79*, 2470–2473. [CrossRef]
43. Jia, J.; Sarker, M.; Steinmetz, M.G.; Shukla, R.; Rathore, R. Photochemical elimination of leaving groups from zwitterionic intermediates generated viaelectrocyclic ring closure of alpha, beta-unsaturated anilides. *J. Org. Chem.* **2008**, *73*, 8867–8879. [CrossRef]
44. Jaik, T.G.; Ciubini, B.; Frascella, F.; Jonas, U. Thermal Response and Thermochromism of Methyl Red-Based Copolymer Systems—Coupled Responsiveness in Critical Solution Behaviour and Optical Absorption Properties. *Polym. Chem.* **2022**, *13*, 1186–1214. [CrossRef]
45. Gianneli, M.; Roskamp, R.F.; Jonas, U.; Loppinet, B.; Fytas, G.; Knoll, W. Dynamics of swollen gel layers anchored to solid surfaces. *Soft Matter* **2008**, *4*, 1443–1447. [CrossRef]

Electronic Supporting Information (ESI)

Photomotion of Hydrogels with Covalently Attached Azobenzene Moieties – Thermoresponsive and Non-Thermoresponsive Gels

Thorben G. Jaik[1], Assegid M. Flatae[2], Navid Soltani[2], Philipp Reuschel[2], Mario Agio[2,3], Emiliano Descrovi[4], Ulrich Jonas[1]*

[1] Department Chemistry - Biology, University of Siegen, Adolf-Reichwein-Strasse 2, 57076, Siegen, Germany

[2] Department Physics, University of Siegen, Walter-Flex-Str. 3, 57072 Siegen, Germany

[3] National Institute of Optics (INO), National Research Council (CNR), via Nello Carrara 1, 50019 Sesto Fiorentino, Italy

[4] Department of Applied Science of Technology (DISAT), Politecnico di Torino, Corso Duca degli Abruzzi 24, 10129 Torino, Italy

*Corresponding author: Prof. Dr. Ulrich Jonas, jonas@chemie.uni-siegen.de

This document contains experimental details like syntheses and sample preparations, additional optical analysis data, and light microscopy images of polymer films with or without irradiation.

Experimentals

Materials and equipment:

All solvents used were of Milli-Q®, spectroscopic or HPLC-grade. 1,4-Dioxane was dried and distilled over sodium. Absolute ethanol was purchased from VWR Chemicals. *N*-hydroxyethyl acrylamide (97%, Sigma Aldrich) was used as received. *N*-Isopropylacrylamide was recrystallised from n-hexane. Azobisisobutyronitrile was recrystallised from methanol. 4-Benzophenoneacrylamide was synthesised according to literature [43]. The synthesis of the *N*-hydroxyethyl acrylamide ester of *o*-methyl red was described in a previous publication [44]. 4-(3-Triethoxysilyl)-

propoxybenzophenone was synthesised by Mr. Daniel John according to literature [45].

UV-vis measurements were performed on a Thermo Scientific™ Evolution™ 220 UV-Vis-spectrophotometer. If not stated otherwise, the measurements were done with 100 nm/min and a resolution of 1 nm. Cloud point measurements were performed with a heating/cooling rate of 1 K/min at mass per volume concentrations of 1%.

NMR measurements were performed on either a Bruker AV 400 or a Jeol EZC 500.

GPC/SEC was measured on a PSS GRAM linM column (Polymer Standards Service GmbH, Mainz, Germany) in dimethylacetamide with LiBr (0.1 g/L) at 60 °C with PMMA-standards as reference.

Free radical copolymerisations:

The different copolymers were obtained by radical polymerisation. The monomers (0.6 mol L^{-1}) and azobisisobutyronitrile were dissolved in 1,4-dioxane or methanol. The solutions were purged with nitrogen for 30 minutes and heated in an oil bath at 60 °C in methanol or 1,4-dioxane for 24 to 48 hours. The polymers were then precipitated up to three times in a non-solvent. The details are summarised in Table S 1.

P_{NR} (poly(HEAm-co-o-MREAm-co-BPAAm)): δH(500 MHz, MeOD) 8.5-6.5 (br, aromatic H), 4.57 (COOCH_2), 4.38 (Ar-CONHCH_2), 3.66 (CH_2CH_2OH), 3.51-3.12 (CONHCH_2), 2.4-1.25 (backbone)

$P_{22°C}$ (poly(NiPAAm-co-HEAm-co-o-MREAm-co-BPAAm)): δH(400 MHz, MeOD) 8.0-6.75 (br, aromatic H), 4.38 (Ar-COOCH_2), 3.96 (NHCH(CH_3)$_2$), 3.65 (CH_2CH_2OH), 3.12 ($N(Me)_2$), 2.3-1.25 (backbone), 1.16 (NHCH(CH_3)$_2$)

$P_{35°C}$ (poly(NiPAAm-co-HEAm-co-o-MREAm-co-BPAAm)): δH(500 MHz, D_2O) 8.1-6.75 (br, aromatic H), 3.90 (NHCH(CH_3)$_2$), 3.69 (CH_2CH_2OH), 3.37 (CONHCH_2), 2.5-1.25 (backbone), 1.16 (NHCH(CH_3)$_2$)

$P_{45°C}$ (poly(NiPAAm-co-HEAm-co-o-MREAm-co-BPAAm)): δH(400 MHz, D_2O) 8.0-6.75 (br, aromatic H), 3.88 (NHCH(CH_3)$_2$), 3.66 (CH_2CH_2OH), 3.33 (CONHCH_2), 2.3-1.25 (backbone), 1.13 (NHCH(CH_3)$_2$)

Table S 1: Feed composition in mol% and reaction parameters for the different free radical copolymersations.

Polymer	NiPAAm [%]	HEAm [%]	o-MREAm [%]	BPAAm [%]	AIBN [%]	T [°C]	Time [h]	Solvent	Non-solvent
NR	0	96.5	2.5	1	2	60	24	Methanol	Ethyl acetate
22 °C	87.2	9.2	2.6	1	2	60	26	1,4-Dioxane	Diethylether
35 °C	55.9	40.4	2.7	1	2	60	24	Methanol	Diethylether
45 °C	27.7	67.3	2.5	2.5	2	60	48	Methanol	Diethylether

Table S 2: Copolymer characteristics as determined by UV-vis spectroscopy and GPC. The built-in ratios for o-MREAm and BPAAm are given in weight percentages and the percentage of the monomer built-in compared to the feed composition. The HEAm:NiPAAm ratio was determined by ^{1}H NMR spectroscopy.

Polymer	o-MREAm [w%] Built-in to feed (%)	BPAAm [w%] Built-in to feed (%)	HEAm:NipAAm ratio; Built-in to feed (mol%)	M_n [10^3 Da]	M_w [10^3 Da]	*Đ*	Yield [%]
NR	4.5 (65%)	1.9 (94%)	-	17.4	37.7	2.17	79
22 °C	5.2 (67%)	2.1 (96%)	0.14 (133%)	22.1	51.9	2.35	81
35 °C	5.5 (68%)	2.4 (120%)	0.83 (115%)	13.6	26.3	1.94	69
45 °C	4.4 (73%)	4.2 (84%)	2.53 (104%)	12.6	29.0	2.30	85

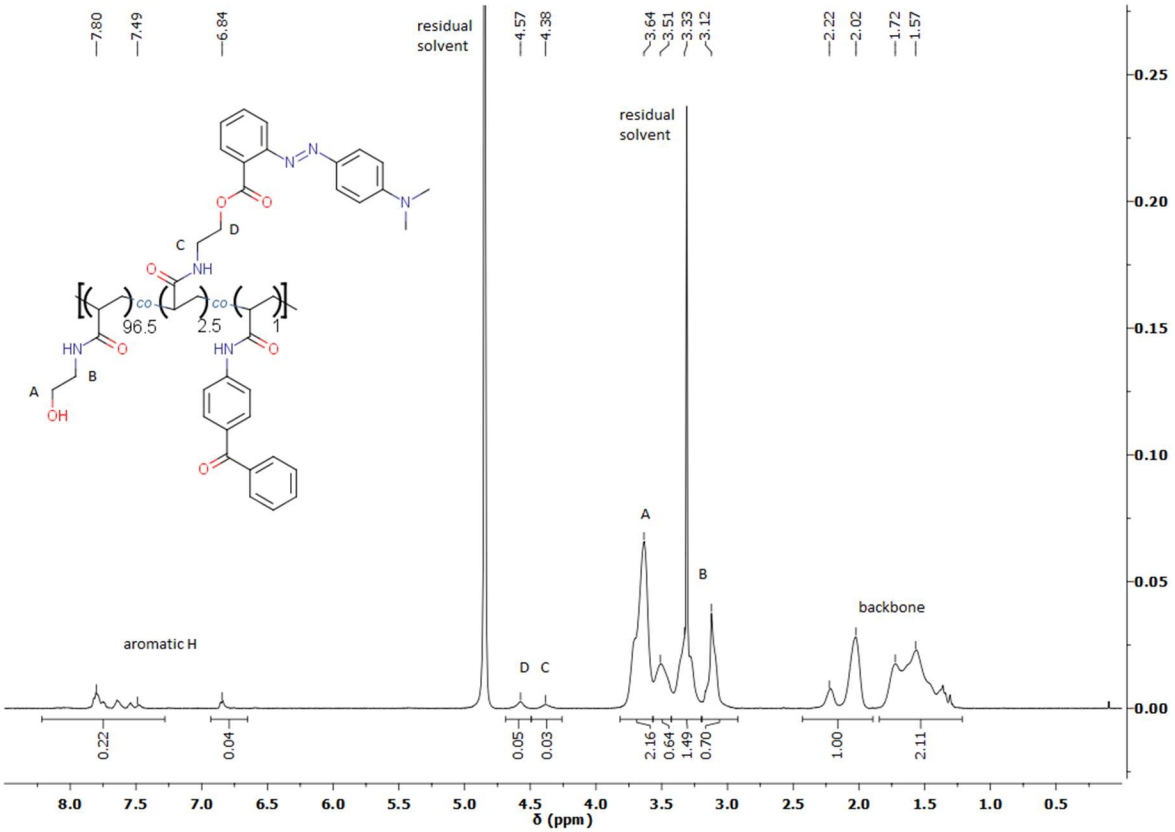

Figure S 1: ^{1}H NMR spectrum (500 MHz) in MeOD of a poly(HEAm-co-o-MREAm-co-BPAAm) copolymer (P_{NR}) (feed: HEAm:o-MREAm:BPAAm 96.5:2.5:1).

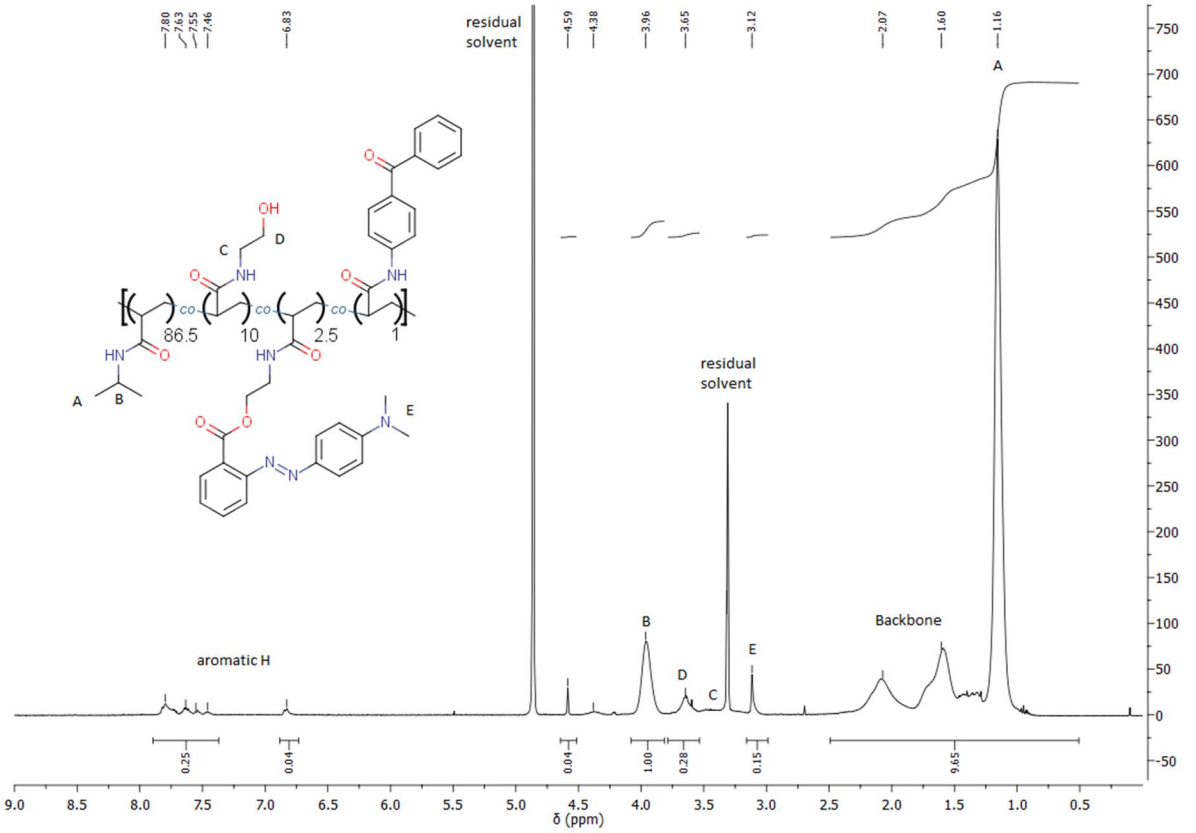

Figure S 2: [1]H NMR spectrum (400 MHz) in MeOD of a poly(NiPAAm-co-HEAm-co-o-MREAm-co-BPAAm) copolymer ($P_{22°C}$) (feed: NiPAAm:HEAm:o-MREAm:BPAAm 87.2:9.2:2.6:1).

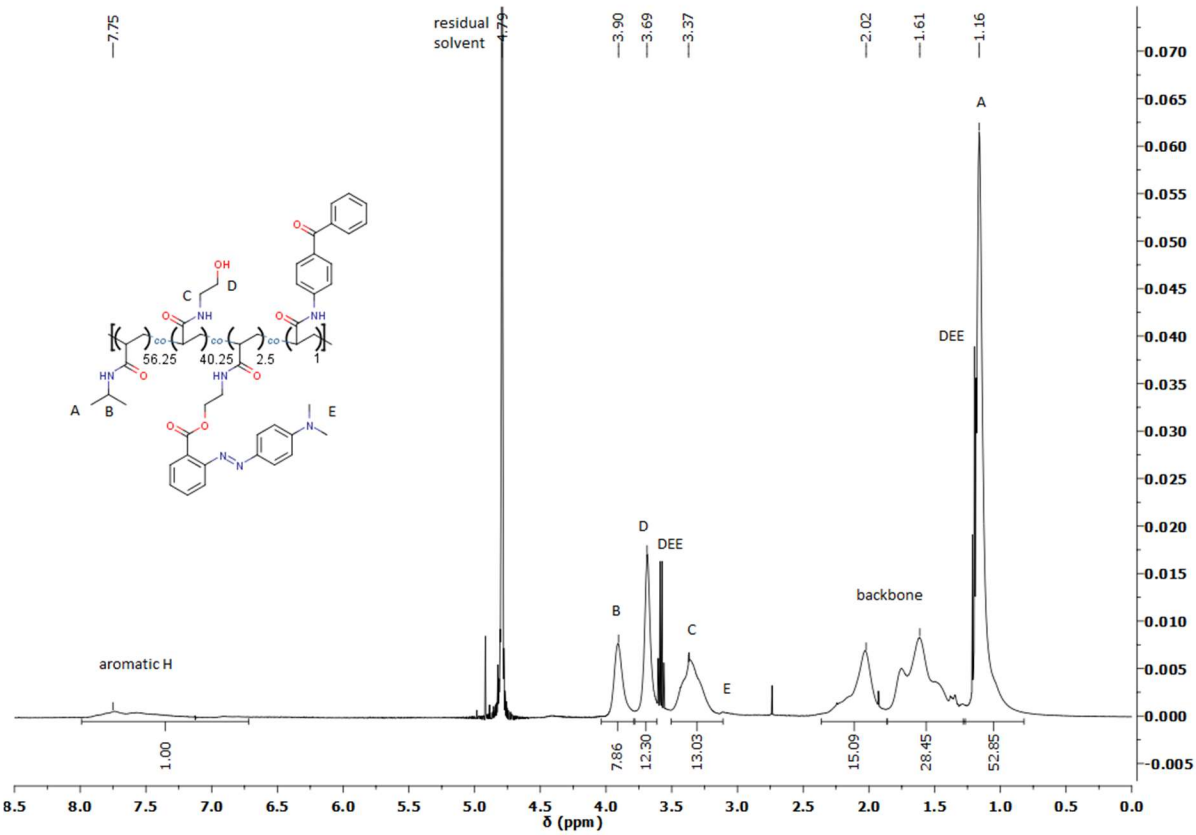

Figure S 3: [1]H NMR spectrum (500 MHz) in D_2O of a poly(NiPAAm-co-HEAm-co-o-MREAm-co-BPAAm) copolymer ($P_{35°C}$) (feed: NiPAAm:HEAm:o-MREAm:BPAAm 55.9:40.4:2.7:1).

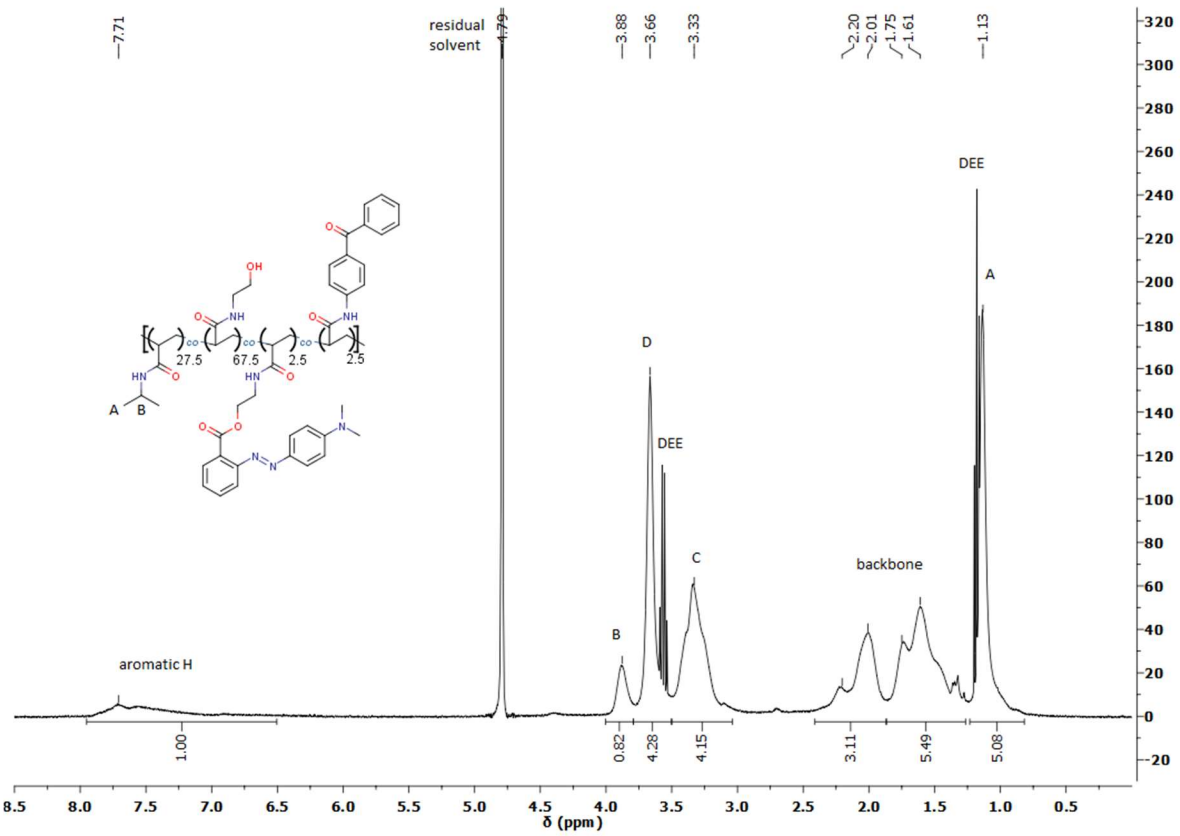

Figure S 4: ^{1}H NMR spectrum (500 MHz) in D_2O of poly(NiPAAm-co-HEAm-co-o-MREAm-co-BPAAm) copolymer ($P_{45°C}$) (feed: NiPAAm:HEAm:o-MREAm:BPAAm 27.7:67.3:2.5:2.5).

Film preparation:

The glass slides used in photoactuation experiments were cleaned with fresh Carothers' acid (sulfuric acid:hydrogen peroxide, 3:1) and rinsed thoroughly with water. The slides were dried under a nitrogen stream. They were submerged in an ethanolic solution of benzophenone silane (1 mmol L^{-1}) for 24 hours before they were rinsed thrice with absolute ethanol and finally dried under a nitrogen stream.

Polymers were drop-casted on the glass slides from MeOH:H_2O (4:1, P_{NR}, $P_{35°C}$, $P_{45°C}$) or aqueous ($P_{22°C}$) solution (2.5 w%, 25 µL). Photocrosslinking was performed at 302 nm with an energy of 20.3 J cm^{-2}. All films were washed with water before further experiments.

Light Microscopy and Photoactuation Set-Up:

The laser used in the experiments is a Class IIIb CW laser with a wavelength of 532 nm and 10 mW power, model MGLIII532, by Changchun New Industries Optoelectronics Tech Co., Ltd., People's Republic of China.

The camera used for imaging is a Zyla sCMOS by Andor Oxford Instruments, UK, with the matching Andor SOLIS software.

Laser power was determined before the objective with a PM100D power meter with a S130c 400 nm - 1100 nm probe by ThorLabs GmbH, Germany.

The objective used is an EC Epiplan-APOCHROMAT 50x/0.95 DIC by ZEISS, Germany.

A 542 nm long-pass filter by ThorLabs GmbH, Germany, was places in front of the camera.

The set-up is sketched in Figure 1 of the main article.

Optical Data and Light Microscopy Images:

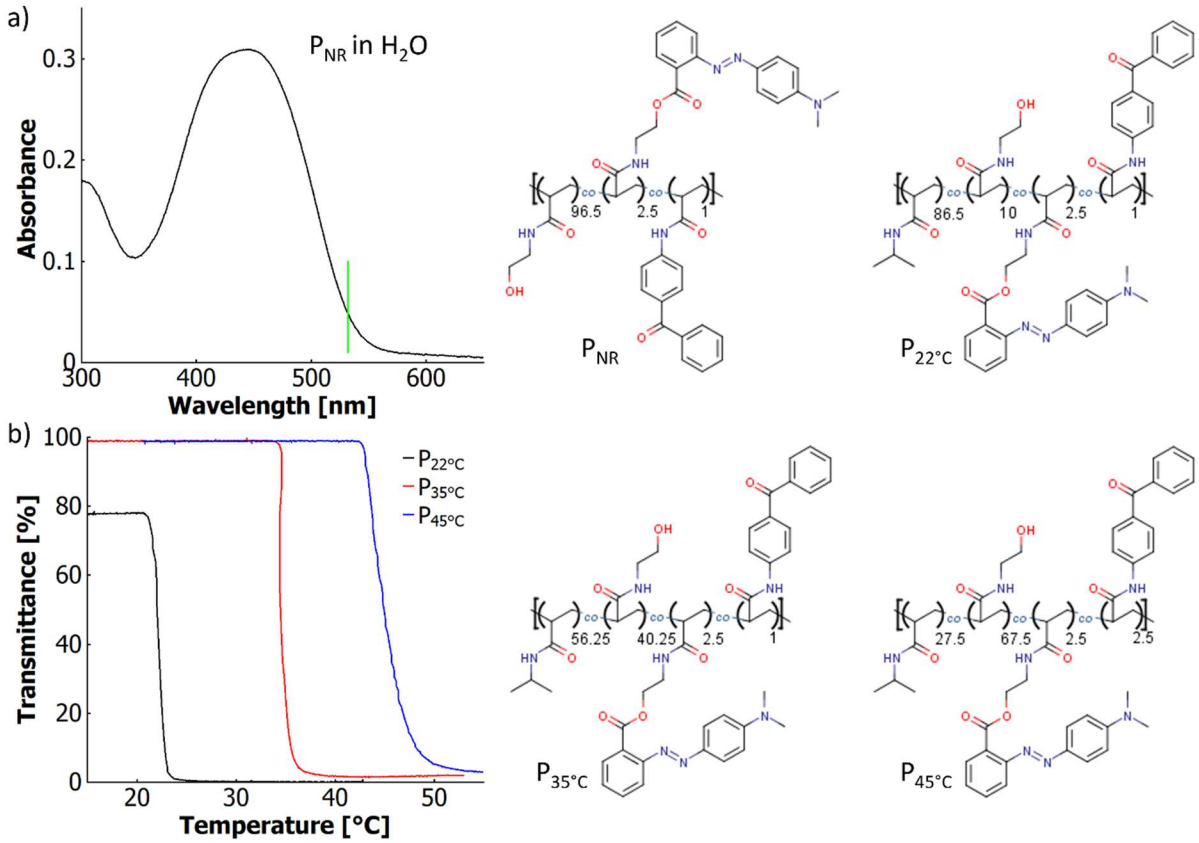

Figure S 5: a) UV-vis spectrum of a photocrosslinked film of poly(HEAm$_{96.5\%}$-co-o-MREAm$_{2.5\%}$-co-BPAAm$_{1\%}$) P_{NR} swollen in water at 26 °C, with the wavelength of the green laser used in this marked with a green vertical line at 532 nm. b) Turbidity measurements at 780 nm of aqueous 1 w% solutions of poly(NipAAm$_{86.5\%}$-HEAm$_{10\%}$-co-o-MREAm$_{2.5\%}$-co-BPAAm$_{1\%}$) $P_{22°C}$, poly(NipAAm$_{56.25\%}$-HEAm$_{40.25\%}$-co-o-MREAm$_{2.5\%}$-co-BPAAm$_{1\%}$) $P_{35°C}$, and poly(NipAAm$_{27.5\%}$-HEAm$_{67.5\%}$-co-o-MREAm$_{2.5\%}$-co-BPAAm$_{2.5\%}$) $P_{45°C}$. On the right: structures of the copolymers used in this study with the feed ratios of monomers in the synthesis.

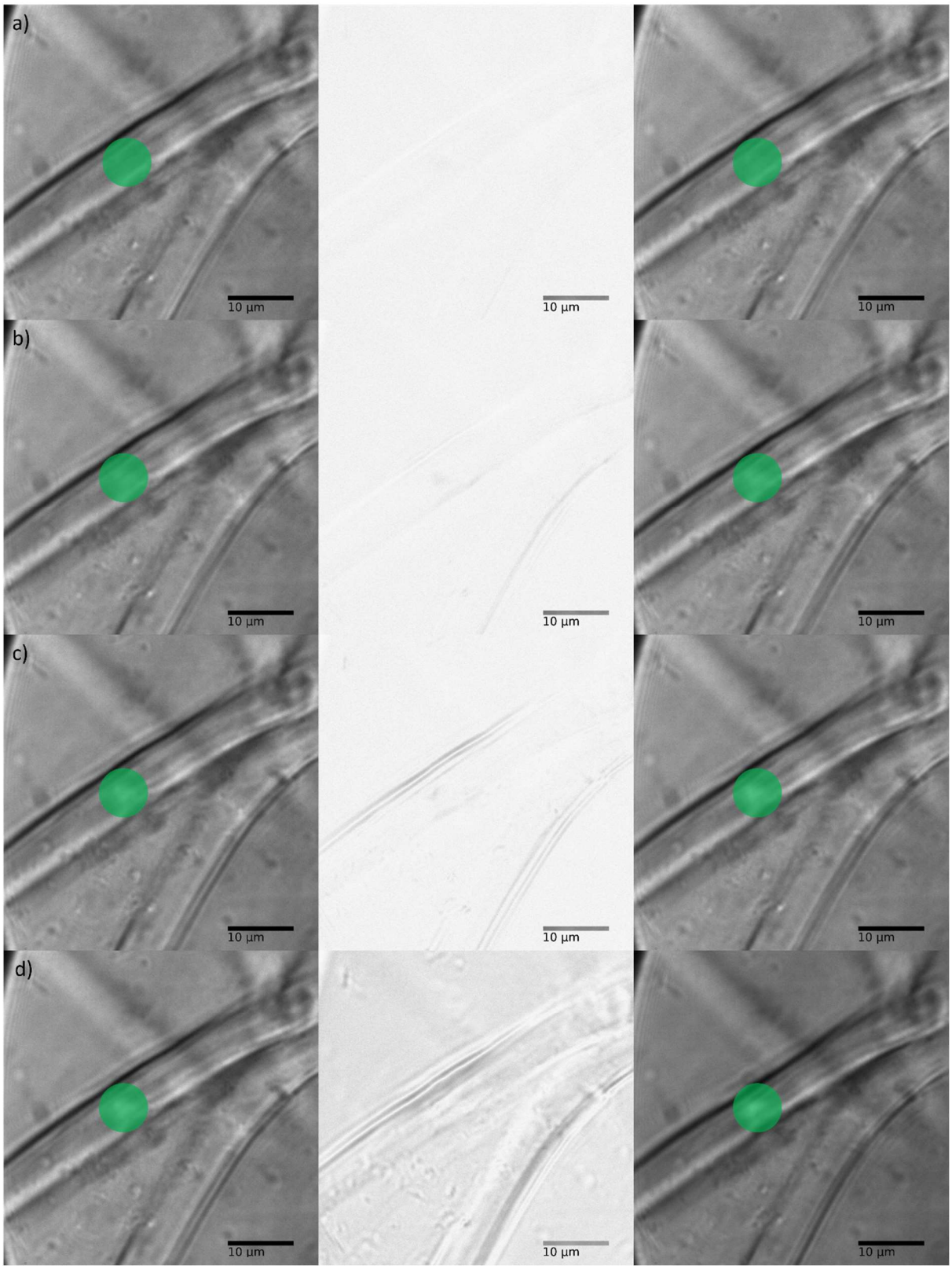

Figure S 6: A series of light microscopy images of a hydrogel of poly(NipAAm$_{86.5\%}$-HEAm$_{10\%}$-co-o-MREAm$_{2.5\%}$-co-BPAAm$_{1\%}$) $P_{22°C}$ showing left: non-irradiated gel with accumulative irreversible change of irradiations at previous stages of power; middle: difference pictures between the non-irradiated and the irradiated gel with inverted colour scheme (laser at λ=532 nm); right: irradiated gel after 3 s at a) 85 µW, b) 376 µW, c) 1210 µW, and d) 3750 µW. The green shaded area shows the approximate dimensions of the laser spot.

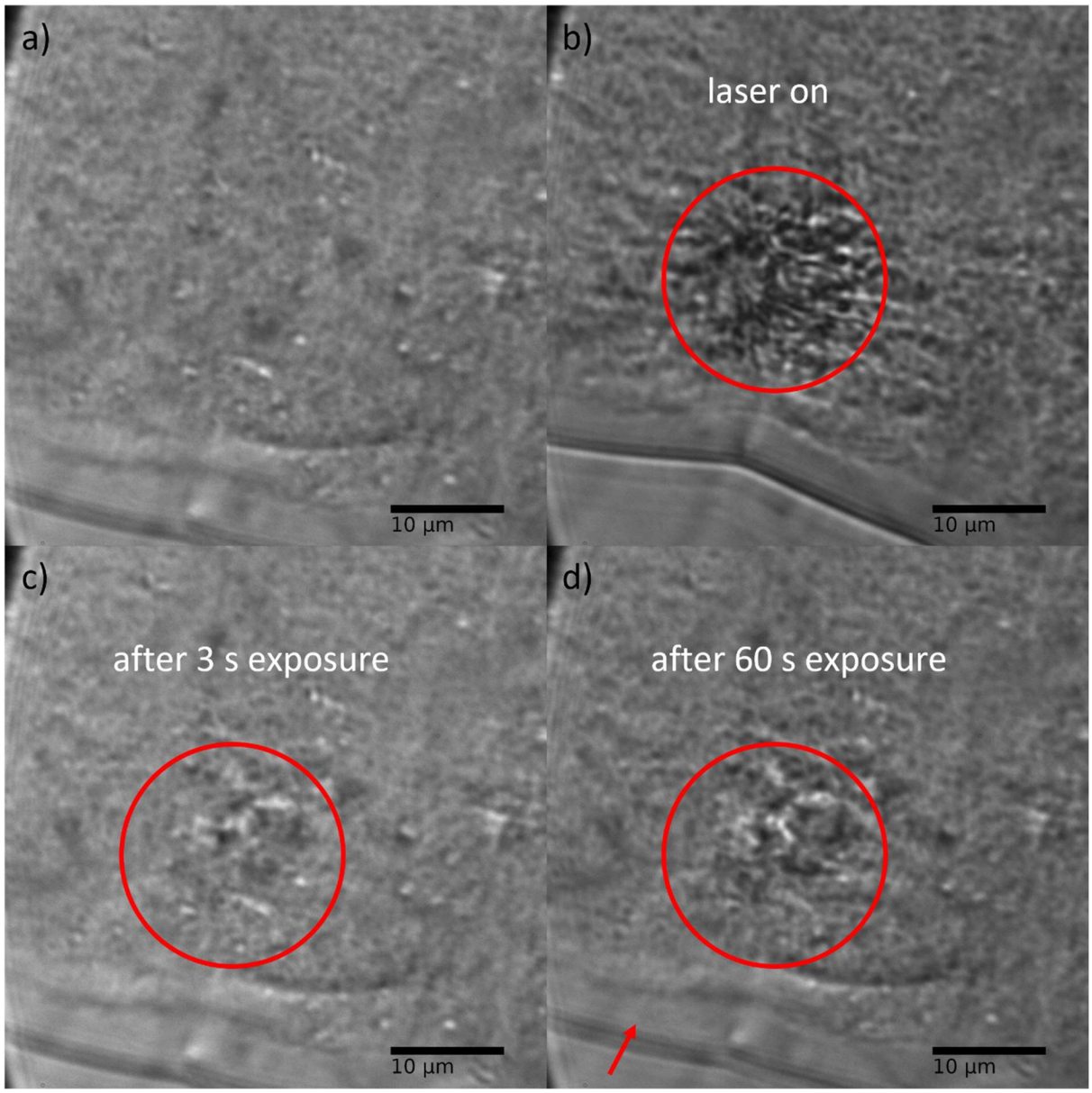

Figure S 7: Light microscopy images of a hydrogel of poly(NipAAm$_{86.5\%}$-HEAm$_{10\%}$-co-o-MREAm$_{2.5\%}$-co-BPAAm$_{1\%}$) P$_{22°C}$ showing a) the pristine hydrogel, b) the hydrogel when irradiated with a laser (λ=532 nm, 3750 µW), c) after 3 s of exposure, and d) after 60 s of exposure.

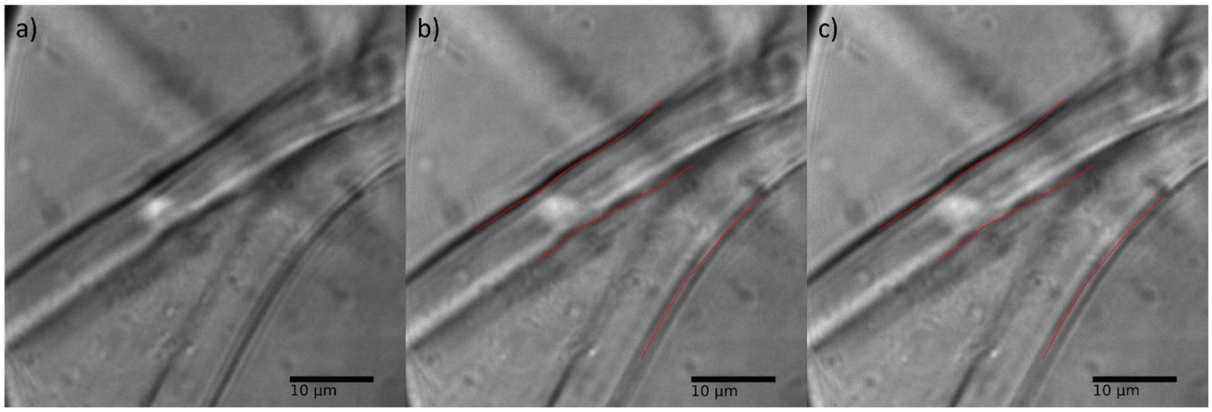

Figure S 8: Light microscopy images of a hydrogel of poly(NipAAm$_{86.5\%}$-HEAm$_{10\%}$-co-o-MREAm$_{2.5\%}$-co-BPAAm$_{1\%}$) P$_{22°C}$ irradiated with laser (λ=532 nm) at 3750 µW a) for the first time, b) after cycling five times between 3 s irradiation intervals and relaxation, c) after cycling twenty times between 3 s irradiation intervals and relaxation. The red lines in b) and c) show the positions of the notable dark features in a).

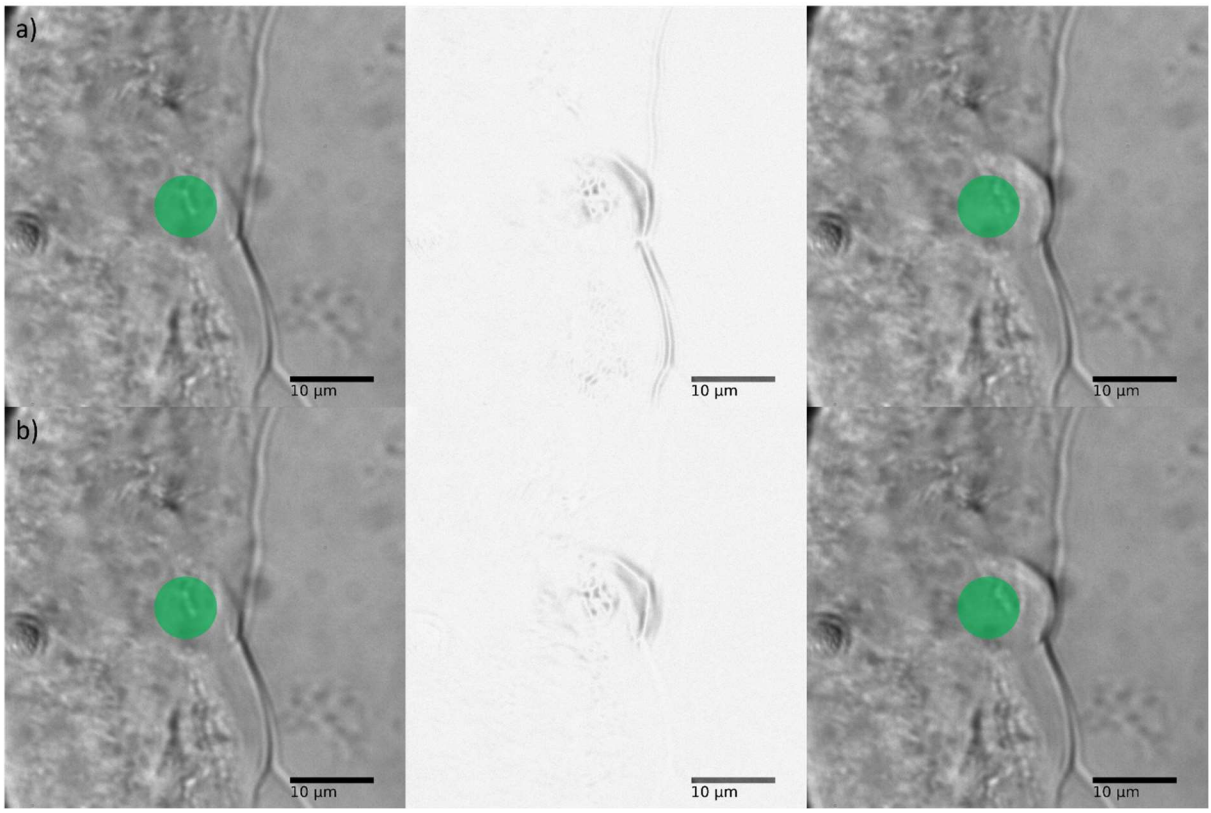

Figure S 9: Light microscopy images of a hydrogel of poly(NipAAm$_{56.25\%}$-HEAm$_{40.25\%}$-co-o-MREAm$_{2.5\%}$-co-BPAAm$_{1\%}$) P$_{35°C}$ showing a) left to right: the pristine gel, a difference picture between the non-irradiated and the irradiated gel, the irradiated gel (laser at λ=532 nm, 3750 µW), and b) left to right: the pristine gel, a difference picture between the non-irradiated gel before and after exposure to laser light, the gel after exposure to laser light. The green shaded area shows the approximate dimensions of the laser spot. The difference pictures are shown with inverted colour scheme.

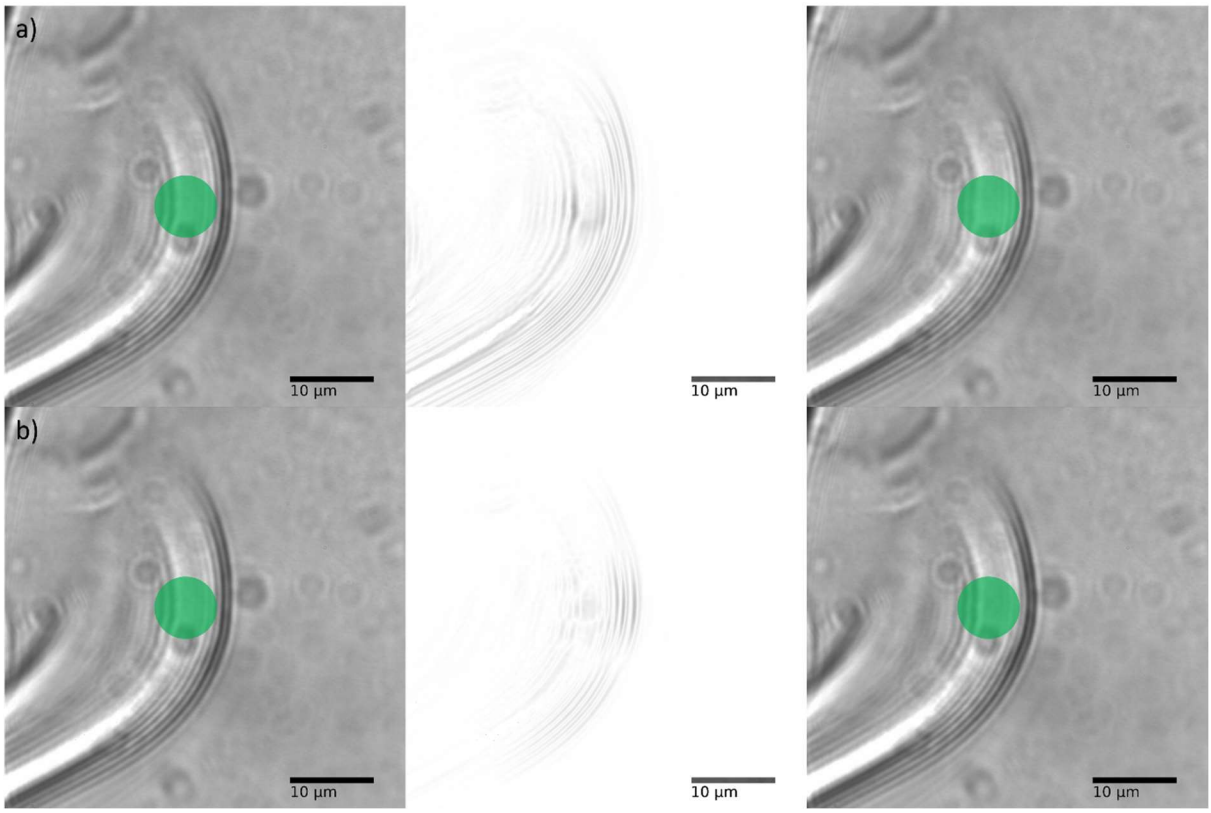

Figure S 10: Light microscopy images of a hydrogel of poly(NipAAm$_{27.5\%}$-HEAm$_{67.5\%}$-co-o-MREAm$_{2.5\%}$-co-BPAAm$_{2.5\%}$) P$_{45°C}$ showing a) left to right: the pristine gel, a difference picture between the non-irradiated and the irradiated gel, the irradiated gel (laser at λ=532 nm, 3750 µW), and b) left to right: the pristine gel, a difference picture between the non-irradiated gel before and after exposure to laser light, the gel after exposure to laser light. The green shaded area shows the approximate dimensions of the laser spot. The difference pictures are shown with inverted colour scheme.

References

43. Jia, J.; Sarker, M.; Steinmetz, M.G.; Shukla, R.; Rathore, R. Photochemical elimination of leaving groups from zwitterionic intermediates generated via electrocyclic ring closure of alpha,beta-unsaturated anilides. *J. Org. Chem.* **2008**, *73*, 8867–8879, doi:10.1021/jo8017445.
44. Jaik, T.G.; Ciubini, B.; Frascella, F.; Jonas, U. Thermal Response and Thermochromism of Methyl Red-Based Copolymer Systems - Coupled Responsiveness in Critical Solution Behaviour and Optical Absorption Properties. *Polym. Chem.* **2022**, *13*, 1186–1214, doi:10.1039/D1PY01361K.
45. Gianneli, M.; Roskamp, R.F.; Jonas, U.; Loppinet, B.; Fytas, G.; Knoll, W. Dynamics of swollen gel layers anchored to solid surfaces. *Soft Matter* **2008**, *4*, 1443–1447, doi:10.1039/b801468j.

7 Topographic Laser Writing with Visible Light in a Dual Photocrosslinked Hydrogel – Proof-of-Principle

This section provides a proof-of-principle for the topic mentioned in the heading and has not been published or submitted to any journal.

External contributions to this project:

- The optical setup used was, as stated in Chapter 6, designed by the Nano-Optics Group of the Department Physics of the University of Siegen under the supervision of Prof. Dr. Mario Agio.
- The sketch of the setup was provided by Dr. Assegid M. Flatae and Mr. Philipp Reuschel.
- The sample preparation for the ^{1}H NMR spectrum in DMSO-d^{6} of the Coumarin 343 monomer I synthesised was done by Ms Fiona Diehl.

Coumarin derivatives are known to undergo photochemically induced [2+2] cycloadditions to form a cyclobutane link (cf. Scheme 1). This reaction is reversible, with the back-reaction being induced by irradiation with shorter wavelengths. In polymeric materials, this process has been exploited to form reversible, covalent crosslinks with a primary focus on the preparation of hydrogel networks.[1–5] Both the photodimerization, as well as the photocleavage, have been shown to proceed by either one- or two-photon excitation.[4,6–9]

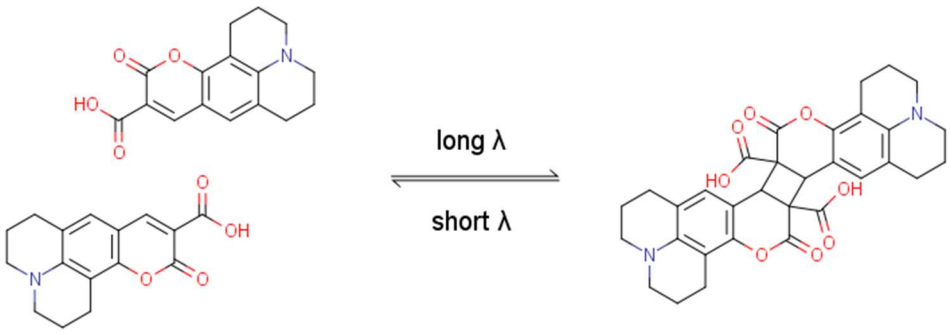

Scheme 1: Reversible [2+2] cycloaddition of a coumarin derivative (here Coumarin 343).

Another widely used photocrosslinker motif for polymers is benzophenone, which forms irreversible covalent bonds and is less selective in its binding partner. Briefly, upon irradiation

a biradical is formed on the carbonyl of benzophenone, which abstracts hydrogen from a second chain, leaving a carbon radical on the chain. This carbon radical and the carbon radical located on the photocrosslinker then combine and connect the two chains by a covalent bond.[10]

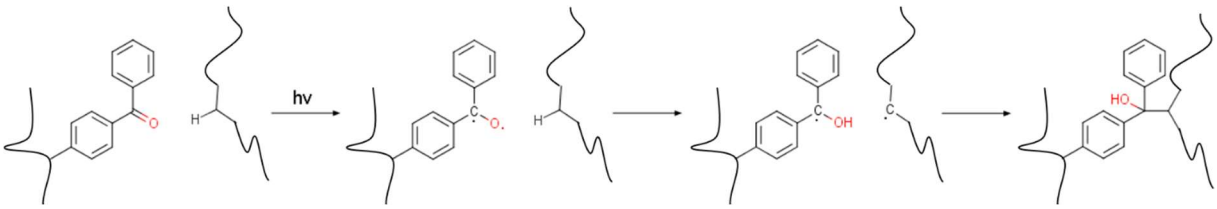

Scheme 2: Schematic crosslinking mechanism of benzophenone moieties attached to a polymeric chain with another chain, including excitation of the carbonyl to a biradical, hydrogen abstraction, and combination.

In order to exploit both crosslinking mechanisms, a hydrophilic copolymer from *N*-isopropylacrylamide (NiPAAm), *N*-hydroxyethyl acrylamide (HEAm), a Coumarin 343 ester of HEAm (C343EAm), and the photocrosslinker 4-benzophenone acrylamide (BPAAm) was prepared by free radical polymerisation. This copolymer was drop-cast on a glass surface that was treated prior with 4-(3-triethoxysilyl)propoxybenzophenone as adhesion promoter and dried. The polymer film was crosslinked at 302 nm (28.4 J cm^{-2}), which activates both the coumarin and the benzophenone crosslinkers, and then swollen in water to yield a hydrogel (cf. Scheme 3 top).

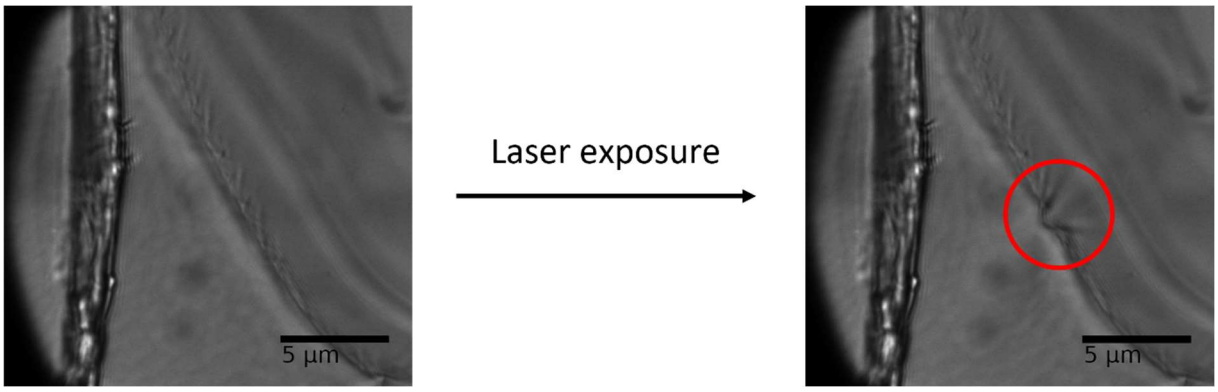

Figure 1: Light microscopy pictures (left) of a pristine hydrogel containing both benzophenone and Coumarin 343 and (right) of the hydrogel after 5 s of laser exposure (532 nm). A red circle marks the region of structural changes.

This hydrogel was subsequently irradiated with a laser (532 nm) at high powers (1 mW), which assumingly cleaves the coumarin dimer, while observing any morphological changes *via* optical microscopy (cf. also Figure S 5). At the focal area of the laser, the hydrogel shows increased swelling in a matter of seconds, which persists when the laser is turned off (cf. Figure 1).

The observed behaviour may be explained by the specific photoresponse of the two different kinds of photocrosslinkers that were employed. In the initial irradiation with UV-light (302 nm), both crosslinker types participate in network formation with the coumarin derivative C343EAm dimerising and the benzophenone moiety BPAAm undergoing the biradical-mediated C-H insertion. When the resulting hydrogel is then irradiated with a laser at long wavelengths (532 nm), the cyclobutane crosslinks from C343EAm dimerization by [2+2] cycloaddition are photocleaved, reducing the crosslink density and allowing increased swelling in turn (cf. Scheme 3 bottom).

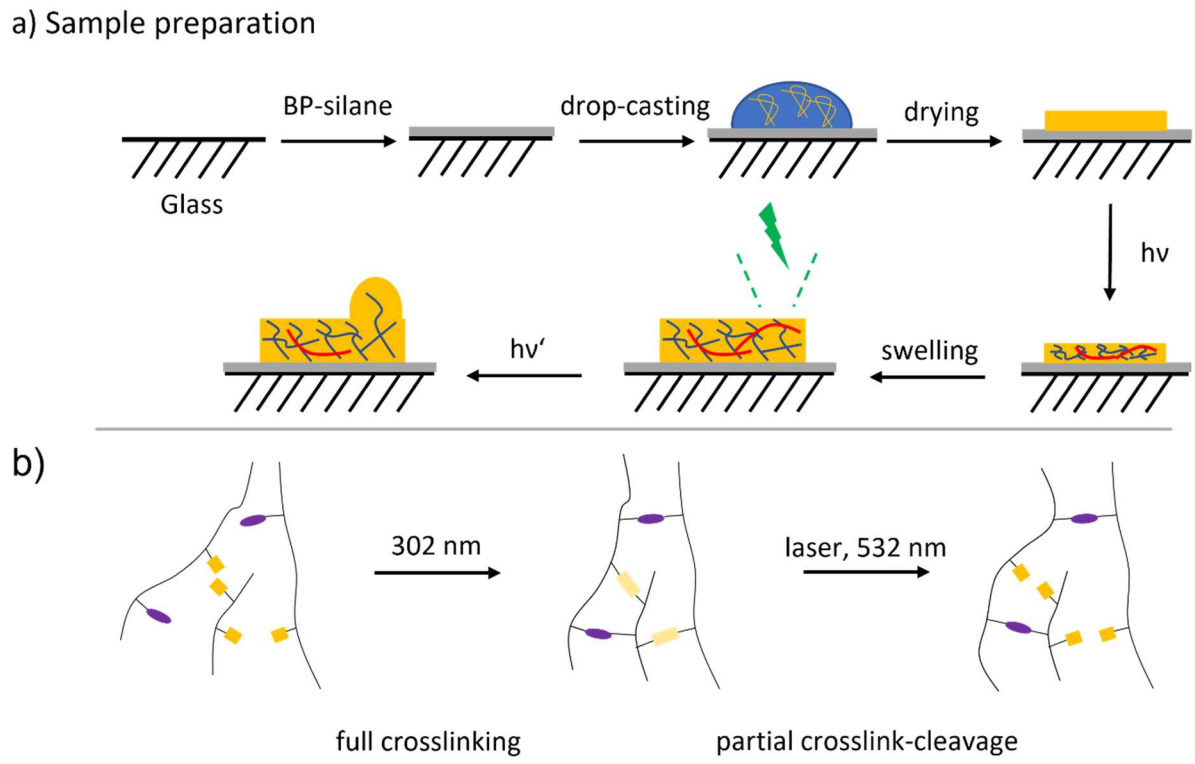

Scheme 3: a) Sample preparation process of hydrogels for topographic laser-writing experiments, involving functionalisation of the glass surface with a silane of the photocrosslinker benzophenone, drop-casting a solution of the respective copolymer, drying, photocrosslinking, subsequent swelling water, and finally irradiation with a laser, resulting in partial photocleavage and anisotropic swelling. Blue lines indicate benzophenone crosslinked network segments, red lines coumarin crosslinked ones. b) Crosslinking and photolithography process of Coumarin 343 (yellow squares) and benzophenone (purple oval) containing copolymers. In the first step, the gel is irradiated with UV-light and both benzophenone and Coumarin 343 crosslink. In the second step, the gel is locally irradiated with a green laser (532 nm) and the Coumarin 343 based crosslinks are cleaved.

However, it is surprising that such photocleavage occurs at such a long wavelength (532 nm) of the laser employed, as the dimerised dye does not show a significant absorption at this wavelength, while the monomeric coumarin chromophore only weakly absorbs (cf. Figure 2). Irradiation of solutions containing either the dye monomer or the C343EAm copolymer at the photocrosslinking wavelength (302 nm, 8.6 J cm^{-2}) leads to photodimersation of the majority of the dye, which is indicated by vanishing of the main absorption band in the visible region at

around 440 nm (cf. Figure 2). In aqueous solution of the copolymer, the evolution of the main absorption band features under irradiation shows an additional process. In the pristine solution, a distinct sub-band structure is visible with a long-wavelength shoulder at 455 nm. The absorption band at 426 nm persists after irradiation, while the long-wavelength shoulder vanishes (cf. Figure 2 b). This suggests that aggregation in solution occurs in the pristine solution, which is known for the parent compound Coumarin 343 and leads to red-shifting of the absorption maximum.[11] Owing to their proximity, aggregates would undergo cycloaddition first, leaving mostly monomers, which absorb further in the blue. While the bulk of the macromolecules are hydrophilic, the dye and photocrosslinker moieties are hydrophobic but are solubilised by the polymer coil. This may lead to the macromolecule acting as a barrier between the C343EAm moieties, resulting in a slower conversion compared to the monomer (cf. comparing Figure 2 a,b black and red lines).

If these solutions are irradiated with a shorter wavelength (254 nm, 8.6 J cm^{-2}), as usually done to photocleave the cyclobutane link of crosslinked coumarin dimers,[1–5] interestingly no photocleavage occurs but rather the few monomers still in solution crosslink as well. This is indicated by the disappearance of the residual absorption in the visible region of the spectra (cf. Figure 2 blue line).

In contrast, when irradiating at the long wavelength (532 nm) of the high power, continuous wave laser, apparently photocleavage the coumarin dimers does occur, as evidenced by the increased swelling of the hydrogels. This suggests a two-photon absorption process, which leads to photocleavage.

In summary, these systems may introduce a new class of writeable hydrogels, in which the crosslinking density can be adjusted with a visible light laser. As Coumarin 343 is a fluorescent dye in its monomeric form, it should also be possible to write fluorescence into the 3D hydrogel in this manner.

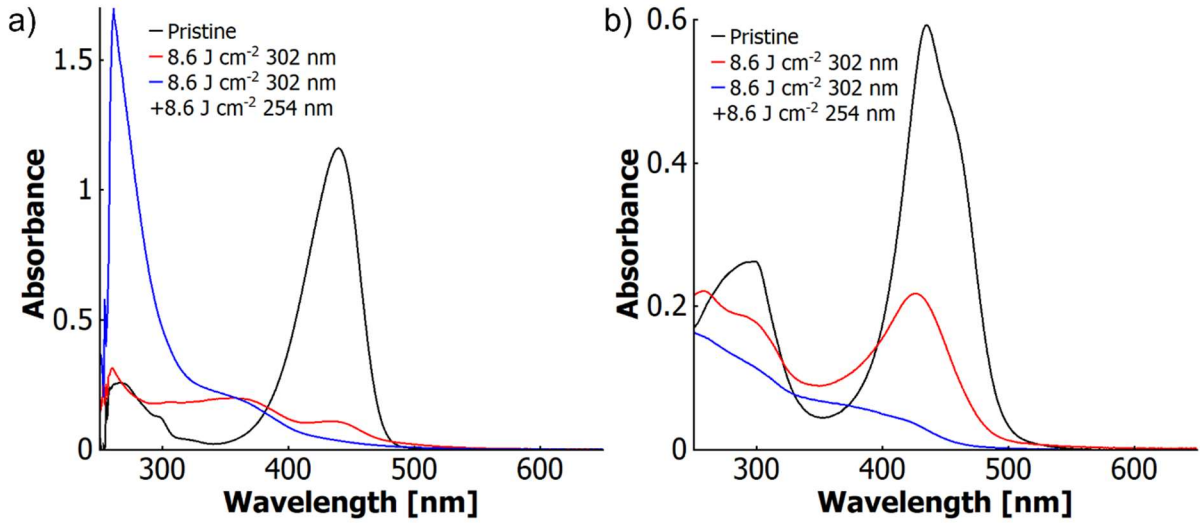

Figure 2: UV-vis spectra at room temperature (23.5 °C) of a) a Coumarin 343 ester of N-hydroxyethyl acrylamide (C343EAm) in dimethylsulfoxide ($2.6*10^{-5}$ $molL^{-1}$, 0.01 gL^{-1}) and b) a poly(NiPAAm-co-HEAm-co-C343EAm-co-BPAAm) copolymer in aqueous solution (0.1 gL^{-1}).

Experimentals

Materials and equipment:

All solvents used were of Milli-Q®, spectroscopic or HPLC-grade. 1,4-Dioxane was dried and distilled over sodium. Absolute ethanol was purchased from VWR Chemicals. Carbonyldiimidazole (97%, Alfa Aesar), Coumarin 343 (Radiant Dyes, Germany), and *N*-hydroxyethyl acrylamide (97%, Sigma Aldrich) was used as received. 1,8-Diazabicyclo[5.4.0]undec-7-ene was distilled under vacuum. *N*-Isopropylacrylamide was recrystallised from n-hexane. Azobisisobutyronitrile was recrystallised from methanol. 4-Benzophenoneacrylamide was synthesised according to literature.[12] 4-(3-Triethoxysilyl)propoxybenzophenone was synthesised by Mr. Daniel John according to literature.[13]

UV-vis measurements were performed on a Thermo Scientific™ Evolution™ 220 UV-Vis-spectrophotometer. If not stated otherwise, the measurements were done with 100 nm/min and a resolution of 1 nm.

NMR-measurements were performed on either a Bruker AV 400 or a Jeol EZC 500.

GPC/SEC was measured on a PSS GRAM linM column (Polymer Standards Service GmbH, Mainz, Germany) in dimethylacetamide with LiBr (0.1 g/L) at 60 °C with PMMA-standards as reference.

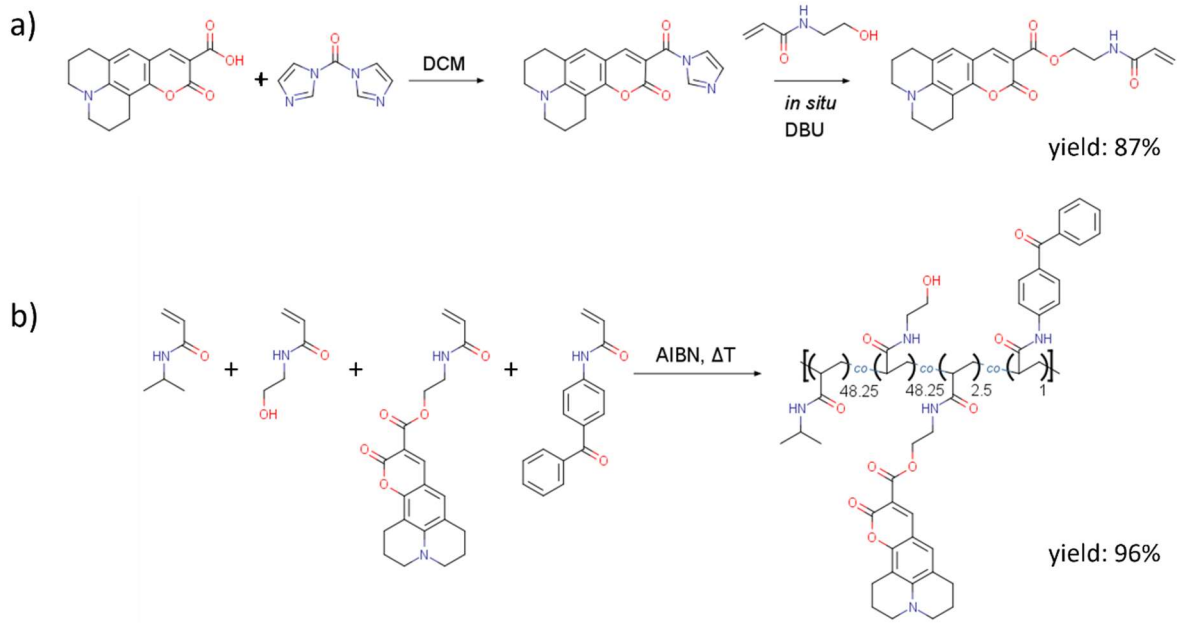

Scheme S 1: a) Functionalisation of Coumarin 343 with N-hydroxyethyl acrylamide via carbonyldiimidazole in a one-pot reaction to yield a Coumarin 343 ester of N-hydroxyethyl acrylamide (C343EAm). b) Free radical copolymerisation of N-isopropylacrylamide, N-hydroxyethyl acrylamide, C343EAm, and 4-benzophenone acrylamide, initiated thermally with azobisisobutyronitrile.

Synthesis of the Coumarin 343 ester of N*-hydroxyethyl acrylamide (C343EAm):*

Coumarin 343 (251 mg, $8.8*10^{-4}$ mol) was dissolved in dichloromethane (25 mL) at room temperature. Carbonyldiimidazole (228 mg, $1.4*10^{-3}$ mol) was added and the solution was stirred for five hours and twenty minutes. *N*-Hydroxyethyl acrylamide (0.18 mL, $1.7*10^{-3}$ mol) and 1,8-diazabicyclo[5.4.0]undec-7-ene (0.25 mL, $1.7*10^{-3}$ mol) were added. This solution was then stirred for sixteen hours at room temperature before water was added. The organic phase was extracted with water, diluted aqueous NaOH and again water. The product was purified *via* column chromatography (silica) in ethyl acetate. The yield was 293 mg or 87%.

δH (400 MHz, $CDCl_3$) 8.32 (s, 1H), 7.54 (s, 1H), 6.93 (s, 1H), 6.26 (dd, J = 17.1, 1.9 Hz, 1H), 6.18 (dd, J = 17.1, 9.9 Hz, 1H), 5.61 (dd, J = 9.9, 1.9 Hz, 1H), 4.35 (t, J = 5.1 Hz, 2H), 3.66 (t, J = 5.1 Hz, 2H), 3.32 (dd, J = 11.3, 5.1 Hz, 4H), 2.83 (t, J = 6.4 Hz, 2H), 2.73 (t, J = 6.1 Hz, 2H), 2.38 (s, 2H), 1.94 (p, J = 11.8, 6.1 Hz, 4H).

δC (101 MHz, $CDCl_3$) 166.24, 165.28, 159.82, 153.54, 150.18, 149.10, 131.01, 130.97, 127.27, 126.37, 119.78, 107.80, 106.30, 105.64, 77.16, 64.08, 50.38, 49.96, 38.32, 27.43, 21.06, 20.09, 20.01.

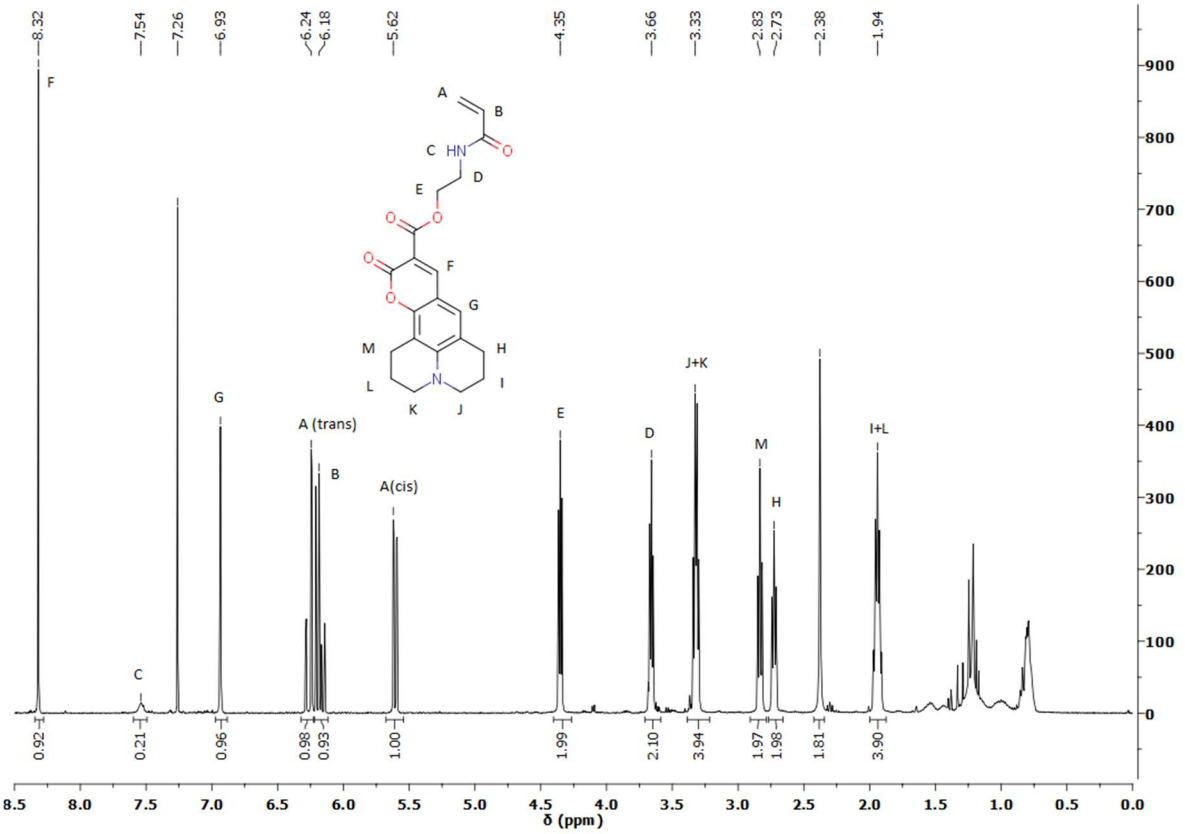

Figure S 1: ^{1}H NMR spectrum (400 MHz) of a Coumarin 343 ester of N-hydroxyethylacrylamide in $CDCl_3$ with 15% MeOD.

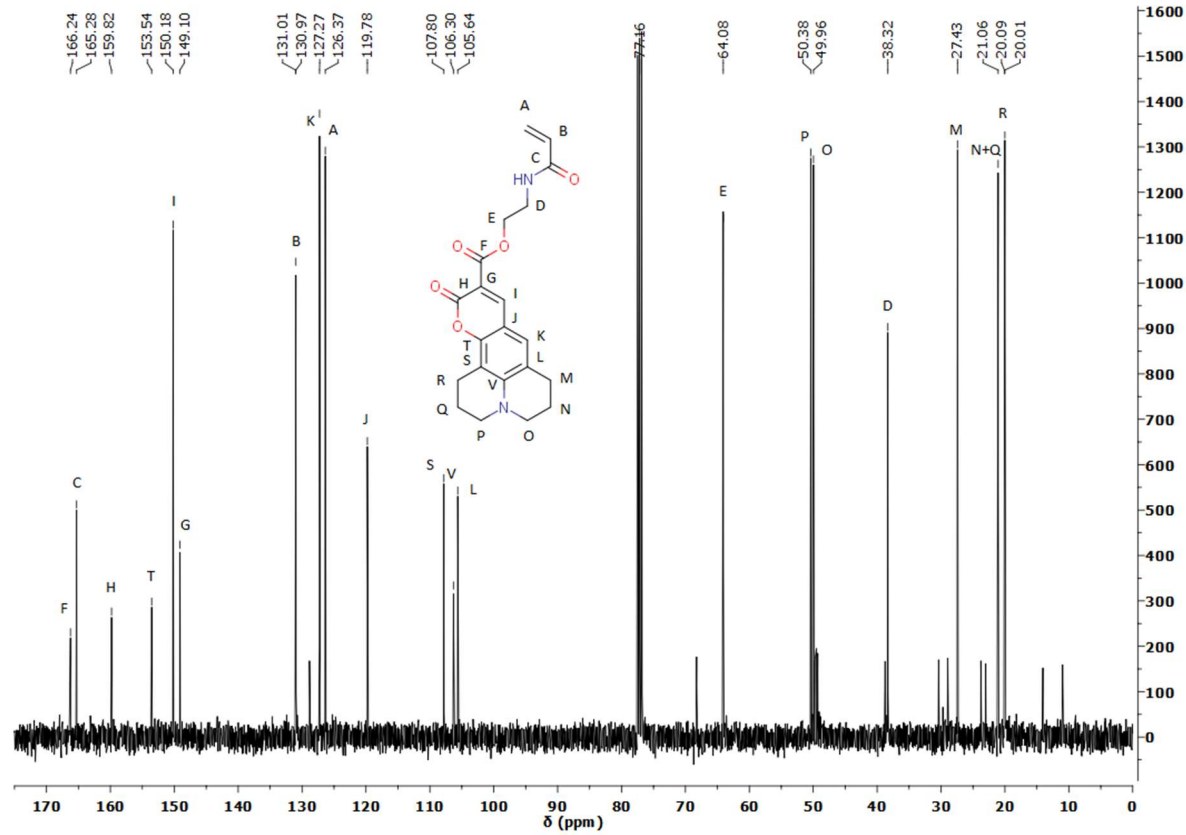

Figure S 2: ^{13}C NMR spectrum (101 MHz) of a Coumarin 343 ester of N-hydroxyethylacrylamide in $CDCl_3$ with 15% MeOD.

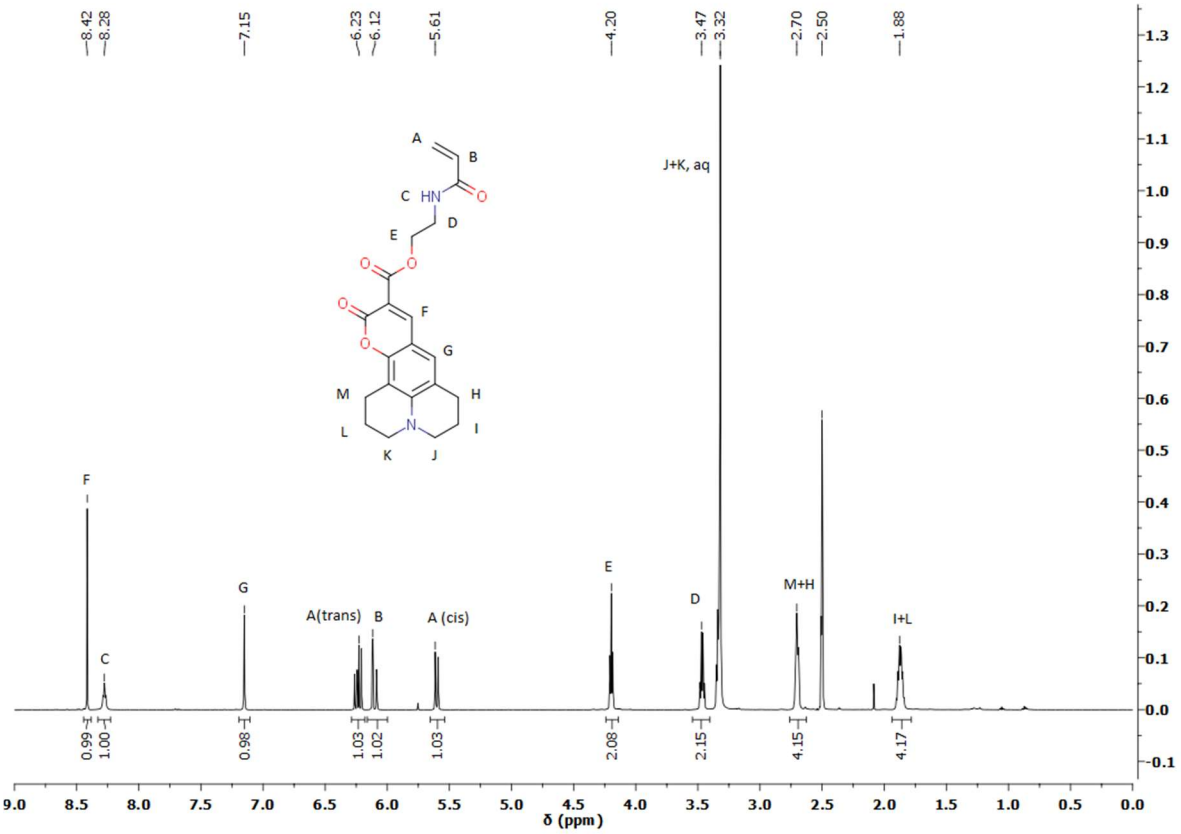

Figure S 3: ^{1}H NMR spectrum (400 MHz) of a Coumarin 343 ester of N-hydroxyethylacrylamide in DMSO-d^{6}. This spectrum serves to demonstrate that the impurities between 0.6 and 1.5 ppm in Figure S 1 are not because of the compound but because of the deuterated solvent used.

Free radical copolymerisations:

N-Isopropylacrylamide (125 mg, 1.1*10^{-4} mol), *N*-hydroxyethyl acrylamide (129 mg, 1.1*10^{-4} mol), a Coumarin 343 ester of *N*-hydroxyethyl acrylamide (22.5 mg, 5.9*10^{-5} mol), 4-benzophenone acrylamide (5.8 mg, 2.3*10^{-5} mol), azobisisobutyronitrile (7.5 mg, 4.6*10^{-5} mol) were dissolved in a 1:1 mixture of chloroform and methanol (6 mL) (NiPAAm:HEAm:C343EAm:BPAAm 47.9:48.6:2.5:1, 2% AIBN). The solutions were purged with nitrogen for 30 minutes and heated in an oil bath at 60 °C in methanol for 24 hours. The polymer was then precipitated twice in diethylether.

The yield was 272 mg or 96%.

δH(500 MHz, MeOD) 8.5-7 (aromatic H), 4.54 (CONHC*H*), 3.90 ($CH_2C\mathit{H}_2OH$), 3.63 ($CONHC\mathit{H}_2$), 2.4-1.25 (backbone), 1.12 ($CONHCH(C\mathit{H}_3)_2$).

Table S 1: Copolymer characteristics as determined by UV-vis spectroscopy and GPC. The built-in ratios for o-MREAm and BPAAm are given in weight percentages and the percentage of the monomer built-in compared to the feed composition.

C343EAm [w%] Built-in to feed (%)	BPAAm [w%] Built-in to feed (%)	M_n [10^3 Da]	M_w [10^3 Da]	$Đ$
6.1 (77%)	2.0 (97%)	23.9	74.5	3.12

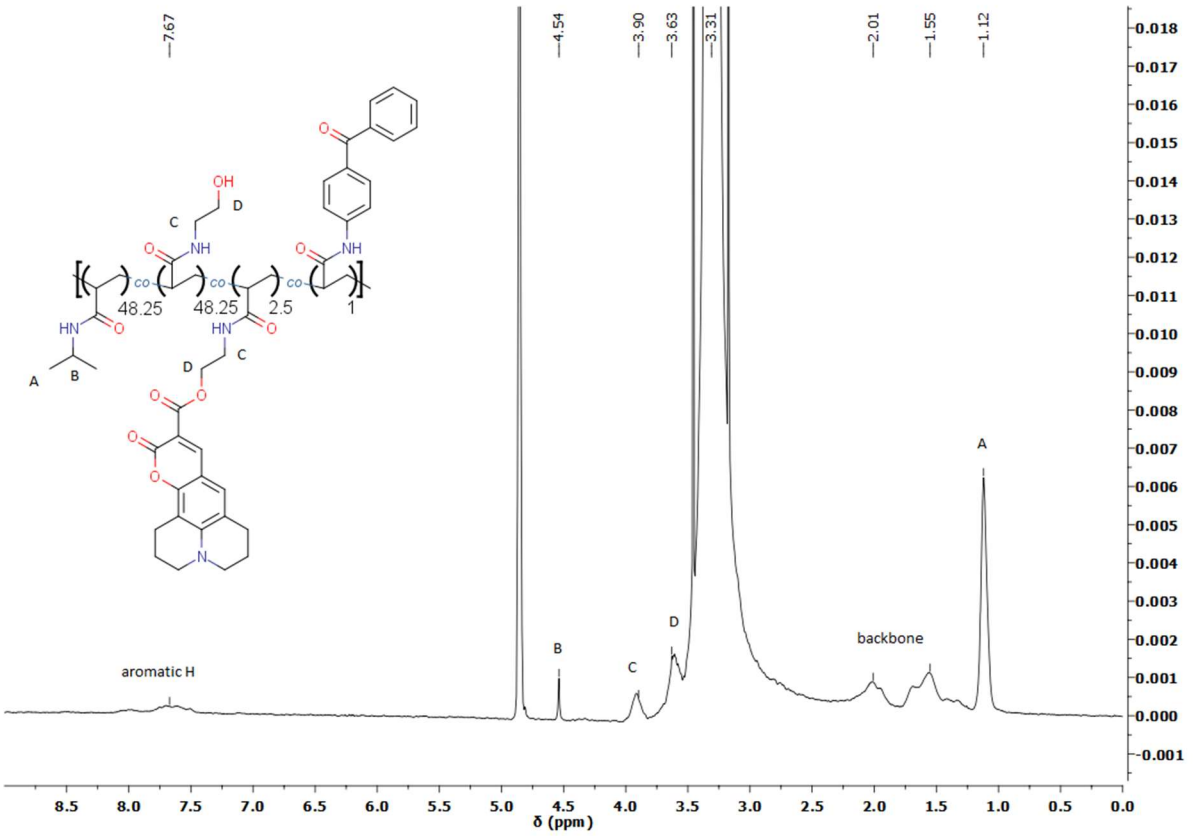

Figure S 4: ^{1}H NMR spectrum (500 MHz) in MeOD of a poly(NiPAAm-co-HEAm-co-C343EAm-co-BPAAm) copolymer (feed: NiPAAm:HEAm:C343EAm:BPAAm 47.9:48.6:2.5:1).

Film preparation:

The glass slides used in photoactuation experiments were cleaned with fresh Carothers' acid (sulfuric acid:hydrogen peroxide, 3:1) and rinsed thoroughly with water. The slides were dried under a nitrogen stream. They were submerged in an ethanolic solution of benzophenone silane (1 mmol/L) for 24 hours before they were rinsed thrice with absolute ethanol and finally dried under a nitrogen stream.

The polymer was drop-casted on the glass slides from MeOH:H_2O (4:1) solution (2.5 w%, 25 µL). Photocrosslinking was performed at 302 nm with an energy of 28.4 J/cm². The films were washed with water before further experiments.

Light Microscopy and Photoactuation Set-Up:

The laser used in the experiments is a Class IIIb CW laser with a wavelength of 532 nm and 10 mW power, model MGLIII532, by Changchun New Industries Optoelectronics Tech Co., Ltd., People's Republic of China.

The camera used for imaging is a Zyla sCMOS by Andor Oxford Instruments, UK, with the matching Andor SOLIS software.

Laser power was determined before the objective with a PM100D power meter with a S130c 400 nm - 1100 nm probe by ThorLabs GmbH, Germany.

The objective used is an EC Epiplan-APOCHROMAT 50x/0.95 DIC by ZEISS, Germany.

A 542 nm long-pass filter by ThorLabs GmbH, Germany, was places in front of the camera.

The set-up is sketched in Figure S 5.

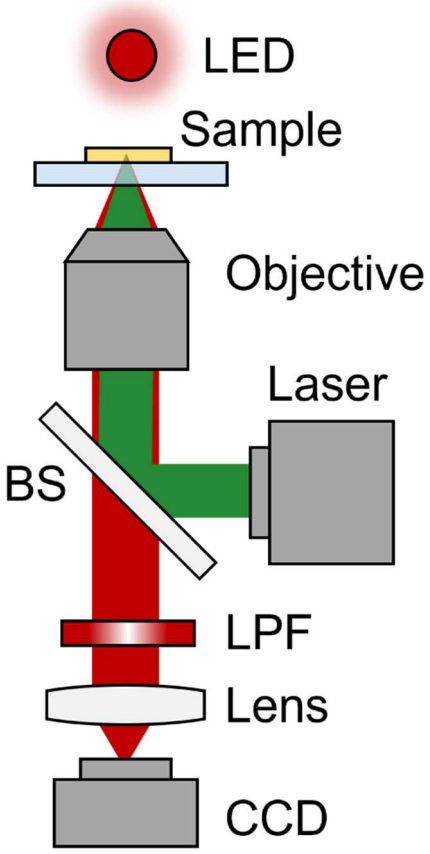

Figure S 5: Sketch of the set-up used in photoactuation experiments including the laser source, objective, sample holder, focussing lenses, filters, and the camera. The schematic was produced and provided by Mr. Philipp Reuschel and Dr. Assegid M. Flatae.

References

1 S. R. Trenor, A. R. Shultz, B. J. Love and T. E. Long, Coumarins in polymers: from light harvesting to photo-cross-linkable tissue scaffolds, *Chem. Rev.*, 2004, **104**, 3059–3077.

2 C. P. Kabb, C. S. O'Bryan, C. C. Deng, T. E. Angelini and B. S. Sumerlin, Photoreversible Covalent Hydrogels for Soft-Matter Additive Manufacturing, *ACS Appl. Mater. Interfaces*, 2018, **10**, 16793–16801.

3 I. Cazin, E. Rossegger, G. La Guedes de Cruz, T. Griesser and S. Schlögl, Recent Advances in Functional Polymers Containing Coumarin Chromophores, *Polymers*, 2020, **13**.

4 K. Iliopoulos, O. Krupka, D. Gindre and M. Sallé, Reversible two-photon optical data storage in coumarin-based copolymers, *J. Am. Chem. Soc.*, 2010, **132**, 14343–14345.

5 Y. Chujo, K. Sada and T. Saegusa, Polyoxazoline having a coumarin moiety as a pendant group. Synthesis and photogelation, *Macromolecules*, 1990, **23**, 2693–2697.

6 T. Buckup, J. Dorn, J. Hauer, S. Härtner, N. Hampp and M. Motzkus, The photoinduced cleavage of coumarin dimers studied with femtosecond and nanosecond two-photon excitation, *Chem. Phys. Lett.*, 2007, **439**, 308–312.

7 T. Buckup, A. Southan, H.-C. Kim, N. Hampp and M. Motzkus, Optimisation of two-photon induced cleavage of molecular linker systems for drug delivery, *J. Photochem. Photobiol. A*, 2010, **210**, 188–192.

8 M. Jiang, N. Paul, N. Bieniek, T. Buckup, N. Hampp and M. Motzkus, Photocleavage of coumarin dimers studied by femtosecond UV transient absorption spectroscopy, *Phys. Chem. Chem. Phys.*, 2017, **19**, 4597–4606.

9 H.-C. Kim, S. Härtner and N. Hampp, Single- and two-photon absorption induced photocleavage of dimeric coumarin linkers: Therapeutic versus passive photocleavage in ophthalmologic applications, *J. Photochem. Photobiol. A*, 2008, **197**, 239–244.

10 G. Dormán, H. Nakamura, A. Pulsipher and G. D. Prestwich, The Life of Pi Star: Exploring the Exciting and Forbidden Worlds of the Benzophenone Photophore, *Chem. Rev.*, 2016, **116**, 15284–15398.

11 X. Liu, J. M. Cole and K. S. Low, Molecular Origins of Dye Aggregation and Complex Formation Effects in Coumarin 343, *J. Phys. Chem. C*, 2013, **117**, 14723–14730.

12 J. Jia, M. Sarker, M. G. Steinmetz, R. Shukla and R. Rathore, Photochemical elimination of leaving groups from zwitterionic intermediates generated via electrocyclic ring closure of alpha,beta-unsaturated anilides, *J. Org. Chem.*, 2008, **73**, 8867–8879.

13 M. Gianneli, R. F. Roskamp, U. Jonas, B. Loppinet, G. Fytas and W. Knoll, Dynamics of swollen gel layers anchored to solid surfaces, *Soft Matter*, 2008, S**4**, 1443–1447.

8 Outlook

The results obtained and hypotheses developed in this thesis lay the groundwork for several directions of research. While it was possible to describe two different modes of photoactuation for azo dye-containing polymers and hydrogels, and to determine the interplay of polymer- and dye-inherent properties, the results are limited to a specific set of polymers and dyes.

In terms of thermochromism, the logical next step is to expand the range of already known azo dyes for the same kind of polymeric environments. However, new directions regarding other types of dyes and polymers should be undertaken as well. In this thesis, only the functional group on the acceptor side of the pseudostilbene was modified. By switching from classical azo dyes to heteroaromatic systems, like thiazole-based dyes, a new protonation site can be introduced, namely the nitrogen in the thiazole ring. While this increases the complexity of a thermo-halochromic process, it should also permit the display of a wider variety of colours, as with each proton addition the electronic structure of the chromophore changes.

On the other hand, by exchanging the donor site from an amine to a phosphine, new opportunities regarding complexation, reactivity, and chromic response may be introduced toward sensing applications. Some precedence for systems involving a phosphonium ion intramolecularly binding to the azo bridge already exists in literature and may be exploited in this context.[1]

Another interesting possibility is to exchange the pseudostilbene to an azo-dye with longer thermal lifetimes of the *cis*-isomer, as this would open opportunities to combine thermochromism with photochromism.

On the side of the polymer, the inherent nature can be modified by appropriate choice of comonomers or architectural design. This thesis focussed on the utilisation of lower critical solution temperature type thermoresponsive copolymers. Yet, it may be hypothesised that upper critical solution temperature type thermoresponsive copolymers must have a profound effect on thermo-halochromism as well. Similarly, thermoresponsiveness and new hydrogen bonding motifs may be introduced in systems containing tertiary amides of *o*-methyl red in order to tune the temperature, at which hydrolysis becomes prevalent.

The low fluorescence efficiency of azobenzenes may be exploited as well in the context of thermo-halochromism. Owing to their own low fluorescence, azobenzenes are excellent quenchers for fluorescent dyes. By careful choice of dyes, it should be possible to only quench fluorescence efficiently with the protonated form of the employed azo dye, but not with the

neutral form. In this way, fluorescence is slowly “switched on” when more of the protonated azo dye is deprotonated at higher temperatures, introducing a new kind of optical thermometer.

Photomotion of azobenzene-containing hydrogels is another topic with high potential. Apart from systematic modification of the hydrogels regarding swelling degree and the degree of dye substitution, the polymeric architecture may be varied as well. In particular, the effect of block copolymers may be studied in detail, as these may introduce self-assembled structures like vesicles, which would be decomposed upon irradiation and photothermal heating. This could provide another handle to influence the photoactuation of the systems, specifically response times and the scale of motion.

By switching the thermoresponsive nature from lower critical solution temperature type to upper critical solution temperature type copolymers, it could be possible to provide irradiation-controlled swelling instead of collapse. Even one step further, complete photoactuated dissolution of reformation of gels may be achieved by using dynamic crosslinkers like hydrogen bonding motifs such as ureidopyrimidinone. The weak crosslinks would be broken either photothermally or through the mechanical stress of the moving gel.

More immediate research opportunities lie in the quantification of the photoactuation. There are three large questions to be answered:

1. What is the mechanical stress generated by the photoactuation?
2. How much does the temperature increase locally upon irradiation?
3. What is the cause for incomplete reversibility in the systems presented in this thesis?

To answer these questions, *in situ* measurements of these parameters are necessary. These may be atomic force microscopy (AFM) to determine the mechanical force, optical thermometers to measure the temperature increase, and a scale-up of the systems and subsequent spectroscopic analysis to determine the cause for irreversibility. Each of these come with their own set of challenges, as the motion is too fast for AFM imaging, optical thermometers may affect the photomotion, and larger scales of the systems may be difficult to achieve.

In summary, the research on these systems is still in its early stages, giving opportunities for many new approaches for responsive dyes, polymers, and gels.

References

1 M. Yamamura, N. Kano and T. Kawashima, Thermal and photocontrol of the equilibrium between a 2-phosphinoazobenzene and an inner phosphonium salt, *Journal of the American Chemical Society*, 2005, **127**, 11954–11955.

Acknowledgements

Many people who deserve gratitude accumulated over the years. To avoid rambling, I will try to keep myself concise.

The first person I want to thank is Prof. Dr. Ulrich Jonas, who introduced me to macromolecular chemistry and sparked my interest in this interdisciplinary field. The countless hours of discussions and corrections, often intertwined with laughter, which made me a better scientist. He made the time as a PhD student a lot easier and allowed me to start on a completely new topic, when the first topic did not work out at the halfway point. Without his generosity and support, I would not have been able to finish this thesis.

Prof. Dr. Emiliano Descrovi, who initiated the first project of photomotion in hydrogels and lent his ear in many discussions.

Prof. Dr. Holger Schönherr, who made me stay in Siegen and is responsible for many laughs.

Prof. Dr. Mario Agio, who was always ready for collaboration, allowed me to work in his labs with his working group, who made me feel right at home.

Prof. Dr. Thomas Lenzer, who first introduced me to spectroscopy during my studies and now went full circle to take a final look at my work.

Prof. Dr. Ralph Jaquet, who taught me theoretical chemistry, helping me understand so much more of the effects I've found in the end, while we had many, many discussions that were sometimes about science but certainly not exclusively.

Prof. Dr. Heiko Ihmels and Prof. Dr. Michael Schmittel, who never evaded questions or discussions.

Dr. Thomas Paululat, who measured countless NMR spectra for me and never lost his humour in the process, even when he took on the task of teaching me how to use an NMR spectrometer.

Dr. Franck Thétiot, who always jumped to my help, when I needed to talk, and introduced me to the art of devouring a crab.

Dr. Véronique Schwartz, who taught me a lot about chemistry and became a friend that never gave up on me.

Dr. Jakub Dostalek, who taught me how to communicate with physicists in quite some discussions over the years and who always loved to play with new ideas.

Dr. Christian Petri, Dr. Cleiton Kunzler, Dr. Niklas Jung, Dr. Maximilian Meier, whom I have shared many fun hours inside and outside the lab with and who had to suffer through my wild attempts to explain phenomena.

Petra Frank, who always knew where everything was and helped wherever she could in the lab.

Fiona Diehl, Jonas Grün, and Aliia Ibramigova, who suffered with me through night shifts for a while during the pandemic and cheered me up quite often.
Gabriel (Pepe) Gomez, whom I became friends with when I hit my head on a wall, accompanying me since then.
Dr. Daniel John, who's been there since day 1 of my chemistry journey.
Anita Akbarzadeh Solbu, for much laughter and many writing sessions.
Dr. Scarlet Milo, who did her best to improve my English and never really succeeded in the end, but never gave up. I make fewer mistakes now.
Dr. Alexander Haseloer. We started out as strangers on a train, planned a conference together, became friends. Bouncing back and forth ideas whenever I needed to.
Melanie Walther, who threw her relentless optimism at me, when I was about to lose hope for a project.
Denisa Soost, Max Heide and Max Müller, who endured my teaching at first but brightened many days since then.
Silvia Freese, who got through many, many night shifts, many day shifts, many weekend shifts, much time outside of the lab with me, read all my attempts of explaining what the hell is going on with my systems and still seemed like she's having fun.
Everybody from Atto-Tec, whom I shared a corridor with for most of the time and who brought a great atmosphere and energy. Jutta Arden-Jacob, Alexander Zilles, and Norbert Kemnitzer are also some of those, who had to discuss my problems with me and were always happy to.
The many people passing through our labs who continued their journey elsewhere or stayed with us.
The many people I've met at university and summer or winter schools, or the JCF. On some days it's the little things.
My parents and siblings, who have always supported my work and tried to understand the things I didn't understand myself yet.

I've met many people on this journey. And each had their small or big share in solving the problems that are now a thesis.
Thank you.